UC Davis
UC Davis Electronic Theses and Dissertations

Title

29Si Nuclear Magnetic Resonance Spectroscopy: Profiling Silyl Sugar Alcohols, Mono, Di-, and Oligosaccharides, and the Development of a Quantification Method via 29Si NMR for Mono- and Disaccharides

Permalink

https://escholarship.org/uc/item/9pp526zt

Author

Vue, Bao

Publication Date

2024

Peer reviewed|Thesis/dissertation

eScholarship.org Powered by the California Digital Library
University of California

^{29}Si Nuclear Magnetic Resonance Spectroscopy: Profiling Silyl Sugar Alcohols, Mono, Di-, and Oligosaccharides, and the Development of a Quantification Method via ^{29}Si NMR for Mono- and Disaccharides

By

BAO VUE

DISSERTATION

Submitted in partial satisfaction of the requirements for the degree of

DOCTOR OF PHILOSOPHY

In

Chemistry

in the

OFFICE OF GRADUATE STUDIES

of the

UIVERSITY OF CALIFORNIA, DAVIS

Approved:

_____
Professor Jacquelyn Gervay-Hague, Chair

_____
Professor Xi Chen

_____
Professor Annaliese Franz

Committee in Charge
2024

Table of Contents

Abstract ..... **vii**

List of Figures ..... **ix**

List of Tables ..... **xxiii**

List of Schemes ..... **xxix**

List of Equations ..... **xxx**

The Abbreviation List ..... **xxxi**

Acknowledgement ..... **xxxv**

Chapter 1: *The Synthesis and ^{29}Si NMR Characterization of Silylated Carbohydrates* **1**

Abstract **1**

1.1.0 Introduction **2**

1.1.1 Carbohydrates Found in Food 2

1.1.2 Carbohydrate Silylation for Quantitative Analysis 8

1.1.3 The Limitations of Available Quantification Techniques 9

1.1.4 Background on Silicon-29 NMR and Peak Assignments 16

1.2.0 Results and Discussion **29**

1.2.1 Optimized Synthesis and Characterization of Silylated Carbohydrates Using ^{29}Si NMR Spectroscopy 29

1.2.2 Assignment of Methyl-2,3,4,6-Tetra-*O*-TMS-α-Glucopyranoside (**13**). 36

1.2.3. Assignment of 1,2,3,4,6-Penta-*O*-TMS- α-Glucopyranoside (per-*O*-TMS glucose) (**14**) 41

1.2.4. Assignment of 1,3,4,6-Tetra-*O*-TMS-α–Mannopyranoside (α-per-*O*- TMS mannose) (**15**) 43

1.2.5. Assignment of 1,2,3,4,6-Penta-*O*-TMS-β-Fructopyranoside (per-*O*-TMS fructose) (**16**). 46

1.2.6. Assignment of 1,2,3,4,5,6-Hexa-*O*-TMS-Sorbitol (per-*O*-TMS sorbitol) (**17**). 50

1.2.7. Assignment of 1,2,3,4,5-Penta-*O*-TMS Ribitol (per-*O*-TMS ribitol) (**18**) 53

1.2.8. Assignment of 1,2,3,4,5 Penta-*O*-TMS Xylitol (per-*O*-TMS xylitol) (**19**).....57

1.2.9. Assignment of 1,3,4,6,2',3',4',6-Octa-*O*-TMS-Sucrose (per-*O*-TMS sucrose) (**20**).60

1.2.10. Assignment of 2,3,4,6,2',3',4',6'-Octa-*O*-TMS-Trehalose (per-*O*-TMS trehalose) (**21**).....67

1.2.11. Assignment of 1,3,4,6,3',4',6',2",3",4",6"-Unde-*O*-TMS-Kestose (per-*O*-TMS kestose) (**22**).....70

1.2.12. Assignment of 1,3,4,6,2',3',4',2",3",4",6"-Unde-*O*-TMS Raffinose (per-*O*-TMS raffinose) (**23**).....79

1.2.13. Assignment of 1,3,4,6,2',3',4',2",3",4",2'",3"',4"',6'"-Tetrade-*O*-TMS-Stachyose (per-*O*-TMS stachyose) (**24**).....91

1.3.0 Conclusion: Comparison and Contrast of the Silicon Signals in all Twelve Compounds. 97

1.4.0 General Procedure 104

1.4.1 Experimental Conditions..... 104

1.4.2 *General procedure for global silylation of per-O-silylated (TMS) of mono and disaccharides using microwave reactor.* 105

References:..... 202

Chapter 2: *Decoding Silicon in Multidimensional Space: 2D Analysis of Per-O-Silylated Sugars in Silicon vs. Carbon Graph for Accurate Peak Identification* 213

Abstract.....213

2.1.0 Introduction: 214

2.2.0 Result and Discussion 215

2.2.1. Selected Si Signals Overlapping from Various Compounds Pose a Challenge When Assigning Them in Mixtures. 215

2.2.3 A Theoretical Mixture 2D Plot of 12 Persilylate-*O*-Sugars and 1 Internal Standard, per-*O*-TMS DHEA Compound Using Chemical Shift Value from Pure Compound..... 230

2.2.4 Selection of Si2-C2, Si2'-C2', Si2"-C2", and Si4"-C4" NMR chemical shifts as Potential Diagnostic Signals in Mixture..... 234

Upon careful analysis of the 2D graph, it is evident that Si2 signals (indicated by the arrow) from different compounds are notably more dispersed compared to other signals, Figure 2.8. For instance, the Si2 signal (red arrow) from compound **16** is positioned further to the left (upfield), while the Si2 (green arrow) signals from compound **14** are situated within the δ 17 ppm region, and those from compounds **15** (orange arrow) and **17** (purple arrow) fall between δ 15 and 16 ppm, further distinguished by their carbon-13 NMR chemical shifts. 234

2.2.5 The Synthesis of Twelve Per-*O*-Silylated Sugars (**13**-**24**) and an Internal Standard (**25**) as Mixture in One Pot Reaction. 238

2.3.0 Conclusion: 250

2.4.0 Experimental Section 252

2.4.1 *Global silylation of per-O-silylated (TMS) mono, disaccharides, trissacharides, tetrasaccharides and free sugars as mixture stirred at room temperature (mixture of stachyose, kestose, raffinose, trehalose, sucrose, sorbitol, ribitol, xylitol, glucose, mannose, methyl glucoside, fructose, DHEA) at room temperature.* 252

2.4.2 *NMR sample preparation of per-O-silylated (TMS) mono, disaccharides, trissacharides, tetrasaccharides and free sugars as a mixture (mixture of stachyose, kestose, raffinose, trehalose, sucrose, sorbitol, ribitol, xylitol, glucose, mannose, methyl glucoside, fructose, DHEA).* 253

References: 312

Chapter 3: *Quantitative ^{29}Si-NMR Spectroscopy as an Efficient Method for Quantification of Carbohydrate Mixtures* 313

Abstract: 313

3.1.0 Introduction: 314

3.2.0 Result and Discussion 322

3.2.1 Introduction to twelve per-*O*-silylated sugars 322

3.2.2 Investigating the sensitivity of ^{29}Si NMR chemical shifts on concentration. 323

3.2.3 Determination of the Integration Ration of α-Per-*O*-TMS Glucose (**14**), β-Per-*O*-TMS Fructose (**16**), and Per-*O*-TMS Sucrose (**20**) from ^{29}Si Integration in a Synthetic. 330

3.2.4 Determine the Mmol of α-Per-*O*-TMS Glucose (**14**), β-Per-*O*-TMS Fructose (**16**), and Per-*O*-TMS Sucrose (**20**) from Si Integration of Known Amount Mixture..... 337

3.2.5 The Use 3-*O*-*Tert*-Butyldiphenylsilyl-Dehydroepiandrosterone (DHEA-TBDPSi) (**25**) as Internal Standard to Calculate the Mmol of Different Per-*O*-Silylated Mixtures. 343

3.2.6 Calculated the Mmol of Per-*O*-TMS Trehalose From Si Integration of Individual NMR Experiment With 3-*O*-Tert-Butyldiphenylsilane-Dehydroepiandrosterone as Internal Standard. 347

3.2.7 Calculating the Mmol of Per-*O*-Silylated-Trehalose (**21**) From Si Integration Individual Run NMR Experiment With 3-*O*-Trimethylsilane-Dehydroepiandrosterone (**25**) as Internal Standard. 352

3.2.8 Determining the Percent Conversion of α-Per-*O*-TMS Glucose (**14**), β-Per-*O*-TMS Fructose (**16**), and Per-*O*-TMS Sucrose (**20**), Per-*O*-TMS Kestose (**22**), Per-*O*-TMS raffinose (**23**), and Per-*O*-TMS Stachysoe (**24**) Using 3-*O*-Trimethylsilane-Dehydroepiandrosterone (**26**) as Internal Standard. 356

3.3.0: Conclusion 360

3.4.0: Experimental Section 361

3.3.1: NMR Experimental Method: 361

*3.3.2: Global silylation of per-O-silylated (TMS) mono and disaccharides as mixture stirred at room temperature (mixture of glucose (**2**), fructose (**4**), glucose (**8**)).* 362

*3.3.3: Global silylation of per-O-silylated (TMS) mono and disaccharides as mixture stirred at room temperature (glucose (**2**), fructose (**4**), sucrose (**8**), raffinose (**10**), kestose (**11**), stachyose (**12**), and DHEA).* 362

3.3.4: Silylation DHEA-TBDPO. 364

This compound was synthesized by Matthew Orellana in Dr. Jacquelyn Gervay-Hague Laboratory as part of his dissertation.[40] 364

References: 430

Bao Vue
March 2024
Chemistry

Abstract

This dissertation delves into the contemporary significance of carbohydrates across diverse life forms and industries, emphasizing their pivotal role in shaping product quality, safety, and regulatory compliance within sectors like food and beverage, pharmaceuticals, and biofuels. The research capitalizes on significant advancements in nuclear magnetic resonance (NMR) spectroscopy, specifically silicon-29 NMR, extending its applications beyond protons to exert influence in fields such as materials science, biochemistry, and environmental science.

A focal point of the study involves the synthesis of twelve per-*O*-silylated sugars using a microwave reactor, strategically reducing reaction time while preserving yield. Advanced NMR experiments identify silicon signals, providing valuable insights into spatial orientation and distinctive structural variations. The analysis of chemical shifts in per-*O*-silylated sugars contributes to the establishment of an extensive silicon NMR database for comprehensive carbohydrate characterization. Noteworthy patterns in per-*O*-silylated sugars, along with the discernible chemical shifts in diverse silylated compounds, further enhance the depth of the database.

Recent strides in the ^{29}Si NMR characterization technique are underscored, with a specific focus on per-*O*-silylated sugars. The characterization of twelve per-silylated sugars using ^{29}Si NMR spectroscopy, complemented by a 2D graph

incorporating ^{13}C NMR chemical shifts, introduces an innovative approach that optimizes visualization and streamlines compound identification. Despite encountering challenges in a mixture synthesis experiment, where silicon chemical shifts undergo slight changes, the study contributes significantly to our understanding of per-*O*-silylated sugars using ^{29}Si NMR spectroscopy.

The dissertation concludes by addressing the limitations of ^{1}H NMR spectroscopy, introducing the prominence of ^{1}H quantitative nuclear magnetic resonance (qNMR). The Gervay-Hague research group employs ^{29}Si NMR spectroscopy to quantify glucose, sucrose, and fructose within mixtures, which could extend the analysis to encompass coffee and tea leaves. Insights derived from ^{29}Si NMR analysis affirm the reliability of integrated resonances, with the incorporation of a novel internal standard leading to a notable reduction in errors. The ^{29}Si NMR signal corresponding to the 2-hydroxyl position emerges as a consistent and promising diagnostic tool for the quantitative assessment of sample mixtures, thereby showcasing the potential for accurate carbohydrate measurement across a spectrum of applications.

List of Figures

Chapter 1:

Figure 1.1: Chemical structure of monosaccharides found in natural products. Note: configuration for each structure is not given by the literature.....5

Figure 1.2: Chemical structure of free oligossacharides found in a natural product. Note: configuration for each structure is not given by the literature.....6

Figure 1.3: Uronic acids that are shown can be detected using gas chromatography with flame ionization detection..... 14

Figure 1.4: The illustration shown the assignment of pentamethyl(phenyl)silane using ^{1}H-^{29}Si HMBCchemical shift correlations in 2D NMR (HMBC) where F2 is ^{1}H and F1 is ^{29}Si.[63] 21

Figure 1.5: Chemical structures of per-*O*-silylated-methyl-α-glucopyranoside, per-*O*-silylated-methyl-α- galactopyranoside, per-*O*-silylated-methyl-α-mannopyranoside, per-*O*-silylated-methyl-α-6-deoxy-galactopyranoside.[64] 22

Figure 1.6: Showed the doublet and triplet splitting pattern of Si to H, which helped to distinguish silicon signal that bond to methylene (Si6) and methine (Si2-Si4) groups of per-*O*-silylated-methyl-α-glucopyranoside, per-*O*-silylated-methyl-α-galactopyranoside, and per-*O*-silylated-methyl-α-mannopyranoside..... 23

Figure 1.7: ^{1}H-^{29}Si 2D correlations illustrate the intensity of cross peaks from methine or ring protons and trimethylsilyl protons to Si nuclei. Stronger cross-peak intensity is generated from trimethylsilyl protons to Si, with weaker cross-peak intensity observed for Si-methine protons.[65] 24

Figure 1.8: Stepwise of assignments ^{29}Si, initiated by assignment of proton peaks using homonuclear (COSY) and heternuclear (HMBC and HSQC) experiments follow by ^{1}H-^{29}Si HMBC experiment to assign ^{29}Si by correlated the 3 bonds correlation to proton. 24

Figure 1.9: The measurement of ^{29}Si NMR spectra using the INEPT pulse sequence modified for $Si(CH_3)_3$ groups. The specific parameters include a 75 ms polarization, 16 ms refocusing delays optimized for polarization transfer, and a relaxation delay of 10 s.[70] 25

Figure 1.10: The INEPT–gHMQC combination, a modification of the ^{29}Si,^{13}C gHMQC pulse sequence with the substitution of the first ^{29}Si pulse by an INEPT pulse train. The gHMQC portion is adjusted by incorporating a silicon refocusing 180° pulse in the middle to maintain its ^{29}Si refocusing property. This is synchronized with a simultaneous 180° carbon pulse to ensure the desired magnetization development during the T delay. The T delay and the initial 90° ^{13}C pulse facilitate polarization transfer from ^{29}Si to ^{29}Si,^{13}C. The optimal T delay is equal to $1/[^{2}J(Si,C)]$.[70] 26

Figure 1.11: 3 *O*-TMS derivatives of flavone and polyphenol that had been elucidated using long-range coupling constant, (Si,C) gCOSY, and INEPT–gHMQC. 26

Figure 1.12: A study of polyphenol structure assignment based on the long-range ^{29}Si-^{13}C *J* coupling constant from C1-C4. 26

Figure 1.13: The long-range *J* coupling constant of different ^{29}Si-^{13}C on polyphenols para substituents. The substituents on para position showed little influence on the *J* coupling constant. Note, the *J* values were written as they are shown in the literature. 27

Figure 1.14: ^{2}J and ^{3}J coupling constants of $J_{(Si,C)}$ of per-*O*-silylated polyphenols and using these values can help identify the relative assignment of the Si signal such in quercetin. 28

Figure 1.15: The Fermi contact calculated values of ^{2}J (Si-*O*-C1) and ^{3}J (Si-*O*-C1-C2) coupling constants of ^{29}Si-^{13}C for *para* substitutes of different X groups and *O*-TMS. 28

Figure 1.16: Three internal standards, dehydroepiandrosterone-*O*-TMS (**25**), dehydroepiandrosterone-*O*-TBDPSi (**26**), and hexamethydisilazane (HMDS **27**) were synthesized in the lab to use for quantification. 34

Figure 1.17: Pulse sequence of ^{29}Si DEPT experiment; f1 channel is the silicon and f2 channel is proton with 2 s delay relaxation and pulse length of 14 μs and 28 μs on both channels. 35

Figure 1.18: COSY of methyl-2,3,4,6-tetra-*O*-TMS-α-glucopyranoside (**13**), showed cross peak correlation between H1 to H2. 37

Figure 1.19: COSY of methyl-2,3,4,6-tetra-*O*-TMS-α-glucopyranoside (**13**), showed cross peak correlation between H2 to H3. 38

Figure 1.20: COSY of methyl-2,3,4,6-tetra-*O*-TMS-α-glucopyranoside (**13**), showed cross peak correlation between H3 to H4, H4 to H5, and H5 to H6. 38

Figure 1.21: ^{1}H-^{13}C HMBC of methyl-2,3,4,6-tetra-*O*-TMS-α-glucopyranoside (**13**), showed the cross peak correlation between C3 to H4, C4 to H3 and H5, and C5 to H4. 40

Figure 1.22: ^{1}H-^{29}Si HMBC of methyl-2,3,4,6-tetra-*O*-TMS-α-glucopyranoside (**13**) showed cross peak correlation between Si3 to H3 and Si4 to H4, Si to H2 and Si6 to H6ab. 40

Figure 1.23: The ^{1}H-^{29}Si HMBC spectrum of per-*O*-TMS glucose (**14**) showed cross-peak correlations between the proton and silicon signals, which was used to assign the silicon signals. 41

Figure 1.24: The ^{1}H-^{29}Si HMBC spectrum of per-*O*-TMS glucose (**14**) showed cross-peak correlations between the signals of trimethyl groups to the silicon signals. 42

Figure 1.25: The ^{1}H-^{29}Si HMBC spectrum of α-per-*O*-TMS mannose (**15**) showed a cross-peak correlation between the proton and silicon signals, which was used to assign the silicon signal. 44

Figure 1.26: The ^{1}H-^{29}Si HMBC spectrum of α-per-*O*-TMS mannose (**15**) showed a cross-peak correlation between the signals of trimethyl groups to the silicon signal. 45

Figure 1.27: COSY spectrum of β-per-*O*-TMS fructose (**16**) showed the cross-peak correlations between H3 to H4, H1a and H1b, and H6a, H6b and H5 to H6a. 47

Figure 1.28: ^{1}H-^{29}Si HMBC spectrum of β-per-*O*-TMS fructose (**16**) showed the cross-peak correlation of H3 to Si3 and H1a, H1b to Si1. 48

Figure 1.29: ^{29}Si NMR spectrum of β-per-*O*-TMS fructose showed the five signals of Si2 (most upfield at 10.72 ppm) while Si3 is the most downfield at 18.33 ppm. 49

Figure 1.30: The COSY of per-*O*-TMS sorbitol (**17**) showed the cross-peak correlation between H2 to H1a, H1b and H2 to H3 51

Figure 1.31: ^{1}H-^{29}Si HMBC of per-*O*-TMS sorbitol (**17**) showed the cross peaks correlation of H1a, H1b to Si1 and H6a, H6b to Si6. 52

Figure 1.32: COSY spectrum of per-*O*-TMS ribitol (**18**) showed cross peak correlations of H1ab, and H5ab to H2 and H4. 54

Figure 1.33: ^{1}H-^{29}Si HMBC of per-*O*-TMS ribitol (**18**) showed the cross-peak correlation between proton and silicon. 56

Figure 1.34: ^{29}Si spectrum of per-*O*-TMS ribitol (**18**), showed the integration and peak assignment. 56

Figure 1.35: COSY of per-*O*-TMS xylitol (**19**) showed the cross-peak correlation between H2 and H4 to H1ab and H5ab and H2 & H4 to H3. 58

Figure 1.36: ^{1}H-^{29}Si HMBC per-*O*-TMS xylitol (**19**) showed the cross-peak correlation between H1ab and H5ab to Si1, Si5. 58

Figure 1.37: COSY spectrum of per-*O*-TMS sucrose (**20**) showed the cross-peak correlation between H1' to H2', from H2' to H3' and H3' to H4'. 61

Figure 1.38: ^{1}H-^{13}C HMBC of per-*O*-TMS sucrose (**20**) showed the long-range coupling between H1' to C2 and C2' and H5' and H3' to C4', indicated the neighboring proton assignments are correct. 62

Figure 1.39: COSY spectrum of per-O-TMS sucrose (**20**) showed the cross-peak correlation between H3 to H4 and H4 to H5 and the correlation between two H1a and H1b. 63

Figure 1.40: ^{1}H-^{13}C HMBC spectrum of per-*O*-TMS sucrose (**20**) showed the long-range coupling between H1a and H1b to C2 and C5 to H4 and H6. The spectrum showed long-range coupling between H4 and H5 to C3. 64

Figure 1.41: ^{1}H-^{29}Si HMBC spectrum of per-*O*-TMS sucrose (**20**) showed the cross-peak correlation from Si signal from Glcp ring. 65

Figure 1.42: ^{1}H-^{29}Si HMBC spectrum of per-*O*-TMS sucrose (**20**) showed the cross-peak correlation from Si from Fruf rings. 66

Figure 1.43: ^{1}H-^{29}Si HMBC spectrum of per-*O*-TMS trehalose (**21**) showed the cross-peak correlation of proton to silicon for assignment of the 4 signals, Si3, Si2, Si6 and Si4 68

Figure 1.44: ^{1}H-^{29}Si HMBC spectrum of per-*O*-TMS trehalose showed the cross-peak correlation of silicon to CH_3 proton for the assignment of the CH_3 signals 70

Figure 1. 45: Overlap spectra of per-*O*-TMS kestose (**22**), per-*O*-TMS sucrose (**20**), and per-*O*-TMS glucose (**15**) showing the signal of H1", H1' and H1 from each silyl derivatives. The signals are from the equatorial H from the Glc*p* ring. 71

Figure 1.46: TOSCY spectrum of per-*O*-TMS kestose (**22**), showed cross peak correlation of H2" to H1", H3", H5", H6a, and 6b" or from H1" to H2", H4". 72

Figure 1.47: ^{1}H-^{13}C HMBC spectrum of per-*O*-TMS kestose (**22**): showed the cross-peak correlation from H3' to C2', which distinguish between H3 and H3' 73

Figure 1.48: ^{1}H-^{13}C HMBC spectrum of per-*O*-TMS kestose (**22**): showed the cross-peak correlation from H1" to C2', which helped distinguish C2 and C2' 74

Figure 1.49: Per-*O*-TMS kestose (**22**): ^{1}H-^{29}Si HMBC showed the cross-peak correlation between Si1 and H1ab. 77

Figure 1. 50: Overlap of carbon spectra between per-*O*-TMS raffinose (**23**), per-*O*-TMS kestose (**22**), and per-*O*-TMS sucrose (**20**), illustrates similar chemical shift of the carbon signals 78

Figure 1.51*:* ^{1}H-^{13}C HMBC of per-*O*-TMS raffinose (**23**) showed the correlation of H1" to C6' and C2" to distinguish H1" and H1' from 81

Figure 1.52: COSY of per-*O*-TMS raffinose (**23**): Glc*p* ring illustrated the cross-peak correlation between proton assignments of H1" to H2", H4" to H5" and H5" to H6". 82

Figure 1.53: TOCSY of per-*O*-TMS raffinose (**23**) correlation of H1' to H2', H3', H4', & H5' and H1" to H2", H3" &H4"..... 82

Figure 1.54: COSY of per-*O*-TMS raffinose (**23**) of Glc*p* ring: showed the cross peaks correlation of H1' to H2' and H2' to H3'. 83

Figure 1.55: 1D 1H NMR spectrum of per-*O*-TMS sucrose (**20**), per-*O*-TMS raffinose (**23**) and per-*O*-TMS kestose (**22**), showed the H3 chemical shift of Fru*f* ring. 84

Figure 1.56: COSY of per-*O*-TMS raffinose (**23**) of Fru*f* ring: showed cross peak correlation of H3 to H4 and H1a and H1b. 85

Figure 1.57: TOCSY of per-*O*-TMS raffinose (**23**) of Fru*f* ring: showed correlation of H3 to H4, H5, and H6ab. 85

Figure 1.58: ^{1}H-^{29}Si HMBC of per-*O*-TMS raffinose (**23**) of Fru*f* ring-showed the cross peaks of H1a and H1b to one Si signal, Si1..... 87

Figure 1.59: ^{1}H-^{29}Si HMBC of per-*O*-TMS raffinose (**23**) showed the cross peak of TMS-methyl groups correlated with Si signals. 88

Figure 1.60: Overlapped of ^{13}C spectra of three per-*O*-TMS sugars (per-*O*-TMS raffinose (**23**), per-*O*-TMS kestose (**22**), and per-*O*-TMS sucrose (**20**) of Fru*f* rings and their corresponding chemical shifts of C2, C1', and C5 were shown. 90

Figure 1.61: ^{1}H-^{13}C HSQC of per-*O*-TMS raffinose (**23)**, showed the cross peaks correlation of H3 and H4 to their corresponding carbon atoms, C3 and C4 in $CDCl_3$. 90

Figure 1.62: ^{13}C NMR spectra overlapped of per-*O*-TMS kestose (**22**), per-*O*-TMS raffinoses (**23**), and per-*O*-TMS stachyose (**24**); showed the chemical shift of C2, C1''', C1", C1' and C5 from per-*O*-TMS stachyose (**24**) have similar chemical shift values as the corresponding carbon in per-*O*-TMS kestose (**22**) and per-*O*-TMS raffinoses (**23**). 93

Figure 1.63: The ^{1}H-^{13}C HSQC spectrum of per-*O*-TMS stachyose (**24**); showed cross peak correlation of C1''', C1'', C1', C5, C4, and C3 to it corresponding protons. 94

Figure 1.64: Expanded COSY spectrum of per-*O*-TMS stachyose (**24**) showed the cross-peak correlation between H1' to H2', H1" to H2", H1''' to H2''' and H3 to H4. . 95

Figure 1.65: ^{1}H-^{29}Si HMBC spectrum of per-*O*-TMS stachyose (**24**) showed the cross-peak correlation between proton and silicon nuclei. 96

Figure 1.66: 1D ^{29}Si NMR spectra overlap of twelve per-*O*-TMS derivatives (twelve sugars with per-*O*-TMS DHEA as internal standard). The chemical shift reference used was TMS. All spectra acquired in $CDCl_3$. 98

Chapter 2

Figure 2.1: Per-*O*-silylated derivatives that have chemical shift values close to each other. Per-*O*-TMS-α-methylglucoside (**13**), per-*O*-TMS fructose (**16**), per-*O*-TMS ribitol (**18**), per-*O*-TMS sucrose (**20**), per-*O*-TMS trehalose (**21**), per-*O*-TMS kestose

(**22**), per-*O*-TMS raffinose (**23**), and per-*O*-TMS stachyose (**24**). The color codes indicate the chosen *O*-TMS signals used in the studies.....216
Figure 2.2: 2D graph of per-*O*-TMS fructose (**16**) illustrated the NMR chemical shifts of silicon-29 and carbon-13 in 2 dimensional analyses to spread out chemical shifts that are close proximity (C1 and C6 and Si1 and Si3) using the data in Table 2.2...219
Figure 2.3: 2D graph of per-*O*-TMS sorbitol (**17**) illustrated the NMR chemical shifts of silicon-29 and carbon-13 (C1 and C6) in 2 dimensional analyses to spread out NMR chemical shifts that are close proximity using the data from Table 2.3.....221
Figure 2.4: 2D graph of per-*O*-TMS sucrose (**20**) illustrated the NMR chemical shifts of silicon-29 and carbon-13 in 2 dimensional analyses to spread out chemical shifts that are close proximity (Si3 and Si4; C2';C3', and C3:C4) using the data in Table 2.4. 222
Figure 2.5: 2D graph of per-*O*-TMS kestose (**22**); ^{29}Si NMR signals on x-axis and ^{13}C signal on y-axis. Each dot represents the correlation of C atom to Si atom on its chemical shift. The graph illustrated 2D dispersion of close proximity signals (Si2"-Si3"Si6; Si4'-Si4"; Si1-Si4 and C6-C6', C1-C6") using the data from Table 2.5. 224
Figure 2.6: 2D graph of per-*O*-TMS raffinose (**23**) illustrated the NMR chemical shifts of silicon-29 and carbon-13 in 2 dimensional analyses to spread out chemical shifts that are close proximity (Si3'-Si2'-Si3"-Si2"; Si3-Si1-Si6'; Si4"-Si4 and C2"-C4"-C4'-C2-C3"-C3') using the data from Table 2.6.....226
Figure 2.7: 2D graph representation of δ ^{29}Si NMR (axis) vs. ^{13}C NMR (y-axis) of mono, di, tri- and tetra-saccharides. The numbers on the dots represent the Si and C atom and the abbreviation are as follow: per-*O*-TMS methylglucoside (MG-**13**), per-*O*-TMS

glucose (G-**14**), per-*O*-TMS mannose (M-**15**), per-*O*-TMS fructose (F-**16**), per-*O*-sorbitol (S-**17**), per-*O*-ribitol (R-**18**), per-*O*-TMS xylitol (X-**19**), per-*O*-TMS sucrose (Su-**20**), per-*O*-TMS trehalose (T-**21**), per-*O*-TMS kestose (K-**22),** per-*O*-TMS raffinose (Ra-**23**), per-*O*-TMS kestose (K-**22**), per-*O*-TMS stachyose (St-**24**), and per-*O*-TMS DHEA (D-**25**). See Table 1 SI. 231

Figure 2.8: 2D graph representation of δ ^{29}Si NMR (axis) vs. ^{13}C NMR (y-axis) of mono, di, tri- and tetra-saccharides. Selected of Si2 signals indicated by the arrow further analysis. 234

Figure 2.9: 2D graph representation of δ ^{29}Si2 NMR (axis) vs. ^{13}C2 NMR (y-axis) of mono, di, tri- and tetra-saccharides. The graph showed the diagnostic signal of Si_2 and $Si_{2''}$ from twelve per-*O*-silylated sugars derivatives (**13-24**) and the internal standard per-*O*-TMS DHEA (D-**25**). This graph showed only the Si2 or 2" signals from each compound. 236

Figure 2.10: 2D graph representation of δ ^{29}Si NMR (axis) vs. ^{13}C NMR (y-axis) of mono, di, tri- and tetra-saccharides. The graph showed the diagnostic signal Si2 and Si4 of twelve per-*O*-silylated sugars derivatives (**13-24**) and the internal standard DHEA-*O*-TMS (D-**25**). 238

Figure 2.11: ^{29}Si NMR spectra between pure per-*O*-TMS glucose (**14**) and mixture sample of all twelve per-silylated derivatives. The spectra showed small Δ values of the chemical shifts Si1 and Si6 between the pure and mixture compound. 240

Figure 2.12: ^{29}Si NMR spectra between pure per-*O*-TMS glucose (**14**) and mixture sample of all twelve per-silylated derivatives. The spectra showed small Δ values of the chemical shifts Si3 and Si2 between the pure and mixture compound. 241

Figure 2.13: ^{13}C NMR spectra overlapped between pure per-*O*-TMS glucose (**14**) and mixture sample of all twelve per-silylated derivatives. The spectra showed there is no Δ value (deviation) of the chemical shift between the pure and mixture compound. 241

Figure 2.14: ^{29}Si NMR spectra between pure per-*O*-TMS kestose (**22**) and mixture sample of all twelve per-*O*-silylated derivatives. The spectra showed small Δ values of the chemical shifts Si4' and Si4" between the pure and mixture compound. 243

Figure 2.15: ^{29}Si NMR spectra between pure per-*O*-TMS kestose (**22**) and mixture sample of all twelve per-*O*-silylated derivatives. The spectra showed small Δ values of the chemical shifts Si1 and Si4 between the pure and mixture compound. 244

Figure 2.16: ^{13}C NMR spectra overlapped between pure per-*O*-TMS kestose (**22**) and mixture sample of all twelve per-*O*-silylated derivatives. The spectra showed there is no Δ value (deviation) of the chemical shift between the pure and mixture compound. 244

Figure 2.17: The overlapped spectra of mixture per-*O*-TMS fructose (**16**) and its pure compound (bottom). The spectra show distinct signals for each ^{29}Si NMR signal, facilitating the assignment of Si4, Si6, and Si2 in the mixture.....247

Figure 2.18: 2D graph representation of δ ^{29}Si NMR (axis) vs. ^{13}C NMR (y-axis) of mono, di, tri- and tetra-saccharides from Table 2.9. This graph shows the signals that could be assigned from the reaction mixture of free sugar to per-*O*-silylated derivatives (**13-25**).....249

Chapter 3:

Figure 3. 1: ^{1}H NMR spectrum of a sample mixture containing per-*O*-TMS glucose (**14**), per-*O*-TMS fructose (**16**), and per-*O*-TMS sucrose (**20**).....320

Figure 3.2: ^{29}Si NMR spectrum of a sample mixture containing per-*O*-TMS glucose (**14**), per-*O*-TMS fructose (**16**), and per-*O*-TMS sucrose (**20**). These spectra illustrated the difference of peak overlapped between ^{1}H and ^{29}Si spectra. All peaks are resolved in ^{29}Si NMR. 321

Figure 3.3:Pulse sequence of ^{29}Si DEPT experiment; f1 channel is the silicon and f2 channel is proton with 2 s delay relaxation and pulse length of 14 μs and 28 μs on both channels. 324

Figure 3.4: Optimizing ^{29}Si NMR quantification: a comprehensive guide to stepwise sample preparation and data processing. 324

Figure 3.5: The three internal standard uses for the study of ^{29}Si NMR quantification. Internal standard **25** and **26** were synthesized in the lab as solids and HMDS (**26**) was purchased as a liquid.....325

Figure 3.6: Stacked spectra of different concentrations from 0.0125 M to 0.500 M of α-per-*O*-TMS-glucose (**14**) spectra zoom in region of Si signal from glucose ring..327

Figure 3.7: Stacked spectra of different concentrations from 0.0125 M to 0.500 M of α-per-*O*-TMS-glucose (**14**) spectra zoom in region of reference Si signals, HMDS and TMS.....327

Figure 3. 8: ^{13}C stacked spectra of different concentrations from 0.0125 M to 0.500 M of α-per-*O*-TMS glucose (**14**) in the HMDS δ 2.45 and TMS region.....329

Figure 3. 9: ^{13}C stacked spectra of different concentrations from 0.0125 M to 0.500 M of α-per-*O*-TMS glucose (**14**) in the $CDCl_3$ region where the middle peak at δ 76.98. 329

Figure 3.10: (4) is ^{29}Si NMR spectra of a reaction mixture containing (**14**), (**16**), and (**20**) in 1:1:1 ratio in $CDCl_3$ stirred at room temperature for 24 h. (3), (2), and (1) are pure ^{29}Si spectra of per-*O*-TMS sucrose (**20**), β-per-*O*-TMS fructose (**16**), and α-per-*O*-TMS glucose (**14**) respectively.....331

Figure 3.11: NMR samples preparation for ratio study of reaction mixture contained α-per-*O*-TMs glucose (**14**), β-per-*O*-TMS fructose (**16**), and per-*O*-TMS sucrose (**20**). 332

Figure 3.12: NMR samples preparation for calculating mmol (quantification study) of mixture contained α-per-*O*-TMS glucose (**14**), β-per-*O*-TMS fructose (**16**), and per-*O*-TMS sucrose (**20**).....338

Figure 3.13: 3-*O*-tert-butyldiphenylsilane-dehydroepiandrosterone (**26**) is the internal standard used for the mmol calculated from per-*O*-TMS-sugars (left) and the ^{29}Si NMR of this IS on the right. 344

Figure 3.14: 3-*O*-trimethylsilane-dehydroepiandrosterone (**25**) is the internal standard used for the mmol calculated from per-*O*-TMS trehalose (**21**) and the ^{29}Si NMR of this IS. 353

Figure 3.15: ^{29}Si NMR spectrum of α-per-*O*-TMS glucose (**14**), β-per-*O*-TMS fructose (**16**), per-*O*-TMS sucrose (**20**), per-*O*-TMS kestose (**22**), per-*O*-TMS raffinose (**23**),

and per-*O*-TMS stachysoe (**24**) with internal standard, DHEA-*O*-TMS (**26**) as a mixture synthesized from free sugar and DHEA. 358

List of Tables

Chapter 1:

Table 1.1: Fruits, vegetables and drinks that contain common sugars like glucose, fructose, and surcose. [1,2,3,4,5] 3

Table 1.2: The ^{29}Si chemical shift for silyl derivative. These chemical shifts help illustrate that there is no peak overlap between these compounds, even when just two junctions at positions 3 or 4 are different.[56] 18

Table 1. 3: The twelve per-*O*-silylated sugars studied. 30

Table 1.4: The ^{1}H, ^{13}C, ^{29}Si NMR chemical shifts (δ) methyl-2,3,4,6-tetra-*O*-TMS-α-glucopyranoside (per-*O*-TMS methylglucosdie) (**13**) in $CDCl_3$. 39

Table 1.5: The ^{1}H, ^{13}C, ^{29}Si NMR chemical shifts (δ) 1,2,3,4,6-penta-*O*-TMS- α-glucopyranoside (**14**) (per-*O*-TMS glucose) in $CDCl_3$. 43

Table 1.6: The ^{1}H, ^{13}C, ^{29}Si chemical shifts (δ) 1,2,3,4,6-penta-*O*-TMS- α-mannopyranoside (**15**) (per-*O*-TMS-mannose) in $CDCl_3$. 46

Table 1.7: The ^{1}H, ^{13}C, ^{29}Si NMR chemical shifts (δ) 1,2,3,4,6-penta-*O*-TMS-β-fructopyranoside (per-*O*-TMS fructose) (**16**) in $CDCl_3$. 50

Table 1. 8: The ^{1}H, ^{13}C, ^{29}Si NMR chemical shifts (δ) of 1,2,3,4,5,6-hexa-*O*-TMS-sorbitol (**17**) (per-*O*-TMS sorbitol) in $CDCl_3$. 53

Table 1.9: The ^{1}H, ^{13}C, ^{29}Si NMR chemical shifts (δ) of 1,2,3,4,5 penta-*O*-TMS ribitol (**18**) (per-*O*-TMS ribitol) in $CDCl_3$. 55

Table 1.10: The ^{1}H, ^{13}C, ^{29}Si NMR chemical shifts (δ) of 1,2,3,4,5 penta-*O*-TMS xylitol (**19**) (per-*O*-xylitol) in $CDCl_3$. 60

Table 1.11: The ^{1}H, ^{13}C, ^{29}Si NMR chemical shifts (δ) of 1,3,4,6,2',3',4',6-octa-*O*-TMS-sucrose (per-O-TMS sucrose) (**20**) in$CDCl_3$..... 67

Table 1.12: The ^{1}H, ^{13}C, ^{29}Si NMR chemical shifts (δ) of 2,3,4,6,2',3',4',6'-octa-*O*-TMS-trehalose (per-*O*-TMS trehalose) (**21**) in$CDCl_3$. 69

Table 1.13: Comparison of chemical shift of δ ^{1}H, δ ^{29}Si, and δ ^{13}C between per-*O*-TMS ketose and per-*O*-TMS sucrose. The Δ of δ ^{1}H, and δ ^{13}C between two compounds are small, however the Δ for δ ^{29}Si is large. 75

Table 1.14: The ^{1}H, ^{13}C, ^{29}Si NMR chemical shifts (δ) of 1,3,4,6,2',3',4',2",3",4",6"-unde-*O*-TMS-raffinose (per-*O*-TMS raffinose) (**23**) 91

Table 1.15: The ^{1}H, ^{13}C, ^{29}Si NMR chemical shifts (δ) of 1,3,4,6,2',3',4',2",3",4",2'",3"',4"',6'" -tetrade-*O*-TMS-stachyose (per-*O*-TMS stachyose) (**24**)..... 97

Table 1.16: **Δ** values of ^{29}Si NMR between per-*O*-TMS mannose (**15**) and per-*O*-TMS glucose (**14**) 99

Table 1. 17: Sugars' purity and hydrates contents are as described below:.....105

Chapter 2:

Table 2.1: The ^{29}Si NMR signal values from different per-*O*-TMS compounds exhibit close proximity in chemical shift. These signals are so closely aligned, with a range of +/- 0.01, that they can fully overlap in the spectrum. 217

Table 2.2: The δ values of ^{29}Si NMR and ^{13}C NMR, along with the integration values* for per-*O*-TMS fructose (**16**). *The integration values were measured by referencing

Si_2 as a standard with a value of 1.00, not an internal standard integration reference. 220

Table 2.3: The δ values of ^{29}Si NMR and ^{13}C NMR signals, along with the integration values* for per-*O*-TMS sorbitol (**17**). *The integration values were measured by referencing Si_2 as a standard with a value of 1.00, not an internal standard integration reference. 220

Table 2.4: The δ values of ^{29}Si NMR and ^{13}C NMR, along with the integration values* for per-*O*-TMS sucrose (**20**). *The integration values were measured by referencing Si_2 as a standard with a value of 1.00, not an internal standard integration reference. 223

Table 2.5: The δ values of ^{29}Si NMR and ^{13}C NMR, along with the integration values* for per-*O*-TMS kestose (**22**). *The integration values were measured by referencing Si_2 as a standard with a value of 1.00, not an internal standard integration reference. 225

Table 2.6: The δ values of ^{29}Si NMR and ^{13}C NMR, along with the integration values* for per-*O*-TMS raffinose (**23**). *The integration values were measured by referencing Si_2 as a standard with a value of 1.00, not an internal standard integration reference. 227

Table 2.7: The δ values of ^{29}Si NMR and ^{13}C NMR, along with the integration values* for the remaining 7 compounds. The^{29}Si NMR and ^{13}C NMR, values could be used to show their dispersion in 2D plot. *The integration values were measured by referencing Si_2 as a standard with a value of 1.00, not an internal standard integration reference. 228

Table 2.8: The alternative chemical shifts of ^{29}Si NMR and ^{13}C NMR that are used for the 2D graph to eliminate overlapped of compound **12**, **14**, **15**, and 16. 237

Table 2.9: The assignable silicon signals for compound **13-26** from a reaction mixture of these thirteen free sugars with DHEA. The Δ values calculated indicated the deviation of the mixture from the pure compound. The integration values integrated respected to compound **26**, internal standard synthesized with the mixture. The chemical shifts reported to the thousandth place to illustrate the Δ values between pure and mixture per-*O*-silylated sugars.....245

Table 2.10: The table below contains the theoretical values (mmol and mass) of each derivative. Using the theoretical values, the overall percentage yield was calculated as shown.....253

Chapter 3:

Table 3.1: ^{29}Si NMR integration values obtained from an equal mole ratio sample contained α-per-*O*-TMs glucose (**14**), β-per-*O*-TMS fructose (**16**), and per-*O*-TMS sucrose (**20**). Triplicate experiments were conducted in $CDCl_3$. HMDS was used as internal standard and set as reference at 1.00.....333

Table 3.2: The relative ratio obtained used ^{29}Si NMR integration values from an equal mole ratio sample containing α-per-*O*-TMS-glucose (**14**), β-per-*O*-TMS-fructose (**16**), and per-*O*-TMS-sucrose (**20**). Three experiments were conducted in $CDCl_3$. HMDS was used as internal standard and set as reference at 1.00.....335

Table 3.3: The integrations of α-per-*O*-TMs glucose (**14**), β-per-*O*-TMS fructose (**16**), and per-*O*-TMS sucrose (**20**) from mixtures of triplicate ^{29}Si NMR experiment at different ratios. 339

Table 3.4: The calculated mmol from ^{29}Si NMR integration in a mixture contained α-per-*O*-TMS glucose (**14**), β-per-*O*-TMS fructose (**16**), and per-*O*-TMS sucrose (**20**) at different mol ratio and HMDS (**27**) was used as internal standard. 341

Table 3. 5: The calculated mmol from ^{29}Si NMR integration in a mixture contained α-per-*O*-TMS glucose (**14**), β-per-*O*-TMS fructose (**16**), and per-*O*-TMS sucrose (**20**) with DHEA-TBDPSi (**25**) as internal standard. 345

Table 3.6: The calculated mmol from ^{29}Si NMR integration of per-*O*-TMS trehalose (**21**) using DHEA-TBDPSi (**25**) was used as internal standard. The experiments were carried out as 1:1, 0.5:1 and 0.25:1 ratio of per-*O*-TMS trehalose (**21**) to DHEA-TBDPSi (**25**).....349

Table 3.7: The percent error from ^{29}Si NMR integration of per-*O*-TMS trehalose (**21**) using DHEA-TBDPSi (**25**) was used as internal standard. The experiments were carried out as 1:1, 0.5:1 and 0.25:1 ratio of per-*O*-TMS trehalose (**21**) to DHEA-TBDPSi (**25**).....349

Table 3.8: The calculated mmol from ^{29}Si NMR integration of per-*O*-TMS-trehalose (**21**) using DHEA-*O*-TMS (**26**) as internal standard. The experiments were carried out as 1:1 ratio of per-*O*-TMS-trehalose (**21**) to DHEA-*O*-TMS (**26**). The percentage error of each experiment is shown in the right column and each signal shown at bottom. 355

Table 3.9: The integration and chemical shifts (**δ)** from a reaction mixture synthesized from free sugars to produce α-per-*O*-TMS glucose (**14**), β-per-*O*-TMS fructose (**16**), per-*O*-TMS sucrose (**20**), per-*O*-TMS kestose (**22**), per-*O*-TMS raffinose (**23**), per-*O*-TMS stachysoe (**24**) and DHEA-*O*-TMS (**26**). 357

Table 3.10: The mmol of free sugars and theoretical mmol of the per-silylated sugars use to calculate the theoretical concentration of each individual silylated sugar. ... 359

Table 3. 11: The integration and chemical shifts (**δ)** from a reaction mixture synthesized from free sugars to produce α-per-*O*-TMS glucose (**14**), β-per-*O*-TMS fructose (**16**), per-*O*-TMS sucrose (**20**), per-*O*-TMS kestose (**22**), per-*O*-TMS raffinose (**23**), and per-*O*-TMS stachysoe (**24**) and additional 1 equiv. of DHEA-*O*-TMS (**26**) added. 360

Table 3.12: Mass and theoretical mass of free sugars and per-*O*-silylated (TMS) in mg used in synthesis trail 2. 363

Table 3.13: Mass and theoretical mass of free sugars and per-*O*-silylated (TMS) in mg used in synthesis trail 3. 364

List of Schemes

Chapter 1:

Scheme 1.1: A silylation reaction of alcohol was performed using pyridine, TMSCl, and HMDS. 9

Scheme 1. 2: Microwave synthesis of per-*O*-silylated monosacharides, disaccharides, and oligosaccharides. 29

Chapter 3:

Scheme 3.1: Synthesis of α-per-O-TMS glucose (**14**), β-per-O-TMS fructose (**16**), and per-O-TMS sucrose (**20**) as reaction mixture. 330

List of Equations

Chapter 3:

Equation 3.1: Integration Ratio Calculation 334

Equation 3.2: mmol calculation from integration 340

Equation 3.3: Percent Error Calculation 347

The Abbreviation List

Chapter 1:

1. Nuclear Magnetic Resonance (NMR)
2. Distortionless Enhancement by Polarization Transfer (DEPT)
3. Insensitive Nuclei Enhanced by Polarization Transfer (INEPT)
4. Heteronuclear Multiple Bond Correlation (HMBC)
5. Heteronuclear Single Quantum Coherence (HMQC)
6. Heteronuclear Single Quantum Coherence (HSQC)
7. Corelated Spectroscopy (COSY),
8. Nuclear Overhauser Effect (NOE)
9. Non-Starch Polysaccharides (NSPs)
10. Seed Polysaccharides (TSPS)
11. Tea Polysaccharides (TPSs)
12. Rhamnose (Rha)
13. Xylose (Xyl)
14. Arabinose (Ara)
15. Glucose (Glc)
16. Galactose (Gal)
17. Glucuronic Acid (GulA)
18. Galacturonic Acid (GalA)
19. Mannuronic Acid (ManA)
20. Guluronic Acid (GulA)
21. Fucose (Fuc)

22. Mannose (Man)

23. Ribose (Rib)

24. Sucrose (Suc)

25. Maltose (Mal)

26. Lactose (Lac)

27. Raffinose (Raf)

28. Fructose (Fru)

29. Stachyose (Sta)

30. Mannitol (Man-ol)

31. Trimethylsilyl (TMS)

32. Trimethylchlorosilane (TMSCl)

33. Hexamethyldisilazane (HMDS)

34. Trimethylsilyl oximes (TMSO)

35. 3,5-Dinitrosalicylic acid (DNS)

36. 1-Phenyl-3-methyl-5-pyrazolone (PMP)

37. High-Performance Liquid Chromatography (HPLC)

38. Gas Chromatography (GC)

39. Association of Official Analytical Chemists (AOAC International)

40. Evaporative Light Scattering Detector (ELSD)

41. Refractive Index Detector (RID)

42. Ultraviolet-Visible (UV-VIS)

43. Near-Infrared (NIR)

44. Mid-Infrared (MIR)

45. Far-Infrared (FIR)
46. Partial Least Square Regression (PLSR)
47. Low Molecular Weight Carbohydrates (LMWC)
48. Supplemental Information (SI)

Chapter 2:

1. per-*O*-TMS methylglucoside (MG-**13**),
2. per-*O*-TMS glucose (G-**14**),
3. per-*O*-TMS mannose (M-**15**),
4. per-*O*-TMS fructose (F-**16**),
5. per-*O*-sorbitol (S-**17**),
6. per-*O*-ribitol (R-**18**),
7. per-*O*-TMS xylitol (X-**19**),
8. per-*O*-TMS sucrose (Su-**20**),
9. per-*O*-TMS trehalose (T-**21**),
10. per-*O*-TMS kestose (K-**22),**
11. per-*O*-TMS raffinose (Ra-**23**),
12. per-O-TMS kestose (K-**22**),
13. per-*O*-TMS stachyose (St-**24**)
14. per-*O*-TMS DHEA (D-**25**)

Chapter 3:

1. Quantitative Nuclear Magnetic Resonance (qNMR)
2. Quantitative Proton NMR (qHNMR)
3. Limit of Detection (LOD)
4. Limit of Quantification (LOQ)
5. Hexamethyldisilsane (HMDSS)
6. Internal Standard (IS)

Acknowledgement

I am deeply grateful for the unwavering support and encouragement I received throughout my education journey, which began alongside my new settlement here in the United States. My heartfelt appreciation goes to my loving parents, Fai Dang Vue and Youa Yang, who instilled in me the belief that education is the key to success. Despite facing numerous challenges with their limited English and knowledge, they never hesitated to provide me with their invaluable support. Without their love and guidance, I would not have achieved this level of academic success.

I am indebted to the numerous advisors who played pivotal roles in guiding me along the path to college. I owe a tremendous debt of gratitude to Irene Buchanan, my migrant counselor at Roosevelt High School, whose unwavering support and inspiration guided me through pivotal moments of my educational journey. She is truly the person whom I consider my educational mother.

My journey was further enriched by the guidance and mentorship of Dr. Saeed Attar, my Bachelor's and Master's research advisor. His belief in my abilities and relentless encouragement pushed me to explore new horizons in research and academia. I am also deeply thankful to the Chemistry Department at Fresno State, which I proudly consider my second home. Their unwavering support and opportunities for research under Dr. QiaoHong Chen's guidance have been instrumental in shaping my academic endeavors.

I am profoundly grateful to the Chemistry Department at UC Davis for their invaluable support and financial assistance throughout my studies. I extend my sincerest appreciation to Dr. Jacquelyn Gervay-Hague for her unwavering guidance,

patience, and support during my Ph.D. journey. Her mentorship and understanding during challenging times empowered me to persevere and complete my research and dissertation.

I am also thankful to my committee members for their insightful suggestions and guidance throughout my dissertation process. Their expertise and dedication have been invaluable assets to my academic journey.

In addition, I extend my heartfelt gratitude to my extended family members and friends whose unwavering belief in me, and steadfast support have been constant sources of strength and inspiration. I am deeply appreciative of everything they have done to help me reach this significant milestone in my education. Their love and support have truly been the cornerstone of my success.

Lastly, I want to acknowledge the funding from the National Science Foundation, Grant Number 1902488, and the University of California, Davis Bridge Program, UC Davis OR, MPS Dean Department of Chemistry for their support of my research under the supervision of Dr. Jacquelyn Gervay-Hague.

Chapter 1:

The Synthesis and ^{29}Si NMR Characterization of Silylated Carbohydrates

Abstract

Carbohydrates (from natural products) are essential for all forms of life, playing crucial roles in both plants and humans. In the food and beverage industry, identifying and quantifying carbohydrates is vital for ensuring product quality and nutritional accuracy. In the pharmaceutical industry, carbohydrate analysis is crucial for drug formulation and efficacy. In the biofuel industry, measuring carbohydrate content is essential for optimizing fuel production. Accurate carbohydrate analysis is also important for maintaining safety and regulatory compliance across these industries. The field of nuclear magnetic resonance (NMR) spectroscopy has made remarkable advancements, especially in the identification and quantification of nuclei beyond protons, broadening its applications in fields such as materials science, biochemistry, and environmental science. With the prevalence of silicon compounds in various applications, Silicon-29 NMR has gained importance. In this study, twelve per-*O*-silylated sugars were synthesized in a microwave reactor, which reduced the reaction time from overnight to 1 hour, while still maintaining the yield compared to room temperature synthesis. The silicon signals were assigned using Distortionless Enhancement by Polarization Transfer (DEPT) and ^{1}H-^{29}Si Heteronuclear Multiple Bond Correlation (HMBC) NMR experiments. The comparison of chemical shifts in per-*O*-silylated mannose and glucose reveals valuable insights into Si2 spatial

orientation, contributing to unique structural variations between the compounds. Consistent patterns of Si4 and Si2 in per-*O*-silylated galactose (literature review) as well mannose and glucose in this study indicated that axial ^{29}Si NMR signal is more upfield than equatorial ^{29}Si NMR signal. The Fru*f* chemical shifts are downfield compared to Glc*p* in di- and trisaccharide silyl derivatives. The presence of a stereocenter influences ^{29}Si NMR chemical shifts, leading to noticeable differences in silylated compounds like per-*O*-silylated-xylitol and per-*O*-silylated-ribitol. This distinctness of chemical shifts led to the creation of an extensive silicon NMR database and characterizes carbohydrates.

1.1.0 Introduction

1.1.1 Carbohydrates Found in Food

The human diet relies heavily on dietary carbohydrates, including monosaccharides, disaccharides, starch, and non-starch polysaccharides (NSPs) to provide energy for the body's metabolic processes. In addition, carbohydrates play a crucial role in many aspects of our lives, from their importance as a source of energy in the human diet to their use as raw materials to produce drugs, cosmetics, and other consumer products. Plant-based foods such as fruits, vegetables, edible seeds, grains, legumes, and wholegrains are considered dependable sources of dietary carbohydrates for humans.[1,2] Carbohydrates such as monosaccharides, α-linked disaccharides, oligosaccharides, and starch are digestible carbohydrates. These are the main sources of human nutrition. Naturally occurring monosaccharides like glucose, fructose, and galactose can be found in many vegetables and fruits as shown

in Table 1.1.[1,2,3,4,5] Meanwhile, disaccharides like sucrose, maltose, and lactose are easily broken down into their monosaccharide components.[1]

Table 1.1: Fruits, vegetables and drinks that contain common sugars like glucose, fructose, and surcose. [1,2,3,4,5]

Fruit/Vegetable	Glucose	Fructose	Sucrose
Apples	☑	☑	☑
Apricots	☑	☑	☑
Avocado	☑	☑	☑
Bananas	☑	☑	☑
Dates	☑	☑	☑
Grapefruit	☑	☑	☑
Grapes	☑	☑	☑
Green figs	☑	☑	☑
Peaches	☑	☑	☑
Persian limes	☑	☑	☑
Pineapples	☑	☑	☑
Plums	☑	☑	☑
Strawberries	☑	☑	☑
Blueberry	☑	☑	☑
Goji Berry	☑	☑	☑
Cocoa beans	☑	☑	☑
Potation	☑	☑	☑
Blackberry	☑	☑	☑
Jucara fruit	☑	☑	☑
Carob	☑	☑	☑
Wofberry fruit	☑	☑	☑
Tea	☑	☑	☑
Coffee	☑	☑	☑
Sweet potatoes	☑	☑	☑

The naturally occurring monosaccharides and disaccharides, including glucose, fructose, and sucrose, are not only abundant in fruits and vegetables, but also represent a significant proportion of the carbohydrates present in teas and coffee.[6,7] In fact, they constitute the majority of the carbohydrate content in these beverages. The quantity of total sugar detected in tea is contingent upon the specific variety of tea and the botanical source of the plant. However, it's worth noting that the

carbohydrate composition of different tea varieties can vary depending on factors such as the growing conditions, harvesting time, and processing methods used.

Tea, made from the leaves of the *Camellia sinensis* plant, has been consumed for thousands of years in many cultures throughout the world, particularly in Asia. *Camellia sinensis* contains a variety of compounds, with polyphenols being the most abundant. Other compounds found in green tea leaves, include carbohydrates, lipids, proteins, minerals, caffeine, and amino acids.[8,9] Tea plants are widely recognized for their potential health benefits and have been the subject of numerous research studies. [6]

The total sugar content in three distinct parts of the tea plant was measured - leaves, seeds, and flowers. The study findings showed that the leaves contained 20.80% of total sugars, the seeds contained 47.58%, and the flowers contained 62.84%.[8] The study also found that tea seed polysaccharides (TSPS) consisted of seven monosaccharide types, namely rhamnose (Rha), xylose (Xyl), arabinose (Ara), glucose (Glc), galactose (Gal), as shown in Figure 1.1, glucuronic acid (GulA), and galacturonic acid (GalA), as shown in Figure 1.3. Although the sugar backbone of TSPS was thought to be glucose, the branched chain may contain rhamnose, xylose, arabinose, and galactose. Furthermore, the tea leaves were found to contain tea polysaccharides (TPSs) at a concentration ranging from 1.5% to 13%, comprising 2-10 monosaccharides such as glucose, rhamnose, arabinose, xylose, galactose, fucose (Fuc), mannose (Man), ribose (Rib), (as shown in Figure 1.1), galacturonic acid, and glucuronic acid.[8,10]

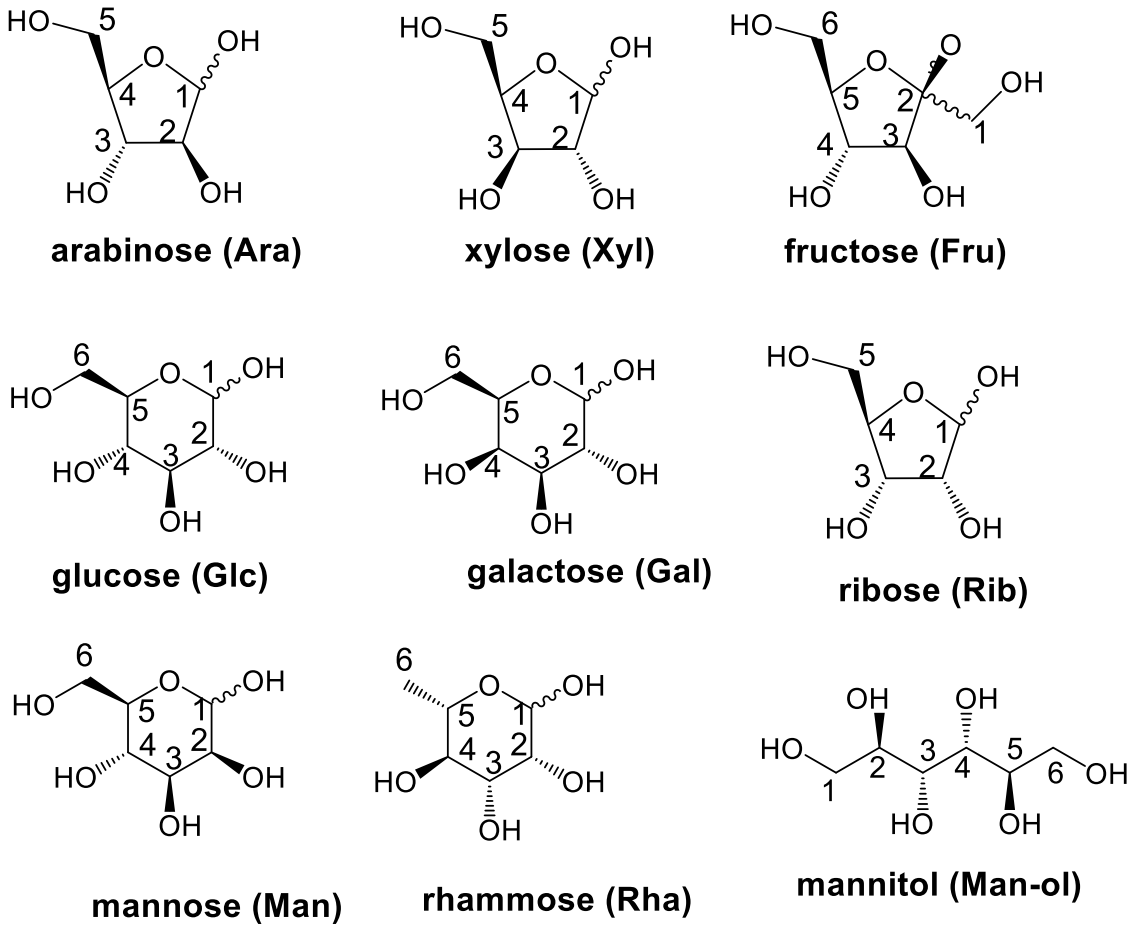

Figure 1.1: Chemical structure of monosaccharides found in natural products. Note: configuration for each structure is not given by the literature.

In another study, it was observed that the sugar profile of tea leaves comprises soluble sugars including fructose, glucose, sucrose (Suc), maltose (Mal), lactose (Lac), and raffinose (Raf) as shown in Figure 1.2. Notably, sucrose was identified as the predominant saccharide, constituting 50-82% of the total sugar pool. More specificity, the content of sucrose increased with the maturity of the tea leaves, with leaves at the bottom of the stem having the highest sucrose content of 37.56±3.12 mg/g dry weight.[11] It has been reported that green tea shoots contain varying amounts of polysaccharides, and low molecular weight carbohydrates.

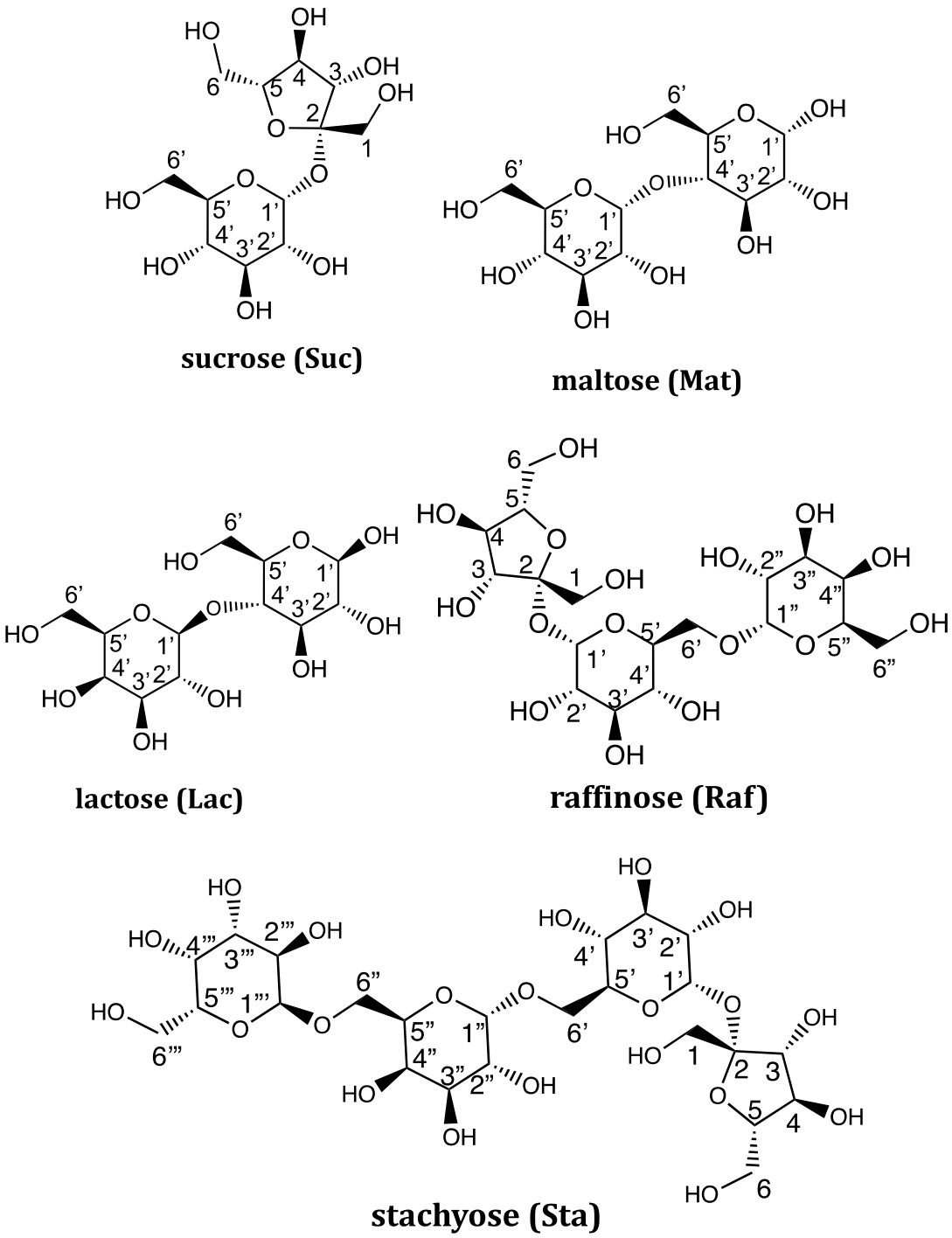

Figure 1.2: Chemical structure of free oligossacharides found in a natural product. Note: configuration for each structure is not given by the literature.

Specifically, green tea shoots consist of 4-10% polysaccharides and 3-5% low molecular weight carbohydrates (LMWC). The free sugars, glucose, fructose (Fru), as shown in Figure 1, sucrose, raffinose (Raf), and stachyose (Sta), as shown in Figure 1.2, are the major types of LMWC found in *Camellia sinensis*.[9] More specific, tea shoot tips were found to have glucose and fructose content ranging from 0.3-0.8%, and sucrose content ranging from 0.9-2.3%. The total soluble carbohydrate content of tea shoot tips, on a dry weight basis, was reported to be between 1.3-3.1%.[12] As previously stated, the sugar concentration in tea can vary depending on factors such as the tea type, freshness, and processing. A conducted study revealed that fresh tea leaves contained significantly higher levels of fructose, glucose, and sucrose compared to the bud and older leaves. Interestingly, the concentration of these sugars was lowest in black tea made using the bud and older leaves. [12]

Sucrose is one of the most important precursors, as it is the major free sugar in green coffee beans, and its amount depends on the coffee species and source. Carbohydrates are the main constituents of Arabica coffee (34-44%) and Robusta coffee (48-55%).[13] Free monosaccharides, including arabinose, fructose, glucose, galactose, mannose, mannitol (Man-ol), as shown in Figure 1.1, rhamnose, ribose, and xylose, as well as the disaccharide sucrose and water-soluble oligosaccharides such as raffinose (trisaccharide) and stachyose (tetrasaccharide) were also found in raw bean.[14] The levels of fructose and glucose in green coffees (Coffea arabica L. var. Acai`a) were found to be higher when using dry processed method (unwashed coffee) compared to using wet processed (washed coffee) methods. Other sugars like galactose, arabinose, and mannose were also decreased using wet method, however,

sucrose, the major low molecular weight sugar, was not significantly impacted by dry processing.[15] Green coffee beans contain significant amounts of sucrose, glucose, and fructose.[16]

1.1.2 Carbohydrate Silylation for Quantitative Analysis

Various methods, such as high-performance liquid chromatography (HPLC) and gas chromatography (GC), have been used to identify and quantify sugars. These methods have limitations and are time-consuming.[17] To analyze sugars using GC, chemical derivatization is required to produce volatile molecules. Literature reviews often mention several typical carbohydrate derivatives, such as methyl ethers, acetates, trifluoroacetates, and trimethylsilyl ethers. Among these, trimethylsilyl (TMS) ethers are the most favored derivatives due to their excellent stability and volatility properties.[18] Trimethylsilyl ethers, obtained through silylation, which is a chemical technique used to convert non-volatile organic compounds, into volatile derivatives, can be analyzed using gas chromatography. The process involves the addition of a silylating agent, such as trimethylchlorosilane (TMSCl) or hexamethyldisilazane (HMDS), to the sample, which reacts with the hydroxyl groups of the compound to form a volatile silylated derivative.[17,19,18]

In Gorwitz's paper, it was mentioned that Sauer conducted the first silylation experiment, in which he used trimethylchlorosilane and pyridine to silylate ethyl and methyl alcohol. Later, Mjorne introduced hexamethyldisilazane for amine silylation, and Spier combined HMDS with TMSCl to silylate alcohols and phenols, Scheme 1.[19] Hexamethyldisilazane and trimethylchlorosilane are common silylation reagents used with pyridine as a solvent.[18,20,21,22,23] Silylation can also be carried out using

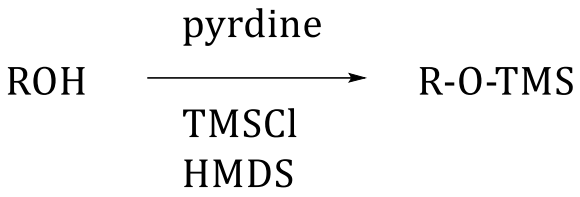

Scheme 1.1: A silylation reaction of alcohol was performed using pyridine, TMSCl, and HMDS.

various other reagent such as *N*-trimethylsilylimidazole, *N*-methyl-*N*-trimethylsilylacetamide, N-trimethylsilyldiethylamine, *N*-trimethylsilyldimethylamin, *N,O*-bis(trimethylsilyl)acetamide, *N,O*-bis(trimethylsilyl)trifluoroacetamide, *N*-methyl-*N*-trimethylsilyltrifluoroacetamide, and *N,O*-bis(trimethylsilyl)acetamide.[17-18,24,5] Polar aprotic solvents such as pyridine, acetonitrile, dimethylformamide, and dimethylsulfoxide are commonly used in silylation synthesis due to the poor solubility of free carbohydrates in other organic solvents.[17,18,25]

1.1.3 The Limitations of Available Quantification Techniques

Colorimetric methods are commonly used for quantifying total carbohydrates in a biological sample. The method involves the reaction of a reducing sugar, such as glucose, with a colorimetric reagent such as phenol-sulfuric acid or 3,5-dinitrosalicylic acid (DNS). The reaction produces a colored complex, which can be quantified spectrophotometrically at a wavelength of 490 nm for the phenol-sulfuric method and at 540 nm for the DNS method.[8,14] These colorimetric methods are simple, sensitive, and relatively inexpensive, making them a popular choice for carbohydrate quantification in various biological samples.[2,14] While this method is suitable for determining carbohydrates that consist of identical repeating units

(homopolymers), it is not effective for analyzing complex carbohydrate.[26] Another method is the anthrone assay. It works by reacting furfural derivatives generated by carbohydrates in the presence of concentrated oxidizing sulphuric acid with anthrone. This produces blue-green complexes with absorption maxima at 625 nm, and the intensity of the color varies depending on the composition of the polysaccharide.[27]

The phenol-sulfuric acid method has several disadvantages, including the use of hazardous phenol and variable absorbance responses to different sugars.[28] Additionally, the method yields glucose-equivalent concentrations that may not accurately quantify non-hexoses such as pentoses.[29] The chemical reactivity of carbohydrates with phenol-sulfuric acid also affects the molar absorption coefficient.[30] The color intensity of polysaccharide analysis is affected by the mixture of uronic acids and hexosamines.. The anthrone reagent's instability affects reliability, so an antioxidant like thiourea is added to prevent oxidative changes. The concentrations of sulphuric acid and reaction period also influence sensitivity, with intensity and absorbance varying depending on hydrolysis conditions for pentoses and hexose sugars.[31] The rate of chromomeric material formation and degradation in a hot acidic medium is crucial for maximum color intensity, but the equilibration point varies for different sugars, with ketoses being more accurate.[32] The DNS method has limitations as it gives different color intensities for different reducing sugars, making it unsuitable for quantifying individual sugars in mixtures. Separate calibration curves are needed for every measured component.[33]

High-performance liquid chromatography is a noteworthy method for analyzing carbohydrate quantities because of its effectiveness and accuracy. It rapidly separates mixed components with high resolution, and is considered a standard technique by the Association of Official Analytical Chemists (AOAC International).[34] Different types of HPLC can be used for carbohydrate analysis, including ion chromatography, reversed phase, and hydrophilic interaction. The most common method is normal phase HPLC, which is useful for separating carbohydrates from complex matrices. Reverse phase mode is also useful for separating mono-, di-, and trisaccharides.[35,36] However, there are difficulties in analyzing monosaccharides due to their similar chemical properties and lack of charge and chromophores. In addition, some drawbacks such as short retention times and the possibility of doubling or broadening peaks due to the presence of anomers.[35]

Several detectors can be used in conjunction with HPLC for more accurate analysis of compounds. The evaporative light scattering detector (ELSD) is commonly used to detect carbohydrates and organic acids due to its non-specific and universal nature.[37] However, ELSD has some limitations. For instance, it requires non-volatile analytes and volatile mobile phases such as mixtures of acetonitrile-water or ethanol-water.[38,39] Additionally, the detector response can be affected by the composition of the mobile phase, with higher organic content resulting in a higher response. Another disadvantage is the non-linear calibration response curve, which can be sigmoidal or exponential in shape.[38] Another conjunction detector often found in pair with HPLC is the refractive index detector. The refractive index detector (RID) finds extensive usage in various applications. It operates by measuring the refractive index of the

eluted sample in comparison to the reference cell.[40] However, one significant limitation of RID is its inability to function in a gradient mode due to its high sensitivity to alterations in the mobile phase composition, which can result in shifts or movements in the baseline.[41]

Carbohydrates, lacking a chromophore or luminophore, require chemical derivatization before detection using ultraviolet-visible (UV/UV-VIS) spectrophotometer and fluorescence detectors. The 1-phenyl-3-methyl-5-pyrazolone (PMP) and *p*-aminobenzoic ethyl ester reagents are popular choices for UV detection, as they react with carbohydrates quantitatively and under mild conditions.[42] Fluorescence detection is also possible but requires derivatization due to the absence of fluorophores.[43] However, the use of UV and fluorescence detection is not commonly preferred for sugar detection due to poor detection sensitivity, time-consuming sample preparation, and potential alterations in sugar chemical structure.[2]

Gas chromatography (GC) is a viable alternative to monosaccharide determination due to its superior separation properties when compared to liquid chromatography. Additionally, GC is capable of detecting chiral components within a relatively short time frame.[2] Various detectors may be coupled with GC, including the flame ionization detector (FID), Mass Spectrometer (MS), and Nitrogen Phosphorus Detector (NPD). FID is an especially sensitive method for carbohydrate determination.[44] GC-FID is well suited for the determination of monosaccharides such as fucose, glucose, galactose, mannose, and ribose, as shown in Figure 1.1, as well as uronic acids including glucuronic acid, galacturonic acid, mannuronic acid (ManA),

and guluronic (GulA) acid, as shown in Figure 1.3. Moreover, it can be used to simultaneously determine neutral and acidic carbohydrates.[35] As previously mentioned, since sugars are non-volatile and thermally unstable, prior derivatization is required for GC analysis. For carbohydrate determination using GC, various derivatives such as methyl ethers, acetates, trifluoroacetates, trimethylsilyl (TMS) ethers, trimethylsilyl oximes (TMSO), aldonitrile and alditol acetates, and dialkyl acetals may be utilized. TMS and TMSO are the most frequently employed derivatives for carbohydrate derivatization in GC analysis.[17,18,19] However, this process has several challenges, including the presence of large amounts of hydroxyl functional groups in the molecule, the existence of tautomeric forms in solution leading to complex chromatograms, and the instability of some molecules.[2] Additionally, the inability to quantify sugars is a significant drawback due to the generation of two peaks from each sugar representing the alpha (anti) and beta (syn) anomer.[45] TMS ether derivatization leads to the formation of different end products for each cyclic tautomer, resulting in a complex chromatogram.[46]

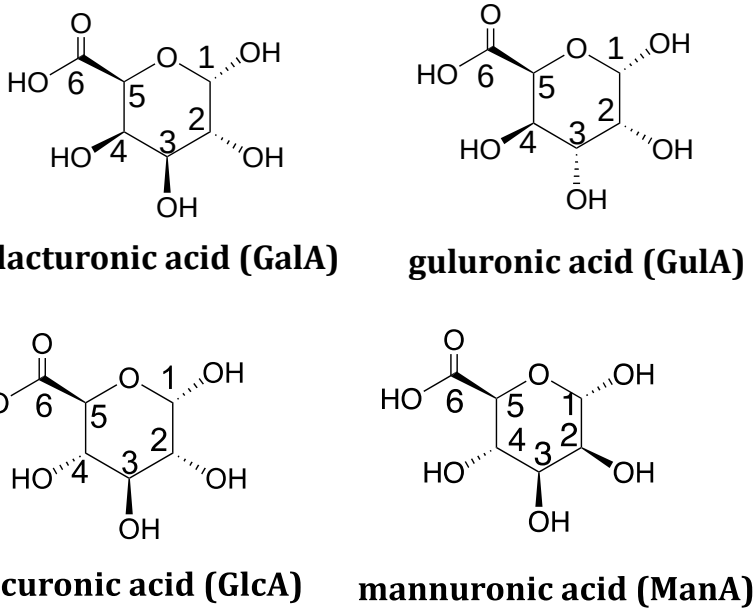

Figure 1.3: Uronic acids that are shown can be detected using gas chromatography with flame ionization detection.

In agriculture and horticulture, Visible and Infrared spectral methods are used to analyze carbohydrate content. Infrared spectroscopy has the advantage of being non-destructive and having a short sample preparation time.[2] The Infrared region is divided into three subranges: Near-infrared (NIR), Mid-infrared (MIR), and Far-infrared. NIR provides information about overtones and combination vibrations, while MIR captures stretching and bending vibrations.[47] Quantitative NIR analysis uses light absorption correlation with the sample's composition.[48] NIR spectra provide information about organic compounds and minerals, but chemometric analyses are necessary for interpretation.[48,49] Synergistic multivariate statistical methods like partial least square regression (PLSR) is required to extract quantitative information from NIR spectra.[50] The disadvantage of the NIR method is its high sensitivity to the sample matrix, which can distort the measurement. This means that the accuracy of the measurement may be affected if the matrix of the test sample is

not similar enough to the calibration standards used.[51] Additionally, although chemometric methods can improve the analysis, they require pre-processing of the NIR spectra to remove physical phenomena and non-linearities, which can be time-consuming and require expertise.[52] Additionally, the large number of combinations and overtone bands in the NIR spectra can make them less specific compared to other types of spectroscopy, such as infrared or Raman spectroscopy. This is because the vibrations that contribute to NIR absorption often involve combinations of multiple bonds or overtones of fundamental vibrations. As a result, many different chemical species can produce similar NIR spectra, which can make it challenging to identify specific compounds or chemical groups.[53]

NMR spectroscopy is a potent and non-destructive tool that enables the quick and simultaneous detection and measurement of organic compounds. This is an advantage over other analytical techniques that may require chemical modifications or destructive processes.[7] It is commonly used for identifying carbohydrates and related compounds in food samples, and to ascertain their purity. NMR spectroscopy can analyze both simple and complex carbohydrates, whether they are isolated or integrated into the sample matrix. The molecular structure of the compounds is determined by chemical shifts and coupling constants in the NMR spectrum.[2]

Quantification of carbohydrates by NMR spectroscopy typically involves the use of internal standards, which are compounds that are added to the sample in a known quantity and have a characteristic NMR signal. The height or area of the peak corresponding to a specific group in the analyte is then compared to that of the internal standard to determine the concentration of the group in the sample.[54] ^{1}H

NMR signal is better for quantification than ^{13}C NMR signals because it is more sensitive. Hydrogen (proton) nuclei have a higher gyromagnetic ratio than carbon-13 nuclei, which means that they can be more easily excited by the magnetic field and radiofrequency radiation used in NMR spectroscopy. This results in stronger signals for ^{1}H NMR signal, which makes it easier to detect and quantify small concentrations of analytes in a sample. In contrast, ^{13}C NMR signal is associated with a longer acquisition time, which can limit its usefulness for high-throughput or rapid analysis. The nuclear Overhauser effect (NOE) can also be a problem in ^{13}C NMR spectra. The NOE occurs when the signals from nearby protons in the sample interfere with the signals from carbon-13 nuclei, which can lead to incorrect quantification of analytes.[55] The technique of using ^{13}C NMR signal to determine the concentration of coffee components has been significantly enhanced by the recent addition of a relaxation agent, which dramatically increases the ability to quantify ^{13}C NMR integration.[7]

Two disadvantages of NMR analysis are peak overlapping and a relatively low sensitivity. Peak overlapping can occur when the NMR spectrum is crowded with many signals, making it challenging to differentiate between individual peaks. This can reduce the accuracy and precision of the analysis. The sensitivity of NMR analysis can also be relatively low, which means that it may not be suitable for detecting low concentrations of analytes in a sample.[54]

1.1.4 Background on Silicon-29 NMR and Peak Assignments

Although many techniques have been established and used for the identification and quantification of sugars, these methods still have limitations that

require further improvements, as discussed earlier. Therefore, the need for new tools or techniques to identify and quantify sugars remains crucial for industries such as food and beverage, pharmaceutical, and biofuels more efficiently and accurately. The development of faster and easier techniques will help overcome the existing limitations and improve the quality control, safety, and regulatory compliance aspects of these industries.

In 1972, it was discovered that the accuracy of hydroxyl and carboxyl group quantification using NMR could be significantly enhanced through the conversion of OH groups into $Si(CH_3)_3$ groups. This conversion helped amplify the ^{1}H NMR signal by a factor of nine, which led to a surge in NMR quantification applications.[56] In addition, there has been remarkable progress in the field of nuclear magnetic resonance spectroscopy for the past few years, particularly in the identification and quantification of nuclei beyond protons. The latest advancements in NMR technology have significantly expanded the range of detectable isotopes, such as ^{29}Si, ^{31}P, and ^{15}N, which were previously undetectable due to their lower natural abundance.[57] This has been made possible through the utilization of higher magnetic field strengths in NMR spectrometers, along with hardware and software improvements that enable more accurate and efficient data acquisition and analysis. As a result, NMR spectroscopy has emerged as an increasingly versatile and powerful analytical tool with broad applications in diverse fields including materials science, biochemistry, and environmental science.

Silicon-29 has become an important nucleus in NMR due to the prevalence of silicon compounds on the earth's surface and in consumer products. Silicones,

silicates, and silanes are used in a variety of applications, such as rubber, glues, and catalyst systems in the chemical industry.[57] The increasing usage of materials containing silicon atoms has led to a rising demand for novel and enhanced techniques for characterizing these compounds. Silicon-29 NMR chemical shifts exhibit high sensitivity to structure, such that even two closely related compounds, such as xylopyranose with differing junctions at positions 3 and 4, generate two distinct spectra with negligible overlap in peaks, Table 1.2.[56] This criterion makes Silicon-29 NMR spectroscopy a valuable technique, but relatively difficult to observe that makes it not widely used until recently. This is due to several characteristics of ^{29}Si isotope including the low natural abundance of ^{29}Si (4.67%), small magnetogyric ratio (γ) and energy difference between spin states, negative NOE effects, and long spin-lattice relaxation times, which make time-average experiment very time-consuming.[57,58]

Table 1.2: The ^{29}Si chemical shift for silyl derivative. These chemical shifts help illustrate that there is no peak overlap between these compounds, even when just two junctions at positions 3 or 4 are different.[56]

Compound	Si-6	Si-4	Si-3	Si-2
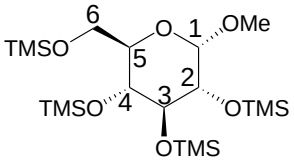	17.04	17.36	16.87	16.12
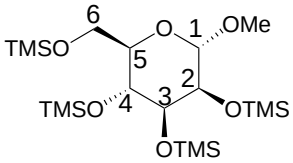	16.86	17.94	17.07	15.72
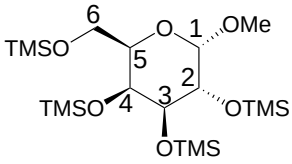	17.03	17.31	16.44	15.97

There are two techniques that can be implemented to decrease the acquisition time when running a ^{29}Si NMR experiment. The first method is by adding a small amount (0.01) of a relaxation reagent that can replace all other relaxation mechanisms with a more efficient electron-nuclear dipole-dipole interaction, shortening T1 to a few seconds. This eliminates the proton-nuclear dipole-dipole relaxation mechanism and the NOE under proton decoupling conditions, producing an absorption spectrum that has sharp signals.[57] Another techniques to enhance the ^{29}Si NMR signal in NMR spectroscopy is the transfer of polarization from protons to ^{29}Si NMR signal when silicon nuclei are coupled to protons. INEPT (insensitive nuclei enhanced by polarization transfer) and DEPT (distortionless enhancement by polarization transfer) are pulse sequences that transfer nuclear spin polarization from protons to other nuclei that are coupled to them. As a result, the signal strength for ^{29}Si NMR signal is significantly increased and allows for data to be acquired much more rapidly, resulting in a timesaving factor of 30 to 300 in ^{29}Si-NMR experiments compared with normal FT-NMR spectroscopy.[58]

The hydroxyl groups on sugar molecules are often protected against undesirable side reactions using trimethylsilyl (TMS). This is frequently achieved by employing trialkylsilyl derivatives as protective agents due to their thermal stability, resistance to air oxidation, low viscosity, and ability to easily recover the parent compound or achieve separation by distillation.[56] Additionally, the TMS group has the potential to enhance compound volatility, and render carbohydrate solubility in organic solvent, thereby facilitating gas chromatography (GC) analysis. As a result,

the techniques and procedures for silylation (TMS) derivatization of hydroxyl groups are widely established and acknowledged in laboratory settings.

^{29}Si NMR spectroscopy is used to determine the structure of polyfunctional compounds such as sugars, steroids, carboxylic acids, amino acids, and peptides by analyzing their trimethylsilyl (TMS) derivatives.[59] A large number of TMS derivatives of sugars, such as the TMS derivatives that are discussed in this dissertation have been prepared for gas chromatography and some have been characterized by proton and carbon NMR. However, only a few derivatives had been characterized using ^{29}Si NMR signal and most were not fully assigned in ^{29}Si NMR signals. The introduction of the ^{1}H-^{29}Si heteronuclear multiple bond correlation (HMBC) technique, which uses two-bond proton (H2' to Si_{ii}) or three-bond proton (H3 to Si_{ii}) correlations for silicon peak assignment (Figure 1.4), has facilitated the identification of silicon signals for silyl derivatives, as illustrated in the figure below. Before this method, several empirical and experimental techniques were used to assign ^{29}Si NMR chemical shifts. The empirical rules have been derived from observed changes in ^{29}Si NMR chemical shifts caused by substituent effects.[60] In addition, techniques such as selective proton decoupling experiments,[61,62] specific deuteriations, studies using shift reagents, refocused INEPT experiments, modified INDOR or INADEQUATE experiments had also been used to improve the accuracy and reliability of analyzing and assigning ^{29}Si chemical shift.[60]

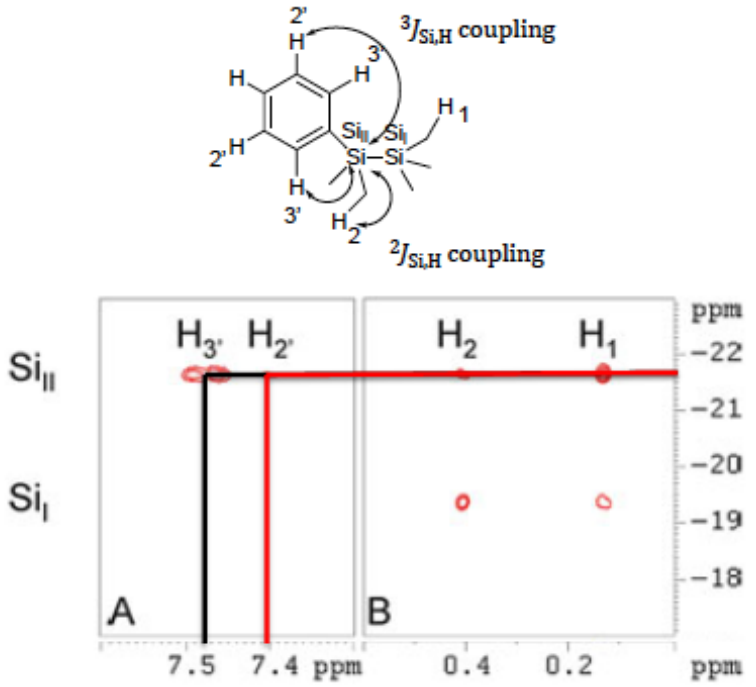

Figure 1.4: The illustration shown the assignment of pentamethyl(phenyl)silane using ^{1}H-^{29}Si HMBCchemical shift correlations in 2D NMR (HMBC) where F2 is ^{1}H and F1 is ^{29}Si.[63]

The following study used single-frequency proton decoupling to identify and assign ^{29}Si NMR chemical shifts. The ^{29}Si NMR chemical shifts for per-*O*-silylated-methyl-α-glucopyranoside, per-*O*-silylated-methyl-α-galactopyranoside, per-*O*-silylated-methyl-α-mannopyranoside, per-*O*-silylated-methyl-α-6-deoxy-galactopyranoside in Figure 1.5 showed all expected peaks. However, peak assignment was not obvious, thus single frequency proton decoupling was performed

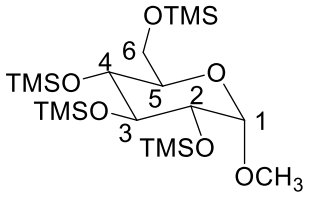

per-*O*-silylated-methyl-α-glucopyranoside

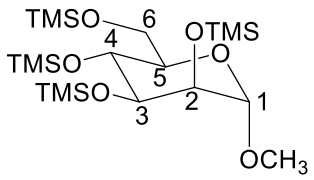

per-*O*-silylated-methyl-α-mannopyranoside

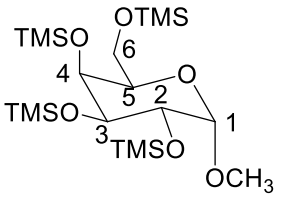

per-*O*-silylated-methyl-α-galactopyranoside

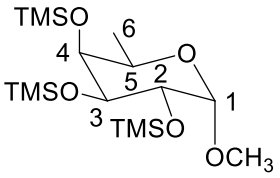

per-*O*-silylated-methyl-α-6-deoxy-galactopyranoside

Figure 1.5: Chemical structures of per-*O*-silylated-methyl-α-glucopyranoside, per-*O*-silylated-methyl-α- galactopyranoside, per-*O*-silylated-methyl-α-mannopyranoside, per-*O*-silylated-methyl-α-6-deoxy-galactopyranoside.[64]

to solve this issue. Though not all (Si, H) coupling effects were removed, residual doublets were observed for Me_3SiOCH groups, and triplets (with the central peak unshifted from that given by noise decoupling) were observed for Me_3SiOCH_2, Figure 1.6. The differentiation between doublet and triplets observed for Me_3SiOCH and Me_3SiOCH_2 enables the assignment of ^{29}Si NMR peaks of the methylene (Si6) for per-*O*-silylated-methyl-α-glucopyranoside, per-*O*-silylated-methyl-α-galactopyranoside, per-*O*-silylated-methyl-α-mannopyranoside.[64] For the remaining signals (Si2-Si4), reasoning and assignment were made based on comparison of chemical shifts between per-*O*-silylated-methyl-α-glucopyranoside, per-*O*-silylated-methyl-α-galactopyranoside, per-*O*-silylated-methyl-α-mannopyranoside, per-*O*-silylated-methyl-α-6-deoxy-galactopyranoside.

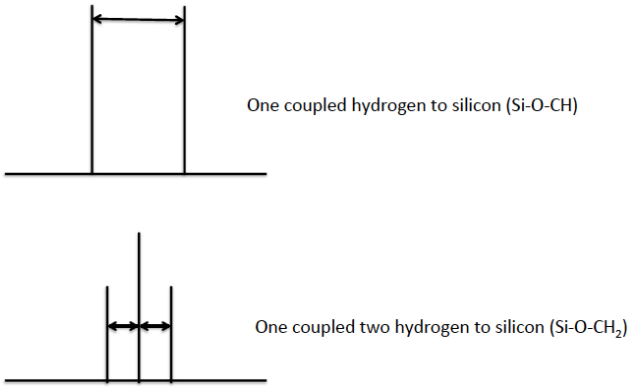

Figure 1.6: Showed the doublet and triplet splitting pattern of Si to H, which helped to distinguish silicon signal that bond to methylene (Si6) and methine (Si2-Si4) groups of per-*O*-silylated-methyl-α-glucopyranoside, per-*O*-silylated-methyl-α-galactopyranoside, and per-*O*-silylated-methyl-α-mannopyranoside.

In recent years, numerous methods have been developed and employed to aid in the assignment of persilylated derivatives, including two-dimensional techniques such as heteronuclear multiple bond coherence and heteronuclear single quantum coherence (HMQC). Extensive research has been conducted on the use and advantages of employing these techniques.[65,66,67,63,68] The strong cross-peaks observed in the 2D ^{1}H-^{29}Si HMBC correlated spectra arise from the correlation between the silicon nuclei (Si2, Si3, Si4) and each trimethylsilyl group (Figure 1.7, right). The correlation of the methine or methylene protons (H2, H3, H4, H6) to silicon nuclei (Si2, Si3, Si4, Si6) exhibits smaller cross-peak intensities, as illustrated in Figure 1.7 (left). The application of 2D Si peak assignment can be utilized to identify the glycosidation site of disaccharide and trisaccharide derivatives, helping to avoid ambiguous assignments.[67] In order to utilize the 2D heteronuclear method, a complete assignment of ^{1}H NMR must be performed on the compound using both homonuclear (^{1}H) and heteronuclear (^{1}H-^{13}C) techniques as illustrated in Figure 1.8.

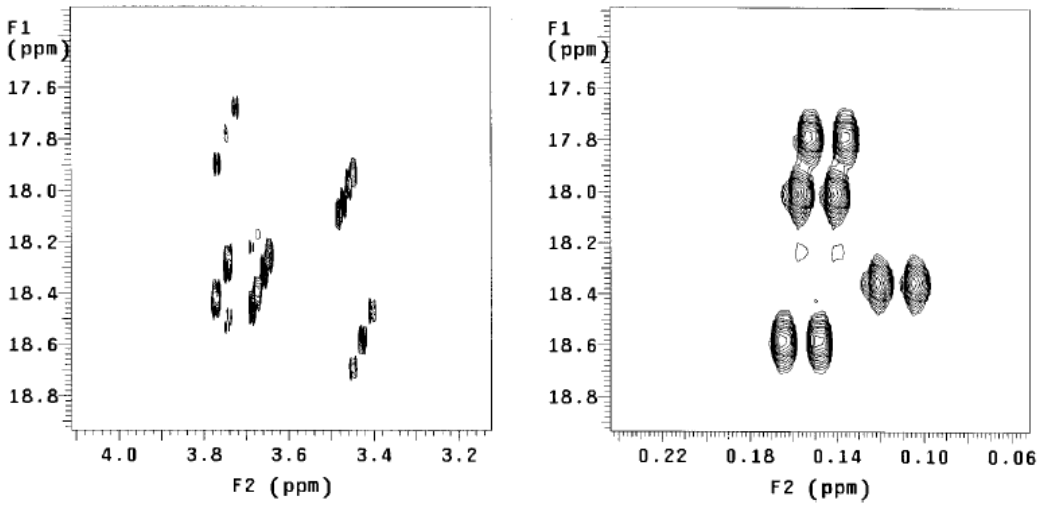

Figure 1.7: ^{1}H-^{29}Si 2D correlations illustrate the intensity of cross peaks from methine or ring protons and trimethylsilyl protons to Si nuclei. Stronger cross-peak intensity is generated from trimethylsilyl protons to Si, with weaker cross-peak intensity observed for Si-methine protons.[65]

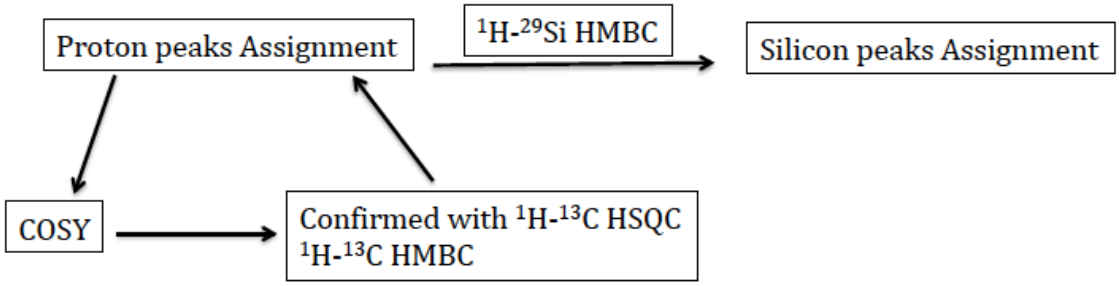

Figure 1.8: Stepwise of assignments ^{29}Si, initiated by assignment of proton peaks using homonuclear (COSY) and heternuclear (HMBC and HSQC) experiments follow by ^{1}H-^{29}Si HMBC experiment to assign ^{29}Si by correlated the 3 bonds correlation to proton.

Furthermore, with the advancement of NMR technology, ^{29}Si NMR peaks assignments can be made for polyphenols, which are natural products containing aromatic rings and no coupling to hydrogen. The precise experimental assignment relies on the coupling between silicon and carbon-13 nuclei ($^{n}J(^{29}Si,^{13}C)$, where n > 1), provided that the ^{13}C NMR spectra have been partially assigned. Two methods have been employed: heteronuclear INADEQUATE and selective ^{29}Si NMR decoupling.

Both methods utilize polarization transfer of the INEPT type to enhance signals and pulsed magnetic field gradients to select coherence pathways. The first method, (Si,C)gCOSY, detects ^{13}C NMR signals, while the second method, (Si,C,Si)gHMQC, detects ^{29}Si NMR signals as illustrated in the pulse sequence shown in Figure 1.9 and 1.10 respectively. These aforementioned methods were used to analyze silyl derivatives of hydroxyflavone, ferulic acid, and quercetin, Figure 1.11.[69]

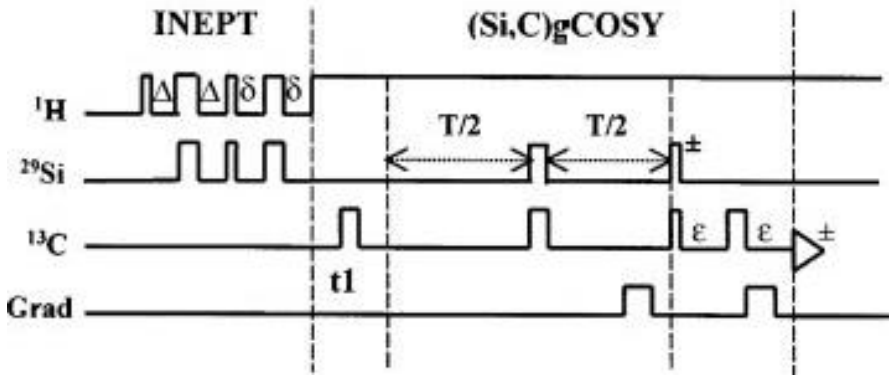

Figure 1.9: The measurement of ^{29}Si NMR spectra using the INEPT pulse sequence modified for $Si(CH_3)_3$ groups. The specific parameters include a 75 ms polarization, 16 ms refocusing delays optimized for polarization transfer, and a relaxation delay of 10 s.[70]

(Si,C,Si)gHMQC methods and narrow ^{29}Si NMR singal lines have been developed to measure and analyze the interactions between silicon (Si) and carbon (C) atoms over up to five bonds, see structure in Figure 1.12. The coupling constants obtained are not only influenced by the number of intervening bonds but also by the substituents attached to the silicon atom. Interestingly, ring substitution in the para position does not alter the two- and three-bond couplings, indicating that substituents on the aromatic ring have no effect on the measured couplings between silicon and carbon atoms, see Figure 1.13 for *J* coupling constant and subsituents.[71]

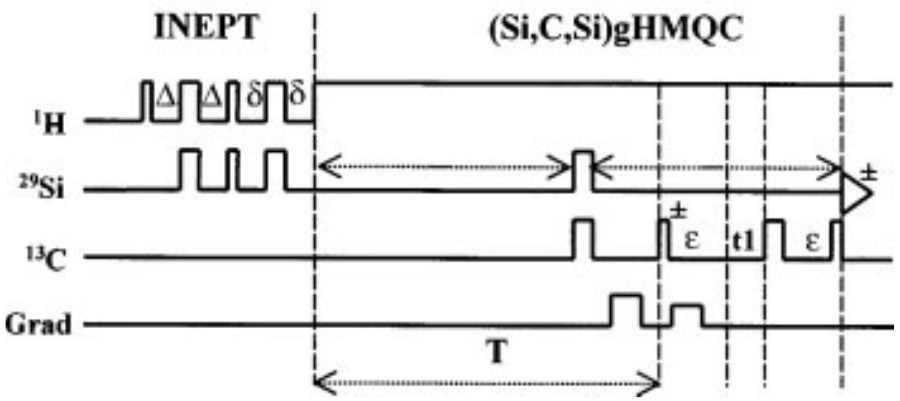

Figure 1.10: The INEPT–gHMQC combination, a modification of the $^{29}Si,^{13}C$ gHMQC pulse sequence with the substitution of the first ^{29}Si pulse by an INEPT pulse train. The gHMQC portion is adjusted by incorporating a silicon refocusing 180° pulse in the middle to maintain its ^{29}Si refocusing property. This is synchronized with a simultaneous 180° carbon pulse to ensure the desired magnetization development during the T delay. The T delay and the initial 90° ^{13}C pulse facilitate polarization transfer from ^{29}Si to $^{29}Si,^{13}C$. The optimal T delay is equal to $1/[^2J(Si,C)]$.[70]

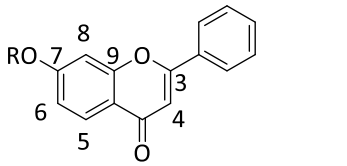

7-Hydroxyflavone (R - TMS)

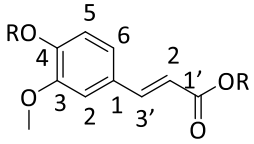

Ferulic acid (R= TMS)

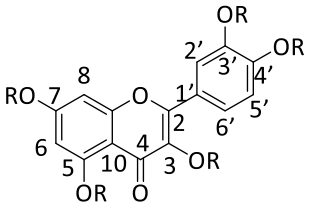

Quercetin (R = TMS)

Figure 1.11: 3 *O*-TMS derivatives of flavone and polyphenol that had been elucidated using long-range coupling constant, (Si,C) gCOSY, and INEPT–gHMQC.[69]

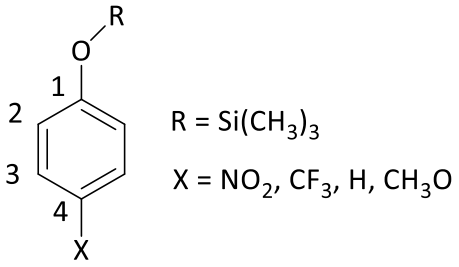

Figure 1.12: A study of polyphenol structure assignment based on the long-range ^{29}Si-^{13}C *J* coupling constant from C1-C4.[71]

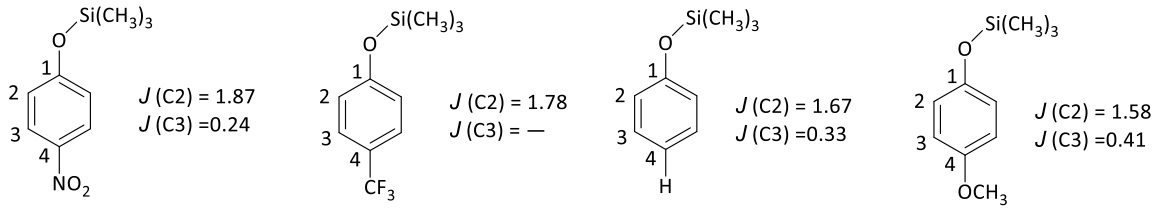

Figure 1.13: The long-range *J* coupling constant of different ^{29}Si-^{13}C on polyphenols *para* substituents. The substituents on *para* position showed little influence on the *J* coupling constant. Note, the *J* values were written as they are shown in the literature.[71]

These $J_{(Si,C)}$ couplings, particularly the two-bond and three-bond couplings, are well suited for identifying and assigning specific spectral lines in the analysis of silylated polyphenols as shown in Figure 1.14.[69] The calculated Fermi contact (FC) contribution determine the magnitudes of the two-bond and three-bond couplings are similar, but their signs are opposite, implying that silicon-carbon interactions separated by two or three bonds have different signs in the coupling constants. The Fermi contact values of ^{2}J and ^{3}J are shown in Figure 1.15. Determining the signs of these geminal and vicinal couplings experimentally would greatly facilitate the line assignment process. Furthermore, the four- and five-bond couplings are influenced in a complex manner by the substituent X (X= H, NO_3, CF_3, CH_3O; Figure 1.13) attached to the silicon atom, highlighting the intricate impact of this substituent on the coupling constants between silicon and carbon atoms separated by four or five bonds.[71,72]

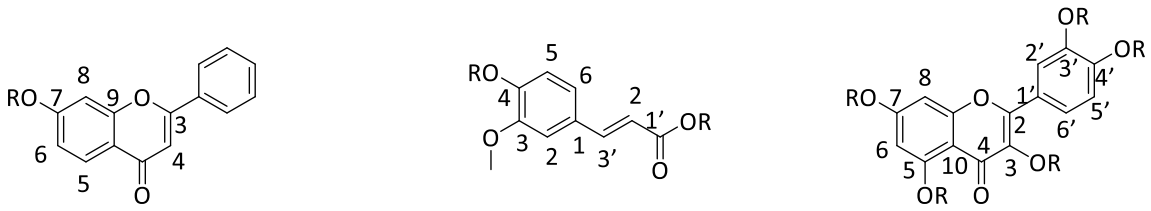

J of Si_7	*J* of Si_4	*J* of Si_5	*J* of $Si_{3'}$
J (C6) = 1.8	*J* (C4) = 2.4	*J* (C5) = 2.1	*J* (C3') = 2.3
J (C7) = 2.0	*J* (C3) = 1.3	*J* (C6) = 1.3	*J* (C2') = 1.3
J (C8) = 1.8	*J* (C5) = 1.6	*J* (C10) = 1.2	*J* (C4') = 1.5
J (C9) = 0.4	*J* (C2) = 0.5	*J* (C7) = 0.6	*J* (C1') = 0.6
	J (C6) = 0.5	*J* (C8) = 0.5	*J* (C6') = 0.5

Figure 1.14: ^{2}J and ^{3}J coupling constants of $J_{(Si,C)}$ of per-*O*-silylated polyphenols and using these values can help identify the relative assignment of the Si signal such in quercetin.[69]

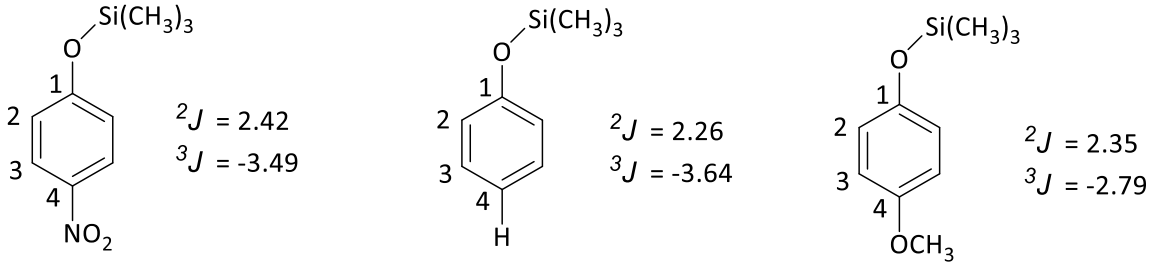

Figure 1.15: The Fermi contact calculated values of ^{2}J (Si-*O*-C1) and ^{3}J (Si-*O*-C1-C2) coupling constants of ^{29}Si-^{13}C for *para* substitutes of different X groups and *O*-TMS.[71]

It should be noted that despite the well-established nature of this method, comprehensive characterization using ^{1}H, ^{13}C, or ^{29}Si nuclear magnetic resonance spectra has not yet been conducted for most of the carbohydrate *O*-silyl derivatives, particularly those involving trisaccharides or tetrasaccharides. In the present study, it is important to highlight that out of the twelve carbohydrate *O*-silyl derivatives examined (Table 1.3), only the *O*-silyl derivative of methylglucoside (**13**) had previously undergone characterization via ^{29}Si NMR analysis. Thus, while the silylation process has demonstrated its efficacy in rendering carbohydrates suitable

for GC-MS analysis, there remains a need for further investigations to fully characterize carbohydrate *O*-silyl derivatives, particularly regarding their chemical shifts and structural information as revealed by ^{1}H, ^{13}C, and ^{29}Si NMR spectroscopy methods.

1.2.0 Results and Discussion

1.2.1 Optimized Synthesis and Characterization of Silylated Carbohydrates Using ^{29}Si NMR Spectroscopy

In this study, twelve per-*O*-silylated (per-*O*-TMS) sugars, Table 1.3, were synthesized using microwave radiation within one hour, following the optimized Scheme 2. This approach significantly reduced the reaction time compared to the previous method, which involved stirring at room temperature overnight.[73,20] Importantly, this modified synthesis method did not affect the percent yield of the sugars.

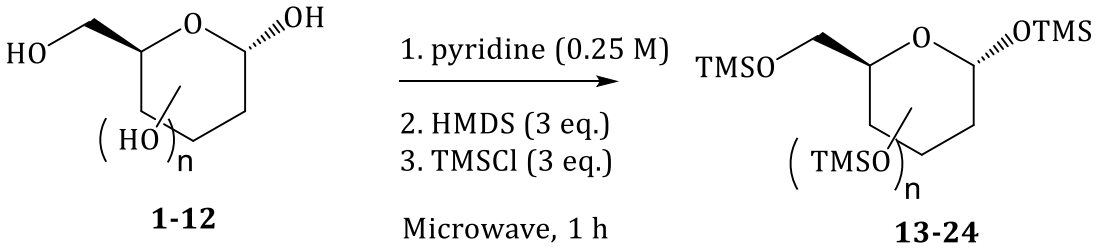

Scheme 1.2: Microwave synthesis of per-*O*-silylated monosacharides, disaccharides, and oligosaccharides.

A comprehensive literature search revealed that all per-*O*-silylated sugars examined in this study had been synthesized before. Some of them had undergone analysis using gas chromatography. However, among the compounds investigated, only per-*O*-TMS-α-methylglucoside (**13**) had been fully assigned in terms of its ^{1}H,

Table 1. 3: The twelve per-*O*-silylated sugars studied.

Chemical Name & Number	Structure
α-methyl-2, 3,4,6-tetra-*O*-TMS-glucopyranoside (**13**)	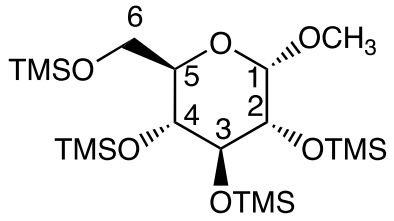
1,2,3,4,6-penta-*O*-TMS- α-glucopyranoside (**14**)	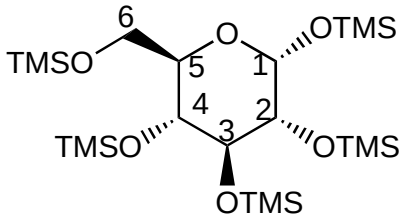
1,2,3,4,6-penta-*O*-TMS- α – mannopyranoside (**15**)	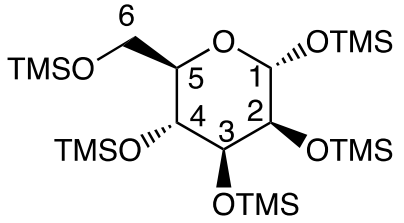
1,2,3,4,6-penta-*O*-TMS-β-fructopyranoside (**16**)	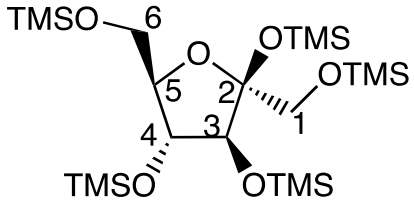

1,2,3,4,5,6-hexa-*O*-TMS-sorbitol (**17**)	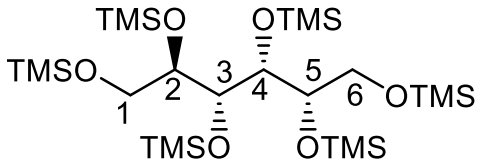
1,2,3,4-tetra-*O*-TMS-ribitol (**18**)	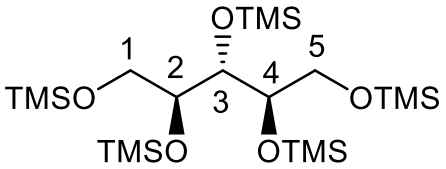
1,2,3,4-tetra-*O*-TMS-xylitol (**19**)	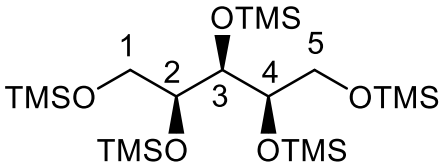
1,3,4,6,2', 3', 4',6-octa-*O*-TMS-sucrose (**20**)	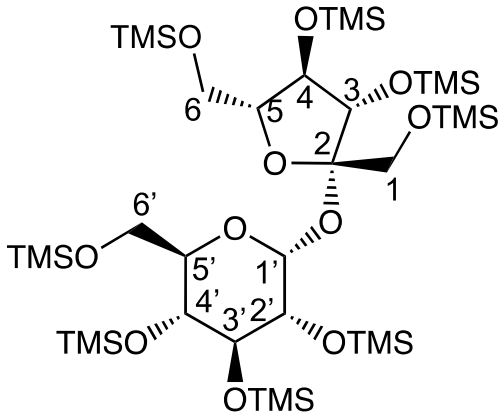

2,3,4,6,2’, 3’, 4’, 6’-octa-*O*-TMS-trehalose (**21**)

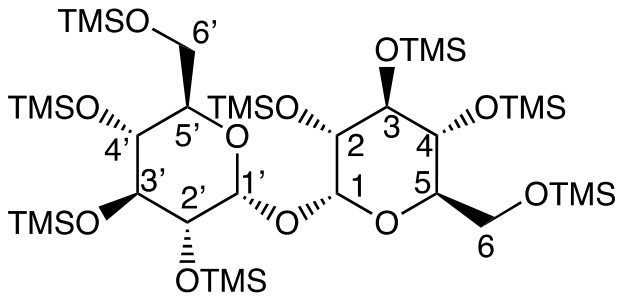

1,3,4,6,3’,4’,6’,2”, 3”, 4”, 6”-unde-*O*-TMS-kestose (**22**)

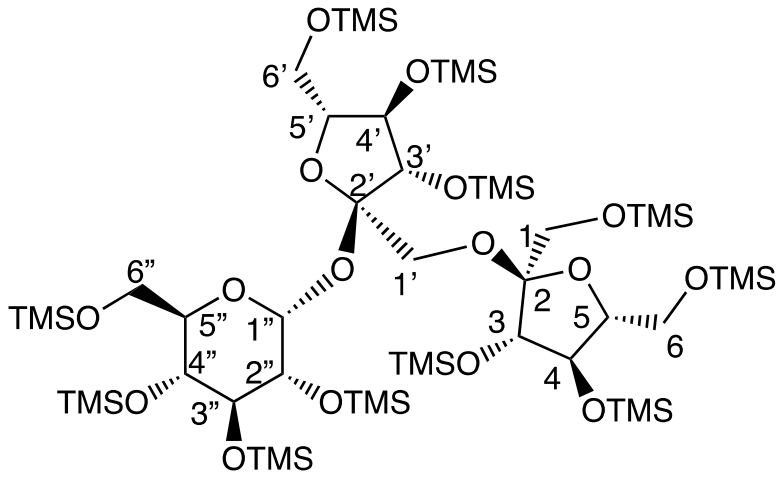

1,3,4,6,2', 3', 4', 2", 3", 4", 6"-unde-*O*-TMS-raffinose (**23**)

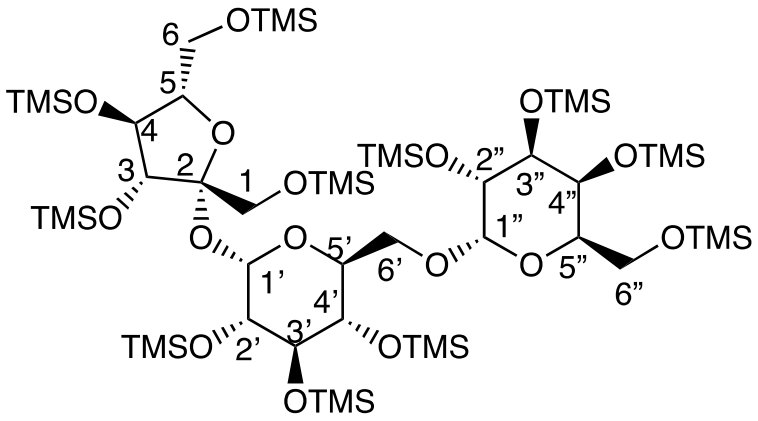

1,3,4,6,2', 3',4',2", 3", 4", 2"', 3"',4"',6"'-tetrade-*O*-TMS-styachose (**24**)

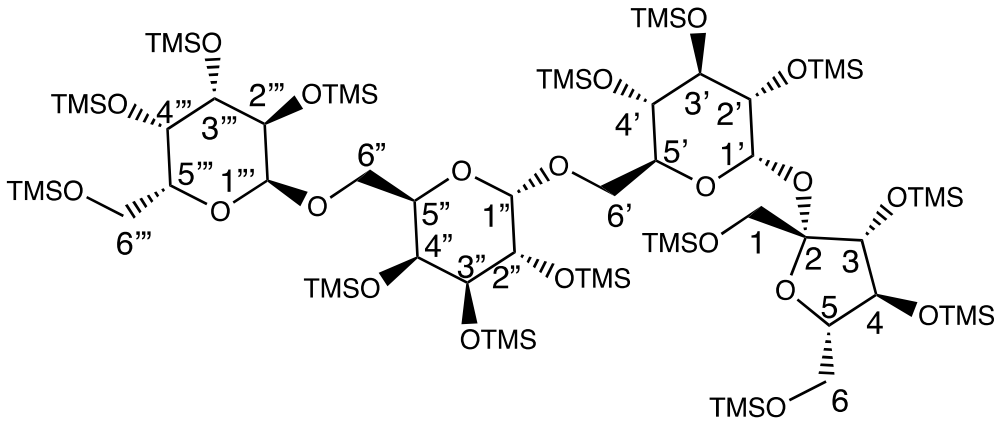

^{13}C, and ^{29}Si NMR spectra. Notably, the NMR results obtained in this study for per-*O*-TMS-α-methylglucoside (**13**) were consistent with the previous findings.[65] Three other per-*O*-persilylated sugars, namely α-per-*O*-TMS-glucose (**14**), α-per-*O*-TMS mannose (**15**), and per-*O*-TMS-trehalose (**21**), had been characterized in terms of their ^{1}H and ^{13}C NMR spectra by the Gervay-Hague lab.[22,73] However, the per-*O*-silylated derivative of methyl-α-mannose and methyl-α-galactose were attempted to be analyzed using ^{29}Si NMR signal. Initially, these sugars were analyzed using "common sense," which was unsuccessful. Later, selective decoupling was employed to assign the remaining signals.[64,60] The ^{29}Si NMR spectra of per-*O*-TMS-sorbitol (**17**) had been published, although a complete assignment had not been performed.[56] Furthermore, the ^{1}H and ^{13}C spectra of β-per-*O*-TMS-fructose (**16**), per-*O*-TMS-sucrose (**20**), and per-*O*-TMS-kestose (**22**) had been analyzed and assigned.[74] Additionally, per-*O*-TMS-ribitol (**18**), per-*O*-TMS-xylitol (**19**), per-*O*-TMS-raffinose (**23**), and per-*O*-TMS-stachyose (**24**) were mentioned in a patent.[75] In our study, we optimized the synthesis method for these compounds and characterized them using the ^{1}H-^{29}Si HMBC. It is worth noting that this characterization method has been validated by other NMR experts and chemists.[65, 76,63]

The ^{1}H, ^{29}Si, and ^{13}C NMR spectra were recorded in solution on a Bruker 400 Spectrometer. The spectrometer operated at frequencies of 399.77 MHz for ^{1}H, 100.52 MHz for ^{13}C, and 79.42 MHz for ^{29}Si NMR measurements. It is an X-Y gradient module with f1 and f2 channels. The spectra were recorded using concentration solutions ranging from 0.0125 M to 0.50 M in $CDCl_3$. To serve as a reference point at δ=0.00, 1% tetramethylsilane (TMS) was added. For quantification purposes, three

internal standards, dehydroepiandrosterone-*O*-TMS (**25**), dehydroepiandrosterone-*O*-SiTBDP (**26**), or hexamethyldisilane (HDMS) (**27**), Figure 1.16, were added for the quantification NMR experiments. All spectra were recorded at 25 °C in a 5 mm NMR tube. The ^{1}H NMR spectra was recorded using zg30 with 16 scans. The spectra width was 7978 Hz, with an acquisition time of 4.10 s and a relaxation delay of 1 s. The spectra were processed using Mnova (Mestrelab) and referenced to TMS at 0.00 ppm.

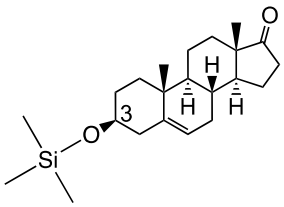

dehydroepiandrosterone-O-TMS (**25**)

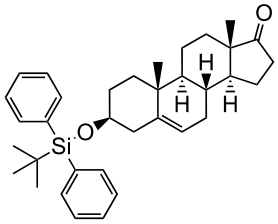

dehydroepiandrosterone-SiTBDP (**26**)

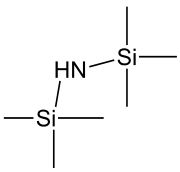

hexamethyldisilazane (HMDS **27**)

Figure 1.16: Three internal standards, dehydroepiandrosterone-*O*-TMS (**25**), dehydroepiandrosterone-*O*-TBDPSi (**26**), and hexamethydisilazane (HMDS **27**) were synthesized in the lab to use for quantification.

The ^{29}Si NMR spectra were recorded using the DEPT pulse sequence for polarization transfer. A pulse length of 180 degrees was used on the f1 channel and 90 degrees on the f2 channel. The pulse lengths were 14 μs and 28 μs respectively. The waltz16 decoupling sequence was applied for a relaxation delay of 2s. The spectra width was 10000 Hz, and 128 scans were performed with an acquisition time of 3.2 s (Figure 1.17). The ^{13}C NMR spectra were recorded using ^{13}C NMR composite pulse decoupling with a pulse length of 30 degrees. The decoupling time was 3.33 μs using the waltz35 decoupling sequence. A total of 1024 scans were performed with a spectral width of 24038 Hz, an acquisition time of 1.3 s, and a relaxation delay of 2.0 s. For the ^{1}H-^{29}Si HMBC correlation experiments, the pulse sequence of ^{29}Si and ^{1}H was used with 4 scans. The spectral width of F2 was 2631.57 Hz, and F1 was 1985.51

Hz. The acquisition times were 0.19 s for F2 and 0.13 s for F1, with relaxation delays of 5 s.

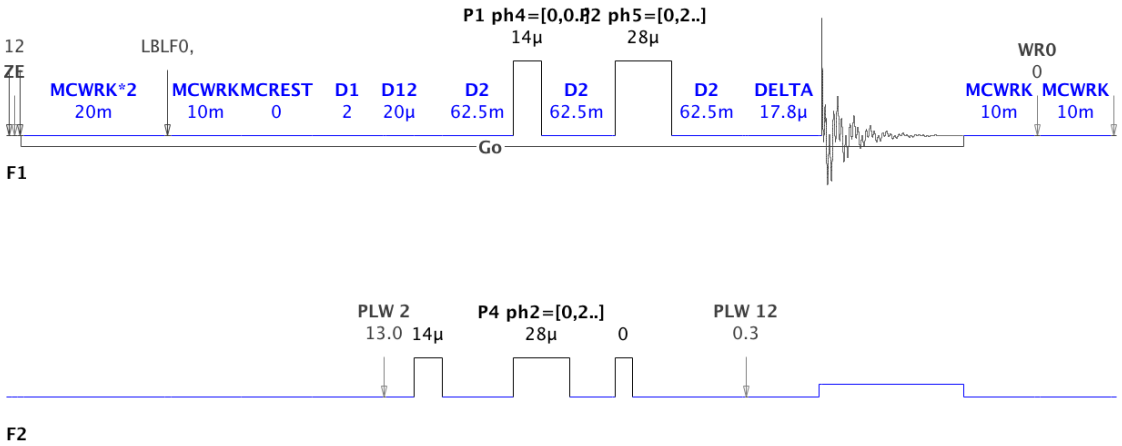

Figure 1.17: Pulse sequence of ^{29}Si DEPT experiment; f1 channel is the silicon and f2 channel is proton with 2 s delay relaxation and pulse length of 14 µs and 28 µs on both channels.

It had been previously mentioned that ^{29}Si NMR spectroscopy has a negative magnetogyric constant, -53.19 (10^6 rad·s^{-1}·T^{-1}) and long relaxation time, making it less desirable to use. However, with the application of non-selective polarization transfer (DEPT or INEPT) experiments, the acquisition time has been reduced, making quantitative ^{29}Si NMR spectroscopy feasible. ^{29}Si NMR spectroscopy has found expanding applications as a diagnostic tool for determining the position of protecting groups[65] and elucidating oligonucleotide structures through silylation (as mentioned in the nucleotide paper). In this study, we obtained ^{29}Si NMR spectra using DEPT for all experiments, which helped reduce the acquisition time by 3 times. We also utilized the DEPT spectrum for ^{1}H-^{29}Si HMBC cross-peak correlations. To initiate the assignment, we started with per-*O*-TMS-α-methylglucoside (**13**) a previously assigned silylated sugar that has been extensively studied in both α and β anomers.[60,76,65]

1.2.2 Assignment of Methyl-2,3,4,6-Tetra-*O*-TMS-α-Glucopyranoside (**13**).

The previously reported assignment methods employed by Mouna Harket involved utilizing a computer program equation to determine the coupling constants, which were then compared to calculated values for assignment. In Mouna's study, the assignment was carried out using acetone-d_6 as the solvent, leading to a different chemical shift order compared to our study where we acquired ^{1}H-^{29}Si HMBC in deuterated chloroform. In Mouna's findings, the chemical shift order was Si4>Si6>Si3>Si2, whereas in our investigation, we observed Si4>Si6>Si2>Si3,[60] thus revealing chemical shift dependance upon solvent.

In another study conducted by Steano Provera, HMQC assignment was employed, and their results indicated the order of Si3>Si6>Si2>Si4,[65] with Si3 and Si4 switched in comparison to our findings in deuterated chloroform. Regrettably, we were unable to obtain the supplemental information from their study, impeding further examination of their assignment for a more precise comparison. It is plausible that the discrepancies observed could be attributed to the choice of solvent, as the solvent used during the experiments can influence the chemical shift of silicon atoms.

Due to disagreement regarding the data obtained and in consideration of previous studies, a thorough examination was conducted on the assignment of H3 and H4 in this study. The purpose is to ensure the accuracy of the findings. The reassignment of proton using ^{1}H-^{1}H Corelated Spectroscopy (COSY), Figures 1.18 & 1.19, confirmed that the signal at δ 4.46 was to H1 and showed a cross peak to H2 (δ 3.33), which was a multiplet (overlapped) from δ 3.38-3.25. H2 showed crossed peak correlation to H3 (δ 3.60) from δ 3.63-3.57 m (overlapped with H6') in the COSY

spectrum, Figure 1.19. The correlation from H3 to H4 (δ 3.29-3.25) a multiple overlapped with H2 and H5 from δ 3.38-3.25 (m) was also observed in Figure 1.20. Furthermore, this zoomed-in spectrum also shows the correlation of H4 (δ 3.29), a multiplet of H5, H4, and H2 from δ 3.38 to 3.25, to H5 (δ 3.35). Additionally, the correlation of H5 to H6 (δ 3.54), appearing as a doublet of doublets, was also displayed.

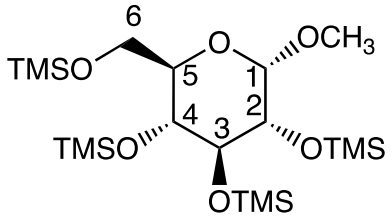

13

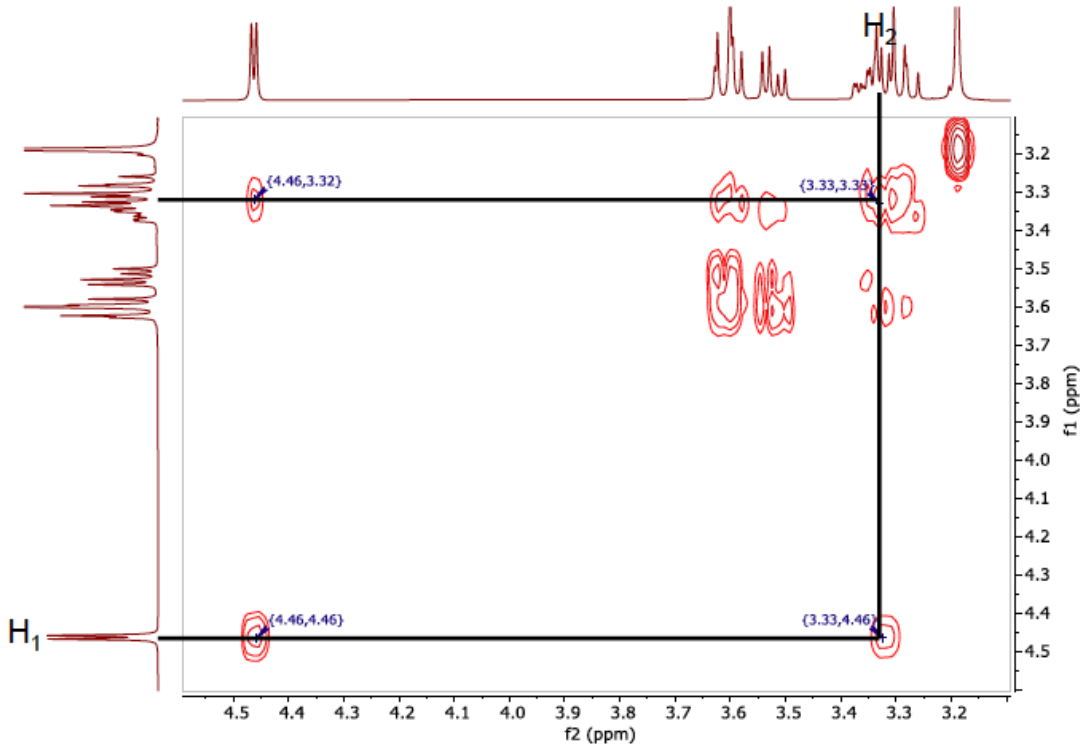

Figure 1.18: COSY of methyl-2,3,4,6-tetra-*O*-TMS-α-glucopyranoside (**13**), showed cross peak correlation between H1 to H2.

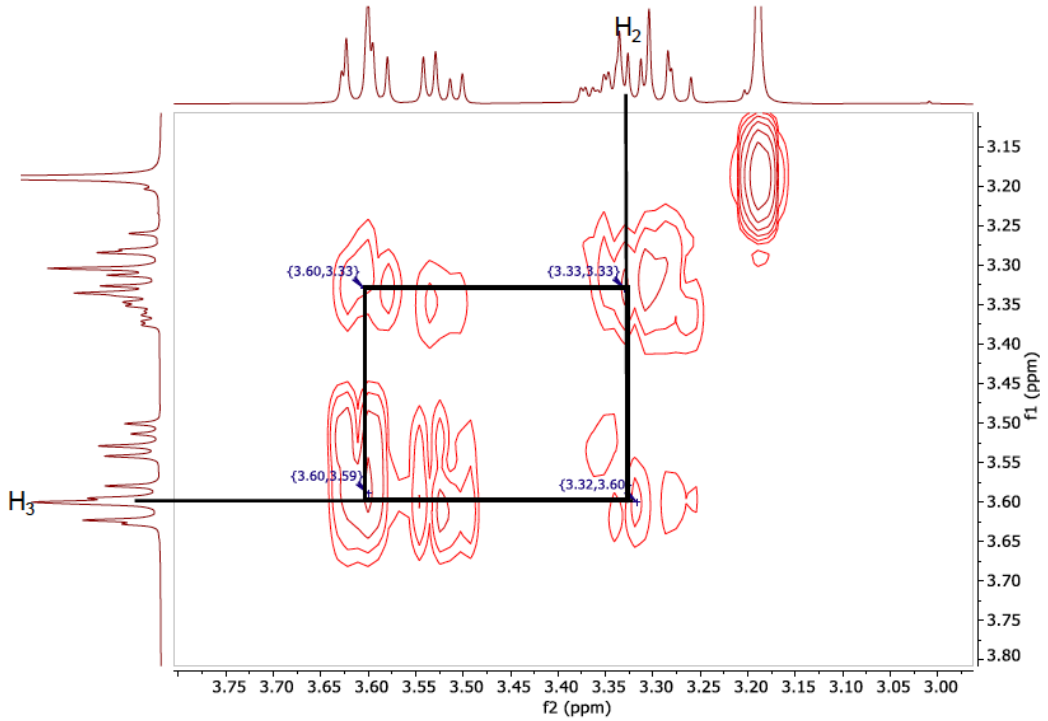

Figure 1.19: COSY of methyl-2,3,4,6-tetra-*O*-TMS-α-glucopyranoside (**13**), showed cross peak correlation between H2 to H3.

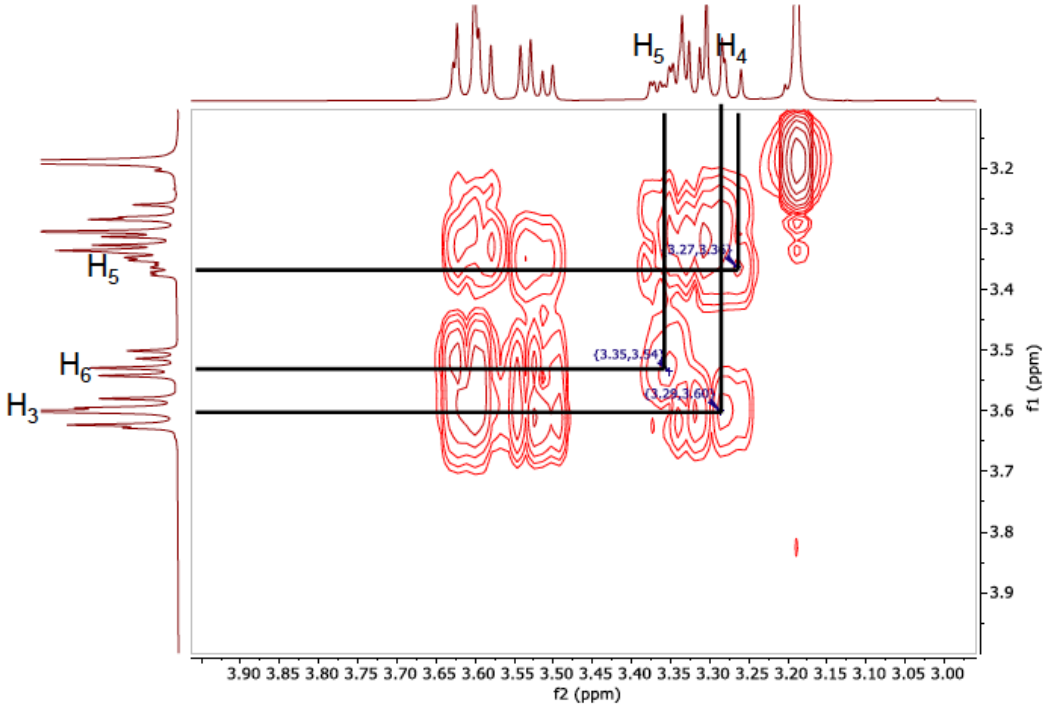

Figure 1.20: COSY of methyl-2,3,4,6-tetra-*O*-TMS-α-glucopyranoside (**13**), showed cross peak correlation between H3 to H4, H4 to H5, and H5 to H6.

To further confirm the assignment of H3, ^{1}H-^{13}C HMBC was used to analyze. In the provided Figure 1.21, a cross peak correlation from C3 (δ 75.3) to both H2 (δ 3.32) and H4 (δ 3.29) was observed. This correlation provided strong evidence for the correct assignment of H3. Additionally, in the same figure, a cross-peak correlation between C4 (δ 72.3) to both H5 (δ 3.36) and H3 (δ 3.60) are also observed. Furthermore, C5 (δ 72.1) showed cross peak correlation to H4 (δ 3.29). These correlations further supported the proximity and connectivity of these atoms within the molecule. Furthermore, to validate the assignment of Si3 and Si4, the Si3 cross peak correlation with H3 and the Si4 cross peak correlation with H4 were confirmed as depicted in the spectrum, Figure 1.22 below. These correlations provided solid evidence for the correct assignment of Si3 and Si4 within the structure. Based on these detailed analyses, it can confidently be stated that the data and assignments (See Table 1.4) have been accurately performed, reinforcing the reliability of the findings.

Table 1.4: The ^{1}H, ^{13}C, ^{29}Si NMR chemical shifts (δ) methyl-2,3,4,6-tetra-*O*-TMS-α-glucopyranoside (per-*O*-TMS methylglucosdie) (**13**) in $CDCl_3$.

Atom	**δ ^{1}H**	**δ ^{13}C**	**δ ^{29}Si**
1	4.63	99.6	--
2	3.55-3.42	72.2	17.9
3	3.80-3.74	75.3	17.7
4	3.55-3.42	73.9	18.5
5	3.55-3.42	72.0	--
6	3.80-3.74	62.2	18.3
6’	3.69	--	--
OCH3	3.36 (s)	54.5	--
O-TMS_2	0.17	1.30	--
O-TMS_3	0.17	0.94	--
O-TMS_4	0.18	-0.25	--
O-TMS_6	0.14	0.56	--

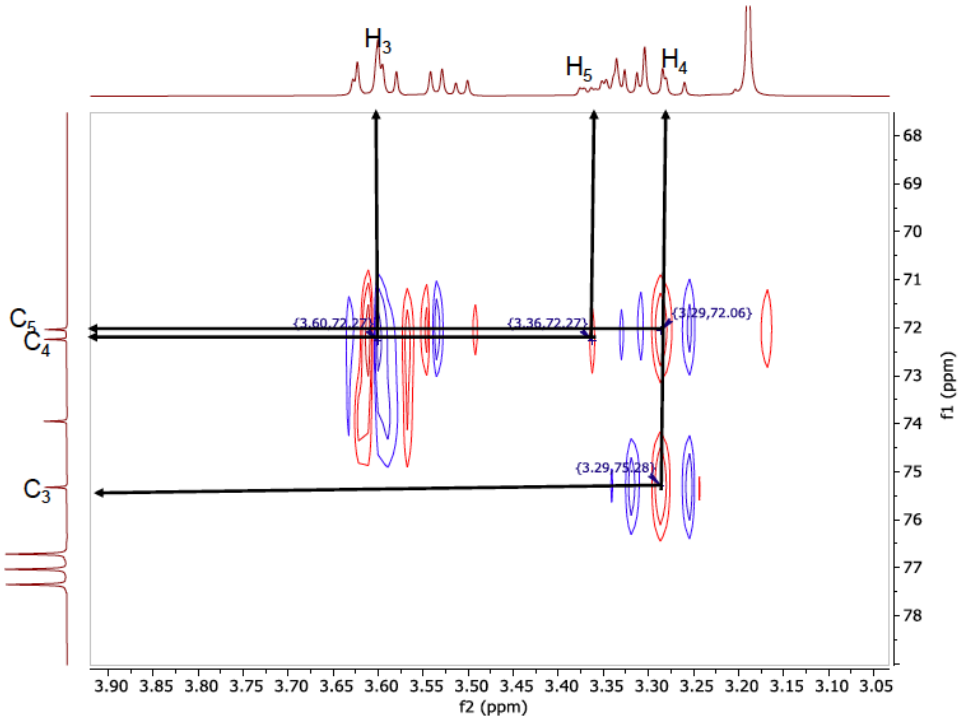

Figure 1.21: ^{1}H-^{13}C HMBC of methyl-2,3,4,6-tetra-*O*-TMS-α-glucopyranoside (**13**), showed the cross peak correlation between C3 to H4, C4 to H3 and H5, and C5 to H4.

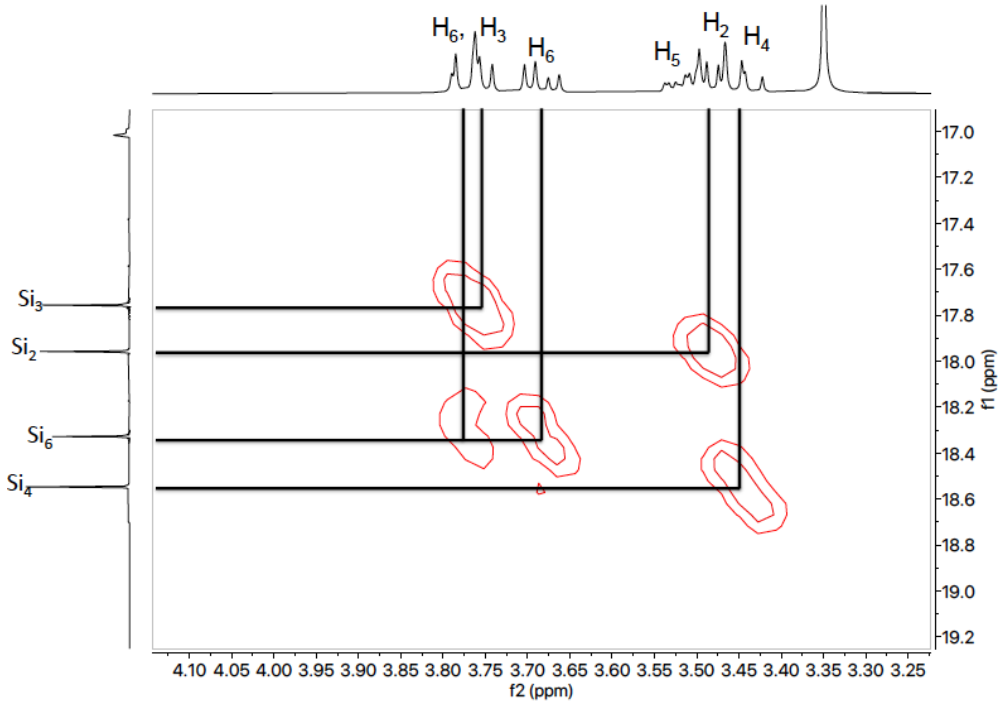

Figure 1.22: ^{1}H-^{29}Si HMBC of methyl-2,3,4,6-tetra-*O*-TMS-α-glucopyranoside (**13**) showed cross peak correlation between Si3 to H3 and Si4 to H4, Si to H2 and Si6 to H6ab.

1.2.3. Assignment of 1,2,3,4,6-Penta-*O*-TMS- α-Glucopyranoside (per-*O*-TMS glucose) (**14**)

The Gervay-Hague research group successfully determined the ^{1}H NMR and ^{13}C NMR peaks assignment for per-*O*-silylated glucose.[73] The obtained ^{1}H NMR and ^{13}C NMR spectra aligned with their published data, confirming the accuracy of this finding. Building upon their research, this study aimed to assign the ^{29}Si nuclei present in the compound. To accomplish this, a ^{1}H-^{29}Si HMBC experiment was utilized, Figure 1.23 and Figure 1.24.

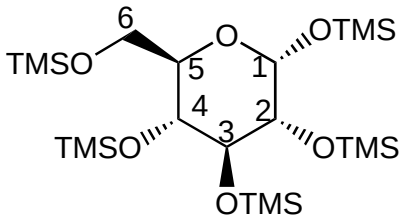

14

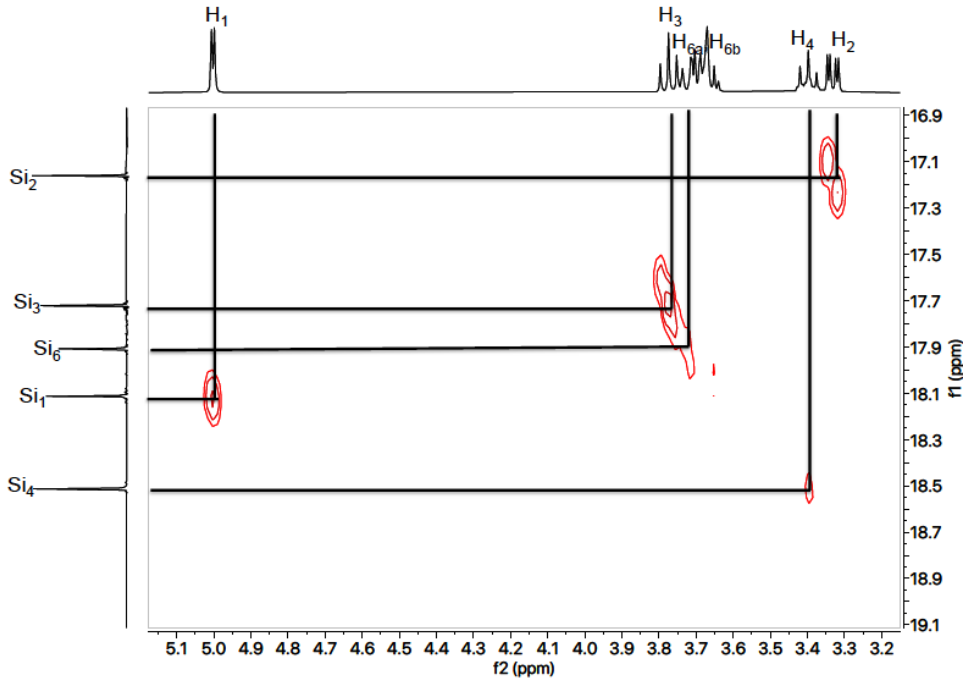

Figure 1.23: The ^{1}H-^{29}Si HMBC spectrum of per-*O*-TMS glucose (**14**) showed cross-peak correlations between the proton and silicon signals, which was used to assign the silicon signals.

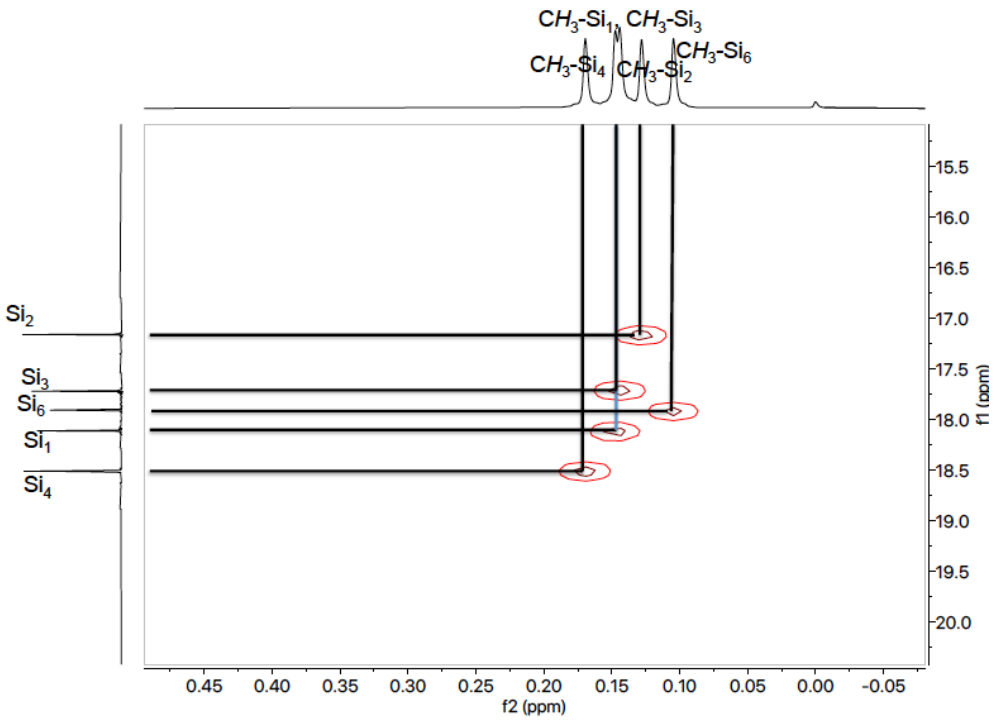

Figure 1.24: The ^{1}H-^{29}Si HMBC spectrum of per-*O*-TMS glucose (**14**) showed cross-peak correlations between the signals of trimethyl groups to the silicon signals.

The signal observed at δ 18.5 ppm was confidently assigned to Si4 using ^{1}H-^{29}Si HMBC, while the signal at δ 18.1 ppm was attributed to Si1. Furthermore, Si6 was assigned a chemical shift of δ 18.0 ppm, Si3 was assigned δ 17.7 ppm, and Si2 was assigned δ 17.2 ppm. The assignment can be visualized in Figure 1.23 above.

In this study, the assignment of the CH_3 protons and their corresponding carbon signals were successfully accomplished. Specifically, the signal at δ 0.17 (9H) was confidently assigned to the $(CH_3)_3$ groups linked to Si4. Additionally, the signals at δ 0.15, consisting of 18H, were attributed to the $(CH_3)_3$ groups connected to Si1 and Si3. Furthermore, the remaining two $(CH_3)_3$ groups associated with Si2 and Si6 were assigned to the signals at δ 0.13 and 0.10, respectively. The assignment was shown in Figure 1.24 above.

Similarly, the TMS-CH_3 from Si carbon signals were also effectively assigned using HSQC after the trimethyl protons were assigned. The carbon-13 signals observed at δ 1.28, 0.97, 0.47, and 0.19 were confidently assigned to the $(CH_3)_3$ groups attached to Si1, Si4, Si3, and Si2, respectively. However, the remaining $(CH_3)_3$ group, bonded to the silicon atom at Si6, exhibited a notable upfield shift and appeared in the negative region at δ -0.23. The table contains the chemical shifts, and their corresponding protons, carbons, and silicon can be found in Table 1.5. Full assignments can be found in the Supplemental Information on page 118-125.

Table 1.5: The ^{1}H, ^{13}C, ^{29}Si NMR chemical shifts (δ) 1,2,3,4,6-penta-*O*-TMS- α-glucopyranoside (**14**) (per-*O*-TMS glucose) in $CDCl_3$.

Atom	**δ ^{1}H**	**δ ^{13}C**	**δ ^{29}Si**
1	5.00	93.9	18.2
2	3.33	74.2	17.2
3	3.77	74.0	17.8
4	3.40	72.3	18.6
5	3.74-3.63	72.5	--
6	3.74-3.63	62.3	18.0
6’	3.74-3.63	--	--
O-TMS_1	0.15	1.28	--
O-TMS_2	0.13	0.19	--
O-TMS_3	0.15	0.47	--
O-TMS_4	0.17	0.97	--
O-TMS_6	0.10	-0.23	--

1.2.4. Assignment of 1,3,4,6-Tetra-*O*-TMS-α–Mannopyranoside (α-per-*O*- TMS mannose) (**15**).

The proton and carbon signals of per-*O*-silylated mannose (**15**) were successfully assigned by the Gervay-Hague research group[73], and the data reported herein are in agreement with their assignment.

The assignment of silicon signals was accomplished using the ^{1}H-^{29}Si HMBC. The cross peaks correlations illustrated in Figure 1.25. The ^{29}Si NMR signal at δ 18.85

was assigned to Si4, as it exhibits a cross-peak correlation with H4. Si4 signal is the most downfield silicon resonance. Additionally, the ^{29}Si NMR chemical shifts at δ 18.43, 17.60, and 17.10 were assigned to Si1, Si6, and Si3, respectively. Interestingly, Si2 was assigned a chemical shift of δ at 16.05, which is further upfield and stands out among the other signals.

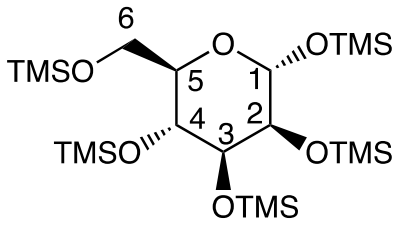

15

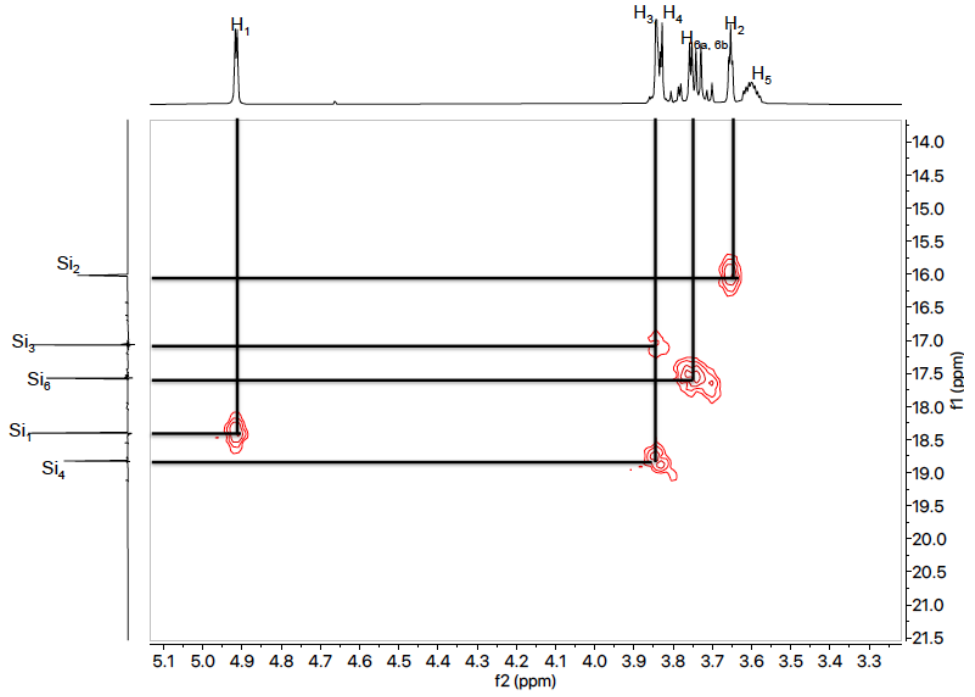

Figure 1.25: The ^{1}H-^{29}Si HMBC spectrum of α-per-*O*-TMS mannose (**15**) showed a cross-peak correlation between the proton and silicon signals, which was used to assign the silicon signal.

Furthermore, utilizing the ^{1}H-^{29}Si HMBC techniques, the assignment of the CH_3 group, Figure 1.26 and its corresponding ^{13}C NMR signals was successfully accomplished. The signal at δ 0.15 (9H) was assigned to the $(CH_3)_3$ groups attached

to Si3. Likewise, the signals at δ 0.14, consisting of 18H, were attributed to the $(CH_3)_3$ groups connected to Si1 and Si4. The remaining two $(CH_3)_3$ groups, belonging to Si2 and Si6, were assigned to the signals at δ 0.11 and 0.10, respectively.

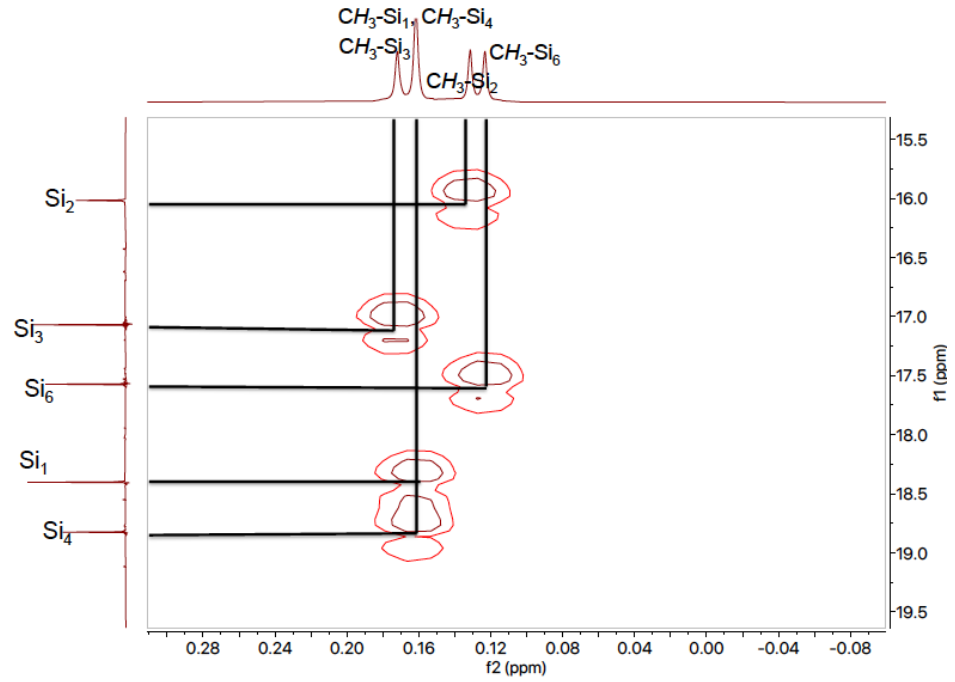

Figure 1.26: The ^{1}H-^{29}Si HMBC spectrum of α-per-*O*-TMS mannose (**15**) showed a cross-peak correlation between the signals of trimethyl groups to the silicon signal.

Using the same method applied to per-*O*-silylated glucose and per-*O*-silylated methylglucoside, the assignment of ^{13}C NMR signals of CH_3 group was achieved using HSQC after the TMS-protons were successfully assigned. The peaks at δ 0.72, 0.61, and 0.39 were assigned to the $(CH_3)_3$ groups bonded to Si6, Si1, and Si4, respectively. In contrast, the two remaining $(CH_3)_3$ groups that are bonded to the silicon atom at Si2 and Si3 exhibited slightly upfield shifts, appearing in the negative region at δ -0.09 and -0.14, respectively. The spectrum assignment can be found in the Supplemental Information section, page 126-133 and the chemical shifts and their corresponding protons, carbons, and silicon can be found in Table 1.6.

Table 1.6: The ^{1}H, ^{13}C, ^{29}Si chemical shifts (δ) 1,2,3,4,6-penta-*O*-TMS- α-mannopyranoside (**15**) (per-*O*-TMS-mannose) in $CDCl_3$.

Atom	δ ^{1}H	δ ^{13}C	δ ^{29}Si
1	4.89	95.6	18.4
2	3.63	75.2	16.1
3	3.87-3.87	72.2	17.1
4	3.87-3.87	64.3	18.8
5	3.60-3.55	74.6	--
6	3.74-3.63	62.5	17.6
6’	3.74-3.63	--	--
O-TMS_1	0.14	0.61	--
O-TMS_2	0.11	-0.09	--
O-TMS_3	0.15	-0.14	--
O-TMS_4	0.14	0.39	--
O-TMS_6	0.10	0.72	--

1.2.5. Assignment of 1,2,3,4,6-Penta-*O*-TMS-β-Fructopyranoside (per-*O*-TMS fructose) (**16**).

The proton of per-*O*-silylated fructose (**16**) was previously assigned in acetone-d6.[74] In this study it was performed in deuterated chloroform. The chemical shifts are similar, except for H4. In acetone-d6, H4 (δ 4.18) is more downfield, and in deuterated chloroform, H4 (δ 3.74, dd) is more upfield. The most downfield signal was assigned to H3 at δ 4.023, a doublet with J = 9.2 Hz. Using COSY NMR spectrum, it was confirmed that the signal at δ 3.74, a doublet of doublets was H4, which is shown in Figure 1.27.

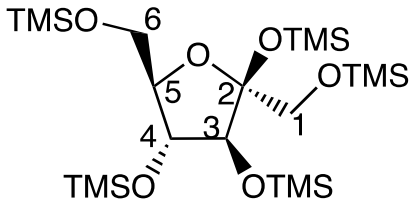

16

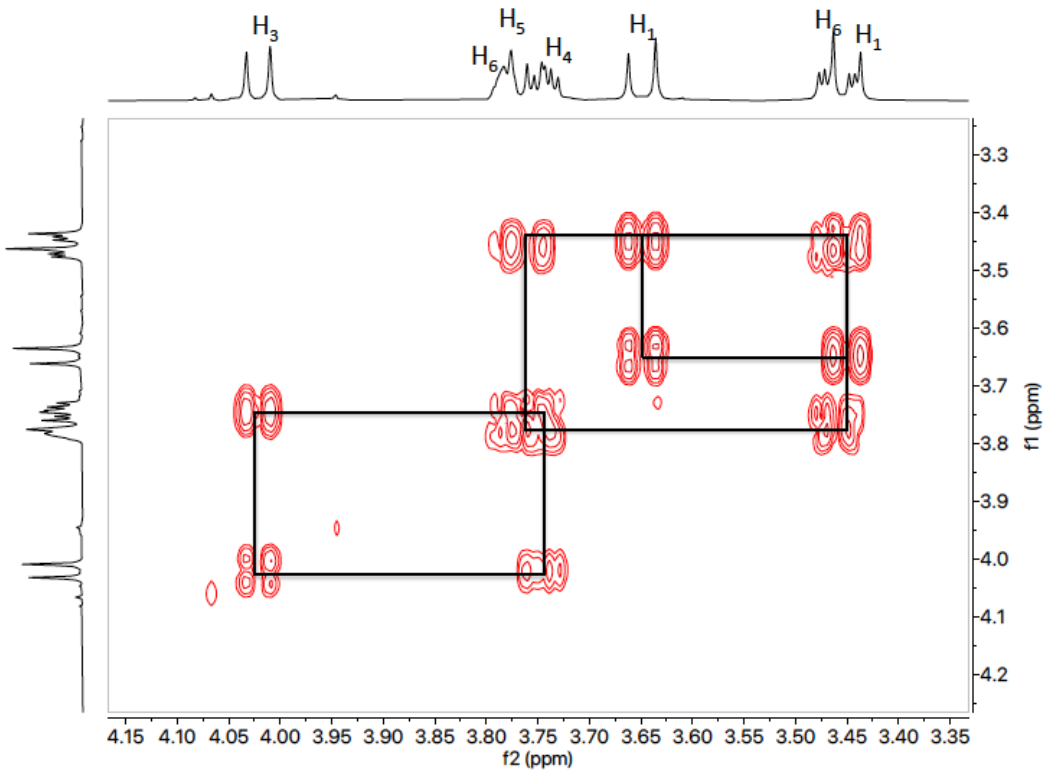

Figure 1.27: COSY spectrum of β-per-*O*-TMS fructose (**16**) showed the cross-peak correlations between H3 to H4, H1a and H1b, and H6a, H6b and H5 to H6a.

The assignment was further confirmed by ^{1}H-^{13}C HMBC, where C4 (δ 71.3) showed cross peak correlations to both H3 (δ 4.02) and H5 (δ 3.78-3.75), shown at the Supplemental Section page 141. H5 is a multiplet (partially overlapped peak) with H6b at δ 3.80-3.78. Meanwhile H6a is at δ 3.46-3.48, which also overlapped with H1a. The doublet at δ 3.65 was assigned to H1a, which was confirmed by COSY, Figure 1.27 and ^{1}H-^{29}Si HMBC showed in Figure 1.28.

For the assignment of the CH_3 groups from the TMS (trimethylsilyl) group, the signal at δ 0.14 (18H) was assigned to the $(CH_3)_3$ groups attached to Si2 and Si4. The signal at δ 0.13 (9H) was assigned to the $(CH_3)_3$ groups attached to Si3. The most upfield signal at δ 0.11 (18H) was assigned to the $(CH_3)_3$ groups attached to Si1 and

Si6. The full spectrum for all assignments can be found in the Supplemental Information Section, page 139.

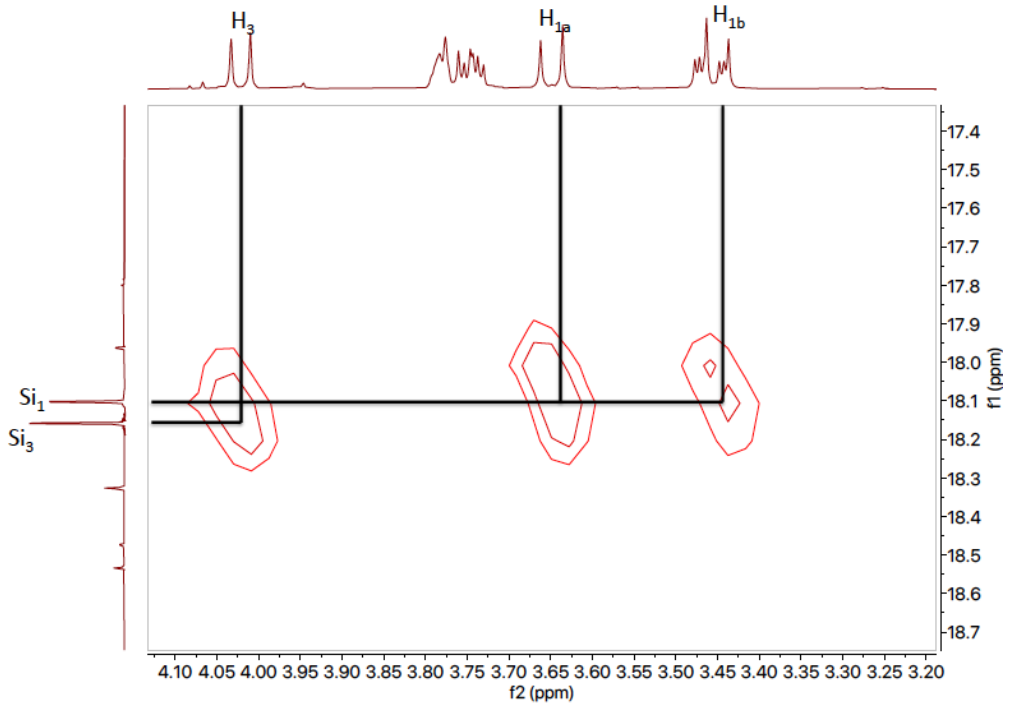

Figure 1.28: ^{1}H-^{29}Si HMBC spectrum of β-per-*O*-TMS fructose (**16**) showed the cross-peak correlation of H3 to Si3 and H1a, H1b to Si1.

The assignment for ^{29}Si NMR signal was achieved using ^{1}H-^{29}Si HMBC after the successful proton assignment. The ^{1}H-^{29}Si HMBC techniques showed direct cross-peak correlations between protons and silicon, thereby eliminating any ambiguity in signal assignment. The signals were assigned as follows: Si3 was the most downfield at δ 18.2, Figure 1.29. The signal at δ 18.1 was assigned to Si1, and these two signals nearly overlapped. Si4 was assigned to the signal at δ 16.6, and Si6 was assigned to δ 15.0. The most upfield signal at δ 10.7 was assigned to Si2 as shown in Figure 1.29. The full spectrum ^{1}H-^{29}Si HMBC assignments can be found in the Supplemental Information Section page 138.

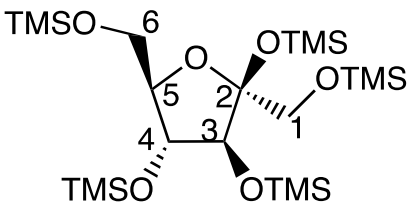

16

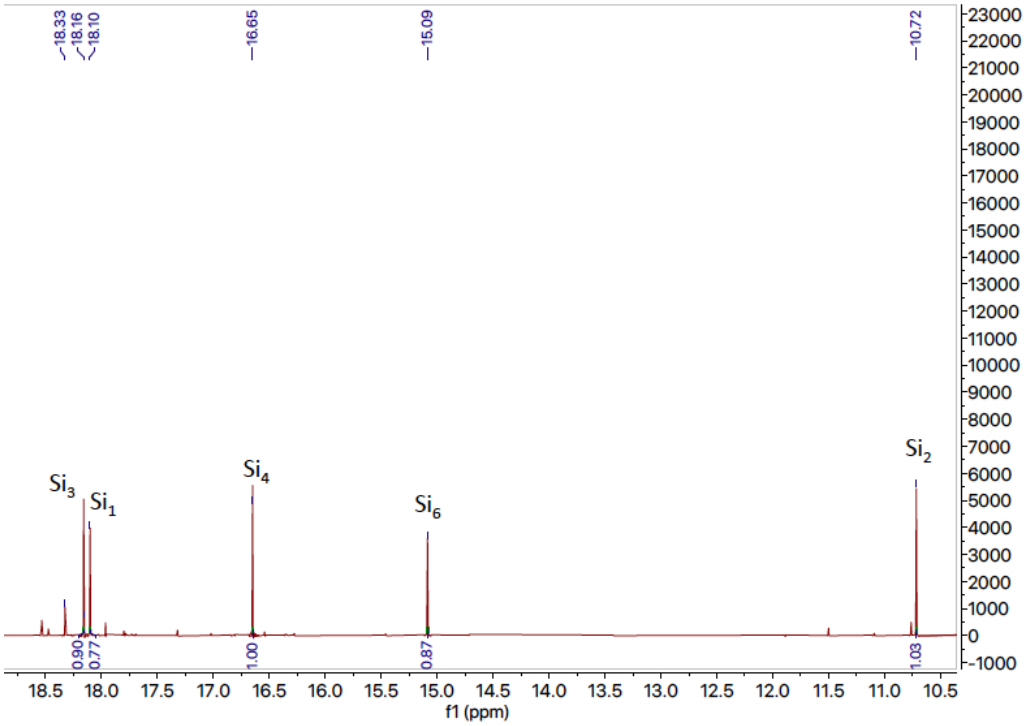

Figure 1.29: ^{29}Si NMR spectrum of β-per-*O*-TMS fructose showed the five signals of Si2 (most upfield at 10.72 ppm) while Si3 is the most downfield at 18.33 ppm.

The carbon assignment was accomplished by using ^{1}H-^{13}C HSQC, which provides direct cross-peak correlations from proton to carbon. With the successful assignment of protons, carbon assignment was performed without ambiguity and confirmed with ^{1}H-^{13}C HMBC. The signal at δ 101.8 was assigned to C2, which does not exhibit proton correlation. C4 and C5 were assigned to signals at δ 72.2 and δ 71.3, respectively. C3 was assigned to δ 69.07, while C1 and C6 were assigned to δ 65.5 and δ 65.1, respectively. Both C1 and C6 were found to be close to each other in terms of chemical shift. Interesting, the TMS carbon cannot be assigned due to significant

overlap between each signal. Therefore, a higher resolution NMR instrument will be required to obtain better cross-peak signals. The full assignment can be found in the Supplemental Information section, page 134-141. The chemical shifts and their corresponding proton, carbon, and silicon atoms can be found in Table 1.7.

Table 1.7: The ^{1}H, ^{13}C, ^{29}Si NMR chemical shifts (δ) 1,2,3,4,6-penta-*O*-TMS-β-fructopyranoside (per-*O*-TMS fructose) (**16**) in $CDCl_3$.

Atom	δ ^{1}H	δ ^{13}C	δ ^{29}Si
1	3.49-3.46	65.5	18.1
1’	3.65	---	
2	--	101.8	10.7
3	4.02	69.1	18.2
4	3.74	71.3	18.6
5	3.78-3.75	72.2	--
6	3.49-3.46	65.2	15.0
6’	3.80-3.78	--	--
O-TMS_1	0.11	--	--
O-TMS_2	0.14	2.21	--
O-TMS_3	0.13	--	--
O-TMS_4	0.14	--	--
O-TMS_6	0.11	--	--

1.2.6. Assignment of 1,2,3,4,5,6-Hexa-*O*-TMS-Sorbitol (per-*O*-TMS sorbitol) (**17**).

It had previously been mentioned that per-*O*-silylated sorbitol (**17**) had been synthesized.[56] However, a full assignment was not found through literature search, specifically the supporting data that provided complete proton, carbon, and silicon assignment. Therefore, the assignments for proton and carbon signals were performed in deuterated chloroform. Using COSY and *J* values, the signal at δ 3.90, a double of triplets with *J* values of 7.8 and 2.5 Hz, was assigned to H2, Figure 1.30. It was observed to have two cross peaks correlating to δ 3.80 (H3) and δ 3.48 (H1a), as well as δ 3.74 (H1b). The overlapped peak from δ 3.82 to 3.73 consisted of four

signals: H3, H6b, H4, and H1b. To distinguish between H1b and H6b from H4 and H3, it was confirmed with ^{1}H-^{29}Si HMBC cross peak correlation. In this case, a single silicon signal would exhibit two cross peaks correlating to H6b and H6a and similar to H1b and H1a, Figure 1.31. H3 had already been assigned using COSY, the signal showed a cross peak correlation to δ 3.63 (J = 6.0, 4.4 Hz), which corresponds to H5. H5 also displayed cross peak correlation to H6a and H6b. Further confirmation was performed using ^{1}H-^{13}C HMBC, which the spectrum can be found at the Supplemental Information Section page 148.

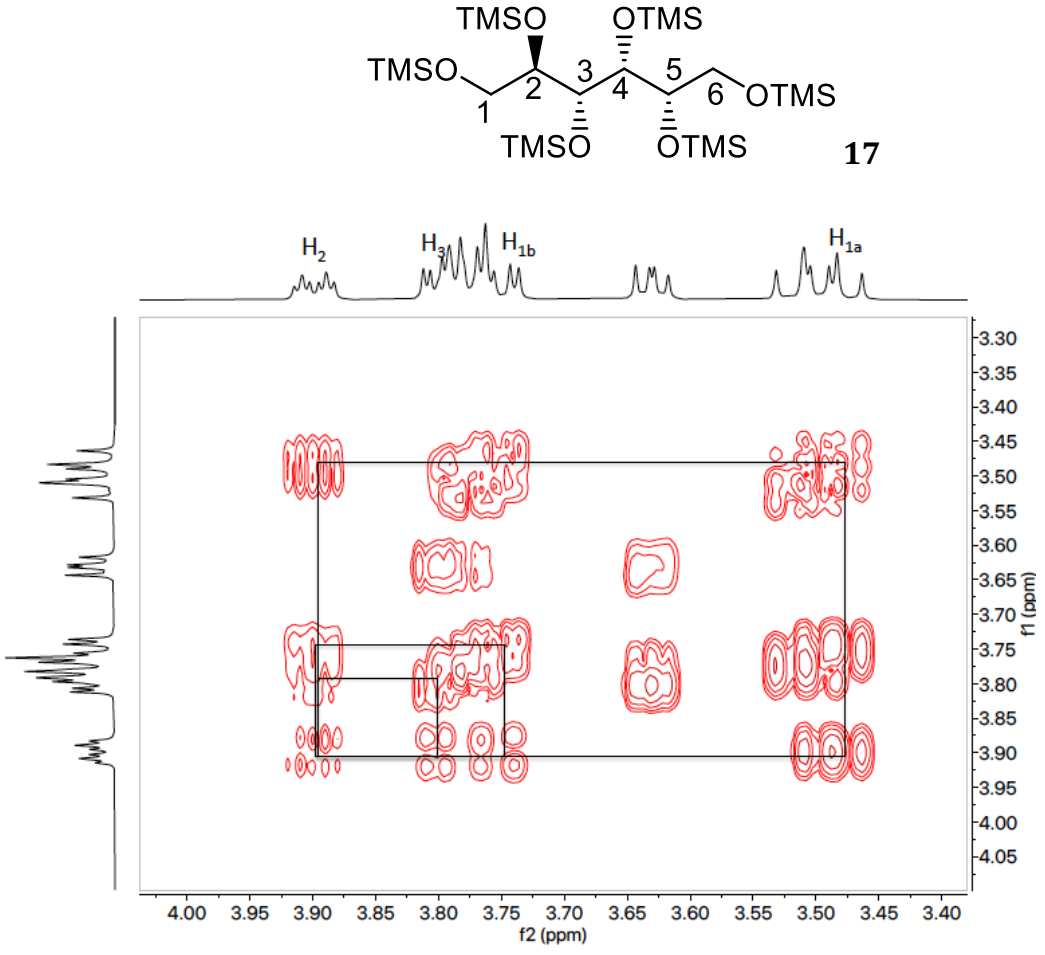

Figure 1.30: The COSY of per-*O*-TMS sorbitol (**17**) showed the cross-peak correlation between H2 to H1a, H1b and H2 to H3

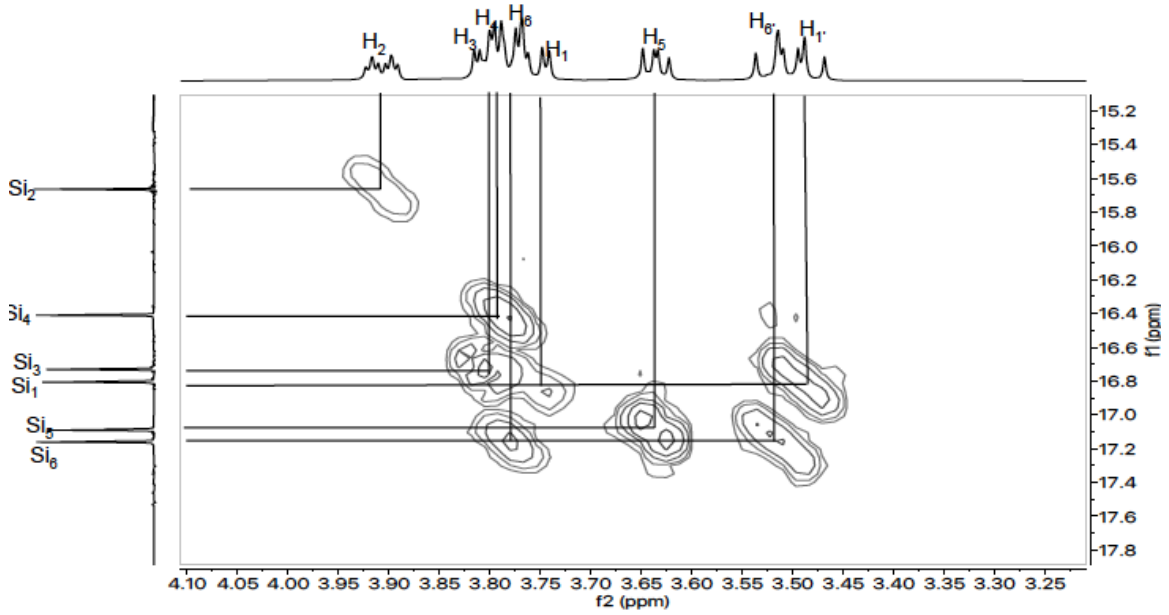

Figure 1.31: ^{1}H-^{29}Si HMBC of per-*O*-TMS sorbitol (**17**) showed the cross peaks correlation of H1a, H1b to Si1 and H6a, H6b to Si6.

After assigning the silicon signal, the protons from the CH_3 groups can be assigned as follows: δ 0.16 (18H) was assigned to the proton from CH_3 attached to Si5 and Si3. Furthermore, the peaks at δ 0.15, 0.14, 0.12, and 0.11 were assigned to the protons from the CH_3 attached to Si4, Si2, Si6 and Si1, respectively.

Carbon assignment was performed using ^{1}H-^{13}C HSQC, which provides direct correlation to its corresponding proton signal. Of particular importance, the carbons from CH_3 groups were assigned as follows: the carbon-CH_3 group bonded to Si2 was assigned to the signal at δ 0.92, while the carbon-CH_3 bonded Si5 was assigned to δ 0.64. Additionally, CH_3 bonded Si3 and Si4 shared the same signal at δ 0.63. The carbon-CH_3 groups bonded to Si1 and Si6 appeared in the negative region at δ -0.44 and -0.50, respectively. The full ^{13}C NMR assignment can be found in the Supplemental Information section on page 144.

The ^{29}Si NMR signal was assigned using ^{1}H-^{29}Si HMBC, as previously employed for the above compound. Since the proton signals were successfully assigned as shown above, silicon assignment was facilitated. The cross-peak correlation between Si and H was evident. There are six silicon signals, which were assigned as follows: Si6 was assigned to δ 17.20, Si5 to δ 17.1, Si1 to δ 16.9, Si3 to δ 16.8, Si4 to δ 16.4, and Si2 to δ 15.7. The full assignment can be found in Figure 1.31, and Table 1.8 below.

Table 1. 8: The ^{1}H, ^{13}C, ^{29}Si NMR chemical shifts (δ) of 1,2,3,4,5,6-hexa-vi-TMS-sorbitol (**17**) (per-*O*-TMS sorbitol) in $CDCl_3$.

Atom	**δ ^{1}H**	**δ ^{13}C**	**δ^{29}Si**
1	3.50	63.7	16.9
1’	3.83-3.73	---	
2	3.90	75.9	15.7
3	3.83-3.73	76.3	16.8
4	3.83-3.73	76.2	16.4
5	3.63	74.5	17.1
6	3.50	63.7	17.2
6’	3.83-3.73	--	--
O-TMS_1	0.11	-0.44	--
O-TMS_2	0.13<u>5</u>	0.92	--
O-TMS_3	0.15	0.63	--
O-TMS_4	0.14<u>5</u>	0.63	--
O-TMS_5	0.15	0.64	--
O-TMS_6	0.12	-0.50	--

Note: The underline values indicate 3 digits to distinguish between TMS2, TMS3, TMS4 and TMS5.

1.2.7. Assignment of 1,2,3,4,5-Penta-*O*-TMS Ribitol (per-*O*-TMS ribitol) (**18**).

Through a literature search, we were unable to find a complete ^{1}H and ^{13}C assignment for per-*O*-TMS ribitol (**18**). The assignment for per-*O*-TMS ribitol (**18**) followed the same method as previously mentioned for all other compounds. Since this is a symmetrical sugar alcohol, the number of protons, carbon, and silicon signals is also reduced. The signal at δ 3.84 was assigned to H2 and H4, while δ 3.72 was

assigned to H1' and H5'. The cross-peak correlation on the COSY, Figure 1.32 confirmed the assignment. The signal at δ 3.64 was assigned to H3. H1 and H5 were assigned to the signal at δ 3.47, which showed correlation to H1' and H5' and H2 and H4, Figure 1.32 (COSY).

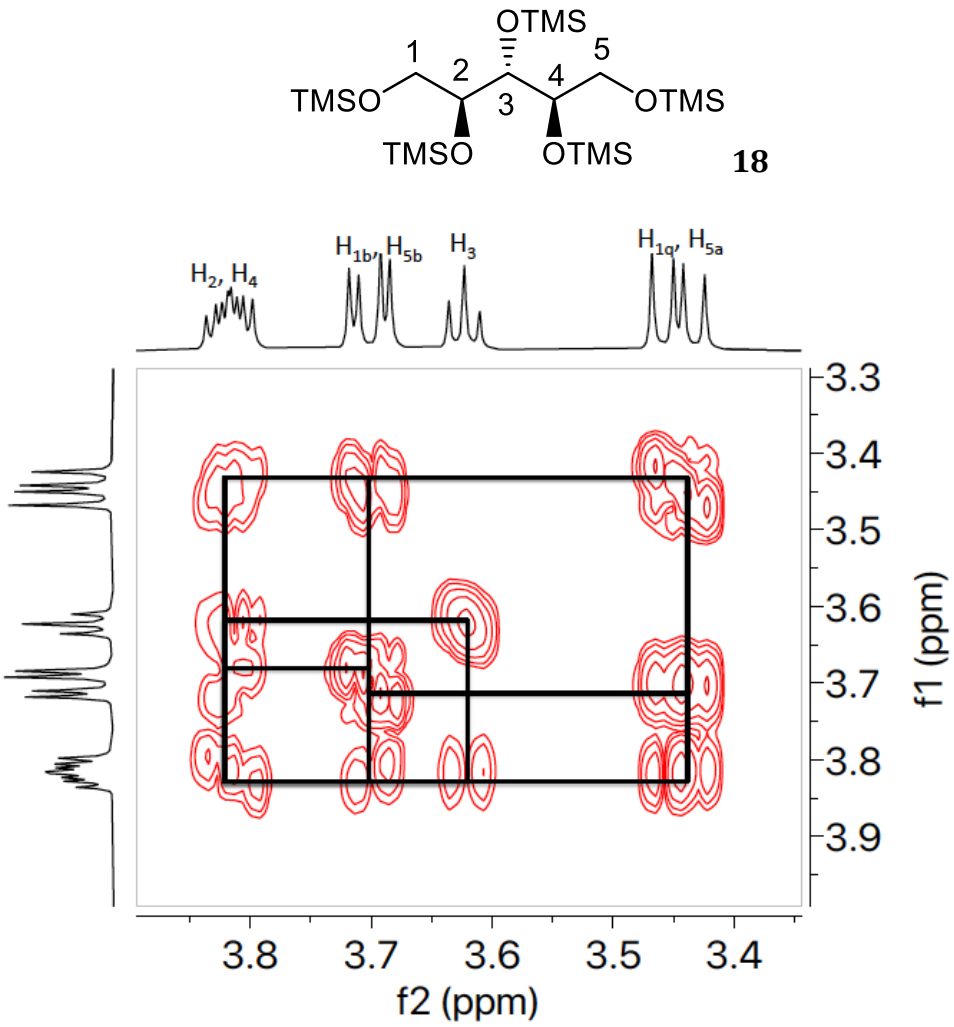

Figure 1.32: COSY spectrum of per-*O*-TMS ribitol (**18**) showed cross peak correlations of H1ab, and H5ab to H2 and H4.

The protons of the CH3 groups generated only three signals: CH3 from Si2 and Si4 was assigned to the signal at δ 0.12 (18H), CH3 from Si3 was assigned to δ 0.11 (9H). Meanwhile CH3 from Si5 and Si1 was assigned to δ 0.10 (18H). The complete

full proton assignment can be found on the back of the Supplemental Information, page 150, and Table 1.9.

There are six carbon signals: three from the symmetrical carbons (1-5) and three from the $(CH_3)_3$ attached to Si. The signal at δ 76.73 was assigned to C3, while C2 and C4 shared the same signal at δ 74.35. Similar to C1 and C5, which shared the signal at δ 64.19. The signal at δ 0.53 was assigned to carbon the $(CH_3)_3$ attached Si2 and Si4, δ 0.42 was assigned to $(CH_3)_3$ attached Si3 in the negative region, and δ -0.53 was assigned to $(CH_3)_3$ attached Si1 and Si5. The full assignment can be found in the Supplemental Information section on page, page 152.

The ^{29}Si NMR signal also consists of three peaks. Si3 was assigned to the most downfield peak at δ 17.68, while Si1 and Si5 were assigned to the peak at δ 17.39. The most upfield peak at δ 16.71 was assigned to Si2 and Si4, Figure 1.33. The integration of each signal corresponds to the number of silicon atoms in the peak. For example, the peak at δ 16.71 integrated to 1.91, Figure 1.34, which is approximately 2.00, indicating the presence of two silicon atoms in this peak.

Table 1.9: The ^{1}H, ^{13}C, ^{29}Si NMR chemical shifts (δ) of 1,2,3,4,5 penta-*O*-TMS ribitol (**18**) (per-*O*-TMS ribitol) in $CDCl_3$.

Atom	**δ ^{1}H**	**δ ^{13}C**	**δ ^{29}Si**
1	3.47	64.1	17.3
1’	3.72	---	
2	3.84	74.3	16.7
3	3.65	76.7	17.6
4	3.84	74.3	16.7
5	3.47	64.1	17.3
5’	3.72	--	--
O-TMS_1	0.10	-0.53	--
O-TMS_2	0.12	0.53	--
O-TMS_3	0.11	0.52	--
O-TMS_4	0.12	0.53	--
O-TMS_5	0.10	-0.53	--

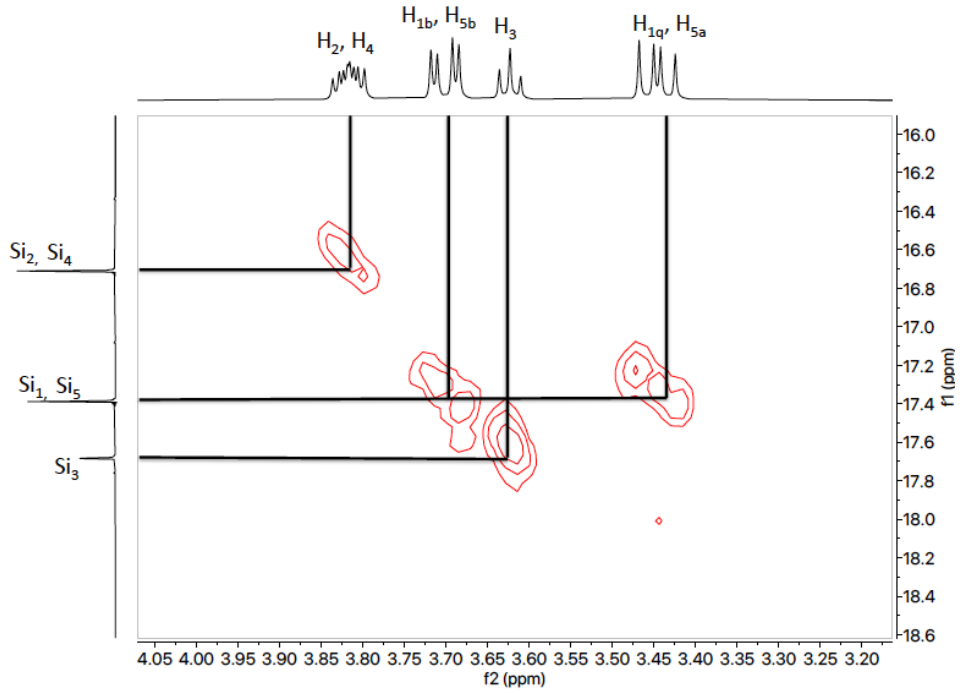

Figure 1.33: ^{1}H-^{29}Si HMBC of per-*O*-TMS ribitol (**18**) showed the cross-peak correlation between proton and silicon.

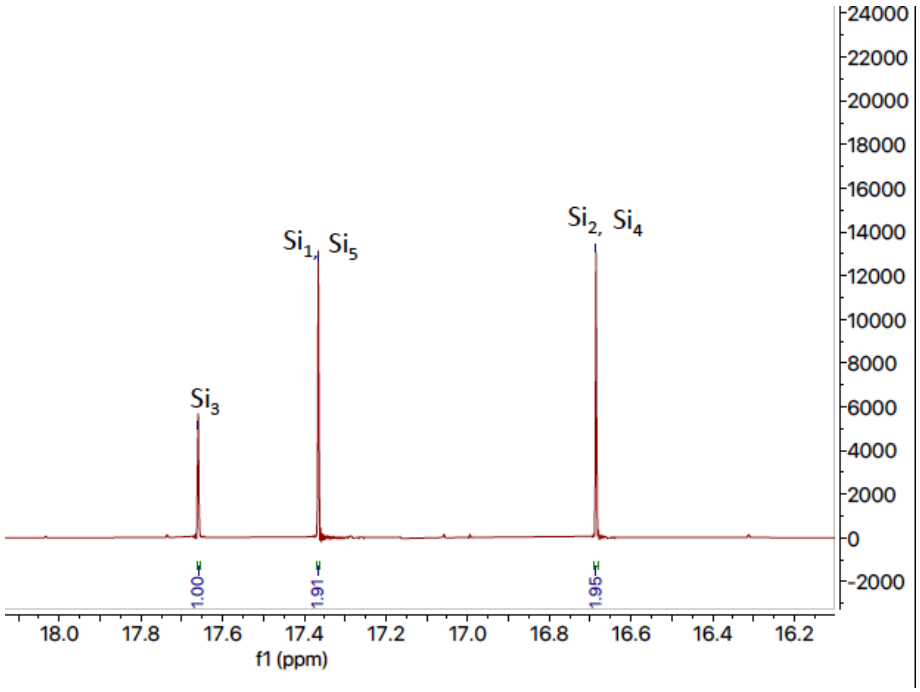

Figure 1.34: ^{29}Si spectrum of per-*O*-TMS ribitol (**18**), showed the integration and peak assignment.

1.2.8. Assignment of 1,2,3,4,5 Penta-*O*-TMS Xylitol (per-*O*-TMS xylitol) (**19**).

The silyl derivatives of xylitol were mentioned in a patent.[75] However, a complete assignment of proton, carbon, and silicon NMR signals could not be found in the literature search. Therefore, a full assignment was conducted using the method previously employed for compounds **17** and **18**, and other silyl compounds in this study. As a symmetrical compound, the number of protons, carbon, and silicon peaks is reduced. The signal at δ 3.82 was assigned to H2 and H4 and showed cross peak correlation to H3. H3 was assigned to a triplet at δ 3.74 (*J* = 4.12 Hz), which partially overlapped with H1b and H5b in the range of δ 3.70-3.69 (multiplet), which also showed cross peak correlation to H2 and H4. The signal at δ 3.52 was assigned to H1a and H5a, which appeared as a doublet of doublets and showed correlation to H2 and H4 as well as H1b and H5b, Figure 1.35. These assignments were confirmed by ^{1}H-^{13}C HMBC and further supported by silicon assignment. The silicon atom exhibited two cross-peak correlations: one with H1' and H5' and another with H1 and H5, indicating the presence of separate peaks for these protons, Figure 1.36. The full assignment can be found in the Supplemental Information section on page 157-163.

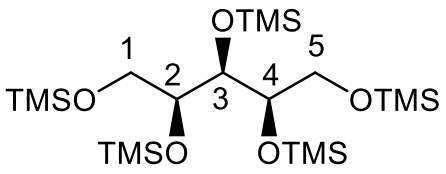

19

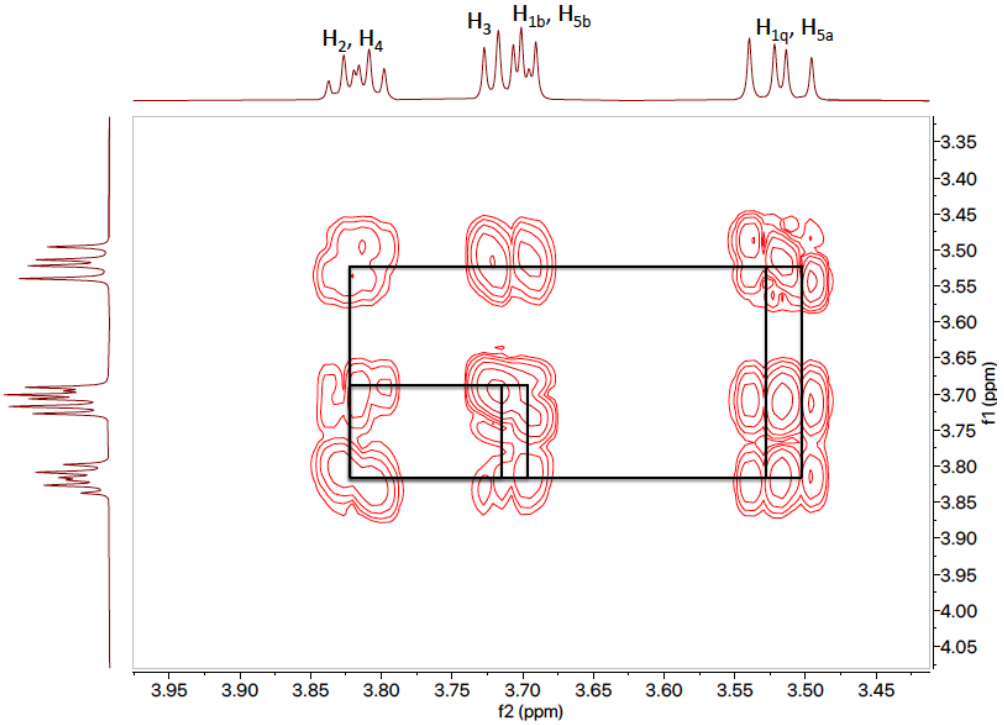

Figure 1.35: COSY of per-*O*-TMS xylitol (**19**) showed the cross-peak correlation between H2 and H4 to H1ab and H5ab and H2 & H4 to H3.

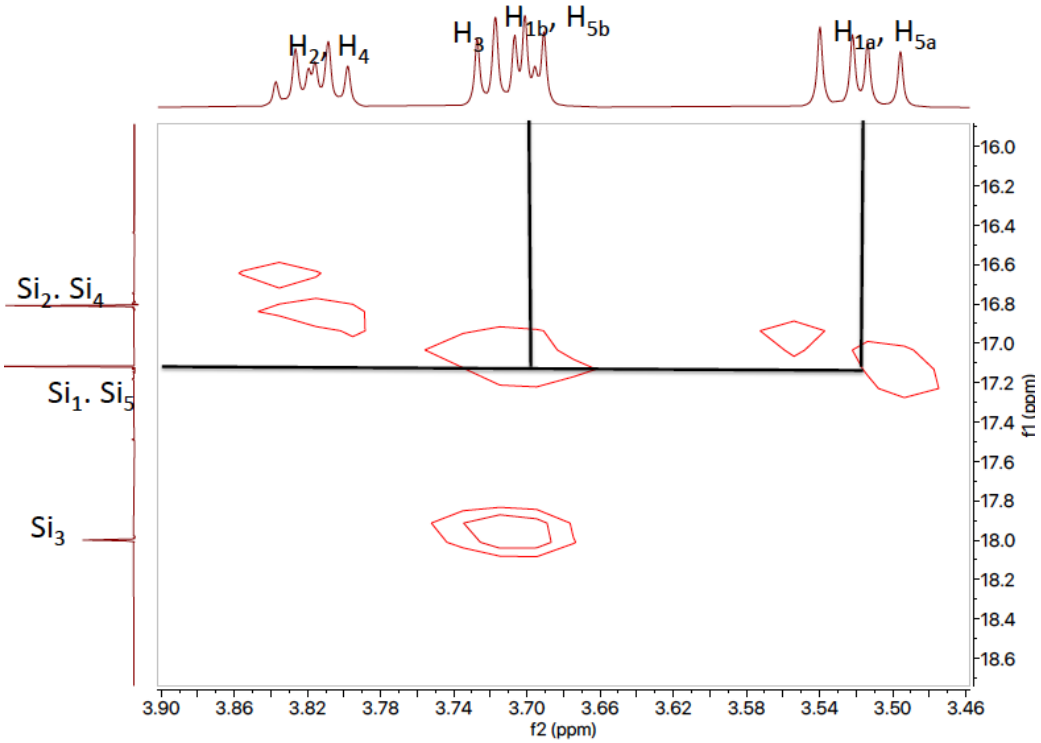

Figure 1.36: ^{1}H-^{29}Si HMBC per-*O*-TMS xylitol (**19**) showed the cross-peak correlation between H1ab and H5ab to Si1, Si5.

The peaks assigned following CH_3 protons attached to the silicon were assigned as the following. The $(CH_3)_3$ groups bonded to Si3 were assigned to δ 0.14 (9H), the signal at δ 0.13 (18H) was assigned to $(CH_3)_3$ groups attached Si2 and Si4, and the $(CH_3)_3$ groups attached Si1 and Si5 were assigned to the peak at δ 0.10. The full assignment can be found in the Supplemental Information section on page 157.

There are six peaks observed in the carbon spectrum: three downfield peaks corresponded to the three carbons from the symmetrical carbons (1-5), and three peaks for the $(CH_3)_3$ groups attached Si, which are upfield and close to 0 ppm. The peak at δ 74.36 was assigned to C2 and C4, while C3 was assigned to δ 73.39. The signal at δ 63.68 was assigned to C1 and C5. The carbon $(CH_3)_3$ groups attached to Si were assigned in the following order: $(CH_3)_3$ carbons attached Si1 and Si5 were assigned at δ 0.70 ppm, while $(CH_3)_3$ carbons attached Si2 and Si4 appeared upfield in the negative region at δ -0.44 ppm, and $(CH_3)_3$ carbons attached Si3 were assigned to the signal at δ 0.45 ppm. The full ^{13}C NMR spectrum assignment can be found in the Supplemental Information section on page 153.

There are only three silicon signals in the compound due to its symmetry. By utilizing the cross-peak correlation of ^{1}H-^{29}Si HMBC, see Supplemental Information section on page 158 and 161, it was confidently assigned Si3 at δ 18.0 and Si1 and Si5 at δ 17.1. Si2 and Si4 were assigned to the signal at δ 16.8, see Table 1.10. Similar to per-*O*-TMS ribitol (**18**), the integration of each signal aligns with the number of atoms represented in the signal.

Table 1.10: The ^{1}H, ^{13}C, ^{29}Si NMR chemical shifts (δ) of 1,2,3,4,5 penta-*O*-TMS xylitol (**19**) (per-*O*-xylitol) in $CDCl_3$.

Atom	δ ^{1}H	δ ^{13}C	δ ^{29}Si
1	3.52	63.6	17.1
1’	3.70-3.69	---	
2	3.82	74.3	16.8
3	3.73	73.3	18.0
4	3.82	74.3	16.8
5	3.52	63.6	17.1
5’	3.70-3.69	--	--
O-$TMS_{1,5}$	0.10	0.70	--
O-$TMS_{2,4}$	0.13	-0.44	--
O-TMS_3	0.14	0.45	--

1.2.9. Assignment of 1,3,4,6,2’,3’,4’,6-Octa-*O*-TMS-Sucrose (per-*O*-TMS sucrose) (**20**).

The proton assignment of per-*O*-TMS sucrose (**20**) was previously assigned in acetone-d6.[74] The assignment of per-*O*-silylated sucrose (**20**) started with the use of COSY, which revealed a *J* coupling constant of *J* = 3.30 Hz for a doublet at δ 5.22, assigned to H1' from the Glc*p* ring. This was further confirmed using ^{1}H-^{13}C HMBC, which displayed a cross peak to C2' (δ 72.99) and C2 (δ 103.2) from the Fru*f* ring, Figure 1.37. This signal also showed a cross-peak correlation to δ 3.33, representing a doublet of doublets, indicating H2'. H2' exhibited a cross-peak correlation to H3' at δ 3.88-3.78, a multiplet that overlapped with H6b and H6b'. The signal at δ 3.50 (triplet) was assigned to H4' since it displayed a cross-peak correlation to H3' on COSY. Furthermore, H5’ was assigned to the signal at δ 3.77-3.74, a multiple that overlapped with H6a, Figure 1.37. The confirmation of H3' and H5' was supported by a cross-peak correlation to C4' at δ 71.68 in the ^{1}H-^{13}C HMBC, which indicated the

correct assignment, Figure 1.38. Full COSY assignment can be found in the Supplemental Information section on page 167 and on Table 1.11.

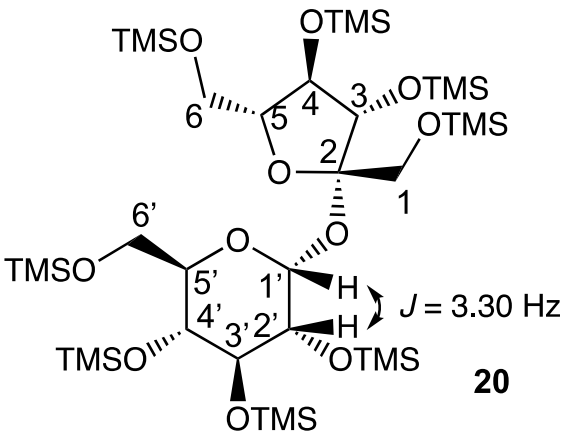

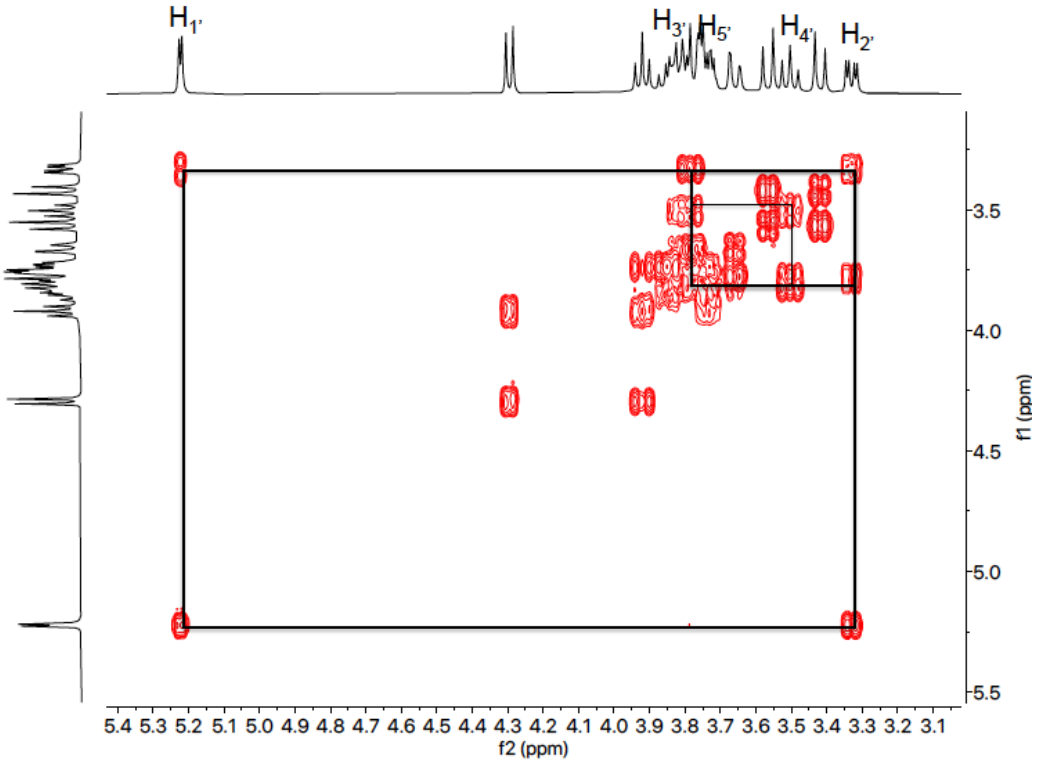

Figure 1.37: COSY spectrum of per-*O*-TMS sucrose (**20**) showed the cross-peak correlation between H1' to H2', from H2' to H3' and H3' to H4'.

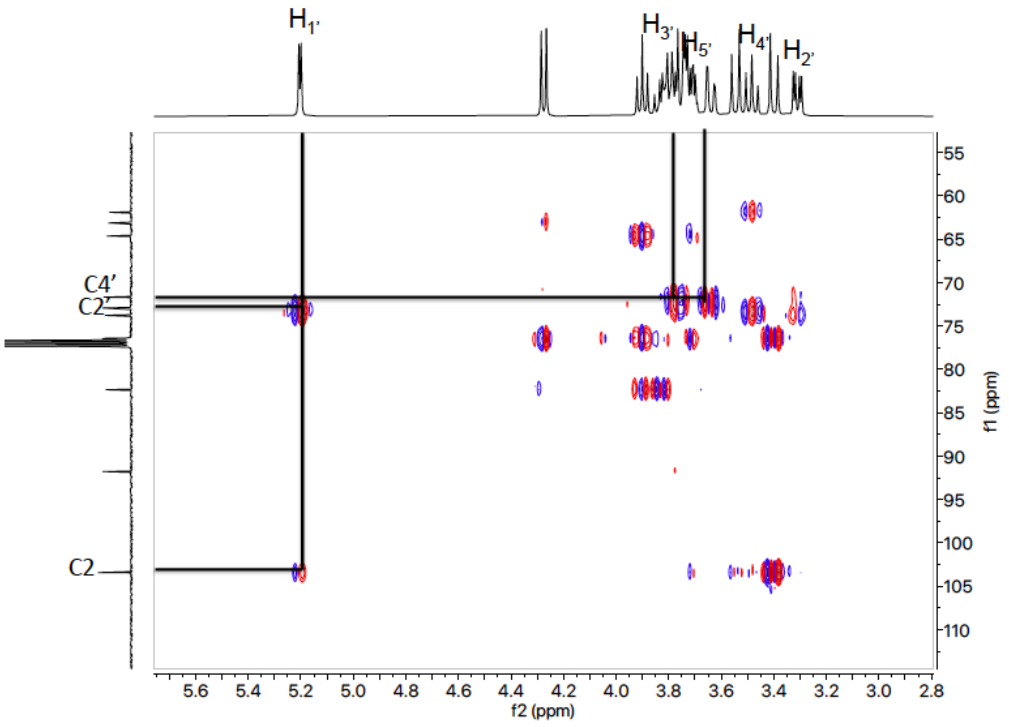

Figure 1.38: ^{1}H-^{13}C HMBC of per-*O*-TMS sucrose (**20**) showed the long-range coupling between H1' to C2 and C2' and H5' and H3' to C4', indicated the neighboring proton assignments are correct.

For the Fru*f* ring, the assignment began with the signal at δ 4.30, assigned to H3, a doublet with *J* = 7.90 Hz, which agreed with the *J* value of a cis-trans coupling constant. From the COSY spectrum, H3 exhibited a cross-peak correlation to H4 at δ 3.92, a triplet, Figure 1.39. The signal at δ 3.73 was assigned to H5, which was confirmed by COSY and ^{1}H-^{13}C HMBC, showing cross-peaks correlated to C4 (δ 76.42) and C6 (δ 64.63), respectively, Figure 1.40. H6a and H6b appeared as two separate signals at δ 3.88-3.78 (m) and δ 3.77-3.74 (m), both of which overlapped with other signals. The signals H1a and H1b were observed separately at δ 3.42 and δ 3.33, respectively, which were confirmed by using ^{1}H-^{13}C HMBC, which displayed a weak cross peak correlated to C2 (δ 103.4). In addition, H1ab also showed two cross peaks correlations to Si1, Figure 1.40. Full proton, COSY, and ^{1}H-^{13}C HMBC

assignments can be found at the Supplemental Information section on page 167 and 170 and on Table 1.11.

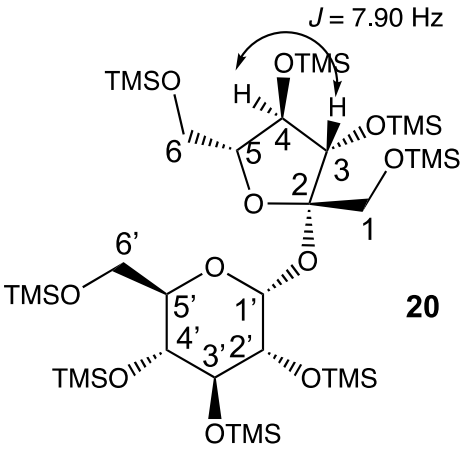

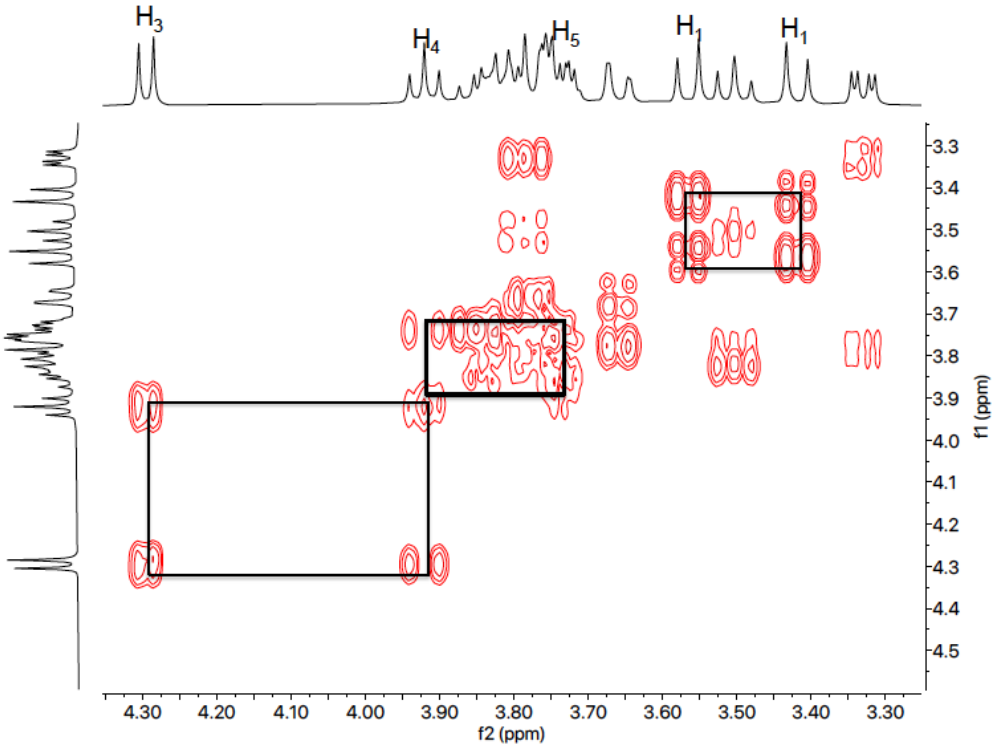

Figure 1.39: COSY spectrum of per-*O*-TMS sucrose (**20**) showed the cross-peak correlation between H3 to H4 and H4 to H5 and the correlation between two H1a and H1b.

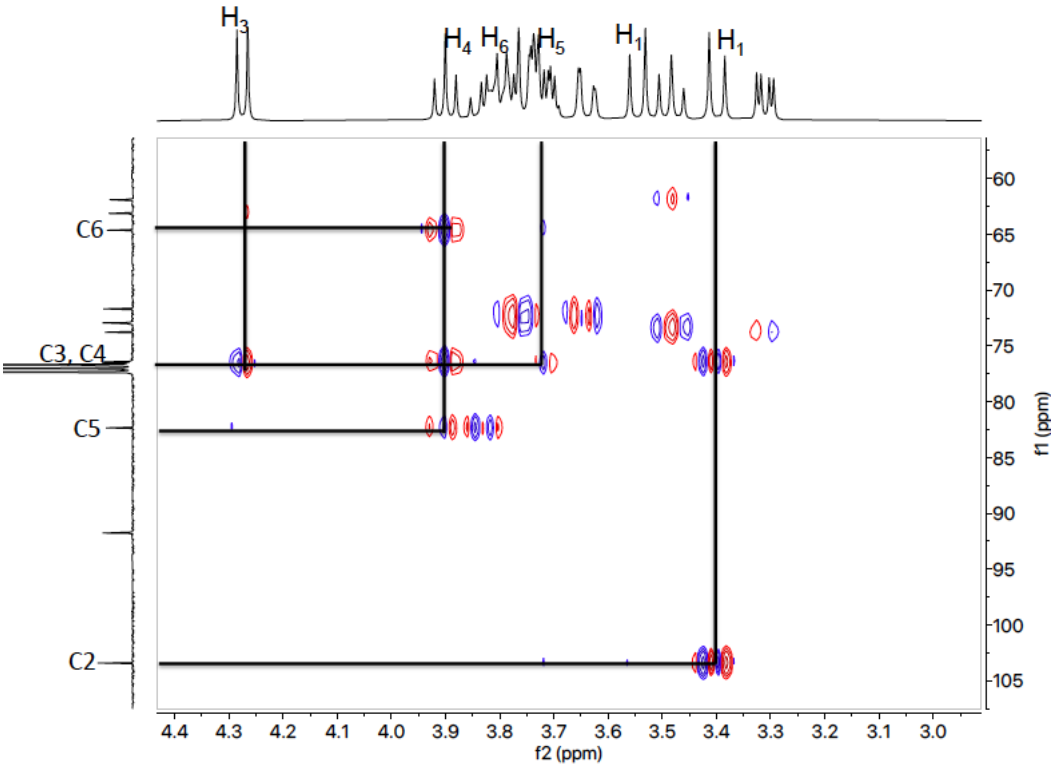

Figure 1.40: ^{1}H-^{13}C HMBC spectrum of per-*O*-TMS sucrose (**20**) showed the long-range coupling between H1a and H1b to C2 and C5 to H4 and H6. The spectrum showed long-range coupling between H4 and H5 to C3.

The assignment of CH_3 protons was performed after assigning the silicon signals. The signal at δ 0.19 was assigned to the CH_3 protons at Si4', while δ 0.17 was assigned to CH_3 protons at Si3. The signal at δ 0.16 (18H) was assigned to two CH_3 protons at Si4 and Si2'. Similarly, the signal at δ 0.15 was assigned to the CH_3 protons at Si3'. Furthermore, the signal at δ 0.14 (18H) was assigned to two CH_3 protons at Si6 and Si6'. The CH_3 protons at Si1 were assigned to the signal at δ 0.13. The completed assignment can be found in the Supplemental Information section on page 164.

The assignment of ^{29}Si nuclei was facilitated by the prior assignment of protons above. To assign the ^{29}Si NMR peaks, the ^{1}H-^{29}Si HMBC technique was

employed, taking advantage of the previously mentioned cross-peak correlations between protons and silicon. The ^{29}Si NMR signals at δ 18.7, 18.2, 18.1, and 17.9 were confidently assigned to Si4, Si1, Si3, and Si6, respectively, which showed in Figure 1.41. Likewise, the ^{29}Si NMR signals at δ 18.0, 17.7, 17.5, and 17.4 were attributed to Si4', Si3', Si2', and Si6', respectively as shown in Figure 1.42. Notably, it was observed that the Si signals originating from the Fru*f* rings appeared further downfield compared to those originating from the Glc*p* ring. This distinction in chemical shifts could be due to the structural differences and electronic environment surrounding the silicon atoms in the respective ring systems. Full assignment can be found in the Supplemental Information section on 165 and 168 on Table 1.11.

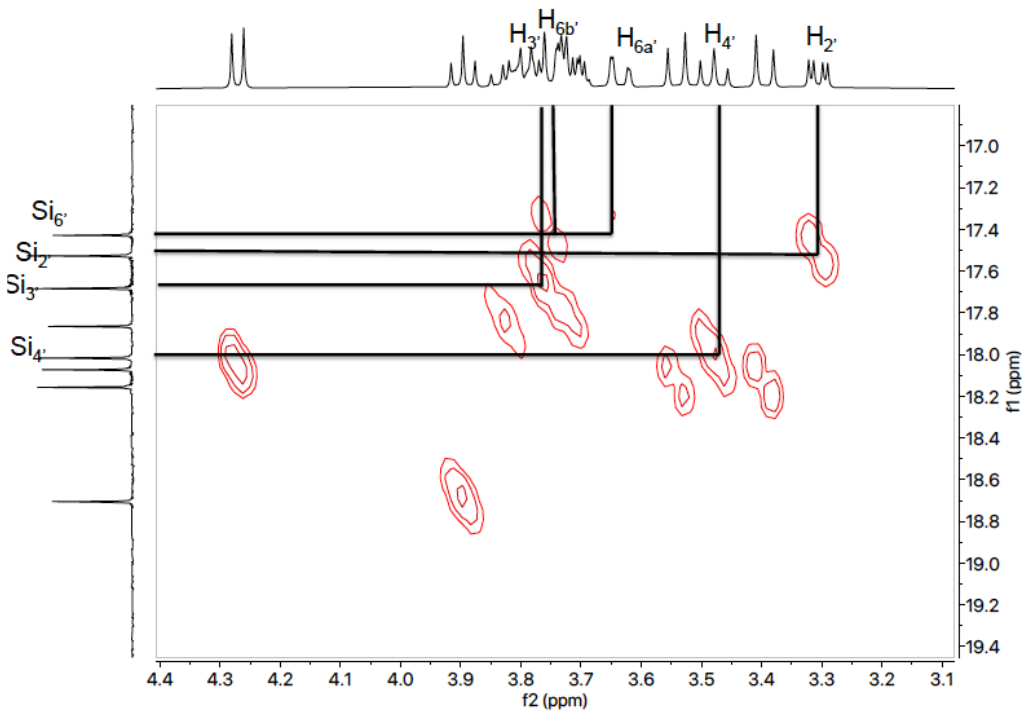

Figure 1.41: ^{1}H-^{29}Si HMBC spectrum of per-*O*-TMS sucrose (**20**) showed the cross-peak correlation from Si signal from Glc*p* ring.

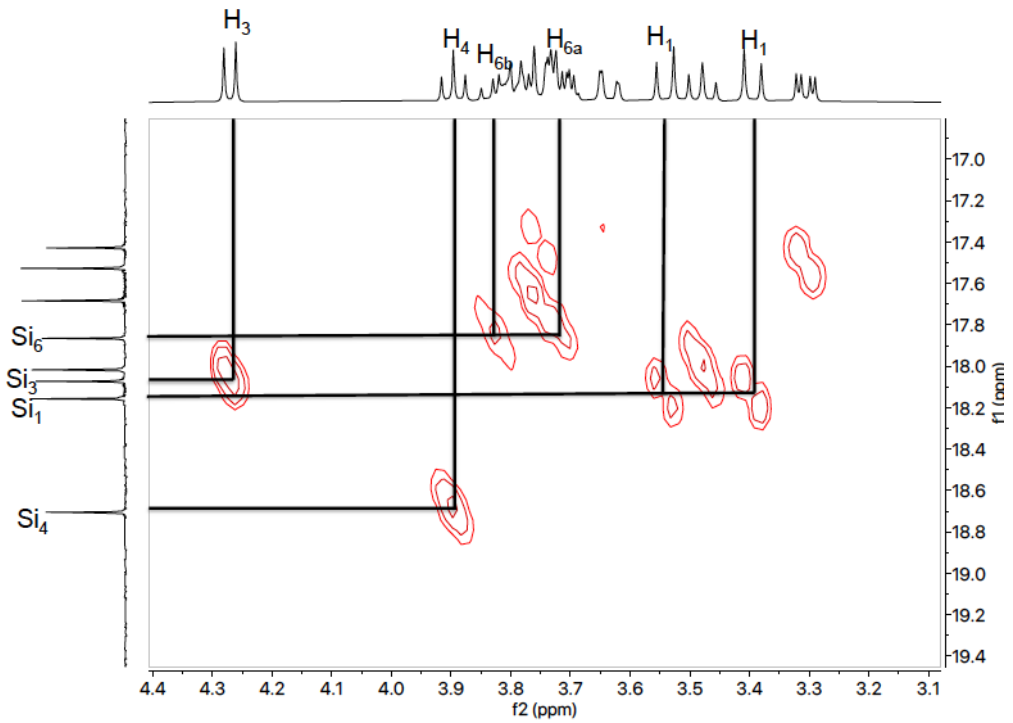

Figure 1.42: ^{1}H-^{29}Si HMBC spectrum of per-*O*-TMS sucrose (**20**) showed the cross-peak correlation from Si from Fru*f* rings.

Similar to the assignment of Si signals, the assignment of carbon signals was accomplished by utilizing the ^{1}H-^{13}C HSQC techniques and analyzing the cross-peak correlations. For specific details regarding the assigned carbon signals, please refer to the Supplementary Information (SI) section page 169. It is crucial to note that caution must be exercised when interpreting the peaks corresponding to C4 at δ 76.42 and C3 at δ 76.54, as they are situated in close proximity to the solvent peaks of $CDCl_3$. Similarly, C2' at δ 72.99 and C5' at δ 72.92 exhibit overlapping signals. The remaining peaks were assigned based on their respective cross-peaks with protons. The carbon from CH_3 groups cannot be assigned due to the overlapping cross peaks that cannot be separated and distinguished.

Table 1.11: The ^{1}H, ^{13}C, ^{29}Si NMR chemical shifts (δ) of 1,3,4,6,2',3',4',6-octa-*O*-TMS-sucrose (per-*O*-TMS sucrose) (**20**) in$CDCl_3$.

Atoms	δ ^{1}H	δ ^{13}C	δ ^{29}Si
1a	3.57	63.1	18.2
1b	3.42	--	--
2	--	103.4	--
3	4.30	76.5	18.1
4	3.92	76.4	18.7
5	3.73	82.3	--
6a	3.88-3.78	64.6	17.9
6b	3.77-3.74	--	--
1'	5.22	91.8	--
2'	3.33	73.0	17.5
3'	3.88-3.78	73.8	17.7
4'	3.50	71.7	18.0
5'	3.77-3.74	72.9	--
6a'	3.88-3.78	61.9	17.4
6b'	3.66	--	--
O-TMS_1	0.13	--	--
O-TMS_3	0.17	--	--
O-$TMS_{2',4}$	0.16<u>5</u>	--	--
O-$TMS_{6,6'}$	0.14	--	--
O-$TMS_{3'}$	0.15	--	--
O-$TMS_{4'}$	0.19	--	--

Note: The underline values distinguish between TMS3, TMS2' and TMS4

1.2.10. Assignment of 2,3,4,6,2',3',4',6'-Octa-*O*-TMS-Trehalose (per-*O*-TMS trehalose) (**21**)

The proton and carbon assignments were previously assigned by the Gervay-Hague's research group and the obtained proton and carbon spectra were consistent with the previous assignment.[22] In the case of per-*O*-silylated trehalose (**21**), only four ^{29}Si signals were observed. This can be attributed to the fact that trehalose possesses symmetrical rings, resulting in identical chemical shifts for both rings. In the proton spectrum, it is evident that H3 and H3' share the same chemical shift at δ 3.91. These protons exhibit a cross-peak correlation with the silicon signal at δ 18.37, which is assigned as Si3 and Si3'. The signals at δ 18.08, 18.01, and 17.52 were

assigned to Si2 and Si2', Si3 and Si3', Si4 and Si4', respectively which shown in Figure 1.43. Interestingly, the Si4 signal in trehalose appears as the most upfield, whereas in other polysaccharides, the Si4 signal is often observed as the most downfield. This discrepancy may arise from the electronic and structural differences surrounding Si4 in this symmetrical ring system. The full ^{1}H-^{29}Si HMBC and ^{29}Si assignment can be found at the Supplemental Information section on page 172 and 175 and Table 1.12

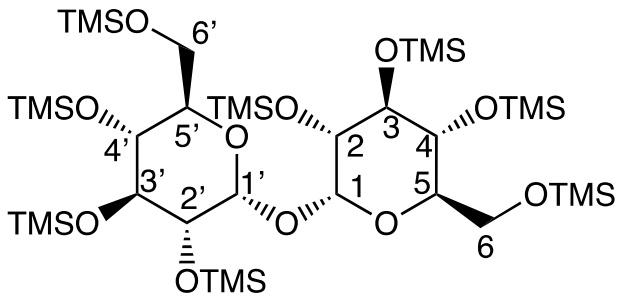

21

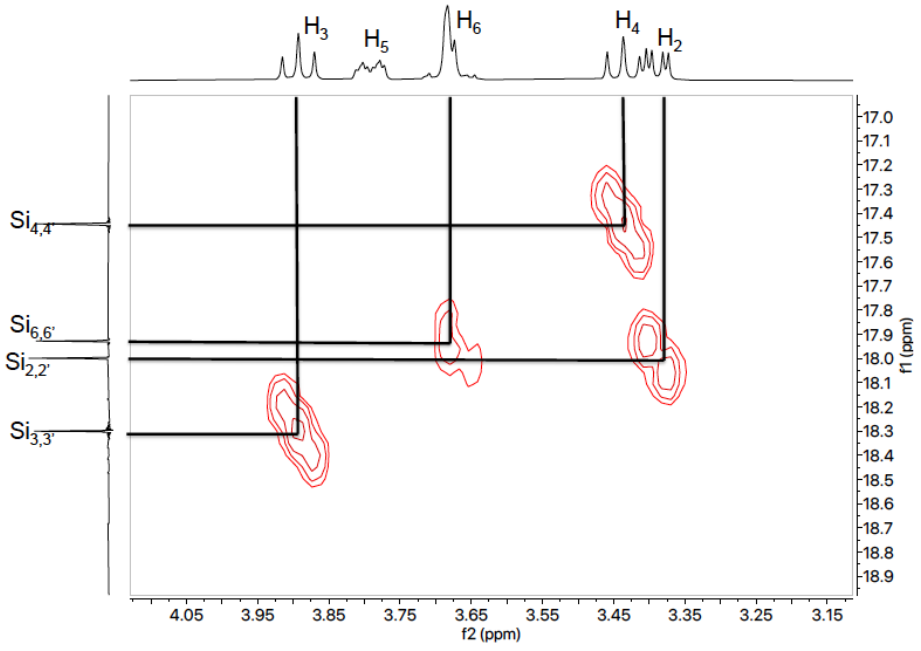

Figure 1.43: ^{1}H-^{29}Si HMBC spectrum of per-*O*-TMS trehalose (**21**) showed the cross-peak correlation of proton to silicon for assignment of the 4 signals, Si3, Si2, Si6 and Si4.

Table 1.12: The ^{1}H, ^{13}C, ^{29}Si NMR chemical shifts (δ) of 2,3,4,6,2',3',4',6'-octa-*O*-TMS-trehalose (per-*O*-TMS trehalose) (**21**) in$CDCl_3$.

Atoms	**δ ^{1}H**	**δ ^{13}C**	**δ^{29}Si**
1,1'	4.92	94.3	--
2,2'	3.39	72.9	18.1
3,3'	3.89	73.6	18.4
4,4'	3.45	71.8	17.5
5,5'	3.81-3.77	73.2	--
6,6'	3.72-3.64	62.2	18.0
O-$TMS_{3,3'}$	0.14	0.94	--
O-$TMS_{4,4'}$	0.14	1.07	--
O-$TMS_{2,2'}$	0.12	0.15	--
O-$TMS_{6,6'}$	0.10	-0.27	

Furthermore, using the ^{1}H-^{29}Si HMBC techniques, the $(CH_3)_3$ proton attached to Si and the corresponding carbon signals were successfully assigned. In total, there were four $(CH_3)_3$ groups. The signal at δ 0.17 (36H) was assigned to the protons of $(CH_3)_3$ groups attached to Si3, Si3' and Si4, Si4'. Likewise, the signals at δ 0.15 and 0.12 were assigned to the protons of $(CH_3)_3$ groups attached to Si2, Si2' and Si6, Si6', respectively, which can be shown in Figure 1.44. Similarly, the carbon of the $(CH_3)_3$ signals were assigned using ^{1}H-^{13}C HMBC from the CH_3 protons correlations. The peaks at δ 1.07, 0.94, 0.15, and -0.27 were assigned to the $(CH_3)_3$ carbon that are bonded to Si4, Si4', Si3', Si2, Si2', and Si6, Si6', respectively. The full spectra assignment can be found in the Supplemental Information section on page 171-177 and Table 1.12.

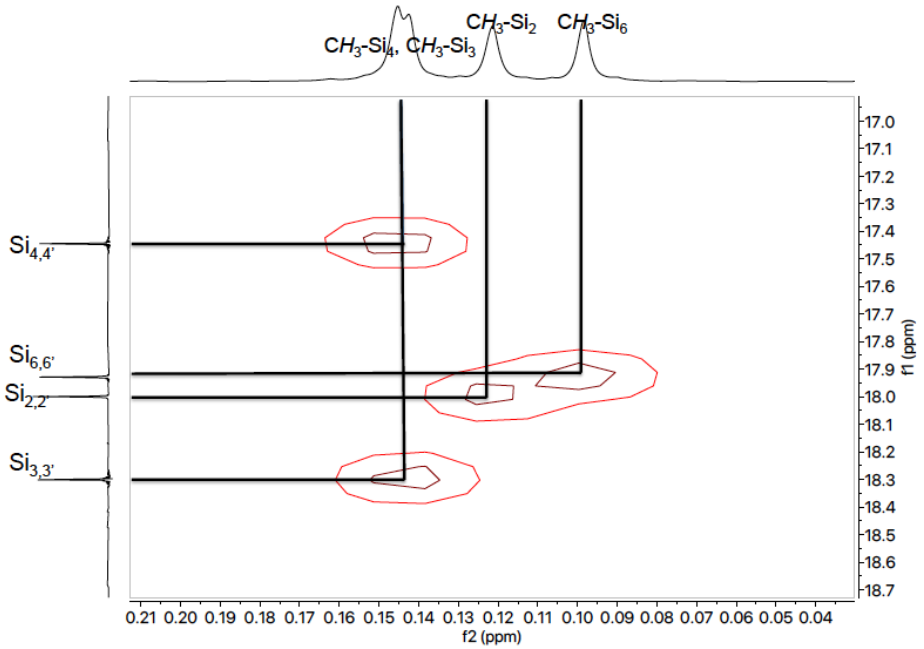

Figure 1.44: ^{1}H-^{29}Si HMBC spectrum of per-*O*-TMS trehalose (**21**) showed the cross-peak correlation of silicon to CH_3 proton for the assignment of the CH_3 signals.

1.2.11. Assignment of 1,3,4,6,3',4',6',2",3",4",6"-Unde-*O*-TMS-Kestose (per-*O*-TMS kestose) (**22**)

The assignment of per-*O*-TMS kestose (**22**) was greatly facilitated by comparing it with the assignments of per-*O*-TMS sucrose (**20**), β-per-*O*-TMS fructose (**16**), and the ^{1}H NMR analysis conducted by Dirk Streefkerk in acetone-d_6 in Table 1.13.[74] In addition to the comparison, successful assignment of the proton and carbon was achieved using homonuclear correlation, COSY, and ^{1}H-^{13}C HSQC, HMBC techniques. Furthermore, the ^{29}Si NMR peaks were successfully assigned using the ^{1}H-^{29}Si HMBC correlation by utilizing the fully assigned proton.

Using COSY and the previous assignment,[74] the signal at δ 5.22 was assigned to H-1", which in agreement with the coupling constant, *J*=3.43 and the relative location of H-1 from free per-*O*-silylated glucose (**14**) or in H-1' in the Glc*p*, per-*O*-silylated sucrose (**20**) also appears close to δ 5.00, Figure 1.45. The peak correlation

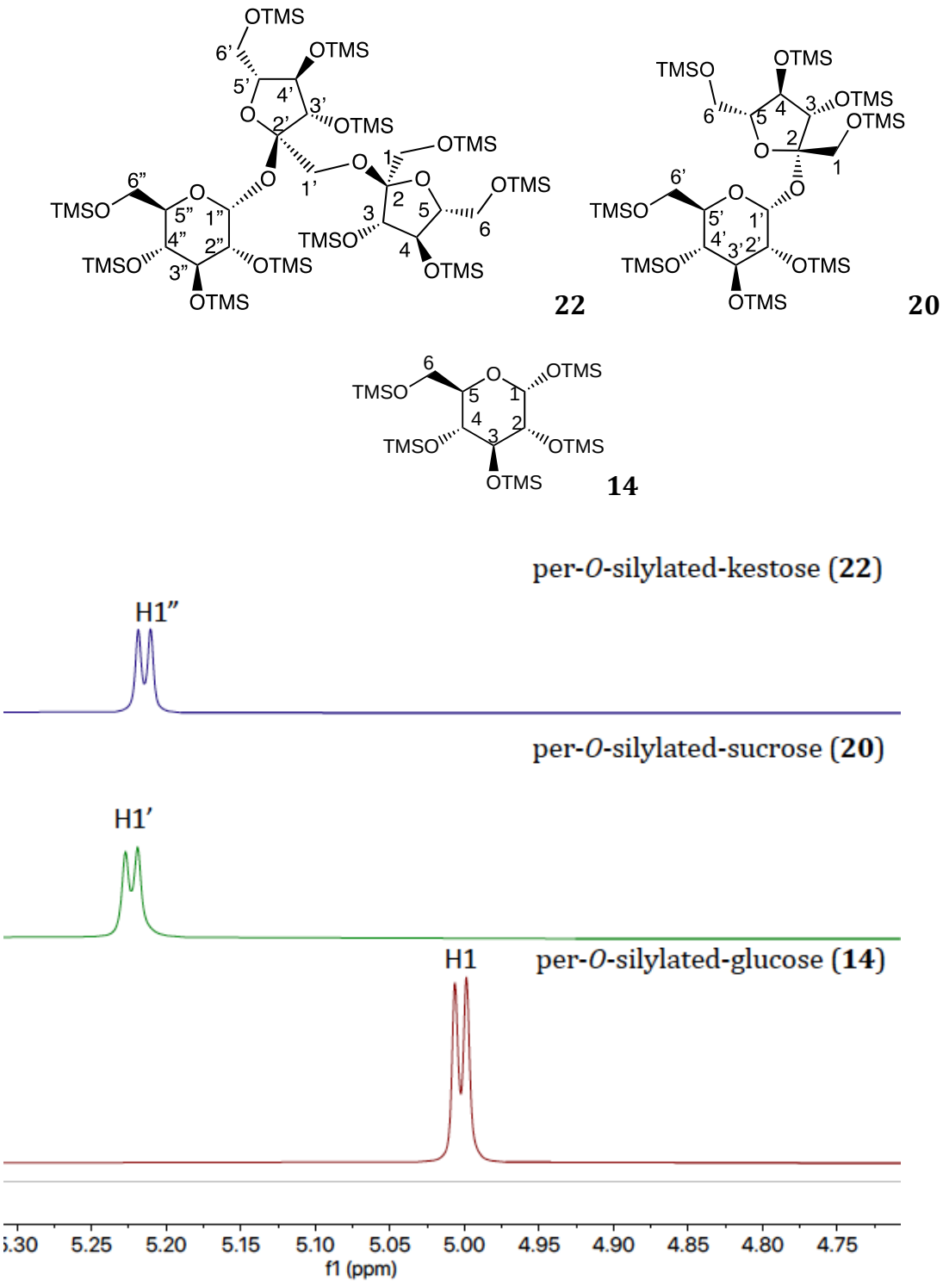

Figure 1.45: Overlap spectra of per-*O*-TMS kestose (**22**), per-*O*-TMS sucrose (**20**), and per-*O*-TMS glucose (**15**) showing the signal of H1”, H1’ and H1 from each silyl derivatives. The signals are from the equatorial H from the Glc*p* ring.

at 5.22 and 3.30 on COSY led to the assignment of H-2" at δ 3.32-3.27, a multiplet, an overlap with H1'. The cross-peak correlation between 3.32-3.27 and 3.81-3.77 led to the assignment of H3" at δ 3.81-3.77; this multiplet signal overlapped with other signals. Although the correlation of H3"- H4'" overlapped with other signals on COSY, it can be confirmed that the signal at δ 3.75-3.73, an apparent doublet of doublets, corresponds to H4". This confirmation is supported by TOCSY and is consistent with the previous assignment. Using the TOCSY spectrum, Figure 1.46, it was confirmed that H5", H3", and H6a" overlapped with H6' peaks from the Fru*f* rings, while H6b" (which has two different chemical shifts) also overlapped with other signals from the Fru*f* rings and agreed with the carbon assignment. The fully assigned COSY and TOCSY spectra assignment can be found in the Supplemental Information section on page 181, and 185.

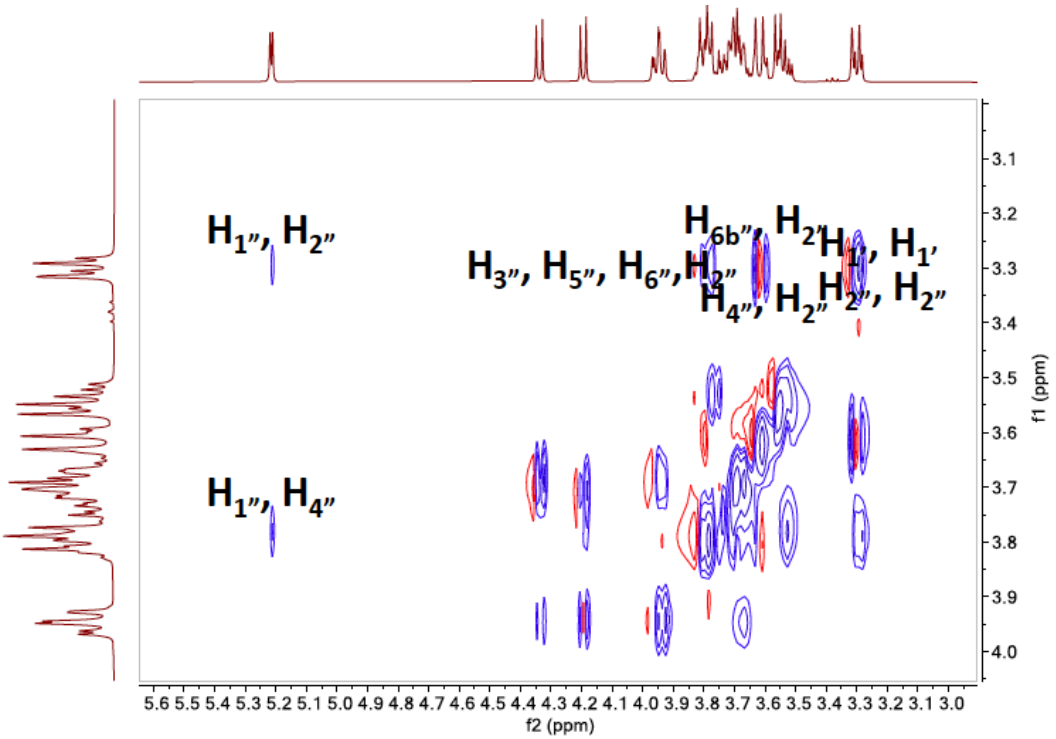

Figure 1.46: TOSCY spectrum of per-*O*-TMS kestose (**22**), showed cross peak correlation of H2" to H1", H3", H5", H6a, and 6b" or from H1" to H2", H4".

The signals at δ 4.34 and δ 4.19 were assigned to H3 and H3', respectively. The signal from H3 correlated to C-3, and H3' correlated to C3'. This assignment further confirmed with ^{1}H-^{13}C HMBC, where H3' showed cross peak correlation to C2', Figure 1.47 and identify of C2' using cross peak correlation between H1" and C2', Figure 1.48. Additional methods were used to help the assignment included using spectral overlap between per-*O*-silylated sucrose (**20**) and per-*O*-silylate-kestose (**23**) to help identify similar regions of proton and carbon signals. This is because sucrose has 1 Glc*p* and 1 Fru*f* ring and kestose has 1 Glc*p* and 2 Fru*f* rings.

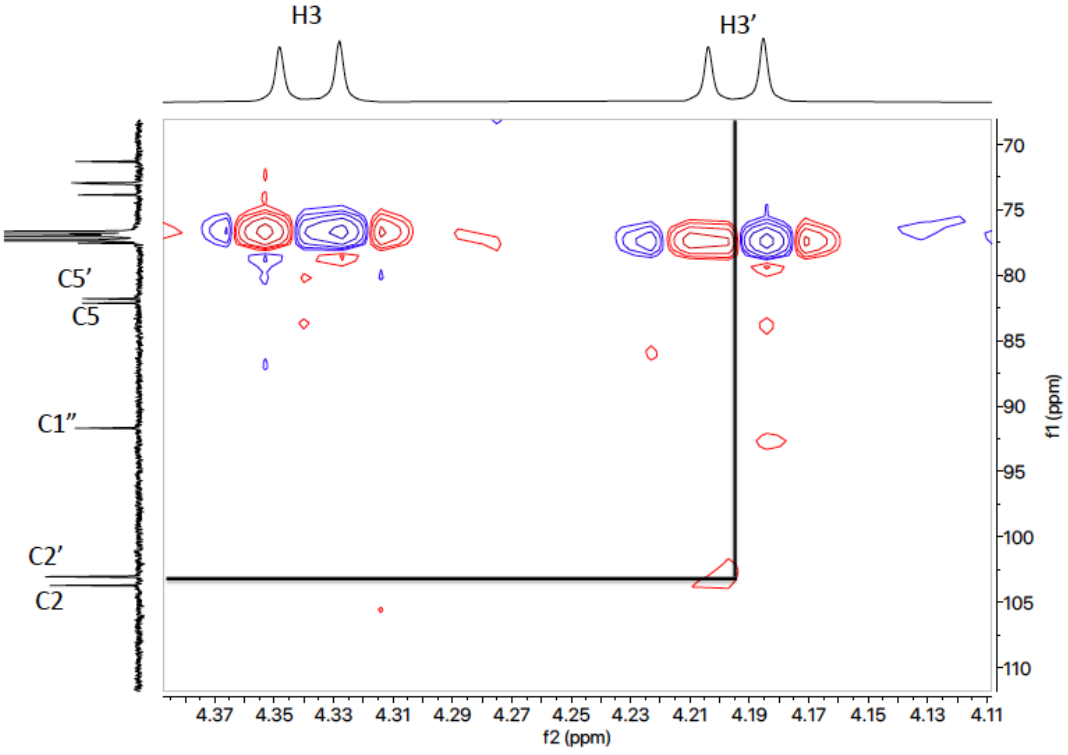

Figure 1.47: ^{1}H-^{13}C HMBC spectrum of per-*O*-TMS kestose (**22**): showed the cross-peak correlation from H3' to C2', which distinguish between H3 and H3'.

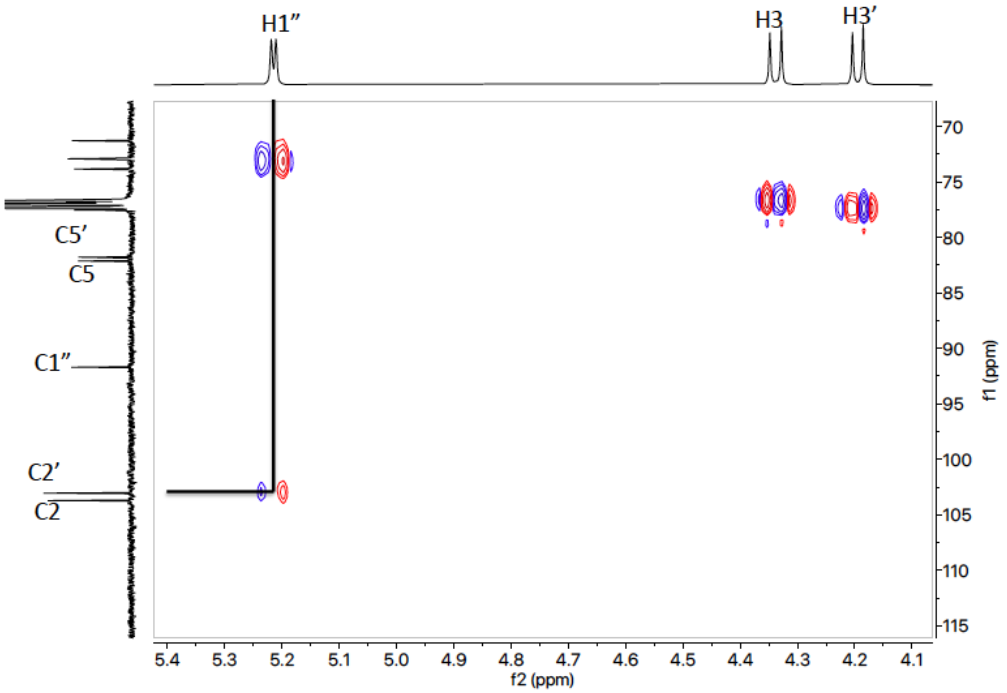

Figure 1.48: ^{1}H-^{13}C HMBC spectrum of per-*O*-TMS kestose (**22**): showed the cross-peak correlation from H1” to C2’, which helped distinguish C2 and C2’.

The comparison of proton and carbon between per-*O*-silylated kestose and per-*O*-silylated sucrose aided in distinguishing between H3' and H3. It is important to note that the chemical shift of the carbons in Glc*p* and Fru*f*(1) from per-*O*-TMS kestose (**22**) did not change significantly compared to per-*O*-TMS sucrose (**20**) (Table 1.13), unlike the silicon chemical shift. Through the use of COSY, HSQC, HMBC, and TOCSY, it was confirmed that the peak at δ 3.97-3.93 (td) was assigned to H4' and H4. Although the signals from H5’ and H5 overlapped with other signals, their identification at δ 3.70 and δ 3.69 was possible using COSY, HSQC, HMBC, and TOCSY. A similar procedure was employed to assign H6 and H6'. The full assignment can be found in the Supplement Information section from page 178-185.

Table 1.13: Comparison of chemical shift of δ ^{1}H, δ ^{29}Si, and δ ^{13}C between per-*O*-TMS ketose and per-*O*-TMS sucrose. The Δ of δ ^{1}H, and δ ^{13}C between two compounds are small, however the Δ for δ ^{29}Si is large.

	22*	**22**	**20**	**22**	**20**	**22**	**20**
Atom	δ ^{1}H*	δ ^{1}H	δ ^{1}H	δ ^{13}C	δ ^{13}C	δ ^{29}Si	δ ^{29}Si
1a, 1b	x	3.58-3.51	3.57, 3.42	62.14	63.12	18.70	18.20
2	x	X		103.72		X	
3	4.0-4.4	4.34		76.95		18.10	
4	4.0-4.4	3.95		77.54		18.80	
5	x	3.72-3.65		82.13		X	
6a	3.7-3.9	3.74		64.48		17.40	
6b		3.72-3.65					
1a’	X	3.64-3.59		61.05		X	
1b’	X	3.32-3.27				X	
2’	X	X	X	103.05	103.42	X	X
3’	4.0-4.4	4.19	4.30	76.90	76.54	18.44	18.1
4’	4.0-4.4	3.95	3.92	76.82	76.42	17.86	18.70
5’	X	3.72-3.65	3.73	81.79	82.34	X	X
6’a	3.7-3.9	3.81-3.77	3.88-3.78	63.98	64.63	17.59	17.9
6b’		3.72-3.65	3.77-3.74				
1”	5.33	5.21 (d)		91.70	91.77	X	
2”	3.36	3.32-3.27	3.33	72.99	72.99	17.52	17.50
3”	3.7-3.9	3.81-3.77	3.88-3.78	73.85	73.77	17.58	17.70
4”	3.59	3.58-3.51	3.50	71.39	71.68	17.81	18.00
5”	3.7-3.9	3.81-3.77	3.77-3.74	72.92	72.92	X	X
6”a,	3.7-3.9	3.81-3.77	3.88-3.78	61.67	61.89	17.17	17.4
6b”		3.64-3.59	3.66				
O-TMS$_{2”}$		0.16	--				
O-TMS$_{4’}$		0.16	0.19				
O-TMS$_{3’}$		0.15	0.15				
O-TMS$_{3}$		0.14	0.17				
O-TMS$_{4}$		0.14	0.16<u>5</u>				
O-TMS$_{2’}$		--	0.16<u>5</u>				
O-TMS$_{3”}$		0.13					
O-TMS$_{4”}$		0.13					
O-TMS$_{6”}$		0.11					
O-TMS$_{6’}$		0.11	0.14				
O-TMS$_{6}$		0.10	0.14				
O-TMS$_{1}$		0.10	0.13				

* Solvent is actone-d$_6$

Note: The underline values distinguish between TMS3, TMS2’ and TMS4 in per-*O*-silylated sucrose (**20**)

What is unique about H6' and H6 is that the chemical shift of their methylene hydrogen signals is separated. However, through the use of TOCSY, ^{1}H-^{13}C HMBC, and HSQC, both chemical shifts of H6a', H6b' and the signals for H6a, H6b could be identified. Distinguishing between H1 and H1' posed a challenge, but the ^{1}H-^{29}Si HMBC spectrum aided in differentiating the two signals. It is evident that H1' should not exhibit any ^{29}Si NMR signals correlation, which aligns with the absence of ^{29}Si NMR signals at δ 3.61-3.59 and δ 3.32-3.29 (two different signals) corresponding to H1'. Meanwhile, the signal at δ 3.57-3.55, which was assigned as H1ab, displayed a ^{29}Si NMR signal correlation at δ 18.7 ppm, Si1, Figure 1.49.

The assignment of the $(CH_3)_3$ groups from the TMS (trimethylsilyl) groups was performed after assigning all silicon signals. By correlating the ^{29}Si NMR signals to the $(CH_3)_3$ groups using the ^{1}H-^{29}Si HMBC experiment, the following chemical shifts were assigned as the signal at δ 0.16 (18H) was assigned to the $(CH_3)_3$ protons bonded to Si2" and Si4'; the signal at δ 0.15 was assigned to the $(CH_3)_3$ protons bonded to Si3. Meanwhile, the peak at δ 0.14 (18H) was assigned to $(CH_3)_3$ protons bonded to Si4, Si3'. The $(CH_3)_3$ protons bonded to Si3" and Si4" were assigned at δ 0.13. The $(CH_3)_3$ protons bonded to Si6"and Si6 were assigned to the signal at δ 0.11. The signal at δ 0.10 (18H) was assigned to the $(CH_3)_3$ protons bonded Si1 and Si6'. The full assignment can be found in the Supplemental Information section on page 178 and 182.

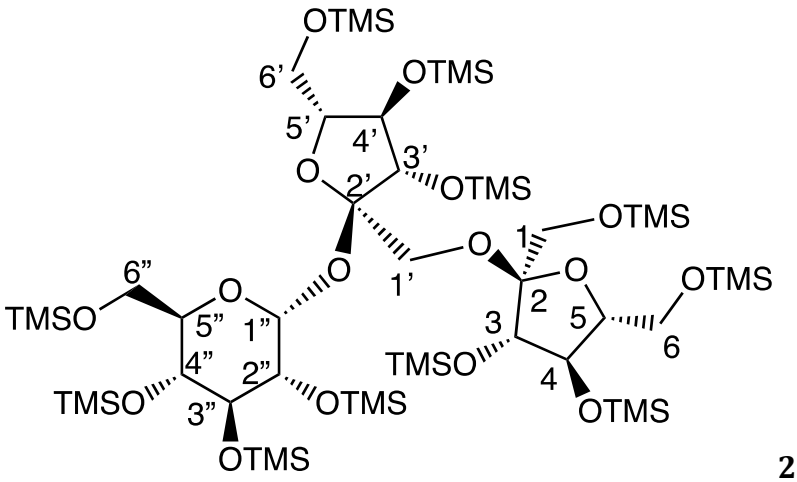

22

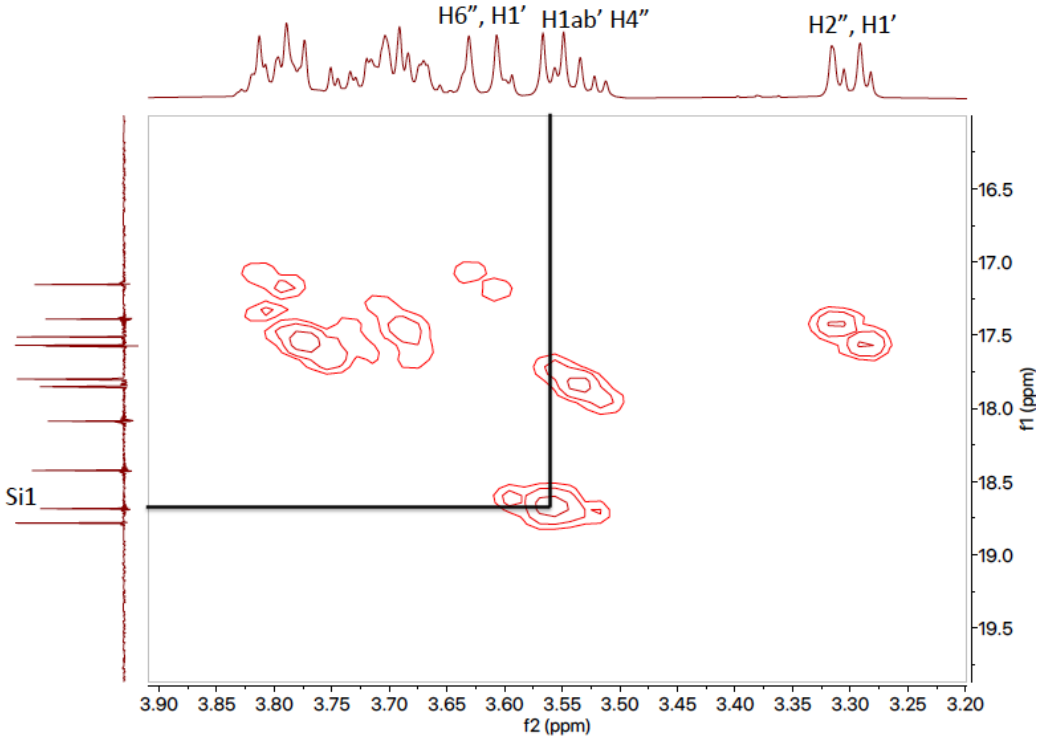

Figure 1.49: Per-*O*-TMS kestose (**22**): ^{1}H-^{29}Si HMBC showed the cross-peak correlation between Si1 and H1ab.

The assignment of carbon was much easier after successfully analyzing and assigning the proton. As previously mentioned, the carbon spectrum and chemical shift did not change significantly when compared to per-*O*-silylated sucrose (**20**) and per-*O*-silylated-raffinose (**23**) Figure 1.50. The spectral consistencies were used to

help with some initial carbon assignment, which were confirmed using proton and ^{1}H-^{13}C HMBC of per-*O*-silylated kestose (**22**). The cross peaks of the HSQC spectrum, C2 and C2' showed no cross-peak correlation to the H, which made the assignment unambiguous. The assignment was further confirmed by the ^{1}H-^{13}C HMBC. The full assignment of HSQC can be found in the Supplemental Information section from page 183-184.

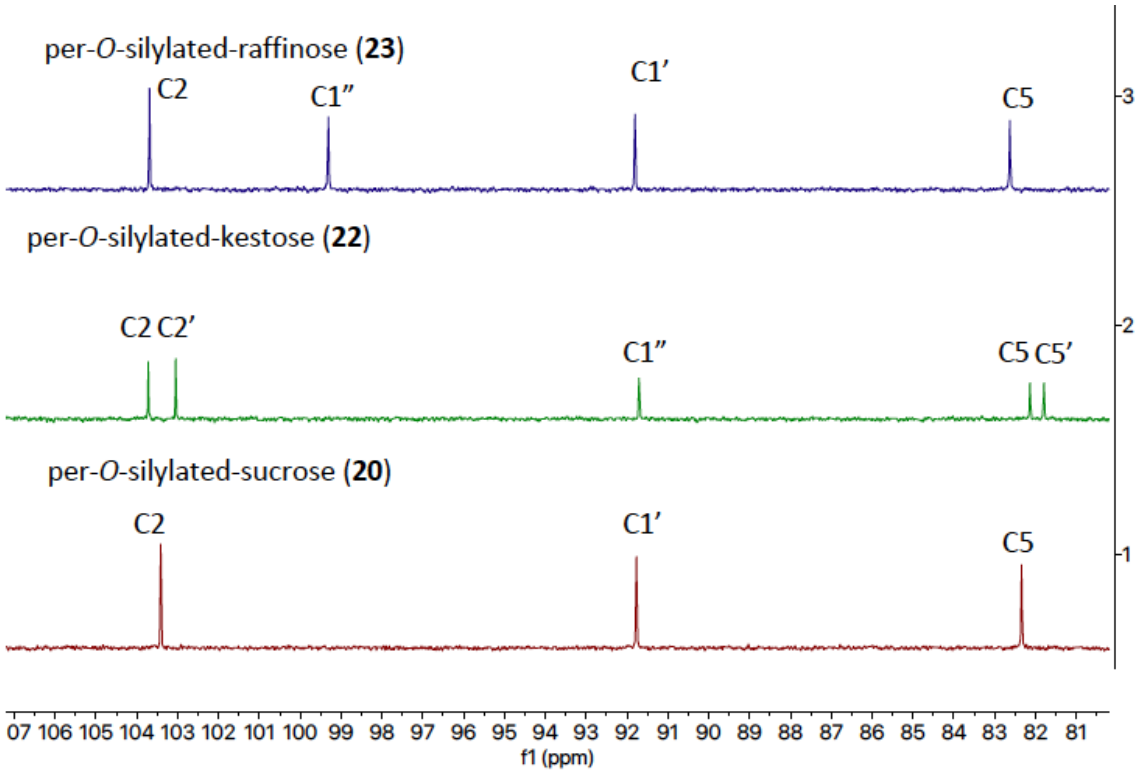

Figure 1.50: Overlap of carbon spectra between per-*O*-TMS raffinose (**23**), per-*O*-TMS kestose (**22**), and per-*O*-TMS sucrose (**20**), illustrates similar chemical shift of the carbon signals.

The assignment of the ^{29}Si NMR peaks was also facilitated by the successful assignment of the proton. The ^{1}H-^{29}Si HMBC technique was utilized to establish three-bond correlations between ^{1}H and ^{29}Si, aiding in the assignment of the ^{29}Si NMR peaks. Most of the observed cross-peaks were direct cross peak correlations

with the proton and did not overlap with other cross-peaks, except for Si6', Si6, and Si3". The ^{29}Si NMR signals at δ 18.80 and δ 17.86 were assigned to Si4 and Si4', respectively, due to their cross-peaks with H4 at δ 3.97-3.93. The differentiation between Si4 and Si4' can be attributed to the steric effect and shielding from neighboring groups. ^{29}Si NMR signals surrounded by *O*-TMS groups tend to exhibit more upfield shifts compared to ^{29}Si NMR signals with fewer neighboring *O*-TMS groups. The steric effect of *O*-TMS causes ^{29}Si NMR to shift upfield, which agrees with the shielding effect.[57] The signals at δ 18.70, 18.44, 18.10, 17.81, 17.52, and 17.17 were assigned to Si1, Si3, Si3', Si4", Si2", and Si6," respectively, as their cross-peaks are directly correlated with the corresponding protons. The signal at δ 17.59 was assigned to Si6', which exhibited a weak cross peak and low intensity with H6ab. Similarly, the signal at δ 18.44 displayed a weaker cross peak with H3' and partially overlapped with the cross peak of Si6'-H6ab'. The signal at δ 17.40 was assigned to Si6, which had a weak cross peak correlation to H6ab. The peak assignment can be found in Table 1.13 above or ^{1}H-^{29}Si HMBC spectrum in the Supplemental Information Section on page 182.

1.2.12. Assignment of 1,3,4,6,2',3',4',2",3",4",6"-Unde-*O*-TMS Raffinose (per-*O*-TMS raffinose) (**23**)

The compound, per-*O*-silylated-raffinose (**23**), is a trisaccharide, consisting of fructose (1), glucose (1'), and galactose (1'') rings. The spectral assignment of **23** was accomplished by employing spectral overlapping of the spectra of per-*O*-TMS sucrose (**20**) (in this study), methyl-per-*O*-TMS galactose from litarure,[60] per-*O*-TMS glucose (**14**) (in this study), and per-*O*-TMS fructose (**16**) (in this study). By

analyzing the chemical shifts of their carbon atoms, valuable insights were gained into the relative positions of these shifts in per-*O*-TMS raffinose (**23**). In addition, various techniques such as COSY, ^{1}H-^{29}Si HMBC, HSQC, ^{1}H-^{13}C HMBC, and TOCSY were employed to achieve a comprehensive assignment.

The assignment initiated with COSY and ^{1}H-^{13}C HMBC experiments starting from the most downfield proton. Since there are two anomeric protons in close proximity, ^{1}H-^{13}C HMBC was utilized to differentiate between the proton from ring 1' (glucose anomeric proton) and the proton from ring 1'' (galactose anomeric proton). According to the structural information, a correlation between H1'' and C6', as well as C2'', in the ^{1}H-^{13}C HMBC spectrum was anticipated (see Figure 1.51). Conversely, H1' only showed correlation with C2'. This allowed the assignment of H1' to 5.15 and H1'' to 5.10.

Using COSY, H2'' was assigned to the signal at δ 3.85-3.83, which overlapped with H5' and H3'', Figure 1.52. The assignment of these protons was further confirmed by ^{1}H-^{13}C HMBC and TOCSY, Figure 1.53. The signal at δ 3.89 was assigned to H4'', while H5'' and H6b'' appeared as a doublet at δ 3.65 (but overlapped). H6a'' appeared upfield at δ 3.57-3.49 (multiplet) and overlapped with H1b, Figure 1.52. This assignment was supported by COSY, Figure 1.52 and ^{1}H-^{13}C HMBC, where C4'' correlated with H5'' and H6''ab (at δ 3.62, with δ 71.98-C4'' and δ 3.49 with δ 71.98), see full assignment on Supplemental Information, page 186.

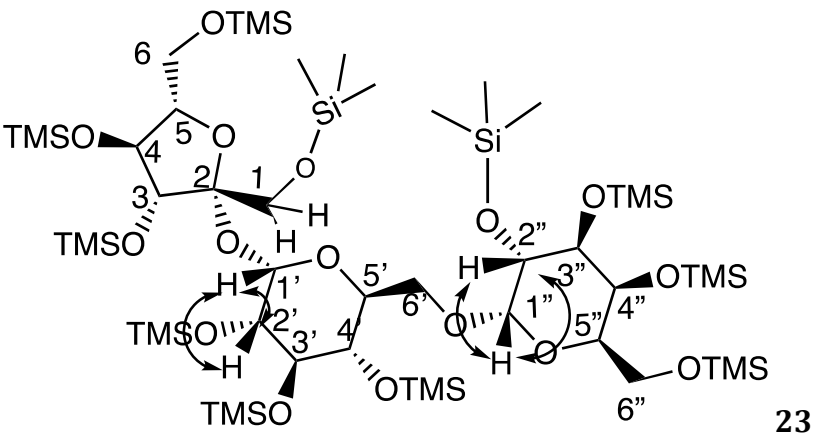

23

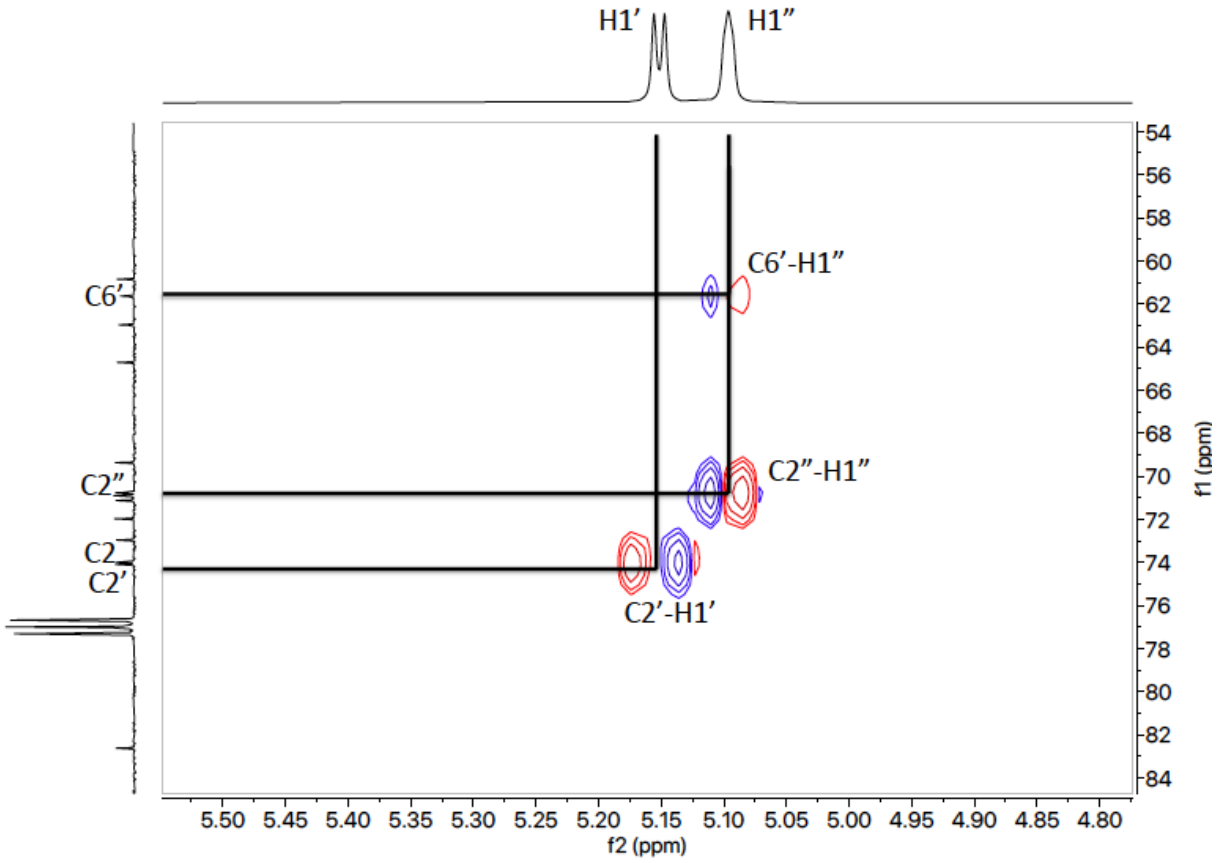

Figure 1.51*:* ^{1}H-^{13}C HMBC of per-*O*-TMS raffinose (**23**) showed the correlation of H1" to C6' and C2" to distinguish H1" and H1' from

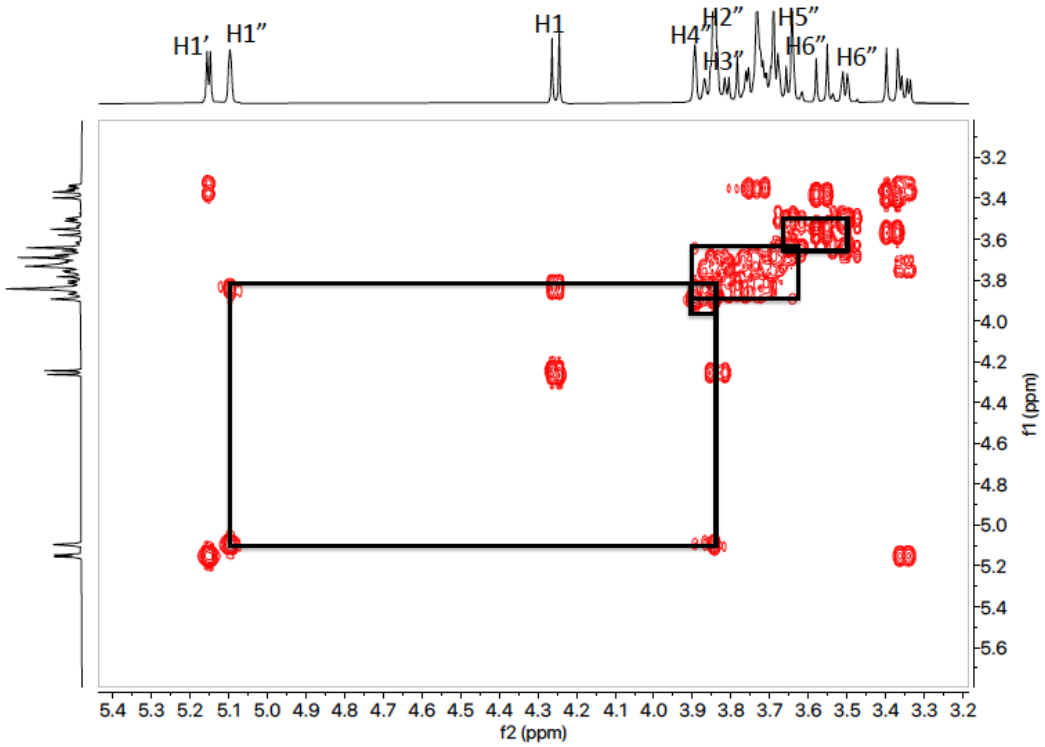

Figure 1.52: COSY of per-*O*-TMS raffinose (**23**): Glc*p* ring illustrated the cross-peak correlation between proton assignments of H1" to H2", H4" to H5" and H5" to H6".

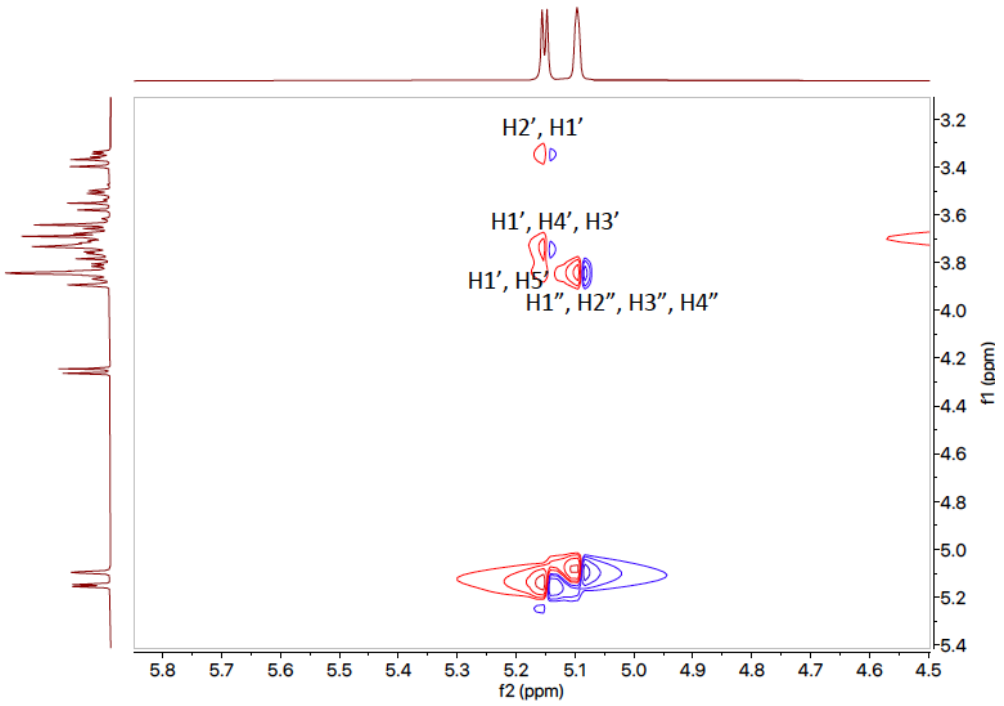

Figure 1.53: TOCSY of per-*O*-TMS raffinose (**23**) correlation of H1' to H2', H3', H4', & H5' and H1" to H2", H3" &H4".

Using COSY (Figure 1.54), H1’ showed cross peak correlation to H2' at δ 3.41-3.33, which overlapped with H1a. Starting from H2', it was confirmed that the peak at δ 3.77-3.67 corresponded to H4', while H3' and H6ab', appeared as a multiplet, overlapping with H5 shown in the COSY spectrum, can be found on page 189. This assignment was further supported by the TOCSY experiment shown in Figure 1.53, above, as well as the ^{1}H-^{13}C HMBC, where the region at δ 3.77-3.71 displayed correlations with C2' and C5' at δ 72.97 and δ 70.77, respectively. As previously mentioned, H5' overlapped with H3'' and H2'' at δ 3.85-3.83. This assignment was once again confirmed by the TOCSY spectrum depicted in Figure 1.53.

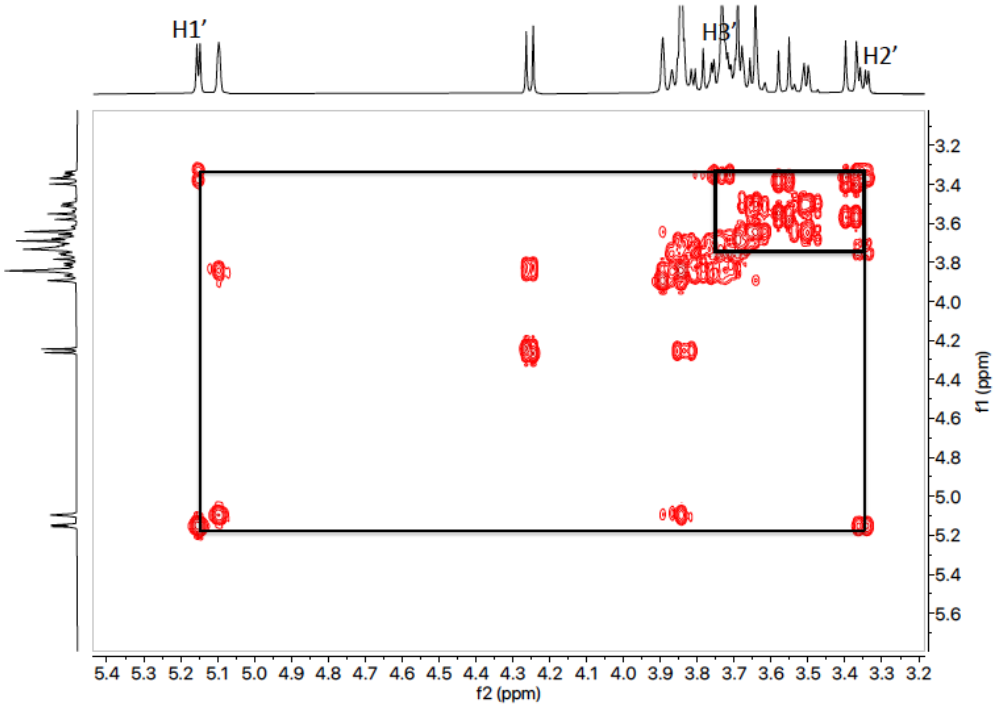

Figure 1.54: COSY of per-*O*-TMS raffinose (**23**) of Glc*p* ring: showed the cross peaks correlation of H1’ to H2’ and H2’ to H3’.

The assignment for the fructose ring began with H3. The chemical shift of H3 from the fructose ring in compound **20** and **22** also appeared at this relative position (Figure 1.55). From H3, it was identified H4 at δ 3.81, Figure 1.56 appeared as a

triplet, and H5 at δ 3.77-3.71, overlapping with H3', H4', and H6ab'. This assignment was confirmed by the expand TOCSY region shown in Figure 1.53 as well as the ^{1}H-^{13}C HMBC, page 192. In the TOCSY region shown in Figure 1.57, H3 had cross peaks

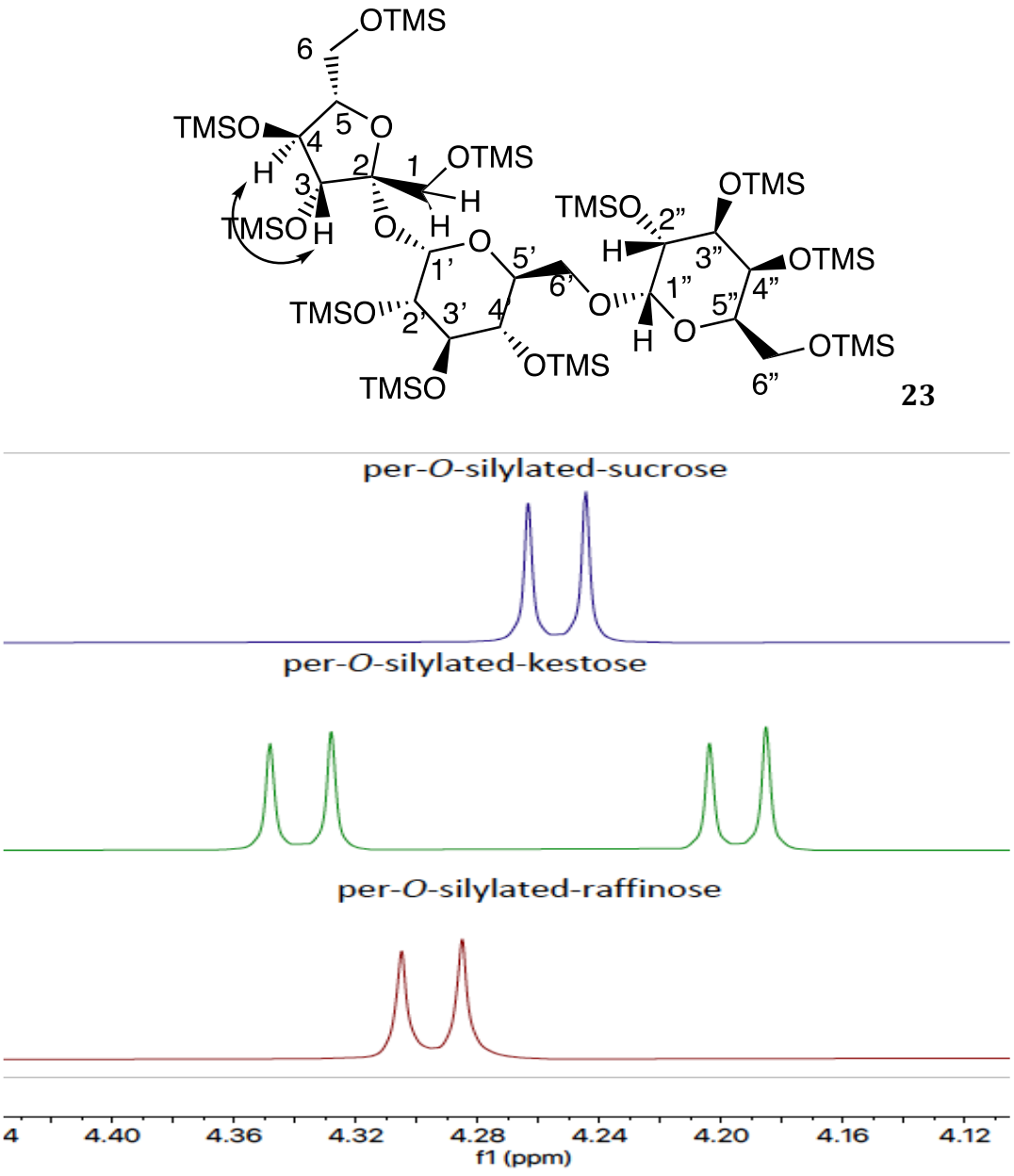

Figure 1.55: 1D 1H NMR spectrum of per-*O*-TMS sucrose (**20**), per-*O*-TMS raffinose (**23**) and per-*O*-TMS kestose (**22**), showed the H3 chemical shift of Fruf ring.

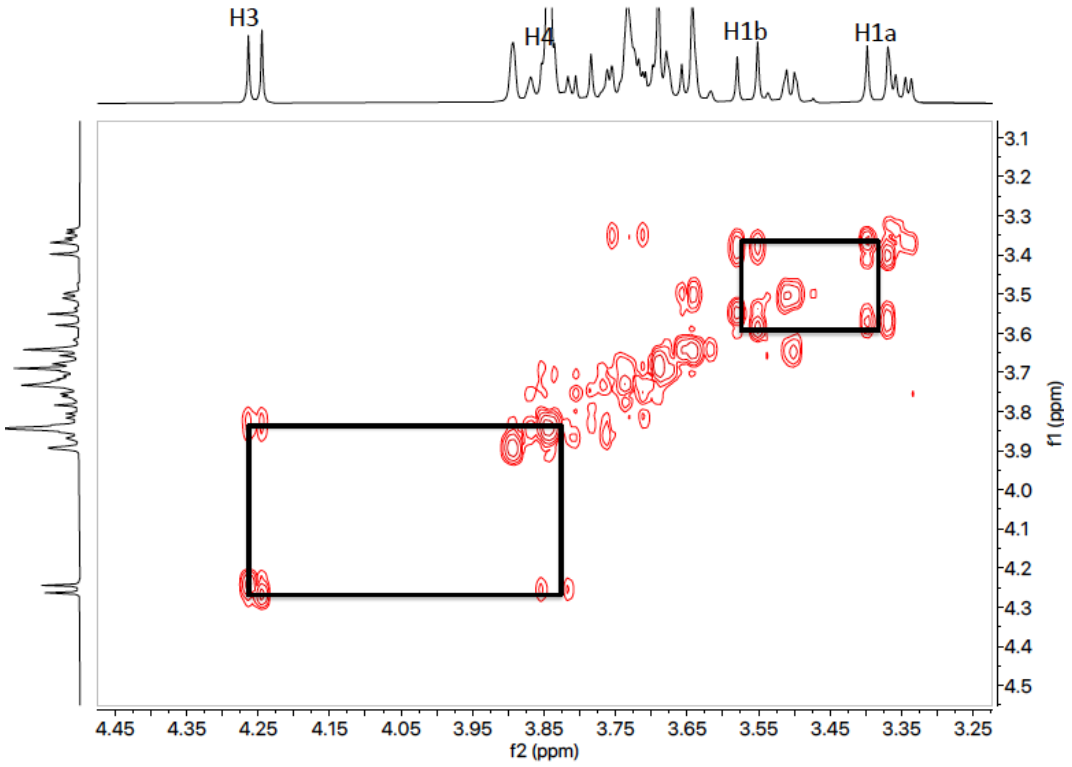

Figure 1.56: COSY of per-*O*-TMS raffinose (**23**) of Fru*f* ring: showed cross peak correlation of H3 to H4 and H1a and H1b.

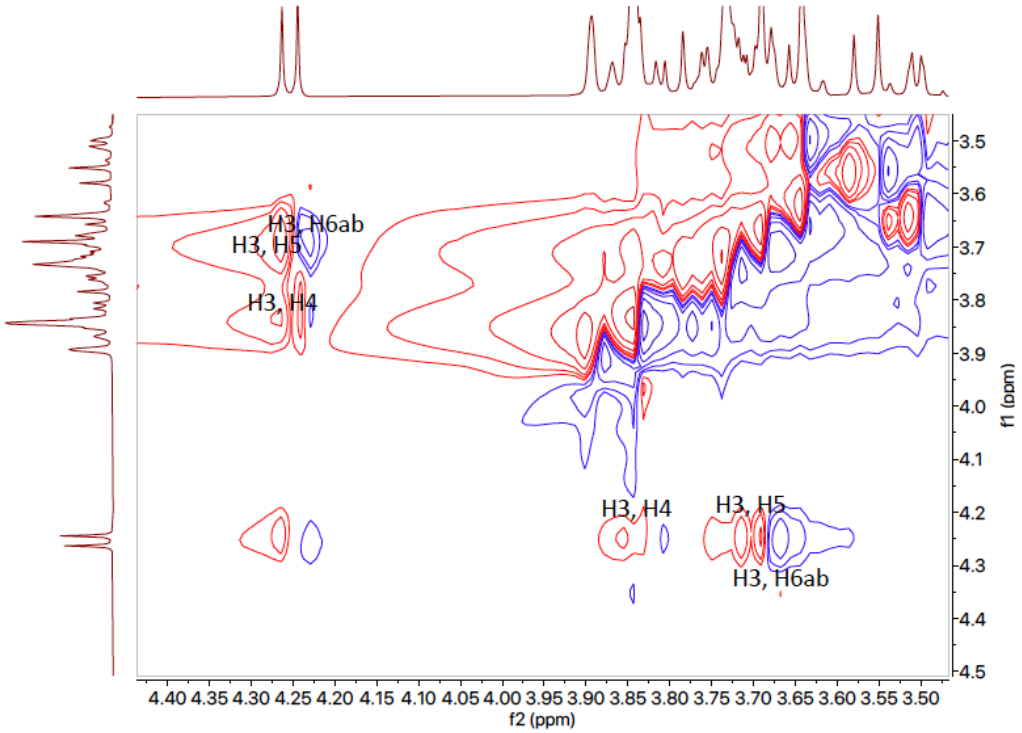

Figure 1.57: TOCSY of per-O-TMS raffinose (**23**) of Fru*f* ring: showed correlation of H3 to H4, H5, and H6ab.

with H4, H5, and H6ab. H6ab was assigned to the peak at δ 3.69, which was supported by the TOCSY data in Figure 1.57 and ^{1}H-^{13}C HMBC, as δ 3.69 correlated with C5 at δ 82.88 shown in the SI page 192. This correlation was observed in the ^{1}H-^{13}C HMBC, as well as the ^{1}H-^{29}Si HMBC (page 190), which only displayed one correlation peak of δ 18.3 to Si3. For the assignment of H1, it was split into two signals: H1a at δ 3.41-3.33, overlapping with H2', and H1ab at δ 3.57-3.49, overlapping with H6a''. These peaks were confirmed to be H1ab through ^{1}H-^{13}C HMBC, showing a correlation to C2 at δ 103.50. This assignment was further corroborated by the ^{1}H-^{29}Si HMBC, as depicted in

Figure 1.58 showed Si signal correlated to two protons (H1a, H1b) as illustrated below in the structure, which were not H6a,b". A complete assignment can be found in the Supplemental Section from page 186-193 and Table 1.13.

The assignment of the CH_3 protons was performed after assigning all silicon signals. By correlating the ^{29}Si NMR signals to the CH_3 groups using the ^{1}H-^{29}Si HMBC experiment. It was assigned as the following, the chemical shifts at δ 0.21 were assigned to $(CH_3)_3$ protons bonded to Si4'; δ 0.15 was assigned to two $(CH_3)_3$ protons bonded to Si3 and Si2''. Meanwhile, the signal at δ 0.14 (24H) was assigned to $(CH_3)_3$ protons bonded to Si4, Si4'', and Si2'. The $(CH_3)_3$ protons bonded to Si3' were assigned the peak at δ 0.13. The $(CH_3)_3$ protons bonded to Si2 were assigned to the signal at δ 0.12. The signal at δ 0.11 (18H) was assigned to the $(CH_3)_3$ protons bonded Si6 overlapping with Si6''. The signal at δ 0.10 was assigned to $(CH_3)_3$ proton bonded to Si1. The assignment can be found in Figure 1.59.

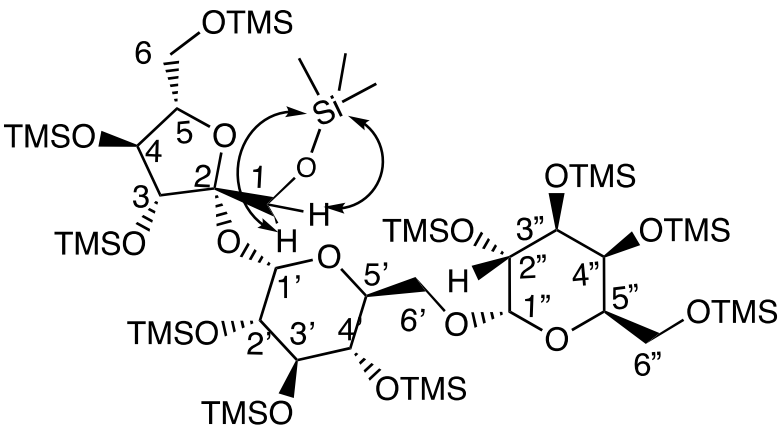

23

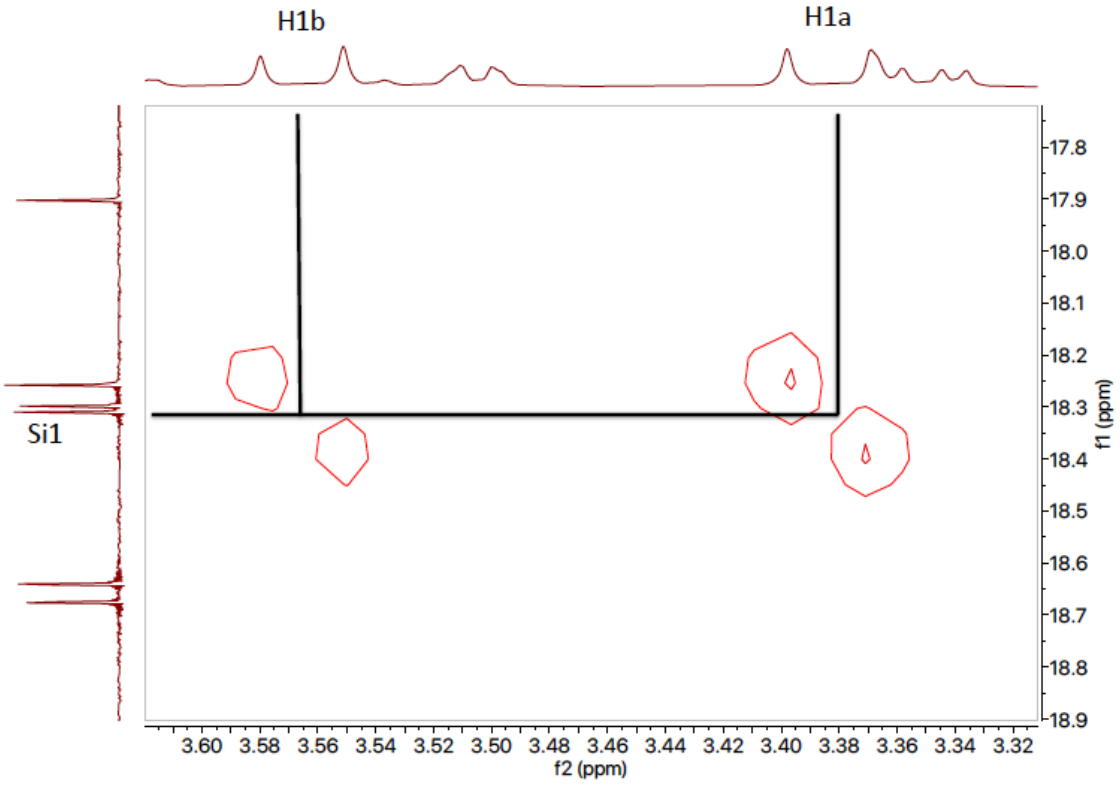

Figure 1.58: ^{1}H-^{29}Si HMBC of per-*O*-TMS raffinose (**23**) of Fru*f* ring-showed the cross peaks of H1a and H1b to one Si signal, Si1.

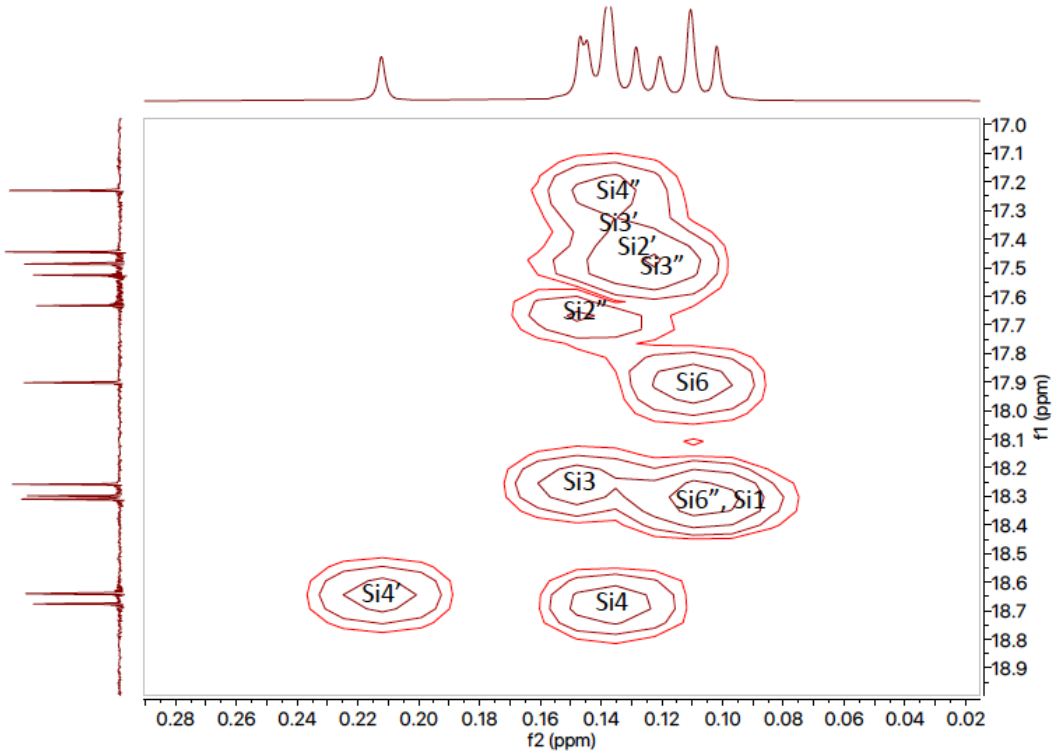

Figure 1.59: ^{1}H-^{29}Si HMBC of per-*O*-TMS raffinose (**23**) showed the cross peak of TMS-methyl groups correlated with Si signals.

The assignment of silicon and carbon is facilitated by the completed assignment of protons. Using the ^{1}H-^{29}Si HMBC experiment, Si4 and Si4' were assigned to the peak at δ 18.73 and δ 18.70, respectively, based on the cross peaks of H4 and H4' with the silicon signals. The assignment of Si6" and Si1, both having two protons, is also aided by their close proximity. However, the cross-peak intensity of Si6-H6ab is weaker compared to the cross peak of Si1 with H1ab. The stronger cross peak between Si1 and H1ab makes the correlation evident and facilitates the assignment of Si1 to H1ab. Meanwhile, the cross-peak involving Si signals interacting with two protons was assigned to Si6. The peak of Si1-H1ab leads to the assignment of δ 18.37 and δ 18.36 for Si and Si6", respectively. The signals at δ 18.32, δ 17.96, δ 17.69, δ 17.58, δ 17.54, δ 17.50, and δ 17.29 are assigned to Si3, Si6, Si2", Si3", Si2',

Si3', and Si4", respectively. The assignment can be found in the Supplemental Information section on page 1897(^{29}Si NMR spectrum) & 190 (^{1}H-^{29}Si HMBC) and Table 1.14.

The assignment of carbon was performed using ^{1}H-^{13}C HSQC experiment. The cross-peaks between carbon and proton were unambiguous. Interestingly, some chemical shifts from per-*O*-TMS raffinose (**23**) exhibited similar shift values to those of the corresponding carbon types in per-*O*-TMS kestose (**22**), per-*O*-TMS sucrose (**20**), or per-*O*-TMS fructose (**16**). Specifically, C2, C1', and C5 were all in close proximity to each other, as depicted in Figure 1.60. Although C4 and C3 overlapped with the $CDCl_3$ peak, their cross-peaks displayed stronger intensities, enabling us to determine which peak from $CDCl_3$ they overlapped with, as shown in Figure 1.61. The assignment of the other signals was based on their cross-peaks, indicating correlations of carbon to proton. The completed assignment of carbon can be found in the SI on page 188 (^{13}C NMR spectrum) and 191 (^{1}H-^{13}C HSQC).

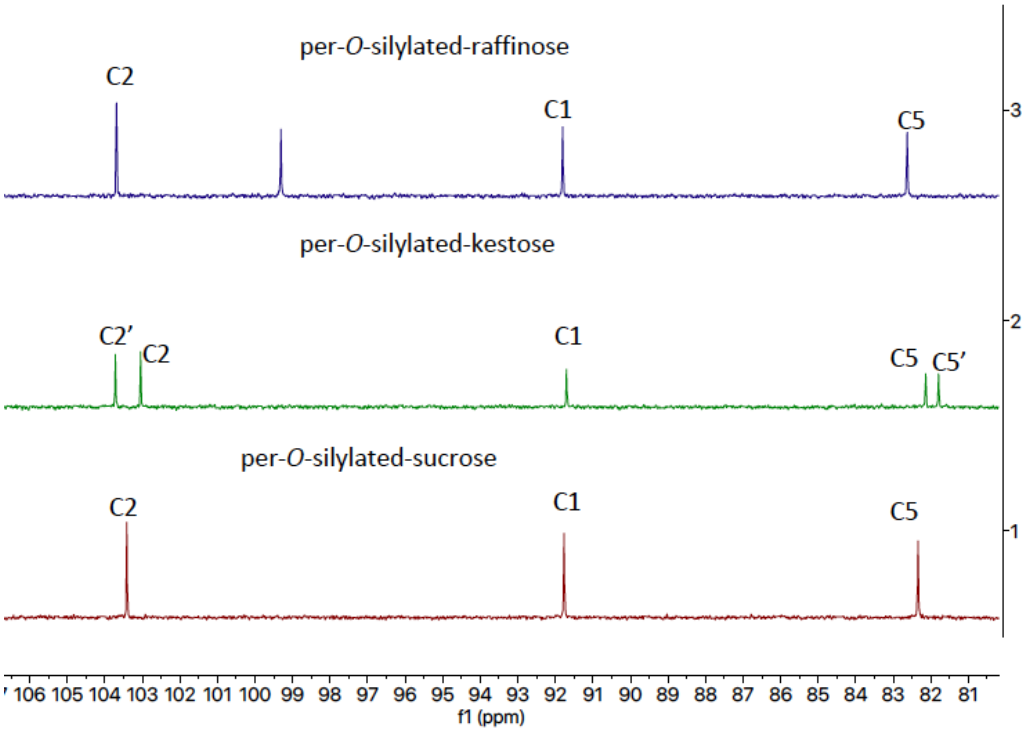

Figure 1.60: Overlapped of ^{13}C spectra of three per-*O*-TMS sugars (per-*O*-TMS raffinose (**23**), per-*O*-TMS kestose (**22**), and per-*O*-TMS sucrose (**20**) of Fruf rings and their corresponding chemical shifts of C2, C1', and C5 were shown.

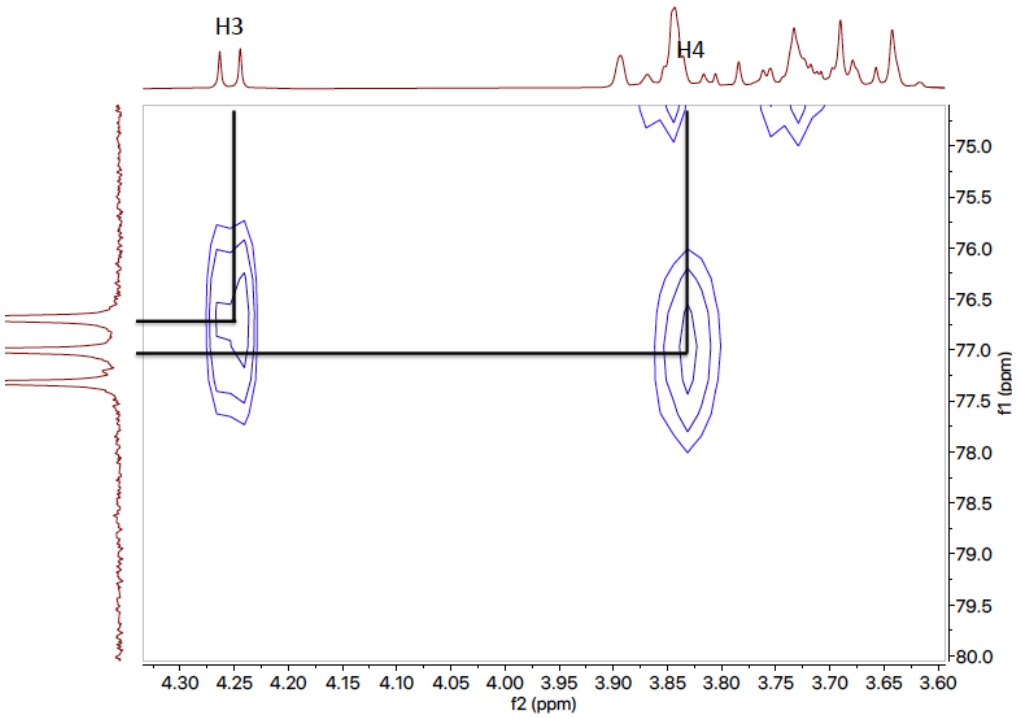

Figure 1.61: ^{1}H-^{13}C HSQC of per-*O*-TMS raffinose (**23**), showed the cross peaks correlation of H3 and H4 to their corresponding carbon atoms, C3 and C4 in $CDCl_3$.

Table 1.14: The ^{1}H, ^{13}C, ^{29}Si NMR chemical shifts (δ) of 1,3,4,6,2',3',4',2",3",4",6"-unde-O-TMS-raffinose (per-O-TMS raffinose) (**23**)

Atom	δ ^{1}H*	δ ^{13}C	δ ^{29}Si
1a*	3.41-3.33	62.98	18.3<u>7</u>
1b*	3.57-3.49	--	--
2	--	103.69	--
3	4.25	76.72	18.3<u>2</u>
4	3.81	77.21	18.7<u>3</u>
5*	3.77-3.71	82.63	--
6a	3.69	64.72	17.9<u>6</u>
6b	3.69		
1'	5.15	91.81	--
2'*	3.41-3.33	72.9<u>7</u>	17.5<u>4</u>
3'*	3.77-3.71	74.10	17.5<u>0</u>
4'*	3.77-3.71	71.13	18.7<u>0</u>
5'*	3.85-3.83	70.77	--
6'a*	3.77-3.71	61.64	--
6'b*	3.77-3.71		
1"	5.10	99.31	--
2"*	3.85-3.83	74.00	17.6<u>9</u>
3"*	3.85-3.83	70.90	17.5<u>8</u>
4"	3.89	71.98	17.2<u>9</u>
5"	3.65	69.37	--
6"a*	3.57-3.49	60.86	18.3<u>6</u>
6b"	3.65		
O-$TMS_{4'}$	0.21	--	--
O-$TMS_{3,2'}$	0.15	--	--
O-$TMS_{4,4",2"}$	0.14	--	--
O-$TMS_{3'}$	0.13	--	--
O-TMS_{2}	0.12	--	--
O-$TMS_{6,6"}$	0.11	--	--
O-TMS_{1}	0.10	--	--

*most case protons are overlapping,
<u>underline</u> indicate chemical shift values are too close for rounding

1.2.13. Assignment of 1,3,4,6,2',3',4',2",3",4",2'",3"',4"',6'"-Tetrade-*O*-TMS-Stachyose (per-*O*-TMS stachyose) (**24**)

Overlapping the carbon spectra from per-*O*-silylated kestose (**22**), per-*O*-silylated raffinoses, (**23**) and per-*O*-silylated stachyose (**24**) was used for the initial assignment of the peaks. As previously discussed for per-*O*-silylated kestose (**22**)

and per-*O*-silylated raffinoses (**23**), the carbon chemical shift of the two compounds did not change significantly. Using this method, it was concluded that the per-*O*-silylated stachyose (**24**) signal at δ 100.7 ppm was C2, followed by C1''' at δ 100.1 and C1'' at δ 99.7 ppm. The signal at δ 91.7 was assigned to C1', and C5 was assigned to the signal at δ 82.5 ppm. The comparisons of three 1D carbon spectra are shown in Figure 1.62 and the expanded ^{1}H-^{13}C HQSC spectrum shown in Figure 1.63 Utilizing the HSQC spectrum of per-*O*-silylated stachyose (**24**), the signal at δ 74.1 was assigned to C2', and C3' was assigned to δ 73.9 ppm. The signal at δ 92.9 was assigned to C2', and C2''' was assigned to the signal at δ 71.9. Meanwhile, C4' was assigned to the signal at δ 91.83 ppm. The signals for C3 and C4 overlapped with the solvent, $CDCl_3$ peaks, where C4 was assigned to δ 77.2 ppm and C3 was at δ 76.7 ppm. The primary carbon spectrum was also used for comparison to help make some initial assignments, and it confirmed ^{1}H-^{29}Si HMBC and ^{1}H-^{13}C HQSC. The signals at δ 64.9 and δ 64.6 were assigned to C6''' and C6, respectively. The signals at δ 63.0, 62.0, and 60.4 were assigned to C1, C6', and C6", respectively. The ^{1}H-^{13}C HQSC can be found in the Supplemental Information on 196, 198, and 199.

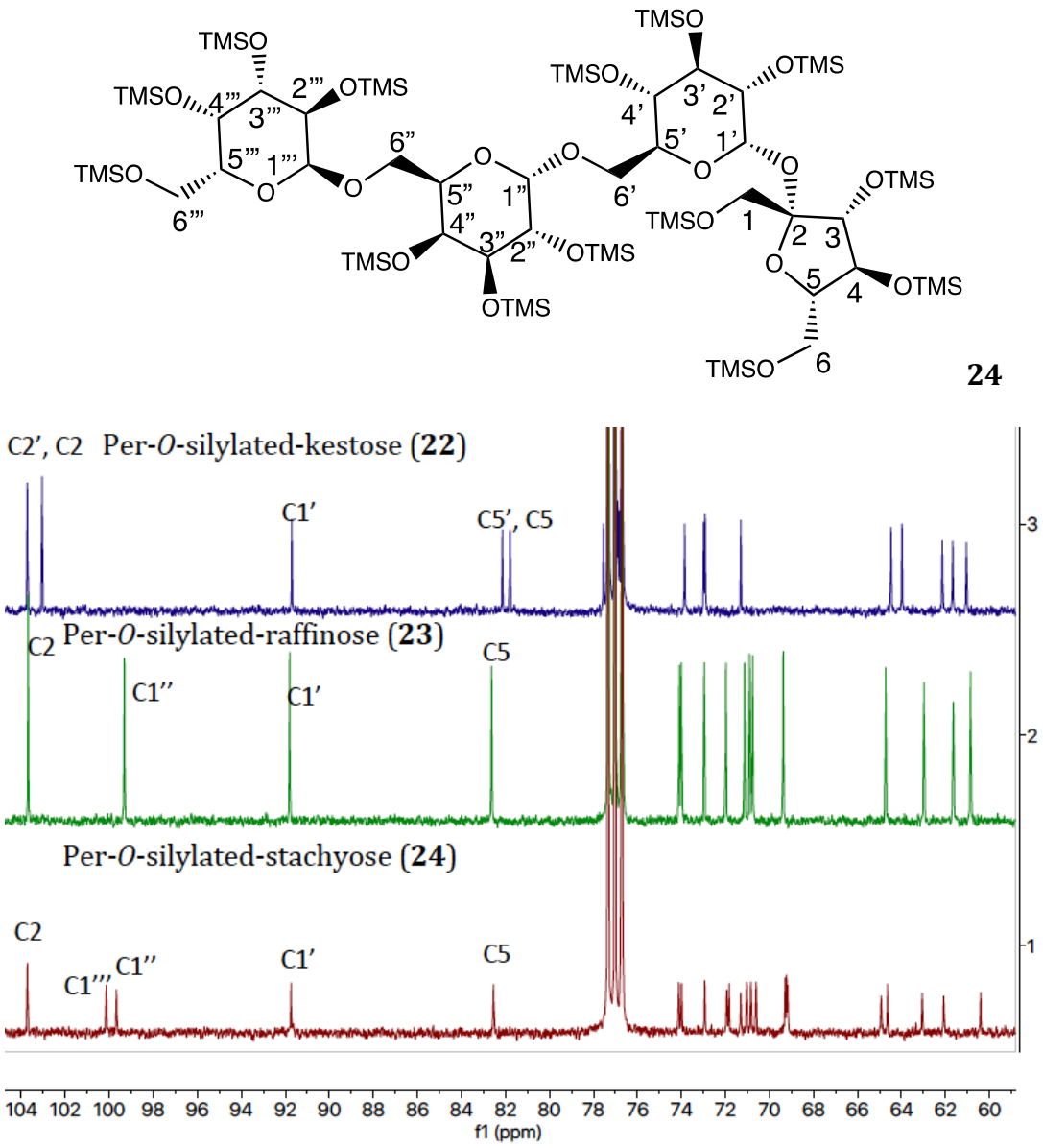

Figure 1.62: ^{13}C NMR spectra overlapped of per-*O*-TMS kestose (**22**), per-*O*-TMS raffinoses (**23**), and per-*O*-TMS stachyose (**24**); showed the chemical shift of C2, C1''', C1", C1' and C5 from per-*O*-TMS stachyose (**24**) have similar chemical shift values as the corresponding carbon in per-*O*-TMS kestose (**22**) and per-*O*-TMS raffinoses (**23**).

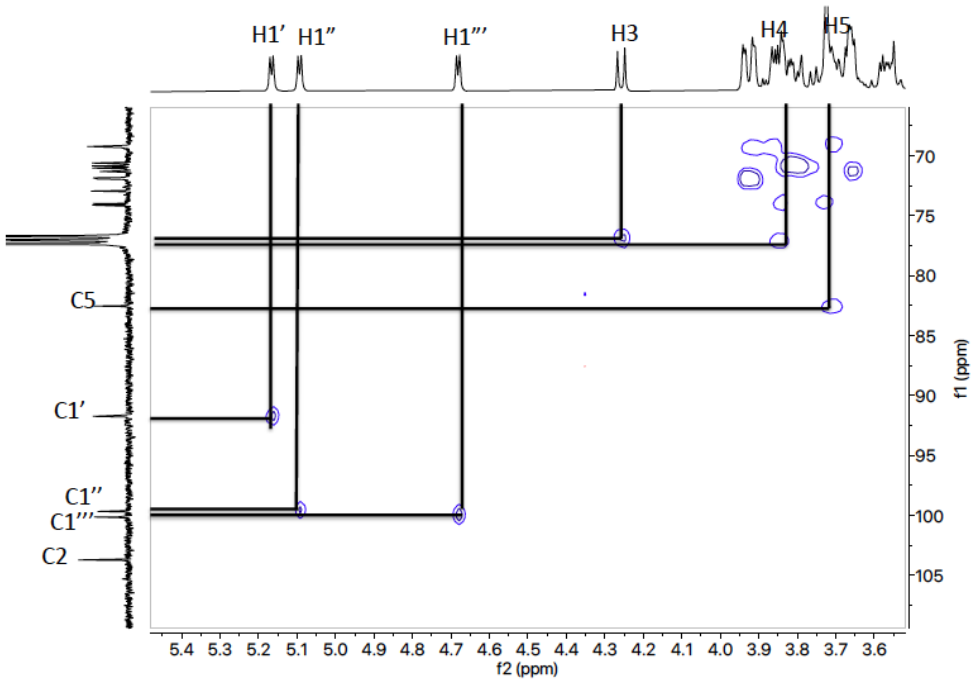

Figure 1.63: The ^{1}H-^{13}C HSQC spectrum of per-*O*-TMS stachyose (**24**); showed cross peak correlation of C1''', C1'', C1', C5, C4, and C3 to it corresponding protons.

Using the initial assignments from carbon spectra comparisons, COSY was performed to assign the proton signals for some peaks that were not overlapped. Starting from H3 at δ 4.26, a doublet with J = 7.32 Hz, this signal showed cross-peak correlation to H4 at δ 3.84 in COSY (see Figure 1.64 below), which had an overlapped peak with H2" and other protons. Although it was difficult to use COSY to identify H5, using ^{1}H-^{13}C HQSC, H5 was assigned to δ 3.71 as shown above (Figure 1.63). Similar to H5, the signal for H6ab at 3.66 was assigned using ^{1}H-^{13}C HQSC correlations from C6. There were two separate peaks for H1a and H1b, which appeared at δ 3.58-3.55 (m) and δ 3.34-3.38 (m), respectively. From the ^{1}H-^{13}C HQSC, the signal at δ 5.17 was identified as H1', and this signal showed cross-peak correlation to H2' at δ 3.34-3.38, appearing as a multiplet and overlapping with H1a. On the other hand, the other

signals, H3' to H5', could not be assigned. Meanwhile, using ^{1}H-^{13}C HSQC, H6ab was assigned to the proton signal at δ 3.71. The signal at δ 5.09 was assigned to H1" because it exhibited cross-peak correlation to C1" as shown in Figure 1.63. This signal also showed cross-peak correlation to H2" at δ 3.86, with overlapped peaks observed in COSY (Figure 1.64). Further correlations could not be identified to assign H3" to H5". Similarly, H6" was assigned to δ 3.65 (H6b") and δ 3.50 (H6a") using ^{1}H-^{13}C HSQC. For H1"', it was assigned to 4.68, a doublet, and showed cross-peak correlation to H2"' at δ 3.91; this signal also overlapped with other unassigned proton signals. Using ^{1}H-^{13}C HSQC, H6ab"' was assigned to δ 3.56 ppm. TOCSY was performed, but the 400 MHz NMR spectrometer cannot provide good resolution to separate the congestion overlapped of these signals. The partial spectrum assignment can be found in the Supplemental Information section on page 194-201.

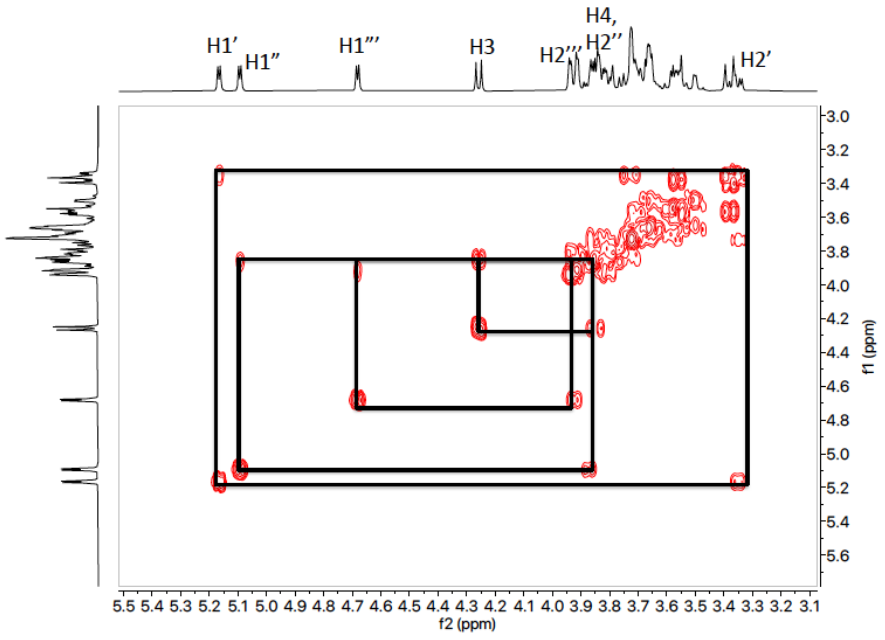

Figure 1.64: Expanded COSY spectrum of per-*O*-TMS stachyose (**24**) showed the cross-peak correlation between H1' to H2', H1" to H2", H1"' to H2"' and H3 to H4.

Similar to the proton and carbon spectra, not all silicon peaks were assigned. The signals that had been assigned showed cross-peak correlation to the assigned proton peaks. Additionally, the cross-peaks also overlapped, further complicating the assignment. As shown in Figure 1.65, the ^{1}H-^{29}Si HMBC spectrum revealed that Si4, at δ 18.7 ppm, was the most downfield and showed cross-peak correlation to H4. Meanwhile, Si1 at δ 18.4 ppm showed two cross-peaks to the two proton signals H1a and H1b. The signal at δ 18.3 ppm was assigned to Si3. The signal at δ 17.4 ppm was assigned to Si2', which showed cross-peak correlation to H2'. Although some H2'', H2''', H6', H6", and H6'" had been assigned, the cross-peak could not provide clear correlation to assign all the silicon signals. A table showing the partial assigned peaks can be found in Table 1.15. Higher resolution is required to give a full spectrum assignment for proton, carbon, and silicon.

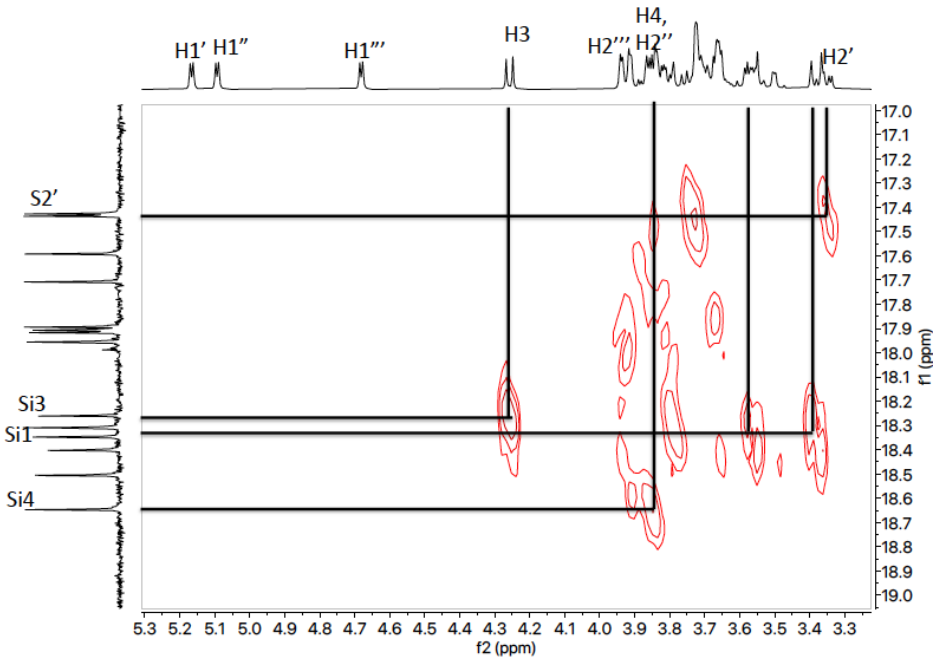

Figure 1.65: ^{1}H-^{29}Si HMBC spectrum of per-*O*-TMS stachyose (**24**) showed the cross-peak correlation between proton and silicon nuclei.

Table 1.15: The ^{1}H, ^{13}C, ^{29}Si NMR chemical shifts (δ) of 1,3,4,6,2',3',4',2",3",4",2'",3'",4'",6'" -tetrade-O-TMS-stachyose (per-O-TMS stachyose) (**24**)

Atom	δ ^{1}H*	δ ^{13}C	δ ^{29}Si
1a	3.61-3.54	63.06	18.36
1b	3.41-3.33	--	--
2	--	103.72	17.48
3	4.26	76.76	18.30
4	3.89-3.78	76.94	18.70
5	3.77-3.68	82.54	--
6a	3.66	64.62	17.76
6b	3.66		
1'	5.17	91.74	--
2'*	3.41-3.33	72.94	x
3'*	3.77-3.68	73.99	x
4'*	X	71.83	x
5'*	X	x	--
6'a*	3.77-3.68	62.08	--
6'b*	3.77-3.68		
1"	5.09	99.67	--
2"*	3.89-3.78	74.12	x
3"*	X	x	x
4"	X	x	18.45
5"	X	x	--
6"a*	3.54-347	60.40	--
6b"	3.66		
1'"	4.68	100.14	--
2'"	3.96-3.90	71.94	x
3'"	X	x	18.01
4'"	X	x	18.56
5'"	X	x	-
6a'"	3.61-3.54	64.92	x
6b'"	3.61-3.54	--	

1.3.0 Conclusion: Comparison and Contrast of the Silicon Signals in all Twelve Compounds.

The overlay spectra in Figure 1.66 showed twelve per-*O*-silylated sugars and the internal standard cholesterol that have been synthesized. From top to bottom, the following compounds were observed: per-*O*-silylated DHEA (**25**) (also commercially available through Sigma), per-*O*-TMS α-methylglucoside (**13**), α-per-

O-TMS glucose (**14**), α-per-*O*-TMS mannose (**15**), β-per-*O*-TMS fructose (**16**), per-*O*-TMS sorbitol (**17**), per-*O*-TMS ribitol (**18**), per-*O*-TMS xylitol (**20**), per-*O*-TMS sucrose (**20**), per-*O*-TMS trehalose (**21**), α-per-*O*-TMS kestose (**22**), α-per-*O*-TMS raffinoses (**23**), and α-per-*O*-TMS stachyose (**24**) (shown in Figure 66). Analyzing all the spectra, it can be stated that the 29 silicon signals of the α-anomer chemical shifts appear to be downfield compared to the β-anomer. This trend is observed in the spectrum between β-per-*O*-TMS fructose (**16**) and α-fructose ring in per-*O*-TMS sucrose (**20**), α-per-*O*-TMS kestose (**22**), and α-per-*O*-TMS raffinose (**23**). This pattern is further supported by the signals of per-*O*-TMS α-methylglucoside (**13**) in this study, which are more downfield compared to the per-*O*-TMS β-methylglucoside published previously.[76]

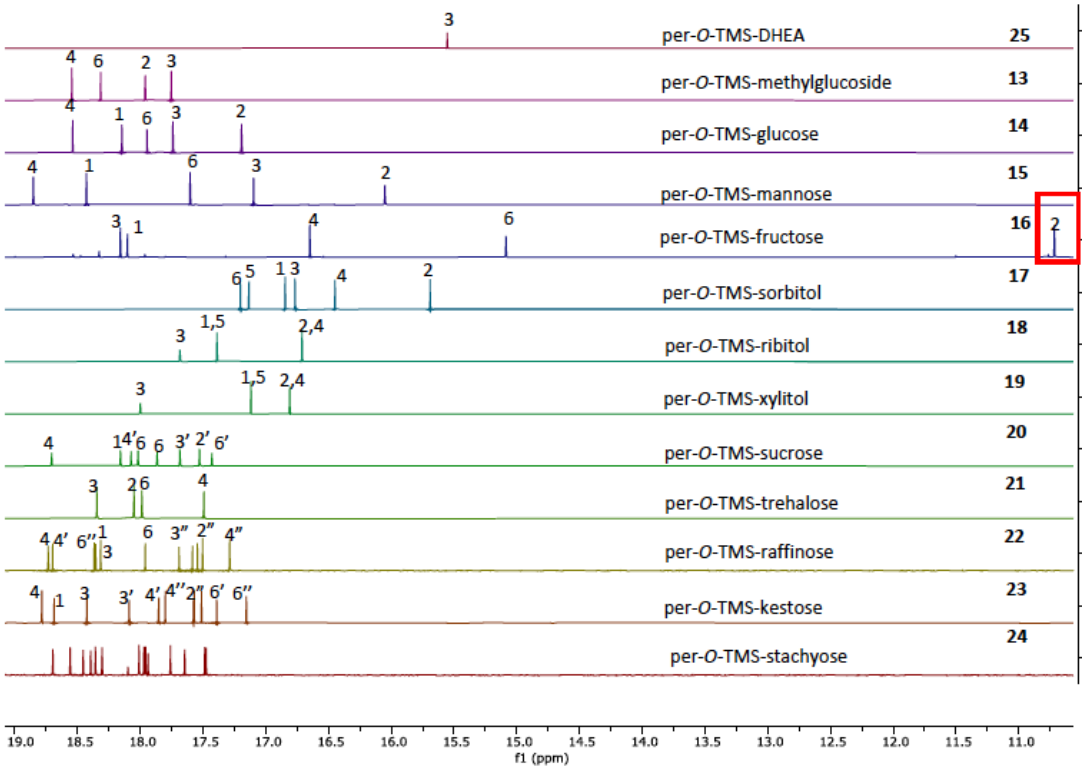

Figure 1.66: 1D ^{29}Si NMR spectra overlap of twelve per-*O*-TMS derivatives (twelve sugars with per-*O*-TMS DHEA as internal standard). The chemical shift reference used was TMS. All spectra acquired in $CDCl_3$.

An interesting observation arises when comparing the chemical shift order of per-*O*-TMS glucose (**14**) and per-*O*-TMS mannose (**15**). In both compounds, the order of the chemical shifts remained consistent: Si4 > Si1 > Si6 > Si3 > Si2. However, it is important to highlight a significant difference in the chemical shift of Si2 between per-*O*-silylated glucose (**14**) and per-*O*-silylated mannose (**15**). The shift exhibited a variation of Δ 1.17 ppm, as clearly indicated in the Table 1.16 below. In contrast, the chemical shifts of the other silicon nuclei showed changes ranging from 0.67 to 0.26 ppm. This discrepancy in the chemical shift of Si2 provides valuable insight into the stereocenter, specifically the spatial orientation (between equatorial and axial positions) of the Si atom, contributing to the structural variations between per-*O*-silylated glucose (**14**) and per-*O*-silylated mannose (**15**).

Table 1.16: **Δ** values of ^{29}Si NMR between per-*O*-TMS mannose (**15**) and per-*O*-TMS glucose (**14**)

Compound	**δ Si4**	**δ Si1**	**δ Si6**	**δ Si3**	**δ Si2**
Glucose (**14**)	18.57	18.17	17.97	17.77	17.22
Mannose (**15**)	18.85	18.43	17.60	17.10	16.05
Δ	0.28	0.26	0.37	0.67	1.17
Galactose[60]	16.60	--	18.10	17.70	18.70
Δ	2.74		0.50	0.40	2.65

Another notable observation was that the axial silicon (^{29}Si NMR) chemical shift appears more upfield compared to the equatorial ^{29}Si NMR chemical shift. This pattern was observed for Si2 in per-*O*-TMS glucose (**14**) and per-*O*-silylated galactose compared to the Si2 in per-*O*-TMS mannose (**15**) as shown in Table 1.16. This pattern was also confirmed for Si4 (axial position) from methyl-per-*O*-TMS galactose (δ 16.60)[60] which is the most upfield signal when compared to all other

chemical shifts from per-*O*-silylated galactose as well as has large Δ values with Si4 in per-*O*-TMS glucose (**14**) and per-*O*-TMS mannose (**15**) as shown in Table 1.16.

It is also important to note that the chemical shifts from Fru*f* are downfield compared to the chemical shifts from Glc*p* in di- and trisaccharide silyl derivatives, as observed in the spectrum overlapped in Figure 1.66. The signals of mannose, glucose, and methylglucoside silyl derivatives followed the same order of chemical shifts from Si4 as the most downfield, and Si2 as the most upfield. However, the chemical shifts of mannose derivatives are more spread out compared to those of glucose or methylglucoside derivatives. The ^{29}Si NMR signals of per-*O*-TMS xylitol (**19**), per-*O*-TMS ribitol (**18**), and per-*O*-TMS sorbitol (**17**) are slightly upfield compared to the silicon signal from the rings. Interestingly, the chemical shifts of xylitol and ribitol derivatives do not overlap, despite their similar structures, except for C-3, where xylitol has an "R" configuration while ribitol has an "S" configuration. This dissimilarity at the stereocenter leads to a noticeable difference in the chemical shifts of the per-*O*-TMS xylitol (**19**) and per-*O*-TMS ribitol (**18**), as determined by ^{29}Si NMR spectroscopy in Figure 1.66. This observation suggests that the presence of a stereocenter exerts a significant influence on the ^{29}Si NMR chemical shift of the overall structure in acyclic as well as cyclic sugars.

The chemical shift order of per-*O*-TMS trehalose (**21**), which constitutes a symmetrical dimer composed of two α-linked-per-*O*-TMS glucose units, differs from that of α-per-*O*-TMS glucose (**14**) or per-*O*-TMS-α-methylglucoside (**13**), which is also a glucose with a methyl group on C-1. However, due to the symmetrical nature

of the ring in per-*O*-TMS trehalose (**21**), only four ^{29}Si signals are generated. In terms of chemical shift order, α-per-*O*-TMS glucose (**14**) shows the following sequence: Si4>Si1>Si6>Si3>Si2. Conversely, per-*O*-TMS trehalose (**21**) has a different order: Si3>Si2>Si6>Si4. Additionally, the chemical shift order for per-*O*-TMS-α-methylglucoside (**13**) is Si4>Si6>Si2>Si3.

Per-*O*-TMS-α-methylglucoside (**13**) and α-per-*O*-TMS glucose (**14**) have a similar chemical shift order, except for Si3 and Si2, which switch positions. A possible explanation for this switch is the deshielding effect of the anomeric carbon, which contains a methyl group instead of a trimethylsilyoxy group in per-*O*-silylated α-methylglucoside. However, further studies may be required to confirm this pattern.

It is interesting to note that the chemical shift order of per-*O*-TMS-α-methylglucoside (**13**) and per-*O*-TMS trehalose (**21**) are reversed, despite both being glucose derivatives differing only at C-1. When analyzing the proton and carbon chemical shifts between the two molecules, the chemical shift order for carbon in per-*O*-TMS trehalose (**21**) is C1>C3>C5>C2>C4>C6, while in per-*O*-TMS-α-methylglucoside (**13**), it is C1>C3>C4>C2>C5>C6. The proton chemical shift values are similar between H2 and H6, for example H4 in per-*O*-TMS trehalose (**21**) has δ 3.45, while in per-*O*-TMS-α-methylglucoside (**13**) is at δ 3.55-3.42 (an overlap). Similar, H3 in per-*O*-TMS trehalose (**21**) has δ 3.89, while in per-*O*-TMS-α-methylglucoside (**13**) is at δ 3.80-3.74 (an overlap). However, the large difference is H1 showing a Δ of 0.29 (refer to Tables 1.4 and 1.12).

Analyzing these chemical shifts from compound **13**, **14** and **21**, it becomes evident that silicon is more sensitive to its surrounding environment. Moreover, the C4 carbon in trehalose is more upfield due to greater shielding compared to methylglucoside, which aligns with the positioning of the silicon atoms in trehalose and methylglucoside. The group attached to C-1 plays a significant role in shielding the atoms connected to C-2, explaining why Si2 is distinct across all three per-silylated sugars.

Furthermore, upon closer examination of the chemical shifts of specific protons, the difference between H4 in per-*O*-TMS glucose (**14**) and per-*O*-TMS trehalose (**21**) is not substantial. H4 in per-*O*-TMS glucose (**14**) exhibits a chemical shift value of δ 3.40, while H4 in per-O-TMS trehalose (**21**) is slightly higher at δ 3.45. Similarly, when comparing the chemical shifts of C4 in both compounds, the difference remains relatively small, with a Δ of 0.52.

The findings of silicon signals between the three per-*O*-silylated sugars highlight the intricate interplay between the symmetrical sugar ring structure and the resulting ^{29}Si NMR chemical shifts, demonstrating the importance of spatial configuration in determining the observable chemical properties of these compounds.

These results indicate that the Si chemical shifts are significantly influenced by the conformation of the structure or the relative steric hindrance of neighboring groups. In other words, the arrangement and spatial interactions of surrounding atoms and groups have a major impact on the observed Si chemical shifts. This

suggests that the local environment and the proximity of other atoms within the molecule strongly contribute to the variations in ^{29}Si NMR chemical shifts. These findings not only confirm the validity of previous research but also emphasize the robustness and consistency of the observed relationships. This knowledge can be leveraged to enhance the accuracy and precision of ^{29}Si NMR chemical shift predictions, facilitating more reliable interpretations and predictions in future studies.

In addition, Figure 1.66 clearly demonstrates the remarkable distinctness of the chemical shifts observed in these silyl carbohydrate derivatives, showcasing minimal overlap with the di- or trisaccharides. This intriguing finding ignited our enthusiasm to create an extensive silicon NMR database, aiming to provide a comprehensive resource for future investigations. Expanding upon this initiative, we undertook the development of a robust methodology capable of quantifying the precise amount of a specific sugar in unknown samples, leveraging the availability of the silicon chemical shift database (see Chapter 2). Through meticulous efforts, we successfully devised a synthesis method that consistently yielded impressive results, boasting an average yield range of 80-90%. This high level of yield not only demonstrates the reproducibility of the approach but also signifies its considerable utility. The combination of our expansive database and reliable synthesis method positions us at the forefront of advancing research in the field, enabling accurate and efficient analysis of sugar content in various samples.

1.4.0 General Procedure

1.4.1 Experimental Conditions

All reagents and solvents used in this work were obtained from commercial sources and used without additional purification. Reactions were conducted under an argon atmosphere, with argon introduced into the reaction vial using a balloon or syringe. For reactions performed at room temperature, a balloon was used for argon delivery, while reactions conducted in a CEM microwave reactor employed closed microwave vessels, with argon injected via syringe before submersion into the reactor. Infrared temperature monitoring was used for microwave reactions. Trimethylsilyl chloride (TMSCl, CAS 999-97-3) and hexamethyldisilazane (HMDS, CAS 75-77-4) were stored at -20°C, while anhydrous pyridine (CAS 110-86-1) was kept at room temperature. All sugars were storage at -20°C (detail contents list in Table 17.1). NMR experiments, including ^{1}H NMR, ^{13}C NMR, ^{29}Si, and 2D NMR, were carried out on 400 MHz and 600 MHz spectrometers. For these experiments, NMR Tube Economy 5mm and NMR Tube Precision 3mm were used. The chemical shifts are reported in parts per million (ppm, δ), and the data are referenced against deuterated chloroform ($CDCl_3$, δ 7.26). The ^{1}H NMR splitting patterns are described as singlet (s), doublet (d), triplet (t), doublet of doublets (dd), doublet of triplets (dt), apparent quartet (app. q.), apparent triplet (app. t.), doublet of doublets of doublets (ddd), and multiplet (m). Coupling constants are expressed in Hertz (Hz).

Table 1.17: Sugars' purity and hydrates contents are as described below:

Sugars/Comp.	Source	CAS Number	Purity (Grade)	Hydrate
α-D-methylglucoside	Arcos Organic	97-30-3	99%	None
α-D-glucose	Arcos Organic	492-62-6	99%	None
D-(+)-mannose	Sigma-Aldrich	3458-28-4	99% (GC)	None
D-(-) fructose	Sigma-Aldrich	57-48-7	99% (HPLC)	None
Sorbitol				
ribitol	Sigma-Aldrich	488-81-3	99%	None
xylitol	Sigma-Aldrich	87-99-0	99%	None
Sucrose	Sigma-Aldrich	57-50-1	99% (GC)	None
D-(+)-trehalose dihydrate	Sigma-Aldrich	6138-23-4	99%	2 hydrate
1-Ketose	Sigma-Aldrich	470-69-9	98% (HPLC)	None
D-(+)-Raffinose pentahydrate	Sigma-Aldrich	17629-30-0	98%	5 hydrate
staychose	Sigma-Aldrich	54261-98-2	98%	None

1.4.2 *General procedure for global silylation of per-O-silylated (TMS) of mono and disaccharides using microwave reactor.*

In a 10 mL microwave vial, 100.0 mg (0.55 mmol) of α-glucose was dissolved in 2.00 mL of pyridine. The vial was sealed and purged with argon gas followed by addition of 350 uL (3 eq) of hexamethyldisilazane and 179 uL (3 eq.) of chlorotrimethylsilane. The vial was then placed in a Biotage Microwave Reactor for 1.5 h at 60 °C. After 1.5 h, the solution removed from the reactor and extracted with hexane (25 mL x 3) and rinsed with deionized water (15 mL x 3) then dried over sodium sulfate. The dried organic layer was concentrated *in vacuo* to produce a clear oil. ^{29}Si, ^{1}H, ^{13}C, ^{1}H-^{13}C & ^{1}H-^{29}Si-HMBC, HSQC, and COSY were taken.

per-*O*-TMS-methyl-α-glucoside (**13**)

^{1}H NMR (400 MHz, $CDCl_3$): δ 4.63 (d, *J* = 3.7 Hz, 1H, H_1), 3.80 – 3.74 (m, 2H, H_3, H_6), 3.69 (dd, *J* = 11.3, 5.2 Hz, 1H, H_6), 3.55 – 3.42 (m, 3H, H_5, H_4, H_2), 3.36 (s, 3H, OCH_3),

0.18 (s, 9H, TMS_4), 0.17 (d, *J* = 1.9 Hz, 18H, TMS_3 &TMS_2), 0.14 (s, 9H, TMS_6). ^{29}Si NMR (79 MHz, $CDCl_3$): δ 18.5 (Si_4), 18.3 (Si_6), 17.9 (Si_2), 17.7 (Si_3). ^{13}C NMR (101 MHz, $CDCl_3$): δ 99.6 (C_1), 75.3 (C_3), 73.9 (C_4), 72.2 (C_2), 72.0 (C_5), 62.2 (C_6), 54.5 (OCH_3), 1.30 (C_2-*O*-TMS_2), 0.940 (C_3-*O*-TMS_3), 0.560 (C_6-*O*-TMS_6), -0.250 (C_4-*O*-TMS_4). Percent yield is 85%.

α-per-*O*-TMS-glucose (**14**)

^{1}H NMR (400 MHz, $CDCl_3$) δ 5.00 (d, *J* = 3.1 Hz, 1H, H_1), 3.77 (t, *J* = 8.9 Hz, 1H, H_3), 3.74 – 3.63 (m, 3H, H_6, H_5, $H_{6'}$), 3.40 (t, *J* = 8.9 Hz, 1H, H_4), 3.33 (dd, *J* = 9.1, 3.1 Hz, 1H, H_2), 0.17 (s, 9H, TMS_4), 0.15 (d, *J* = 1.4 Hz, 18H, TMS_1, TMS_3), 0.13 (s, 9H, TMS_2), 0.10 (s, 9H, TMS_6). ^{29}Si NMR (79.0 MHz, $CDCl_3$) δ 18.5 (Si_4), 18.1 (Si_1), 18.0 (Si_6), 17.7 (Si_3), 17.2 (Si_2). ^{13}C NMR (101 MHz, $CDCl_3$) δ 93.91 (C_1), 74.21 (C_2), 74.03 (C_3), 72.48 (C_5), 72.28 (C_4), 62.33 (C_6), 1.28 (C_1-*O*-TMS_1), 0.97 (C_4-*O*-TMS_4), 0.47 (C_3-*O*-TMS_3), 0.19 (C_2-*O*-TMS_2), -0.23 (C_6-*O*-TMS_6). Percent yield is 89%.

α-per-*O*-TMS-mannose (**15**)

^{1}H NMR (400 MHz, $CDCl_3$) δ 4.89 (d, *J* = 2.1 Hz, 1H, H_1), 3.83 – 3.79 (m, 2H, H_3, H_4), 3.73-3.70 (m, 2H $H_{6ab'}$), 3.63 (t, *J* = 2.20, 1H, H_2), 3.60 – 3.55 (m, 1H, H_5), 0.15 (s, 9H, TMS_3), 0.14 (s, 18H, TMS_4), 0.11 (s, 9H, TMS_2), 0.10 (s, 9H, TMS_6). ^{29}Si NMR (79 MHz, $CDCl_3$) δ 18.85 (Si_4), 18.43 (Si_1), 17.60 (Si_6), 17.10 (Si_3,), 16.05 (Si_2). ^{13}C NMR (101 MHz, $CDCl_3$) δ 95.61 (C_1), 75.23 (C_2), 74.61 (C_5), 72.20 (C_3), 68.43 (C_4), 62.51 (C_6), 0.72 (C_6-*O*-TMS_6), 0.61 (C_1-*O*-TMS_1), 0.39 (C_4-*O*-TMS_4), -0.09 (C_2-*O*-TMS_2), -0.14 (C_3-*O*-TMS_3). Percent yield is 92%.

β-per-*O*-TMS-fructose (**16**)

^{1}H NMR (400 MHz, $CDCl_3$) δ 4.02 (d, *J* = 9.2 Hz, 1H, H_3), 3.80 – 3.78 (m, 1H, $H_{6'}$), 3.78 – 3.75 (m, 1H, H_5), 3.74 (dd, *J* = 4.3, 2.1 Hz, 1H, H_4), 3.65 (d, *J* = 10.6 Hz, 1H, $H_{1'}$), 3.49 – 3.46 (m, 1H, H_6), 3.46 – 3.43 (m, 1H, H_1), 0.14 (d, *J* = 1.3 Hz, 18H, TMS_2, TMS_4), 0.13 (s, 9H, TMS_3), 0.11 (d, *J* = 2.9 Hz, 18H, TMS_1, TMS_6). ^{29}Si NMR (79 MHz, $CDCl_3$) δ 18.2 (S_3), 18.1 (Si_1), 16.6 (Si_4), 15.0 (Si_6), 10.7 (Si_2). ^{13}C NMR (101 MHz, $CDCl_3$) δ 101.8 (C_2), 72.2 (C_5), 71.3 (C_4), 69.07 (C_3), 65.5 (C_1), 65.15 (C_6), 2.21 (C_2-*O*-TMS_2), 0.71, 0.63, 0.50, 0.05. Percent yield is 80%.

per-*O*-TMS-sorbitol (**17**)

^{1}H NMR (400 MHz, $CDCl_3$) δ 3.90 (dt, *J* = 7.8, 2.5 Hz, 1H, H_2), 3.82 – 3.73 (m, 4H, H_3, H_6, H_4, H_1), 3.63 (dd, *J* = 6.0, 4.4 Hz, 1H, H_5), 3.50 (dt, *J* = 10.4, 8.3 Hz, 2H, $H_{6'}$, $H_{1'}$), 0.15 (d, *J* = 1.2 Hz, 18H, TMS_5, TMS_3), 0.15 (s, 9H, TMS_4), 0.14 (s, 9H, TMS_2), 0.12 (s, 9H, TMS_6), 0.11 (s, 9H, TMS_1). ^{29}Si NMR (79 MHz, $CDCl_3$) δ 17.20 (S_6), 17.1 (S_5), 16.9 (Si_1), 16.8 (S_3), 16.4 (Si_4), 15.7 (Si_2). ^{13}C NMR (101 MHz, $CDCl_3$) δ 76.3 (C_3), 76.2 (C_4), 75.9 (C_2), 74.5 (C_5), 63.7 (C_1), 63.7 (C_6), 0.92 (C_2-*O*-TMS_2), 0.64 (C_5-*O*-TMS_5), 0.63 (C_3-*O*-TMS_3, C_4-*O*-TMS_4), -0.44 (C_1-*O*-TMS_1), -0.50 (C_6-*O*-TMS_6). Percent yield is 82%.

per-*O*-TMS-ribitol (**18**)

^{1}H NMR (400 MHz, $CDCl_3$) δ 3.84 (ddd, *J* = 7.0, 5.1, 3.1 Hz, 2H, H_2, H_4), 3.72 (dd, *J* = 10.3, 3.0 Hz, 2H, $H_{1'}$, $H_{5'}$), 3.65 (t, *J* = 5.1 Hz, 1H, H_3), 3.47 (dd, *J* = 10.3, 7.0 Hz, 2H, H_1, H_5), 0.12 (s, 18H, TMS_2 TMS_4), 0.11 (s, 9H, TMS_3), 0.10 (s, 18H, TMS_1, TMS_5). ^{29}Si NMR (79 MHz, $CDCl_3$) δ 17.68 (Si_3), 17.39 (Si_1, Si_5), 16.71 (Si_2, Si_4). ^{13}C NMR (101 MHz, $CDCl_3$) δ 76.73 (C_3), 74.35 (C_2, C_4), 64.19 (C_1, C_5), 0.53 (C_2-*O*-TMS_2, C_4-O-TMS_4), 0.42 (C_3-*O*-TMS_3), -0.53 (C_1-O-TMS_1, C_5-*O*-TMS_5). Percent yield is 76%.

per-*O*-TMS-xylitol **(19)**

^{1}H NMR (400 MHz, $CDCl_3$) δ 3.82 (dt, *J* = 7.2, 4.3 Hz, 2H, H_2, H_4), 3.73 (t, J = 4.12 Hz, 1H, H3), 3.70– 3.69 (m, 2H, $H_{1'}$, $H_{5'}$), 3.52 (dd, *J* = 10.4, 7.1 Hz, 2H, H_1, H_5), 0.14 (s, 9H, TMS_3), 0.13 (s, 18H, TMS_2, TMS_4), 0.10 (s, 18H, TMS_1, TMS_5). ^{29}Si NMR (79 MHz, $CDCl_3$) δ 18.00 (Si_3), 17.12 (Si_1, Si_5), 16.81 (Si_2, Si_4). ^{13}C NMR (101 MHz, $CDCl_3$) δ 74.36 (C_2, C_4), 73.39 (C_3), 63.68 (C_1, C_5), 0.70 (C_1-O-TMS_1, C_5-*O*-TMS_5), 0.45 (C_3-*O*-TMS_3), -0.44 (C_2-*O*-TMS_2, C_4-O-TMS_4). Percent yield is 89%.

per-*O*-TMS-sucrose (**20**)

^{1}H NMR (400 MHz, $CDCl_3$) δ 5.22 (d, *J* = 3.3 Hz, 1H, $H_{1'}$), 4.30 (d, *J* = 7.9 Hz, 1H, H_3), 3.92 (t, *J* = 7.9 Hz, 1H, H_4), 3.88 – 3.78 (m, 3H, H_{6b} 1, $H_{3'}$, $H_{6b'}$), 3.77 – 3.74 (m, 2H, H_{6a}, $H_{5'}$), 3.73 (dd, *J* = 4.8, 3.1 Hz, 1H, H_5), 3.66 (dd, *J* =1.2, 1.7 Hz, 1H, $H_{6a'}$), 3.57 (d, *J* = 11.5 Hz, 1H, H_{1b}), 3.50 (t, *J* = 9.1 Hz, 1H, $H_{4'}$), 3.42 (d, *J* = 11.5 Hz, 1H, H_{1a}), 3.33 (dd, *J* = 9.3, 3.3 Hz, 1H, $H_{2'}$), 0.19 (s, 8H, $TMS_{4'}$), 0.17 (s, 9H, TMS_3), 0.17 (s, 18H, TMS_4, $TMS_{2'}$), 0.15 (s, 9H, $TMS_{3'}$), 0.14 (s, 18H, TMS_6, $TMS_{6'}$), 0.13 (s, 9H, TMS_1). ^{29}Si NMR (79 MHz, $CDCl_3$): δ 18.7 (Si_4), 18.2 (Si_1), 18.1 (Si_3), 18.0 ($Si_{4'}$), 17.9 (Si_6), 17.7 ($Si_{3'}$), 17.5 ($Si_{2'}$), 17.4 ($Si_{6'}$). ^{13}C NMR (101 MHz, $CDCl_3$) δ 103.42 (C_{2f}), 91.77 (C_{1g}), 82.34 (C_{5f}), 76.54 (C_{3f}), 76.42 (C_{4f}), 73.77 (C_{3g}), 72.99 (C_{2g}), 72.92 (C_{5g}), 71.68 (C_{4g}), 64.63 (C_{6f}), 63.12 (C_{1f}), 61.89 (C_{6g}), 1.20, 0.96, 0.78, 0.58, 0.37, -0.12, -0.14, -0.19. Percent yield is 85%.

per-*O*-TMS-trehalose (**21**)

^{1}H NMR (400 MHz, $CDCl_3$) δ 4.92 (d, *J* = 3.1 Hz, 2H, $H_{1,1'}$), 3.89 (t, *J* = 9.0 Hz, 2H, $H_{3,3'}$), 3.81 – 3.77 (m, 2H, $H_{5,5'}$), 3.72 – 3.64 (m, 4H, $H_{6,6'}$), 3.45 (d, *J* = 9.0 Hz, 2H, $H_{4,4'}$), 3.39 (dd, *J* = 9.3, 3.2 Hz, 2H, $H_{2,2'}$), 0.14 (d, *J* = 1.3 Hz, 36H, TMS_4, TMS_3), 0.12 (s, 18H, TMS_2), 0.10 (s, 18H, TMS_6). ^{29}Si NMR (79 MHz, $CDCl_3$) δ 18.37 ($Si_{3,3'}$), 18.07 ($Si_{2,2'}$), 18.00

($Si_{6,6'}$) 17.52 ($Si_{4,4'}$). ^{13}C NMR (101 MHz, $CDCl_3$) δ 94.34 ($C_{1,1'}$), 73.59 ($C_{3,3'}$), 73.23 ($C_{5,5'}$), 72.87 ($C_{2,2'}$), 71.75 ($C_{4,4'}$), 62.15 ($C_{6,6'}$), 1.07 ($C_{4,4'}$-*O*-$TMS_{4,4'}$), 0.94 ($C_{3,3'}$-O-$TMS_{3,3'}$), 0.15 ($C_{2,2'}$-*O*-$TMS_{2,2'}$), -0.27 ($C_{6,6'}$-O-$TMS_{6,6'}$). Percent yield is 92%.

per-O-TMS-kestose (**22**)

^1H NMR (400 MHz, $CDCl_3$) δ 5.21 (d, *J* = 3.3 Hz, 1H,$H_{1''}$), 4.34 (d, *J* = 8.0 Hz, 1H, $H_{3'}$), 4.19 (d, *J* = 7.4 Hz, 1H, H_3), 3.95 (td, *J* = 7.6, 1.8 Hz, 2H, H_4, $H_{4'}$), 3.80 (ddd, *J* = 10.1, 5.6, 3.1 Hz, 4H, $H_{6a''}$, H_{6a}, $H_{3''}$, $H_{5''}$), 3.74 (dd, *J* = 6.5, 2.2 Hz, 1H, $H_{6a'}$), 3.72 – 3.65 (m, 4H, H_5, $H_{5'}$, H_{6b}, $H_{6b'}$), 3.64 – 3.59 (m, 2H,$H_{6b''}$, $H_{1a'}$), 3.58 – 3.51 (m, 3H, H_{1ab}, $H_{4''}$), 3.32 – 3.27 (m, 2H, $H_{2''}$, $H_{1'b}$), 0.16 (d, *J* = 2.3 Hz, 18H, $TMS_{2''}$, $TMS_{4''}$), 0.15 (s, 8H, $TMS_{3'}$), 0.14 (d, *J* = 1.0 Hz, 18H, TMS_4, TMS_3), 0.13 (d, *J* = 1.5 Hz, 18H, $TMS_{4''}$, $TMS_{3''}$), 0.11 (d, *J* = 1.6 Hz, 18H, $TMS_{6''}$, $TMS_{6'}$), 0.10 (d, *J* = 1.5 Hz, 18H, TMS_1, TMS_6). ^{29}Si NMR (79 MHz, $CDCl_3$) δ 18.80 (Si_4), 18.70(Si_1) 18.44 (Si_3), 18.10 ($Si_{3'}$), 17.86 ($Si_{4'}$), 17.81 ($Si_{4''}$), 17.59 ($Si_{6'}$), 17.58 ($Si_{3''}$), 17.52 ($Si_{2''}$), 17.40 (Si_6), 17.17 ($Si_{6''}$). ^{13}C NMR (101 MHz, $CDCl_3$) δ 103.72 ($C_{2'}$), 103.05 (C_2), 91.70 ($C_{1''}$), 82.13 ($C_{5'}$), 81.79 (C_5), 77.54 ($C_{4'}$), 76.95 ($C_{3'}$), 76.90 (C_3), 76.82 (C_4), 73.85 ($C_{3''}$), 72.99 ($C_{2''}$), 72.92 ($C_{5''}$), 71.30 ($C_{4''}$), 64.48 ($C_{6'}$), 63.98 (C_6), 62.14 ($C_{1'}$), 61.67 (C_6), 61.05 ($C_{1''}$), 1.22 (C_{TMS}), 0.91 (C_{TMS}), 0.83 (C_{TMS}), 0.66 (C_{TMS}), 0.65 (C_{TMS}), 0.60 (C_{TMS}), 0.4 (C_{TMS}), 0.03(C_{TMS}), -0.09 (C_{TMS}), -0.34 (C_{TMS}), -0.37 (C_{TMS}). Percent yield is 88%.

per-*O*-TMS-raffinose (**23**)

^1H NMR (400 MHz, $CDCl_3$) δ 5.15 (d, *J* = 3.4 Hz, 1H, $H_{1'}$), 5.10 (appearing t, *J* = 1.5 Hz, 1H, $H_{1''}$), 4.25 (d, *J* = 7.5 Hz, 1H, H_3), 3.89 (appearing s, 1H, $H_{4''}$), 3.85-3.83 (m, 3H, $H_{2''}$, $H_{3''}$, $H_{5'}$), 3.81 (t, *J* = 7.4 Hz, 1H, H_4), 3.77 – 3.71 (m, 5H, $H_{4'}$, $H_{6b'}$, H_5, $H_{3'}$, $H_{6a'}$), 3.69 (d, *J* = 4.48 Hz, 2H, H_{6ab}), 3.65 (appearing (t)d, *J* = 6.0 Hz, 2H, $H_{5''}$, $H_{6b''}$), 3.57-3.49 (m, 2H,

H_{1b}, $H_{6a''}$), 3.41 – 3.33 (m, 2H, H_{1a}, $H_{2'}$), 0.21 (s, 9H, $TMS_{4'}$), 0.15 (d, *J* = 1.0 Hz, 18H, TMS_3, $TMS_{2''}$), 0.14 (d, *J* = 0.7 Hz, 24H, TMS_4, $TMS_{4''}$, $TMS_{2''}$), 0.13 (s, 9H,$TMS_{3'}$), 0.12 (s, 9H, TMS_2), 0.11 (s, 18H, TMS_6, $TMS_{6''}$), 0.10 (s, 9H, TMS_1). ^{29}Si NMR (79 MHz, $CDCl_3$) δ 18.73 (Si_4), 18.70 ($Si_{4'}$), 18.37 (Si_1), 18.36 ($Si_{6''}$), 18.32 (Si_3), 17.96 (Si_6), 17.69 ($Si_{2''}$), 17.58 ($Si_{3''}$), 17.54 ($Si_{2'}$), 17.50 ($Si_{3'}$), 17.29 ($Si_{4''}$). ^{13}C NMR (101 MHz, $CDCl_3$) δ 103.69 (C_2), 99.31 ($C_{1''}$), 91.81 ($C_{1'}$), 82.63 (C_5), 77.21 (C_4), 76.72 (C_3), 74.10 ($C_{3'}$), 74.00 ($C_{2''}$), 72.97 ($C_{2'}$), 71.98 ($C_{4''}$), 71.13 ($C_{4'}$), 70.90 ($C_{3''}$), 70.77 ($C_{5'}$), 69.37 ($C_{5''}$), 64.72 (C_6), 62.98 (C_1), 61.64 ($C_{6'}$), 60.86 ($C_{6''}$), 1.22 ($C\text{-}_{TMS}$), 0.99 ($C\text{-}_{TMS}$), 0.72 ($C\text{-}_{TMS}$), 0.65 ($C\text{-}_{TMS}$), 0.55 ($C\text{-}_{TMS}$), 0.53 ($C\text{-}_{TMS}$), 0.35 ($C\text{-}_{TMS}$), 0.30 ($C\text{-}_{TMS}$), -0.22 ($C\text{-}_{TMS}$), -0.25 ($C\text{-}_{TMS}$), -0.47($C\text{-}_{TMS}$). Percent yield is 87%.

per-*O*-TMS-stachyose (**24**)

^{1}H NMR (400 MHz, $CDCl_3$) δ 5.17 (d, *J* = 3.4 Hz, 1H $H_{1'}$), 5.09 (d, *J* =3.3 Hz, 1H, $H_{1''}$), 4.68 (d, *J*=3.3 Hz, 1H, $H_{1'''}$), 4.26 (d, *J* = 7.5 Hz, 1H, H_3), 3.96-3.90 (m, 3H, $H_{2'''}$, $H_?$, $H_?$), 3.89-3.78 (m, 6H, $H_{2''}$, H_4, $H_?$, $H_?$, $H_?$, $H_?$), 3.77-3.68 (m, 6H, $H_{3'}$, $H6_{ab'}$, H_5, $H_?$, $H_?$), 3.66 (dt, *J* = 5.1, 2.9 Hz, 4H, H_{6ab}, $H_{6b''}$, $H_?$), 3.61-3.54 (m, 3H, H_1, $H_{6ab'''}$), 3.54-3.47 (m, 1H, $H_{6a''}$), 3.41-3.33 (m, 2H, H_1, $H_{2'}$), ^{29}Si NMR (79 MHz, $CDCl_3$) δ 18.70 (Si_4) 18.56 ($Si_{4'''}$), 18.45 ($Si_{4''}$), 18.40 (Si_1), 18.36 (Si?), 18.30 (Si_3), 18.01 ($Si_{2'''}$), 17.97 (Si?), 17.96 (Si?,), 17.94 (Si_6), 17.76 (Si?), 17.65 (Si?), 17.48 (Si_2), 17.48 (Si?).^{13}C NMR (101 MHz, $CDCl_3$) δ 103.72 (C_2), 100.14 ($C_{1'''}$), 99.67 ($C_{1''}$), 91.74 ($C_{1'}$), 82.54 (C_5), 77.22 (C_4), 76.77 (C_3), 74.12 ($C_{2''}$), 73.99 ($C_{3'}$), 72.94 ($C_{2'}$), 71.94 ($C_{2'''}$), 71.83 ($C_{4'}$), 71.30 (C?), 71.03 (C?), 70.85 (C?), 70.61 (C?), 69.29 (C?), 69.22 (C?), 69.17 (C?), 64.92 ($C_{6'''}$), 64.62 (C_6), 63.06 (C_1), 62.08 ($C_{6'}$), 60.40 ($C_{6''}$), 1.94 (C_{TMS}), 1.24 (C_{TMS}), 0.97 (C_{TMS}), 0.83 (C_{TMS}),

0.77 (C_{TMS}), 0.62 (C_{TMS}), 0.56 (C_{TMS}), 0.44 (C_{TMS}), 0.37 (C_{TMS}), 0.34 (C_{TMS}), -0.22 (C_{TMS}), -0.24 (C_{TMS}), -0.39 (C_{TMS}). Percent yield is 77%.

DHEA-*O*-TMS (**25**)

^{1}H NMR (400 MHz, $CDCl_3$) δ 5.37-5.35 (m, 1H, H_6), 3.49 (qt, *J*= 16, 8.0, 4.0 Hz, 1H, H_3), 2.46 (dd, *J* = 19.0, 8.4 Hz, 1H, H_{16}), 2.30 (t, *J*= 11.2 Hz, 1H, H_4), 2.19 (ddd, J=13.3, 7.5, 2.4 Hz, 1H, H_4) , 2.13-2.04 (m, 2H, H_7, H_{16}), 1.98-1.92 (m, 1H, H_{15}), 1.86-1.81 (m, 2H, H_{15}, H_{12}), 1.75-1.43 (m, 7H, H_2, H_2, H_7, H_8, H_{11}, H_{15}), 1.32-1.24 (M, 2H, H_{12}, H_{14}), 1.09 (dd, *J*= 15.2, 3.5 Hz, 1H, H_9), 1.01 (s, 3H, H_{19}), 0.88 (s, 3H, H_{18}), 0.12 (s, 9H, *O*-CH_3), ^{29}Si NMR (79 MHz, $CDCl_3$) δ 15.5, ^{13}C NMR (101 MHz, $CDCl_3$) δ 141.68 (C_5), 120.57 (C_6), 77.23 (C-Si), 72.16 (C_3), 51.82 (C_{14}), 50.35 (C_9), 47.56 (C_{13}), 42.65 (C_4), 37.33 (C_1), 36.72 (C_{10}), 35.85 (C_{16}), 31.92 (C_2), 31.53 (C_{12}), 31.47 (C_8), 30.84 (C_7), 21.89 (C_{15}), 20.36 (C11), 19.41 (C_{19}), 13.56 (C_{18}), 0.25 (C-$_{TMS}$). Percent yield 85%

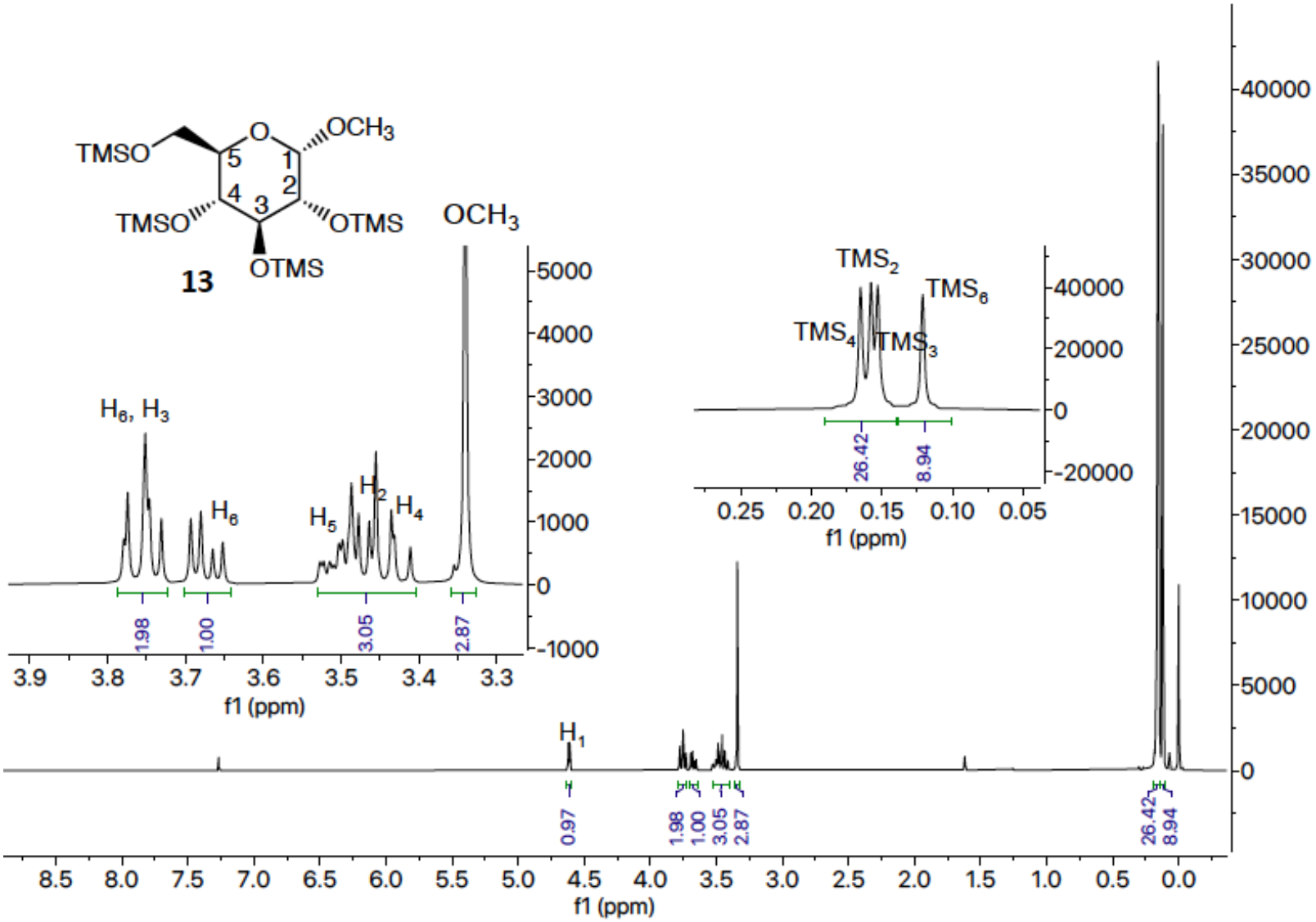

SI-Figure 1.1: per-*O*-TMS-α-methylglucoside (**13**) ^{1}H NMR (400 MHz, $CDCl_3$) spectrum

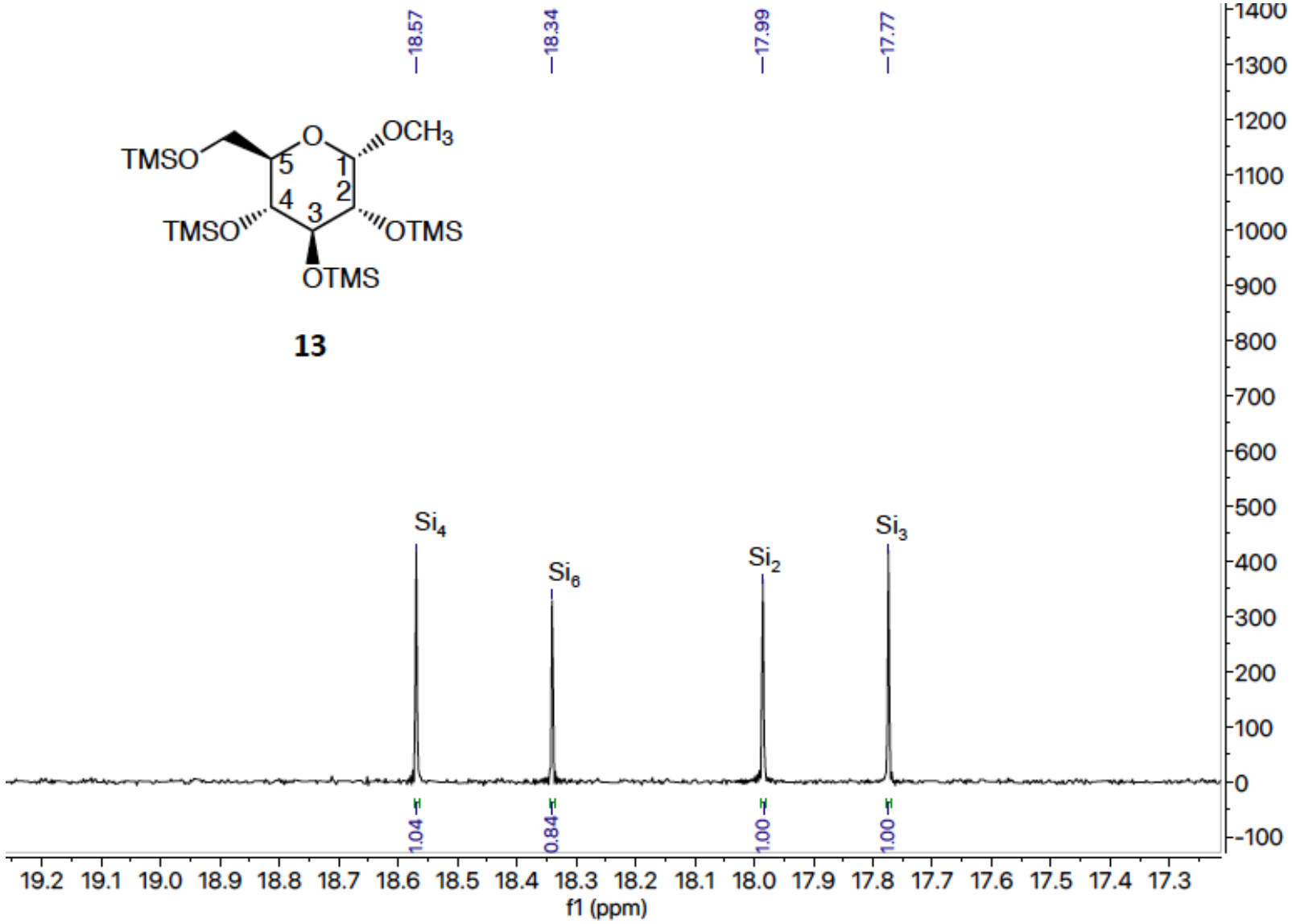

SI-Figure 1.2: per-*O*-TMS-α-methylglucoside (**13**) ^{29}Si NMR (400 MHz, $CDCl_3$) spectrum

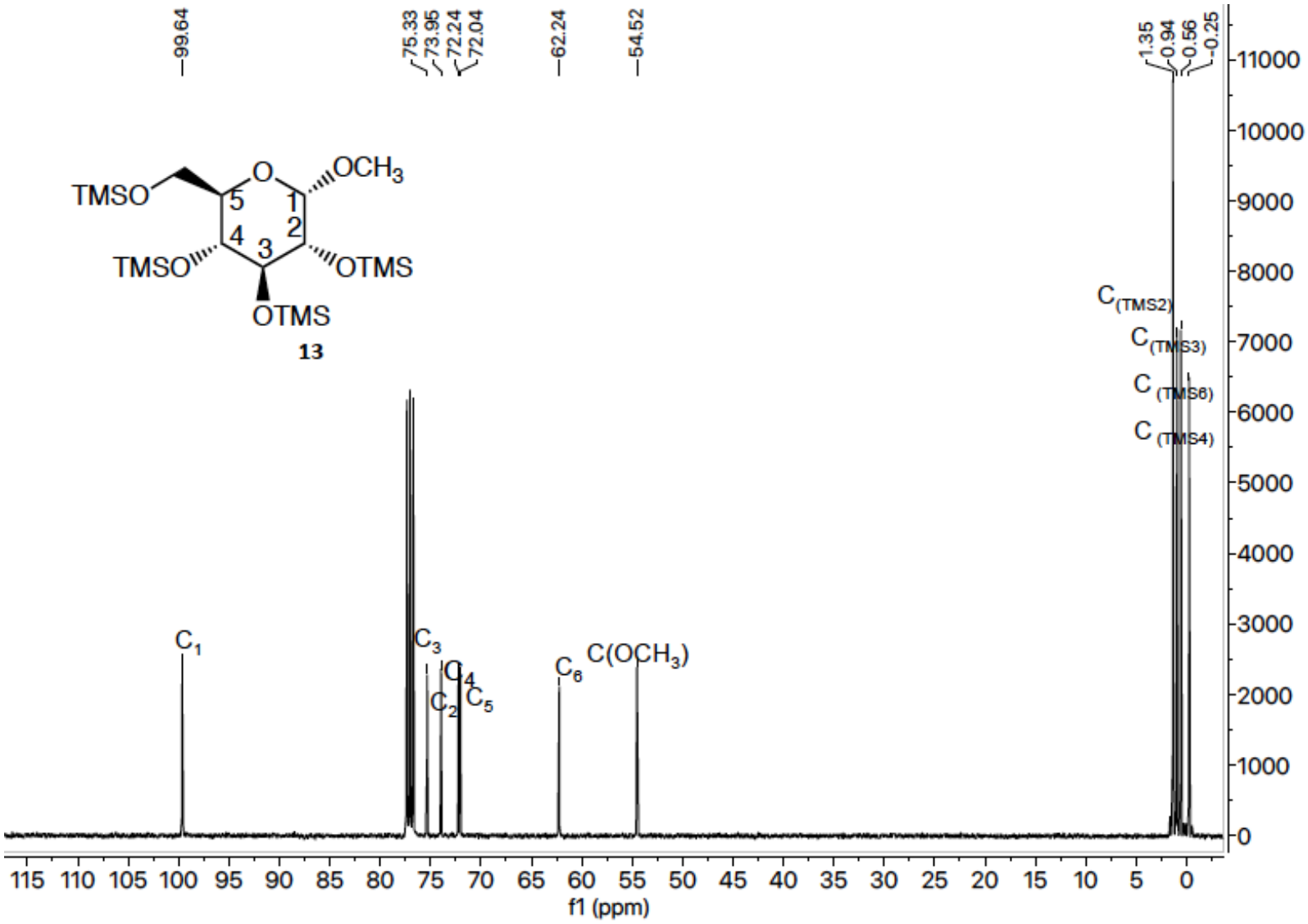

SI-Figure 1.3: per-*O*-TMS-α-methylglucoside (**13**) ^{12}C NMR (400 MHz, $CDCl_3$) spectrum

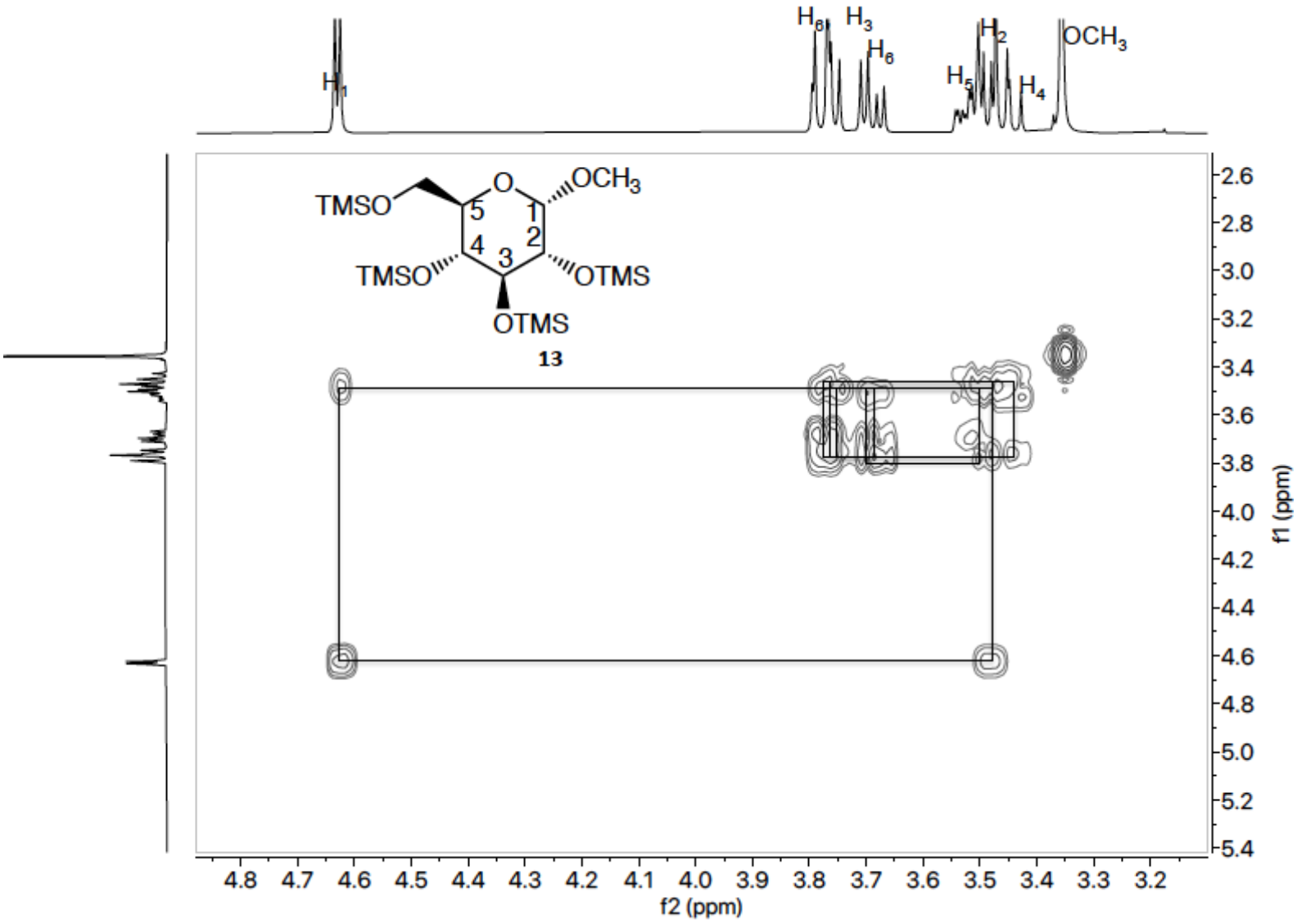

SI-Figure 1.4: per-*O*-TMS-α-methylglucoside (**13**) COSY NMR (400 MHz, $CDCl_3$) spectrum

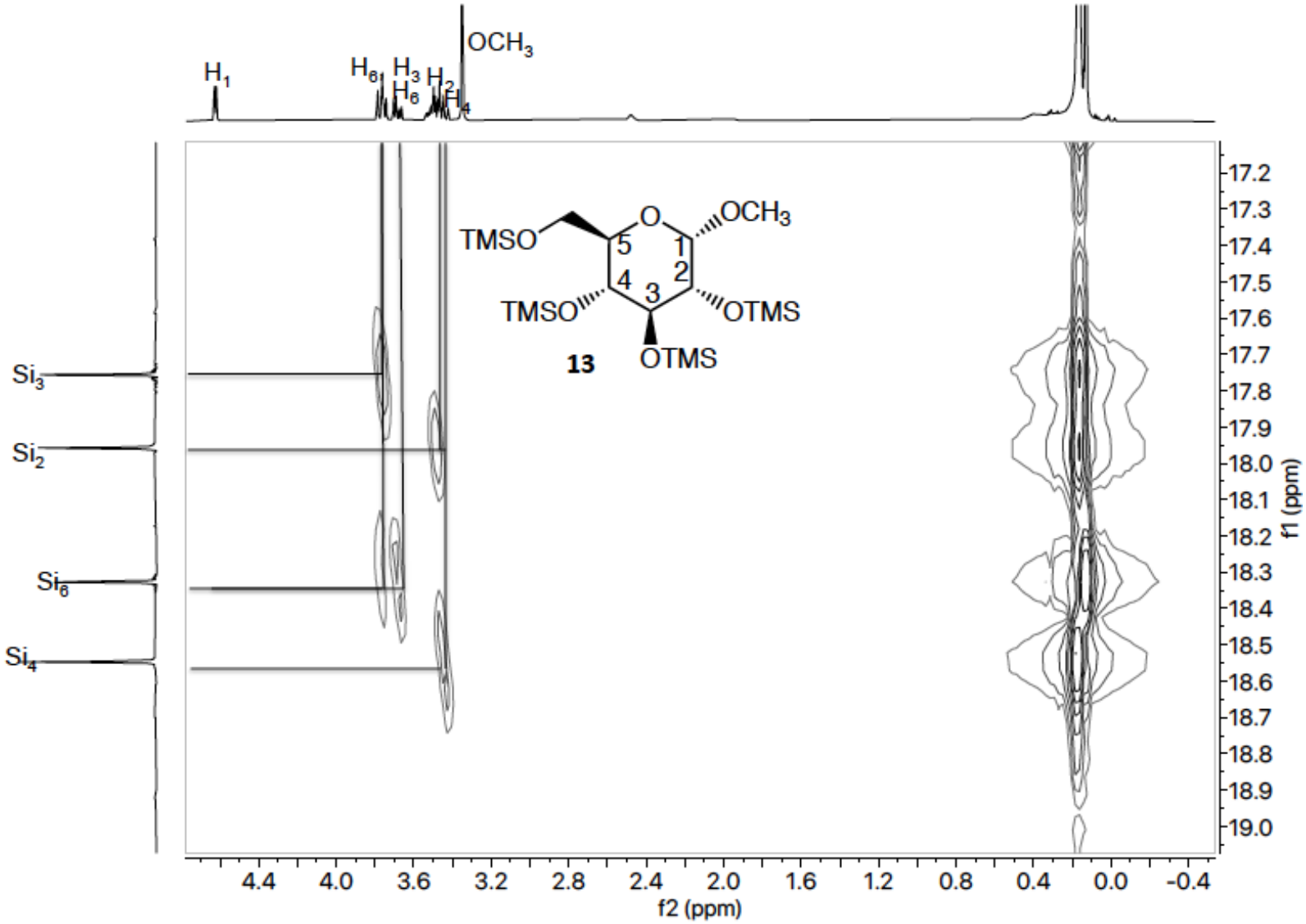

Si-Figure 1.5: per-*O*-TMS-α-methylglucoside (**13**) ^{1}H-^{29}Si HMBC NMR (400 MHz, $CDCl_3$) spectrum

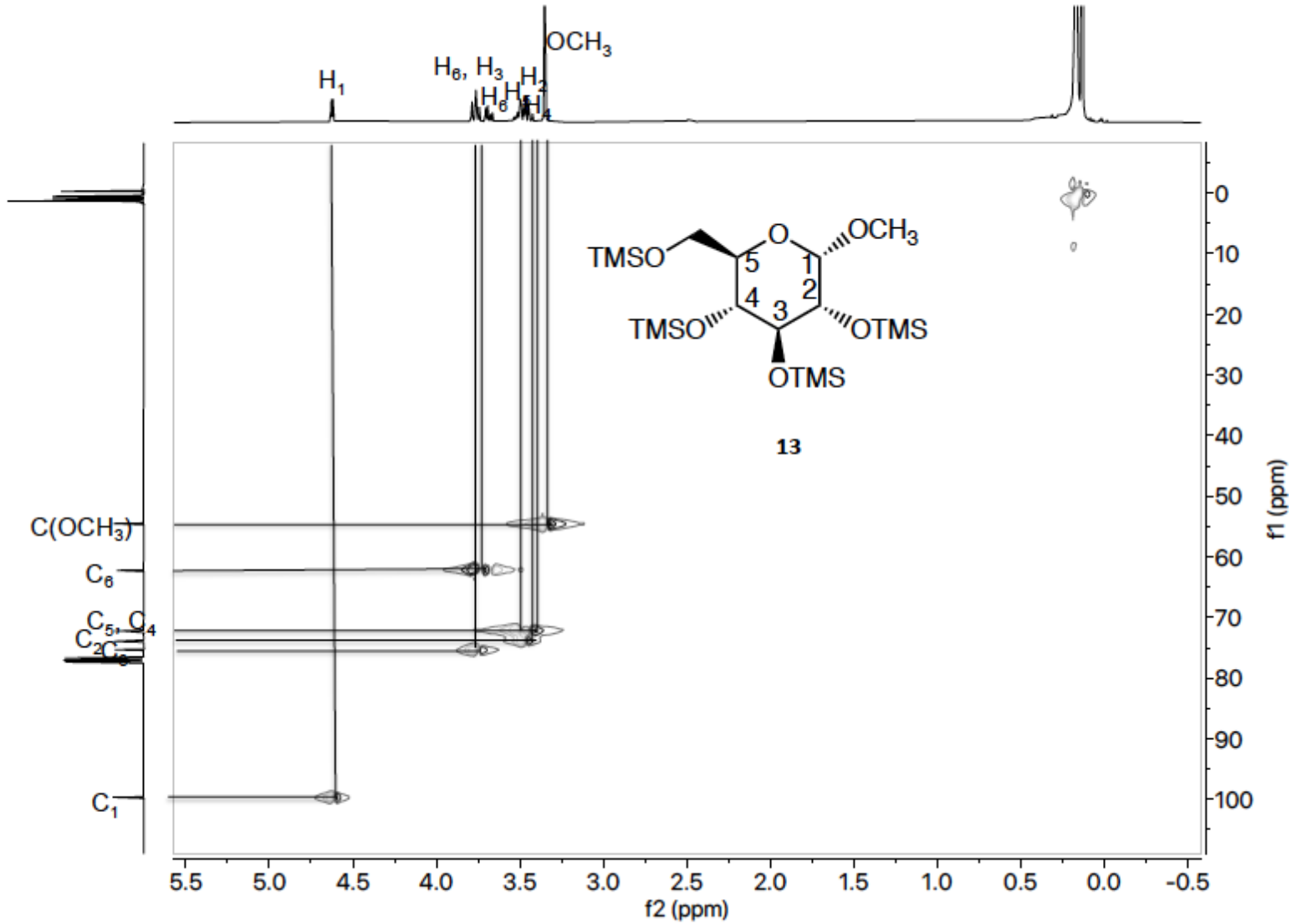

SI-Figure 1.6: per-*O*-TMS-α-methylglucoside (**13**) HSQC NMR (400 MHz, $CDCl_3$) spectrum

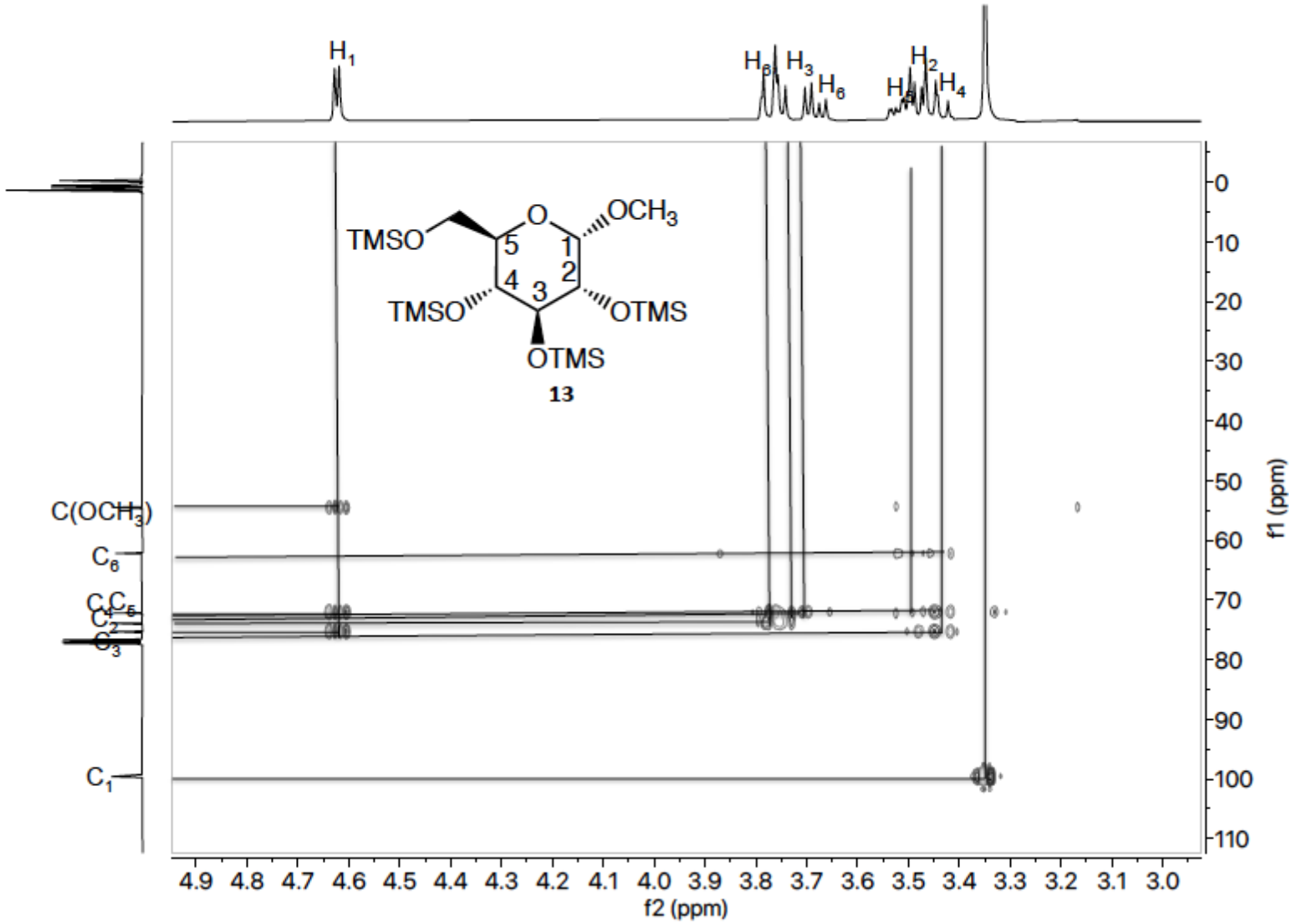

SI-Figue 1.7: per-*O*-TMS-α-methylglucoside (**13**) ^{1}H-^{13}C HMBC NMR (400 MHz, $CDCl_3$) spectrum

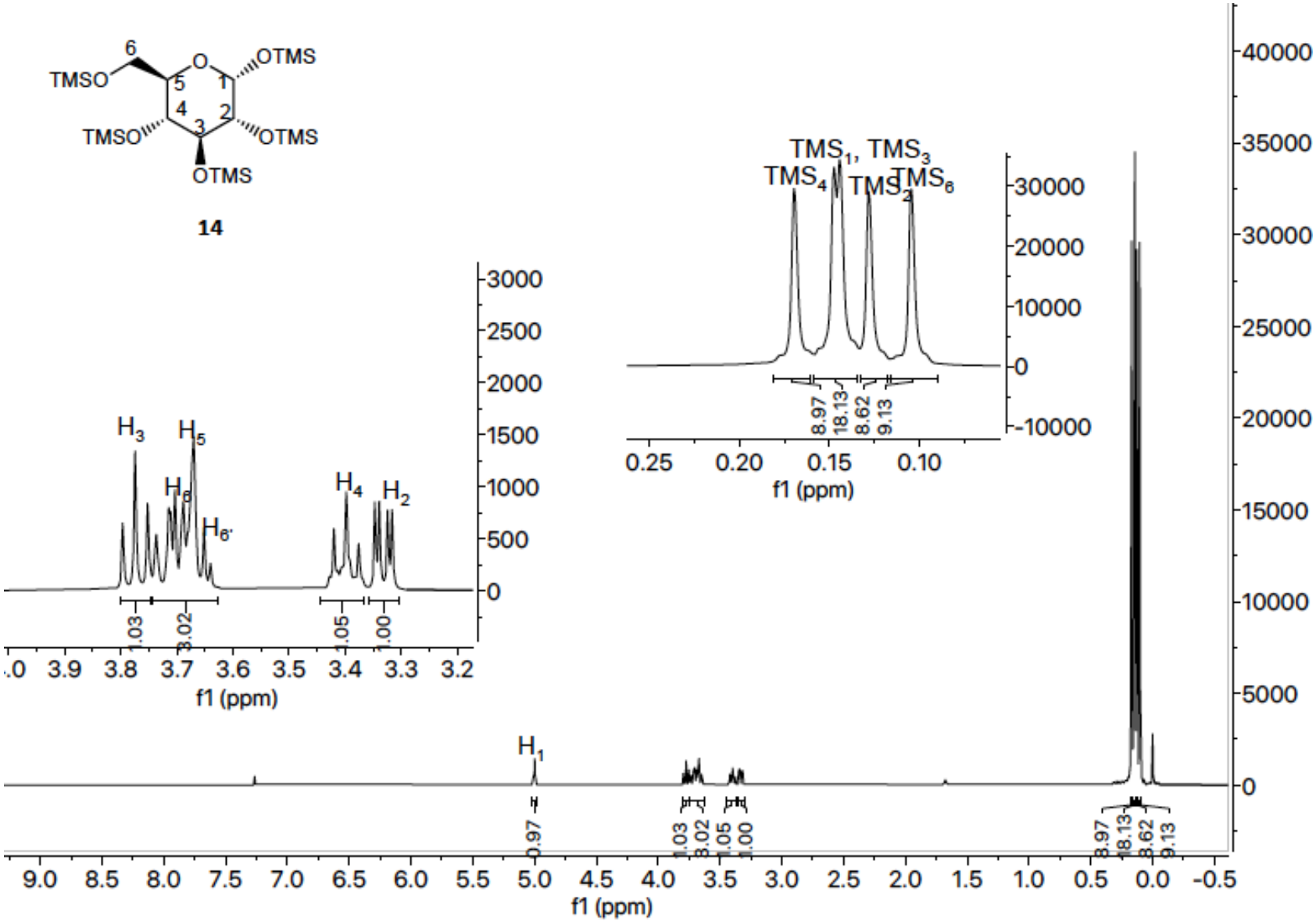

SI-Figure 1.8: per-α *O*-TMS-glucose (**14**) ^{1}H NMR (400 MHz, $CDCl_3$) spectrum

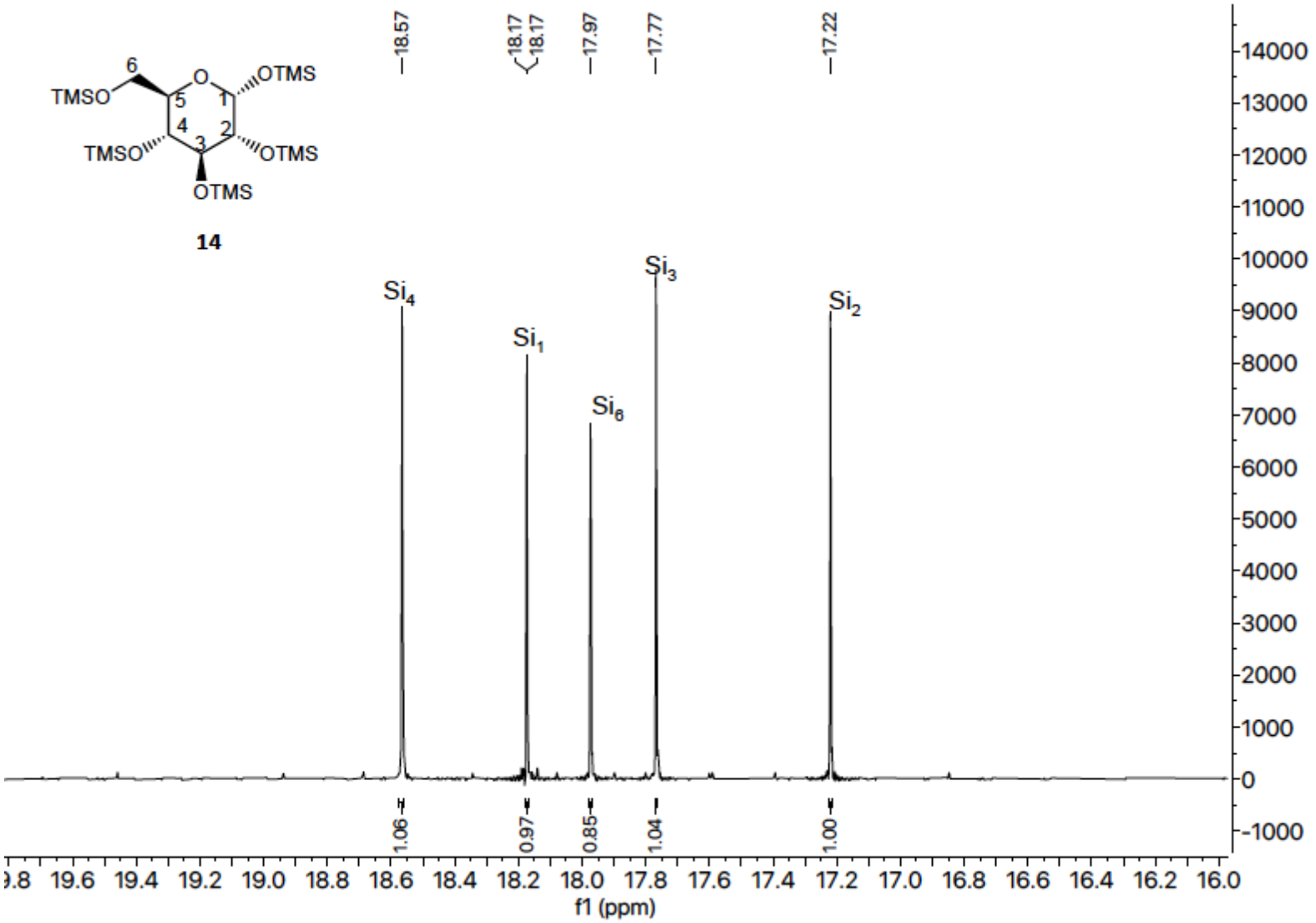

SI-Figure 1.9: per-α *O*-TMS-glucose (**14**) ^{29}Si NMR (400 MHz, $CDCl_3$) spectrum

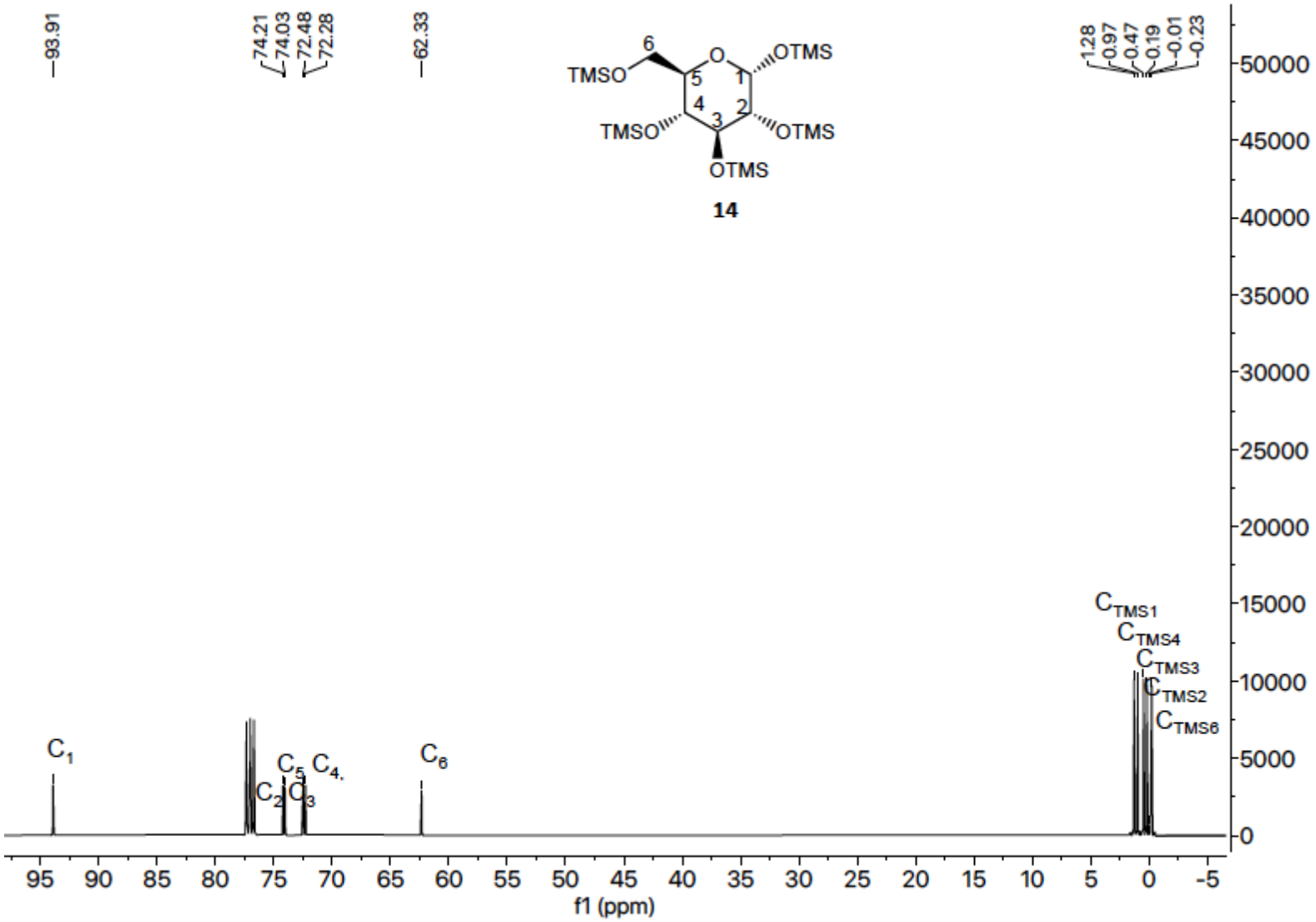

SI-Figure 1.10: per-α *O*-TMS-glucose (**14**) ^{13}C NMR (400 MHz, $CDCl_3$) spectrum

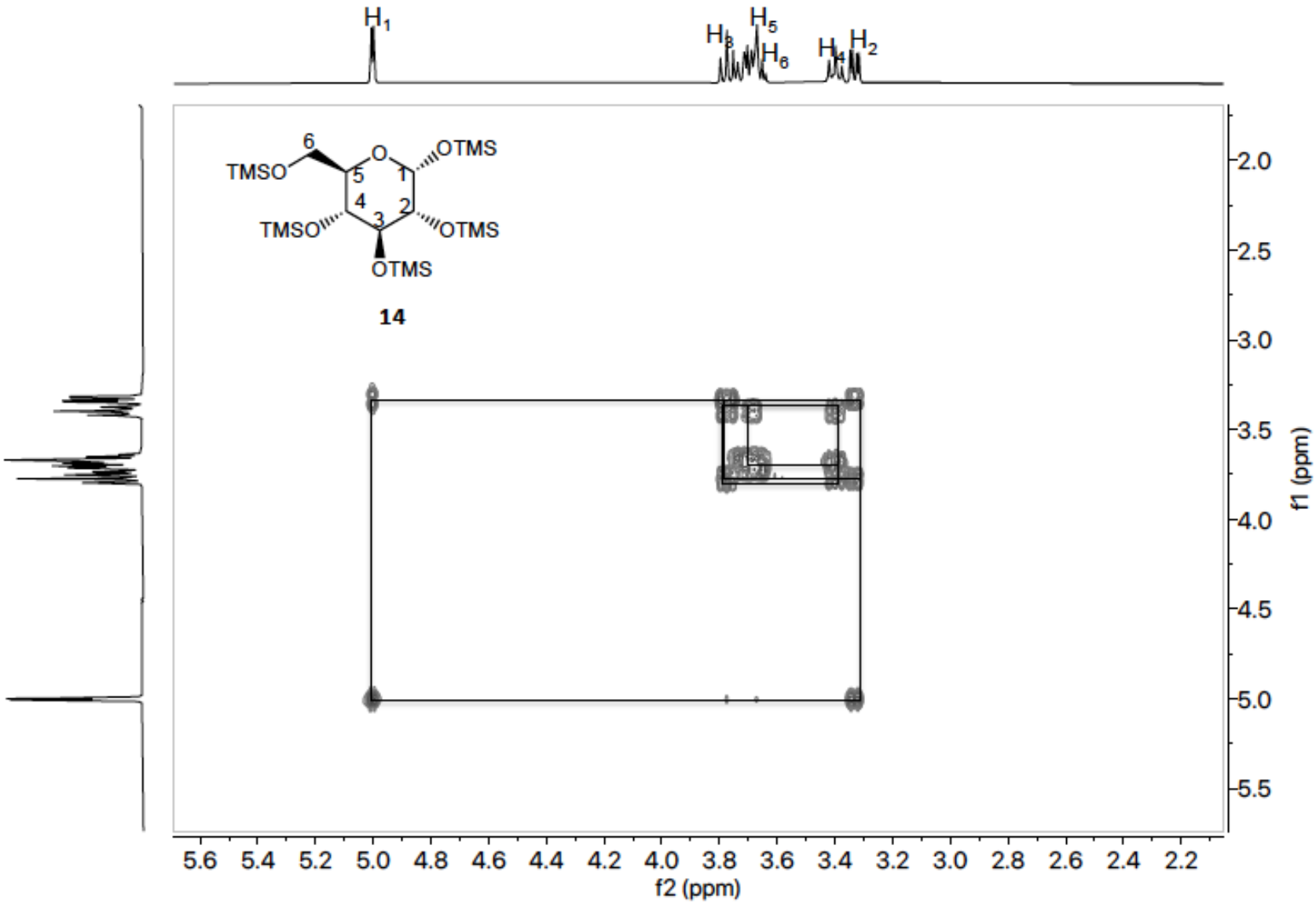

SI-Figure 1.11: per-α *O*-TMS-glucose (**14**) COSY NMR (400 MHz, $CDCl_3$) spectrum

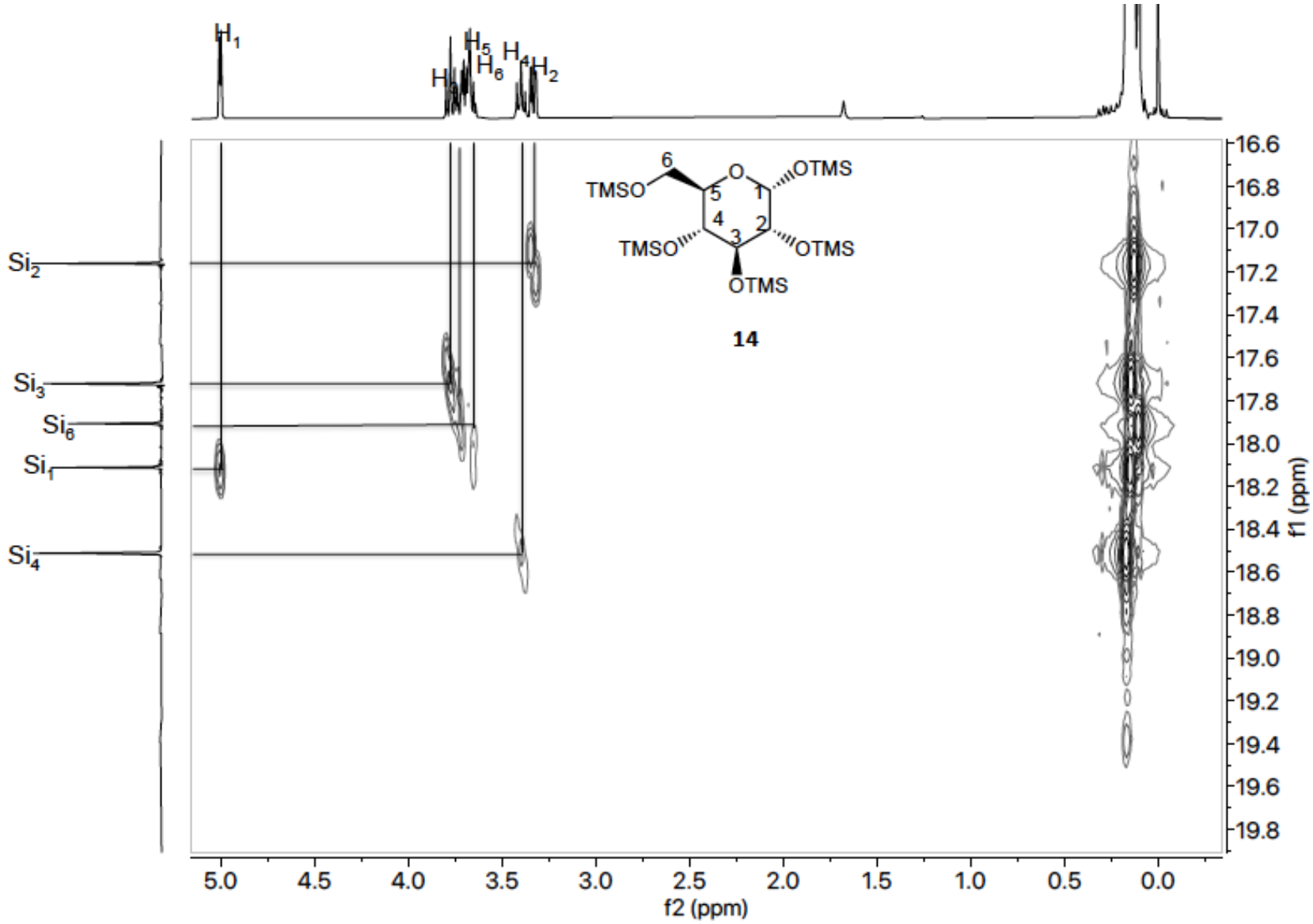

SI-Figure 1.12: per-α *O*-TMS-glucose (**14**) ^{1}H-^{29}Si HMBC NMR (400 MHz, $CDCl_3$) spectrum

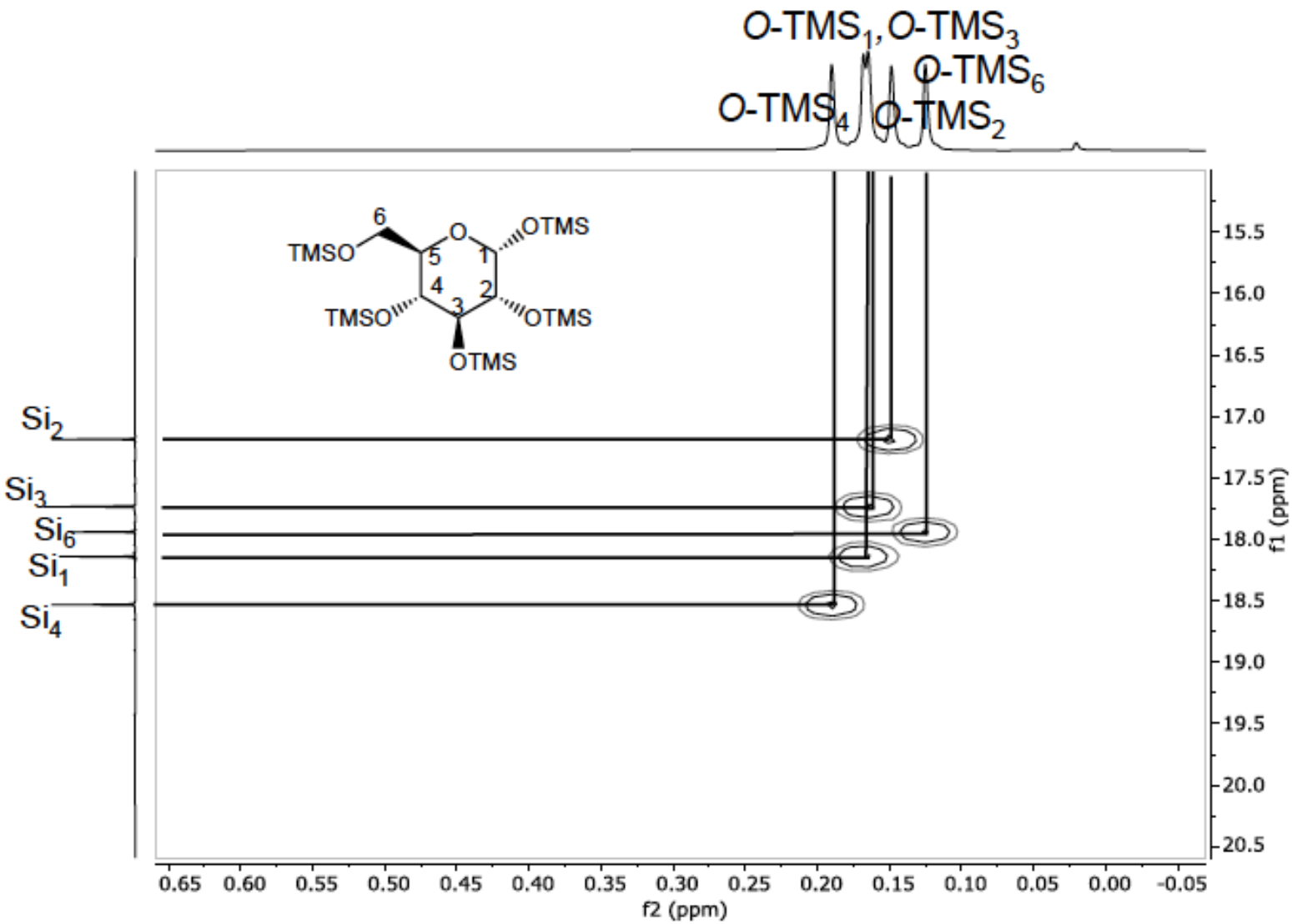

SI-Figure 1.13: per-α *O*-TMS-glucose (**14**) ^{1}H-^{29}Si HMBC NMR (400 MHz, $CDCl_3$) spectrum

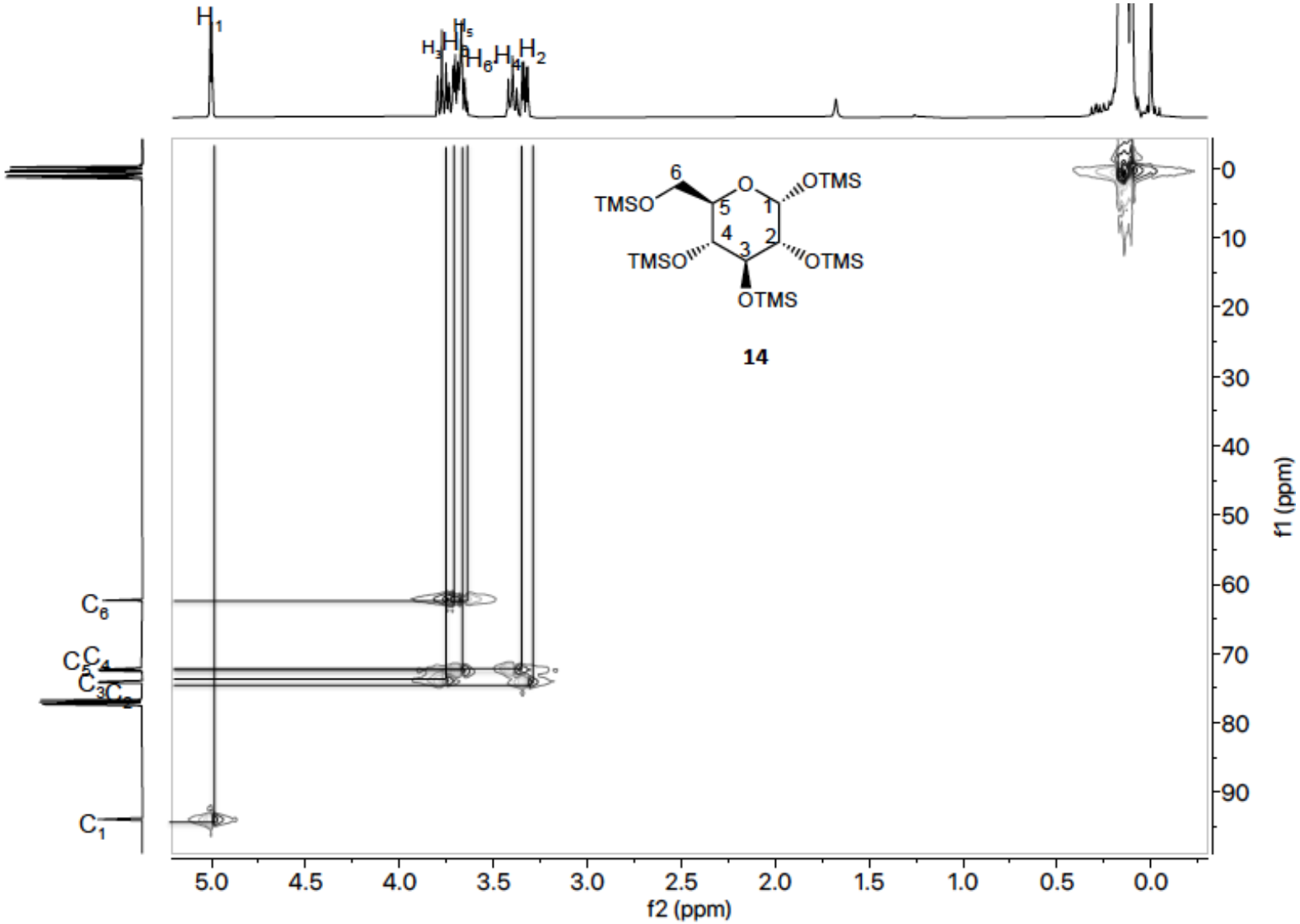

SI-Figure 1.14: per-α *O*-TMS-glucose (**14**) HSQC NMR (400 MHz, $CDCl_3$) spectrum

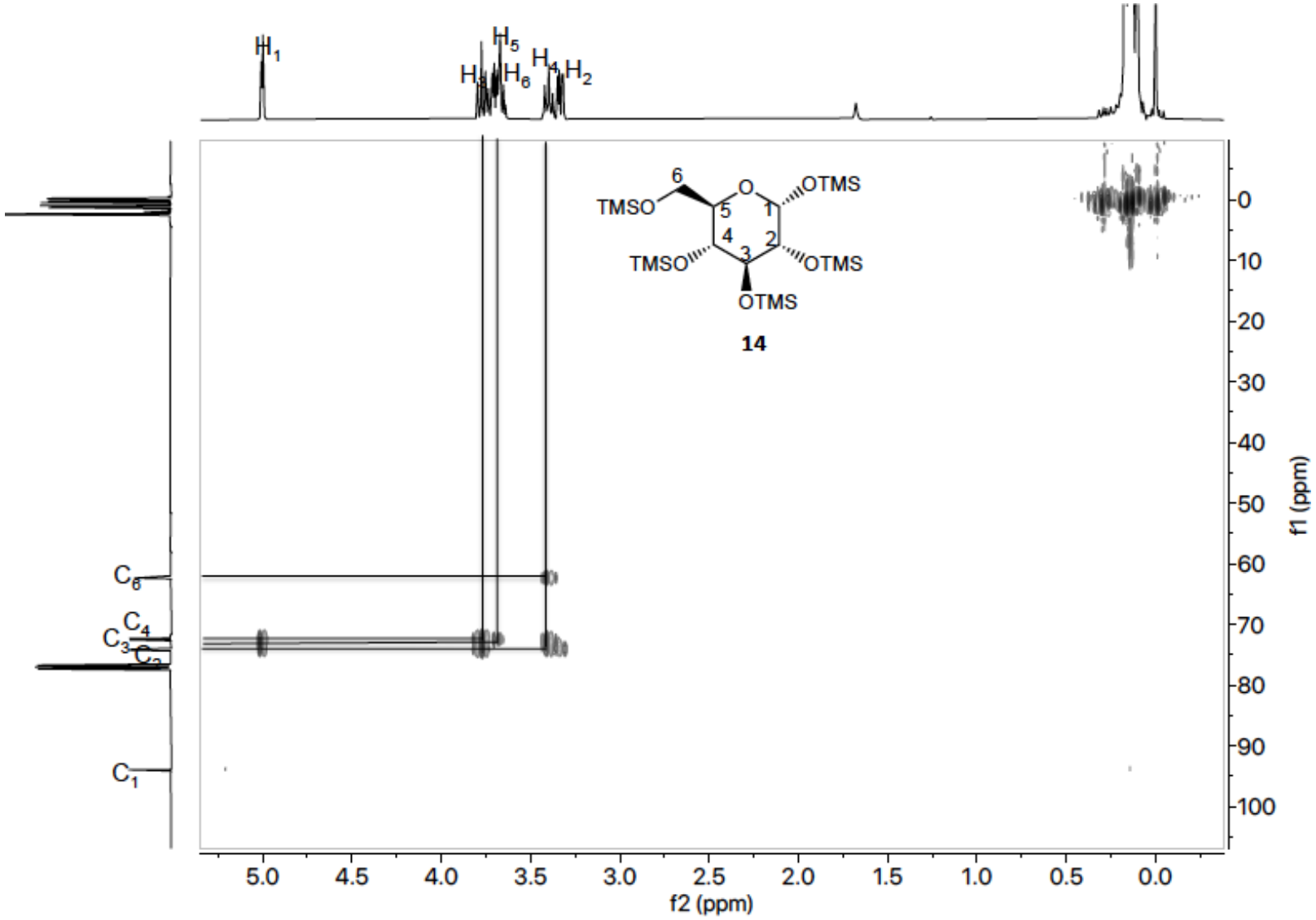

SI-Figure 1.15: per-α *O*-TMS-glucose (**14**) ^{1}H-^{13}C HMBC NMR (400 MHz, $CDCl_3$) spectrum

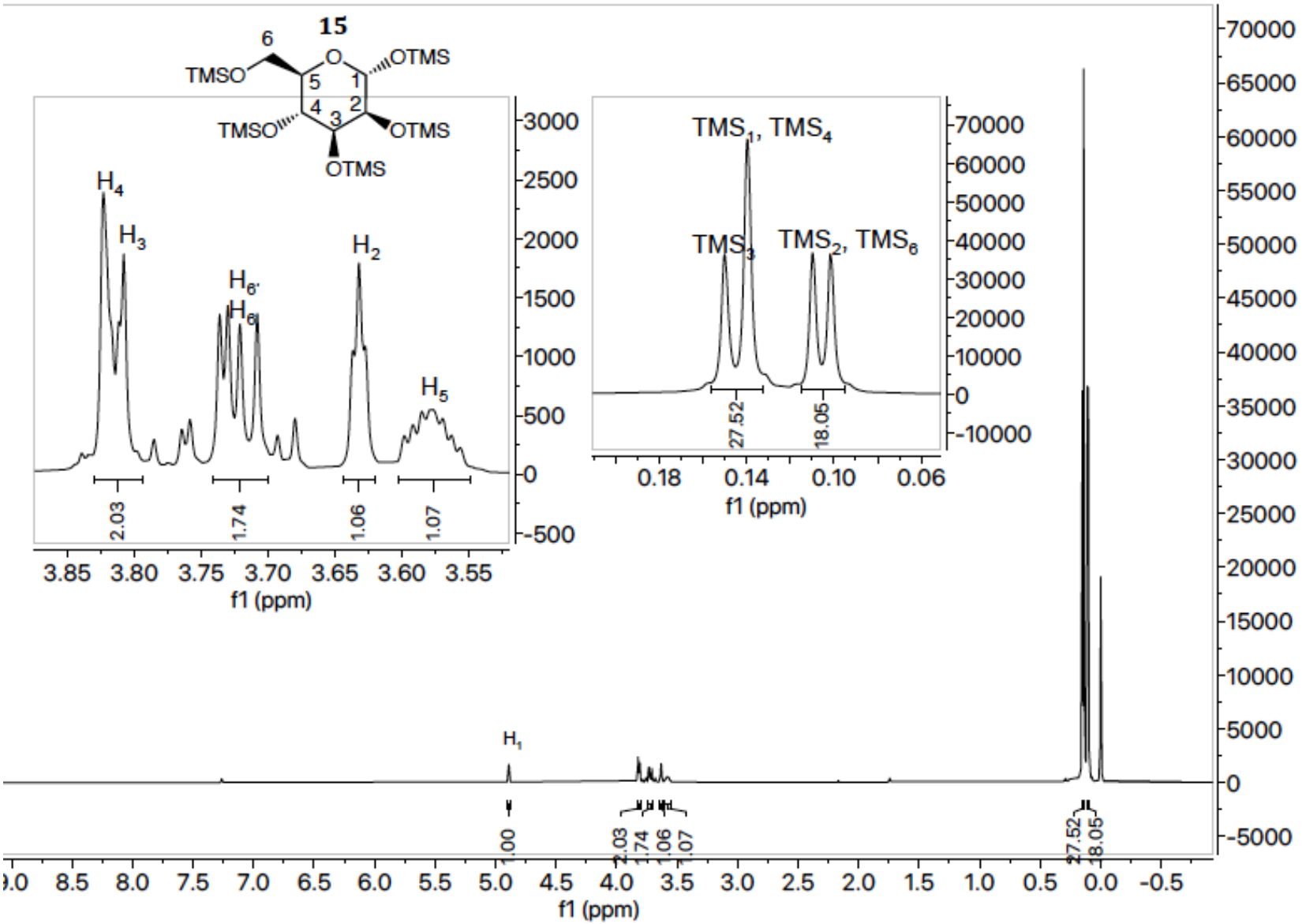

SI-Figure 1.15: per- α -*O*-TMS-mannose (**15**) ^{1}H NMR (400 MHz, $CDCl_3$) spectrum

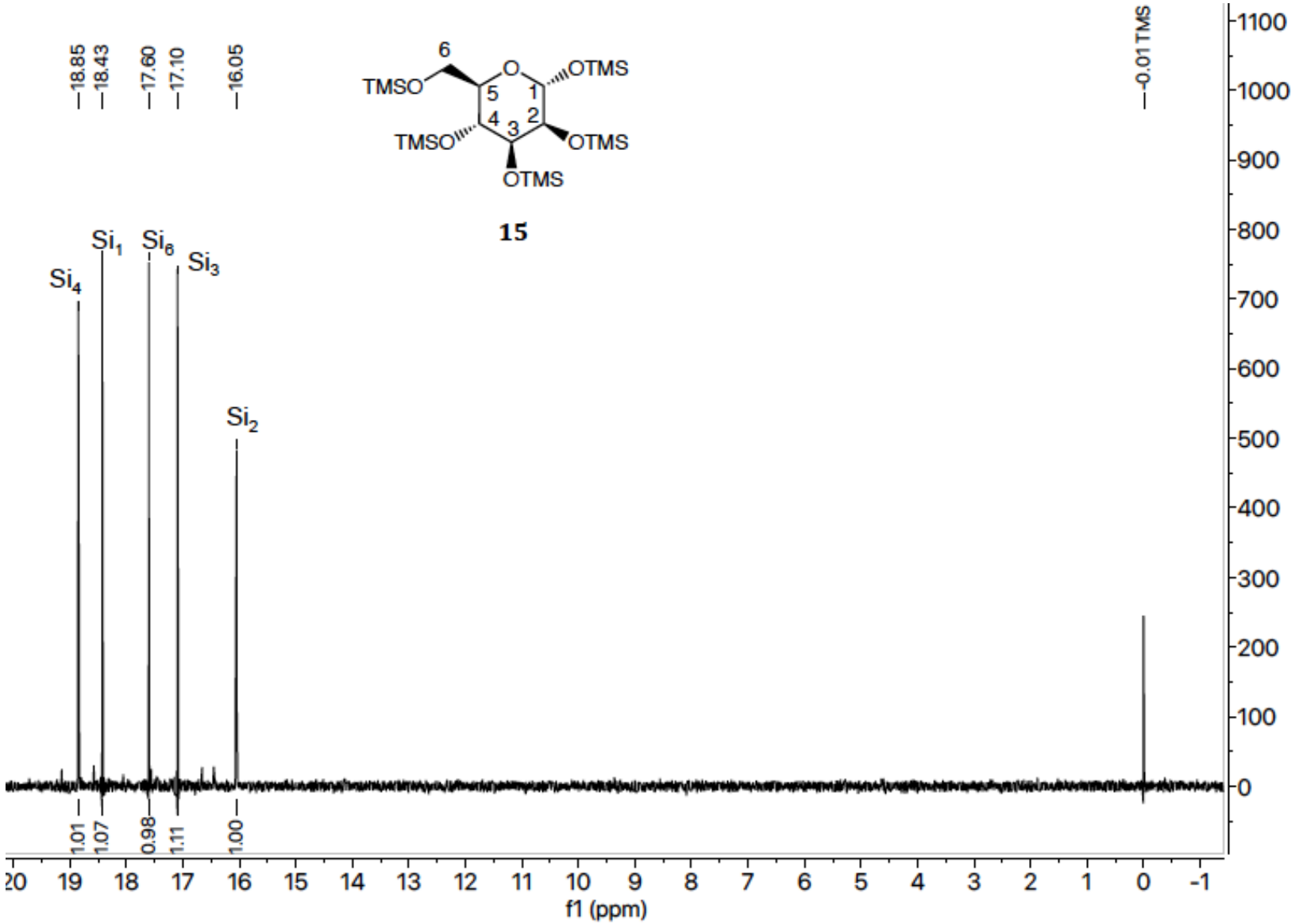

SI-Figure 1.16: per- α -*O*-TMS-mannose (**15**) ^{29}Si NMR (400 MHz, $CDCl_3$) spectrum

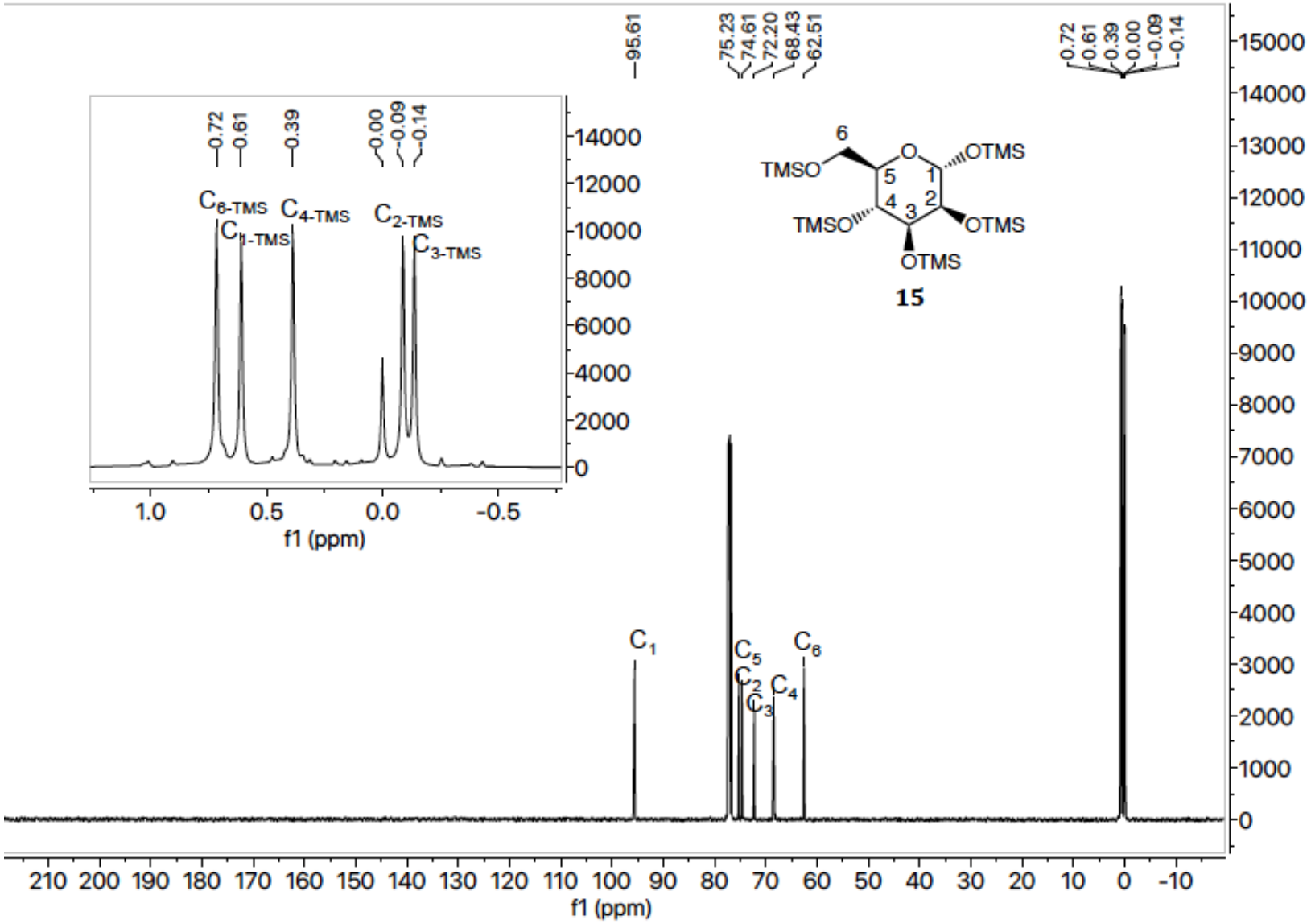

SI-Figure 1.17: per- α -*O*-TMS-mannose (**15**) ^{13}C NMR (400 MHz, $CDCl_3$) spectrum

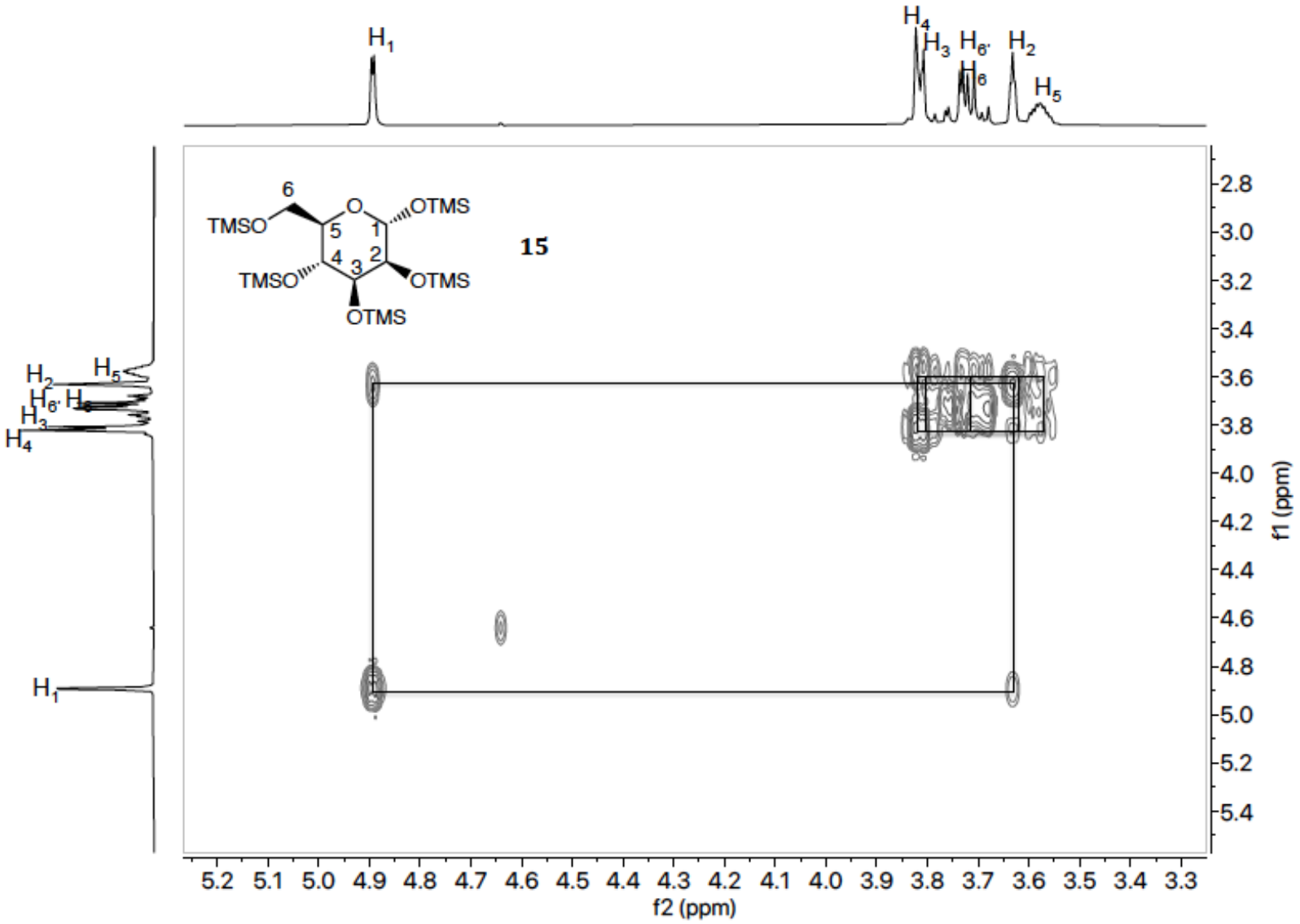

SI-Figure 1.18: per- α -*O*-TMS-mannose (**15**) COSY NMR (400 MHz, $CDCl_3$) spectrum

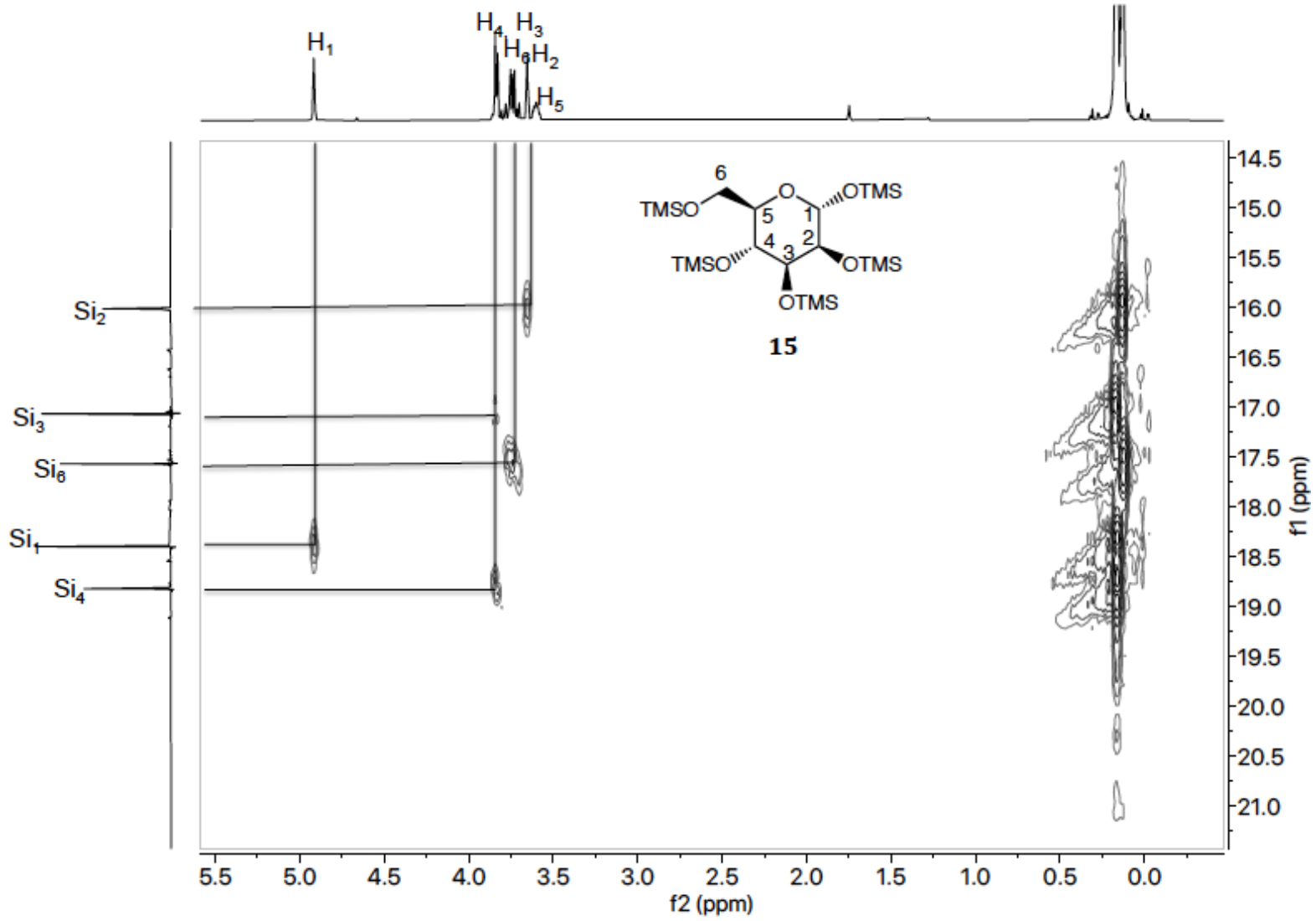

SI-Figure 1.19: per- α -*O*-TMS-mannose (**15**) ^{1}H-^{29}Si HMBC NMR (400 MHz, $CDCl_3$) spectrum

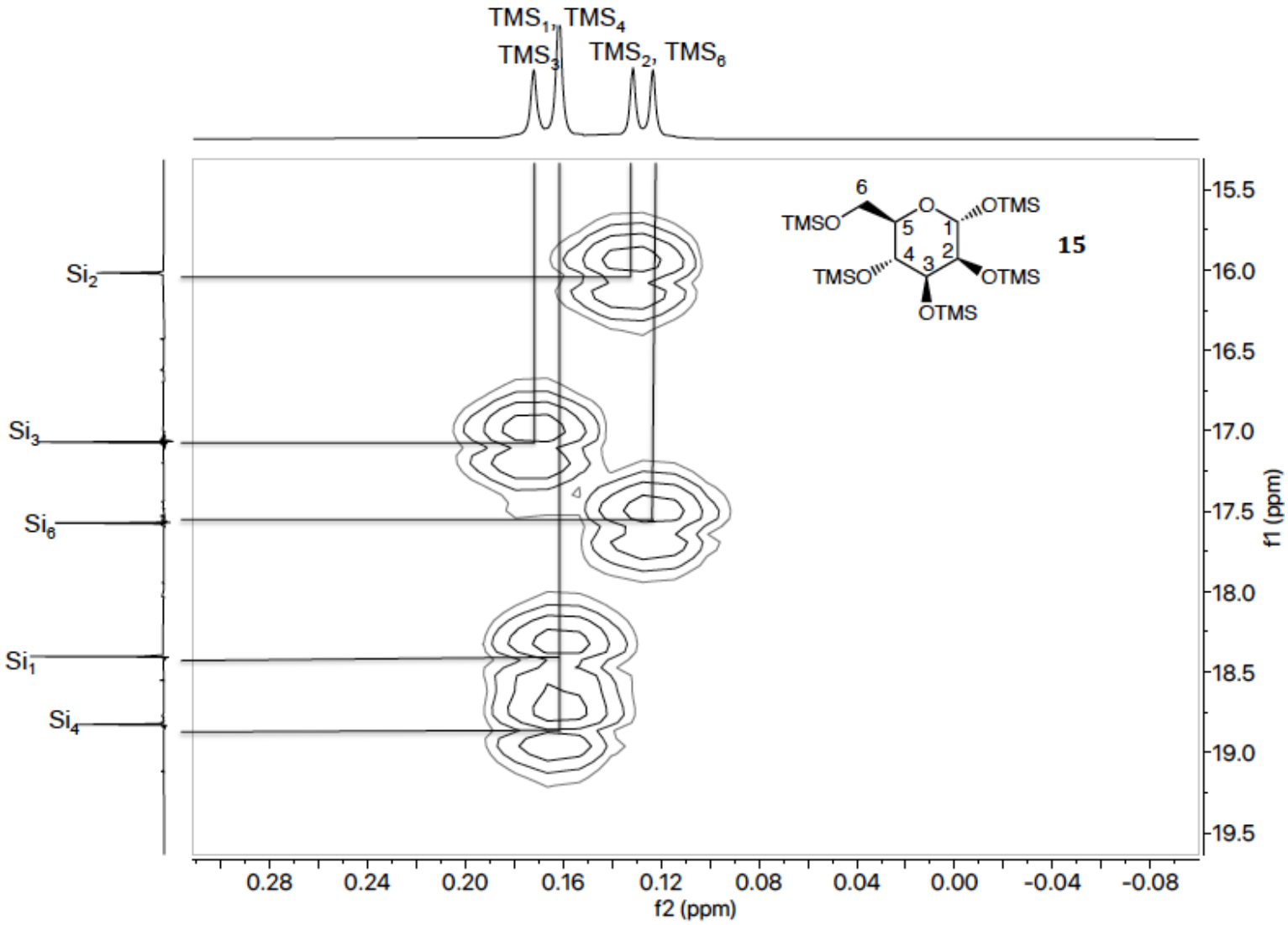

SI-Figure 1.20: per- α -*O*-TMS-mannose (**15**) ^{1}H-^{29}Si HMBC NMR (400 MHz, $CDCl_3$) spectrum (CH_3-Si region)

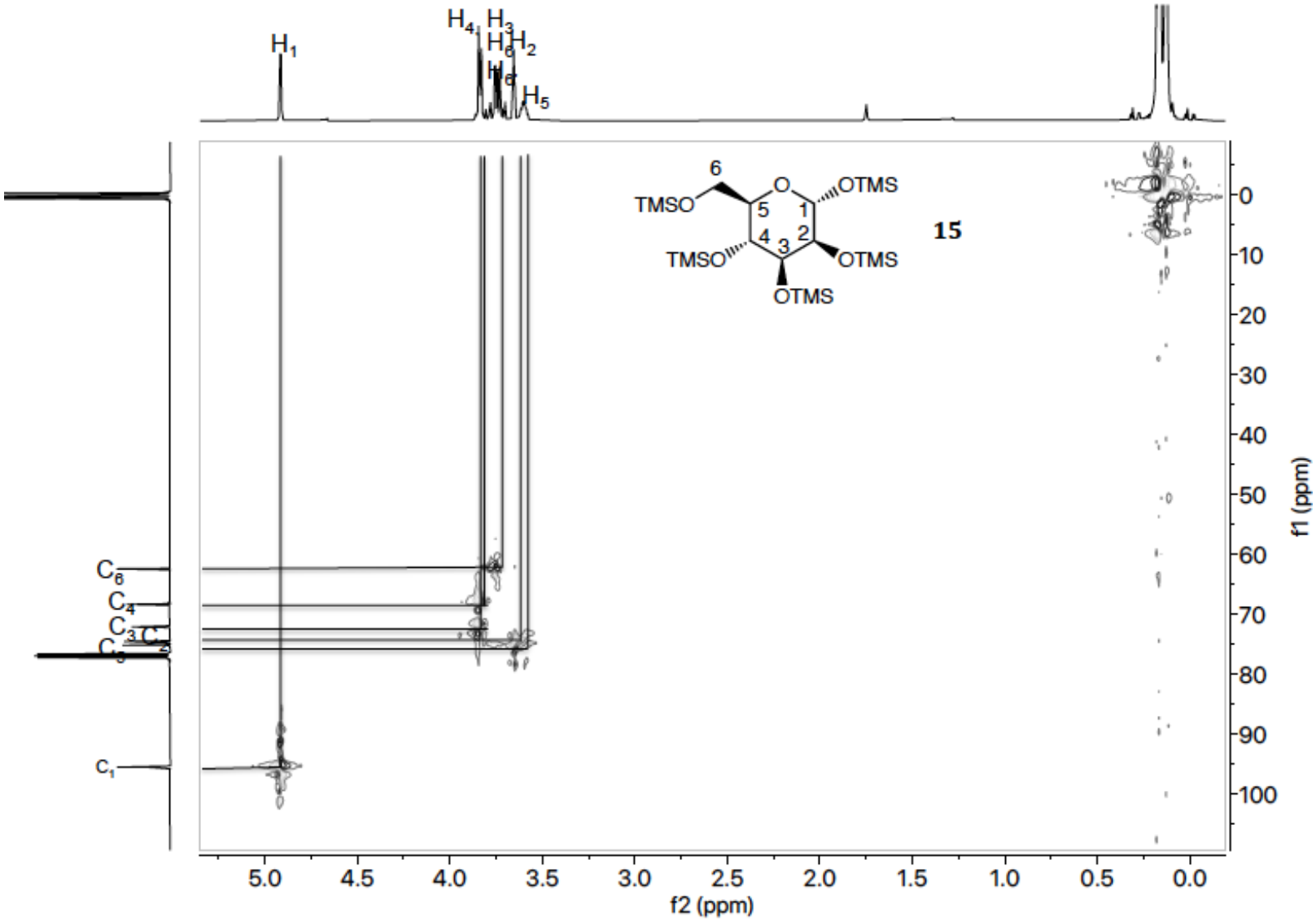

SI-Figure 1.21: per- α -*O*-TMS-mannose (**15**) ^{1}H-^{13}C HSQC NMR (400 MHz, $CDCl_3$) spectrum

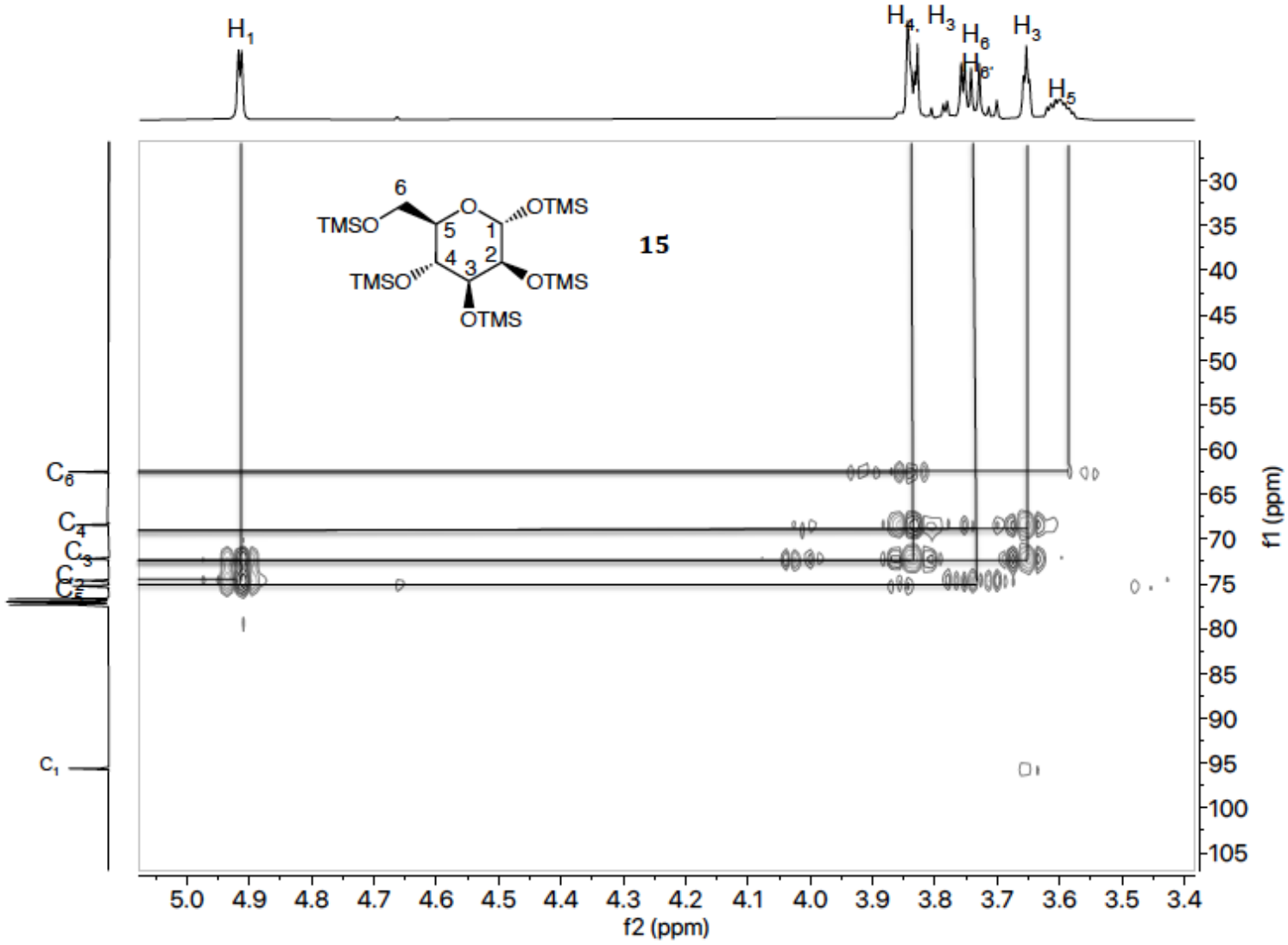

SI-Figure 1.22: per- α -*O*-TMS-mannose (**15**) ^{1}H-^{13}C HMBC NMR (400 MHz, $CDCl_3$) spectrum

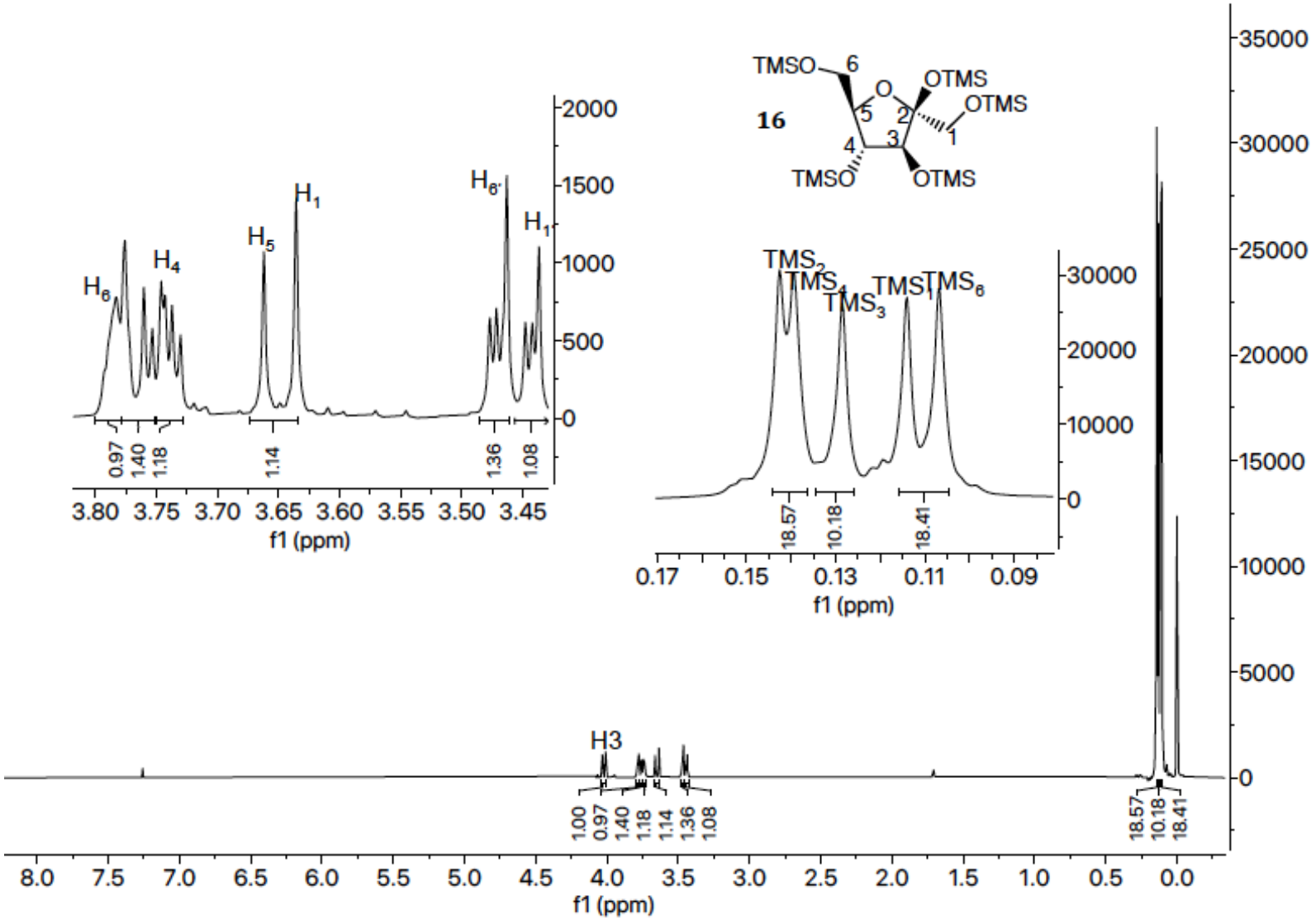

SI-Figure 1.23: β-per-*O*-TMS-fructose (**16**) ^{1}H NMR (400 MHz, $CDCl_3$) spectrum

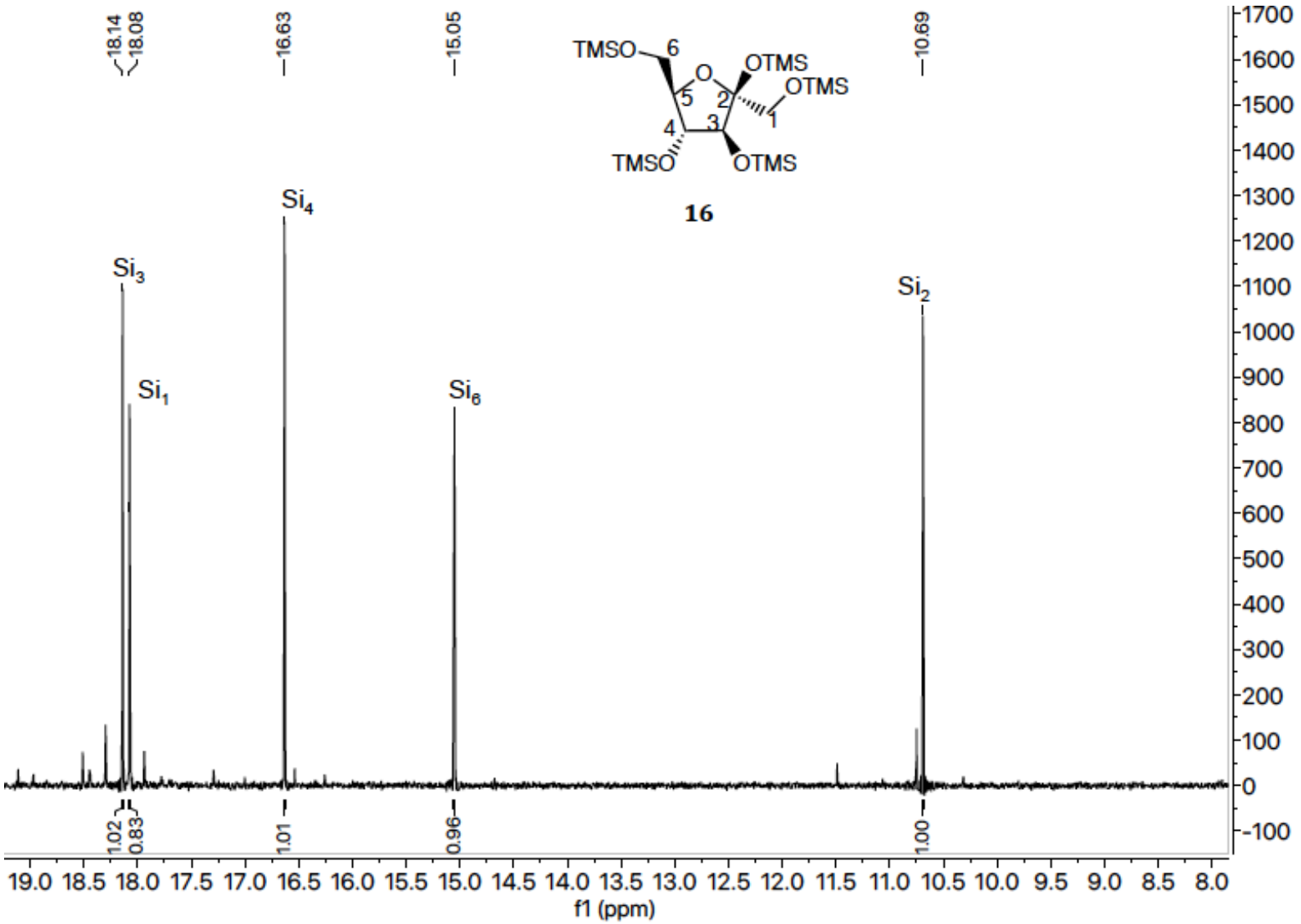

SI-Figure 1.24: β-per-*O*-TMS-fructose (**16**) ^{29}Si NMR (400 MHz, $CDCl_3$) spectrum

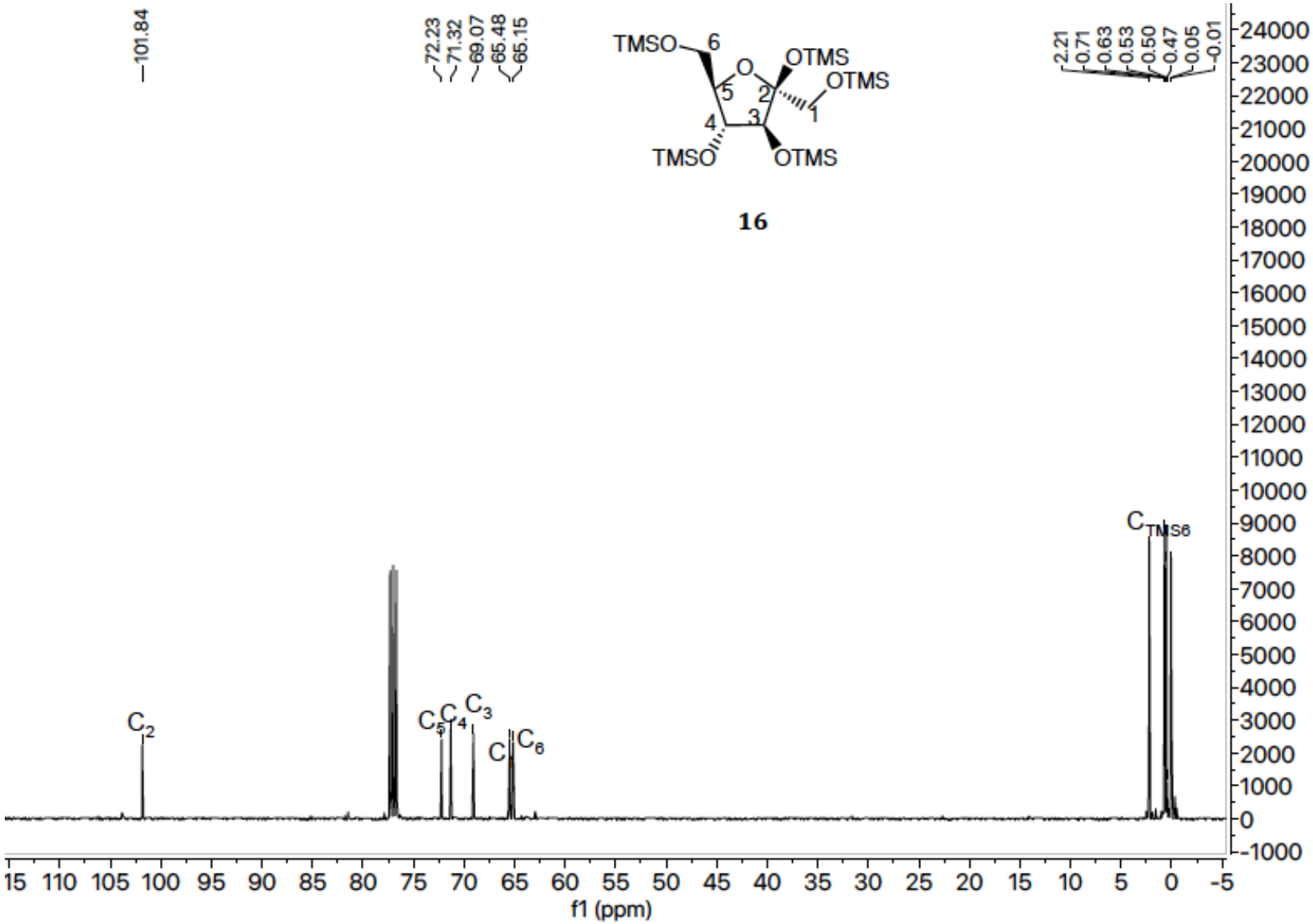

SI-Figure 1.25: β-per-*O*-TMS-fructose (**16**) ^{13}C NMR (400 MHz, $CDCl_3$) spectrum

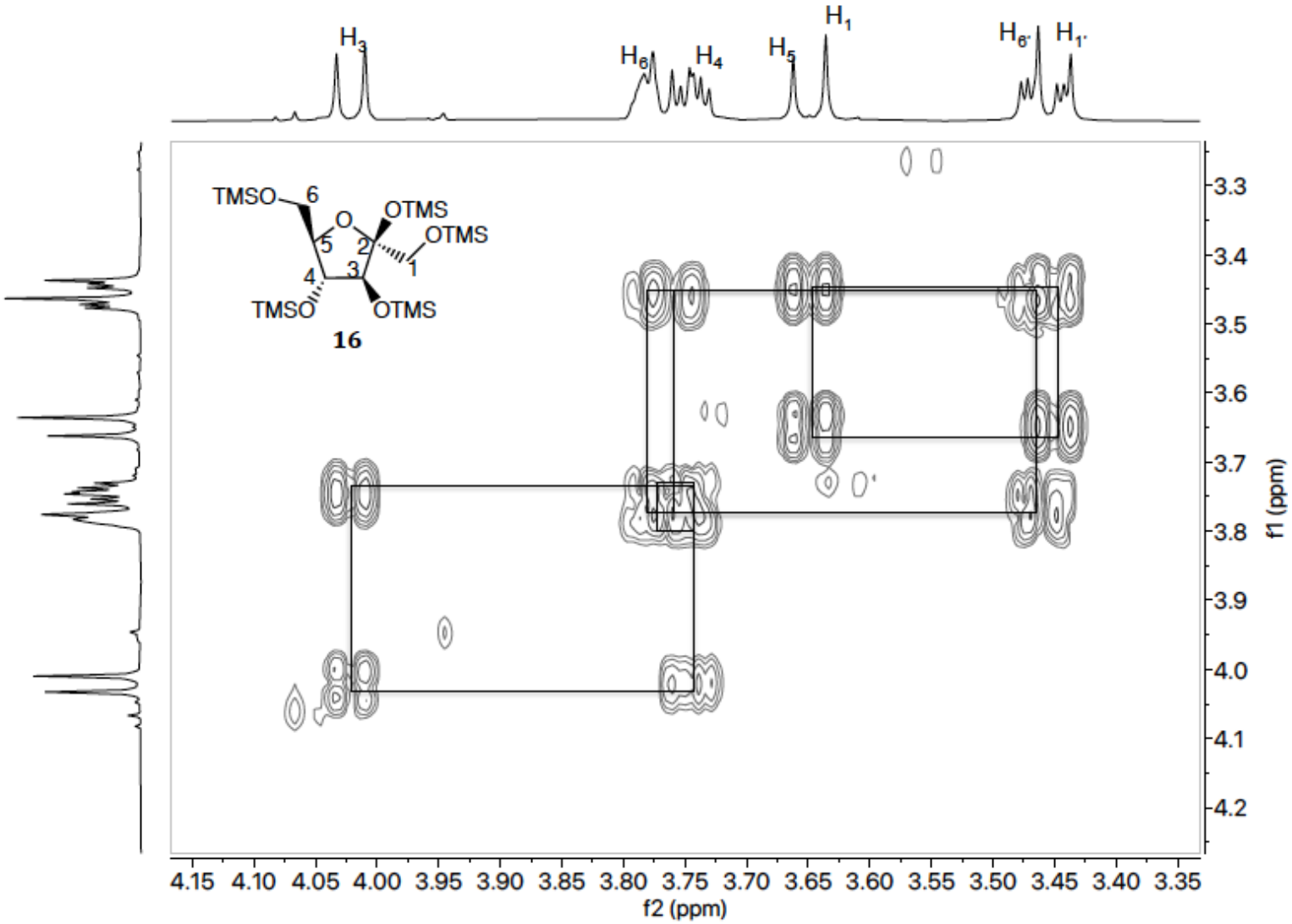

SI-Figure 1.26: β-per-*O*-TMS-fructose (**16**) COSY NMR (400 MHz, $CDCl_3$) spectrum

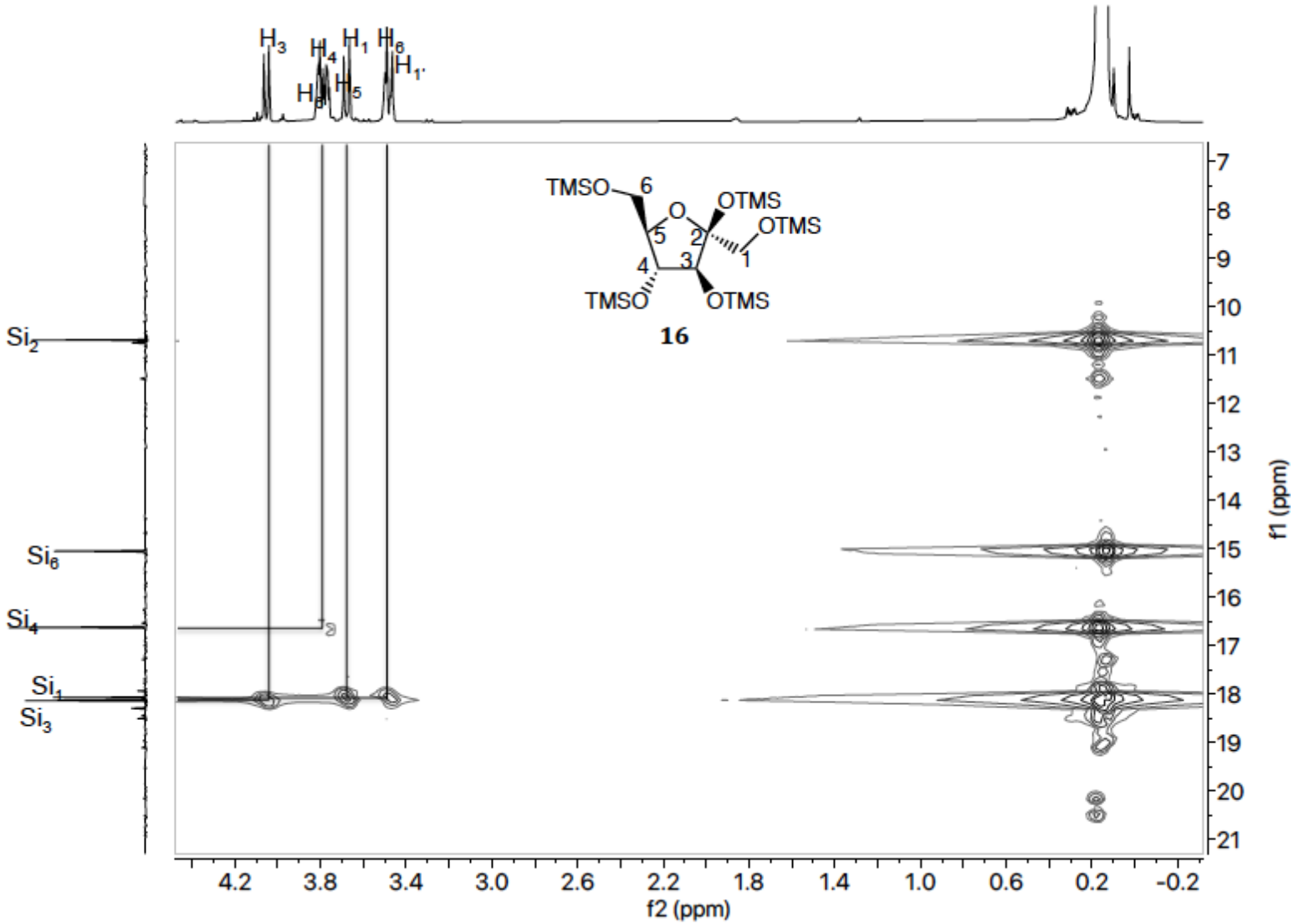

SI-Figure 1.27: β-per-*O*-TMS-fructose (**16**) ^{1}H-^{29}Si HMBC NMR (400 MHz, $CDCl_3$) spectrum

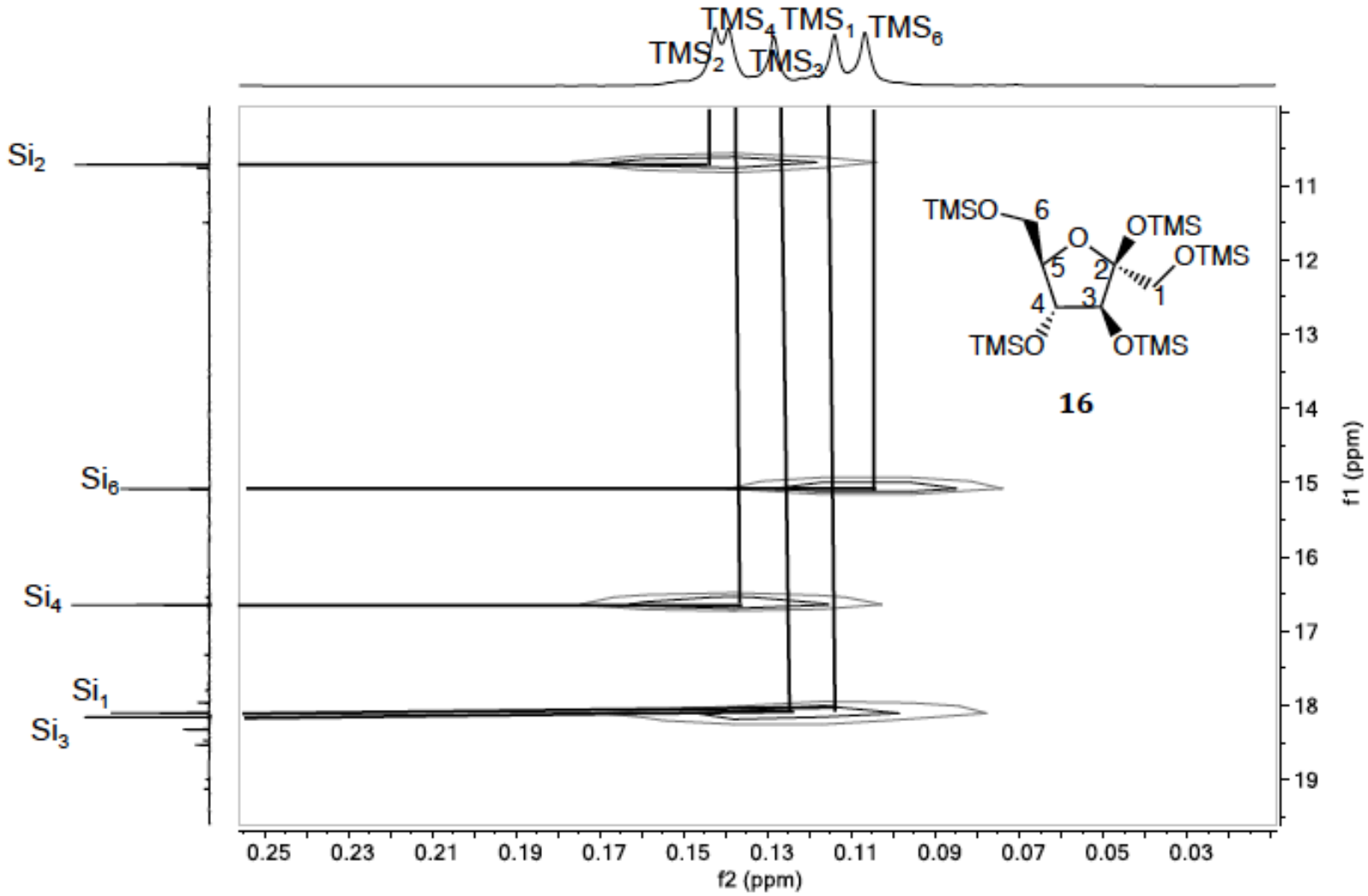

SI-Figure 1.28: β-per-*O*-TMS-fructose (**16**) ^{1}H-^{29}Si HMBC NMR (400 MHz, $CDCl_3$) spectrum (CH_3 region)

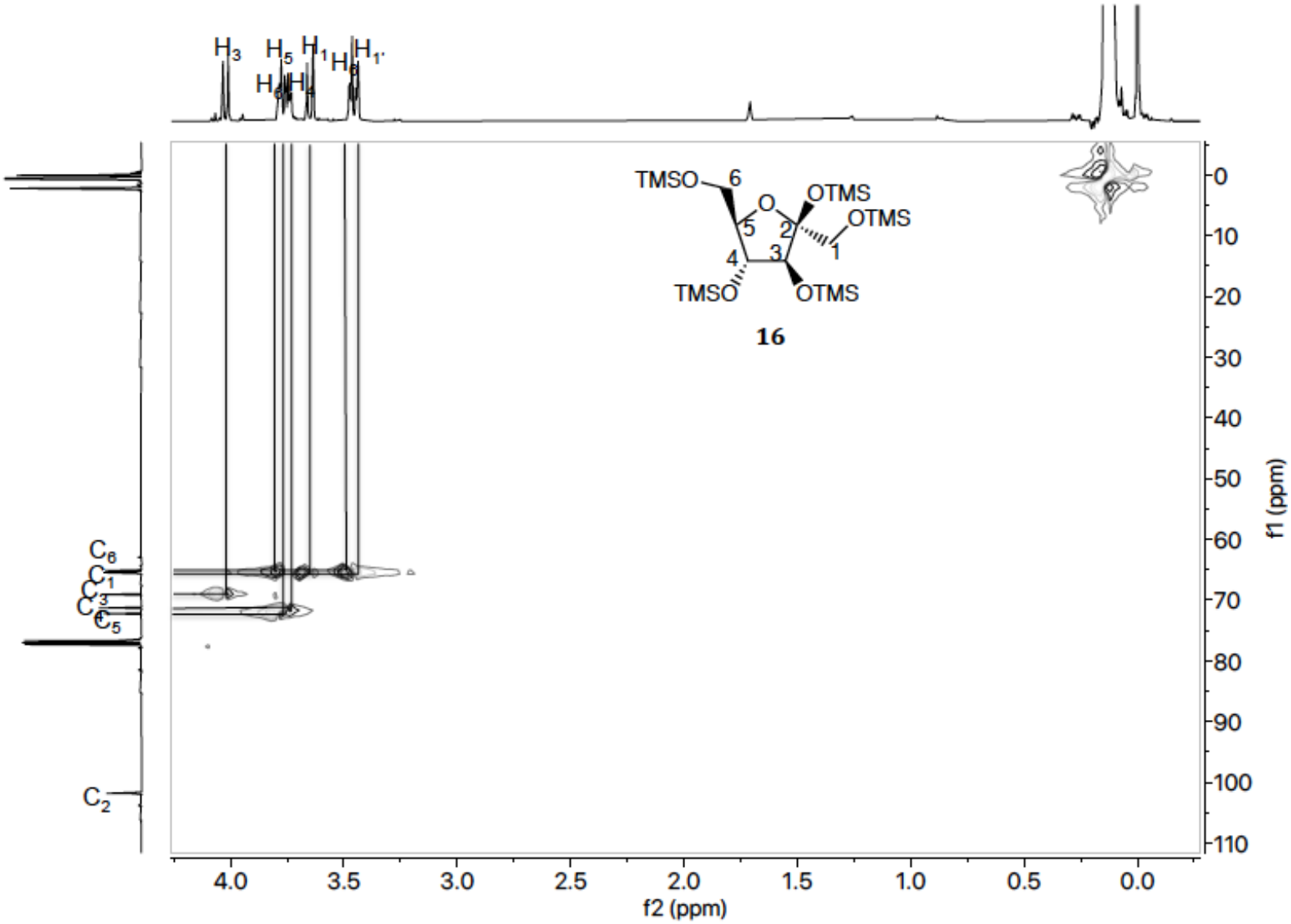

SI-Figure 1.29: β-per-*O*-TMS-fructose (**16**) HSQC NMR (400 MHz, $CDCl_3$) spectrum

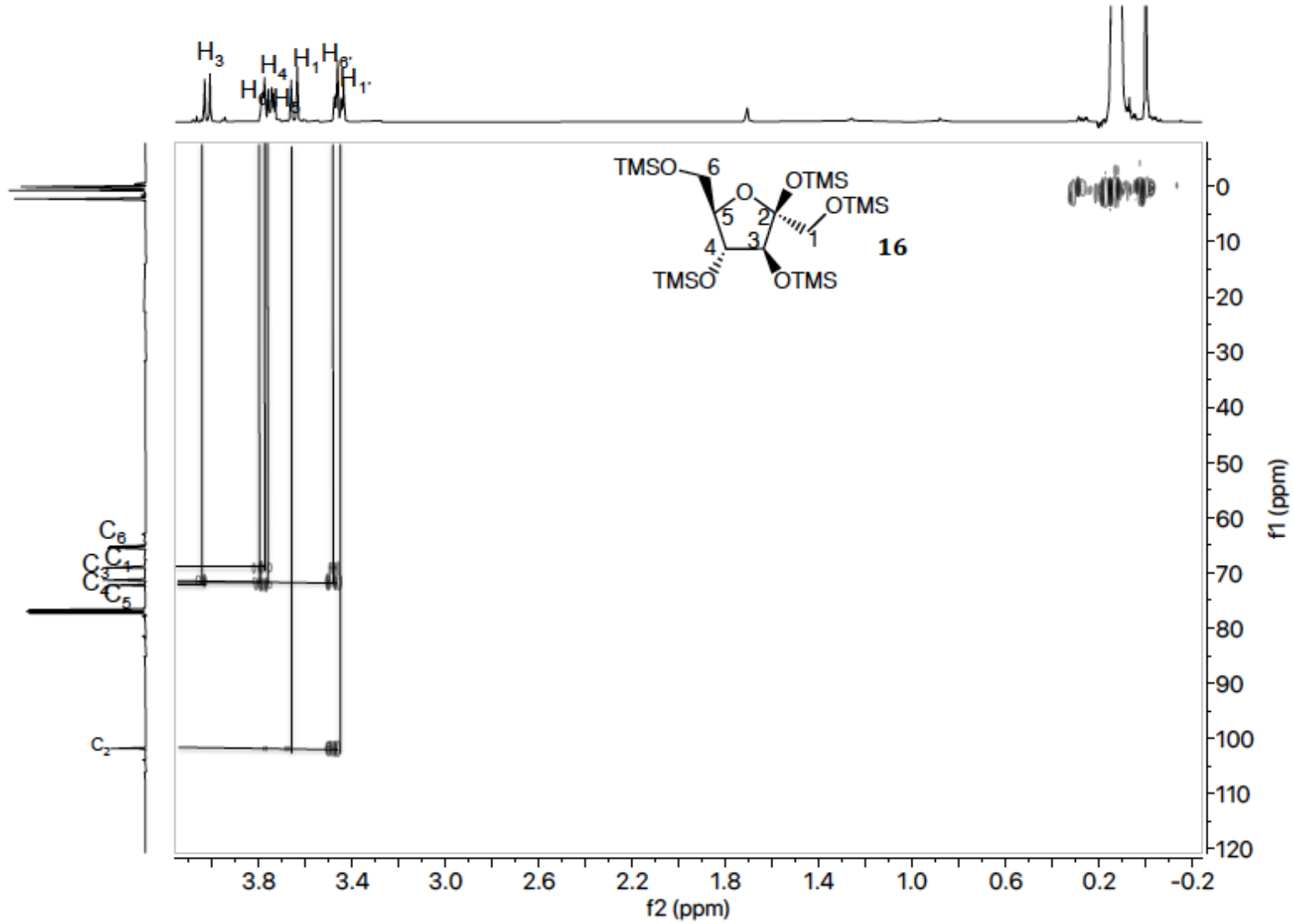

SI-Figure 1.30: β-per-*O*-TMS-fructose (**16**) ^{1}H-^{13}C HMBC NMR (400 MHz, $CDCl_3$) spectrum

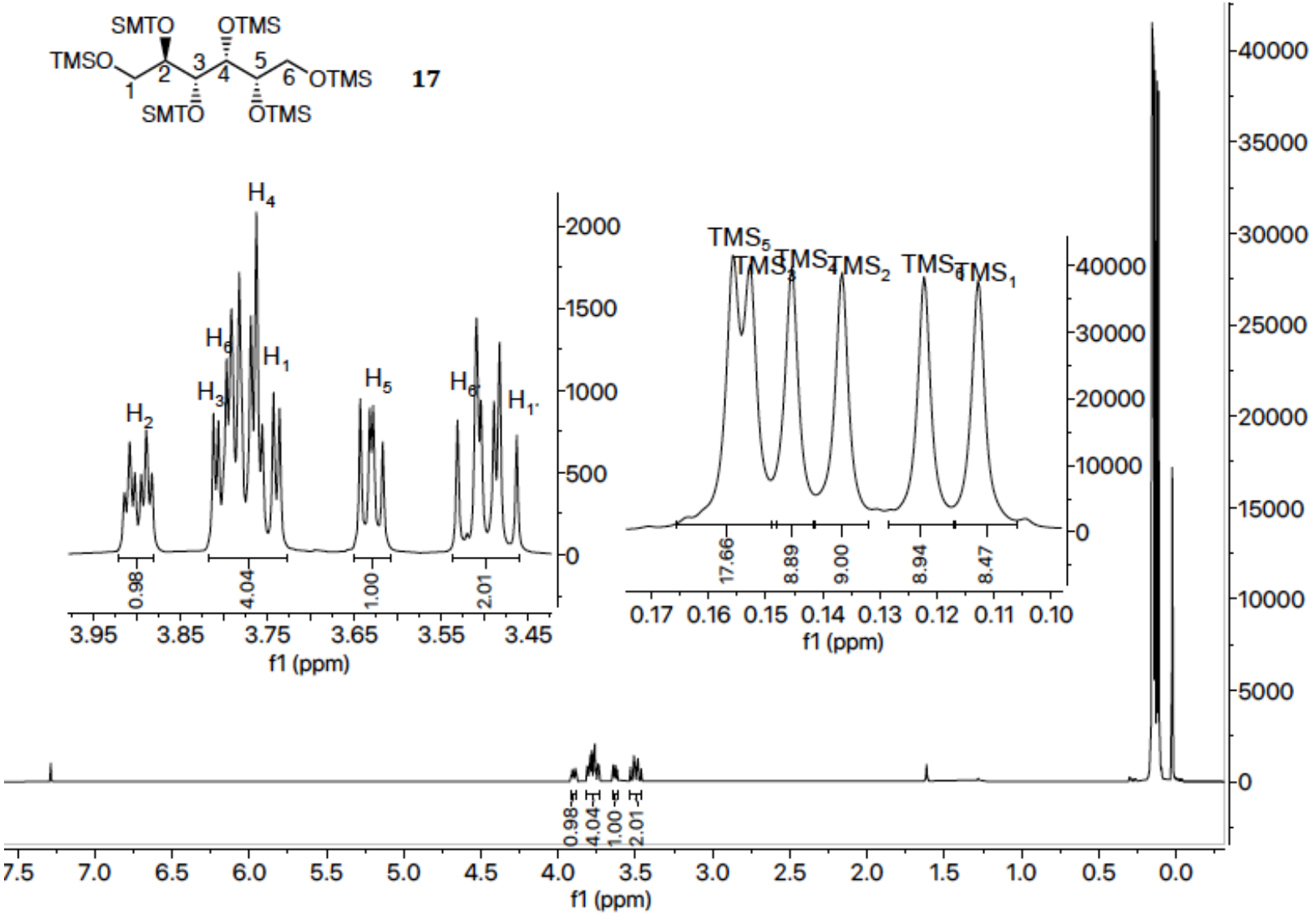

SI-Figure 1.31: per-*O*-TMS-sorbitol (**17**)^{1}H NMR (400 MHz, $CDCl_3$) spectrum

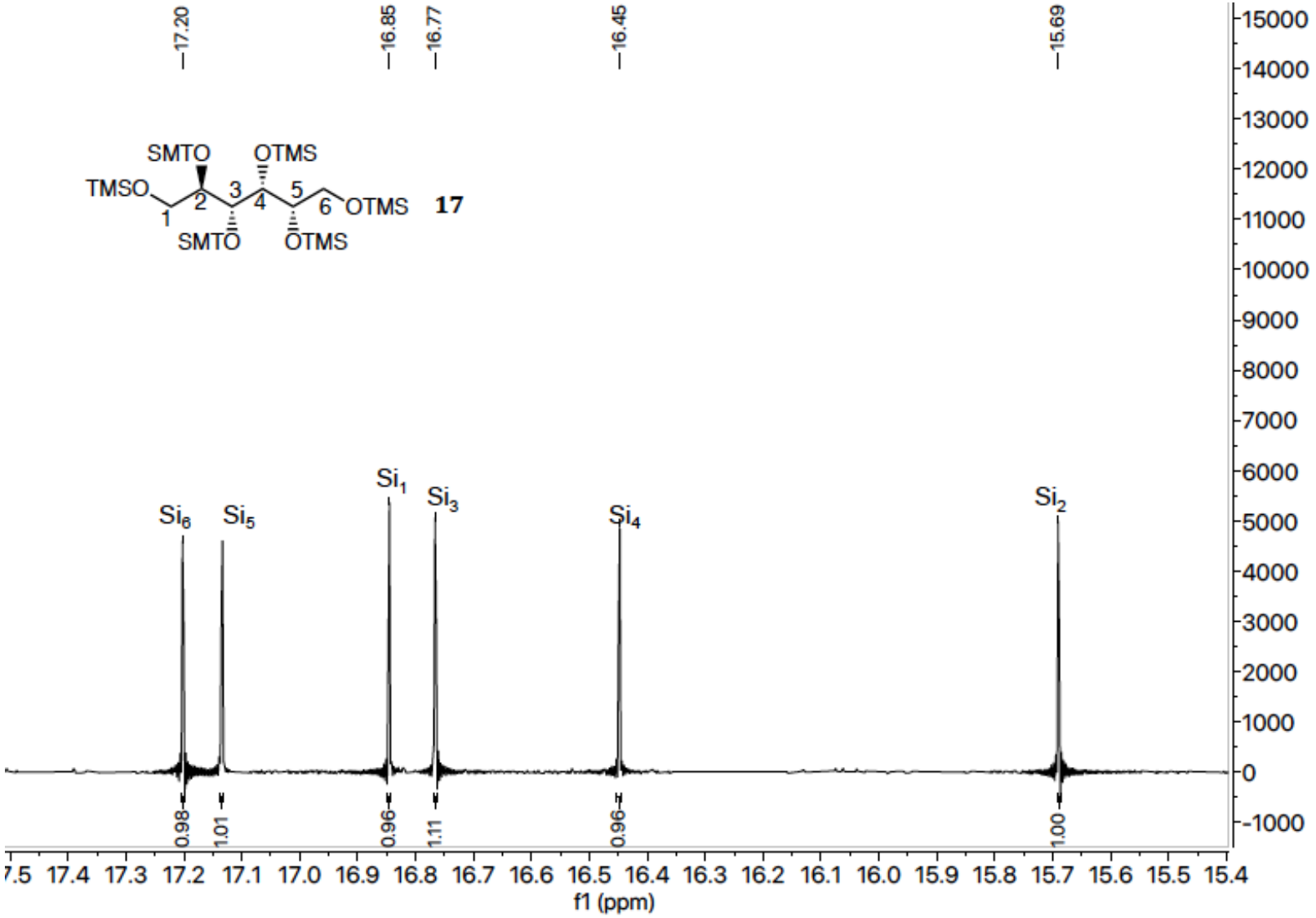

SI-Figure 1.32: per-*O*-TMS-sorbitol (**17**) ^{29}Si NMR (400 MHz, $CDCl_3$) spectrum

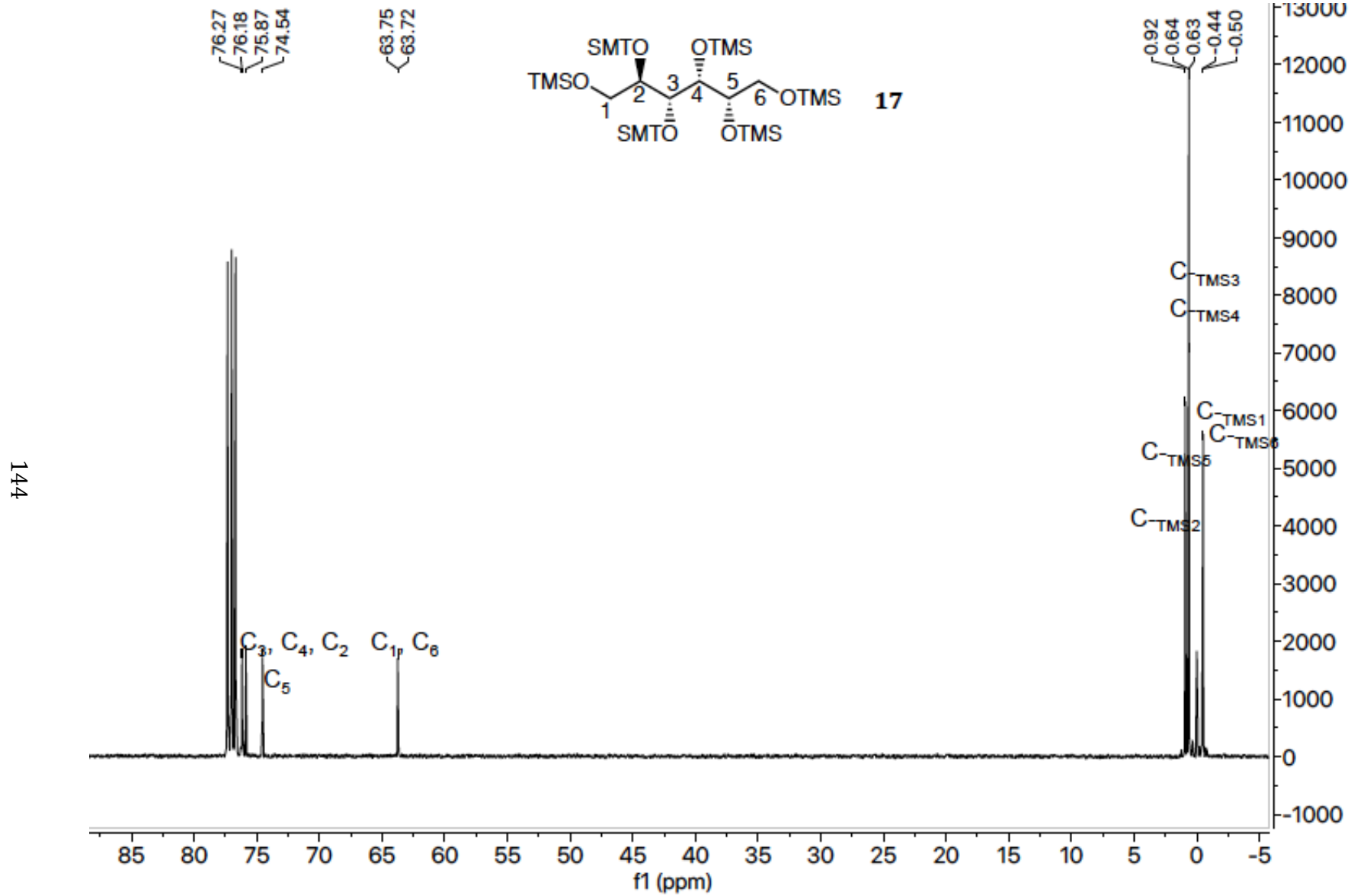

SI-Figure 1.33: per-*O*-TMS-sorbitol (**17**) ^{13}C NMR (400 MHz, $CDCl_3$) spectrum

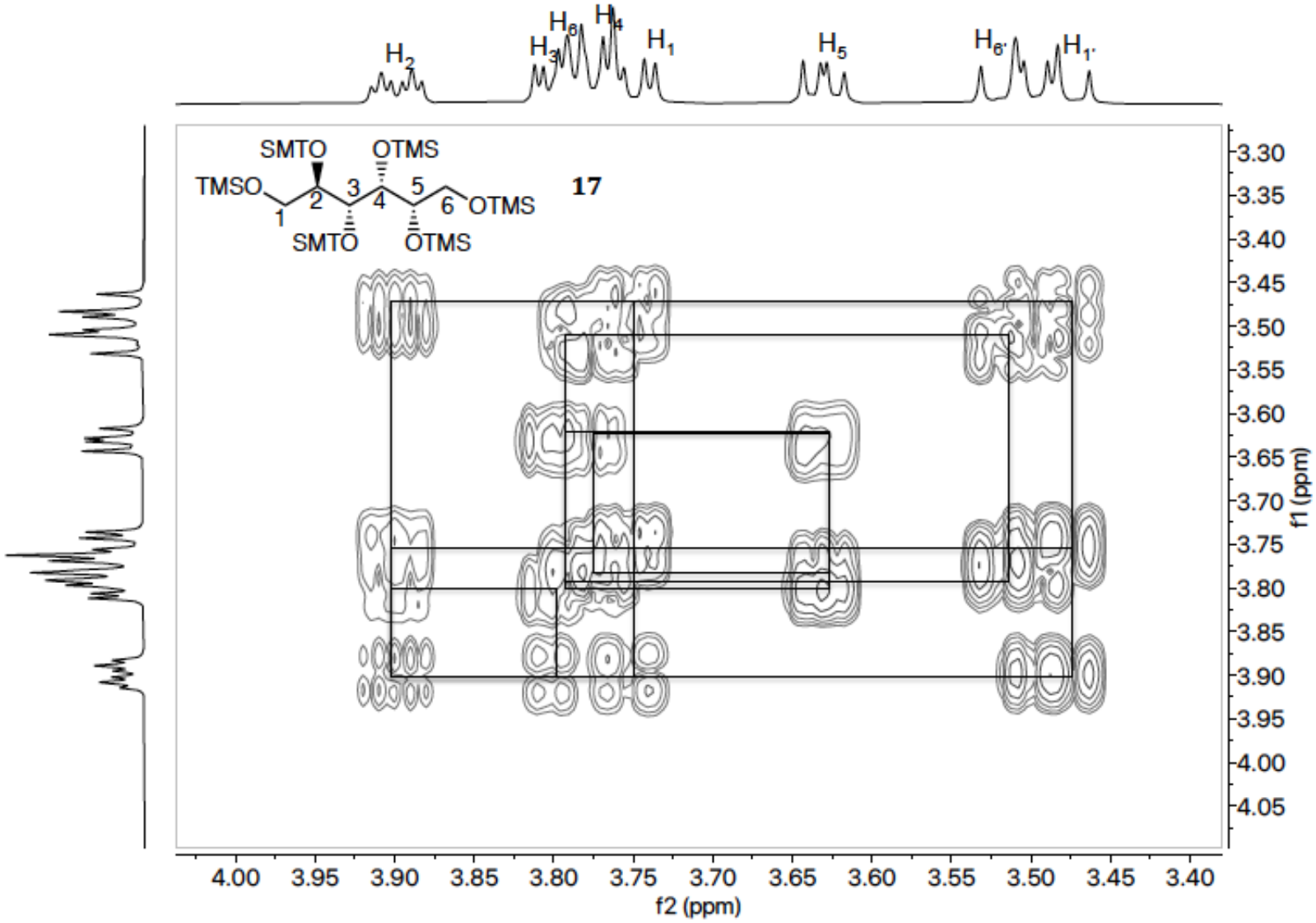

SI-Figure 1.34: per-*O*-TMS-sorbitol (**17**) COSY NMR (400 MHz, $CDCl_3$) spectrum

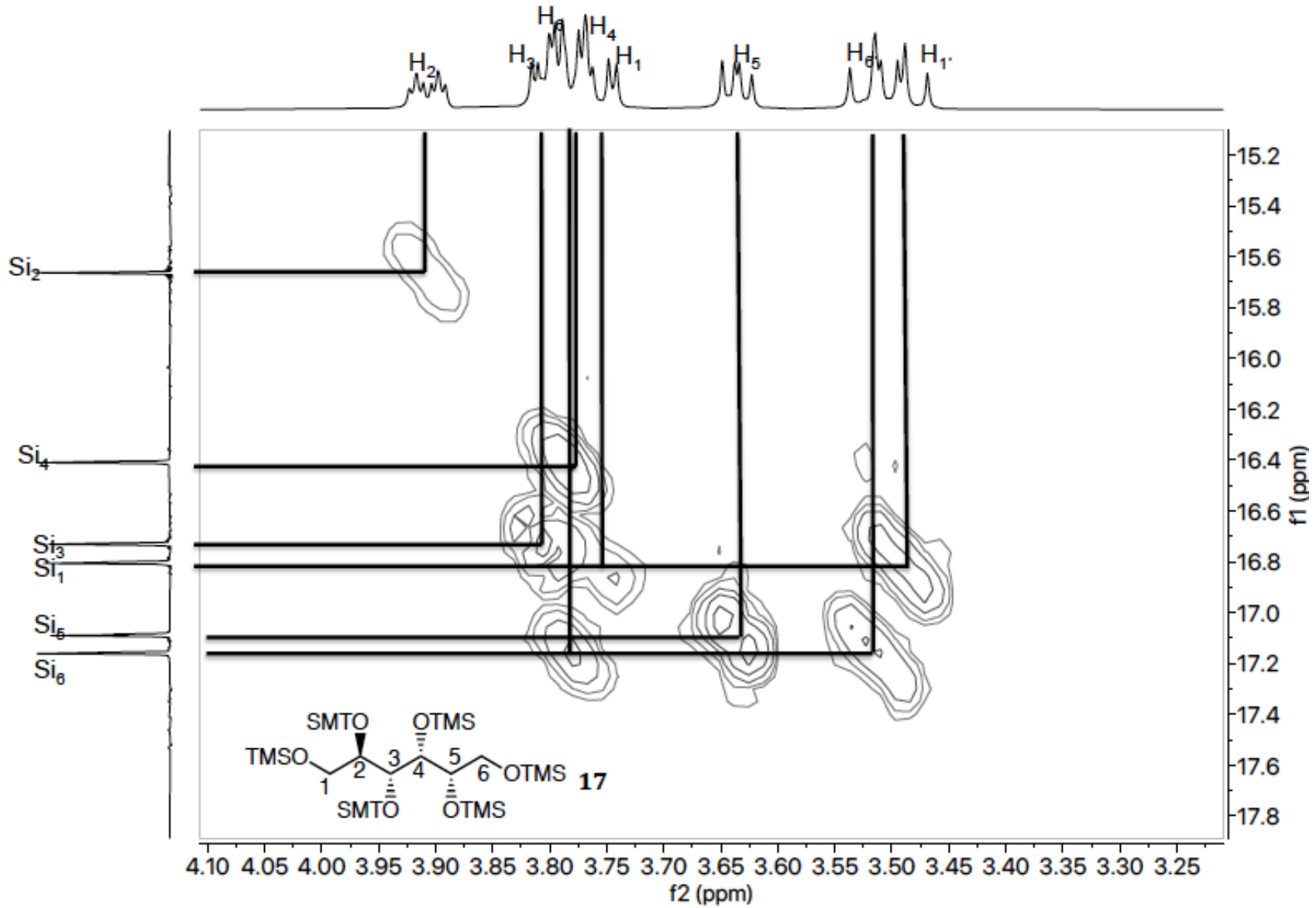

SI-Figure 1.35: per-*O*-TMS-sorbitol (**17**) ^{1}H-^{29}Si HMBC NMR (400 MHz, $CDCl_3$) spectrum

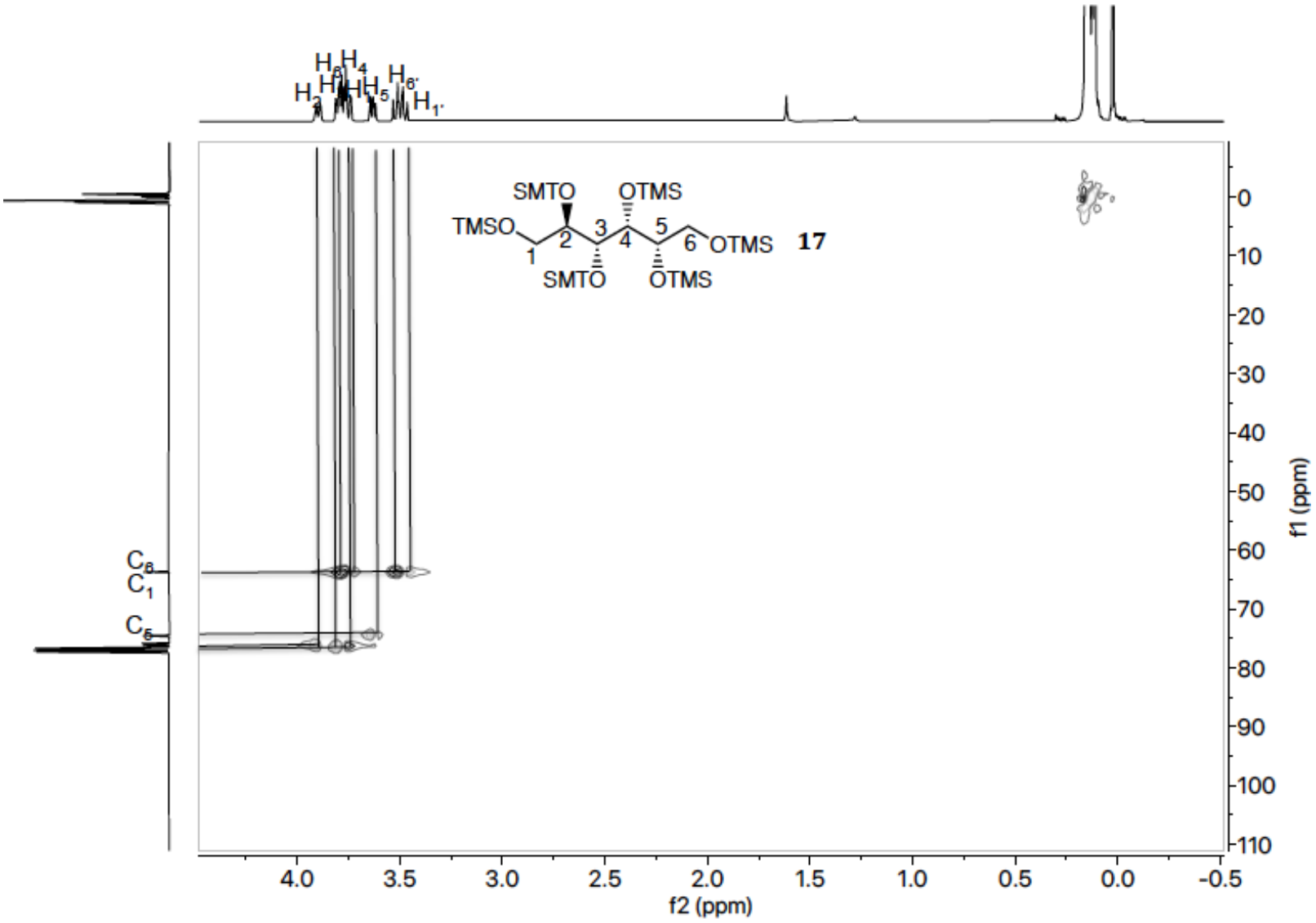

SI-Figure 1.36: per-*O*-TMS-sorbitol (**17**) HSQC NMR (400 MHz, $CDCl_3$) spectrum

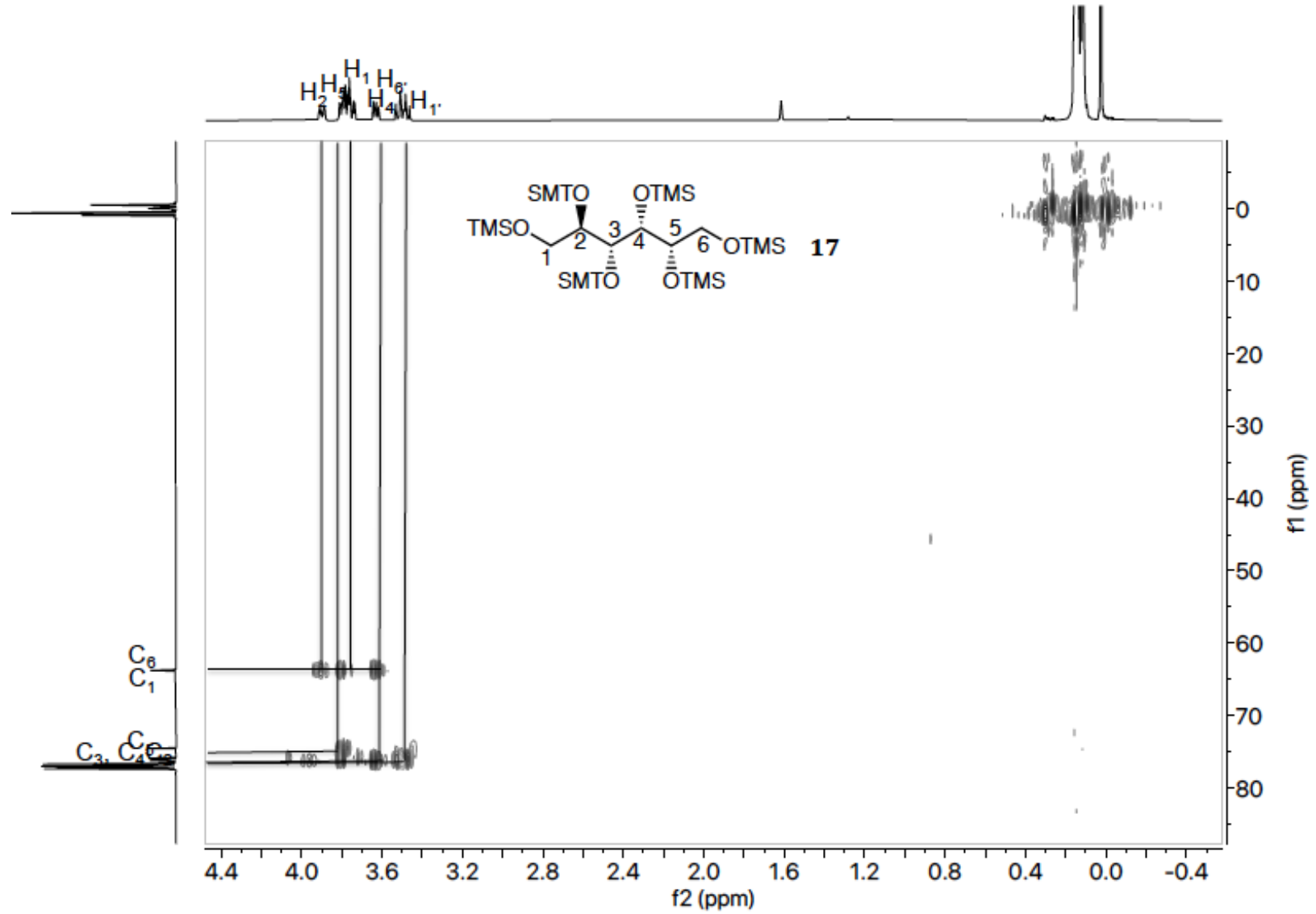

SI-Figure 1.37: per-*O*-TMS-sorbitol (**17**)^{1}H-^{13}C HMBC NMR (400 MHz, $CDCl_3$) spectrum

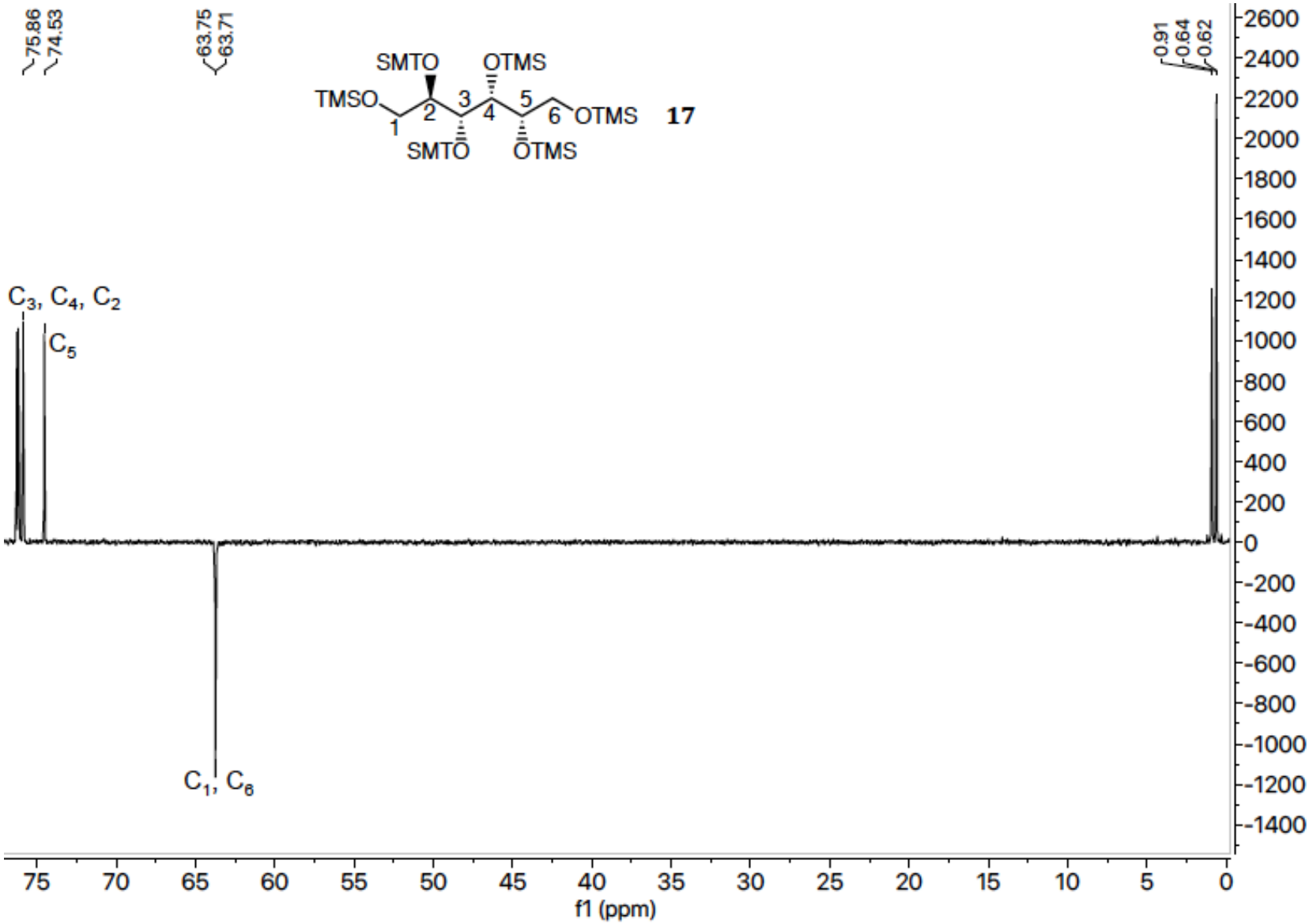

SI-Figure 1.38: per-*O*-TMS-sorbitol (**17**) DEPT-135 NMR (400 MHz, $CDCl_3$) spectrum

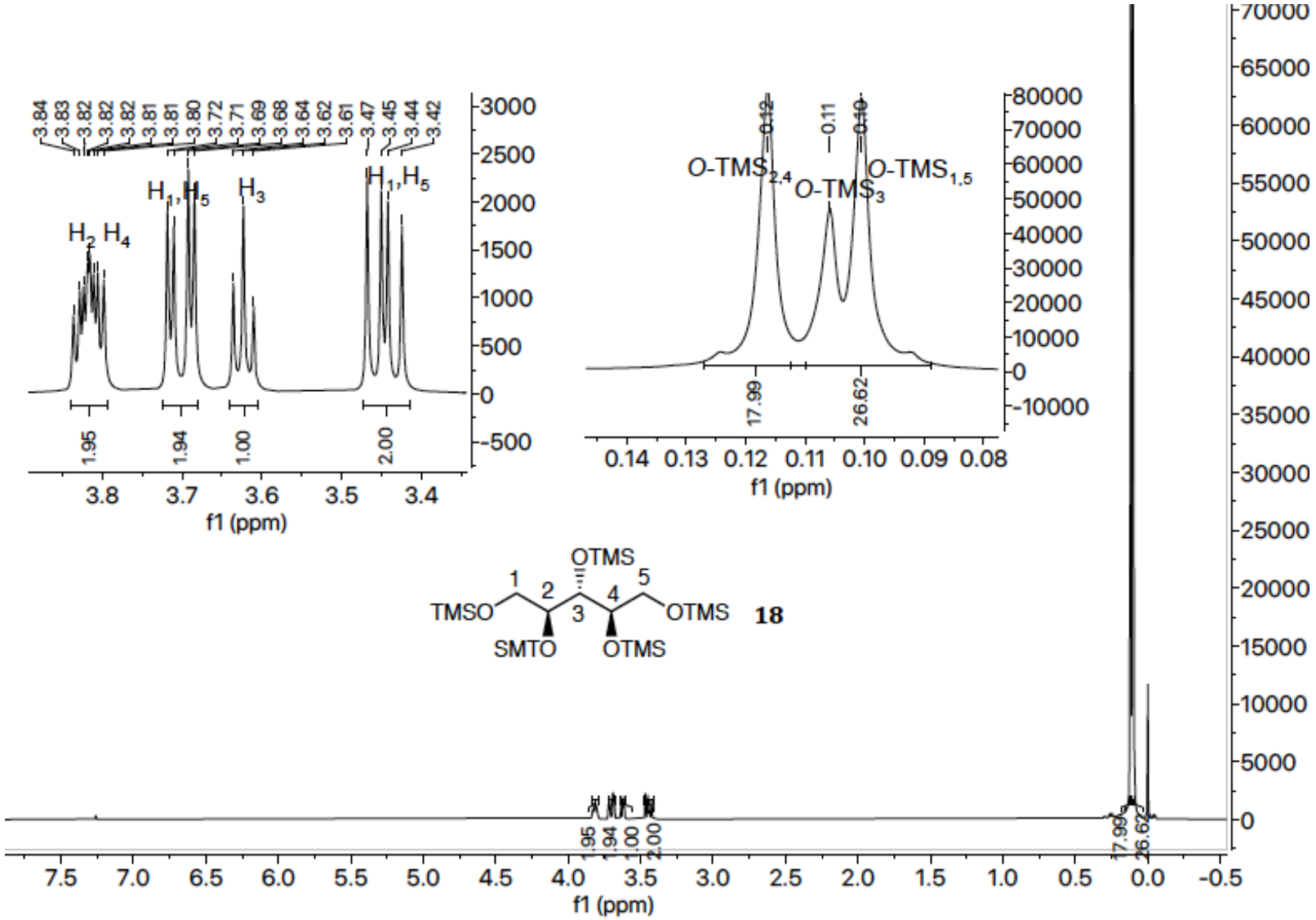

SI-Figure 1.39: per-*O*-TMS-ribitol (**18**) ^{1}H NMR (400 MHz, $CDCl_3$) spectrum

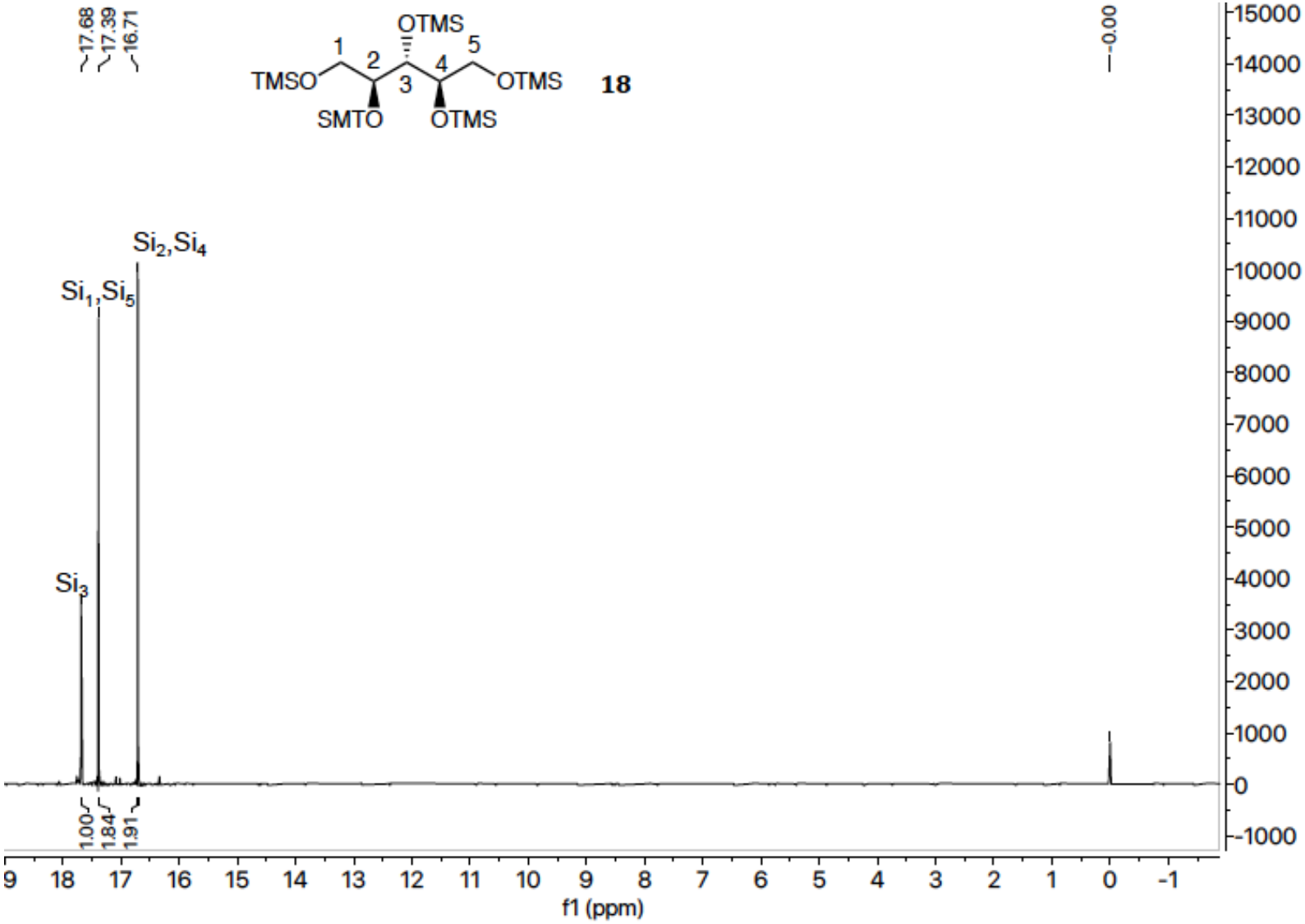

SI-Figure 1.40: per-*O*-TMS-ribitol (**18**) ^{29}Si NMR (400 MHz, $CDCl_3$) spectrum

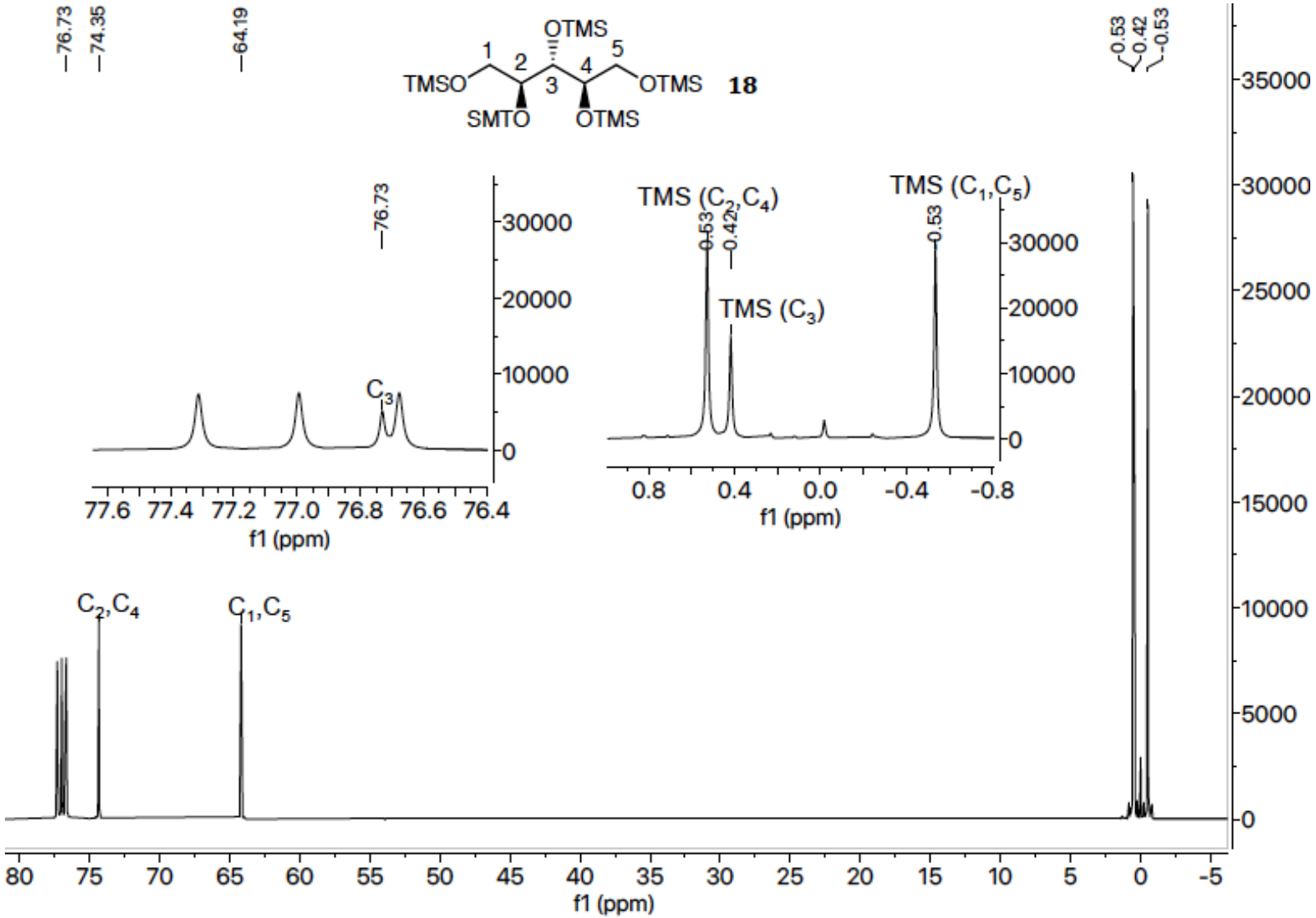

SI-Figure 1.41: per-*O*-TMS-ribitol (**18**) ^{13}C NMR (400 MHz, $CDCl_3$) spectrum

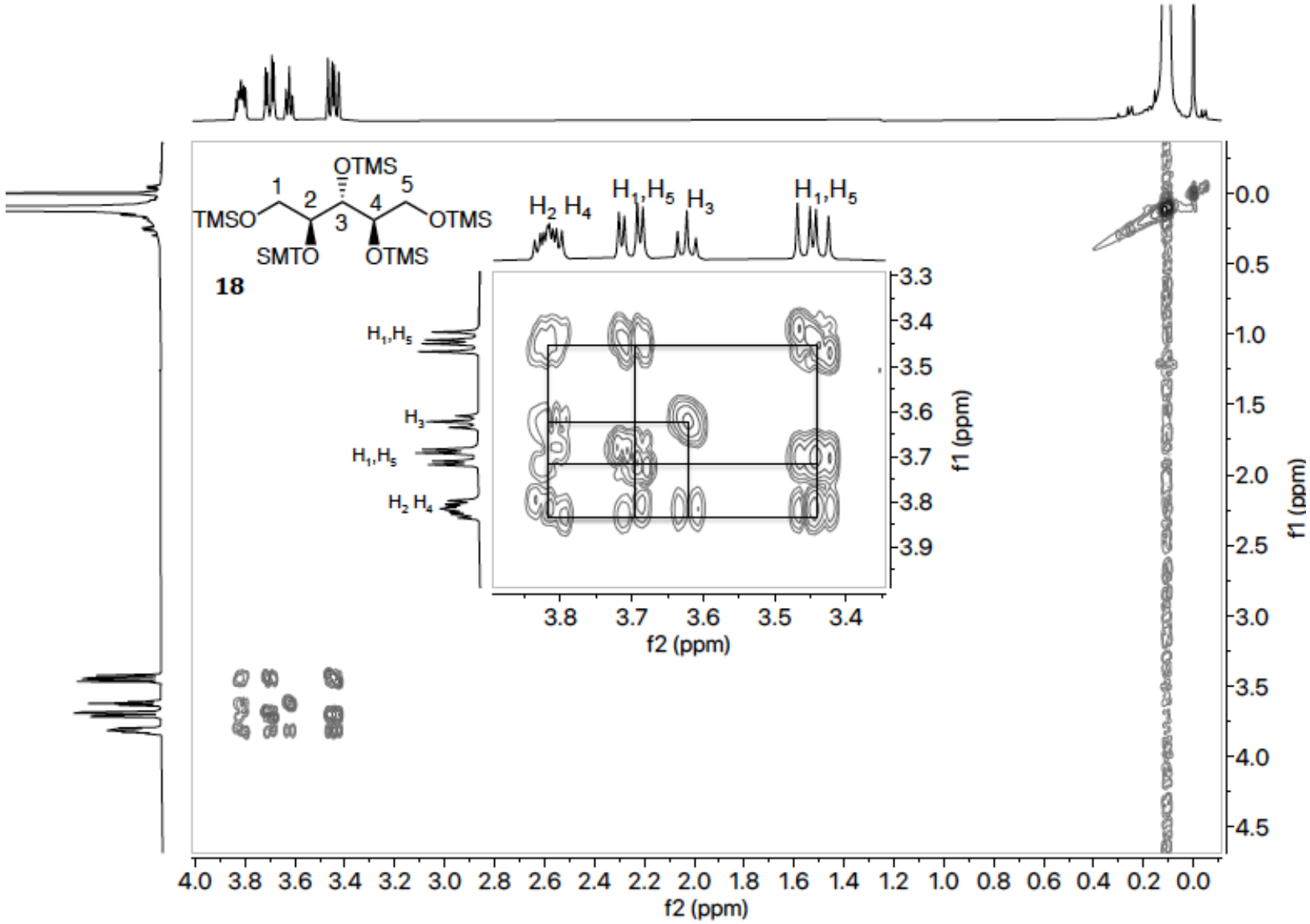

SI-Figure 1.42: per-*O*-TMS-ribitol (**18**) COSY NMR (400 MHz, $CDCl_3$) spectrum

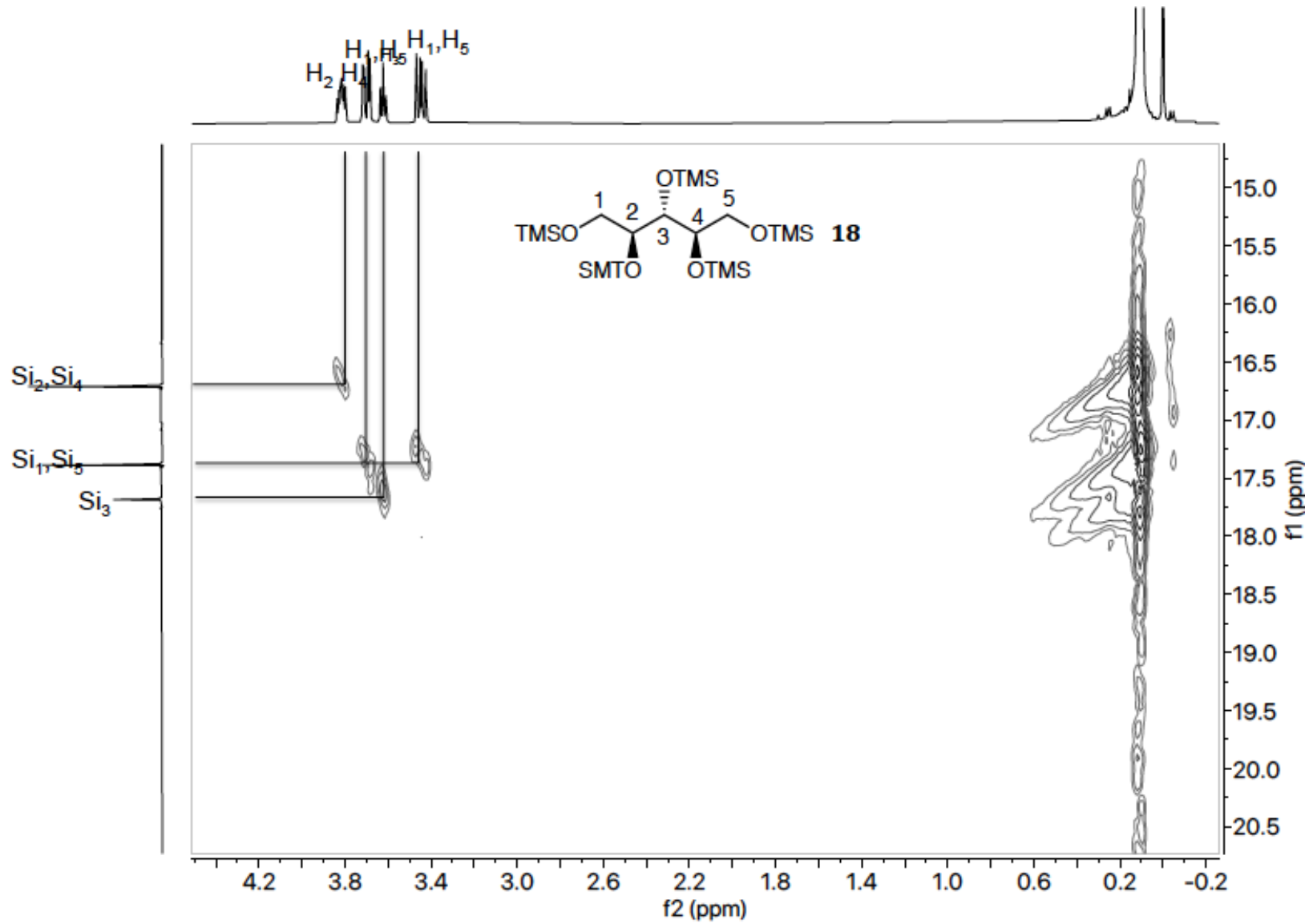

SI-Figure 1.43: per-*O*-TMS-ribitol (**18**) ^{1}H-^{29}Si HMBC NMR (400 MHz, $CDCl_3$) spectrum

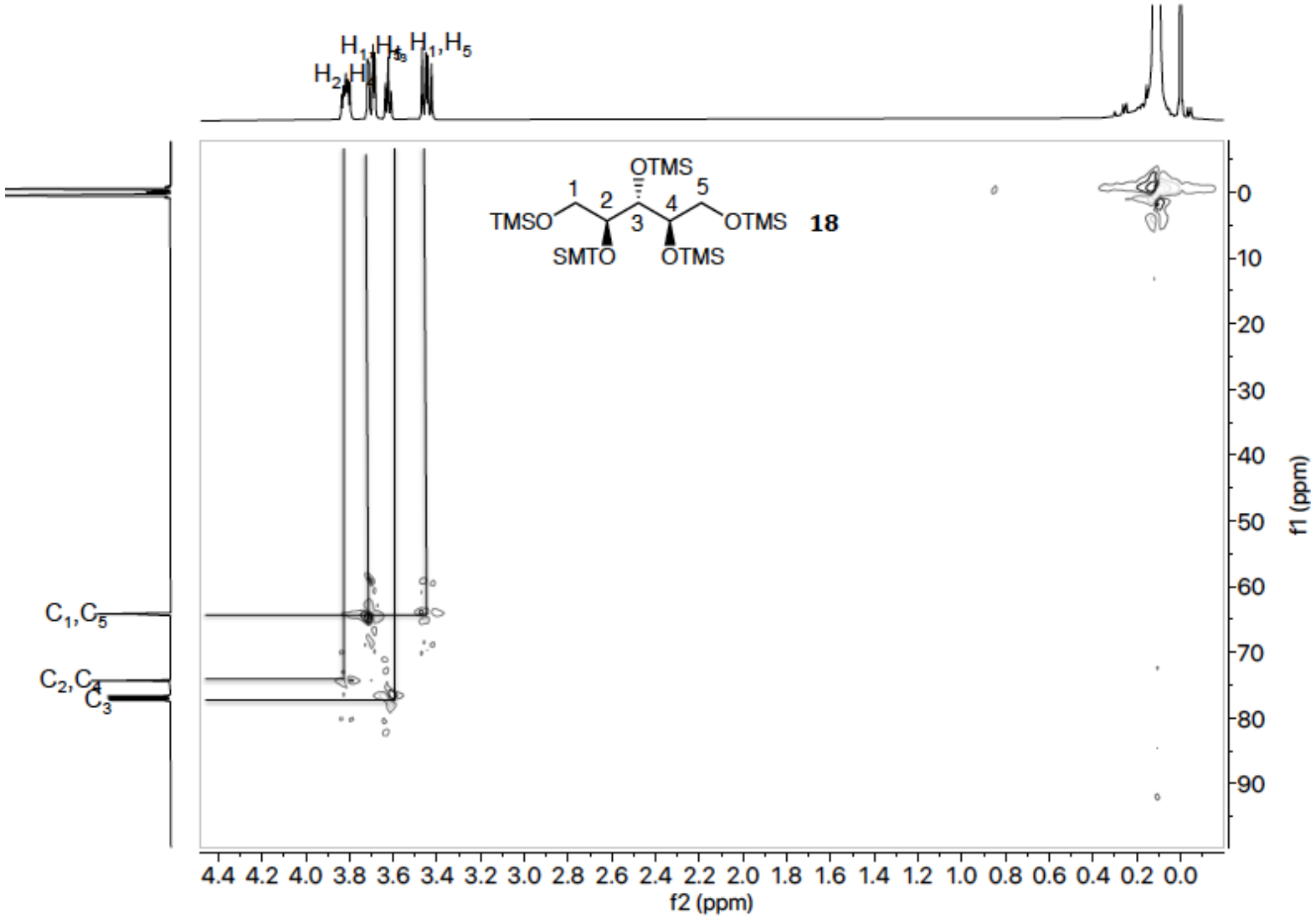

SI-Figure 1.44: per-*O*-TMS-ribitol (**18**) ^{1}H-^{13}C HSQC NMR (400 MHz, $CDCl_3$) spectrum

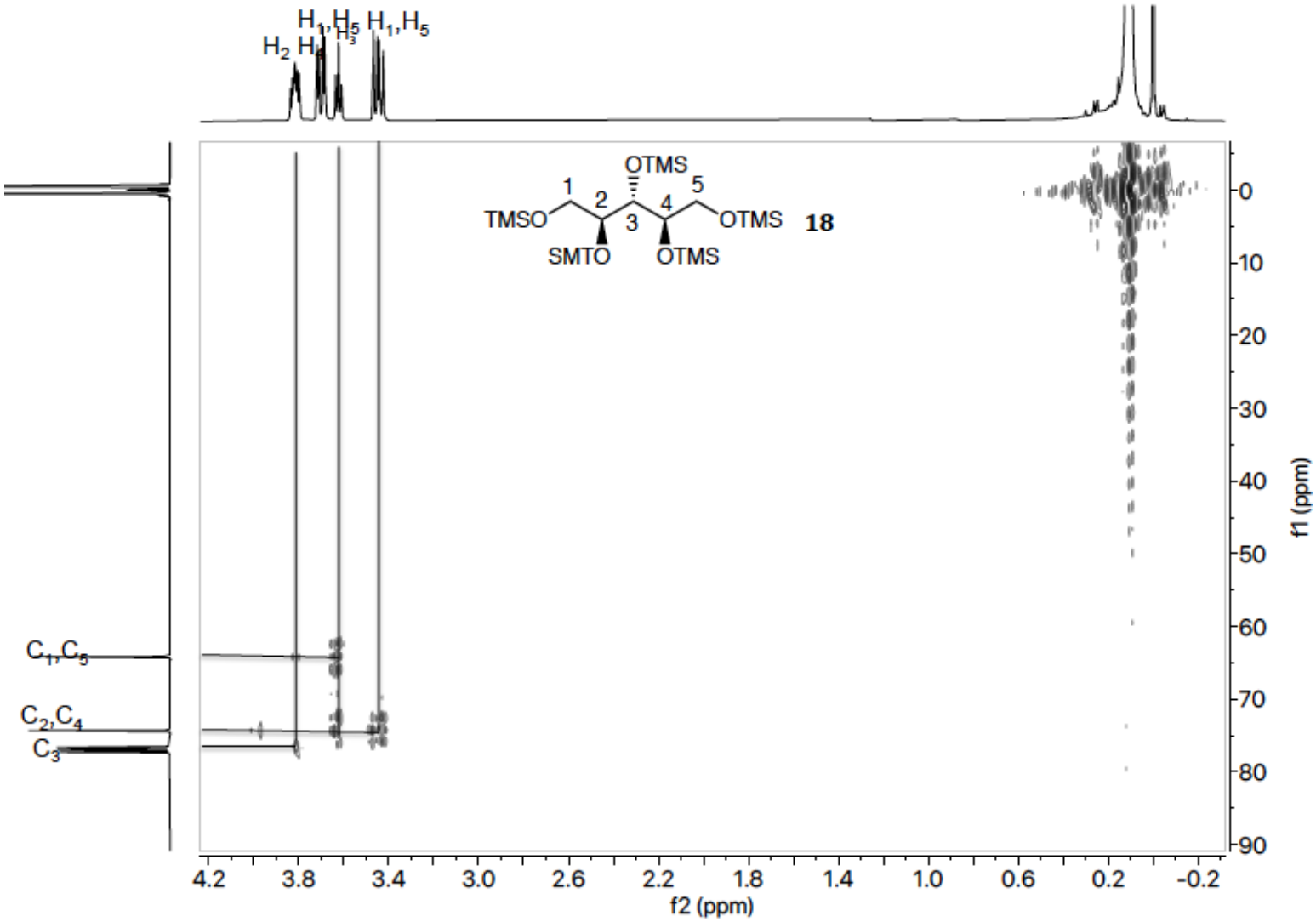

SI-Figure 1.45: per-*O*-TMS-ribitol (**18**) ^{1}H-^{13}C HMBC NMR (400 MHz, $CDCl_3$) spectrum

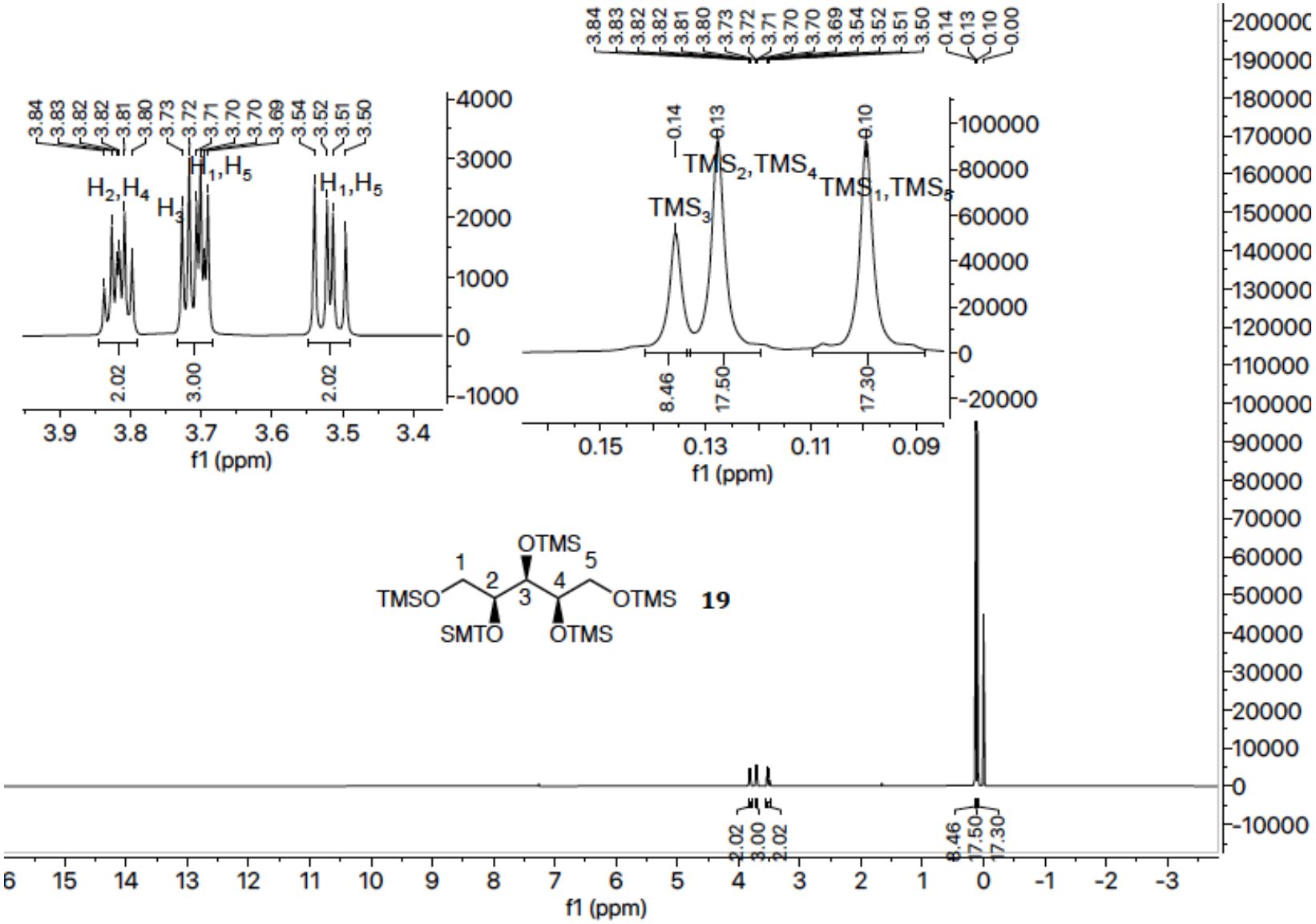

SI-Figure 1.46: per-*O*-TMS-xylitol (**19**) ^{1}H NMR (400 MHz, $CDCl_3$) spectrum

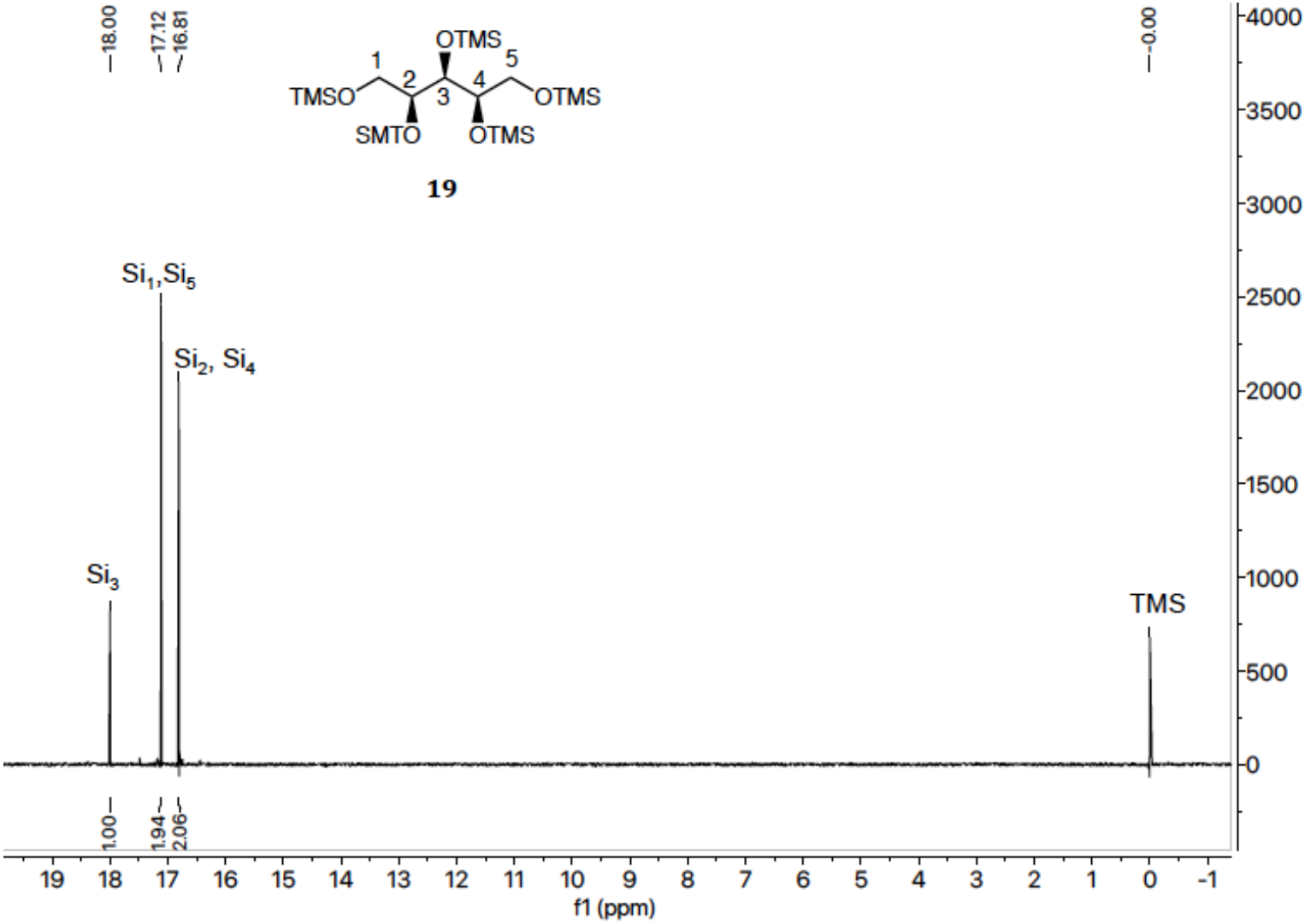

SI-Figure 1.47: per-*O*-TMS-xylitol (**19**) ^{29}Si NMR (400 MHz, $CDCl_3$) spectrum

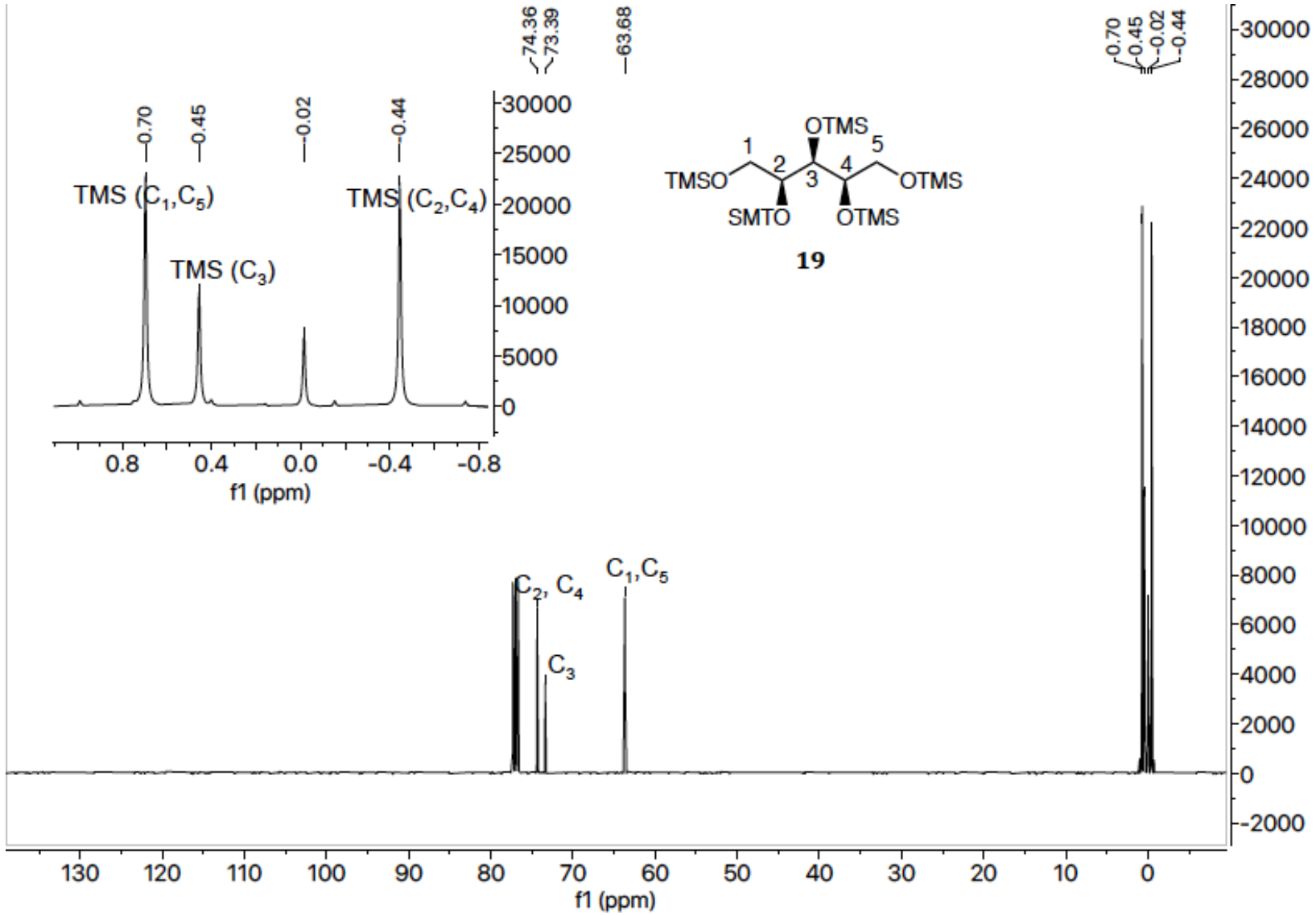

SI-Figure 1.48: per-*O*-TMS-xylitol (**19**) ^{13}C NMR (400 MHz, $CDCl_3$) spectrum

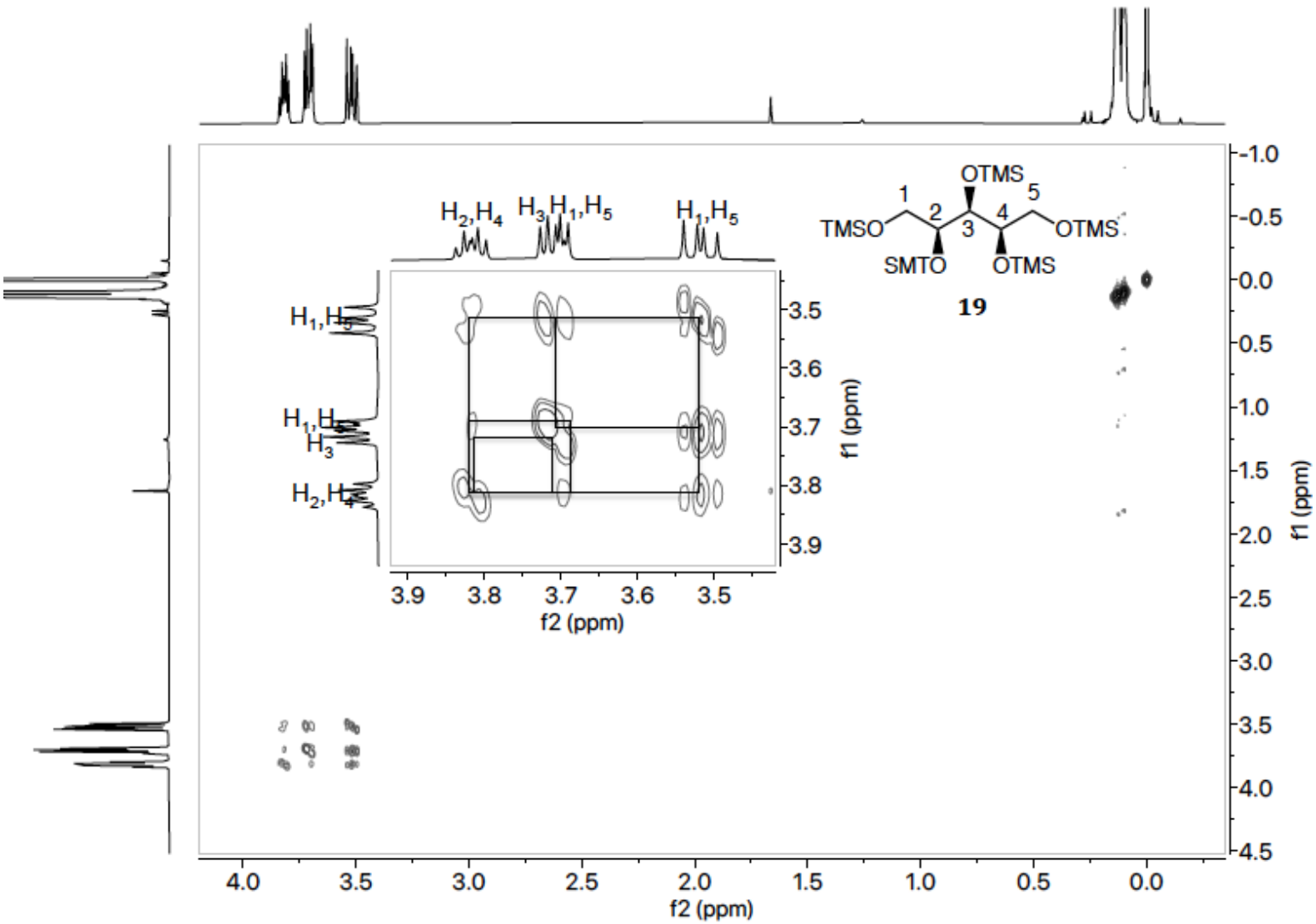

SI-Figure 1.49: per-*O*-TMS-xylitol (**19**) COSY NMR (400 MHz, $CDCl_3$) spectrum

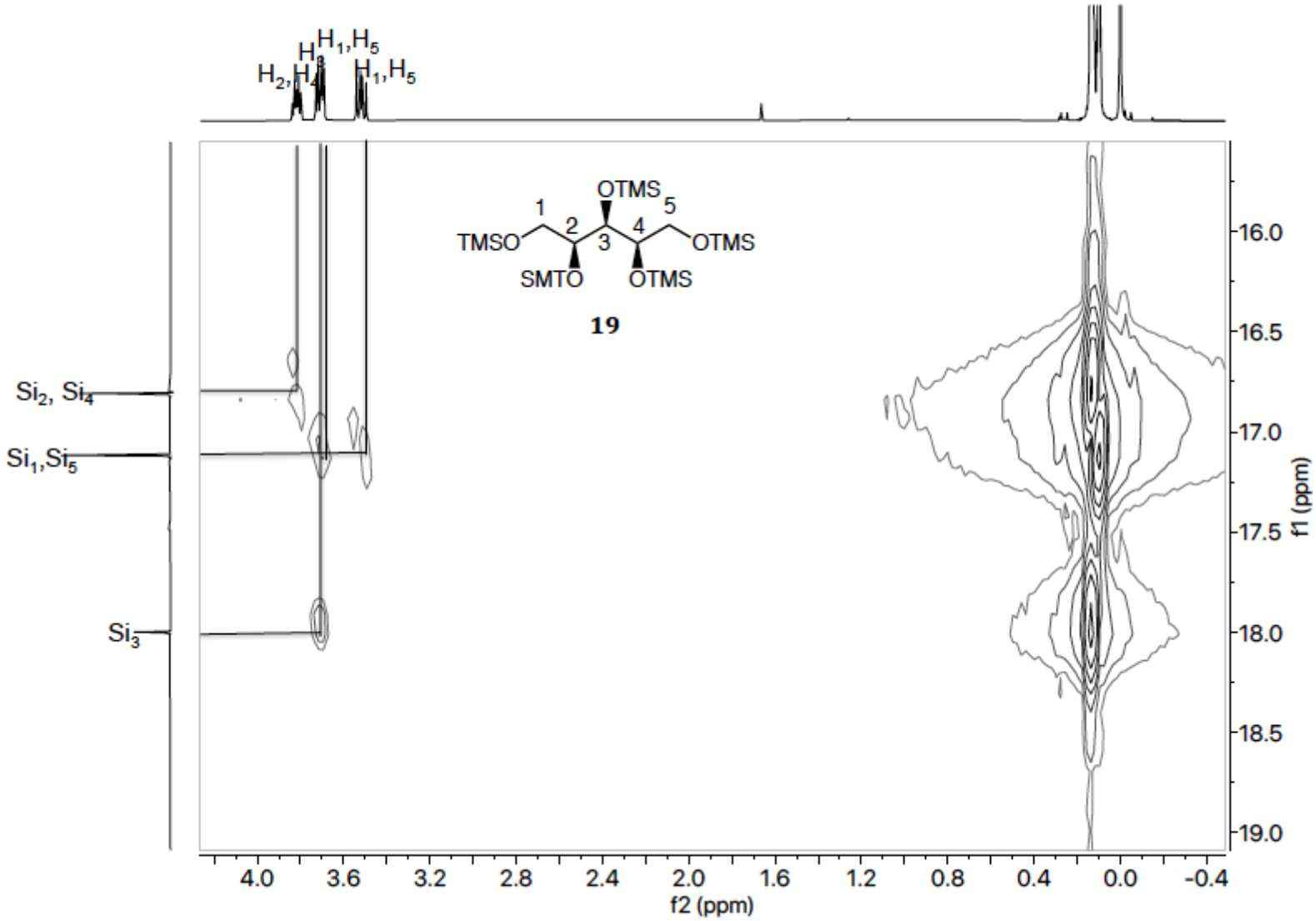

Si-Figure 1.50: per-*O*-TMS-xylitol (**19**) ^{1}H-^{29}Si HMBC NMR (400 MHz, $CDCl_3$) spectrum

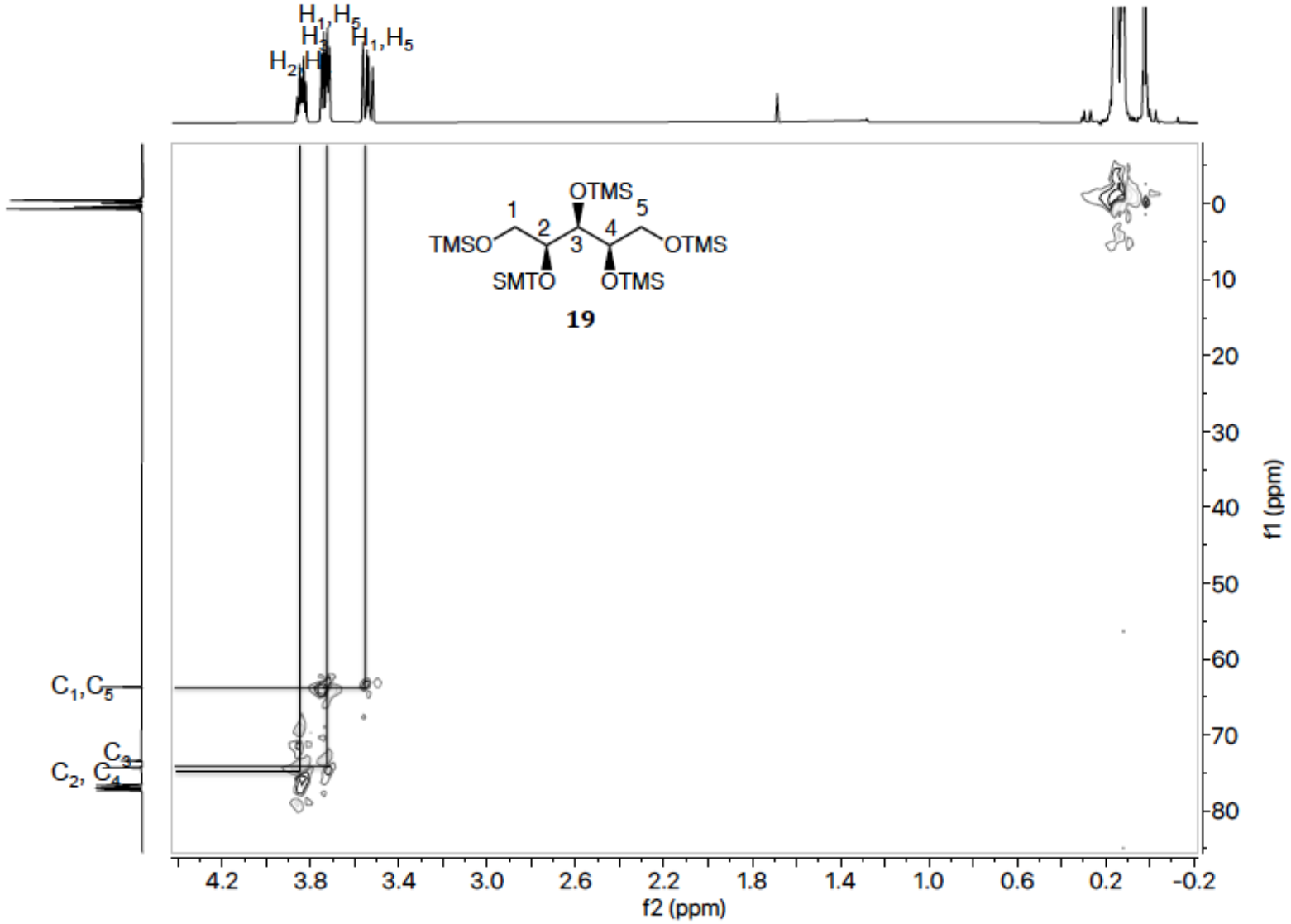

SI-Figure 1.51: per-*O*-TMS-xylitol (**19**) ^{1}H-^{13}C HSQC NMR (400 MHz, $CDCl_3$) spectrum

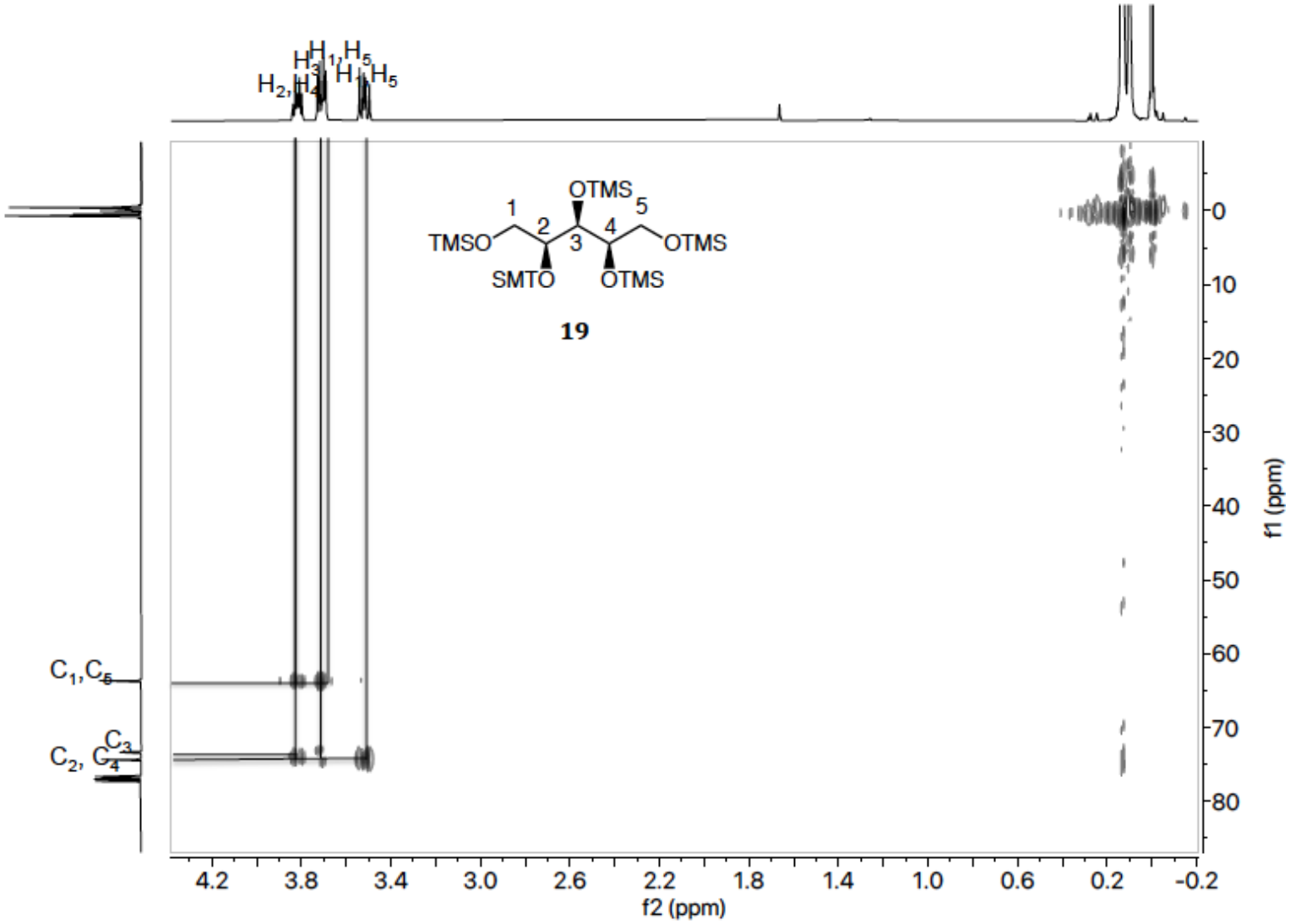

SI-Figure 1.52: per-*O*-TMS-xylitol (**19**) ^{1}H-^{13}C HMBC NMR (400 MHz, $CDCl_3$) spectrum

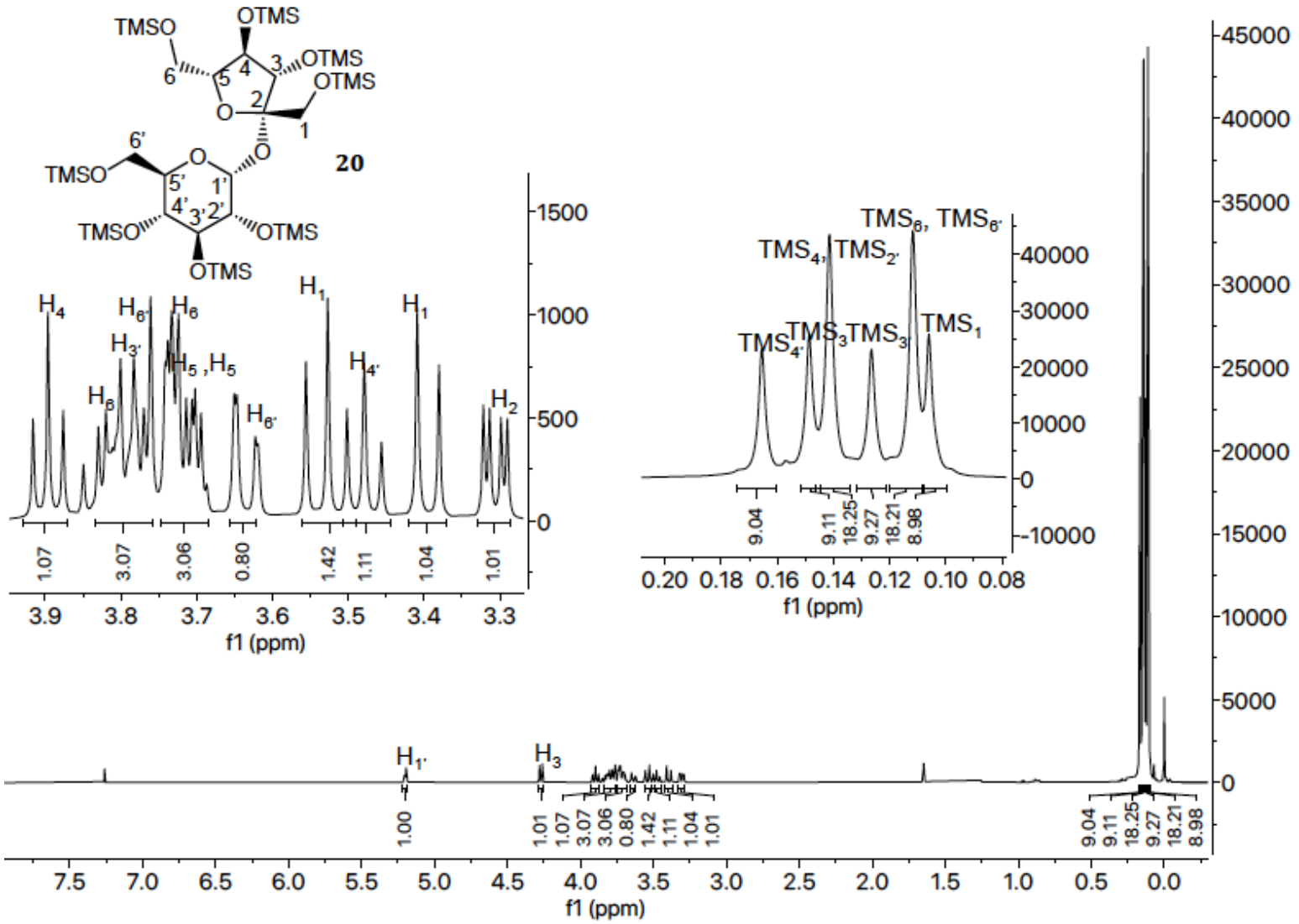

SI-Figure 1.53: per-*O*-TMS-sucrose (**20**) ^{1}H NMR (400 MHz, $CDCl_3$) spectrum

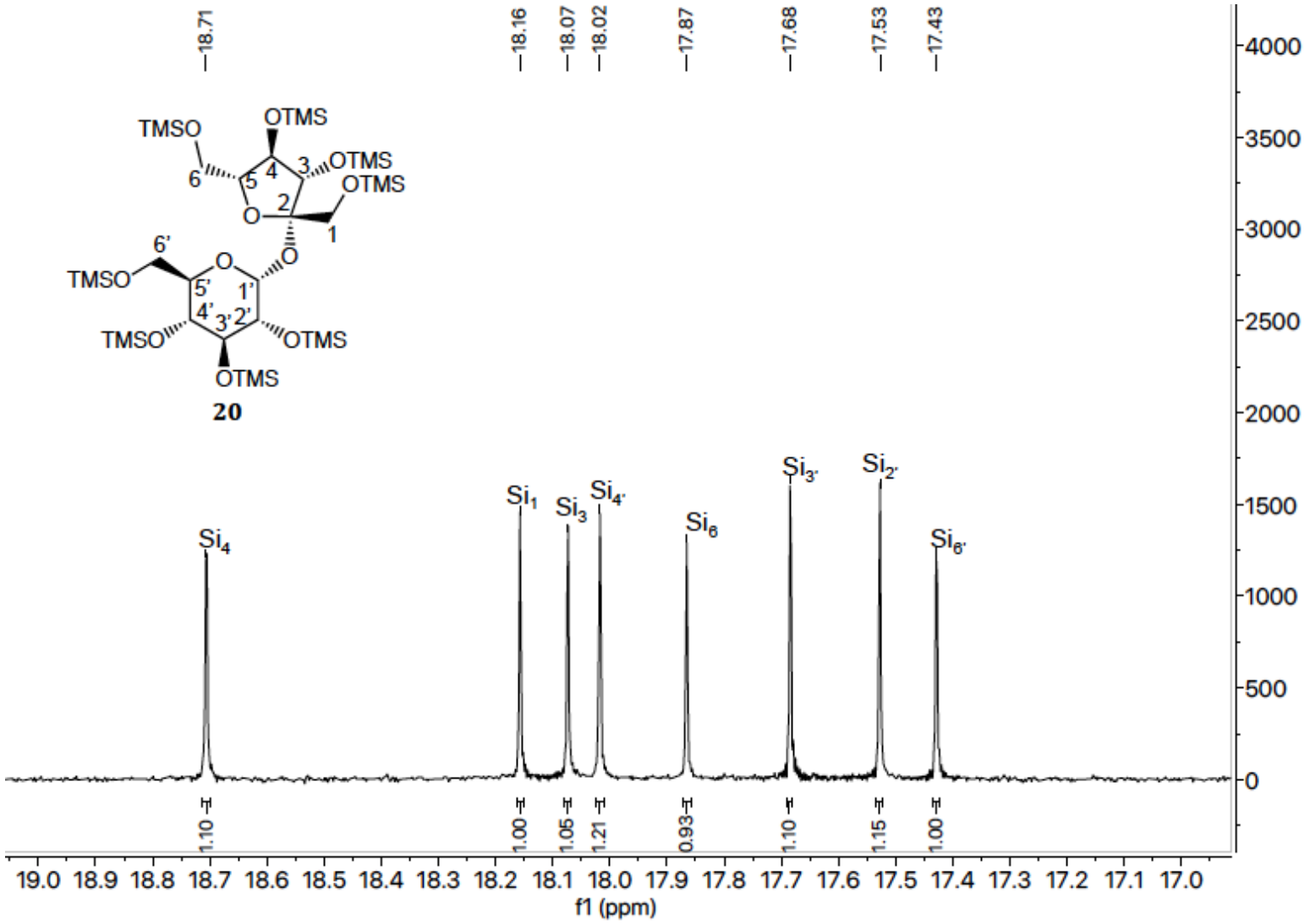

SI-Figure 1.54: per-*O*-TMS-sucrose (**20**) ^{29}Si NMR (400 MHz, $CDCl_3$) spectrum

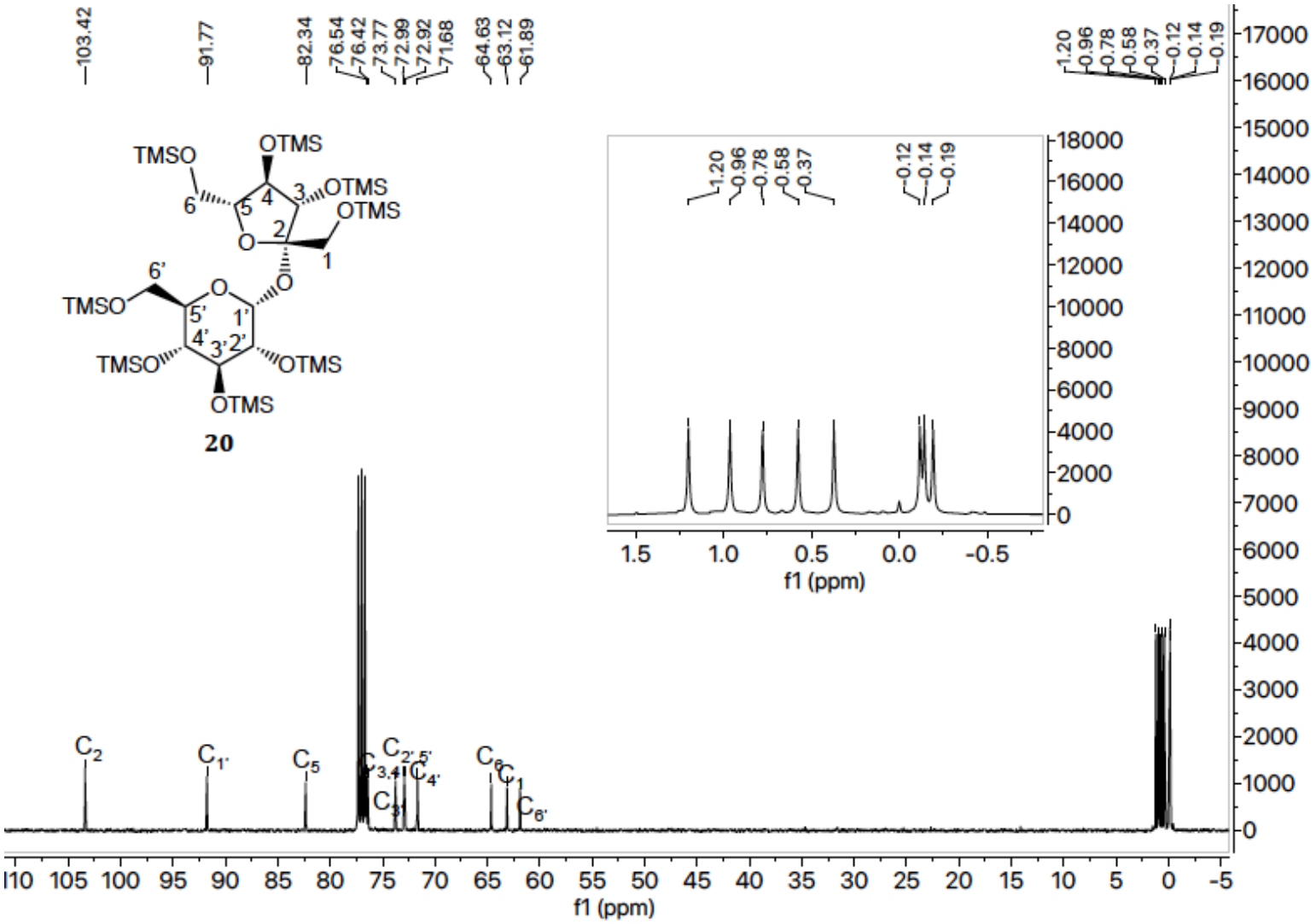

SI-Figure 1.55: per-*O*-TMS-sucrose (**20**) ^{13}CNMR (400 MHz, $CDCl_3$) spectrum

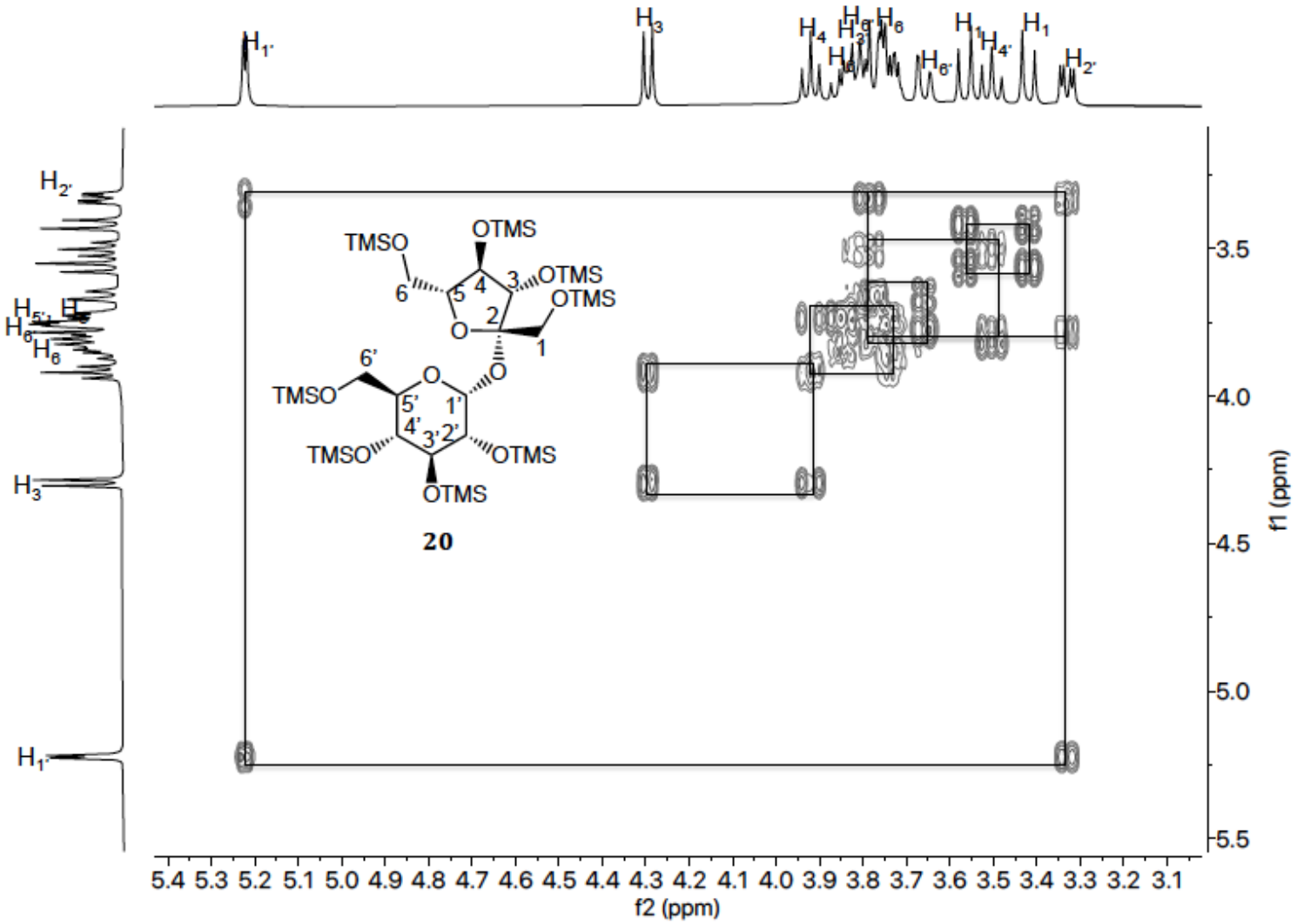

SI-Figure 1.56: per-*O*-TMS-sucrose (**20**) COSY NMR (400 MHz, $CDCl_3$) spectrum

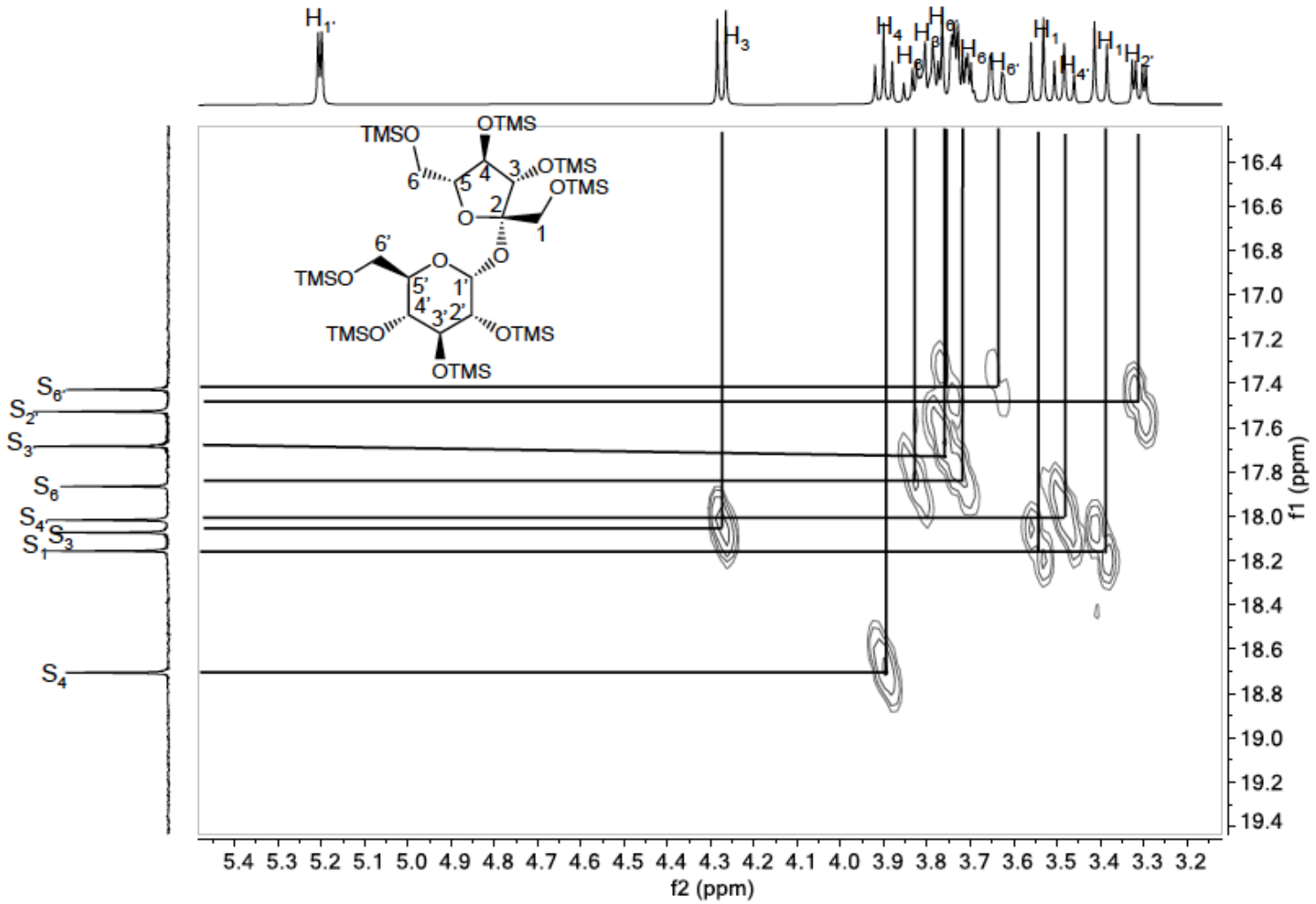

SI-Figure 1.57: per-*O*-TMS-sucrose (**20**) ^{1}H-^{29}Si HMBC NMR (400 MHz, $CDCl_3$) spectrum

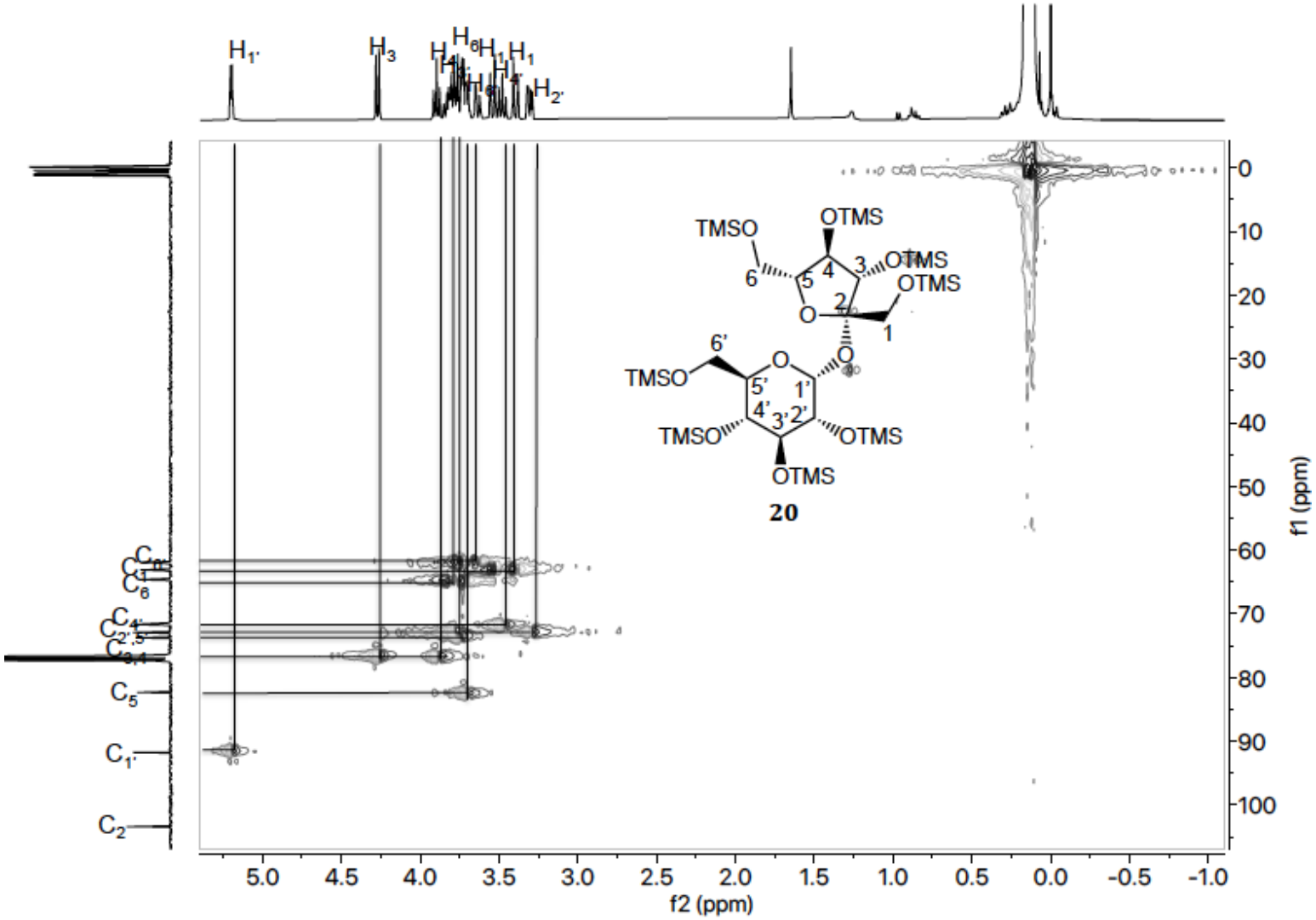

SI-Figure 1.58: per-*O*-TMS-sucrose (**20**) HSQC NMR (400 MHz, $CDCl_3$) spectrum

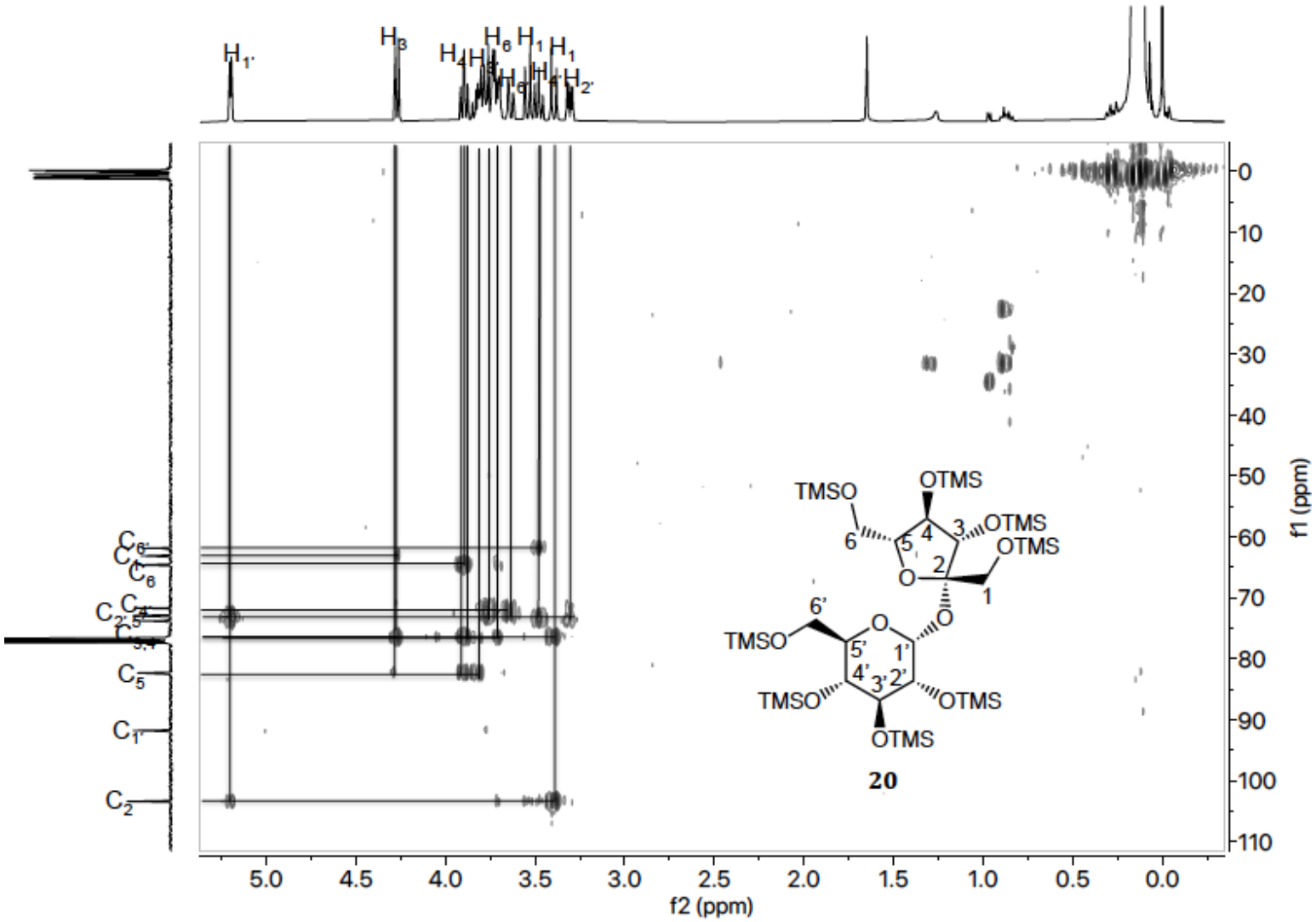

SI-Figure 1.59: per-*O*-TMS-sucrose (**20**) ^{1}H-^{13}C HMBC NMR (400 MHz, $CDCl_3$) spectrum

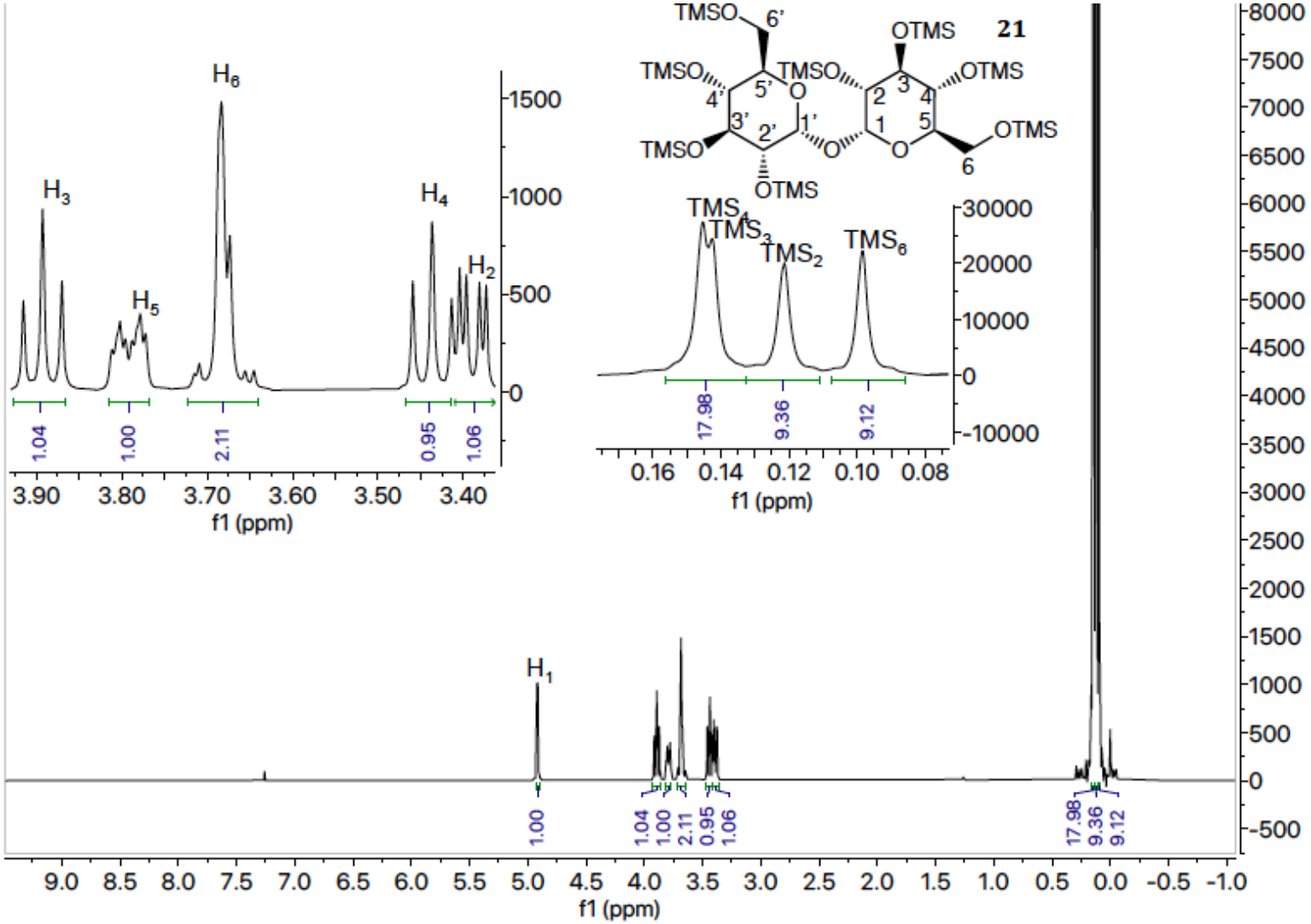

SI-Figure 1.60: per-*O*-TMS-trehalose (**21**) ^{1}H NMR (400 MHz, $CDCl_3$) spectrum

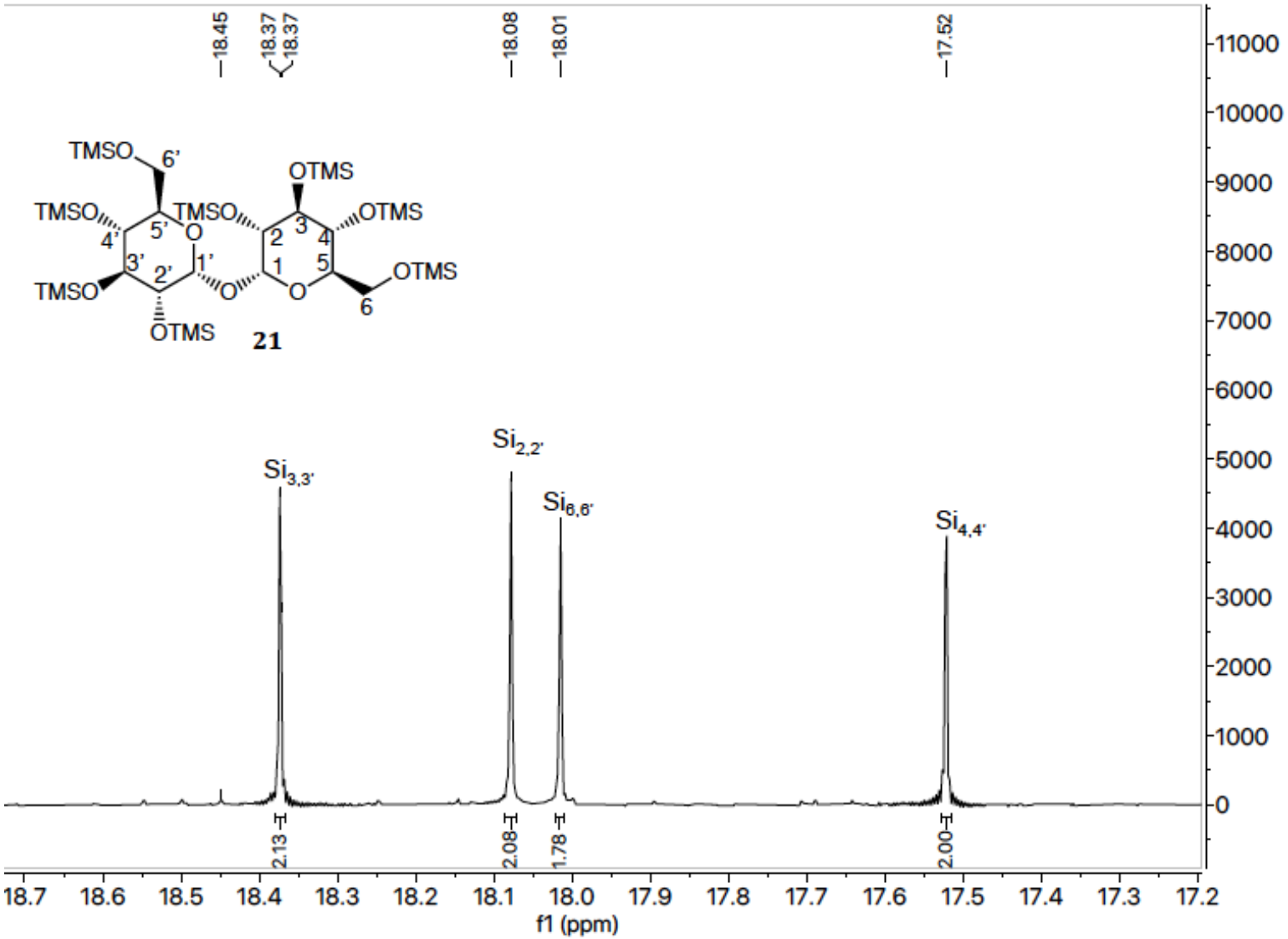

SI-Figure 1.61: per-*O*-TMS-trehalose (**21**) ^{29}Si NMR (400 MHz, $CDCl_3$) spectrum

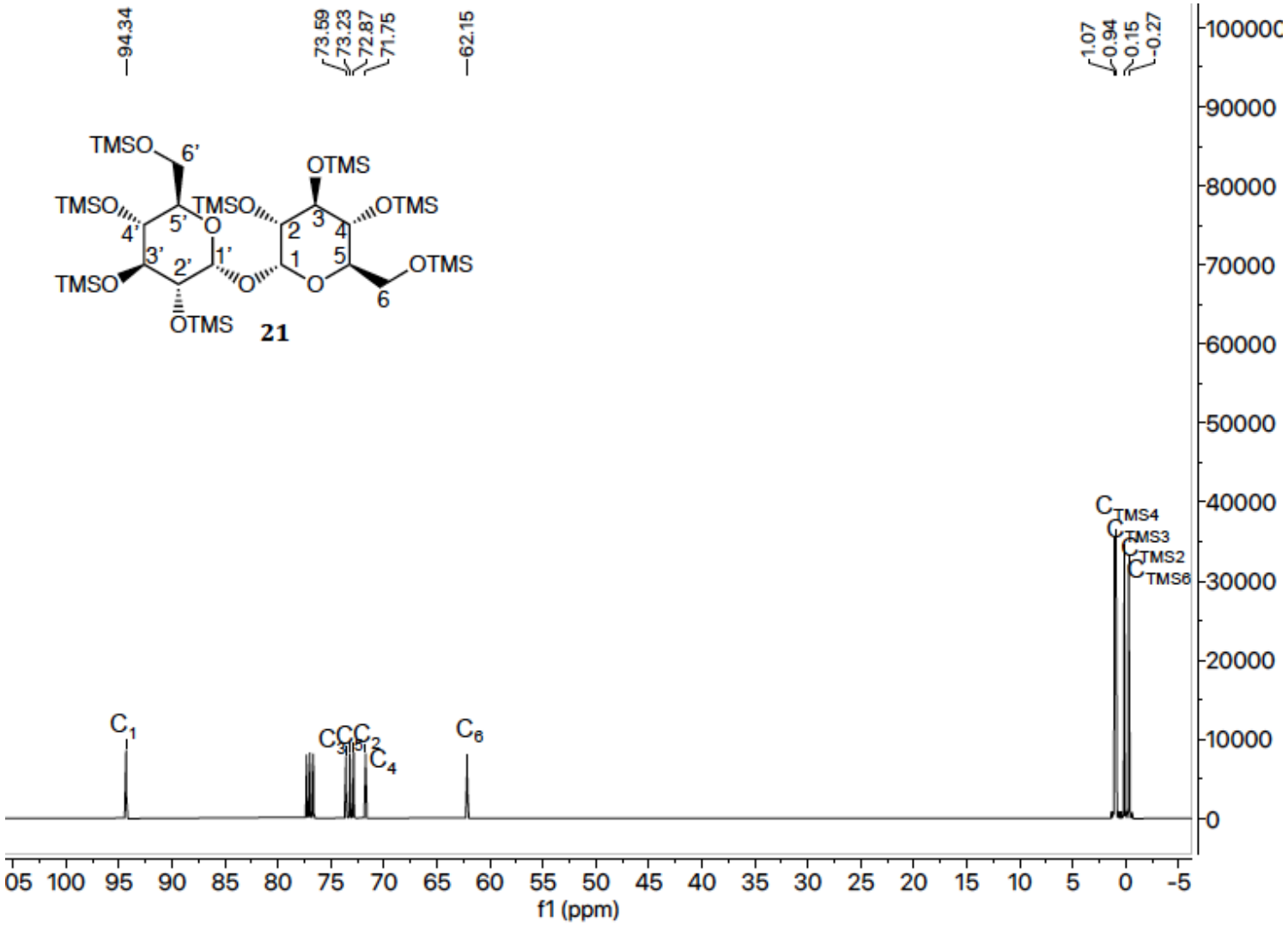

SI-Figure 1.62: per-*O*-TMS-trehalose (**21**) ^{13}C NMR (400 MHz, $CDCl_3$) spectrum

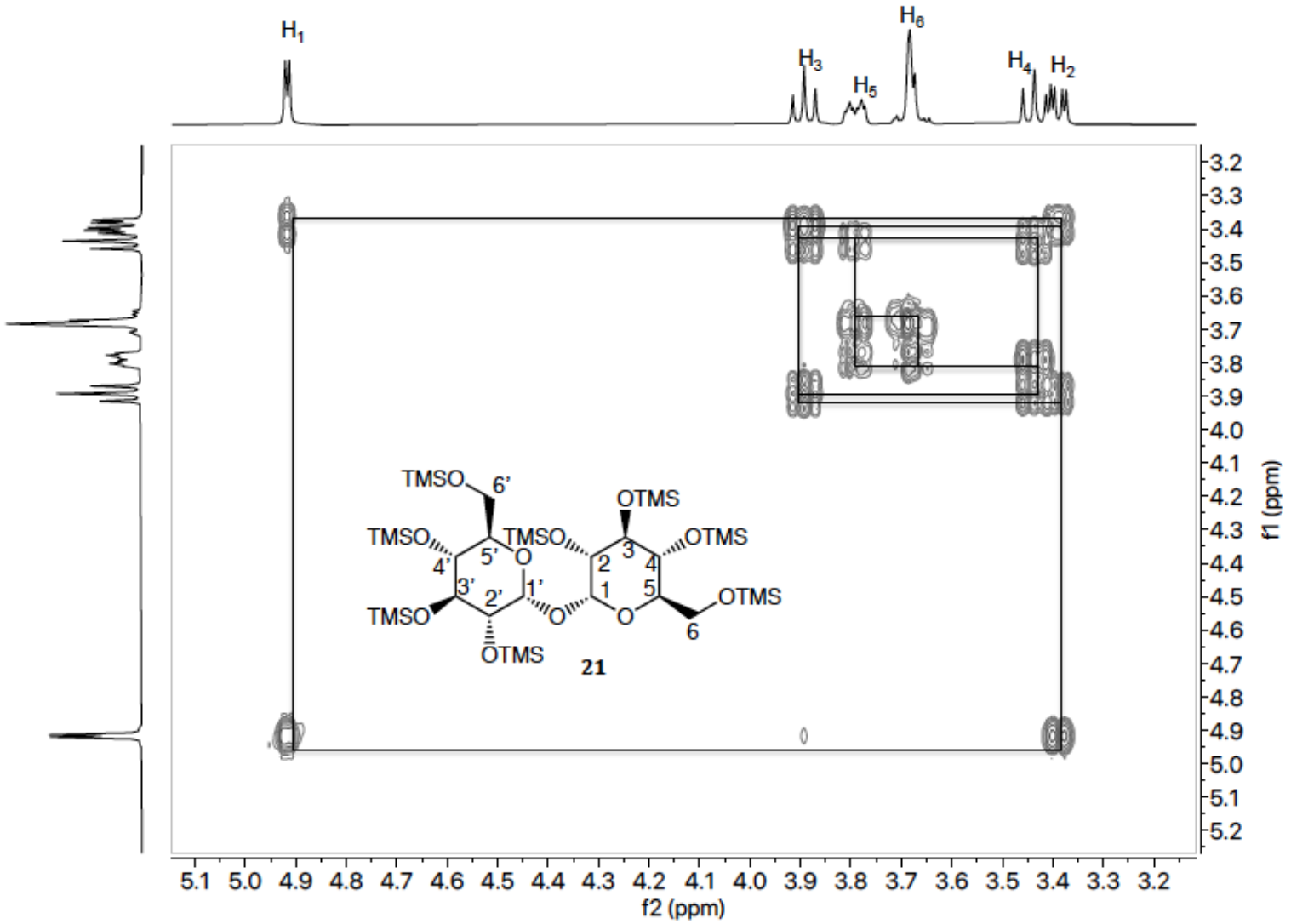

SI-Figure 1.63: per-*O*-TMS-trehalose (**21**) COSY NMR (400 MHz, $CDCl_3$) spectrum

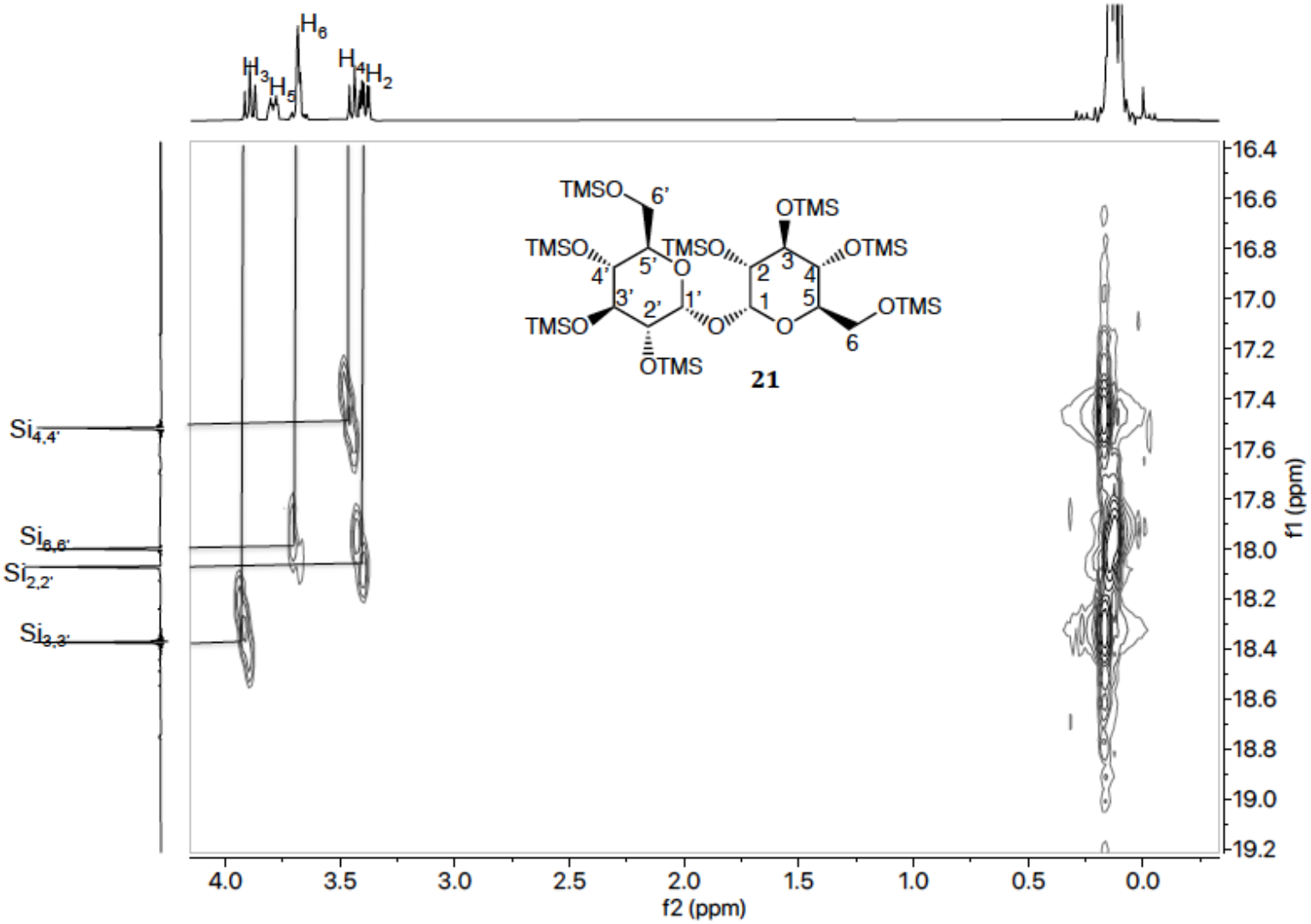

Si-Figure 1.64: per-*O*-TMS-trehalose (**21**) ^{1}H-^{29}Si HMBC NMR (400 MHz, $CDCl_3$) spectrum

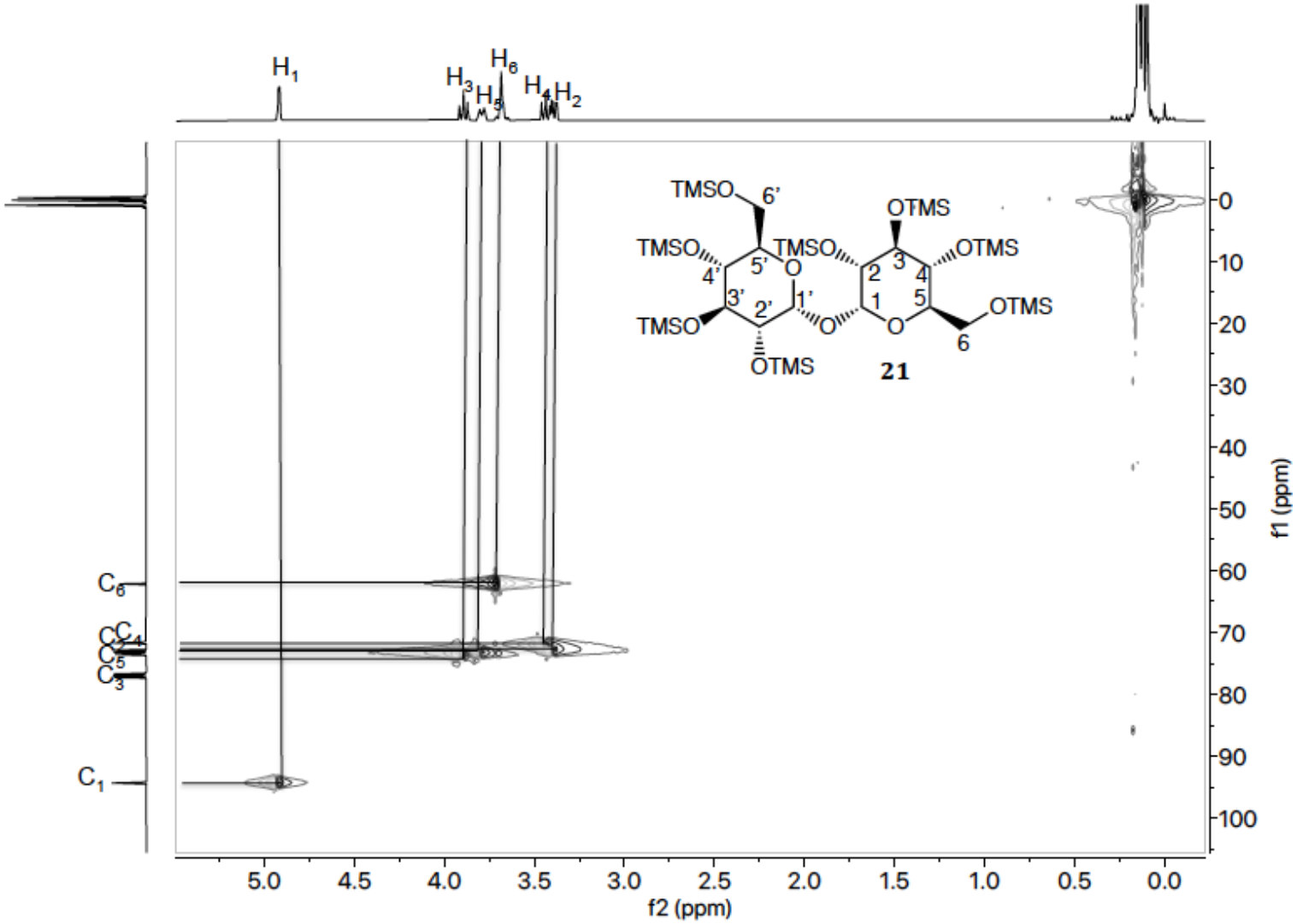

Si-Figure 1.65: per-*O*-TMS-trehalose (**21**) ^{1}H-^{13}C HSCQ NMR (400 MHz, $CDCl_3$) spectrum

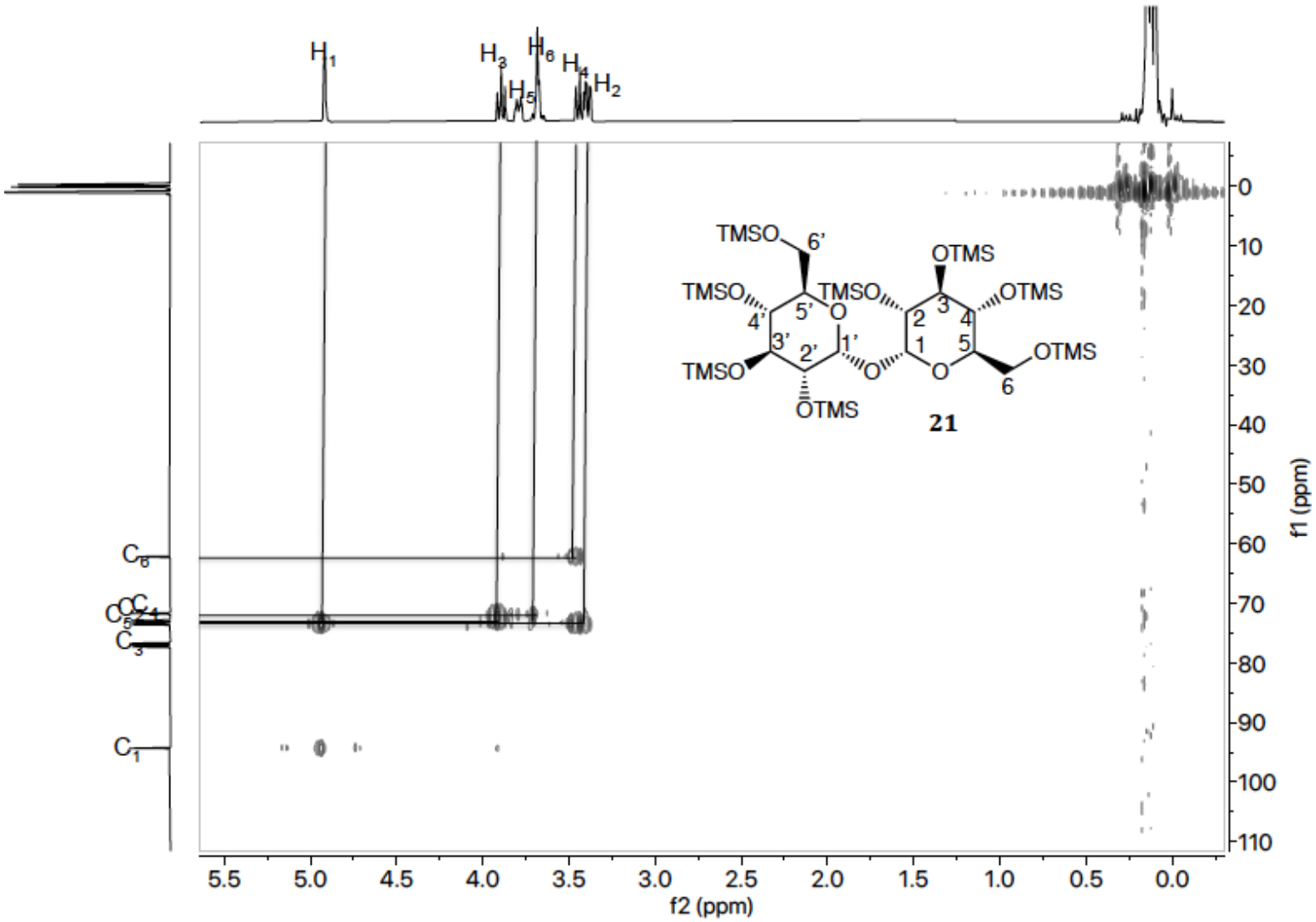

SI-Figure 1.66: per-*O*-TMS-trehalose (**21**) ^{1}H-^{13}C HMBC NMR (400 MHz, $CDCl_3$) spectrum

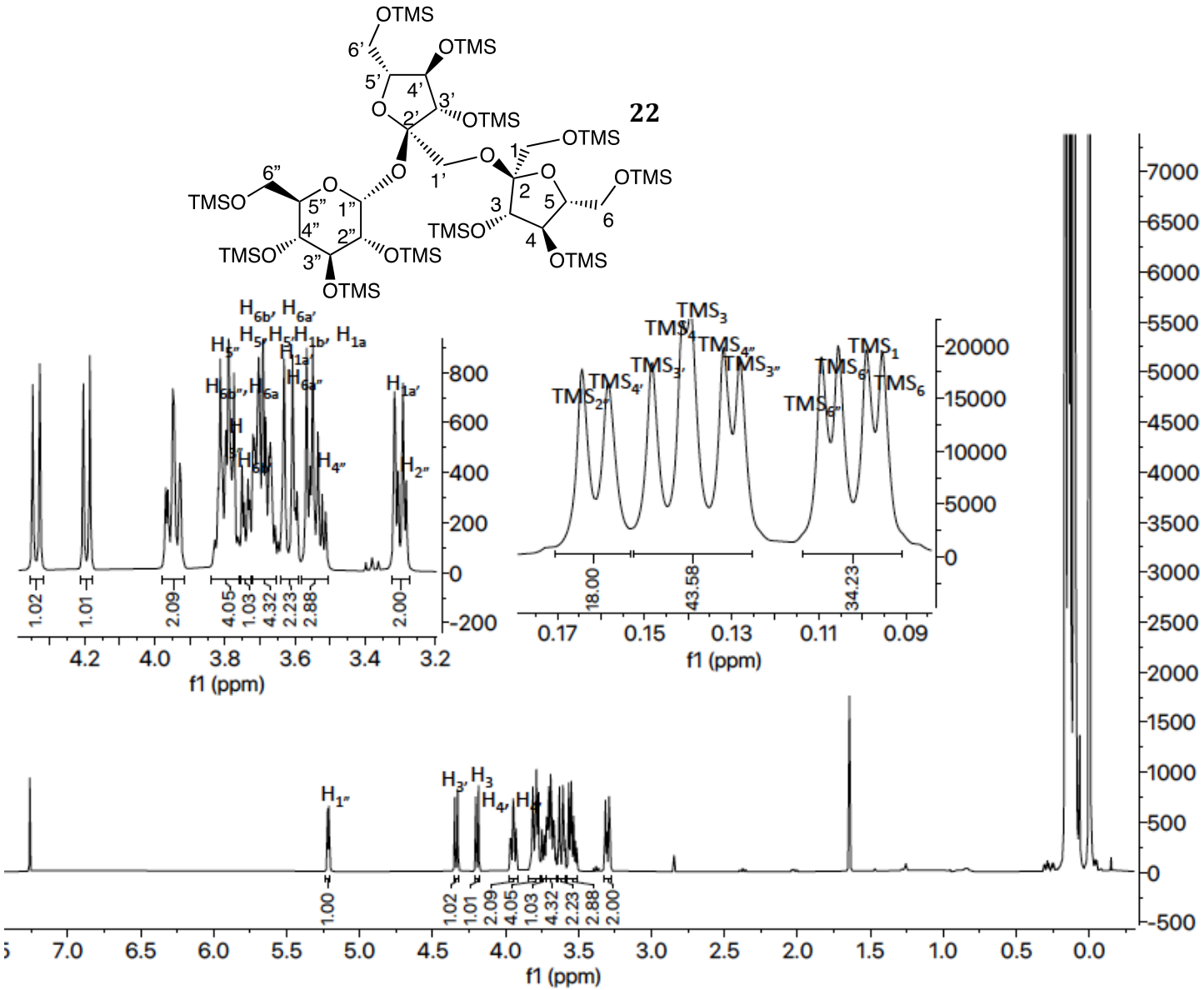

SI-Figure 1.67: per-*O*-TMS kestose (**22**) ^{1}H NMR (400 MHz, $CDCl_3$) spectrum

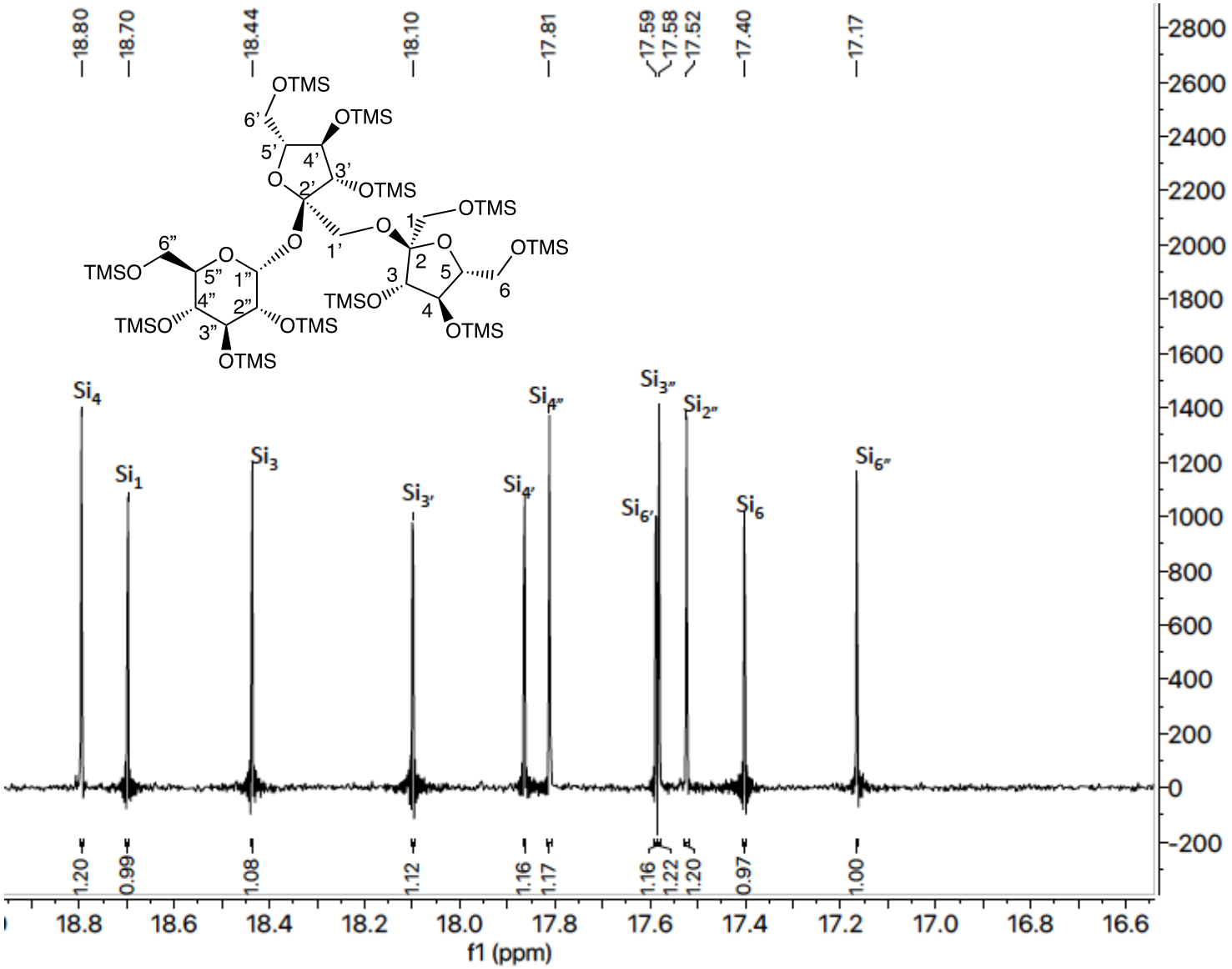

SI-Figure 1.68: per-*O*-TMS kestose (**22**) ^{29}Si NMR (400 MHz, $CDCl_3$) spectrum

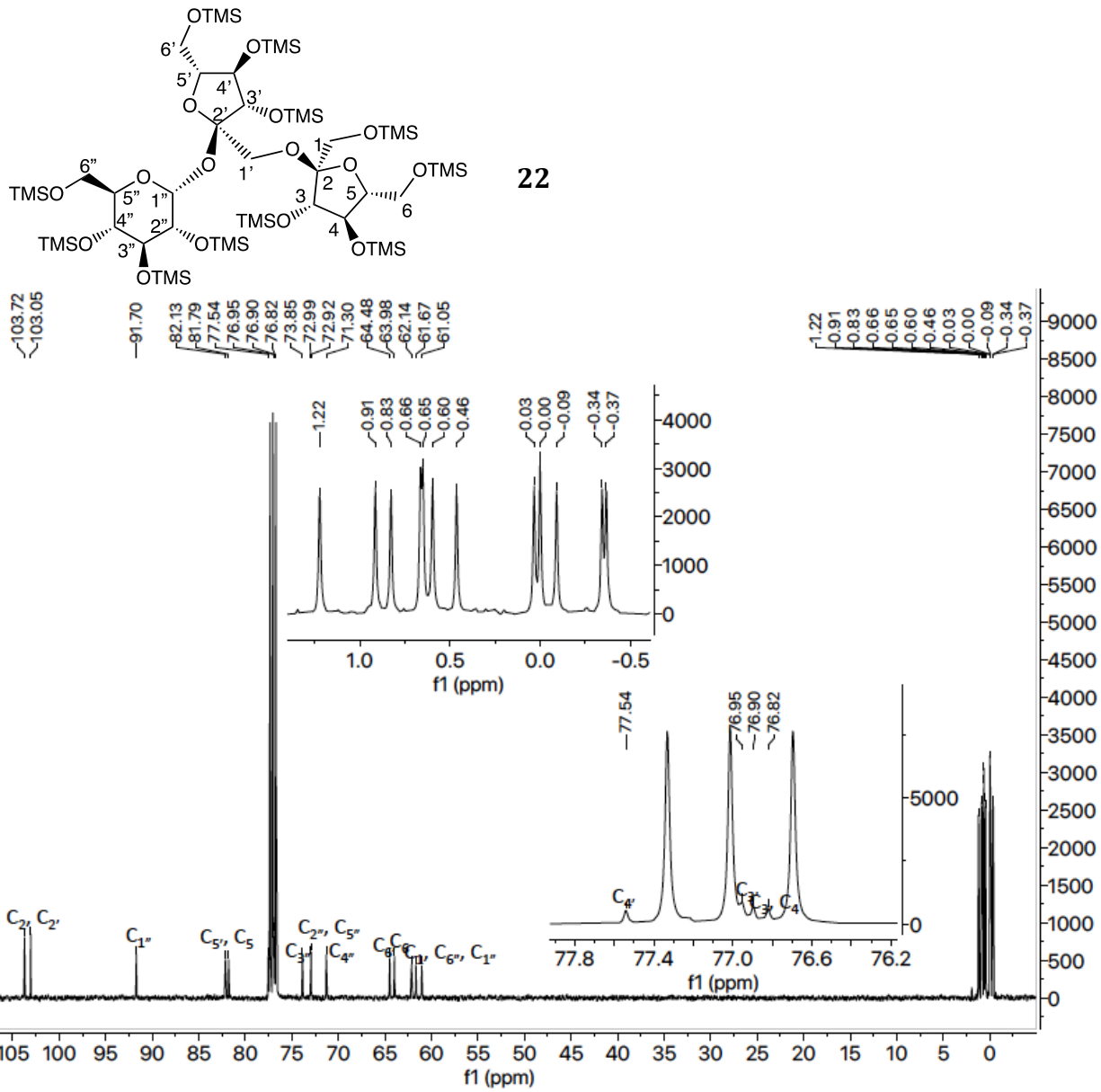

SI-Figure 1.69: per-*O*-TMS kestose (**22**) ^{13}C NMR (400 MHz, $CDCl_3$) spectrum

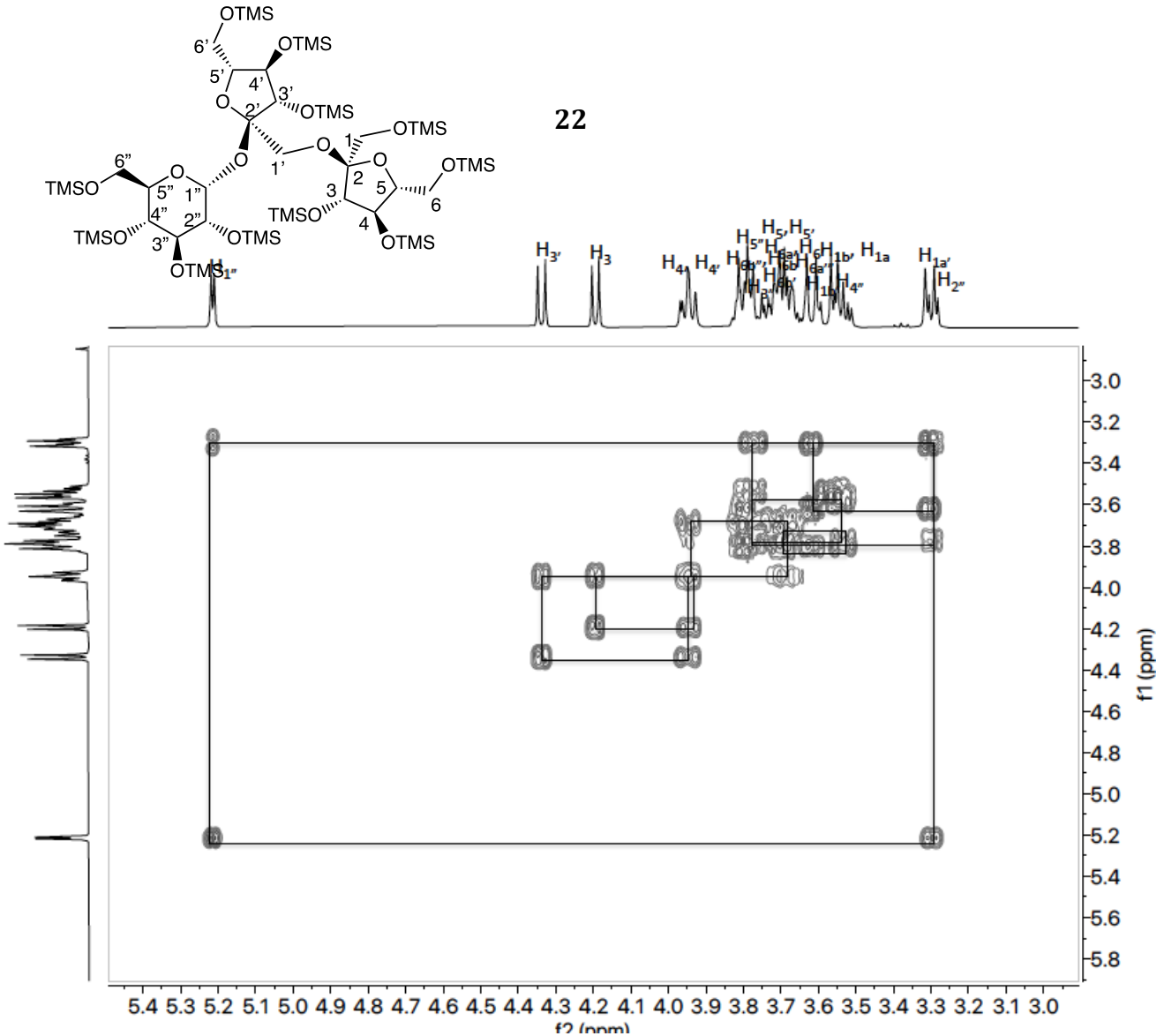

SI-Figure 1.70: per-*O*-TMS kestose (**22**) COSY NMR (400 MHz, $CDCl_3$) spectrum

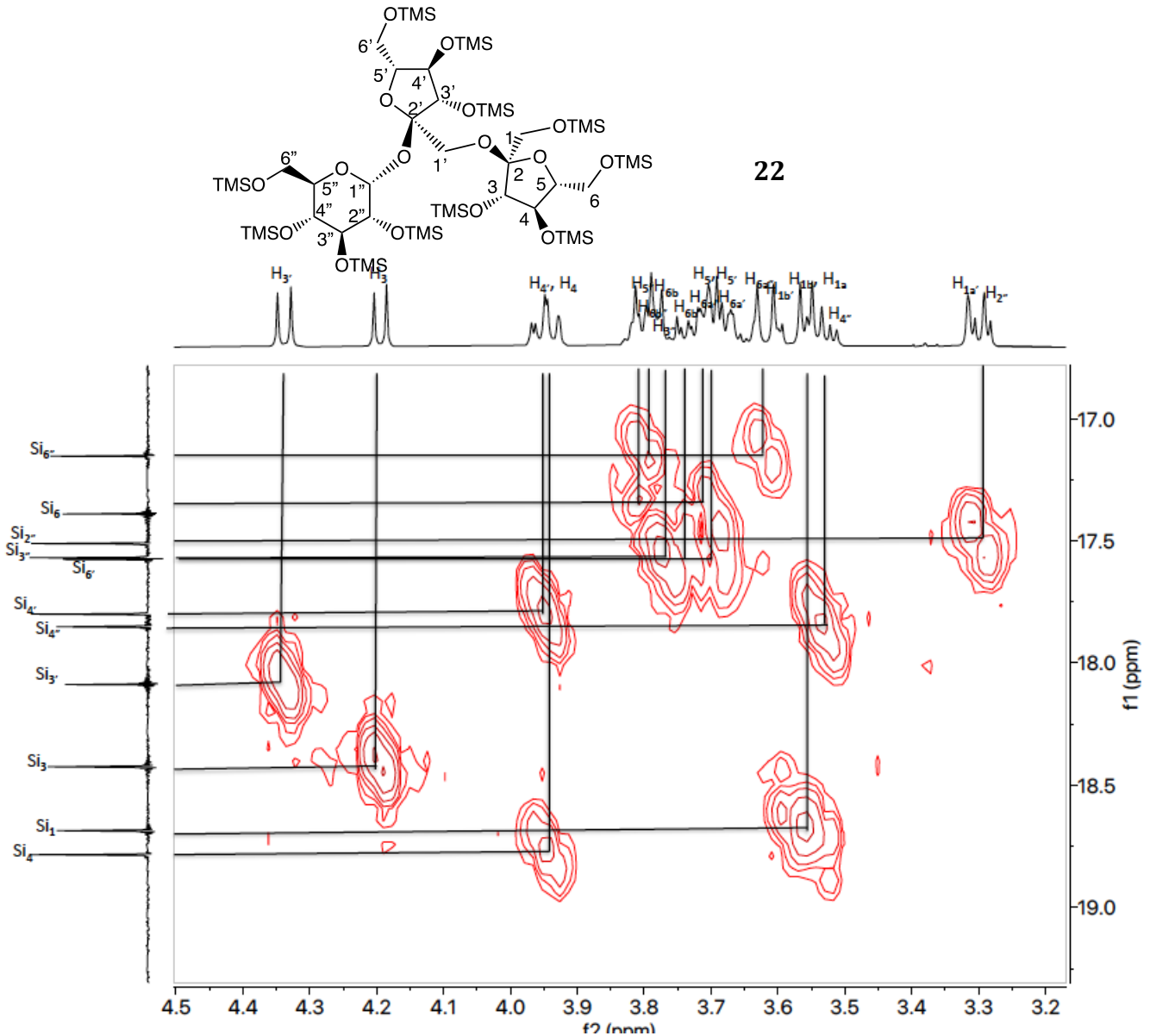

SI-Figure 1.71: per-*O*-TMS kestose (**22**) ^{1}H-^{29}Si HMBC NMR (400 MHz, $CDCl_3$) spectrum

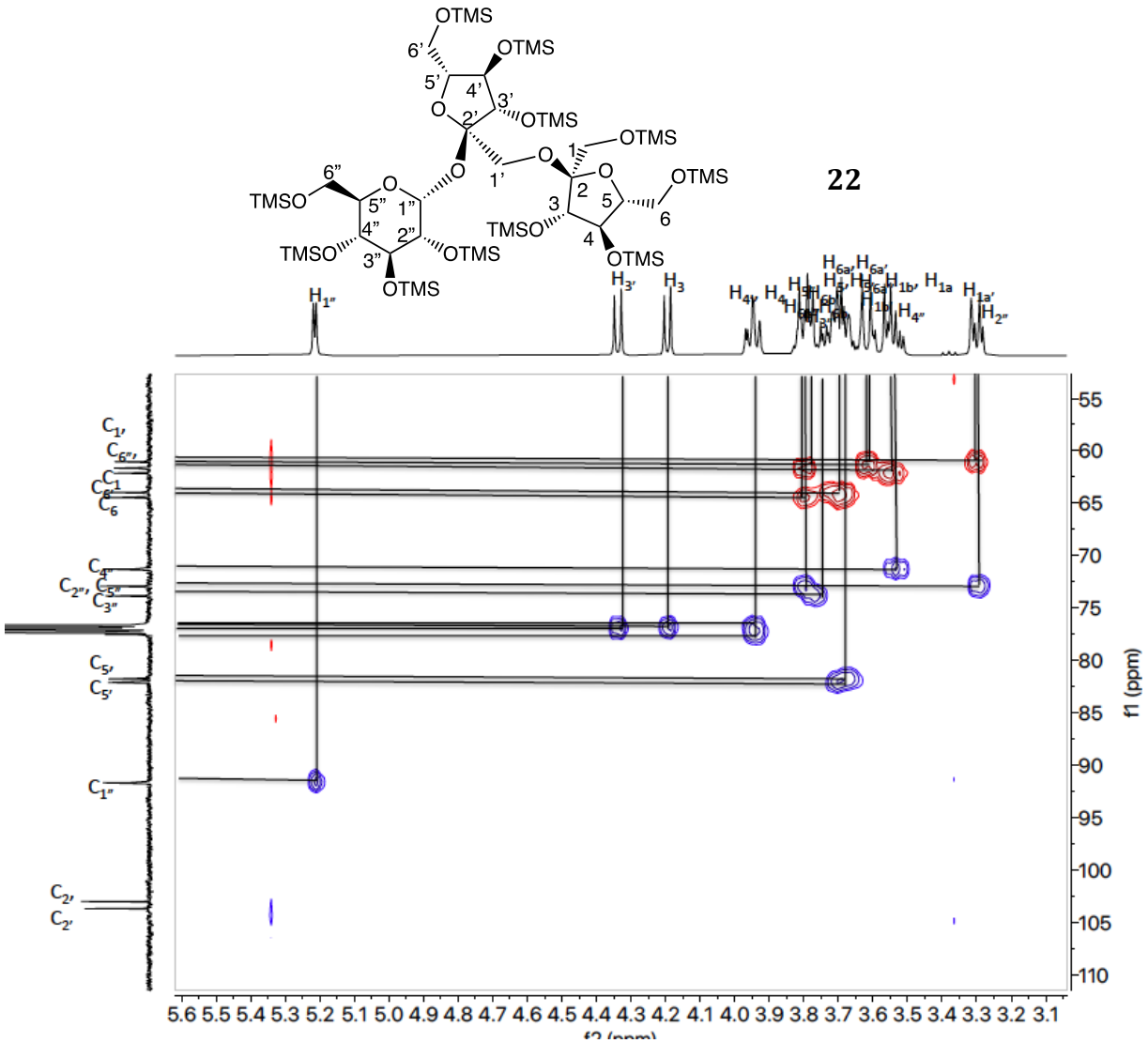

SI-Figure 1.72: per-*O*-TMS kestose (**22**) ^{1}H-^{13}C HSCQ NMR (400 MHz, $CDCl_3$) spectrum

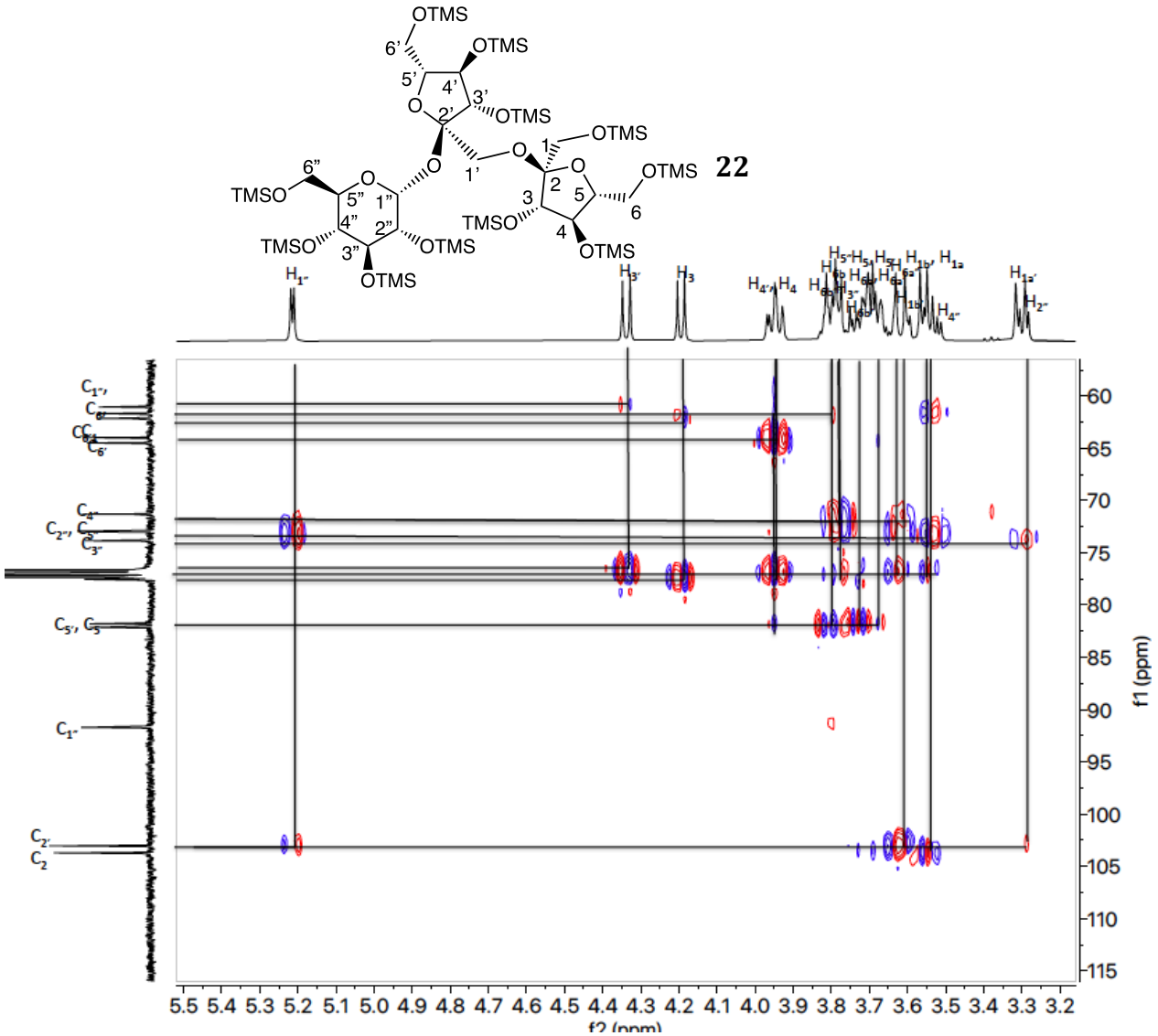

SI-Figure 1.73: per-*O*-TMS kestose (**22**) ^{1}H-^{13}C HMBC NMR (400 MHz, $CDCl_3$) spectrum

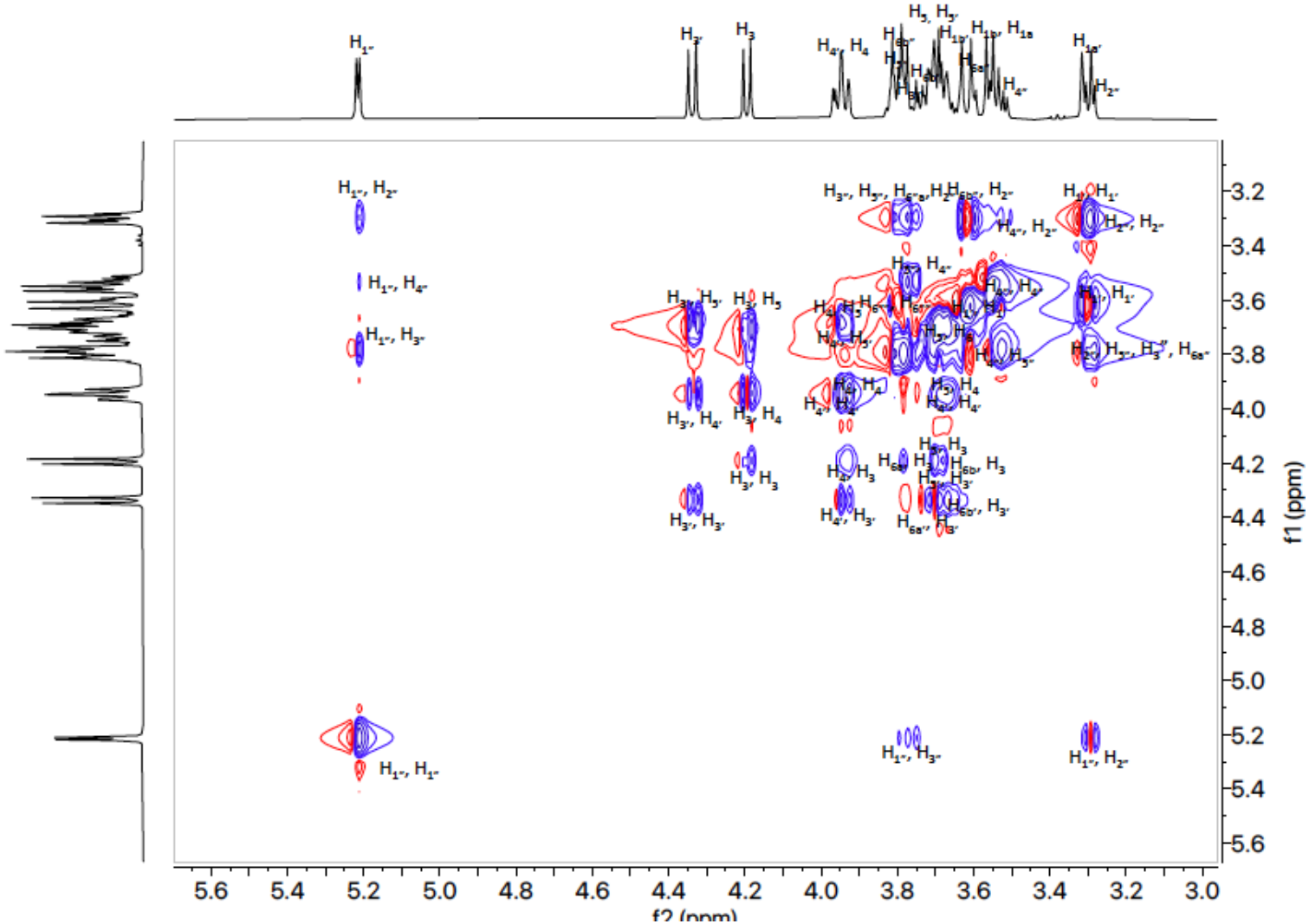

SI-Figure 1.74: per-*O*-TMS kestose (**22**) TOCSY HMBC NMR (400 MHz, $CDCl_3$) spectrum

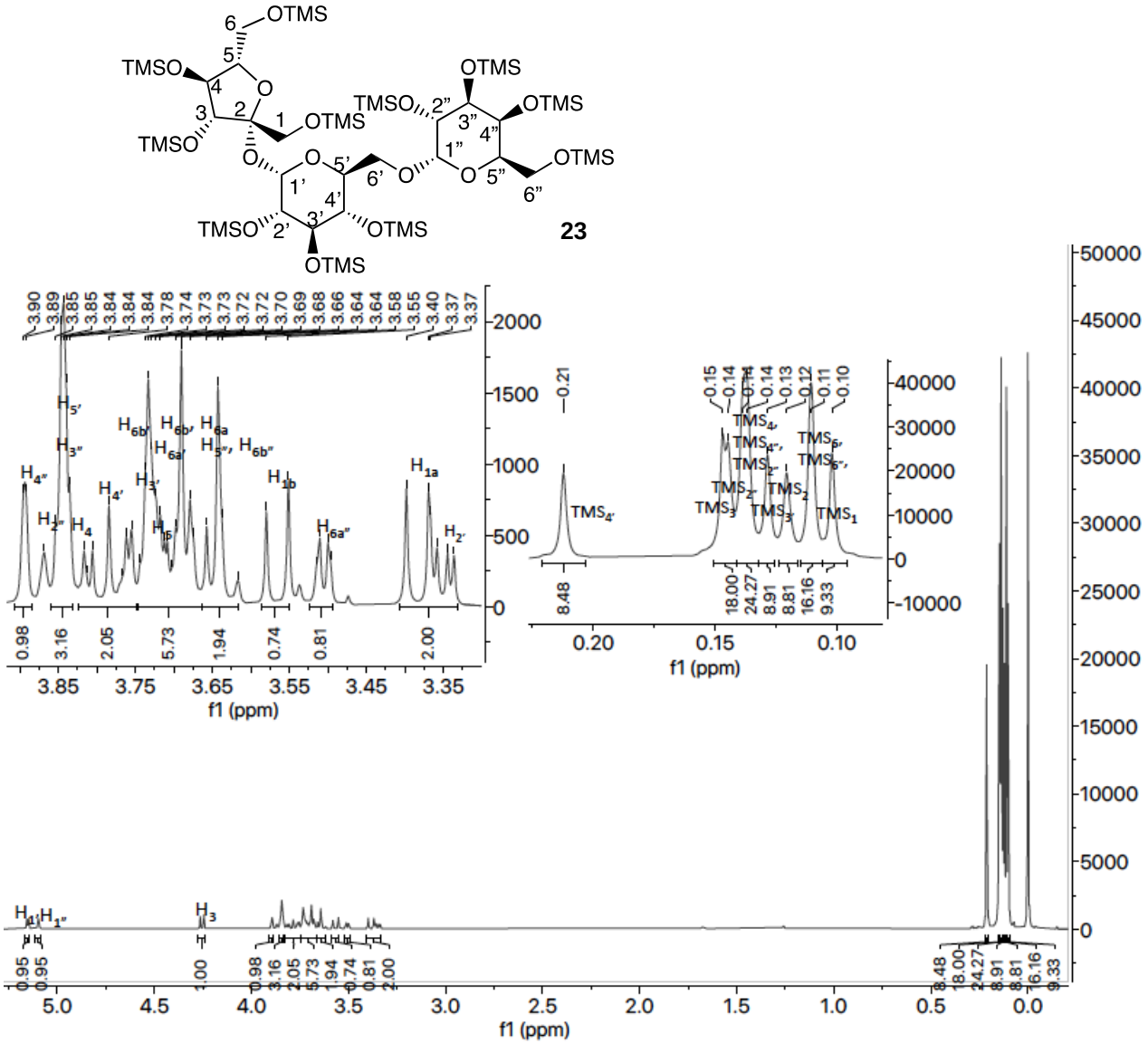

SI-Figure 1.75: per-*O*-TMS-raffinose (**23**) ^{1}H NMR (400 MHz, $CDCl_3$) spectrum

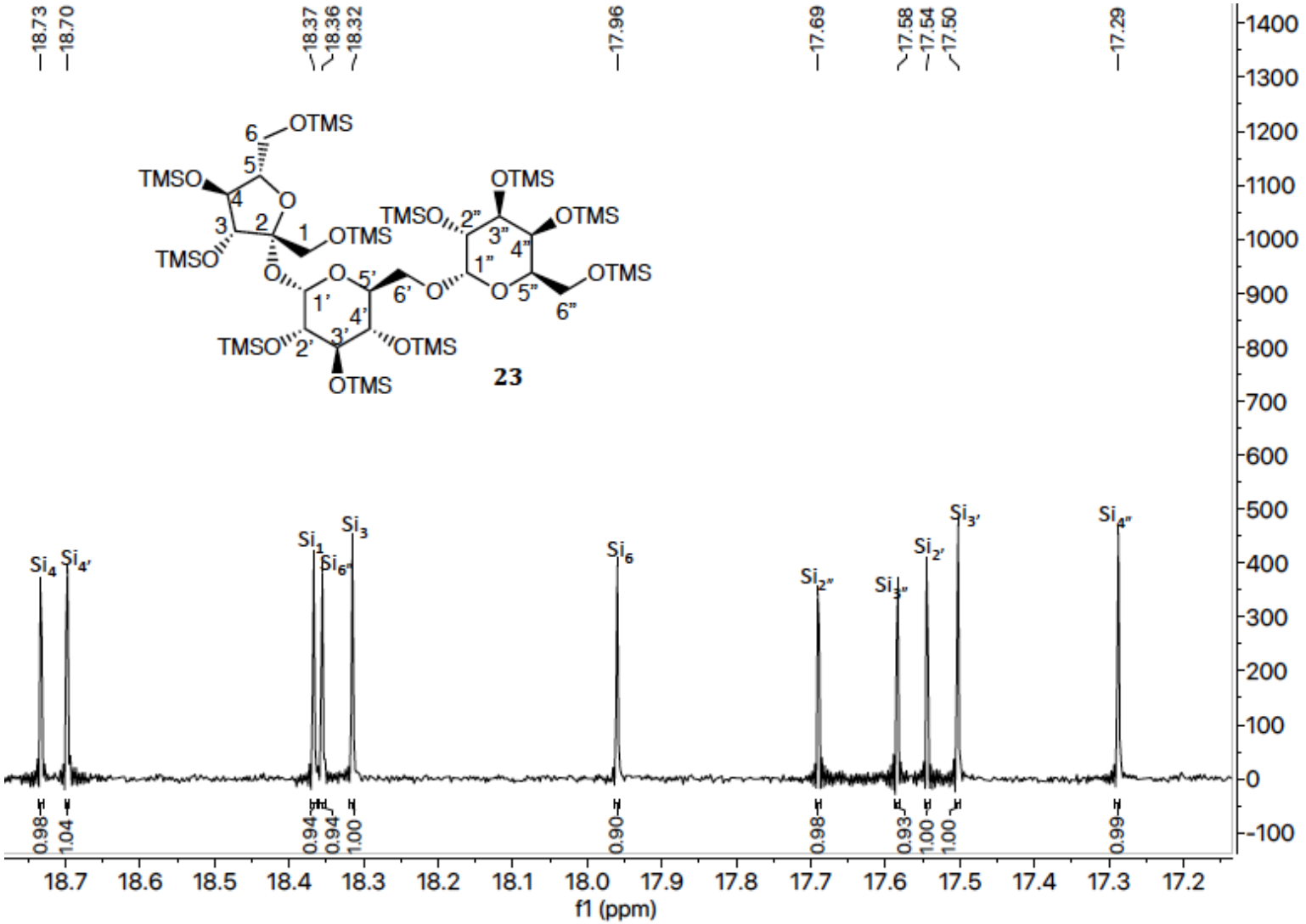

SI-Figure 1.76: per-*O*-TMS-raffinose (**23**) ^{29}Si NMR (400 MHz, $CDCl_3$) spectrum

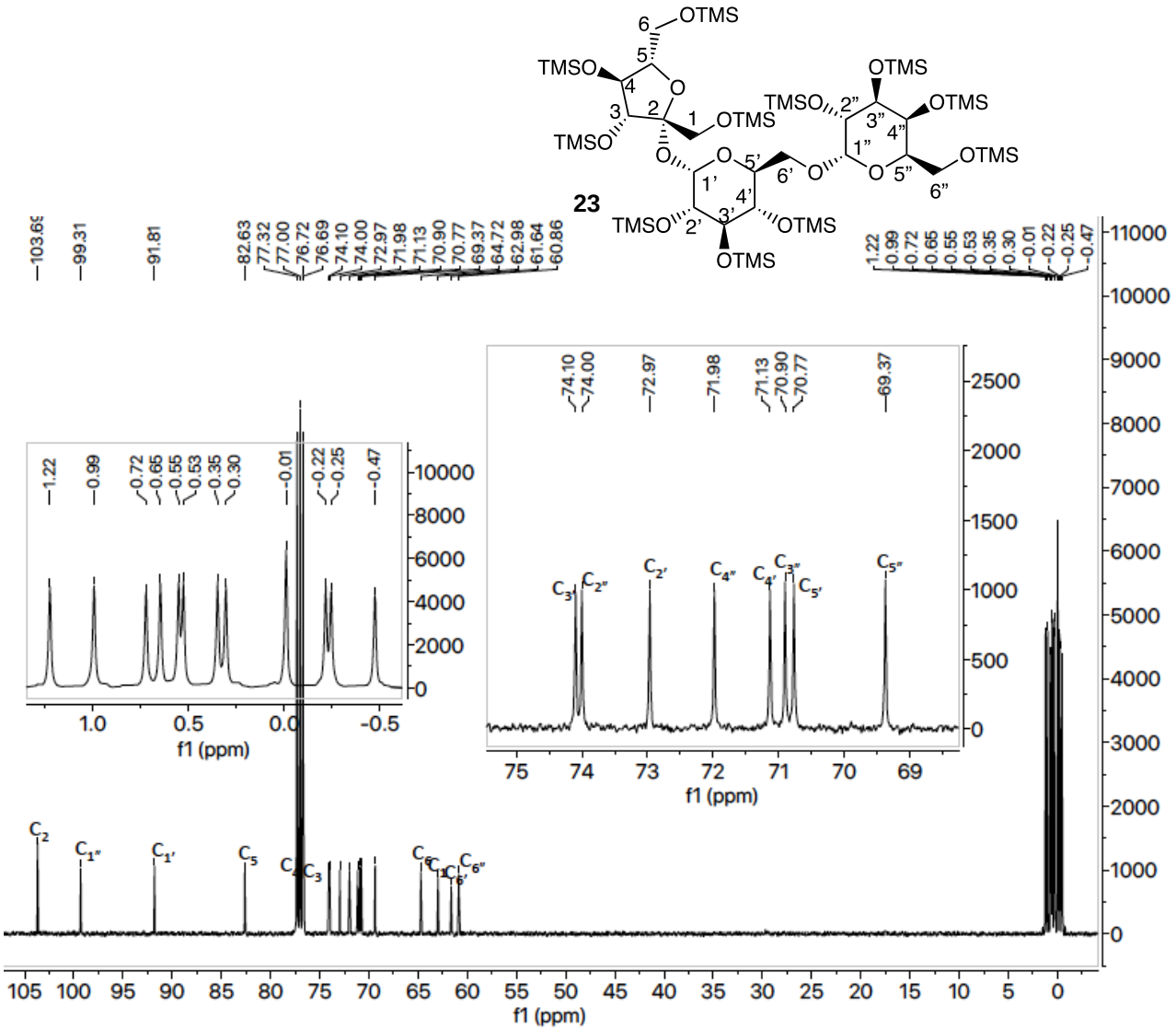

SI-Figure 1.77: per-*O*-TMS-raffinose (**23**) ^{13}C NMR (400 MHz, $CDCl_3$) spectrum

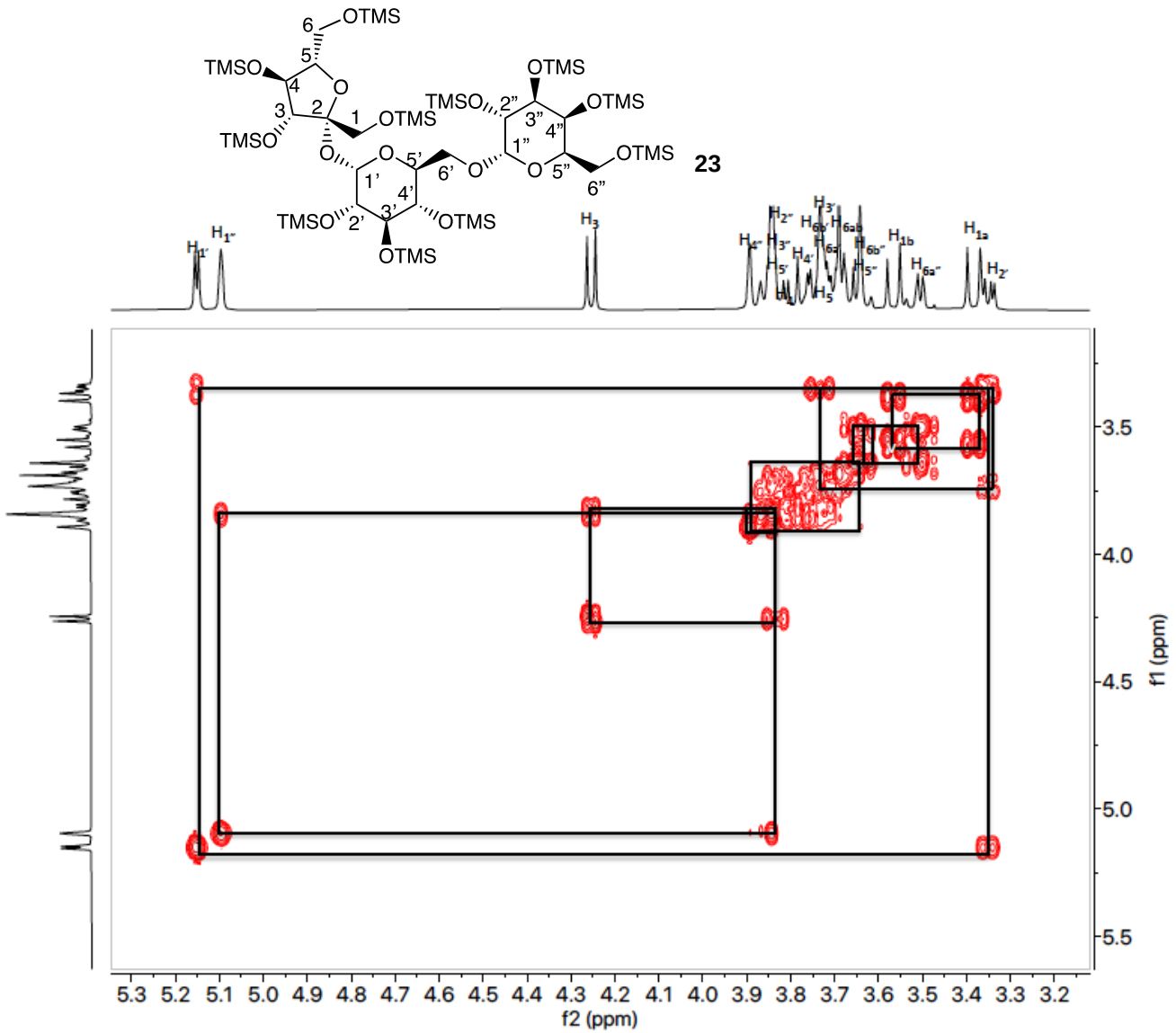

SI-Figure 1.78: per-*O*-TMS-raffinose (**23**) COSY NMR (400 MHz, $CDCl_3$) spectrum

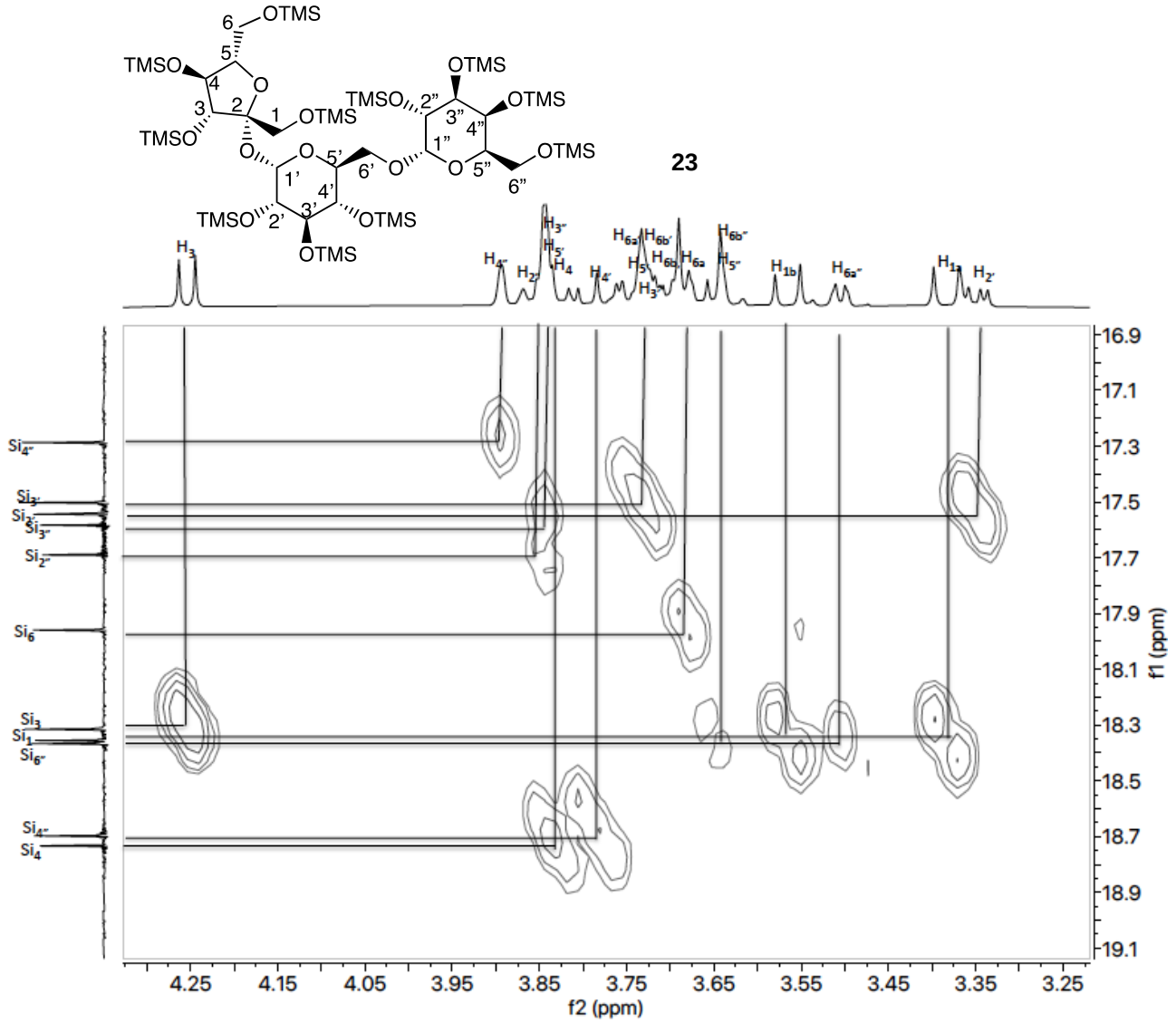

SI-Figure 1.79: per-*O*-TMS-raffinose (**23**) ^{1}H-^{29}Si HMBC NMR (400 MHz, $CDCl_3$) spectrum

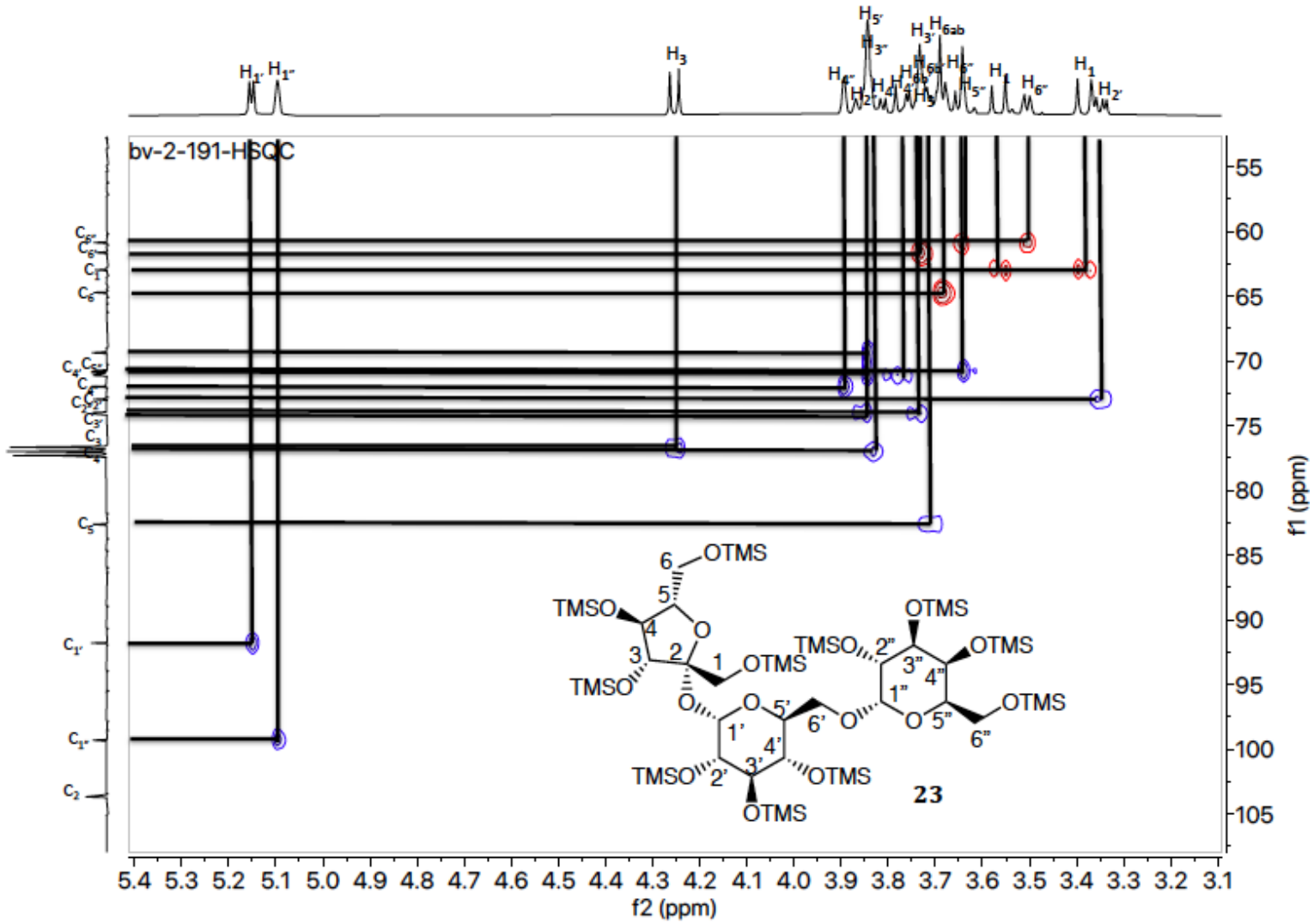

SI-Figure 1.80: per-*O*-TMS-raffinose (**23**) ^{1}H-^{13}C HSCQ NMR (400 MHz, $CDCl_3$) spectrum

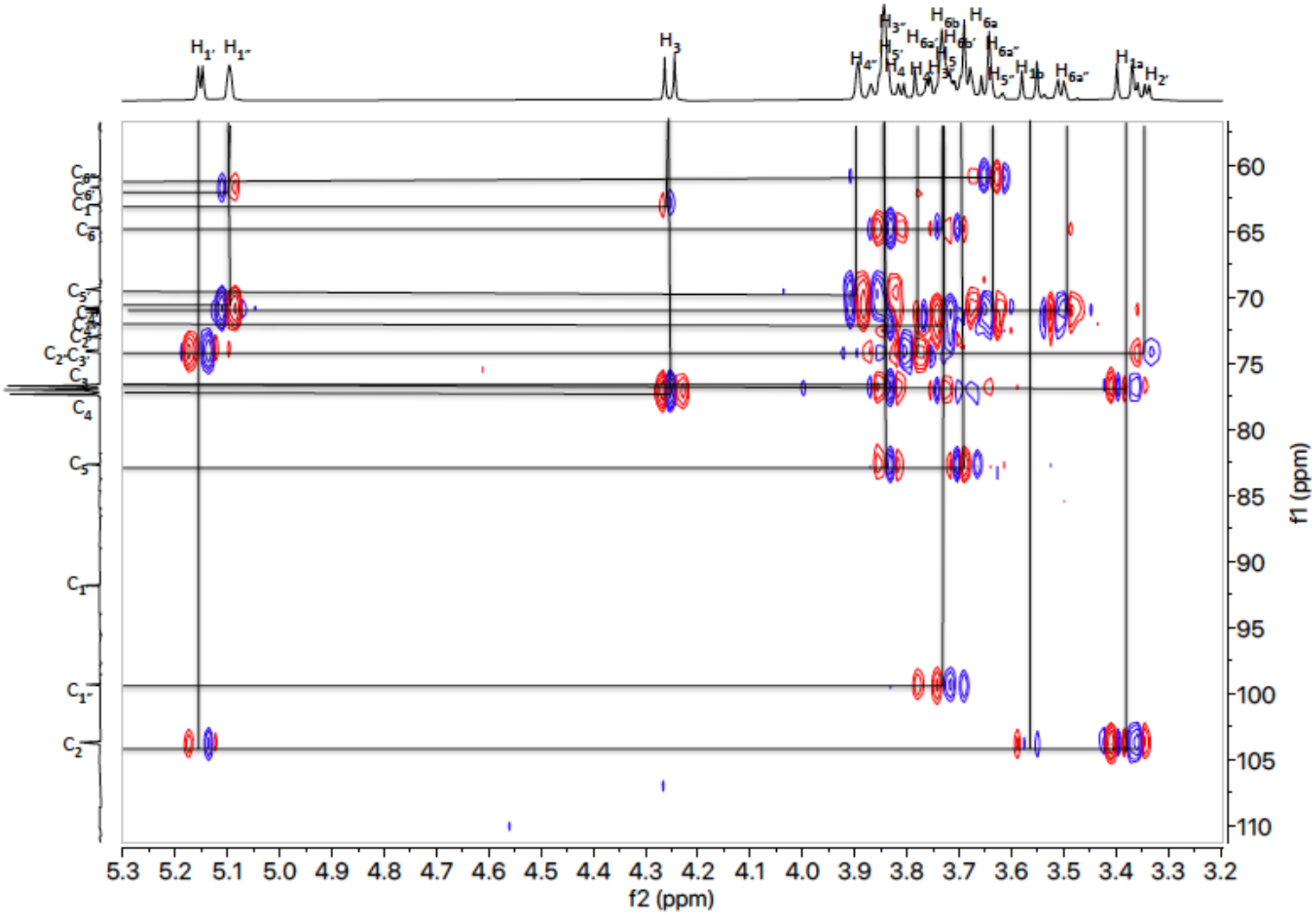

SI-Figure 1.81: per-*O*-TMS-raffinose (**23**) ^{1}H-^{13}C HMBC NMR (400 MHz, $CDCl_3$) spectrum

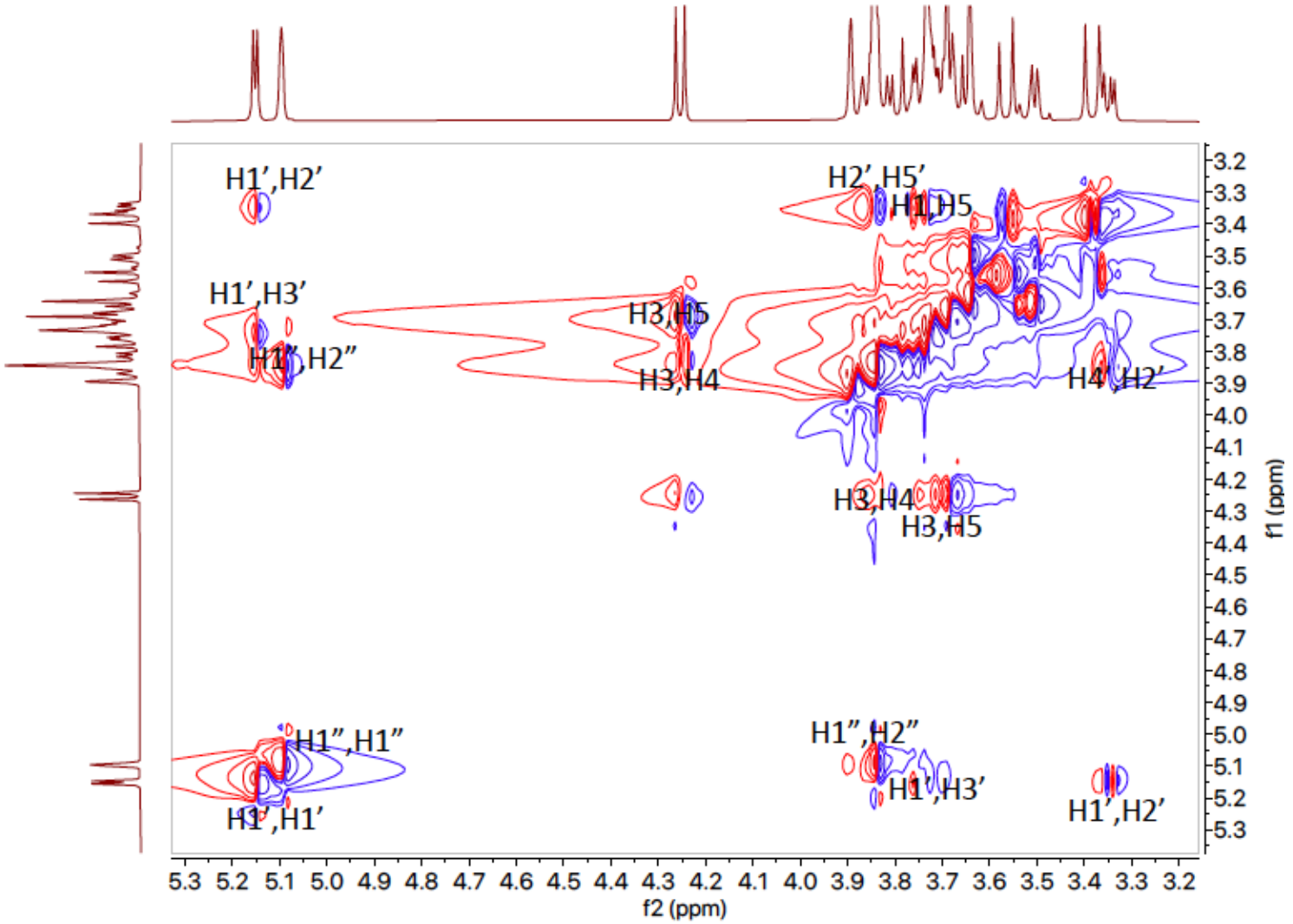

SI-Figure 1.82: per-*O*-TMS-raffinose (**23**) TOCSY NMR (400 MHz, $CDCl_3$) spectrum

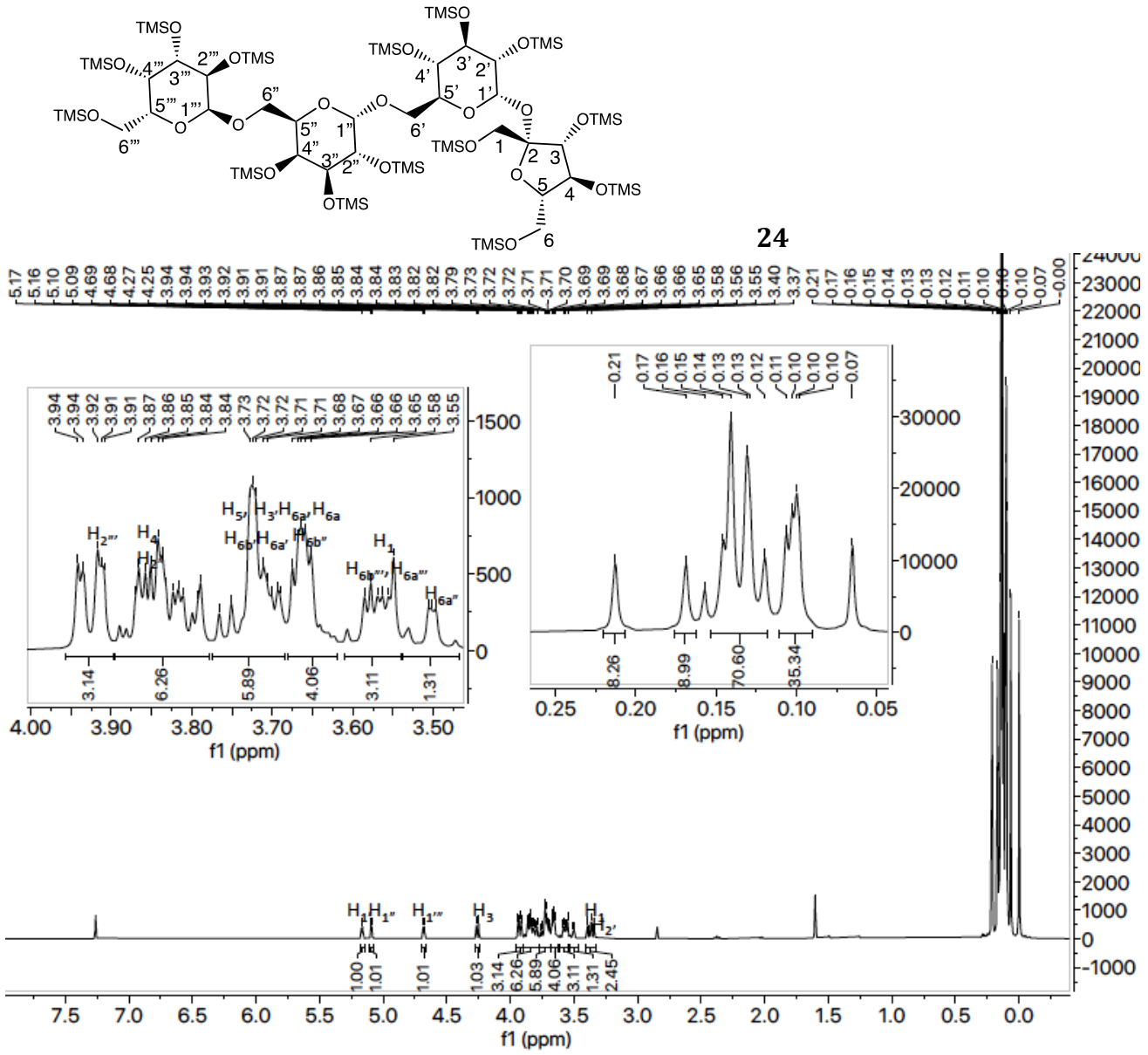

SI-Figure 1.83: per-*O*-TMS- stachyose (**24**) ^{1}H NMR (400 MHz, $CDCl_3$) spectrum

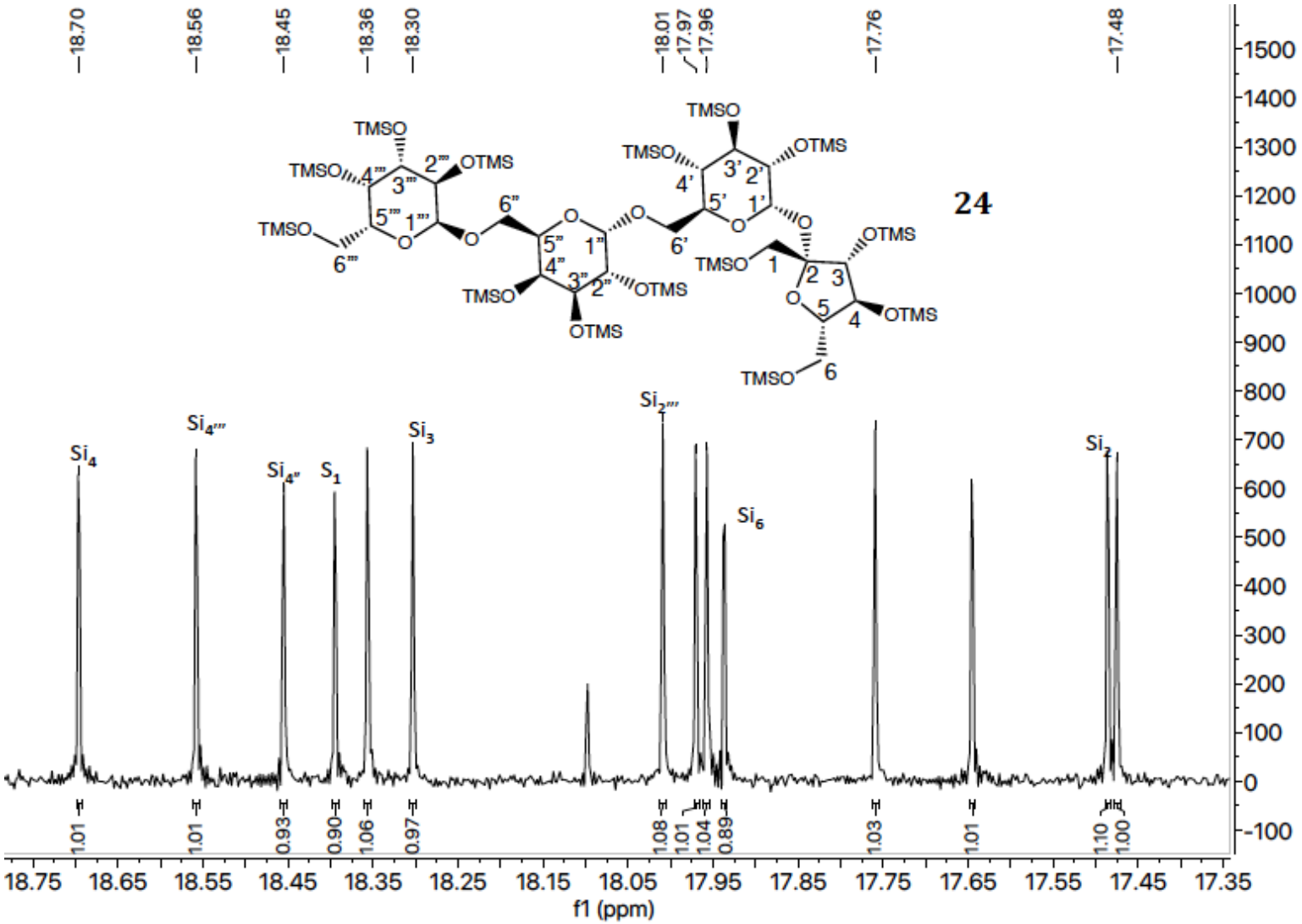

SI-Figure 1.84: per-*O*-TMS- stachyose (**24**) ^{29}Si NMR (400 MHz, $CDCl_3$) spectrum

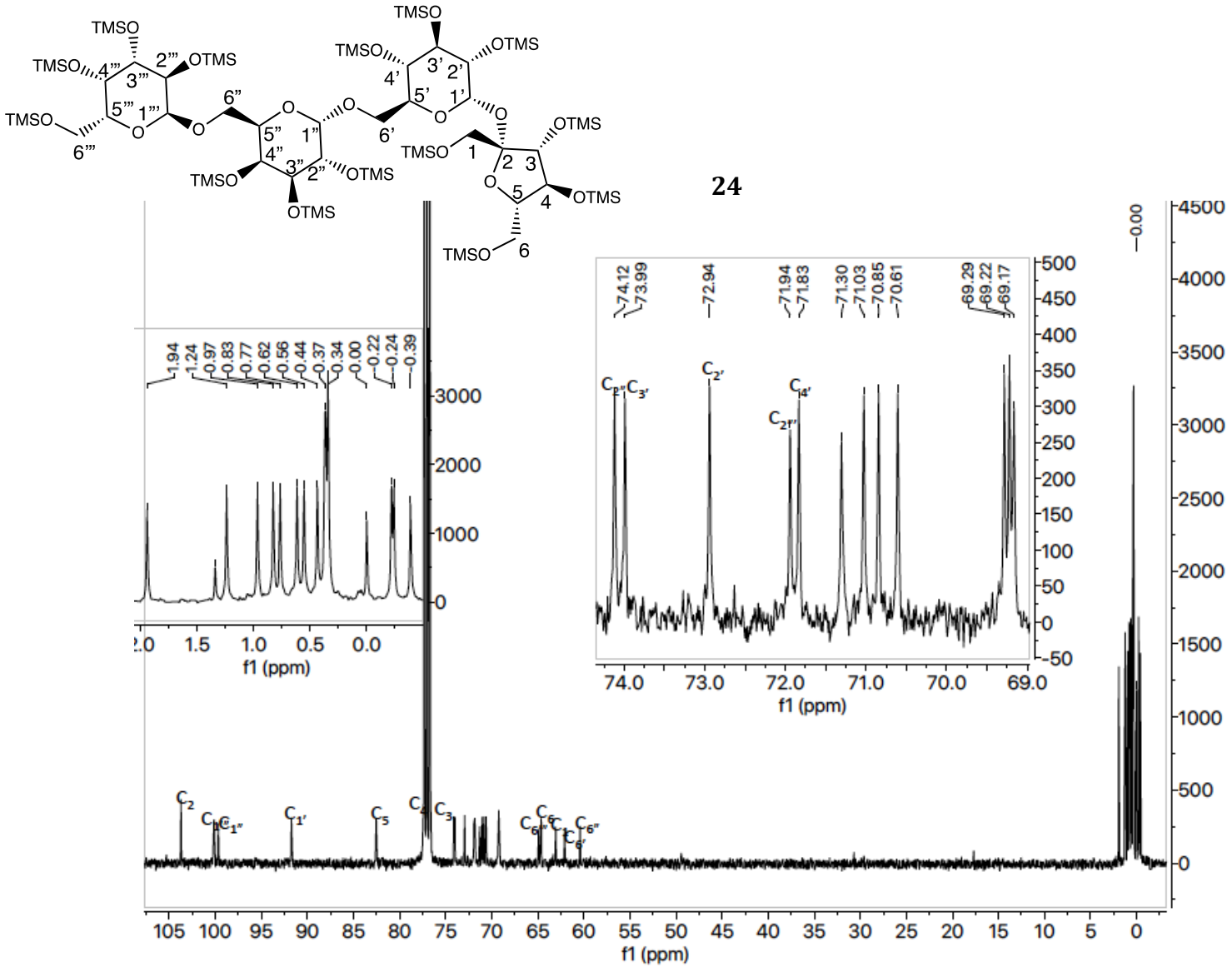

SI-Figure 1.85: per-*O*-TMS- stachyose (**24**) ^{13}C NMR (400 MHz, $CDCl_3$) spectrum

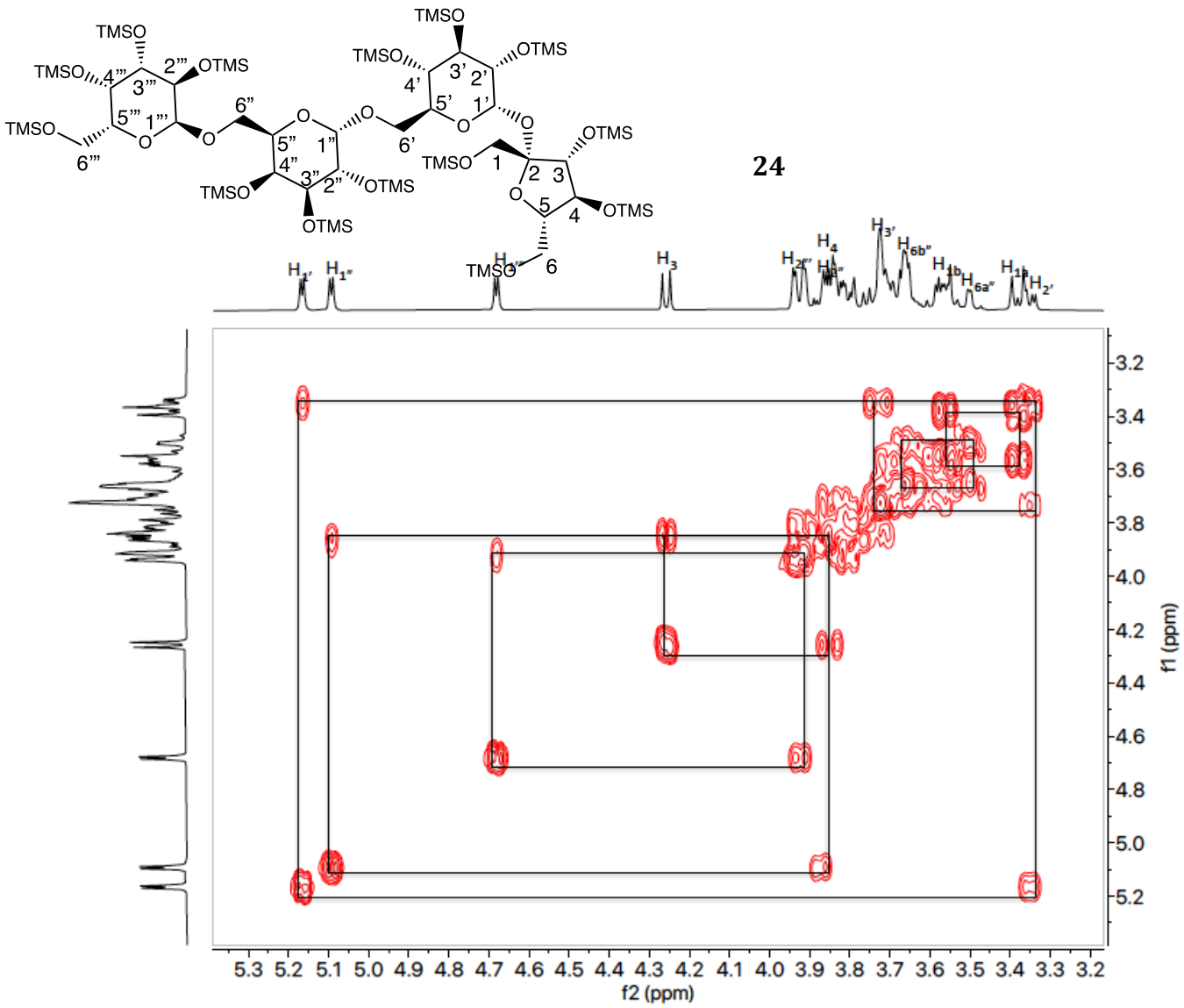

SI-Figure 1.86: per-*O*-TMS- stachyose (**24**) COSY NMR (400 MHz, $CDCl_3$) spectrum

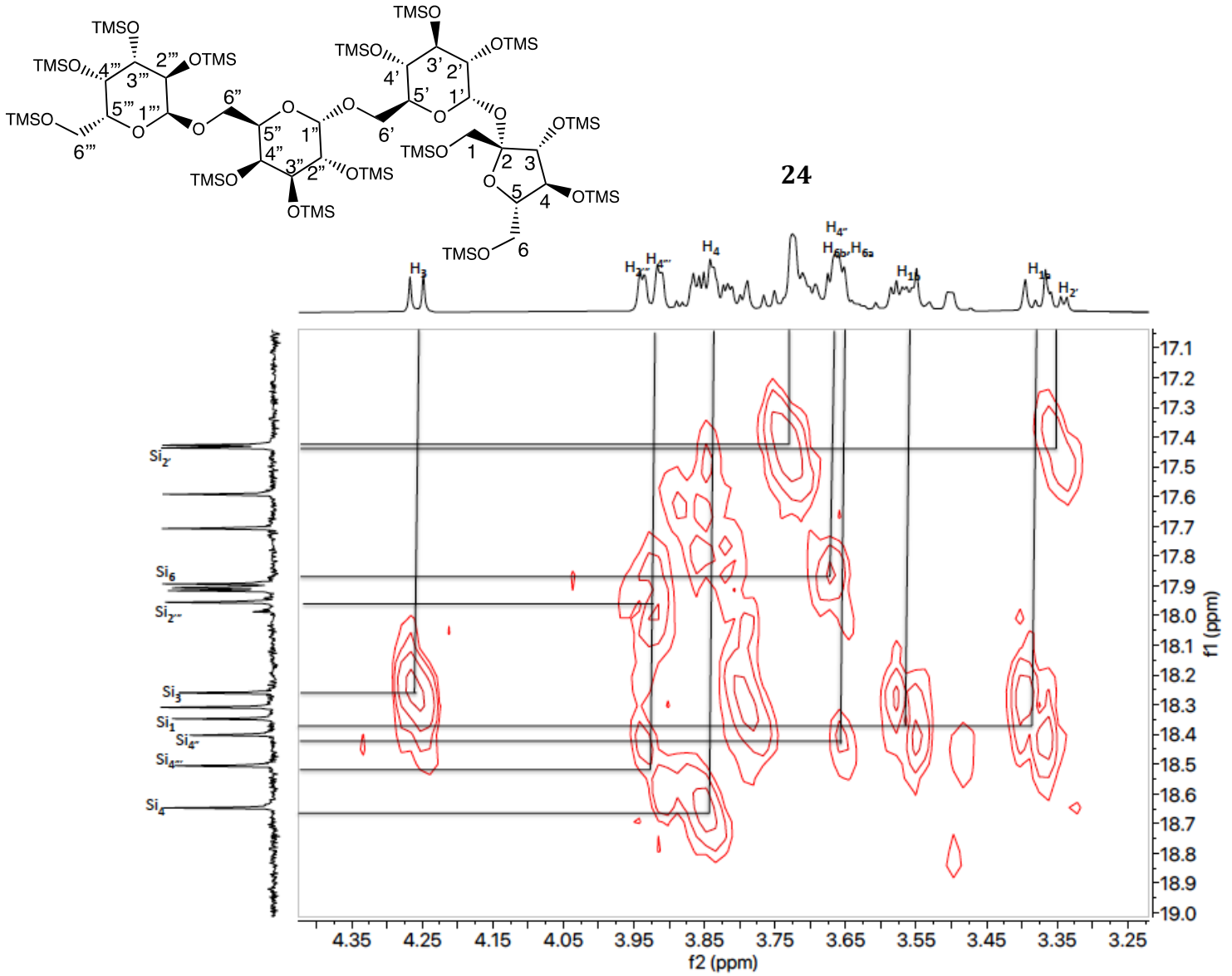

SI-Figure 1.87: per-*O*-TMS- stachyose (**24**) ^{1}H-^{29}Si HMBC NMR (400 MHz, $CDCl_3$) spectrum

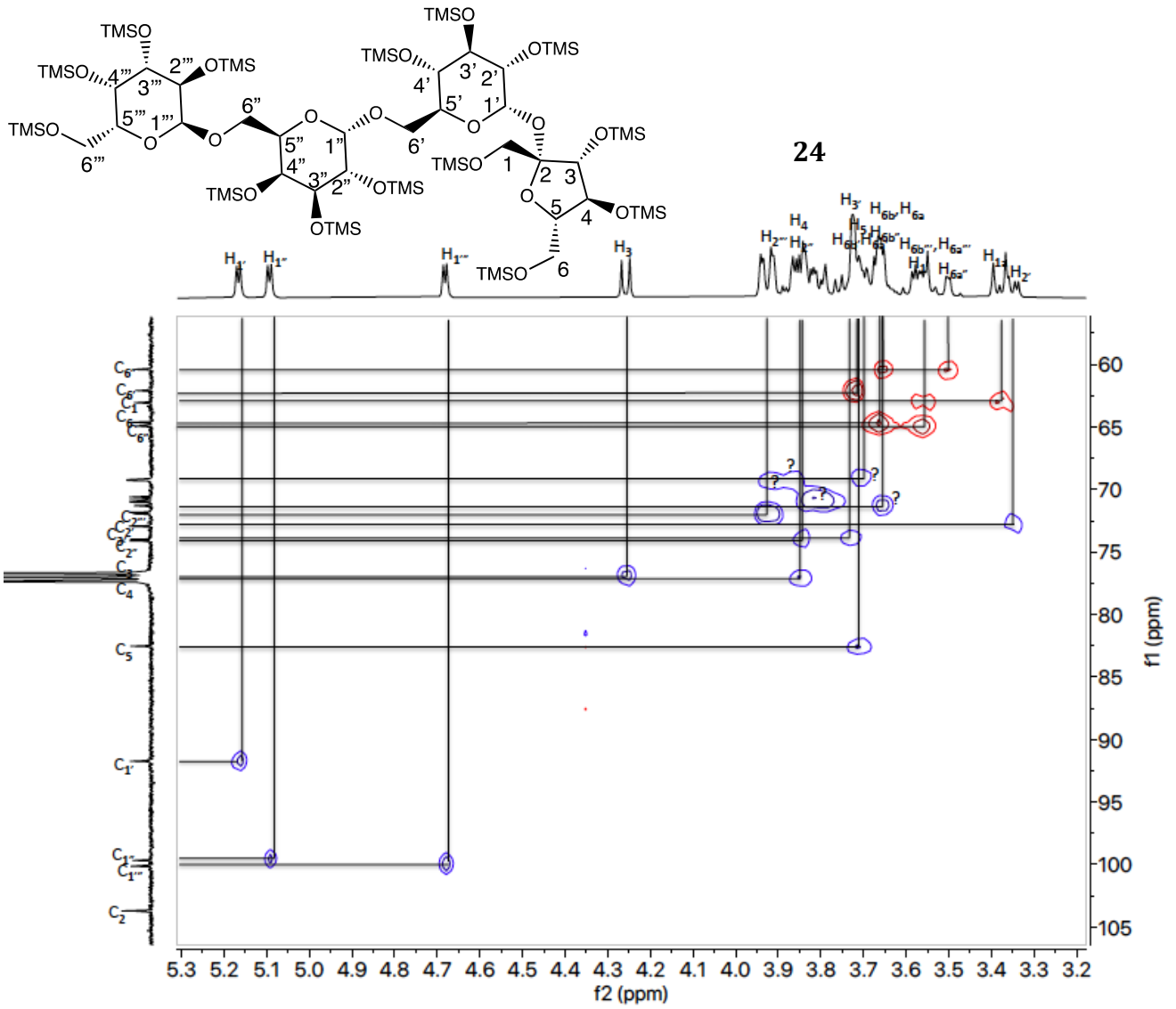

SI-Figure 1.88: per-*O*-TMS- stachyose (**24**) ^{1}H-^{13}C HSCQ NMR (400 MHz, $CDCl_3$) spectrum

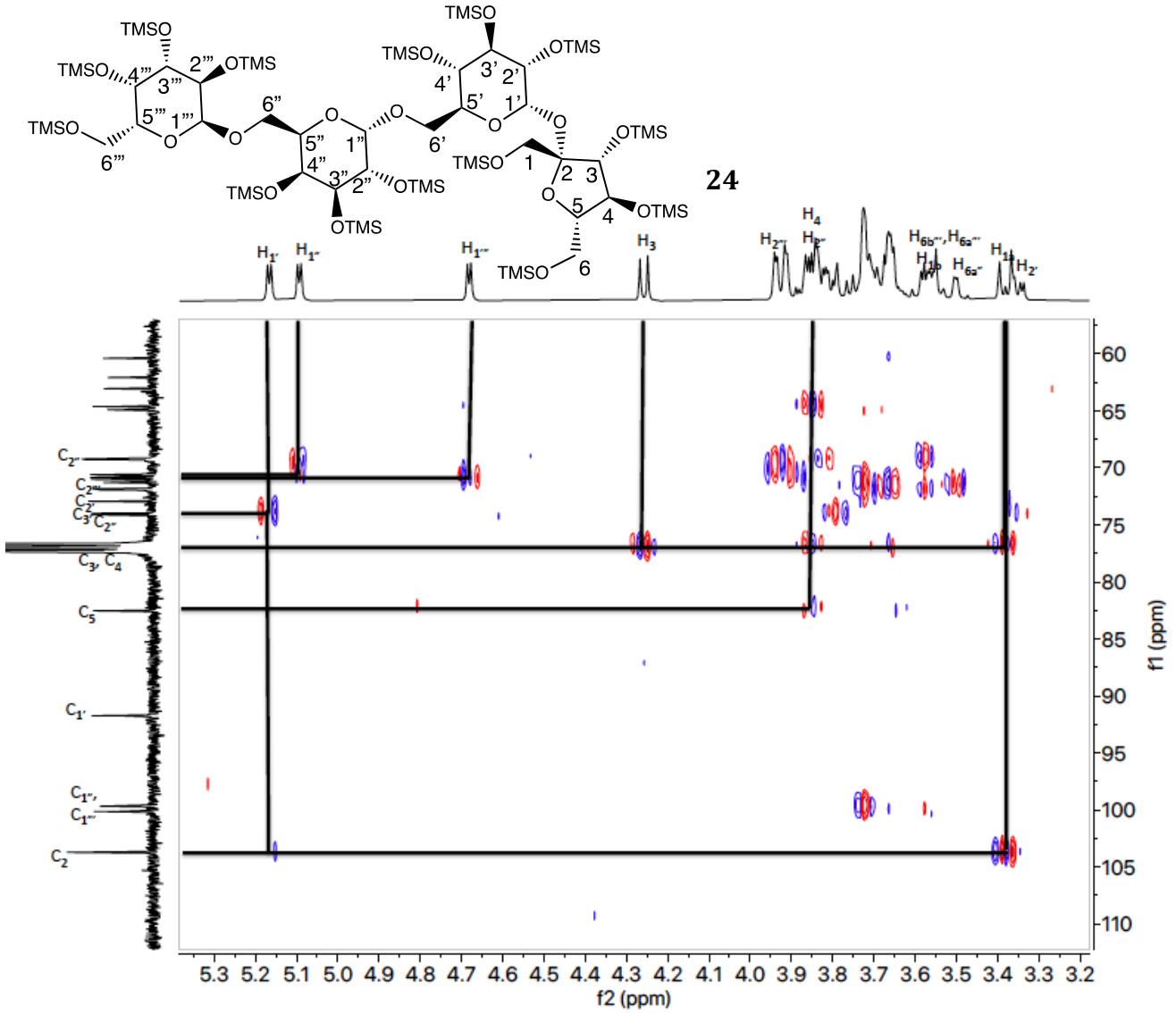

SI-Figure 1.89: per-*O*-TMS –stachyose (**24**) ^{1}H-^{13}C HMBC NMR (400 MHz, $CDCl_3$) spectrum

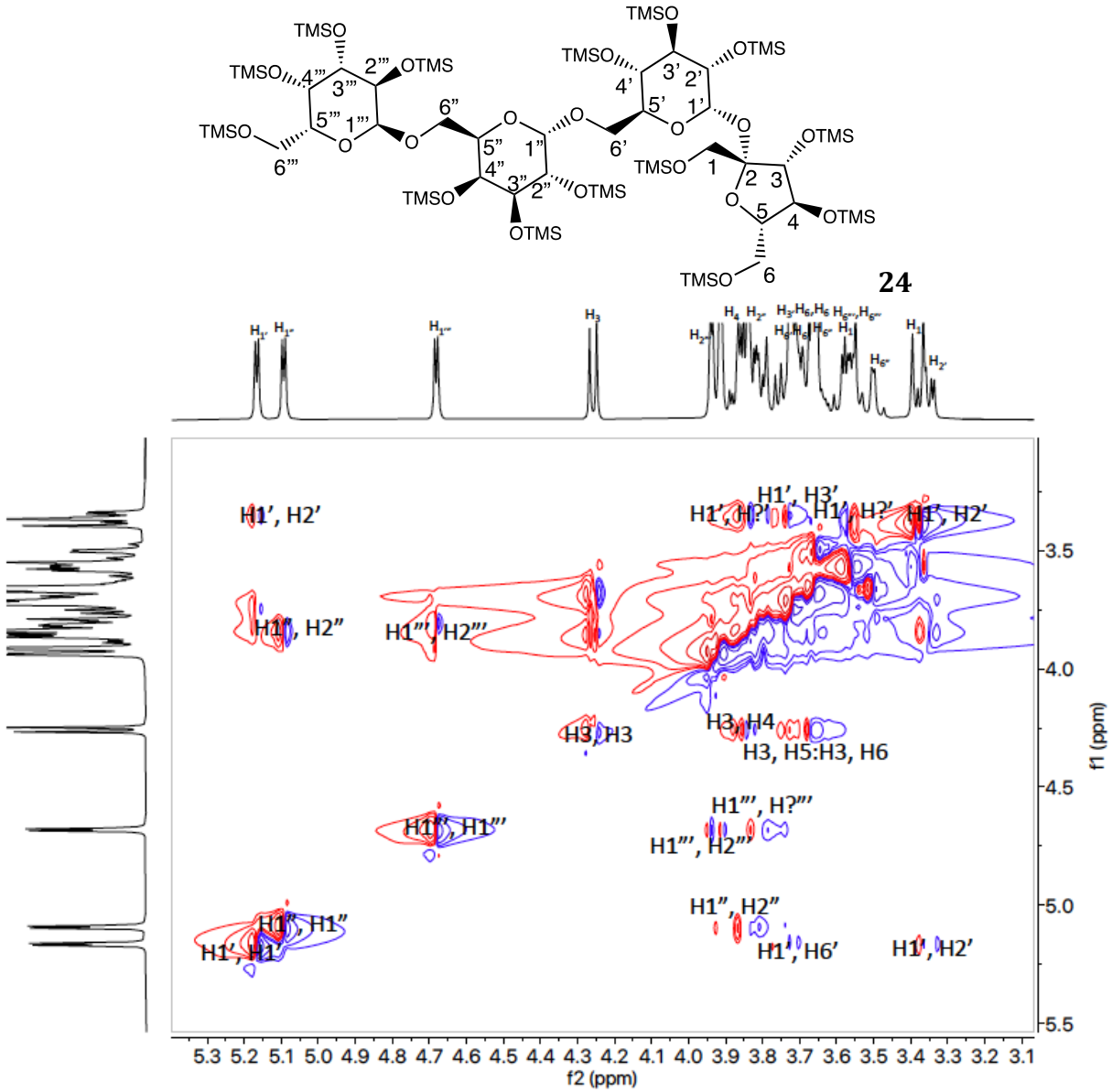

SI-Figure 1.90: per-*O*-TMS –stachyose (**24**) TOCSY HMBC NMR (400 MHz, $CDCl_3$) spectrum

References:

1. Leong, S. Y.; Duque, S. M.; Abduh, S. B. M.; Oey, I., Carbohydrates. In *Innovative Thermal and Non-Thermal Processing, Bioaccessibility and Bioavailability of Nutrients and Bioactive Compounds*, Editorial, M. R. B., Ed. Charlotte Cockle Acquisition: 2019; pp 171-206.

2. Kurzyna-Szklarek, M.; Cybulska, J.; Zdunek, A., Analysis of the chemical composition of natural carbohydrates – An overview of methods. *Food Chemistry* **2022,** *394*, 133466.

3. Yahia, E. M.; Carrillo-López, A.; Bello-Perez, L. A., Carbohydrates. In *Postharvest Physiology and Biochemistry of Fruits and Vegetables*, Maragioglio, N., Ed. Andre Gerharc Wolff Acquisition: 2019; pp 175-205.

4. Al-Mhanna, N.; Huebner, H.; Buchholz, R., Analysis of the Sugar Content in Food Products by Using Gas Chromatography Mass Spectrometry and Enzymatic Methods. *Foods* **2018,** *7* (11), 185.

5. Chapman, G. W.; Horvat, R. J., Determination of nonvolatile acids and sugars from fruits and sweet potato extracts by capillary GLC and GLC/MS. *Journal of Agricultural and Food Chemistry* **2002,** *37* (4), 947-950.

6. Rubel Mozumder, N. H. M.; Lee, Y.-R.; Hwang, K. H.; Lee, M.-S.; Kim, E.-H.; Hong, Y.-S., Characterization of tea leaf metabolites dependent on tea (Camellia sinensis) plant age through 1H NMR-based metabolomics. *Applied Biological Chemistry* **2020,** *63* (1).

7. Wei, F.; Furihata, K.; Hu, F.; Miyakawa, T.; Tanokura, M., Two-Dimensional 1H–13C Nuclear Magnetic Resonance (NMR)-Based Comprehensive Analysis of Roasted

Coffee Bean Extract. *Journal of Agricultural and Food Chemistry* **2011,** *59* (17), 9065-9073.

8. Wei, X.; Mao, F.; Cai, X.; Wang, Y., Composition and bioactivity of polysaccharides from tea seeds obtained by water extraction. *International Journal of Biological Macromolecules* **2011,** *49* (4), 587-590.

9. Shevchuk, A.; Megías-Pérez, R.; Zemedie, Y.; Kuhnert, N., Evaluation of carbohydrates and quality parameters in six types of commercial teas by targeted statistical analysis. *Food Research International* **2020,** *133*, 109122.

10. Yao, J.; Liu, H.; Ma, C.; Pu, L.; Yang, W.; Lei, Z., A Review on the Extraction, Bioactivity, and Application of Tea Polysaccharides. *Molecules* **2022,** *27* (15), 4679.

11. Lv, Y.-Q.; Li, D.; Wu, L.-Y.; Zhu, Y.-M.; Ye, Y.; Zheng, X.-Q.; Lu, J.-L.; Liang, Y.-R.; Li, Q.-S.; Ye, J.-H., Sugar signal mediates flavonoid biosynthesis in tea leaves. *Horticulture Research* **2022,** *9*.

12. Nelum P. Piyasena, K. G.; Hettiarachchi, L. S. K.; D. P. S. Jayawardhane, S. A.; U. Edirisinghe, E. N.; Jayasinghe, W. S., Evaluation of inherent fructose, glucose and sucrose concentrations in tea leaves (Camellia sinensis L.) and in black tea. *Applied Food Research* **2022,** *2* (1), 100100.

13. Caporaso, N.; Whitworth, M. B.; Grebby, S.; Fisk, I. D., Non-destructive analysis of sucrose, caffeine and trigonelline on single green coffee beans by hyperspectral imaging. *Food Research International* **2018,** *106*, 193-203.

14. Portillo, O. R.; Arévalo, A. C., Coffee's carbohydrates. A critical review of scientific literature. *Bionatura* **2022,** *7* (3), 1-12.

15. Knopp, S.; Bytof, G.; Selmar, D., Influence of processing on the content of sugars in green Arabica coffee beans. *European Food Research and Technology* **2005,** *223* (2), 195-201.

16. Constantino, L. V.; Zeffa, D. M.; Koltun, A.; Urbano, M. R.; Santos Sanzovo, A. W.; Nixdorf, S. L., Extraction of soluble sugars from green coffee beans using hot water and quantification by a chromatographic method without an organic solvent. *Acta Chromatographica* **2020,** *32* (4), 242-246.

17. Rojas-Escudero, E.; Alarcón-Jiménez, A. L.; Elizalde-Galván, P.; Rojo-Callejas, F., Optimization of carbohydrate silylation for gas chromatography. *Journal of Chromatography A* **2004,** *1027* (1-2), 117-120.

18. Ruiz-Matute, A. I.; Hernández-Hernández, O.; Rodríguez-Sánchez, S.; Sanz, M. L.; Martínez-Castro, I., Derivatization of carbohydrates for GC and GC–MS analyses. *Journal of Chromatography B* **2011,** *879* (17-18), 1226-1240.

19. Gorwitz, M. Silylation of Carbohydrate Syrups. Western Michigan University, 1979.

20. Park, S. S.; Gervay-Hague, J., Synthesis of partially O-acetylated N-acetylneuraminic acid using regioselective silyl exchange technology. *Org Lett* **2014,** *16* (19), 5044-7.

21. Hsieh, H. W.; Schombs, M. W.; Gervay-Hague, J., Integrating ReSET with glycosyl iodide glycosylation in step-economy syntheses of tumor-associated carbohydrate antigens and immunogenic glycolipids. *J Org Chem* **2014,** *79* (4), 1736-48.

22. Hsieh, H. W.; Schombs, M. W.; Witschi, M. A.; Gervay-Hague, J., Regioselective silyl/acetate exchange of disaccharides yields advanced glycosyl donor and acceptor precursors. *J Org Chem* **2013,** *78* (19), 9677-88.

23. Witschi, M. A.; Gervay-Hague, J., Selective Acetylation of per-O-TMS-Procted Monosaccharides. *Org Lett* **2010,** *12* (19), 4312-4315.

24. Ruiz-Aceituno, L.; Carrero-Carralero, C.; Ramos, L.; Martinez-Castro, I.; Sanz, M. L., Development of a carbohydrate silylation method in ionic liquids for their gas chromatographic analysis. *Analytica Chimica Acta* **2013,** *787*, 87-92.

25. Leblanc, D. J. a. B., A. J.S., A Fast One-Step Method for the Silylation of Sugars and Sugar Phosphates. *Anal. Biochem.* **1978,** *84*, 574-578.

26. Parc, A. L.; Lee, H.; Chen, K.; Barile, D., Rapid Quantification of Functional Carbohydrates in Food Products. *Food and Nutrition Sciences* **2014,** *05* (01), 71-78.

27. Roe, J. H., The Determination of Sugar in Blood and Spinal Fluid with Anthrone Reagent. *Journal of Biological Chemistry* **1955,** *212* (1), 335-343.

28. Wang, Y.; Jing, Y.; Leng, F.; Wang, S.; Wang, F.; Zhuang, Y.; Liu, X.; Wang, X.; Ma, X., Establishment and Application of a Method for Rapid Determination of Total Sugar Content Based on Colorimetric Microplate. *Sugar Tech* **2016,** *19* (4), 424-431.

29. Van Wychen, S.; Long, W.; Black, S. K.; Laurens, L. M. L., MBTH: A novel approach to rapid, spectrophotometric quantitation of total algal carbohydrates. *Analytical Biochemistry* **2017,** *518*, 90-93.

30. Sanz Rodríguez, E.; Díaz-Arenas, G. L.; Makart, S.; Ghosh, D.; Patti, A. F.; Garnier, G.; Tanner, J.; Paull, B., Determination of xylooligosaccharides produced from enzymatic hydrolysis of beechwood xylan using high-performance anion-exchange

chromatography tandem mass spectrometry. *Journal of Chromatography A* **2022,** *1666*, 462836.

31. Haldar, D.; Sen, D.; Gayen, K., Development of Spectrophotometric Method for the Analysis of Multi-component Carbohydrate Mixture of Different Moieties. *Applied Biochemistry and Biotechnology* **2016,** *181* (4), 1416-1434.

32. Jermyn, M. A., Increasing the sensitivity of the anthrone method for carbohydrate. *Anal. Biochem.* **1975,** *68* (1), 332-332.

33. Deshavath, N. N.; Mukherjee, G.; Goud, V. V.; Veeranki, V. D.; Sastri, C. V., Pitfalls in the 3, 5-dinitrosalicylic acid (DNS) assay for the reducing sugars: Interference of furfural and 5-hydroxymethylfurfural. *International Journal of Biological Macromolecules* **2020,** *156*, 180-185.

34. Zaky, A. S.; Pensupa, N.; Andrade-Eiroa, Á.; Tucker, G. A.; Du, C., A new HPLC method for simultaneously measuring chloride, sugars, organic acids and alcohols in food samples. *Journal of Food Composition and Analysis* **2017,** *56*, 25-33.

35. Wang, X.; Zhang, L.; Wu, J.; Xu, W.; Wang, X.; Lü, X., Improvement of simultaneous determination of neutral monosaccharides and uronic acids by gas chromatography. *Food Chemistry* **2017,** *220*, 198-207.

36. Valliyodan, B.; Shi, H.; Nguyen, H. T., A Simple Analytical Method for High-Throughput Screening of Major Sugars from Soybean by Normal-Phase HPLC with Evaporative Light Scattering Detection. *Chromatography Research International* **2015,** *2015*, 1-8.

37. Yan, X., Carbohydrate analysis by high-performance liquid chromatography (HPLC) with evaporative light-scattering detection (ELSD). **2021**, 631-644.

38. Downes, K.; Terry, L. A., A new acetonitrile-free mobile phase method for LC–ELSD quantification of fructooligosaccharides in onion (Allium cepa L.). *Talanta* **2010,** *82* (1), 118-124.

39. Lu, Y.; Guo, S.; Zhang, F.; Yan, H.; Qian, D.-w.; Shang, E.-x.; Wang, H.-q.; Duan, J.-a., Nutritional components characterization of Goji berries from different regions in China. *Journal of Pharmaceutical and Biomedical Analysis* **2021,** *195*, 113859.

40. Raessler, M., Sample preparation and current applications of liquid chromatography for the determination of non-structural carbohydrates in plants. *TrAC Trends in Analytical Chemistry* **2011,** *30* (11), 1833-1843.

41. Hu, X.; Fang, C.; Lu, L.; Hu, Z.; Shao, Y.; Zhu, Z., Determination of soluble sugar profile in rice. *Journal of Chromatography B* **2017,** *1058*, 19-23.

42. Xian, Y.; Dong, H.; Luo, H.; Luo, D.; Wu, Y.; Zhao, M.; Guo, X., Identification of dried shark fins by analysis of seven sugars using pre-column derivatization high-performance liquid chromatography and stable carbon isotope ratio analysis. *Analytical Methods* **2015,** *7* (14), 5973-5980.

43. Račaitytė, K.; Kiessig, S.; Kálmán, F., Application of capillary zone electrophoresis and reversed-phase high-performance liquid chromatography in the biopharmaceutical industry for the quantitative analysis of the monosaccharides released from a highly glycosylated therapeutic protein. *Journal of Chromatography A* **2005,** *1079* (1-2), 354-365.

44. Feng, T.; Sun, M.; Song, S.; Zhuang, H.; Yao, L., Gas chromatography for food quality evaluation. **2019**, 219-265.

45. Han, B.; Park, J. W.; Kang, M.; Kim, B.; Jeong, J.-s.; Kwon, O.-S.; Son, J., Simultaneous analysis of monosaccharides using ultra high performance liquid chromatography-high resolution mass spectrometry without derivatization for validation of certified reference materials. *Journal of Chromatography B* **2020,** *1160*, 122370.

46. Mason, B. S., and Slover, Hal T., Gas-chromatographic method for the determination of sugars in foods. *Journal of Agricultural and Food Chemistry* **1971,** *19* (3), 551-554.

47. Jones, D.; Ormondroyd, G. O.; Curling, S. F.; Popescu, C. M.; Popescu, M. C., Chemical compositions of natural fibres. *Elsevier* **2017**, 23-58.

48. Beghi, R.; Giovenzana, V.; Tugnolo, A.; Guidetti, R., Application of visible/near infrared spectroscopy to quality control of fresh fruits and vegetables in large-scale mass distribution channels: a preliminary test on carrots and tomatoes. *Journal of the Science of Food and Agriculture* **2018,** *98* (7), 2729-2734.

49. Oliveira-Folador, G.; Bicudo, M. d. O.; de Andrade, E. F.; Renard, C. M.-G. C.; Bureau, S.; de Castilhos, F., Quality traits prediction of the passion fruit pulp using NIR and MIR spectroscopy. *Lwt* **2018,** *95*, 172-178.

50. Chudnovsky, A.; Golberg, A.; Linzon, Y., Monitoring complex monosaccharide mixtures derived from macroalgae biomass by combined optical and microelectromechanical techniques. *Process Biochemistry* **2018,** *68*, 136-145.

51. Santos, J. R.; Viegas, O.; Páscoa, R. N. M. J.; Ferreira, I. M. P. L. V. O.; Rangel, A. O. S. S.; Lopes, J. A., In-line monitoring of the coffee roasting process with near infrared

spectroscopy: Measurement of sucrose and colour. *Food Chemistry* **2016,** *208*, 103-110.

52. Rinnan, Å.; Berg, F. v. d.; Engelsen, S. B., Review of the most common pre-processing techniques for near-infrared spectra. *TrAC Trends in Analytical Chemistry* **2009,** *28* (10), 1201-1222.

53. Bellon-Maurel, V.; McBratney, A., Near-infrared (NIR) and mid-infrared (MIR) spectroscopic techniques for assessing the amount of carbon stock in soils – Critical review and research perspectives. *Soil Biology and Biochemistry* **2011,** *43* (7), 1398-1410.

54. Tristán, A. I.; Abreu, A. C.; Aguilera-Sáez, L. M.; Peña, A.; Conesa-Bueno, A.; Fernández, I., Evaluation of ORAC, IR and NMR metabolomics for predicting ripening stage and variety in melon (Cucumis melo L.). *Food Chemistry* **2022,** *372*, 131263.

55. Pieters, L. A. C. a. V., A. J., Applications of quantitative 1H- and 13C-NMR spectroscopy in drug analysis. *Journal of Pharmaceutical and Biomedical Analysis* **1989,** *7* (12), 1405.

56. Schraml, J., 29Si NMR Spectroscopy of Trimethylsilyl Tags. *Progress in NMR Spectroscopy* **1990,** *22*, 289-348.

57. Williams, E. A.; Cargioli, J. D., Silicon-29 NMR Spectroscopy. **1979,** *9*, 221-318.

58. Blinka, T. A.; Helmer, B. J.; West, R., Polarization Transfer NMR Spectroscopy for Silicon-29: The INEPT and DEPT Techniques. **1984,** *23*, 193-218.

59. Vincendon, R. N. a. M., Proton-Silicon-29 Two Dimensional Chemical-Shift Correlation NMR Spectroscopy. *Journal of Magnetic Resonance* **1985,** *61*, 338-342.

60. Mouna Harket, B. D. J., Jean-Claude Lartigue, Michel Petraud, Max Ratier, Application of the 29Si NMR 2D INEPT spin-flip J-resolved technique to the structural analysis of trimethylsilylated glycosides. *Carbohydrate Research* **1994,** *263*, 155-161.

61. Schramal, J., INEPT with selective decoupling of protons used for polarization transfer. Routine assignment technique for 29Si NMR spectra of trimethylsilylated products. *Journal of Magnetic Resonance* **1984,** *59* (3).

62. Knight, C. T. G., On 29Si Scalar Couplings and Spin-Lattice Relaxation Times in 29Si NMR Spectroscopic Studies of the Hydrolysis of Tetramethoxysilane. *Journal of Non-Crystalline Solids* **1988,** *103*, 1515-152.

63. Farjon, J.; Giros, A.; Deloisy, S.; Blanco, L.; Hannedouche, J.; Schulz, E.; Merlet, D., 29Si-1H IMPACT HMBC: a suitable tool for analyzing silylated derivatives. *Magnetic Resonance in Chemistry* **2013,** *51* (4), 230-233.

64. Gale, D. J.; Haines, A. H.; Harris, R. K., 29Si and13C NMR studies of organosilicon chemistry. V—Sugar derivatives. *Organic Magnetic Resonance* **1975,** *7* (12), 635-636.

65. Provera, S.; Davalli, S.; Raza, G. H.; Contini, S.; Marchioro, C., Long-range two-dimensional1H-29Si heteronuclear shift correlation using gradients. Application to tetra-TMS-?-O-methyl-D-glucopyranose and tetra-TES-?-O-methyl-D-glucopyranose. *Magnetic Resonance in Chemistry* **2001,** *39* (1), 38-42.

66. Vincent Baudrillard, D. D., G. Plé, Application of modified selective polarization transfer experiments to the structural analysis of β‐silylated silyl enol ethers by 1H, 13C and 29Si NMR. *Magnetic Resonance in Chemistry* **1994,** *32*, 40-45.

67. Schraml, J., 29Si and 13C NMR spectra of all possible pertrimethylsilylated β‐D‐xylopyranosyl‐substituted methyl 4‐O‐β‐D‐xylopyranosyl‐β‐D‐

xylopyranosides assigned by 2D heteronuclear 1H - 29Si and 1H - 13C chemical shift correlations. *Magnetic Resonance in Chemistry* **1987,** *25*, 75-79.

68. Schoen, B. W.; Holmes, D.; Lee, A., Identification and quantification of cis and trans isomers in aminophenyl double-decker silsesquioxanes using ^{1}H-^{29}Si gHMBC NMR. *Magnetic Resonance in Chemistry* **2013,** *51* (8), 490-496.

69. Schraml, J.; Blechta, V.; Sýkora, J.; Soukupová, L.; Cuřínová, P.; Proněk, D.; Lachman, J., Characterization of polyphenols from plant materials through their silylation and29Si NMR spectroscopy—line assignment through29Si,13C spin-spin couplings. *Magnetic Resonance in Chemistry* **2005,** *43* (10), 829-834.

70. Blechta, V.; Schraml, J., Relative signs of29Si-13C couplings. *Magnetic Resonance in Chemistry* **2008,** *46* (8), 734-738.

71. Sýkora, J.; Blechta, V.; Sychrovský, V.; Hetflejš, J.; Šabata, S.; Soukupová, L.; Schraml, J., 29Si–13C spin–spin couplings over Si–O–Carom link. *Magnetic Resonance in Chemistry* **2006,** *44* (7), 669-674.

72. Sýkora, J.; Blechta, V.; Soukupová, L.; Schraml, J., 29Si□13C spin-spin couplings over an Si–O–Csp3link. *Magnetic Resonance in Chemistry* **2008,** *46* (12), 1112-1118.

73. Bhat, A., S., Gervay-Hague, J. , Efficient Syntheses of B-Cyanosugars Using Glycosyl Iodides Derived from Per-O-Silylated Mono and Disaccharides. *Organic Letters* **2001,** *3* (13), 2081-2081.

74. Dirk G Streefkerk, M. J. A. D., and Johannes F. G. Vliegenthart, Conformational Studies of Per-O-Trimethylsilyl Derivatives of D-Fructoses and Oligosaccharides Containing β -D-Fructofuranose Residues by 200- and 300m MHz P.M R Spectroscopy. *Carbohydrate Research* **1974,** *33*, 249-261.

75. Ma, Z. Z., Ankun Trimethylsilylation of saccharide compound. 2018-04-06, 2017.

76. Nardin, R., Vincendon, M, Proton-Silicon-29 Two-Dimensional Chemical-Shift Correlation NMR Spectroscopy. *Journal of Magnetic Resonance* **1984,** *61*, 338-342.

Chapter 2:

Decoding Silicon in Multidimensional Space: 2D Analysis of Per-O-Silylated Sugars in Silicon vs. Carbon Graph for Accurate Peak Identification

Abstract

Recent advancements in ^{29}Si NMR spectroscopy characterization techniques have captured the attention of chemists. While the characterization of per-*O*-silylated organic derivatives has been a focus in ^{29}Si NMR spectroscopy over the past decades, the application to per-*O*-silylated sugars using ^{29}Si NMR spectroscopy has been limited. Twelve per-silylated sugars were characterized using ^{29}Si NMR spectroscopy in Chapter 1, and in this subsequent chapter, the silicon signals underwent further analysis through a 2D graph with ^{13}C NMR chemical shift. The ^{29}Si NMR and ^{13}C NMR chemical shifts of these sugars were graphed and analyzed. The 2D approach revealed that each signal of closely positioned silicon or carbon signals was spread out, eliminating the congestion of overcrowded signals. The carbon spread the silicon into three regions: the anomeric silicon downfield, away from the primary silicon, and the secondary silicon. The silicon resonances associated with oxygen at the secondary carbon are positioned in the middle of the graph, while the ^{29}Si NMR signals connecting to the primary carbon are at the bottom, reducing congestion. This plotting tool allows for better visualization, easing the identification of compounds in the mixture. Utilizing the obtained data, a mixture synthesis was conducted, intending to identify per-*O*-silylated sugars in the mixture. However, the experiment did not yield the anticipated results, as the silicon chemical shifts in the mixture changed slightly, leading to complications in the identification process.

2.1.0 Introduction:

The synthesis of all twelve per-*O*-silylated sugars has been published or mentioned and while some had been analyzed using gas chromatography. Interesting, the ^{29}Si NMR results for per-*O*-TMS-α-methylglucoside (**13**) is the only ones among the per-silylated derivatives that have undergone full silicon characterization.[1] The remaining eleven compounds were either characterized solely through ^{1}H and ^{13}C NMR spectroscopy analyses (per-*O*-TMS glucose (**14**), per-*O*-TMS mannose (**15**), per-*O*-TMS fructose (**16**), per-*O*-TMS sucrose (**20**), per-*O*-TMS trehalose (**21**), per-*O*-TMS kestose (**22**))[2,3,4,5] or briefly mentioned in publications (per-*O*-TMS sorbitol (**17**))[6] and patent (per-*O*-TMS-ribitol (**18**), per-*O*-TMS-xylitol (**19**), per-*O*-TMS-raffinose (**23**), and per-*O*-TMS-stachyose (**24**)) without specifying their characterization details. In the preceding chapter, a comprehensive characterization of these twelve compounds was performed through ^{1}H, ^{13}C, and ^{29}Si NMR spectroscopy analyses.

In this chapter, a new technique was used for deeper analysis of the correlation of silicon chemical shift with carbon chemical shift, especially those signals that are in close proximity. The advantages offered by ^{29}Si NMR signal, such as its large chemical shift dispersion and reduced spectral congestion, make it a potentially valuable tool for identifying mixtures. This capability arises from the unique chemical environment of silicon atoms in various compounds, allowing for distinct signals in the NMR spectrum. By analyzing these signals, it becomes possible to differentiate between different components within a mixture and gain insights into their structural properties.

However, a comprehensive understanding of the chemical shifts and their respective atom's environment is crucial for accurate interpretation and classification. By examining the specific chemical shifts exhibited by the ^{29}Si NMR peaks, it becomes possible to establish a reliable framework for identifying and characterizing different carbohydrate components within complex mixtures. Interestingly, despite the numerous applications and advantages of ^{29}Si NMR spectroscopy, the search of the existing literature has not revealed any methods that incorporate 2D correlations between ^{29}Si NMR peaks (x-axis), and ^{13}C NMR peaks (y-axis). This knowledge gap emphasizes the importance of conducting further research to explore the possibilities and potential benefits of such correlations. By combining multiple dimensions of NMR data, it may be possible to enhance the accuracy and reliability of carbohydrate mixture identification, providing valuable insights into their composition and structure.

2.2.0 Result and Discussion

2.2.1. Selected Si Signals Overlapping from Various Compounds Pose a Challenge When Assigning Them in Mixtures.

In Chapter 1 and within the existing scientific literature, it has been elucidated that signals emanating from silicon exhibit a pronounced dispersion and tend to exhibit minimal overlap, both within the same molecular structures and among different molecules. However, the present study has revealed a noteworthy phenomenon where a subset of peaks, such as those attributed to per-*O*-silylated monosacharides like *α*-methylglucoside, ribtiol, disaccharides like sucrose or

trehalose, as well as oligosaccharides like raffinose, kestose, and stachyose, Figure 2.1 display an overlap in their respective signals, as visually demonstrated in Table 2.1.

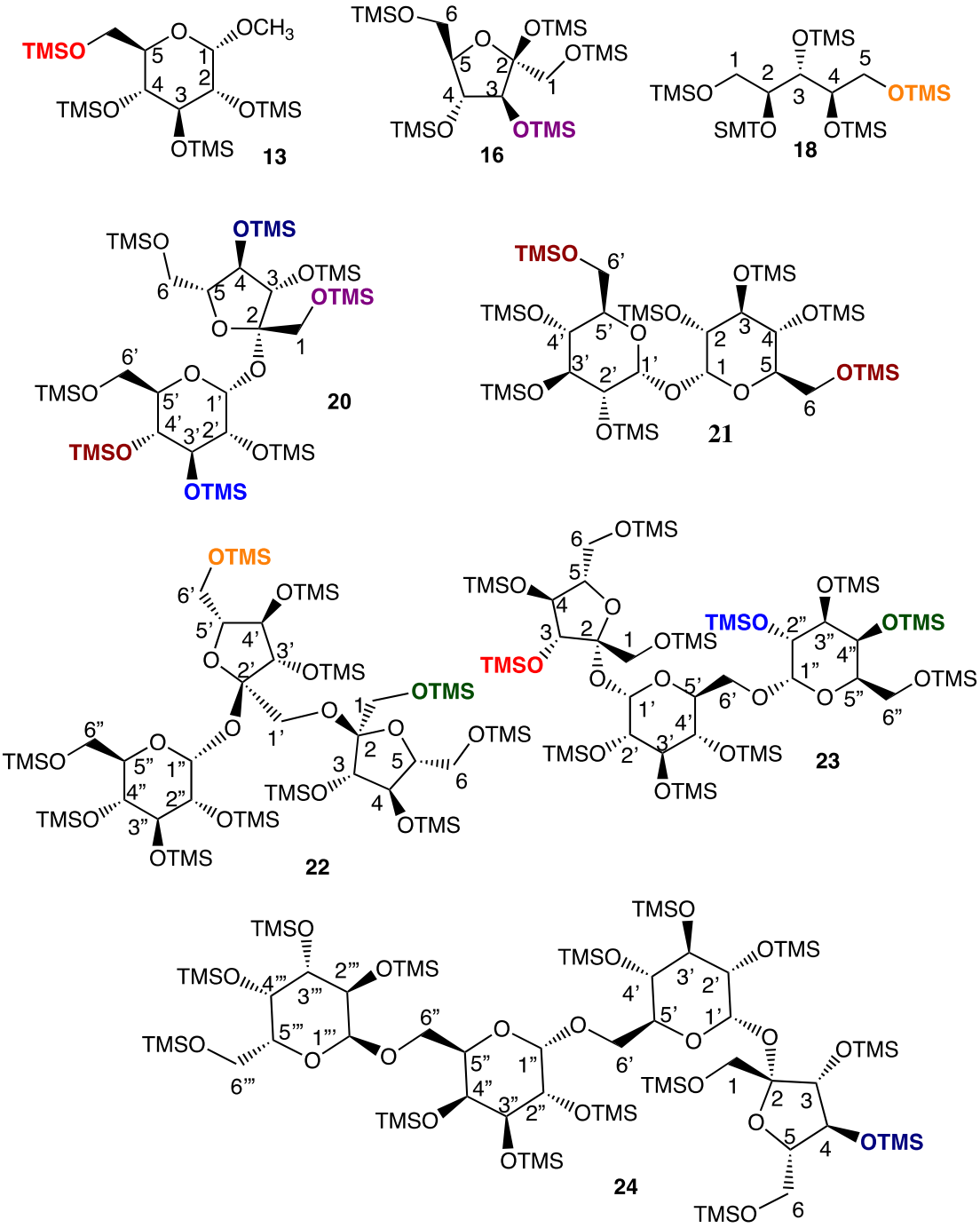

Figure 2.1: Per-*O*-silylated derivatives that have chemical shift values close to each other. Per-*O*-TMS-α-methylglucoside (**13**), per-*O*-TMS fructose (**16**), per-*O*-TMS ribitol (**18**), per-*O*-TMS sucrose (**20**), per-*O*-TMS trehalose (**21**), per-*O*-TMS kestose (**22**), per-*O*-TMS raffinose (**23**), and per-*O*-TMS stachyose (**24**). The color codes indicate the close proximity *O*-TMS signals shown in Table 2.1.

Table 2.1: The ^{29}Si NMR signal values from different per-*O*-TMS compounds exhibit close proximity in chemical shift. These signals are so closely aligned, with a range of +/- 0.01, that they can fully overlap in the spectrum.

δ Si	δ C	Atom	Compound	Compound Number
17.68	73.77	3'-su	sucrose	**20**
17.69	70.9	2"-ra	raffinose	**23**
18.02	71.68	4'-su	sucrose	**20**
18.01	62.15	6-t	trehalose	**21**
18.70	62.21	1-k	kestose	**22**
18.70	71.13	4"-ra	raffinose	**23**
18.70	77.22	4-st	stachyose	**24**
18.71	76.42	4-su	sucrose	**20**
17.39	64.19	5-r	ribitol	**18**
17.40	64.48	6'-k	kestose	**22**
18.16	69.07	3-f	fructose	**16**
18.16	63.12	1-su	sucrose	**20**
18.32	77.21	3-ra	raffinose	**23**
18.31	62.24	6-mg	methylglucoside	**13**
18.36	62.98	1-ra	raffinose	**23**
18.36			stachyose	**24**
18.70	71.13	4"-ra	raffinose	**23**
18.69			stachyose	**24**

Although the degree of overlap may not reach 100%, such a circumstance introduces a considerable challenge in the process of signal assignment, particularly when dealing with mixtures of these two samples. In light of these signal overlaps, it becomes imperative to devise a methodology that effectively organizes these signals in a manner that mitigates issues arising from such overlap in Table 2.1, the chemical

shifts generated from carbon are more spread out when compared among atoms of carbon and silicon with the same number. Using this information, a 2D graph is created to help visualize the dispersion of ^{29}Si NMR chemical shifts.

2.2.2 Using ^{29}Si NMR signal and ^{13}C NMR signal in 2D Graph To Disperse Spatial Overlap

As illustrated above, there are silicon-29 NMR signal peaks that are in close proximity, originating from both different compounds and the same compound, the values are detailed in Table 2.1. Additionally, within the same compound, multiple signals exhibit proximity in their chemical shift (δ) values, such as Si1-17.36 and Si3-17.32 from raffinose. To mitigate peak overlap in mixtures, alternative-graphing methods, such as the 2D approach presented in this study, could resolve the issue. This 2D graph utilizes silicon chemical shift (δ) values for the X-axis and carbon values for the Y-axis. When graphing two values in this 2D format, the signals become more widely separated, as illustrated in Figure 2.2 to Figure 2.5 below with per-*O*-TMS fructose (**18**), per-*O*-TMS sorbitol (**17**), per-*O*-TMS sucrose (**20**), and per-*O*-TMS raffinose (**23**).

The 2D graph, shown on Figure 2.2, was generated for per-*O*-TMS fructose (**16**), illustrating the dispersion of Si1 and Si3 signals (Table 2.2) using the carbon-13 NMR chemical shift (δ). The color code of the structure indicates the carbon atom attached to the *O*-TMS, as indicated by the number. The color in the legend indicates the silicon atoms and carbon atoms (1-6 in compound **16**) of the signals of interest plotted in the graph. This dispersion of the two signals enables a more comprehensive analysis of each signal. The carbon chemical shifts for C1 and C6 (see Table 2.2) are

also close in proximity, but when plotted in a 2D graph, the silicon-29 NMR chemical shift separates the carbon-13 NMR chemical shifts. As a result, the close proximity and potential overlap between C1 and C6 are avoided in this case.

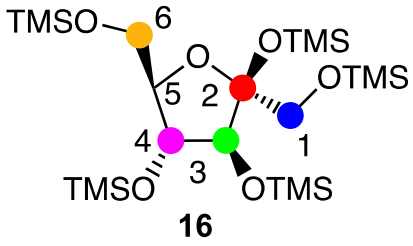

16

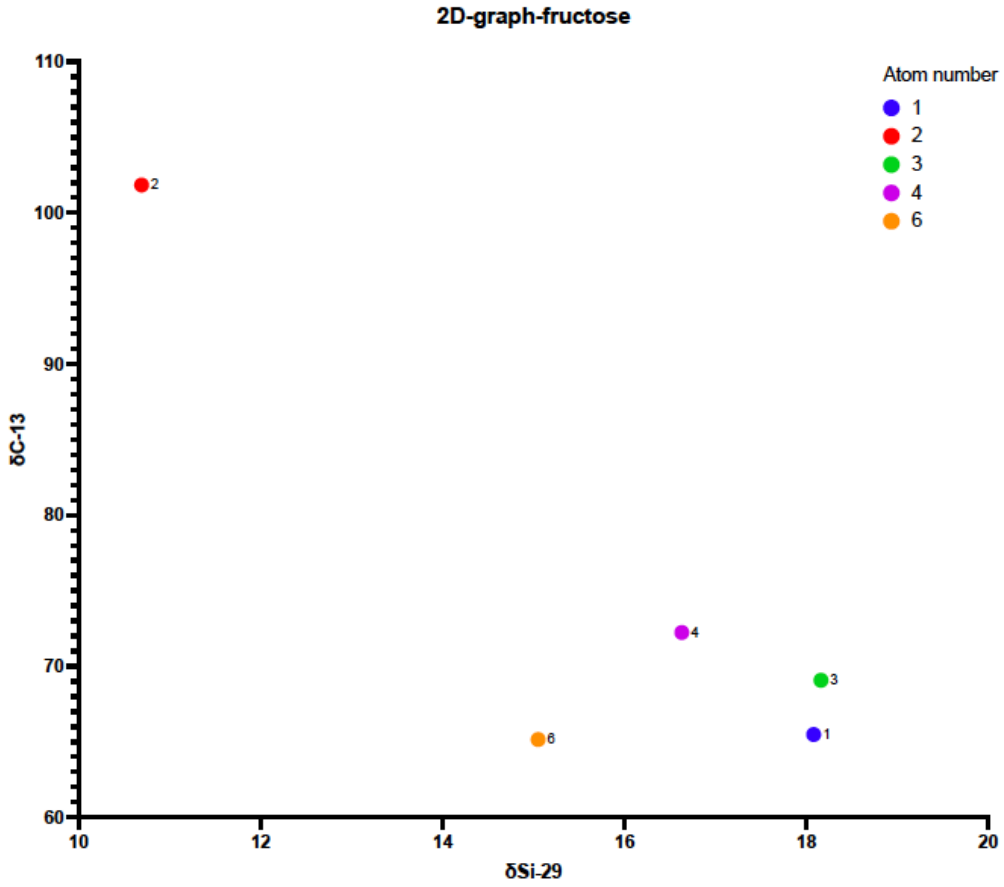

Figure 2.2: 2D graph of per-*O*-TMS fructose (**16**) illustrated the NMR chemical shifts of silicon-29 and carbon-13 in 2 dimensional analyses to spread out chemical shifts that are close proximity (C1 and C6 and Si1 and Si3) using the data in Table 2.2.

Table 2.2: The δ values of ^{29}Si NMR and ^{13}C NMR, along with the integration values* for per-*O*-TMS fructose (**16**). *The integration values were measured by referencing Si_2 as a standard with a value of 1.00, not an internal standard integration reference.

δ Si-29	δ C-13	Measured* Integration	Anticipated Integration	Atom number	Sugars (**16**)
18.08	65.48	0.83	1	1	fructose
10.69	101.84	1.00	1	2	fructose
18.16	69.07	1.02	1	3	fructose
16.63	72.23	1.01	1	4	fructose
15.05	65.15	0.96	1	6	fructose

Similarly, per-*O*-TMS sorbitol (**17**) also benefits from the use of a 2D graph. As shown in Figure 2.3 below, the chemical shifts of several carbon atoms (C) are close in proximity, but their ^{29}Si NMR peaks allow for dispersion, preventing them from clustering too closely together. In particular, the assignment of C1 and C6 as reference in Table 2.3 could be challenging if they were overlapped or mixed, but by utilizing this 2D graph, the plot for C-1 and Si-1 spreads out from C-6 and Si-6. Similarly, it can also be used to distinguish the peaks from C2, C3, and C4, (see Table 2.3) which spread out due to the signals from Si-2, Si-3, and Si-4, reference values in Table 2.3, also spreading out.

Table 2.3: The δ values of ^{29}Si NMR and ^{13}C NMR signals, along with the integration values* for per-*O*-TMS sorbitol (**17**). *The integration values were measured by referencing Si_2 as a standard with a value of 1.00, not an internal standard integration reference.

δ Si-29	δ C-13	Measured* Integration	Anticipated Integration	Atom number	Sugars (**17**)
16.85	63.75	0.96	1	1	sorbitol
15.69	75.87	1.00	1	2	sorbitol
16.77	76.27	1.11	1	3	sorbitol
16.45	76.18	0.96	1	4	sorbitol
17.13	74.54	1.01	1	5	sorbitol
17.20	63.72	0.98	1	6	sorbitol

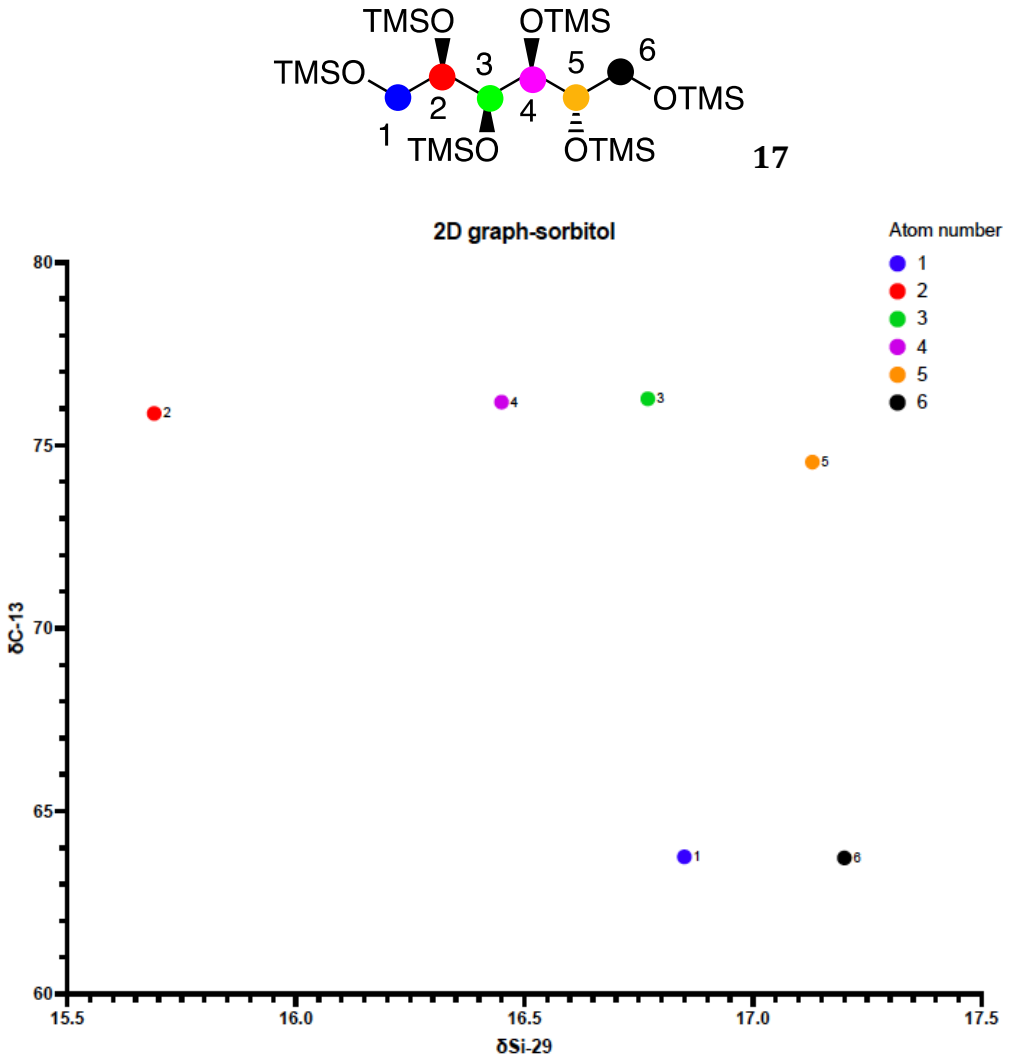

Figure 2.3: 2D graph of per-*O*-TMS sorbitol (**17**) illustrated the NMR chemical shifts of silicon-29 and carbon-13 (C1 and C6) in 2 dimensional analyses to spread out NMR chemical shifts that are close proximity using the data from Table 2.3.

The 2D graph depicted in Figure 2.4 represents the two-dimensional plot of per-*O*-TMS sucrose (**20**). This graph effectively demonstrates the advantages of utilizing 2D plotting, particularly for carbon (C) signals. As observed in Figure 2.4, both C2' and C3', as well as C3 and C4, exhibit significant dispersion when plotted against their respective silicon (Si) signals. While the chemical shifts of C3 and C4 may differ (δ 76.54 and 76.42, respectively), the plotting against ^{29}Si NMR signals results

in the two signals being widely separated from each other, enabling clear assignment and distinct visibility within their own regions. Additionally, Si3 and Si4' are in close proximity, but when their respective ^{13}C NMR signals are used, they become distinct, reducing congestion in the graph as shown in Figure 2.4 and Table 2.4.

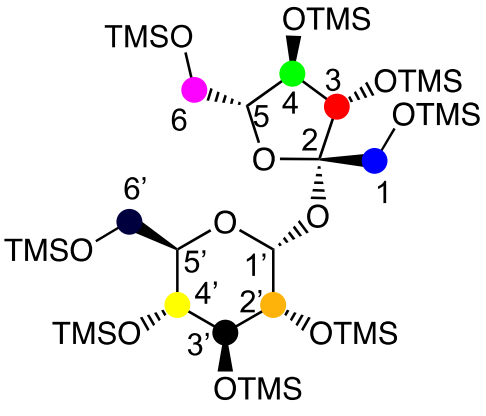

20

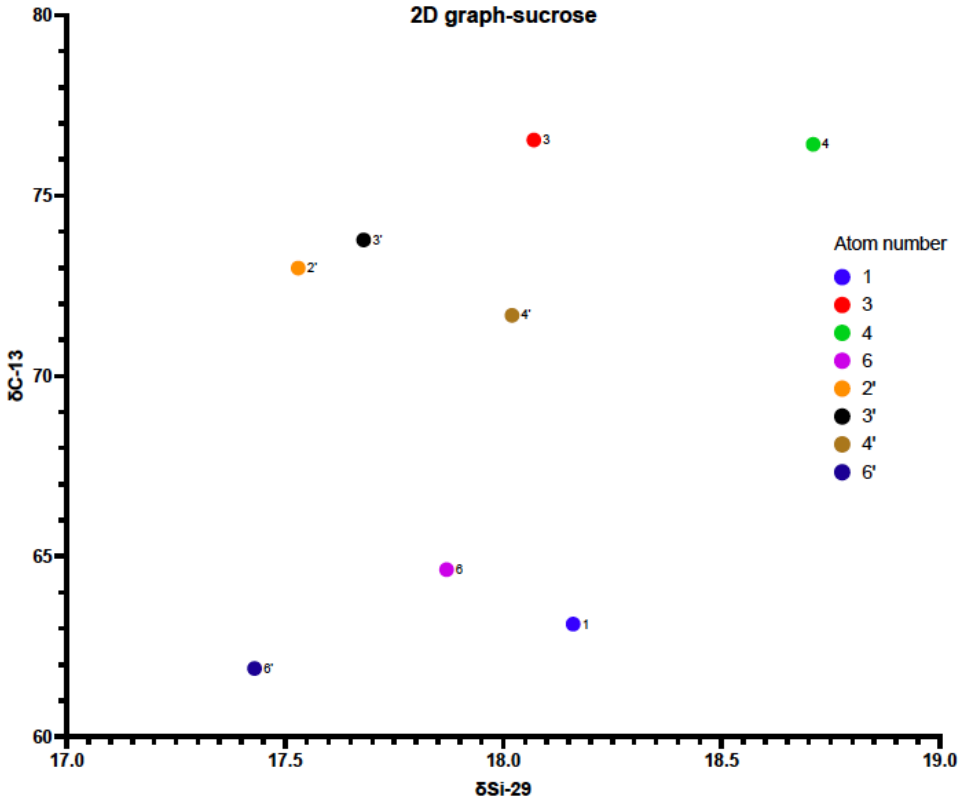

Figure 2.4: 2D graph of per-*O*-TMS sucrose (**20**) illustrated the NMR chemical shifts of silicon-29 and carbon-13 in 2 dimensional analyses to spread out chemical shifts that are close proximity (Si3 and Si4; C2';C3', and C3:C4) using the data in Table 2.4.

Table 2.4: The δ values of ^{29}Si NMR and ^{13}C NMR, along with the integration values* for per-*O*-TMS sucrose (**20**). *The integration values were measured by referencing Si_2 as a standard with a value of 1.00, not an internal standard integration reference.

δ Si-29	δ C-13	Measured* Integration	Anticipated Integration	Atom number	Sugars (**12**)
18.16	63.12	1.00	1	1	sucrose
18.07	76.54	1.05	1	3	sucrose
18.71	76.42	1.10	1	4	sucrose
17.87	64.63	0.93	1	6	sucrose
17.53	72.99	1.12	1	2'	sucrose
17.68	73.77	1.10	1	3'	sucrose
18.02	71.68	1.00	1	4'	sucrose
17.43	61.89	1.00	1	6'	sucrose

The 2D plot presented in Figure 2.5 and chemical shift values in Table 2.5 pertains to per-*O*-TMS kestose (**22**). As illustrated in the plot, the silicon-29 NMR chemical shifts for Si2", Si3", and Si6 are closely proximate. However, when plotted against their respective carbon-13 NMR chemical shifts, these three signals are effectively separated from each other, particularly for Si3" and Si6. This separation is particularly pronounced due to the more downfield carbon chemical shifts for Si3" in comparison to Si6. Furthermore, both the silicon and carbon chemical shifts for Si2" and Si3" exhibit dispersion, contributing to their distinct separation in the plot. Another noteworthy group of signals pertains to the carbon-13 NMR chemical shifts of C3, C4, C3", and C4'. Utilizing their silicon-29 NMR chemical shifts, which are inherently more dispersed compared to the carbon-13 NMR chemical shifts disperses these signals as Si4 is more downfield to Si4’ or Si3’ and Si3.

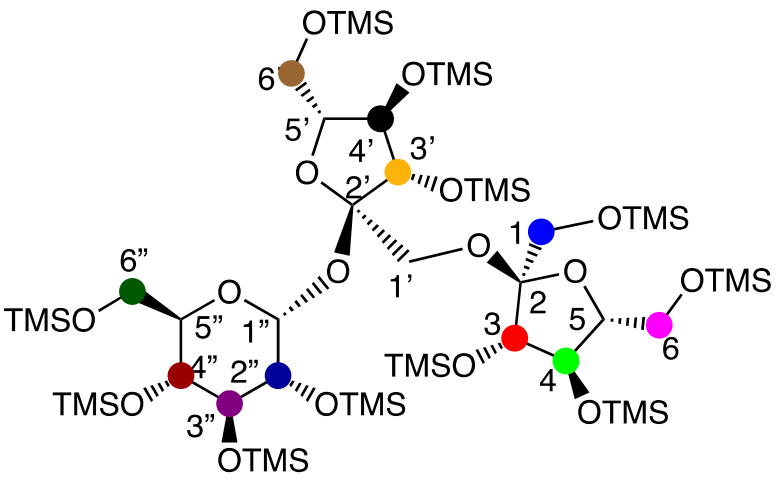

22

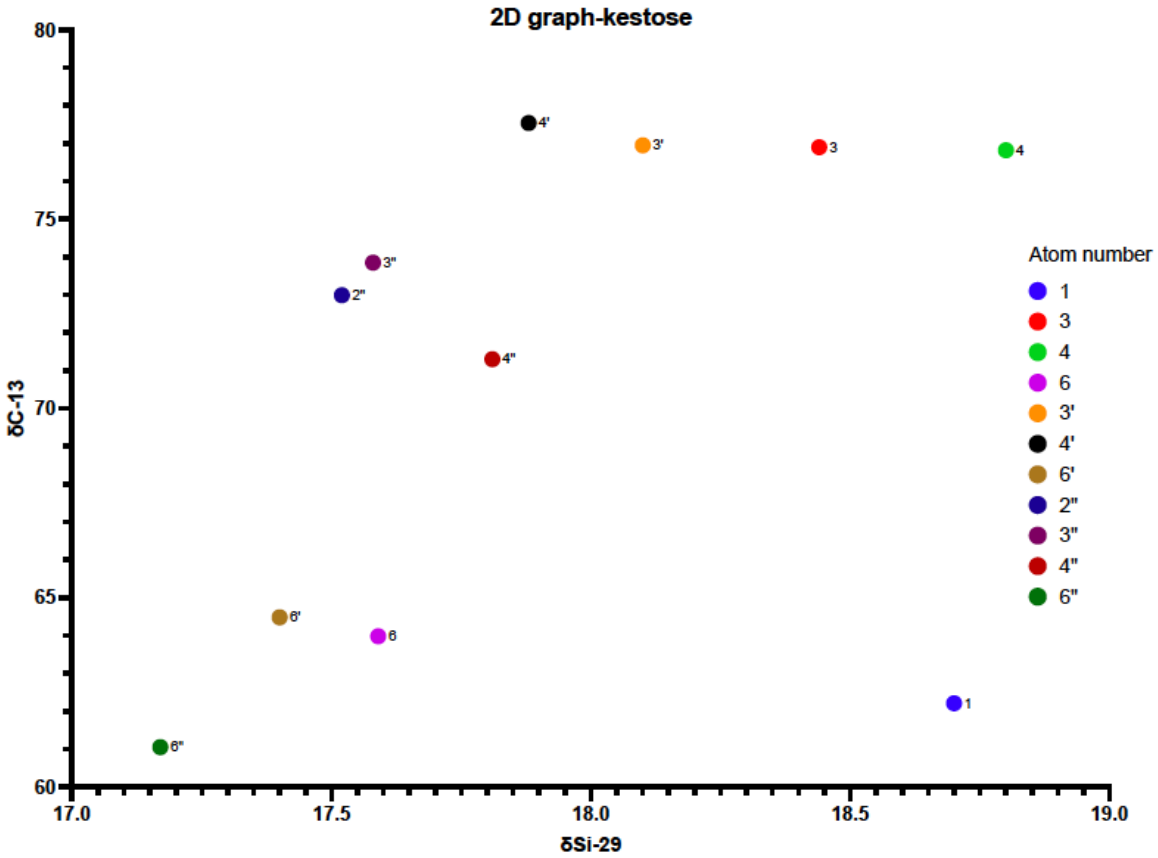

Figure 2.5: 2D graph of per-*O*-TMS kestose (**22**); ^{29}Si NMR signals on x-axis and ^{13}C signal on y-axis. Each dot represents the correlation of C atom to Si atom on its chemical shift. The graph illustrated 2D dispersion of close proximity signals (Si2"-Si3"Si6; Si4'-Si4"; Si1-Si4 and C6-C6', C1-C6") using the data from Table 2.5.

Table 2.5: The δ values of ^{29}Si NMR and ^{13}C NMR, along with the integration values* for per-*O*-TMS kestose (**22**). *The integration values were measured by referencing Si_2 as a standard with a value of 1.00, not an internal standard integration reference.

δ Si-29	δ C-13	Measured* Integration	Anticipated Integration	Atom number	Sugars (**23**)
18.70	62.21	0.99	1	1	kestose
18.44	76.90	1.08	1	3	kestose
18.80	76.82	1.20	1	4	kestose
17.59	63.98	1.16	1	6	kestose
18.10	76.95	1.12	1	3'	kestose
17.88	77.54	1.16	1	4'	kestose
17.40	64.48	0.97	1	6'	kestose
17.52	72.99	1.20	1	2"	kestose
17.58	73.85	1.22	1	3"	kestose
17.81	71.30	1.17	1	4"	kestose
17.17	61.05	1.00	1	6"	kestose

The graph in Figure 2.6 depicts a 2D plot for per-*O*-TMS raffinose (**23**), aiding in the separation of the previously mentioned signals, Si1 and Si3. The dot representing Si1 is located at the bottom of the graph, while Si3 is positioned at the top, despite their closely aligned silicon chemical shifts. However, their carbon-13 NMR chemical shifts differ, and when plotted together, these two signals become more spread out. This same pattern can also be observed for Si4 and Si4', as well as Si1 and Si6''. Furthermore, the cluster located at 17.5 ppm (Si) and 72.00 to 74.00 ppm (C) also demonstrates the dispersion of Si2', Si3', and Si3'' from each other when utilizing their carbon-13 NMR and silicon-29 NMR chemical shifts in 2D plotting. The chemical shift values of ^{29}Si NMR and ^{13}C NMR signals are shown in Table 2.6.

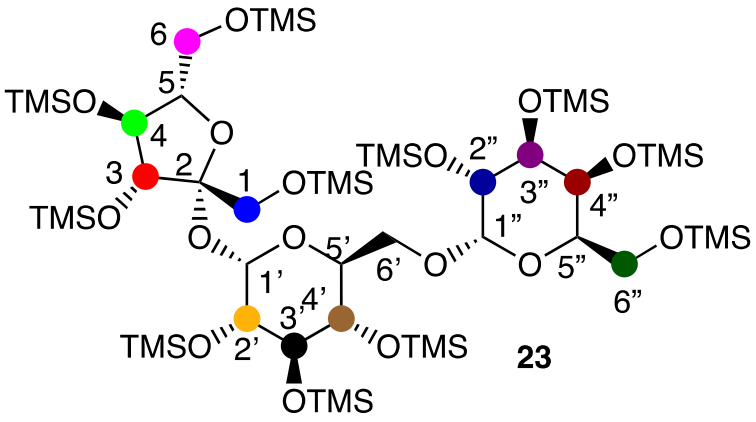

23

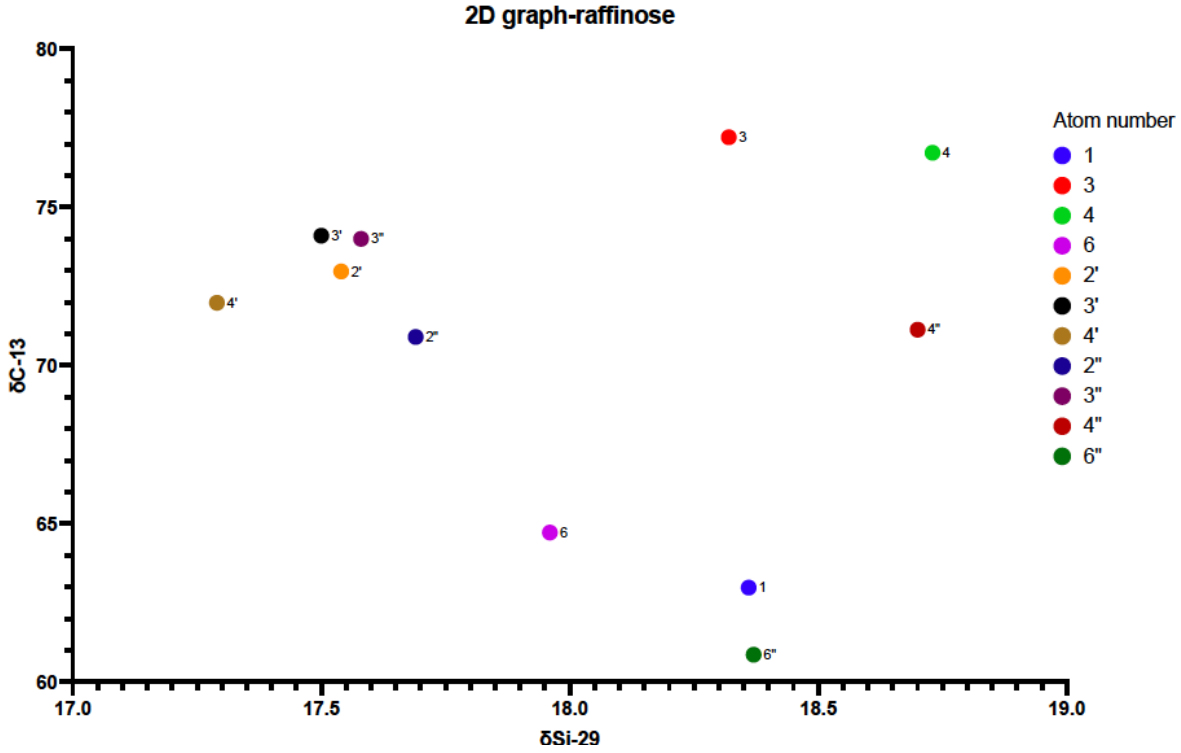

Figure 2.6: 2D graph of per-*O*-TMS raffinose (**23**) illustrated the NMR chemical shifts of silicon-29 and carbon-13 in 2 dimensional analyses to spread out chemical shifts that are close proximity (Si3'-Si2'-Si3"-Si2"; Si3-Si1-Si6'; Si4"-Si4 and C2"-C4"-C4'-C2-C3"-C3') using the data from Table 2.6.

Table 2.6: The δ values of ^{29}Si NMR and ^{13}C NMR, along with the integration values* for per-*O*-TMS raffinose (**23**). *The integration values were measured by referencing Si_2 as a standard with a value of 1.00, not an internal standard integration reference.

δ Si-29	δ C-13	Measured* Integration	Anticipated Integration	Atom number	Sugars (**22**)
18.36	62.98	0.94	1	1	raffinose
18.32	77.21	1.00	1	3	raffinose
18.73	76.72	0.98	1	4	raffinose
17.96	64.72	0.90	1	6	raffinose
17.54	72.97	1.00	1	2'	raffinose
17.50	74.10	0.93	1	3'	raffinose
17.29	71.98	0.99	1	4'	raffinose
17.69	70.90	1.00	1	2"	raffinose
17.58	74.00	0.98	1	3"	raffinose
18.70	71.13	1.04	1	4"	raffinose
18.37	60.86	0.94	1	6"	raffinose

The remaining compounds, including per-*O*-TMS methyl glucoside (**13**), per-*O*-TMS glucose (**14**), per-*O*-TMS mannose (**15**), per-*O*-TMS ribitol (**18**), per-*O*-TMS xylitol (**19**), per-*O*-TMS trehalose (**21**), and per-*O*-TMS stachyose (**24**), were also subjected to 2D plotting. It was observed that their signals exhibited greater dispersion in both carbon-13 NMR and silicon-29 NMR chemical shifts. The 2D plots for these compounds can be referenced in the supplemental information section, specifically in SI-Figure 2.1, SI-Figure 2.2, SI-Figure 2.3, SI-Figure 2.6, SI-Figure 2.7, SI-Figure 2.9, and SI-Figure 2.12 respectively from page 255 to 266. The increased dispersion in their chemical signals, especially silicon, reduces the likelihood of signal overlap, particularly in high-concentration samples (as illustrated in Chapter 1) or mixtures. As evidenced by the 2D plots and the chemical shift table provided (Table 2.7) for these compounds, all peaks are notably separated and spread from each other.

Table 2.7: The δ values of ^{29}Si NMR and ^{13}C NMR, along with the integration values* for the remaining 7 compounds. The^{29}Si NMR and ^{13}C NMR, values could be used to show their dispersion in 2D plot. *The integration values were measured by referencing Si_2 as a standard with a value of 1.00, not an internal standard integration reference.

δ Si-29	δ C-13	Measured* Integration	Anticipated Integration	Atom number	Sugars
Monosaccharide **(13, 14, 15 respectively to the sugar)**					
17.99	72.24	1.00	1	2	methylglucoside
17.77	75.33	1.00	1	3	methylglucoside
18.57	73.95	1.04	1	4	methylglucoside
18.34	62.24	0.84	1	6	methylglucoside
18.17	93.91	0.97	1	1	glucose
17.22	74.21	1.00	1	2	glucose
17.77	74.03	1.04	1	3	glucose
18.57	72.28	1.06	1	4	glucose
17.97	62.33	0.85	1	6	glucose
18.43	95.61	1.07	1	1	mannose
16.05	74.61	1.00	1	2	mannose
17.10	72.20	1.11	1	3	mannose
18.85	68.43	1.01	1	4	mannose
17.60	62.51	0.98	1	6	mannose
Alcohol Sugars **(18, 19 respectively)**					
17.12	63.68	0.97	1	1,5	xylitol
16.81	74.36	1.03	1	2,4	xylitol
18.00	73.39	1.00	1	3	xylitol
17.68	76.73	1.00	1	3	ribitol
17.39	64.19	0.92	1	1,5	ribitol
16.71	74.35	0.96	1	2,4	ribitol
Di-saccharide **(21)**					
18.08	72.87	1.04	1	2,2’	trehalose
18.37	73.59	1.06	1	3,3’	trehalose
17.62	71.75	1.00	1	4,4’	trehalose
18.01	62.15	0.89	1	6,6’	trehalose
Tetra-saccharide **(24)**					
18.40	63.06	0.90	1	1	stachyose
18.30	76.77	0.97	1	3	stachyose
18.70	77.22	1.01	1	4	stachyose
17.96	64.62	0.89	1	6	stachyose
17.48	72.94	1.10	1	2'	stachyose

As demonstrated from Table 2.7 and their respective graphs from the supplemental section, some of these silicon signals are like to be overlapped in 1D. Most importantly, if these ^{29}Si NMR signals are plotted together in one graph, the signals Si3 from per-*O*-TMS methylglucoside (**13**) and per-*O*-TMS glucose (**14**) both resonate at δ 17.77. Similarly, Si4 from per-*O*-TMS methyl glucoside (**13**) and per-*O*-TMS glucose (**14**) resonate at the same chemical shift value of δ 18.57. However, in both cases, their corresponding ^{13}C NMR chemical shifts are different. Other overlapping ^{29}Si NMR signals are also found between per-*O*-TMS mannose (**15**) (δ 17.10, δ 72.20) and per-*O*-TMS xylitol (**18**) (δ 17.12, δ 63.68), where their ^{13}C chemical shifts have different values, which helps distinguish the overlapping ^{29}Si NMR signals.

These individual graphs have demonstrated that the overlapping chemical shifts of silicon-29 can be resolved when plotted against carbon. Similarly, when carbon-13 chemical shifts are closely situated, they can also be resolved or dispersed when plotted in a 2D representation alongside silicon. This distinctive 2D approach enables the dispersion of silicon-29 NMR and carbon-13 NMR signals into a unique region. It has been illustrated that all primary carbon-13 NMR chemical shifts are on the upfield region, effectively distinguishing the silicon-29 NMR signals from other signals. Additionally, secondary carbon-13 NMR signals assist in segregating the silicon-29 NMR signals into specific regions based on the carbon's chemical shift. Further details will be discussed below.

2.2.3 A Theoretical Mixture 2D Plot of 12 Persilylate-*O*-Sugars and 1 Internal Standard, per-*O*-TMS DHEA Compound Using Chemical Shift Value from Pure Compound.

It has been demonstrated above that unique pattern can be obtained from the 2D graph for each individual compound. To further investigate and obtain useful information, all 12 per-*O*-silylated sugars: per-*O*-TMS methylglucoside (MG-**13**), per-*O*-TMS glucose (G-**14**), per-*O*-TMS mannose (M-**15**), per-*O*-TMS fructose (F-**16**), per-*O*-sorbitol (S-**17**), per-*O*-ribitol (R-**18**), per-*O*-TMS xylitol (X-**19**), per-*O*-TMS sucrose (Su-**20**), per-*O*-TMS trehalose (T-**21**), per-*O*-TMS kestose (K-**22**), per-*O*-TMS raffinose (Ra-**23**), per-*O*-TMS stachyose (St-**24**), and an internal standard, per-*O*-TMS DHEA (D-**25**) were graphed in a 2D format. The ^{29}Si NMR and ^{13}C NMR chemical shift values are derived from pure individual compounds and were used to create this graph. The data table can be found in the Supplemental Information on page 310-311. This 2D graph was created to observe a uniform pattern for better analysis. The x-axis of the graph corresponds to the δ values of ^{29}Si NMR, while the y-axis represents the δ values of ^{13}C NMR. Each compound was designated with a color code as illustrated in Figure 2.7.

The primary objective is to meticulously examine and identify any potential signals that do not overlap within all twelve silyl derivatives, which can be used as diagnostic signals for mixture samples. To focus on and amplify specific regions of interest, we strategically removed the x-axis and y-axis in areas where no signals were present. Remarkably, the 2D graph of these 12 compounds revealed the presence of three distinct regions within the y-axis (carbon-13 NMR chemical shifts): the lower region (Figure 2.7, Region A, upfield) for the primary carbon, the middle

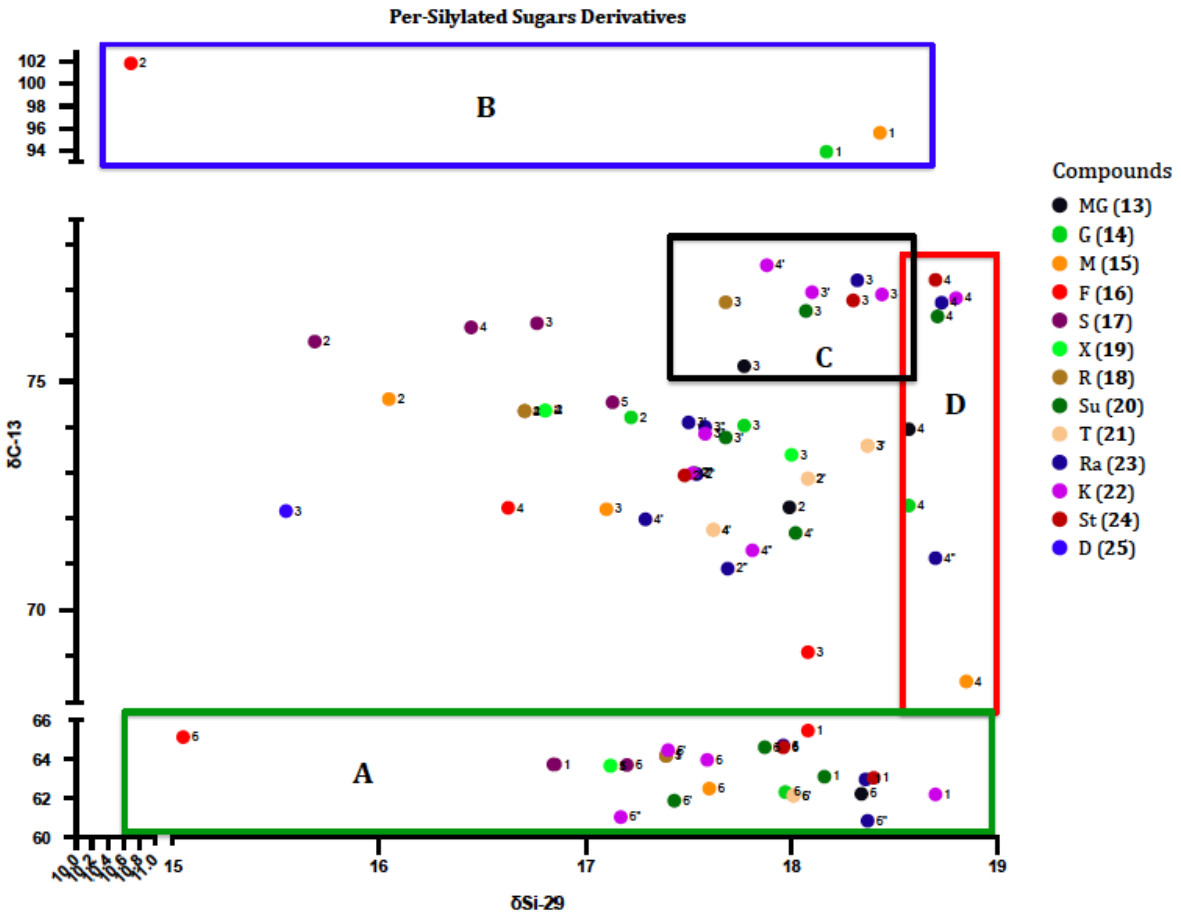

Figure 2.7: 2D graph representation of δ ^{29}Si NMR (axis) vs. ^{13}C NMR (y-axis) of mono, di, tri- and tetra-saccharides. The numbers on the dots represent the Si and C atom and the abbreviation are as follow: per-*O*-TMS methylglucoside (MG-**13**), per-*O*-TMS glucose (G-**14**), per-*O*-TMS mannose (M-**15**), per-*O*-TMS fructose (F-**16**), per-*O*-sorbitol (S-**17**), per-*O*-ribitol (R-**18**), per-*O*-TMS xylitol (X-**19**), per-*O*-TMS sucrose (Su-**20**), per-*O*-TMS trehalose (T-**21**), per-*O*-TMS kestose (K-**22**)**,** per-*O*-TMS raffinose (Ra-**23**), per-*O*-TMS kestose (K-**22**), per-*O*-TMS stachyose (St-**24**), and per-*O*-TMS DHEA (D-**25**). See Table 1 SI.

middle region for secondary carbon, and the upper region (Region B-downfield) for the anomeric carbon. Meanwhile, for the x-axis, most signals appear between 17 to 19 ppm, with the exception of Si2 for compounds **15**, **16**, **17** and Si6 for compound **16**, which are downfield (11-16 ppm) compared to the other signals. Si3 from internal standard per-*O*-TMS DHEA (**25**) is also below 16 ppm.

The carbon-13 NMR chemical shifts contribute to the dispersion of the silicon-29 NMR chemical shifts, as illustrated in Figure 2.7. Chemical shifts originating from primary carbons, such as C-6 and a few C-1 carbons, are found in the upfield or lower region in the region labeled “A” of the 2D graph. This results in all Si6 and Si1 signals from compounds **13, 14, 15, 16**, **17**, **18**, **19**, **20**, **21**, **22**, **23**, and **24** appearing in the lower region, creating distinct separation from the other silicon-29 NMR signals.

Conversely, the top region labeled “B”, which is downfield, primarily contains signals from the anomeric carbon, causing Si2 from compound **18** and Si1 from compounds **14** and **15** to be separated from the other signals originating from secondary carbons.

In the region labeled "C," the signals corresponding to Si3 are from the furanose ring found in oligosaccharides (**20**, **22**, **23**, and **24**), while another signal, Si3', from compound **23**, is also found in this region. Outside of this labeled region, in the range of 69–75 ppm on the y-axis (carbon-13 NMR chemical shift) but with similar values on the x-axis (silicon-29 NMR chemical shift), there are signals corresponding to Si3 from monosaccharides, mainly from pyranose rings.

Interesting, box D is where the majority of Si4 signals are concentrated. However, in this region, the carbon-13 NMR chemical shift differentiates the Si4 from

the furanose ring in di- and oligosaccharides (**21**, **22**, **23**, and **24**) in the upper region, between 74.42 and 77.22 ppm. Meanwhile, the pyranose ring from monosaccharides (**13**, **14**, and **15**) and Si4' from compound **23** are found in the range of 68.43 to 73.94 ppm, which corresponds to the middle to lower part of box D.

The middle region of the graph encompasses the remaining signals from Si_2, Si_3, and Si4, as well as C_2, C_3, and C_4. This particular region appears more condensed compared to others, primarily due to the close proximity of these three signal types. All these signals correspond to secondary carbon atoms and silicon atoms bonded to secondary carbons. While Si_2 and C_2 are scattered farther apart from each other as observed in compound **13**, **14**, **15**, **16**, **17**, **18**, **19** or **20**, intriguingly, Si_3 and Si_4, as well as C_3 and C_4, exhibit a higher degree of clustering. Notably, the upper right region of this middle region is composed of a group of di-, tri-, and tetra-saccharides, characterized by Si_3 and Si_4 signals.

The unique separation achieved through carbon-13 NMR chemical shifts minimizes signal overlap when plotting all compounds together in a single graph. This 2D plot plays a crucial role in segregating and differentiating the primary ^{29}Si NMR signals, anomeric Si signals, and secondary Si signals, thereby enabling more effective and accurate comparisons among various chemical signals. It's also worth noting that the Si3 and Si4 signals from furanose in di- and oligosaccharides are distinct from the Si3 and Si4 signals from pyranose in monosaccharide.

2.2.4 Selection of Si2-C2, Si2'-C2', Si2"-C2", and Si4"-C4" NMR chemical shifts as Potential Diagnostic Signals in Mixture

Upon careful analysis of the 2D graph, it is evident that Si2 signals (indicated by the arrow) from different compounds are notably more dispersed compared to other signals, Figure 2.8. For instance, the Si2 signal (red arrow) from compound **16** is positioned further to the left (upfield), while the Si2 (green arrow) signals from compound **14** are situated within the δ 17 ppm region, and those from compounds **15** (orange arrow) and **17** (purple arrow) fall between δ 15 and 16 ppm, further distinguished by their carbon-13 NMR chemical shifts.

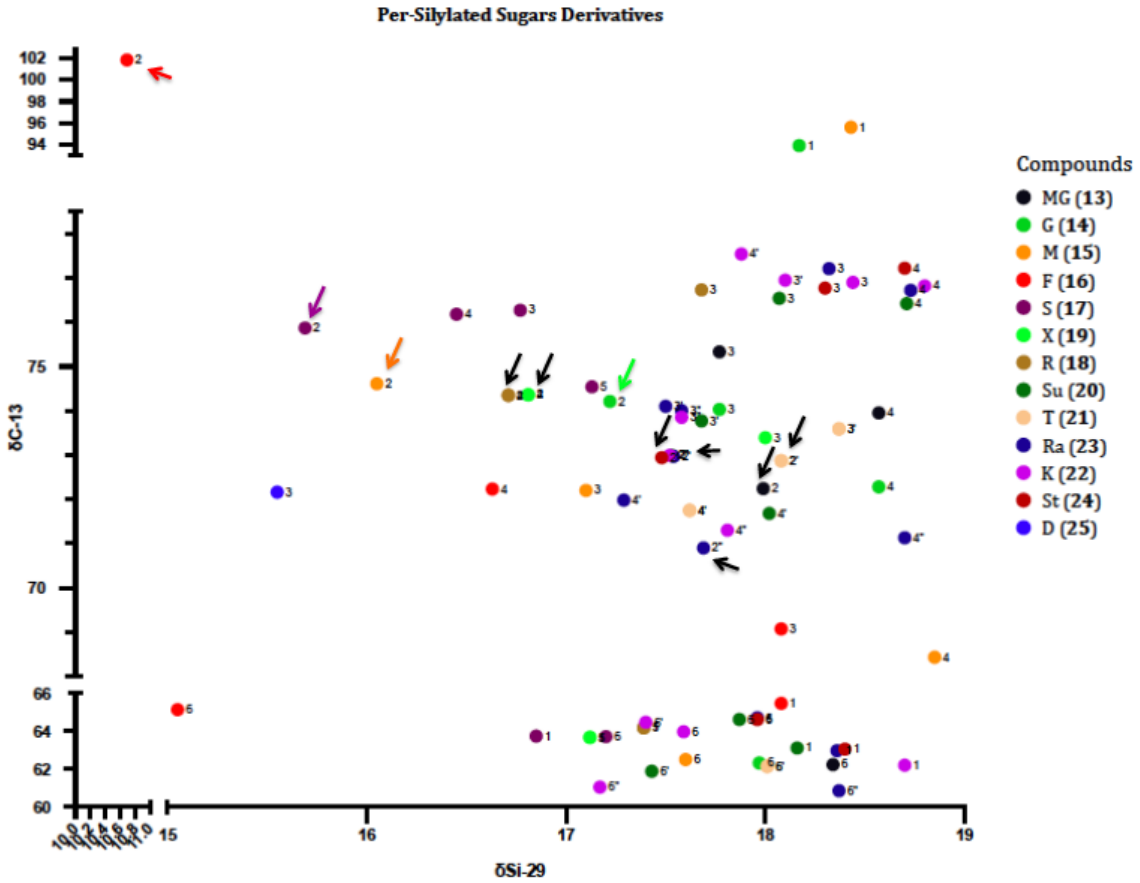

Figure 2.8: 2D graph representation of δ ^{29}Si NMR (axis) vs. ^{13}C NMR (y-axis) of mono, di, tri- and tetra-saccharides. Selected of Si2 signals indicated by the arrow further analysis.

In contrast, the Si2 signals (indicated by black arrows) from the di- and trisaccharides are found in the δ 17 and 18 ppm regions. This observation has led to the extraction of the Si2 signals from all compounds for improved visualization, while minimizing interference from other signals. The purpose of this extraction is to investigate whether Si2 signals can serve as potential tools (or signals) for compound identification within a mixture.

As expected, once Si2 is extracted, it becomes evident that this signal exhibits the most significant dispersion in both carbon-13 NMR chemical shift and silicon-29 NMR chemical shift. Upon examination of Figure 2.9, it is apparent that there are two distinct regions on the carbon-13 NMR chemical shifts of the y-axis, with the C2 signals spanning from δ 70 to 76 ppm and around δ 101 to 103 ppm. On the x-axis, Si2 signals are confined to specific regions, ranging from δ 15.0 to 18.5 ppm for compounds **14** to **15**, and **17** to **24**. However, for compound **16**, Si2 is situated in the approximate range of δ 10 to 11 ppm.

Nevertheless, an overlap is observed among three Si2 signals from per-*O*-TMS kestoses (**22**), per-*O*-TMS raffinose (**23**), and per-*O*-TMS stachyose (**24**), occurring between δ 17.48 to 17.54 ppm on the x-axis and δ 79.94 to 79.99 ppm on the y-axis, as depicted in Figure 2.9. Remarkably, their carbon-13 NMR and silicon-29 NMR chemical shifts are closely aligned, resulting in these signals overlapping. Consequently, it becomes imperative to explore alternative signals from the tri- and tetrasaccharides to identify a suitable diagnostic signal for these compounds.

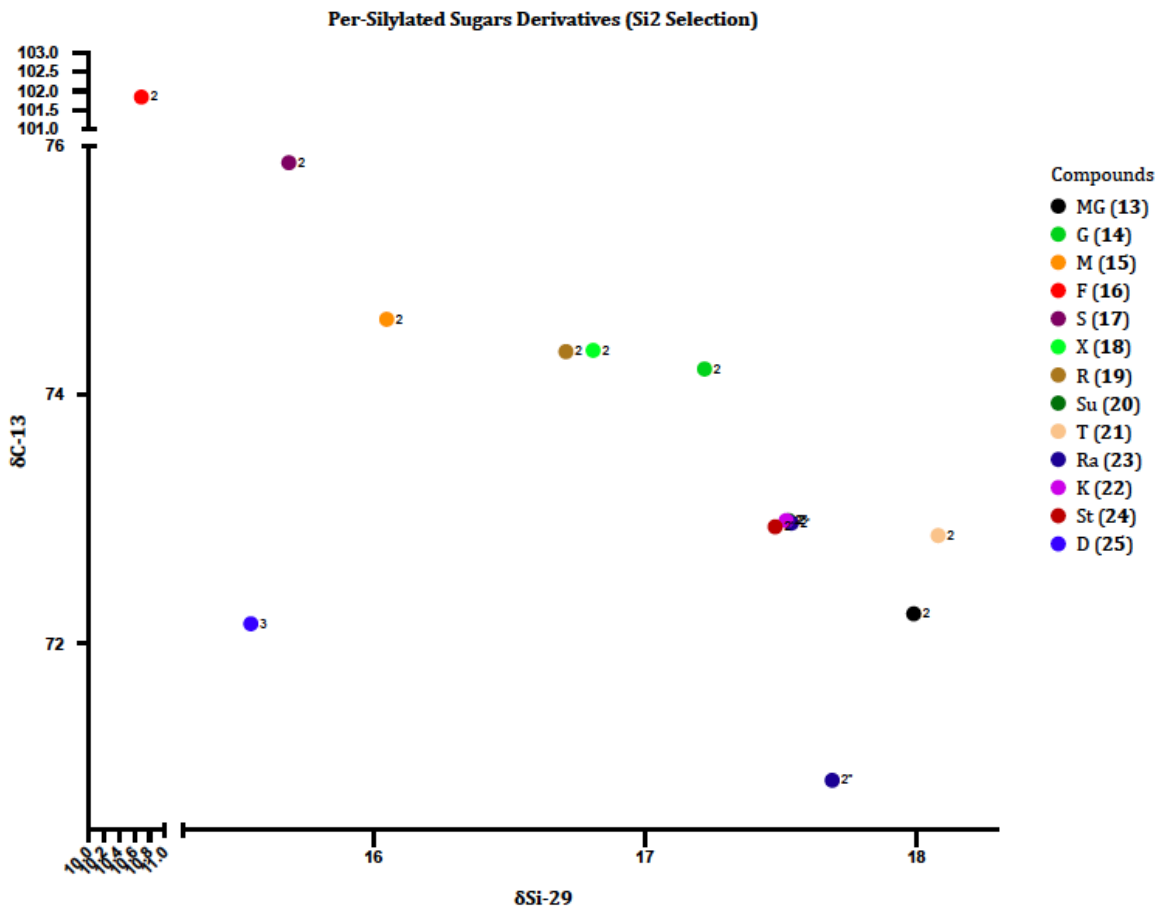

Figure 2.9: 2D graph representation of δ ^{29}Si2 NMR (axis) vs. ^{13}C2 NMR (y-axis) of mono, di, tri- and tetra-saccharides. The graph showed the diagnostic signal of Si_2 and $Si_{2''}$ from twelve per-*O*-silylated sugars derivatives (**13-24**) and the internal standard per-*O*-TMS DHEA (D-**25**). This graph showed only the Si2 or 2" signals from each compound.

Upon closer examination, it was found that Si2" from raffinose was located in the lower region of the graph and further apart from the other Si2" in compounds **22** and **24,** making it a better candidate compared to Si2'. The alternative signal to replace Si2" from compound **22** was the Si4" signal, which appeared in a similar region but was more distant from the Si2" of compounds **23** and **24**. The new signal selections were summarized in Table 2.8 and illustrated in Figure 2.10.

Table 2.8: The alternative chemical shifts of ^{29}Si NMR and ^{13}C NMR that are used for the 2D graph to eliminate overlapped of compound **12**, **14**, **15**, and 16.

Compound	**Si (old)**	**Si (new)**	**C (old)**	**C (new)**
per-*O*-TMS kestose (K-**22**)	Si2”	Si4”	C2”	C4”
	17.52	17.81	72.99	71.30
per-*O*-TMS raffinose (Ra-**23**)	Si2’	S2”	C2’	C2”
	17.54	17.69	72.97	70.90
per-*O*-TMS stachyose (St-**24**)	Si2”	X	C2”	X
	17.48	X	72.94	X

These signals (Si2, Si2', Si2", or Si4) were selected as potential signals to use for the identification of each compound in a mixture. As previously mentioned, there are overlapping signals observed between different compounds, and identifying all signals present in one compound in the mixture could be time-consuming and confusing. 2D graphs were implemented between carbon and silicon, helping to spread out signals by their primary, anomeric, and secondary carbon positions, but some signals still overlapped. To avoid the need for full signal identification, distinguishing signals such as Si2 or 2', 2" were chosen based on their chemical shift in both carbon and silicon and their ability to be more distinguishable compared to other signals (Figure 2.7 above). These selected signals would be used to identify per-*O*-silylated sugars in a mixture through the synthesis of all twelve sugars.

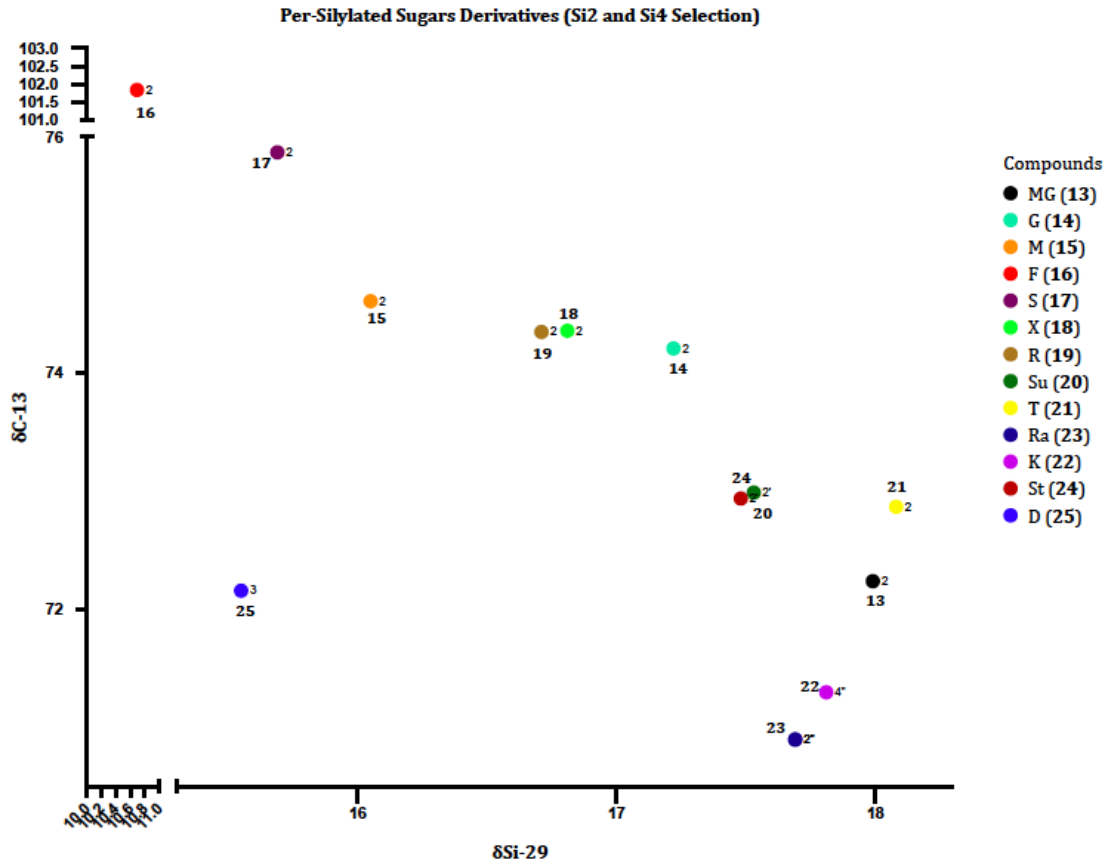

Figure 2.10: 2D graph representation of δ ^{29}Si NMR (axis) vs. ^{13}C NMR (y-axis) of mono, di, tri- and tetra-saccharides. The graph showed the diagnostic signal Si2 and Si4 of twelve per-*O*-silylated sugars derivatives (**13-24**) and the internal standard DHEA-*O*-TMS (D-**25**).

2.2.5 The Synthesis of Twelve Per-*O*-Silylated Sugars (**13-24**) and an Internal Standard (**25**) as Mixture in One Pot Reaction.

To validate whether the 2D graph and its signal selections established above could be used for the identification of per-*O*-silylated compounds, all twelve sugars were synthesized from their free sugars as a mixture. The per-*O*-silylated sugars were prepared in a 1:1 equal mole ratio from their free sugars using the *O*-silylation methods described in Chapter 1. An internal standard, DHEA, was added and synthesized with the free sugars in the reaction. The mixture was diluted in $CDCl_3$ to a concentration of approximately 0.099 M in total (the preparation method can be

found on page 253). The ^{29}Si NMR experiment was performed using DEPT, as mentioned in Chapter 1, and ^{13}C NMR was performed using the same carbon parameters as in Chapter 1. The ^{29}Si NMR spectrum obtained showed changes in the Si chemical shift for all twelve compounds, including the internal standard, compared to their pure spectra at 0.10 M in Chapter 1. However, their carbon spectra did not show significant changes. Utilizing the fact that the carbon-13 NMR chemical shift is constant, a 2D graph can be generated by plotting the ^{13}C NMR chemical shift from the database against the ^{29}Si NMR resonance from experimental data for better visualization.

Changes in the chemical shifts between pure per-*O*-silylated sugars and mixed per-*O*-silylated sugars can be observed in the ^{29}Si NMR spectra. This is illustrated using per-*O*-TMS glucose (1**4**) in Figures 2.11, 2.12, and 2.13, and per-*O*-TMS kestose (**22**) in Figures 2.14, 2.15, and 2.16 as examples. Upon analysis, monosaccharides like per-*O*-TMS glucose (**14**), per-*O*-TMS mannose (**7**), or per-*O*-TMS fructose (**16**) showed small Δ values in chemical shift compared to trisaccharides like per-*O*-TMS kestose (**22**) and per-*O*-TMS raffinose (**23**). As illustrated in Figure 2.11 for per-*O*-TMS glucose (**14**), the Δ values of Si1 chemical shift in the mixture and the pure compound were 0.008; Si2, Si3, Si6 were all within the range of 0.0045 to 0.006, which, upon comparison, was not significantly different. In addition, after thoroughly analyzing the chemical shifts of all per-*O*-silylated sugars, it was found that no silicon-29 NMR signals have values similar to or close to those of these two signals, Si1 and Si6. This further indicated the confidently assigned of Si1 and Si6 from per-*O*-TMS glucose (**14**) to these signals in the mixture. The signals Si2 and Si3 from **14** were

also compared and are shown in Figure 12. Similarly, carbon also showed small Δ value between per-*O*-TMS glucose (**14**) and per-*O*-TMS glucose (**14**) in the mixture. The signals are overlapped between pure and mixture compound as shown in Figure 2.11-2.13. In the figures of these overlapped spectra between pure and mixed compounds, the ^{29}Si NMR δ is shown to the thousandth place to illustrate the Δ between pure and mixed compounds.

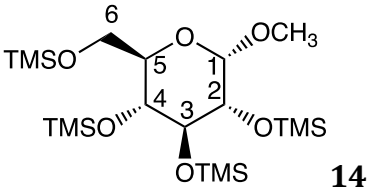

14

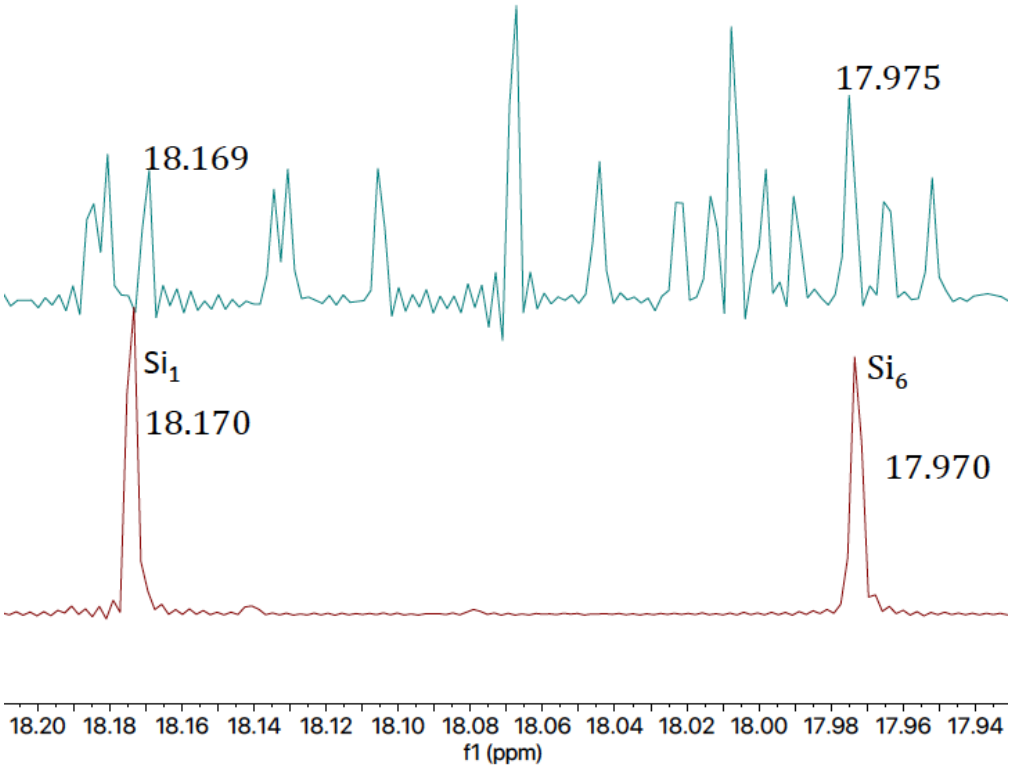

Figure 2.11: ^{29}Si NMR spectra between pure per-*O*-TMS glucose (**14**) and mixture sample of all twelve per-silylated derivatives. The spectra showed small Δ values of the chemical shifts Si1 and Si6 between the pure and mixture compound.

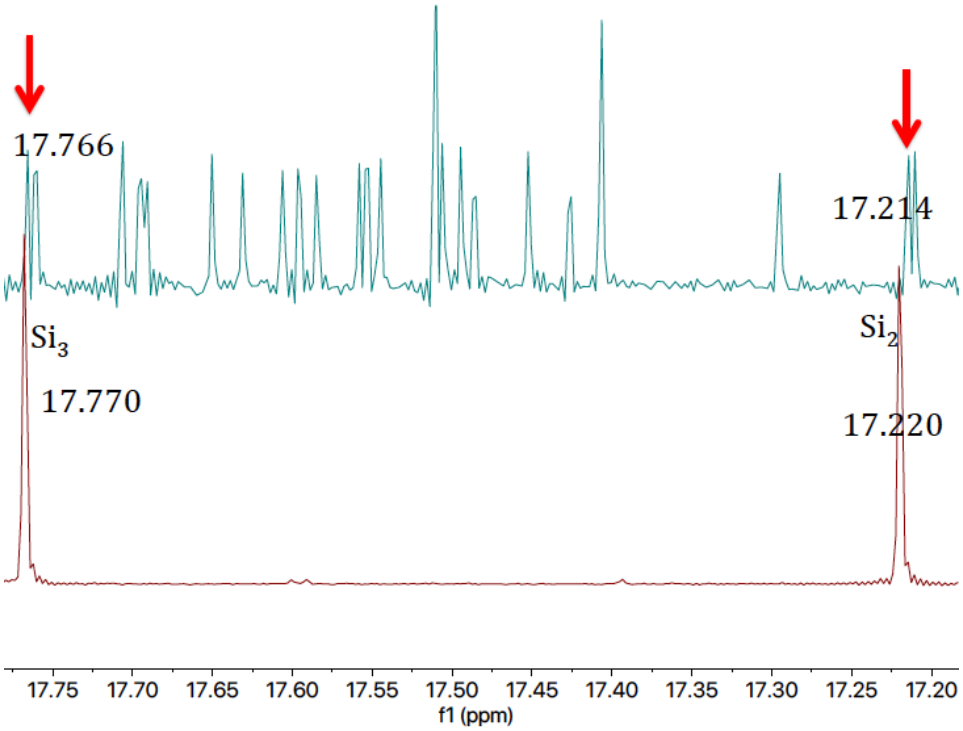

Figure 2.12: ^{29}Si NMR spectra between pure per-*O*-TMS glucose (**14**) and mixture sample of all twelve per-silylated derivatives. The spectra showed small Δ values of the chemical shifts Si3 and Si2 between the pure and mixture compound.

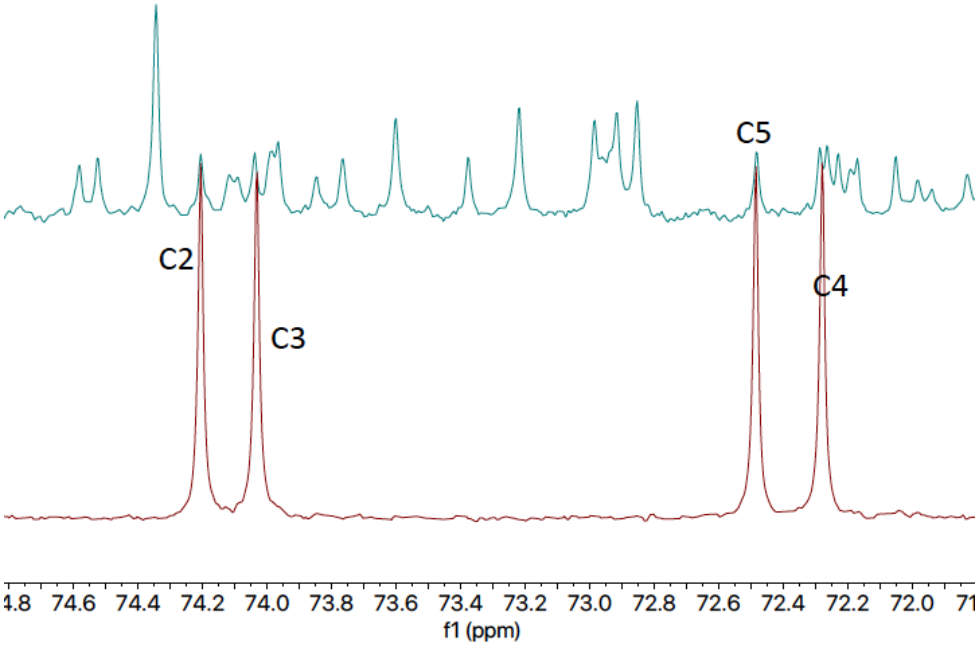

Figure 2.13: ^{13}C NMR spectra overlapped between pure per-*O*-TMS glucose (**14**) and mixture sample of all twelve per-silylated derivatives. The spectra showed there is no Δ value (deviation) of the chemical shift between the pure and mixture compound.

A similar trend was observed for the other three monosaccharides. It is important to note that the signal of each peak can still be identified using the overlap tool of the MestNova software. The full spectra comparison of all monosaccharides and disaccharides can be found at the supplemental section on page 267 to page 284.

When comparing the pure trisaccharide, per-*O*-TMS kestose (**22**), with the same compound in the mixture, it becomes evident that the signals from the mixture exhibit more pronounced deviations from those of the pure compounds. To a certain extent, it becomes challenging to definitively identify which signal in the mixture corresponds to the actual signal, as illustrated in Figure 2.14 with Si4' and Si4". The signal from Si4' could potentially fall within the range of δ 17.845 ppm to δ 17.889 ppm, since the Si4’ signal from the pure compound lies between these two values. Another possibility is that the signal at δ 17.845 ppm may belong to Si4”.

However, not all signals pose challenges for identification. Signals such as Si4 and Si1 can be assigned using overlapping tools with the pure compound. These signals exhibit less deviation when compared to Si4' and Si4". The Δ values of the chemical shift for Si4 are 0.013, and for Si1, it is 0.0079, which is relatively small and doesn't pose a significant risk of potential confusion with nearby signals, Figure 2.15. In the comparison of the carbon spectra of the pure per-*O*-TMS kestose (**22**) with the same compound in the mixture, it is observed that the signals in the pure and mixture samples either overlap or remain unchanged, as depicted in Figure 2.16 with C2' and C2. The carbon spectra or signals of all per-*O*-silylated compounds do not exhibit shifts in their chemical positions, as demonstrated in compounds **22** and **14**. By recognizing that some silicon signals can be confidently identified in the mixture and

that the carbon chemical shift remains constant between the mixture and the pure compounds, a 2D graph can be generated for a mixture of silicon and carbon signals. This data is valuable for future identification of silylated sugars from mixtures and serves as a landmark for artificial intelligence-based programming.

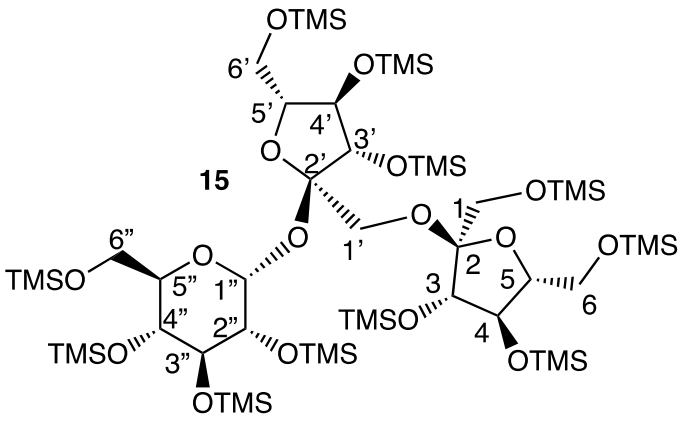

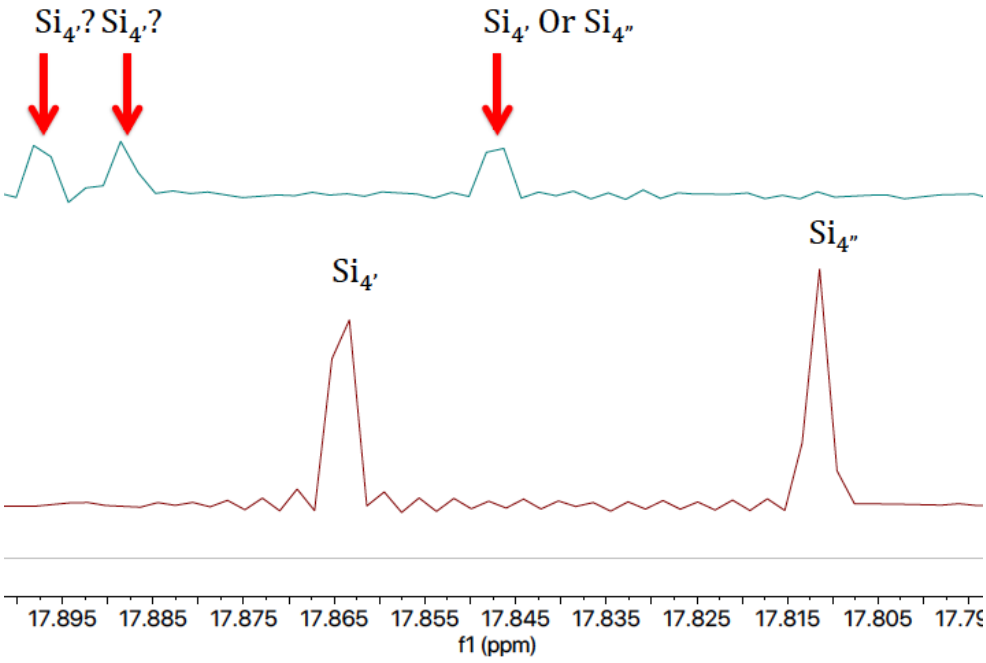

Figure 2.14: ^{29}Si NMR spectra between pure per-*O*-TMS kestose (**22**) and mixture sample of all twelve per-*O*-silylated derivatives. The spectra showed small Δ values of the chemical shifts Si4' and Si4" between the pure and mixture compound.

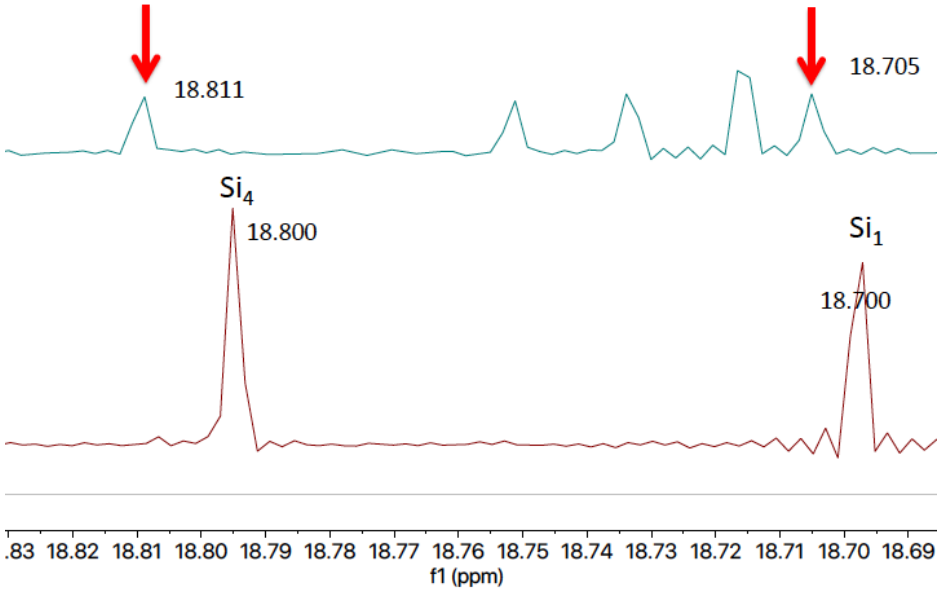

Figure 2.15: ^{29}Si NMR spectra between pure per-*O*-TMS kestose (**22**) and mixture sample of all twelve per-*O*-silylated derivatives. The spectra showed small Δ values of the chemical shifts Si1 and Si4 between the pure and mixture compound.

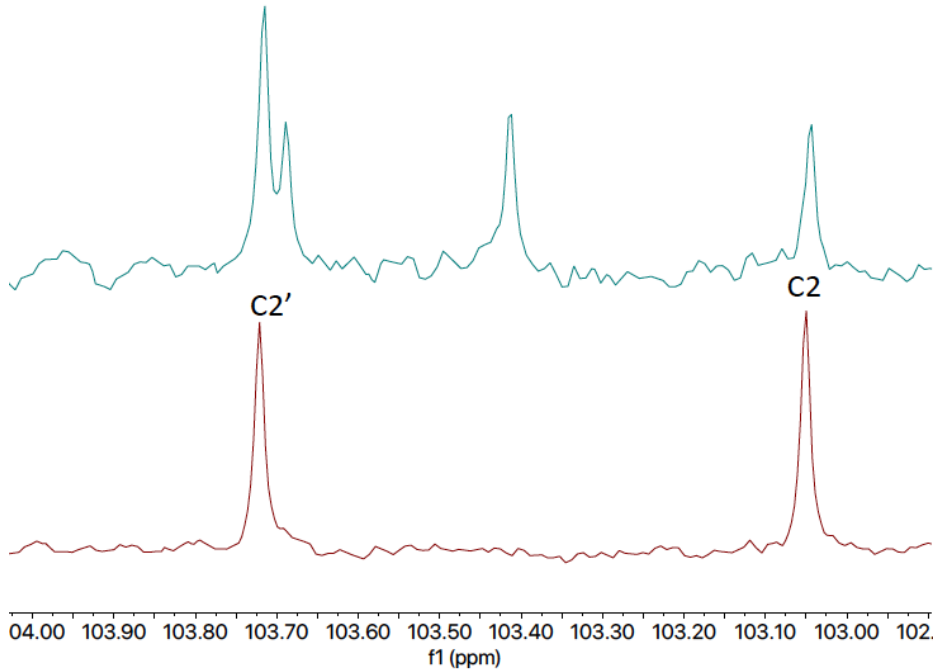

Figure 2.16: ^{13}C NMR spectra overlapped between pure per-*O*-TMS kestose (**22**) and mixture sample of all twelve per-*O*-silylated derivatives. The spectra showed there is no Δ value (deviation) of the chemical shift between the pure and mixture compound.

Using the overlap tool in MestNova, the possible and less ambiguous signals for each compound were assigned and are listed in Table 2.9. The overlap of carbon and silicon spectra can be found in the supplemental section, spanning from SI-Figure 2.13-2.30 starting from page 267 to 285 and SI-Figure 2.43-2.55 297-309. After calculating the Δ (delta) values for all signals, it was found that per-*O*-TMS fructose (**16**) exhibited the greatest deviation within the monosaccharide group. However, this signal was successfully assigned because it was in an isolated region, which cannot be confused with signals from other compounds, Figure 2.17. The other compounds, including the silylated derivative from free sugars, displayed small Δ values, with the exception of per-*O*-TMS xylitol (**18**). For the disaccharide's trehalose and sucrose, the Δ values extended to the thousandth place, which is still relatively small. The signals that could be assigned from the trisaccharides also exhibited small Δ values.

Table 2.9: The assignable silicon signals for compound **13-26** from a reaction mixture of these thirteen free sugars with DHEA. The Δ values calculated indicated the deviation of the mixture from the pure compound. The integration values integrated respected to compound **26**, internal standard synthesized with the mixture. The chemical shifts reported to the thousandth place to illustrate the Δ values between pure and mixture per-*O*-silylated sugars.

Si (Pure)	Si (Mix)	Δ values	Si Inter.	Atom	Compound Abbreviation	Compound #
17.990	17.990	0.0000	1.17	2	MG	**13**
18.340	18.341	0.0012	1.04	6	MG	**13**
18.170	18.169	0.0008	1.14	1	G	**14**
17.220	17.214	0.0058	1.13	2	G	**14**
17.770	17.766	0.0045	1.10	3	G	**14**
18.570	18.564	0.0063	**2.41**	4	G	**14**
17.970	17.975	0.0045	**2.11**	6	G	**14**
16.050	16.082	0.0321	0.93	2	M	**15**
17.100	17.106	0.0058	1.05	3	M	**15**
18.850	18.859	0.0088	0.80	4	M	**15**
17.600	17.606	0.0060	1.09	6	M	**15**

18.080	18.131	0.0513	**2.01**	1	F	**16**
10.690	10.748	0.0575	1.17	2	F	**16**
16.630	16.673	0.0431	1.20	4	F	**16**
16.850	16.854	0.0040	1.12	1	S	**17**
15.690	15.695	0.0045	1.09	2	S	**17**
16.770	16.772	0.0020	1.24	3	S	**17**
16.450	16.456	0.0060	1.10	4	S	**17**
17.130	17.139	0.0090	**2.73**	5	S	**17**
17.200	17.210	0.0103	1.13	6	S	**17**
17.120	17.140	0.0198	2.73	1	X	**18**
17.120	17.140	0.0198	2.73	5	X	**18**
16.810	16.828	0.0180	2.52	2	X	**18**
16.810	16.828	0.0180	2.52	4	X	**18**
18.000	17.998	0.0021	1.17	3	X	**18**
17.680	17.691	0.0108	1.04	3	R	**19**
16.710	16.719	0.0086	2.34	2	R	**19**
16.710	16.719	0.0086	2.34	4	R	**19**
18.070	18.067	0.0029	2.69	3	Su	**20**
18.710	18.705	0.0049	1.15	4	Su	**20**
17.680	17.692	0.0120	1.26	3'	Su	**20**
18.020	18.022	0.0021	1.24	4"	Su	**20**
17.430	17.426	0.0040	0.95	6'	Su	**20**
18.080	18.067	0.0128	2.67	2	T	**21**
18.370	18.368	0.0019	**2.91**	3	T	**21**
17.520	17.511	0.0095	2.68	4	T	**21**
18.010	18.007	0.0030	2.47	6	T	**21**
18.700	18.705	0.0051	1.14	1	K	**22**
18.440	18.440	0.0001	2.10	3	K	**22**
17.400	17.406	0.0064	**2.10**	6	K	**22**
18.800	18.811	0.0105	1.33	4	K	**22**
17.590	17.596	0.0056	1.21	6'	K	**22**
17.580	17.585	0.0051	1.01	3"	K	**22**
18.360	18.368	0.0077	2.10	1	Ra	**23**
18.730	18.734	0.0039	1.33	4	Ra	**23**
17.540	17.545	0.0046	1.09	2'	Ra	**23**
17.502	17.506	0.0038	0.93	3'	Ra	**23**
17.290	17.295	0.0046	1.02	4'	Ra	**23**
17.690	17.691	0.0006	1.25	2"	Ra	**23**
17.580	17.585	0.0051	1.01	3"	Ra	**23**
18.300	18.321	0.0209	1.11	3	St	**24**
18.700	18.705	0.0051	1.15	4	St	**24**
17.480	17.486	0.0059	1.11	2'	St	**24**
15.550	15.572	0.0216	1.00	3	DH	**25**

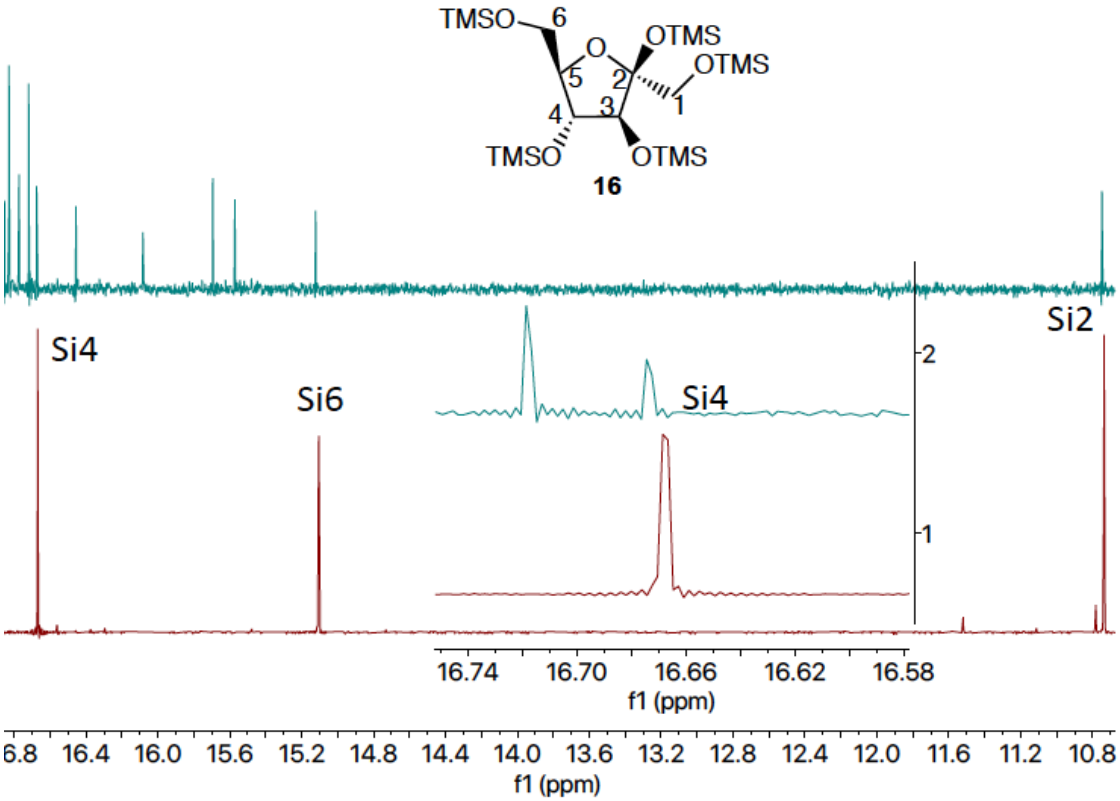

Figure 2.17: The overlapped spectra of mixture per-*O*-TMS fructose (**16**) and its pure compound (bottom). The spectra show distinct signals for each ^{29}Si NMR signal, facilitating the assignment of Si4, Si6, and Si2 in the mixture.

The observed deviations can be categorized into two groups: The first category encompasses signals from the same compound that exhibited a similar range of deviation, approximately to the hundredth place, in contrast to other compounds where deviations were within the range of the thousandth place. The deviation can be explained by differences in concentration between the pure compound and the mixture. The pure compound is more concentrated than the mixture, which can lead to these deviations. As mentioned in Schraml's paper[6], concentration can influence the chemical shift of silicon signals. The pure compound's oily nature, along with the challenges associated with weighing oily compounds, can contribute to uncertainties in mass measurements, leading to concentrations that

may not be as close to the expected 0.10 M of the pure spectrum. Despite some deviations, the data collected from the silicon and carbon chemical shifts have been consistent throughout the study, indicating that the assignment of the silicon signals in the mixture is accurate.

The second category pertains to cases where only one or two signals from a compound exhibited greater deviations compared to other signals within the same compound. A potential explanation for this phenomenon could be that these silicon signals are inherently more sensitive to environmental changes than other signals in the same derivatives. This hypothesis may require further experimental data to validate. For instance, signals like Si4 in per-*O*-TMS kestose (**22**), Si3' in per-*O*-TMS sucrose (**20**), Si2 in per-*O*-TMS trehalose (**21**), Si2 in per-*O*-TMS mannose (**15**), Si6 in per-*O*-TMS sorbitol (**17**), and Si3 in per-*O*-TMS ribitol (**18**) display deviations to the hundredth place when compared to the pure compound, whereas other signals within the same compound exhibit deviations to the thousandth place. Despite these shifts in the signals, they were successfully identified.

The assigned silicon signals were further analyzed by integrating each signal relative to the internal standard, per-*O*-TMS DHEA. As shown in Table 2.9, most of the integration values were close to 1, except for compounds **18**, **19**, and **21**, as these compounds are symmetrical and have two silicon atoms in one signal. Additionally, Si4 and Si6 from compound **21** showed integration values of 2, indicating that these signals are overlapping with other compounds' signals. Similarly, Si1 from compound **16**, Si5 from compound **17**, Si3 from **21** (close to ~3), and Si6 from **22** also had integration values of 2, suggesting that each of these signals contains two silicon

atoms. The majority of the assigned signals had integration values of 1, which correctly represents one silicon atom in one signal. The full integration value of all silicon signals be found from page 285-296 in SI.

The signals obtained were plotted in a 2D graph, as shown in Figure 2.18. After a careful analysis of the silicon signals assigned, it was observed that not all Si2 signals were extracted from the mixture, as expected based on the proposed idea that Si2, Si2', Si2", or Si4' could serve as diagnostic signals for each compound due to their distinctiveness. The signals used in Figure 2.18 were those that could be identified from the spectrum and plotted against the ^{13}C NMR (C) signals.

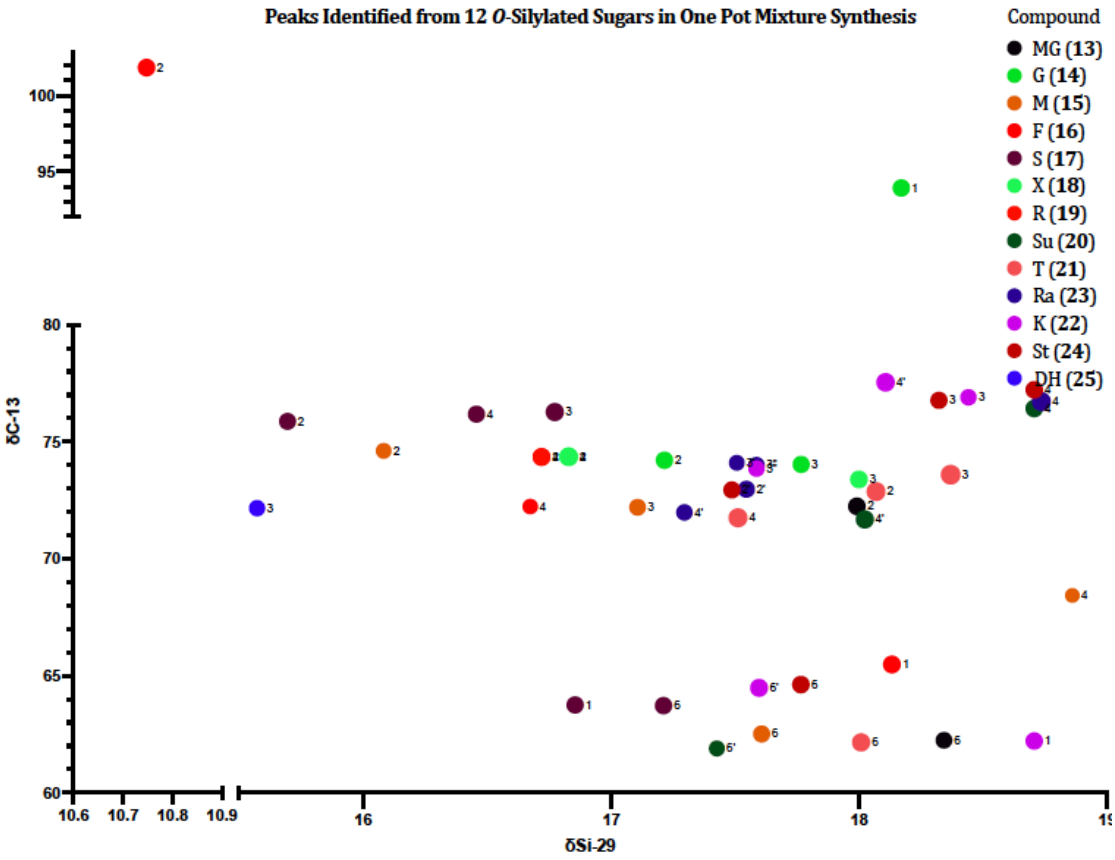

Figure 2.18: 2D graph representation of δ ^{29}Si NMR (axis) vs. ^{13}C NMR (y-axis) of mono, di, tri- and tetra-saccharides from Table 2.9. This graph shows the signals that could be assigned from the reaction mixture of free sugar to per-*O*-silylated derivatives (**13-25**).

2.3.0 Conclusion:

In this study, thirteen individual 2D graphs were created, each dedicated to one of the thirteen silyl derivatives. These 2D plots were constructed with silicon-29 (^{29}Si) NMR chemical shifts on the x-axis and carbon-13 (^{13}C) NMR chemical on the y-axis, facilitating the separation of closely neighboring carbon-13 or silicon-29 NMR signals. An interesting finding was that when two carbon-13 NMR signals were in close proximity, the inclusion of a silicon-29 NMR signal facilitated their separation on a 2D graph. Conversely, closely spaced silicon-29 NBMR signals could be more clearly differentiated when distinct carbon-13 NMR signals were present. This graphing method proved especially valuable for larger molecules like trisaccharides, as it allowed for the clear distinction of various silicon-29 NMR signals in close proximity. For instance, in per-*O*-TMS raffinose (**22**), signals such as Si3', Si3", Si2', and Si2" were effectively separated, and similar distinctions were made in per-*O*-TMS kestose (**23)**, where Si2", Si3", Si4', and Si4" signals were well differentiated based on their corresponding carbon atoms.

Further examination was done on these signals, both silicon and carbon, in a single graph to detect any overlapping points between different compounds. Although some signals were very close, they had not yet overlapped. The resulting 2D graph unveiled three distinct regions: the silicon-29 NMR signals were categorized into anomeric carbon, secondary carbon, and primary carbon regions, while the carbon-13 NMR signals were delineated by their positions in the upfield and downfield regions using silicon-29 NMR signals such as majority of Si4 from both pyranose and furanose are downfield.

Based on these data, Si2, Si2', and Si2" were selected as diagnostic signals for the mixture due to their noticeable separation from one another. However, this initial idea faced a setback when attempting to use Si2 to identify individual compounds within a mixture of thirteen compound syntheses together. The challenge arose from the shifting of silicon-29 NMR signals in the mixture, which did not align with the locations in pure compounds, rendering it impossible to identify all Si2, Si2', or Si2". Nonetheless, the assigned signals were integrated, and the resulting values were found to be consistently close to 1 for each signal. This indicates that the signal assignments were accurate and correct. Furthermore, the corresponding carbon-13 NMR signals remained consistent.

The experimental 2D graph generated from the collected data aligned with the theoretical 2D graph derived from pure compounds, indicating that the silicon-29 NMR signal identification was successful. The integration of the silicon-29 NMR signals from the experimental data further supported this conclusion. However, a more comprehensive analysis of the integration results will be explored in Chapter 3. Since the integration of silicon-29 NMR signal is relatively novel, further validation requires detailed experimental data to ensure accuracy and reliability.

Future research efforts could focus on validating the concentration of pure spectra, especially when dealing with oily samples. The variability of chemical shifts between pure compounds and mixtures complicates signal identification, as does the overlap of closely neighboring signals. To address these challenges, it might be useful to adjust the concentrations in the mixtures as well as in the pure samples. Additionally, determining the Δ shift between each signal in pure compounds ranging

from **13** to **26** could aid in identifying suspected signals within mixtures. This approach could enhance the accuracy of signal assignment in complex samples, contributing to the development of a comprehensive database and potentially enabling the creation of a software program for automated silicon signal identification in mixtures.

2.4.0 Experimental Section

2.4.1 *Global silylation of per-O-silylated (TMS) mono, disaccharides, trissacharides, tetrasaccharides and free sugars as mixture stirred at room temperature {mixture of stachyose, kestose, raffinose, trehalose, sucrose, sorbitol, ribitol, xylitol, glucose, mannose, methyl glucoside, fructose, DHEA) at room temperature.*

In a 10 mL, 2 neck round bottom flask, 2.95 mg (0.0150 mmol) of α-methylglucoside, 2.70 mg (0.0150 mmol) of α-glucose, 2.73 mg (0.0150 mmol) of mannose, 2.70 mg (0.0150 mmol) of fructose, 2.90 mg (0.0150 mmol) of sorbitol, 2.43 mg (0.0150 mmol) of xylitol, 2.58 mg (0.0151 mmol) of ribitol, 5.13 mg (0.150 mmol) of sucrose, 5.89 mg (0.0150 mmol) of trehalose, 7.41 mg (0.0150 mmol) of raffinose, 7.20 mg (0.0150 mmol) of kestose, 10.05 mg (0.0150 mmol) of staychose, and 4.50 mg (0.0150 mmol) of DHEA were dissolved in 3.50 mL of pyridine. The flask purged with argon gas using balloon followed by addition of 0.170 mL (13 x 3 equiv.) of hexamethyldisilazane and 0.10 mL (3 equiv. x 13) of chlorotrimethylsilane. The solution was stirred at room temperature for 24 hours. After 24 hours, the solution was extracted with hexane (10 mL x 3) and raised with deionized water (10 mL x 3) then dried over sodium sulfate. The dried organic layer was concentrated to a clear oil. ^{29}Si NMR, ^{13}C NMR, where ^{1}H NMR were performed, the silicon NMR integration

value match with the total number of silicon atoms in all thirteen compounds. The overall percent yield is 81% without purification.

2.4.2 *NMR sample preparation of per-O-silylated (TMS) mono, disaccharides, trissacharides, tetrasaccharides and free sugars as a mixture (mixture of stachyose, kestose, raffinose, trehalose, sucrose, sorbitol, ribitol, xylitol, glucose, mannose, methyl glucoside, fructose, DHEA).*

Table 2.10: The table below contains the theoretical values (mmol and mass) of each derivative. Using the theoretical values, the overall percentage yield was calculated as shown.

Compound	Amount	MW (reactant)	mmol	MW (product)	Theoretical (mg)
Methylglucoside (**13**)	2.95	194.18	0.0151	482.91	7.33
Glucose (**14**)	2.75	180.18	0.0152	541.07	8.25
Mannose (**15**)	2.73	180.18	0.0151	541.07	8.19
Fructose (**16**)	2.74	180.18	0.0152	541.07	8.22
Xylitol (**17**)	2.32	152.15	0.0152	601.23	9.16
Ribitol (**18**)	2.20	152.15	0.0151	601.23	9.08
Sorbitol (**19**)	2.75	182.17	0.0151	703.45	10.6
Sucrose (**20**)	5.13	342.30	0.0150	919.75	13.8
Trehalose (**21**)	5.25	342.30	0.0153	919.75	14.1
Raffinose (**22**)	7.60	504.42	0.0150	1226.26	18.5
Kestose (**23**)	7.61	504.42	0.0151	1298.44	19.6
Styachose (**24**)	10.10	666.60	0.0151	1677.13	25.4
DHEA (**25**)	4.35	288.42	0.0151	360.61	5.43
Total mmol/mg			0.197		157

Actual (collected) = 127.7

Percent yield = $\frac{127.7\ mg}{157.7}\ x\ 100\ =\ 80.8\%$

Using the percent yield, the mmol of the actual sample were calculated,

mmol of actual yield = % yield value x theoretical mmol

mmol of actual yield = 0.197 mmol *0.8079 = 0.159 mmol

To prepare the NMR sample, 2 dilutions series were performed. The first dilution started with dissolving the 127.7 mg (~0.159 mmol) of actual yield in 0.40 mL $CDCl_3$ to obtain 0.39 M. This molarity was further diluted by 50% to obtain 0.198 M, the last dilution was performed by reduction the molarity by 50% to obtain 0.099 M ~ 0.100 M as needed. The calculation scheme for dilution is shown below. The NMR sample was performed in $CDCl_3$.

0.159 mmol /0.40 mL = 0.39 ~0.40 M → 50% dilution → 0.198 (~0.20 M)→ 50% dilution → 0.099 M (~0.10).

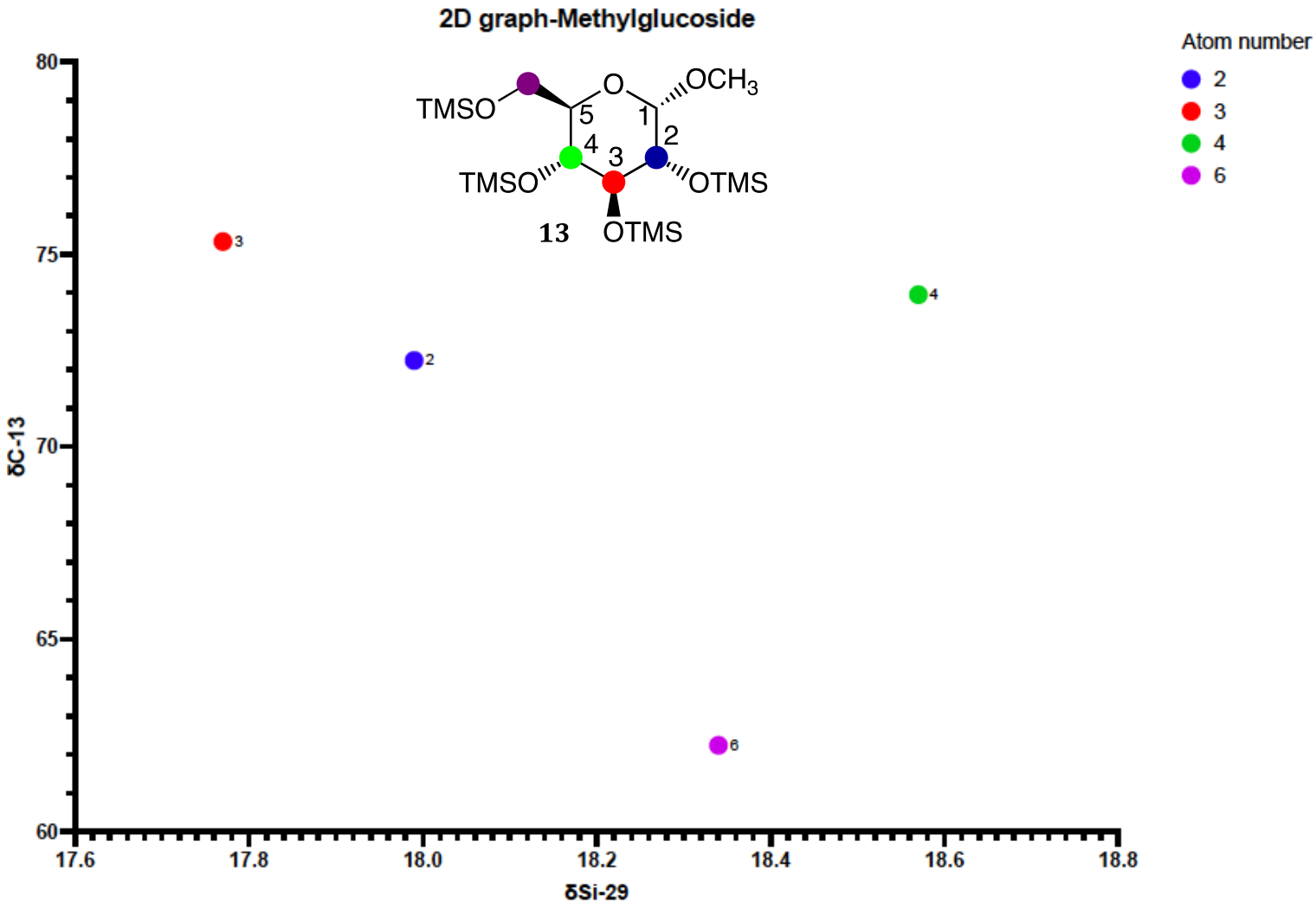

SI-Figure 2.1: 2D graph of per-*O*-TMS methyl glucoside (**13**); Si-29 NMR on x-axis and C-13 NMR on y-axis. Each dot represents the correlation of C atom to Si atom on its chemical shift.

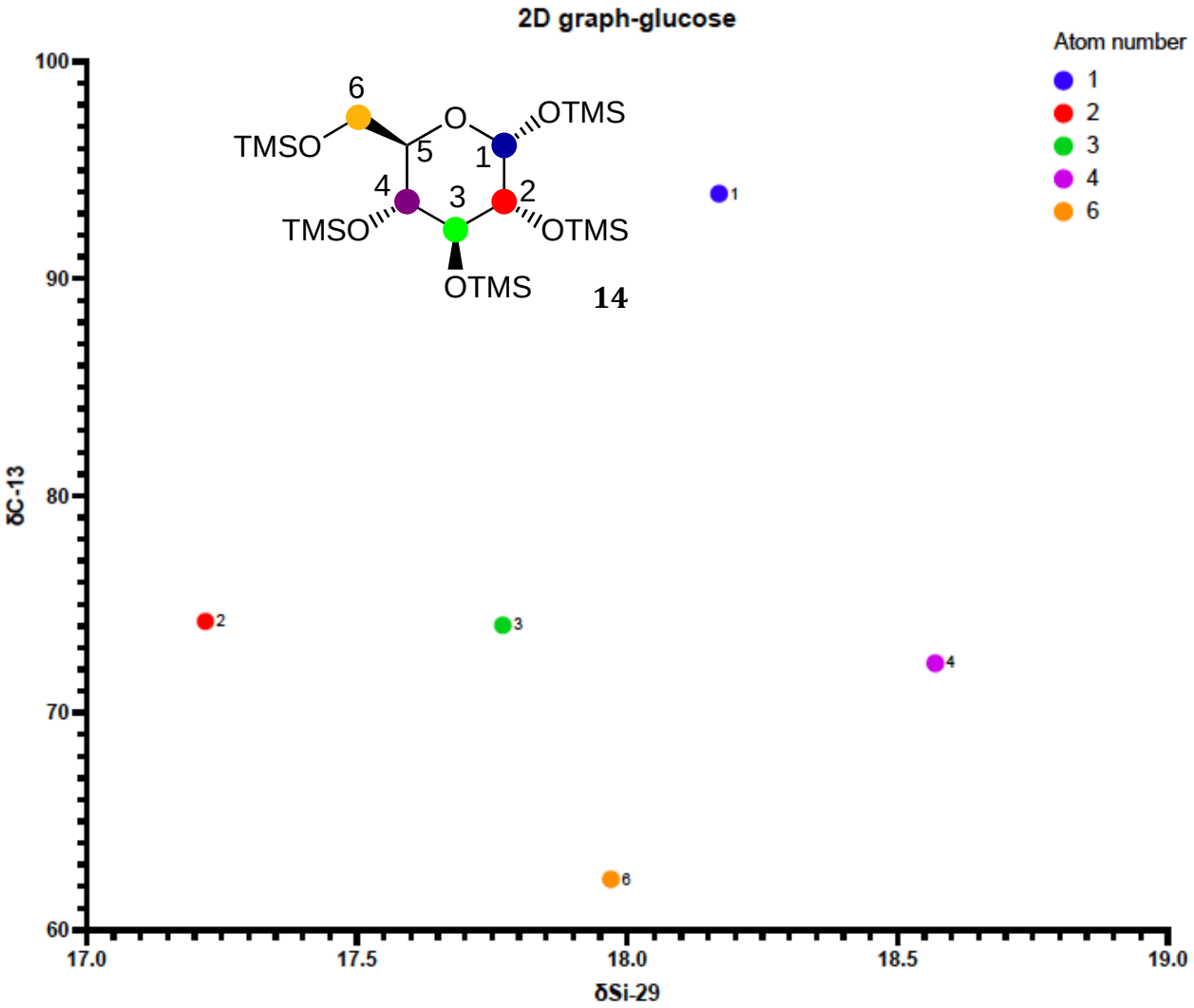

SI-Figure 2.2: 2D graph of per-*O*-TMS glucose (**14**); Si-29 NMR on x-axis and C-13 NMR on y-axis. Each dot represents the correlation of C atom to Si atom on its chemical shift.

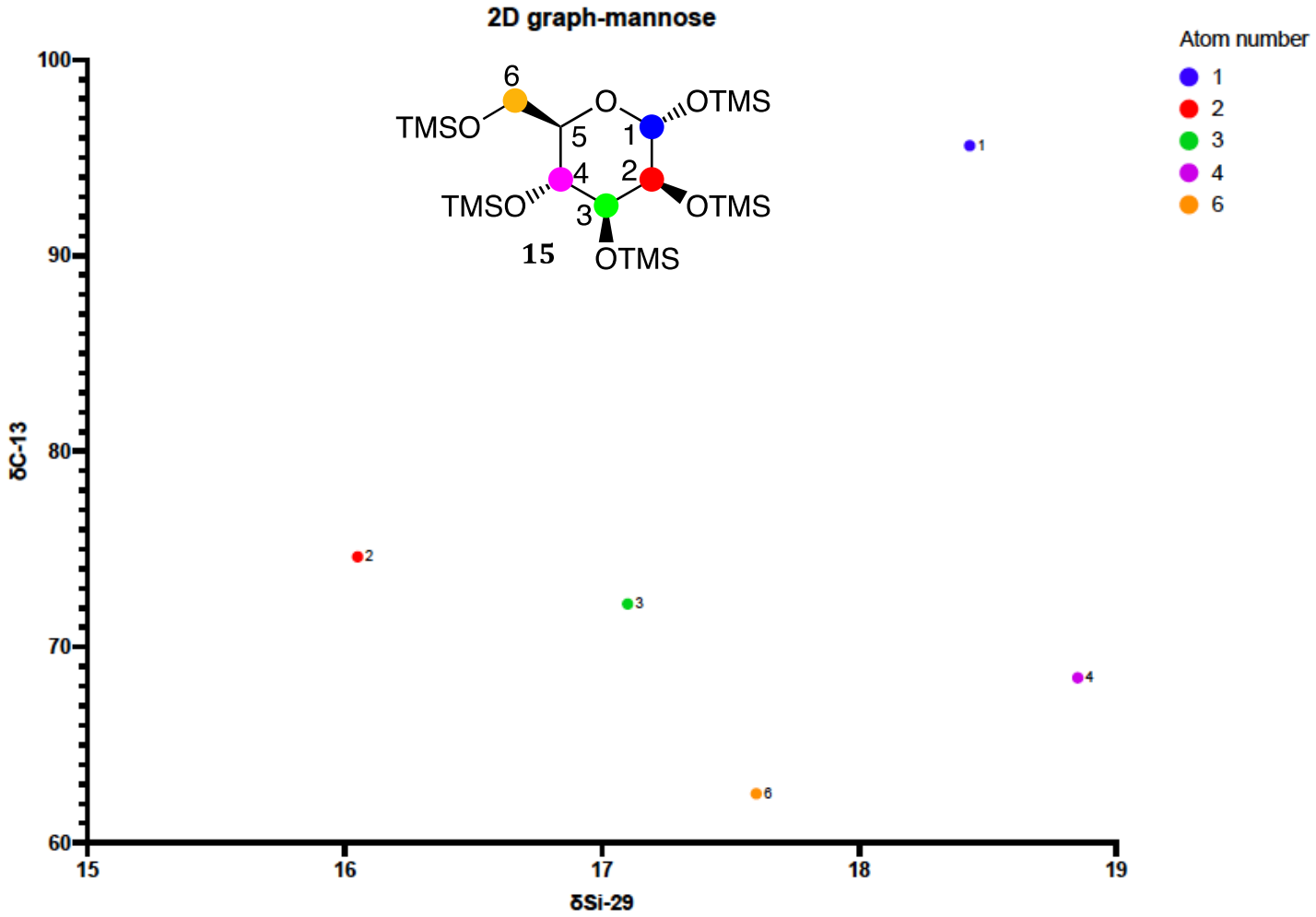

SI-Figure 2.3: 2D graph of per-*O*-TMS mannose (**15**); Si-29 NMR on x-axis and C-13 NMR on y-axis. Each dot represents the correlation of C atom to Si atom on its chemical shift.

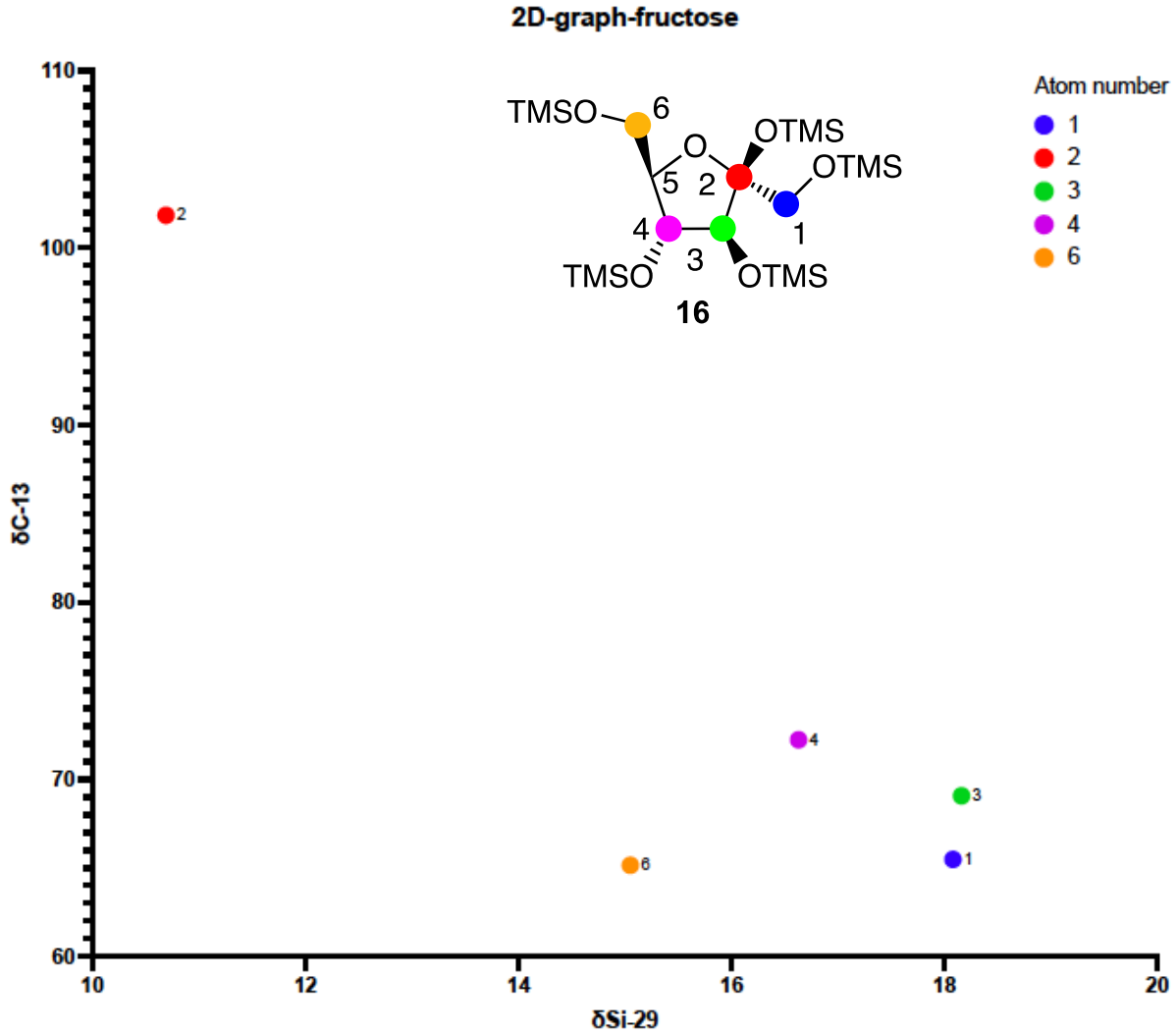

SI-Figure 2.4: 2D graph of per-*O*-TMS fructosse (**16**); Si-29 NMR on x-axis and C-13 NMR on y-axis. Each dot represents the correlation of C atom to Si atom on its chemical shift.

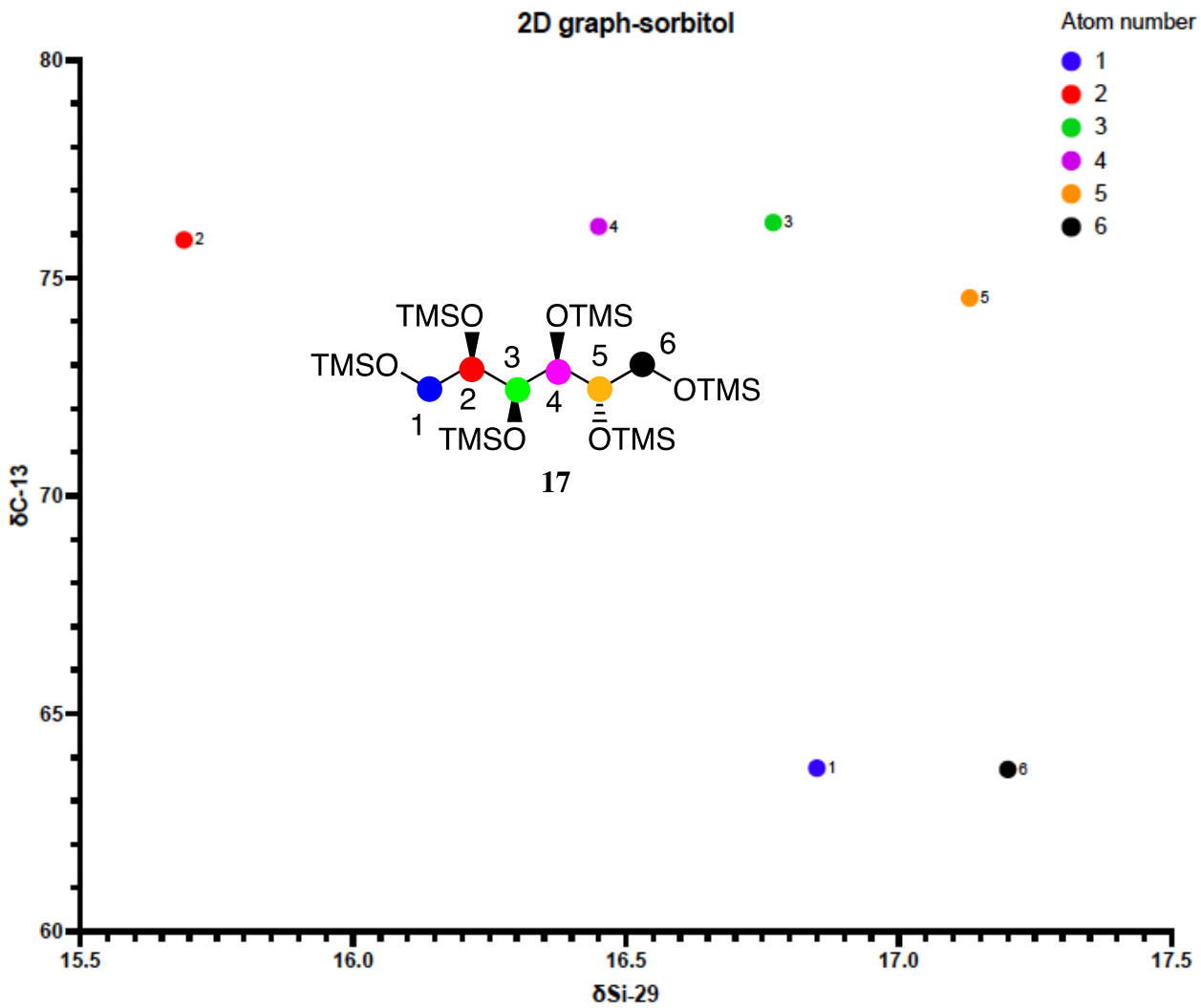

SI-Figure 2.5: 2D graph of per-*O*-TMS sorbitol (**17**); Si-29 NMR on x-axis and C-13 NMR on y-axis. Each dot represents the correlation of C atom to Si atom on its chemical shift.

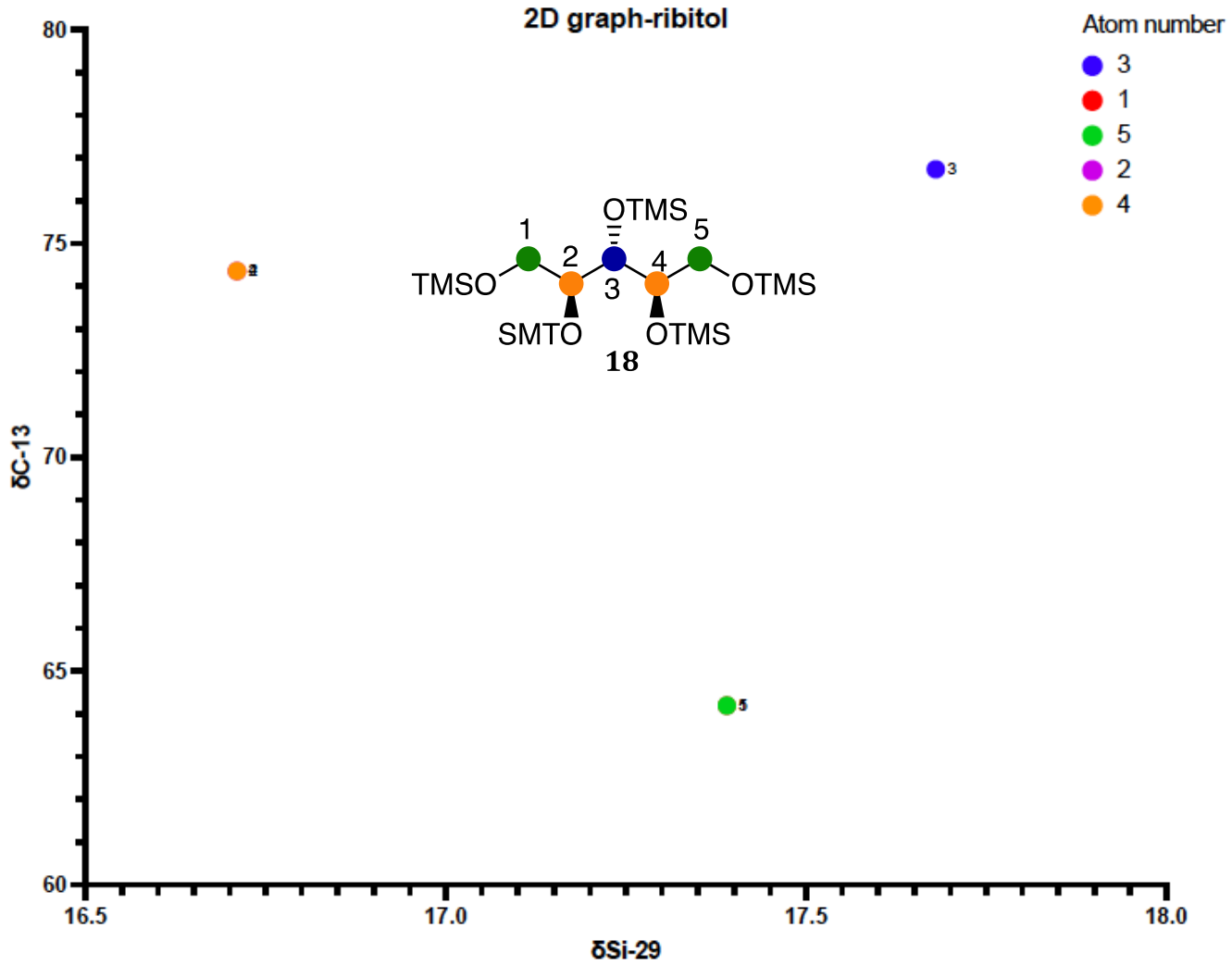

SI-Figure 2.6: 2D graph of per-*O*-TMS ribitol (**18**); Si-29 NMR on x-axis and C-13 NMR on y-axis. Each dot represents the correlation of C atom to Si atom on its chemical shift.

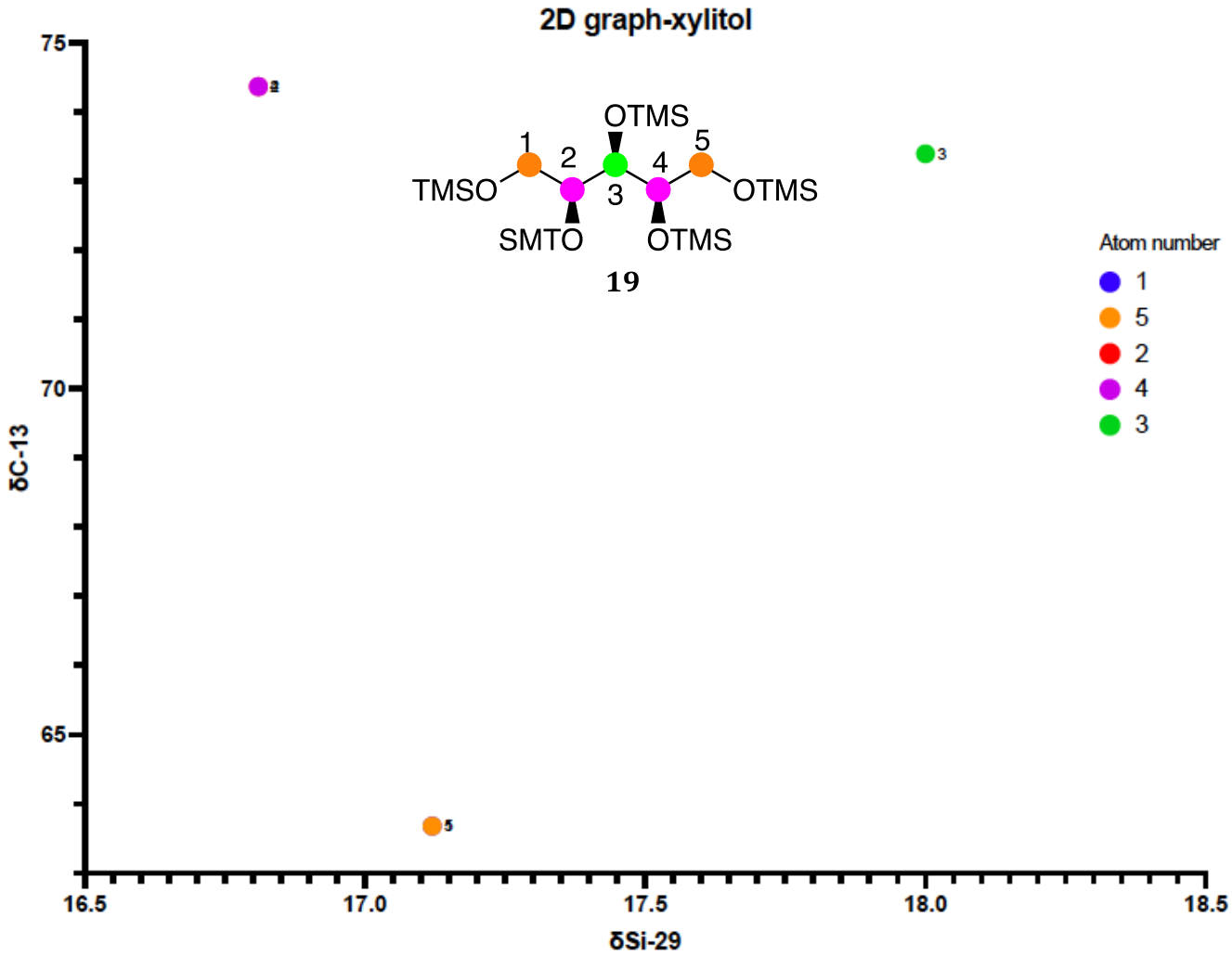

SI-Figure 2.7: 2D graph of per-*O*-TMS xylitol (**19**); Si-29 NMR on x-axis and C-13 NMR on y-axis. Each dot represents the correlation of C atom to Si atom on its chemical shift.

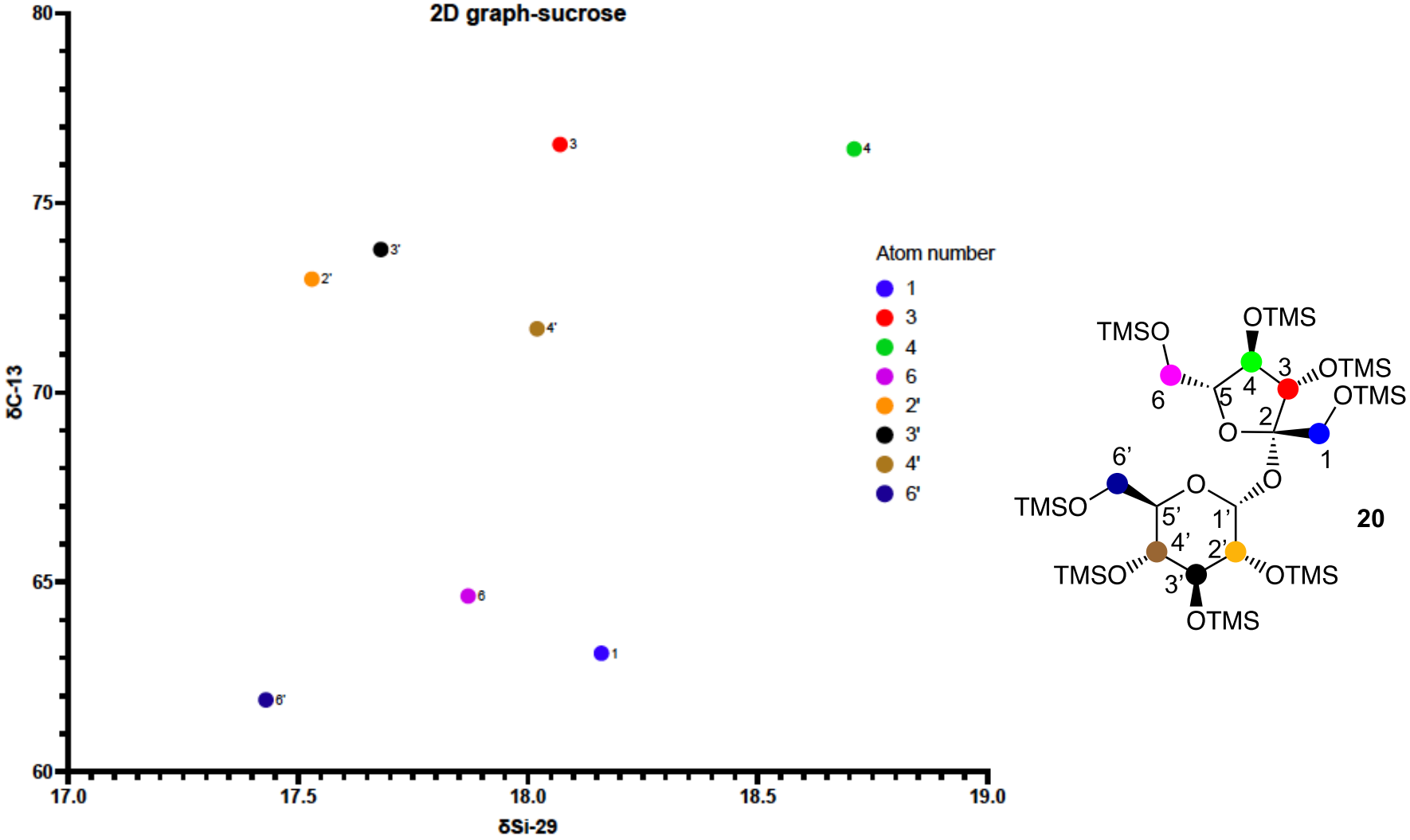

SI-Figure 2.8: 2D graph of per-*O*-TMS sucrose (**20**); Si-29 NMR on x-axis and C-13 NMR on y-axis. Each dot represents the correlation of C atom to Si atom on its chemical shift.

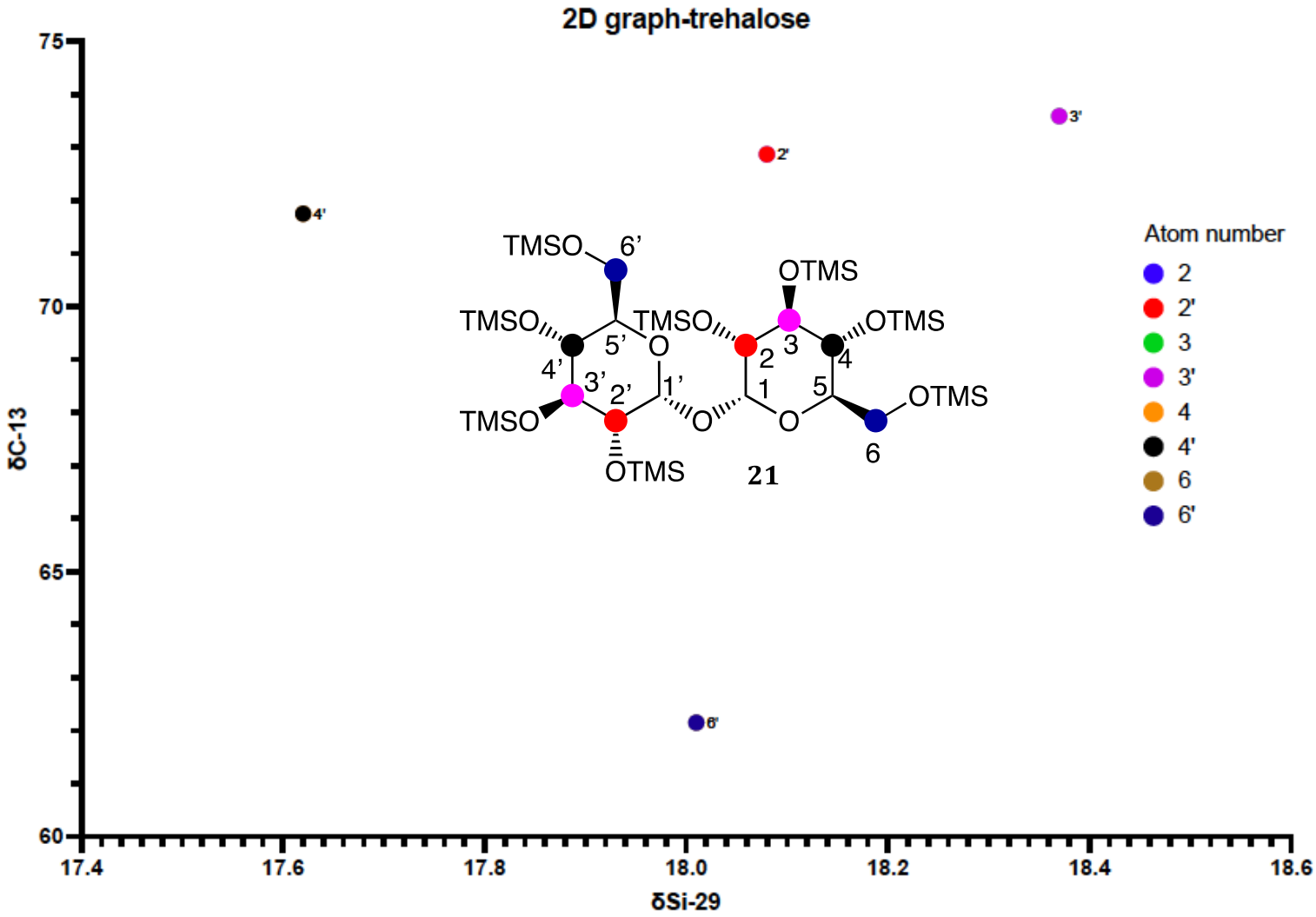

SI-Figure 2.9: 2D graph of per-*O*-TMS trehalose (**21**); Si-29 NMR on x-axis and C-13 NMR on y-axis. Each dot represents the correlation of C atom to Si atom on its chemical shift.

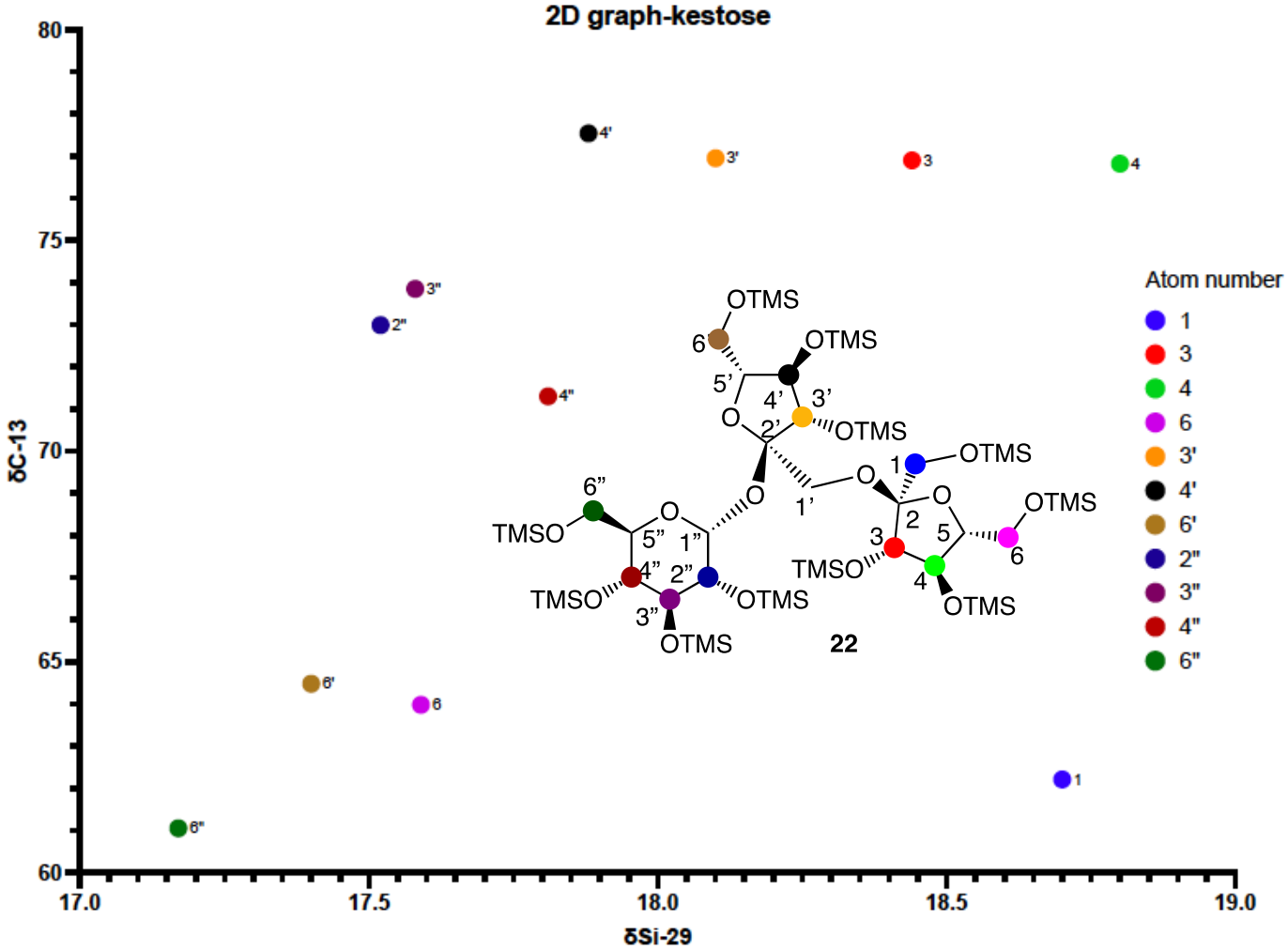

SI-Figure 2.11: 2D graph of per-*O*-TMS kestose (**23**); Si-29 NMR on x-axis and C-13 NMR on y-axis. Each dot represents the correlation of C atom to Si atom on its chemical shift.

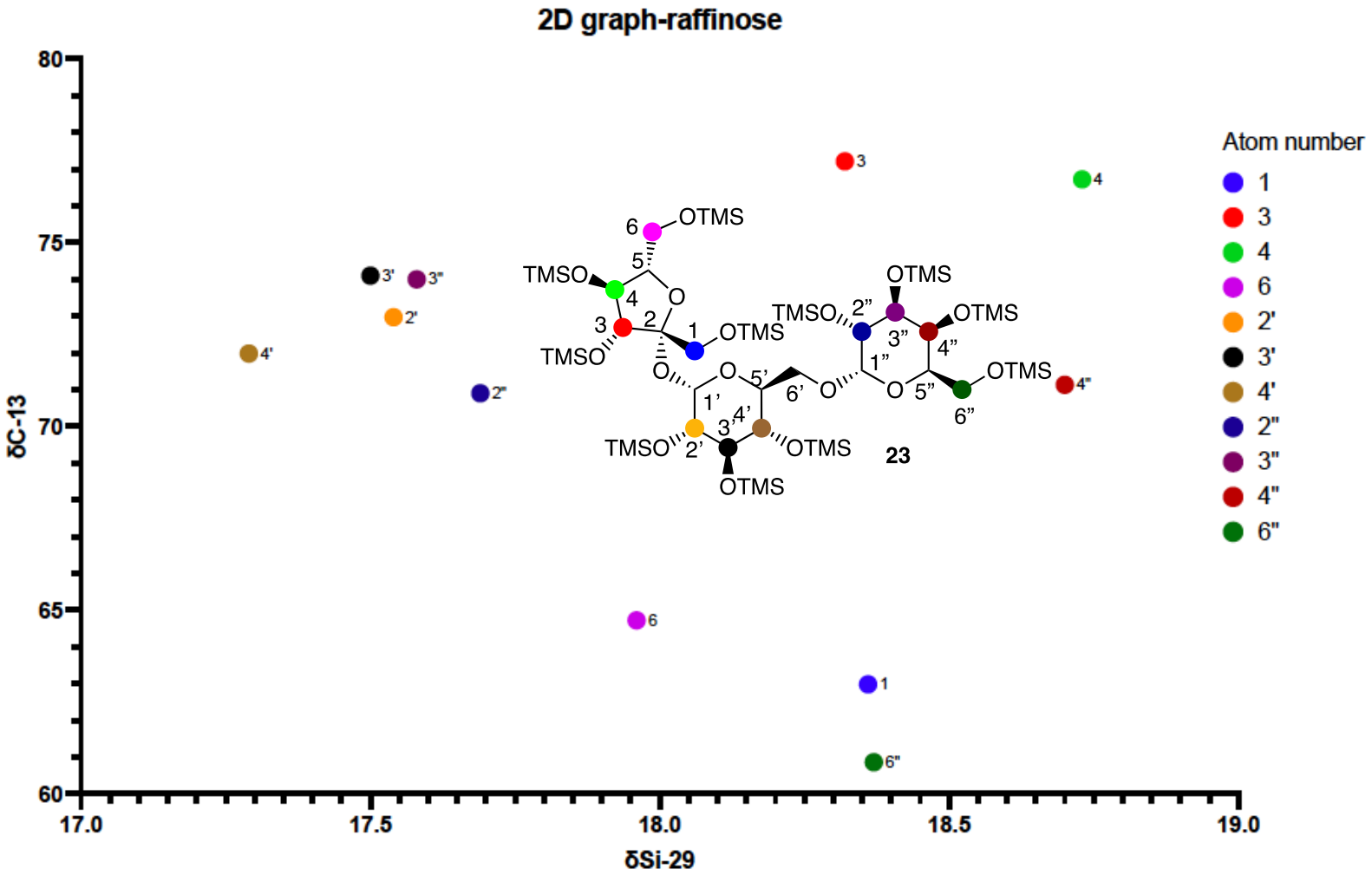

SI-Figure 2.10: 2D graph of per-*O*-TMS raffinose (**22**); Si-29 NMR on x-axis and C-13 NMR on y-axis. Each dot represents the correlation of C atom to Si atom on its chemical shift.

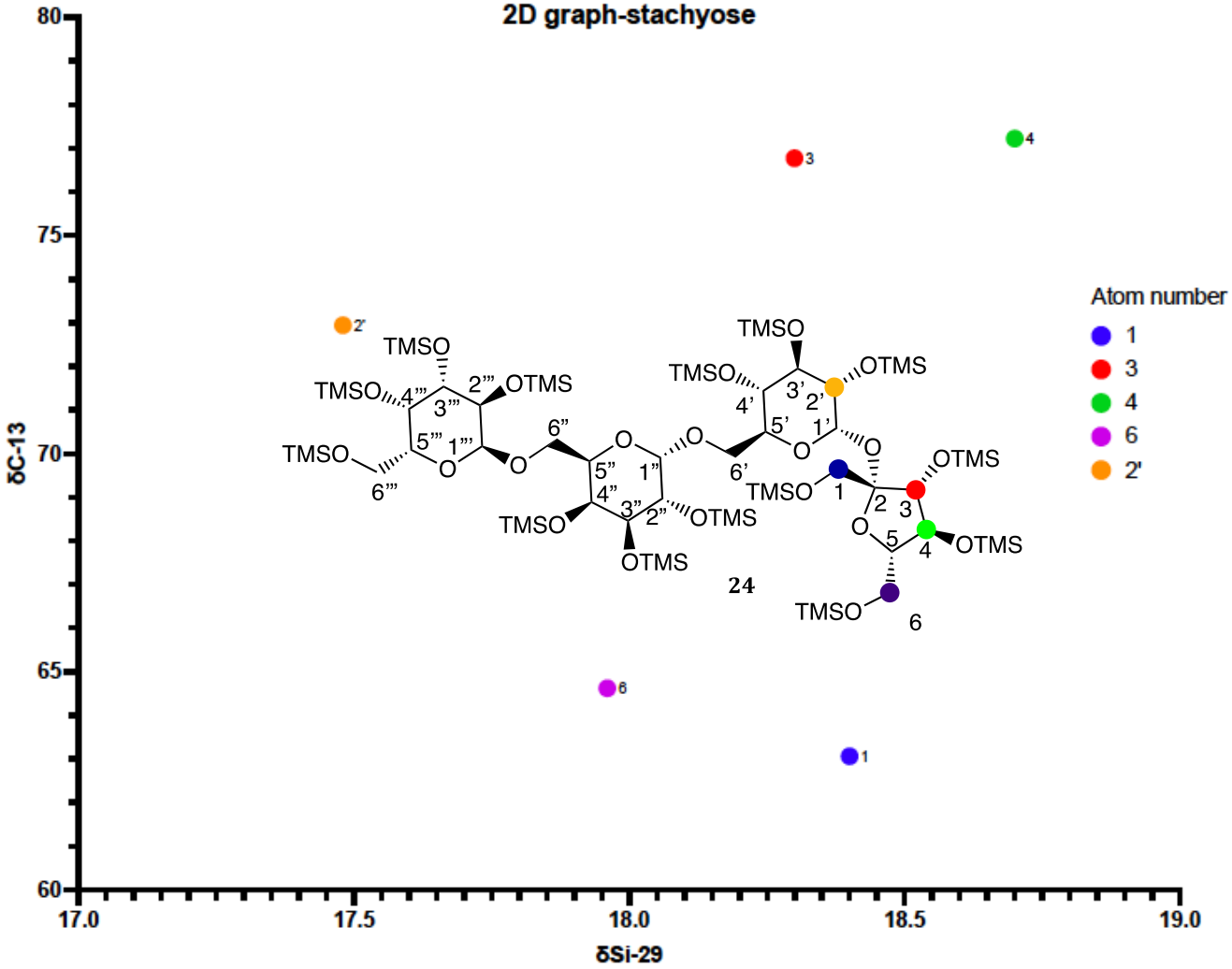

SI-Figure 2.12: 2D graph of per-*O*-TMS stachyose (**24**); Si-29 NMR on x-axis and C-13 NMR on y-axis. Each dot represents the correlation of C atom to Si atom on its chemical shift.

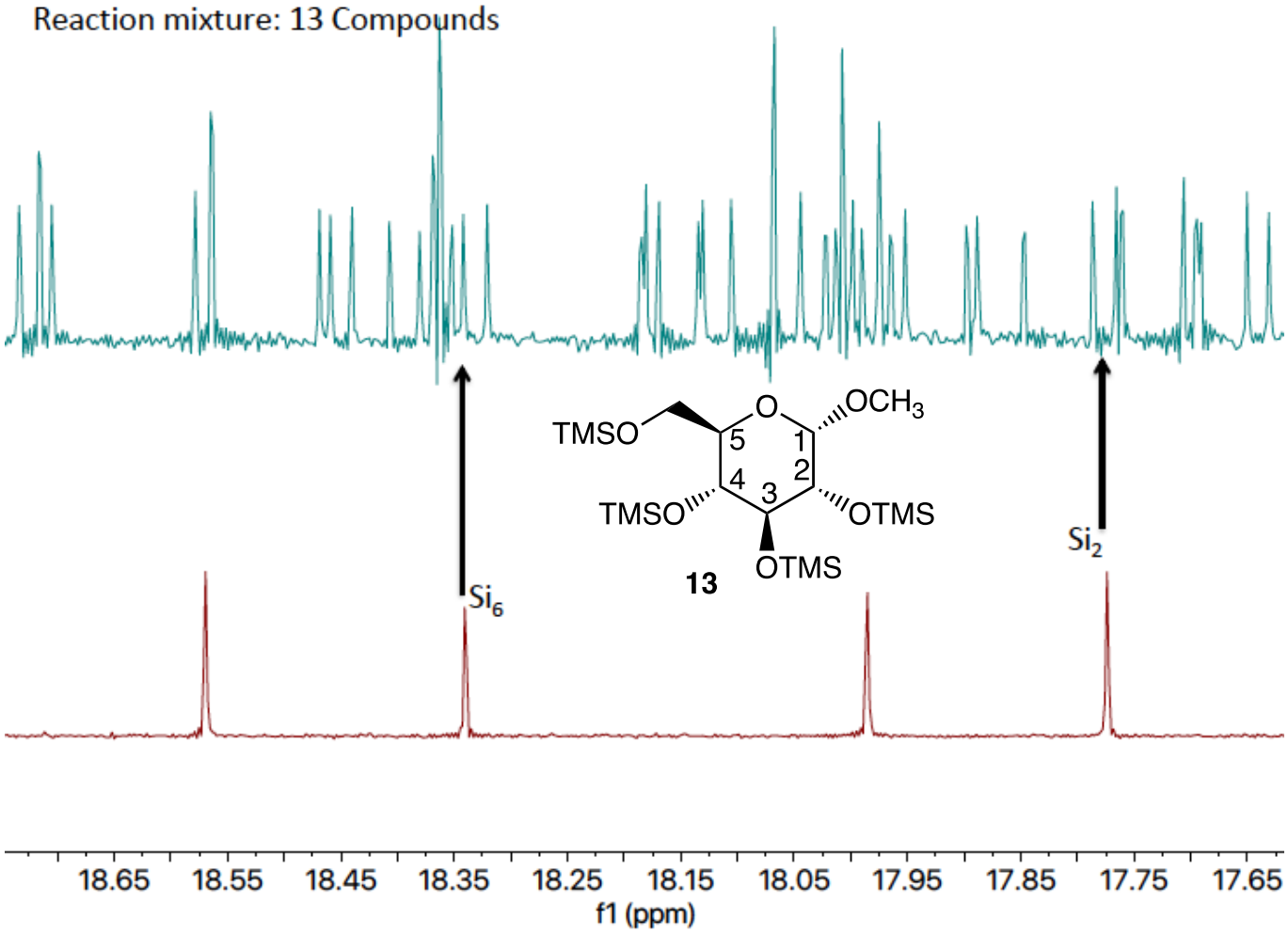

SI-Figure 2.13: The ^{29}Si NMR spectra overlapped between per-*O*-TMS methylglucoside (**13**) and reaction mixture of 13 per-*O*-silylated derivatives.

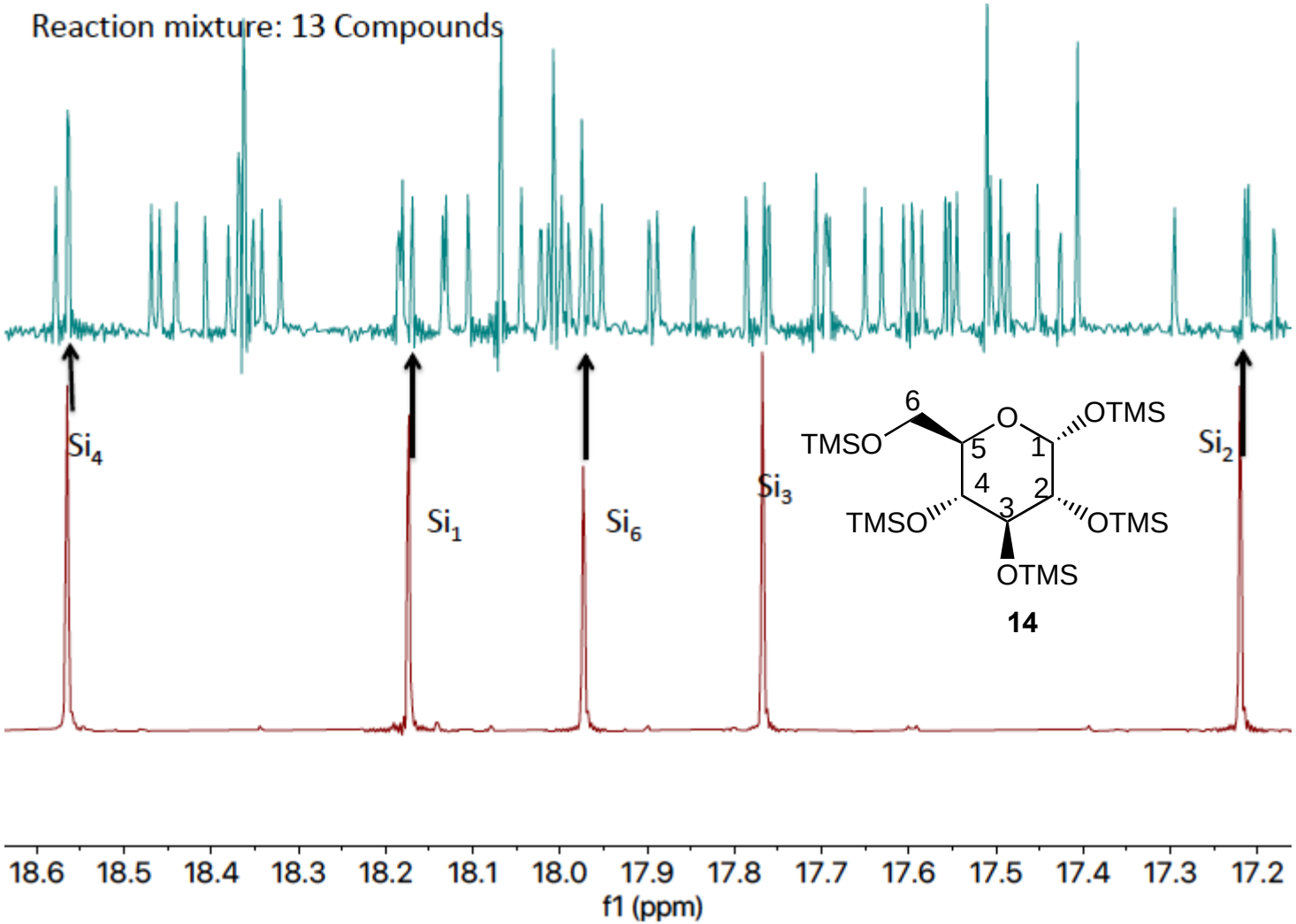

SI-Figure 2.14: The ^{29}Si NMR spectra overlapped between per-*O*-TMS glucose (**14**) and reaction mixture of 13 per-*O*-silylated derivatives.

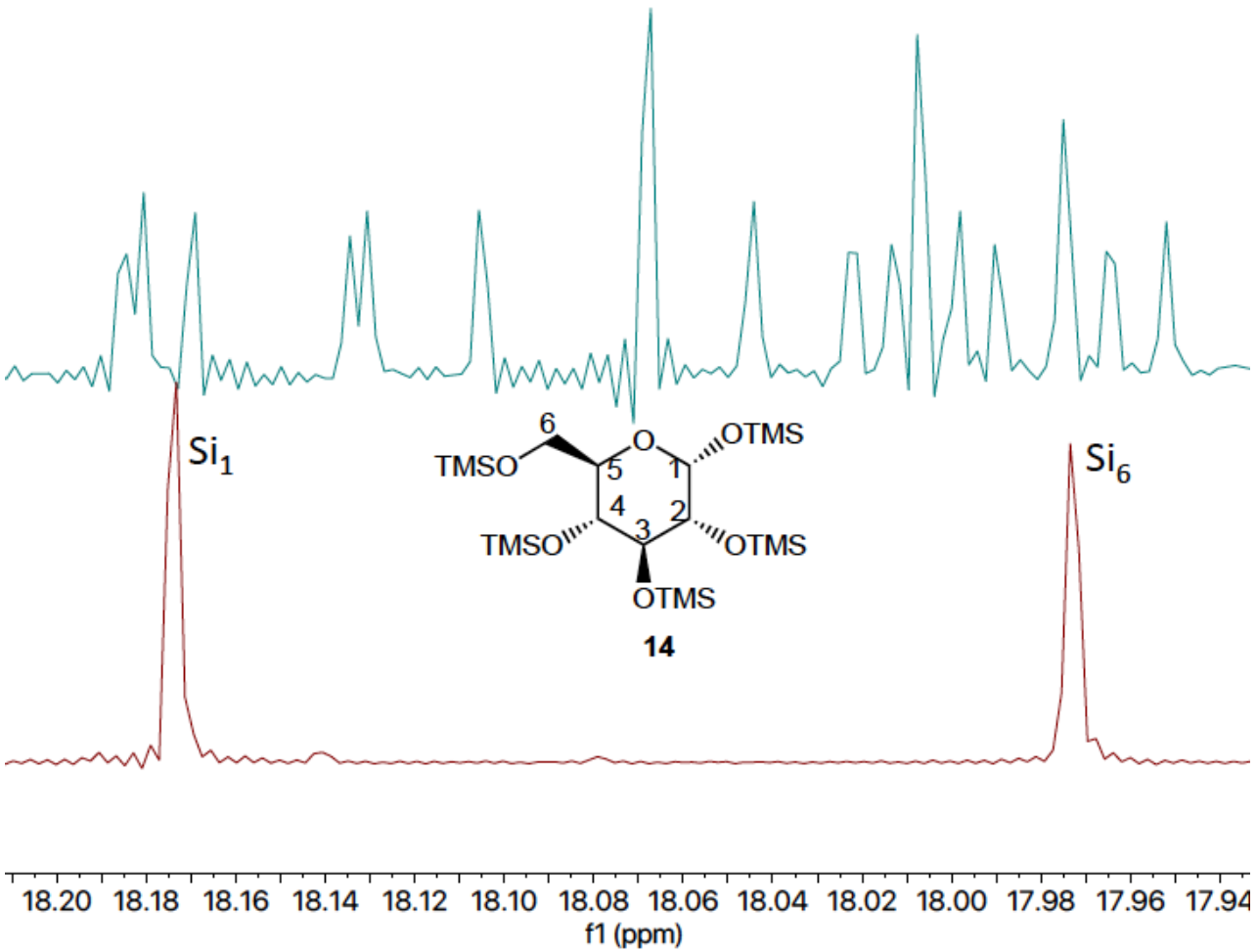

SI-Figure 2.15: The ^{29}Si NMR spectra overlapped between per-*O*-TMS glucose (**14**) and reaction mixture of 13 per-*O*-silylated derivatives in zoom in region of Si1 and Si6 comparison for peak identification.

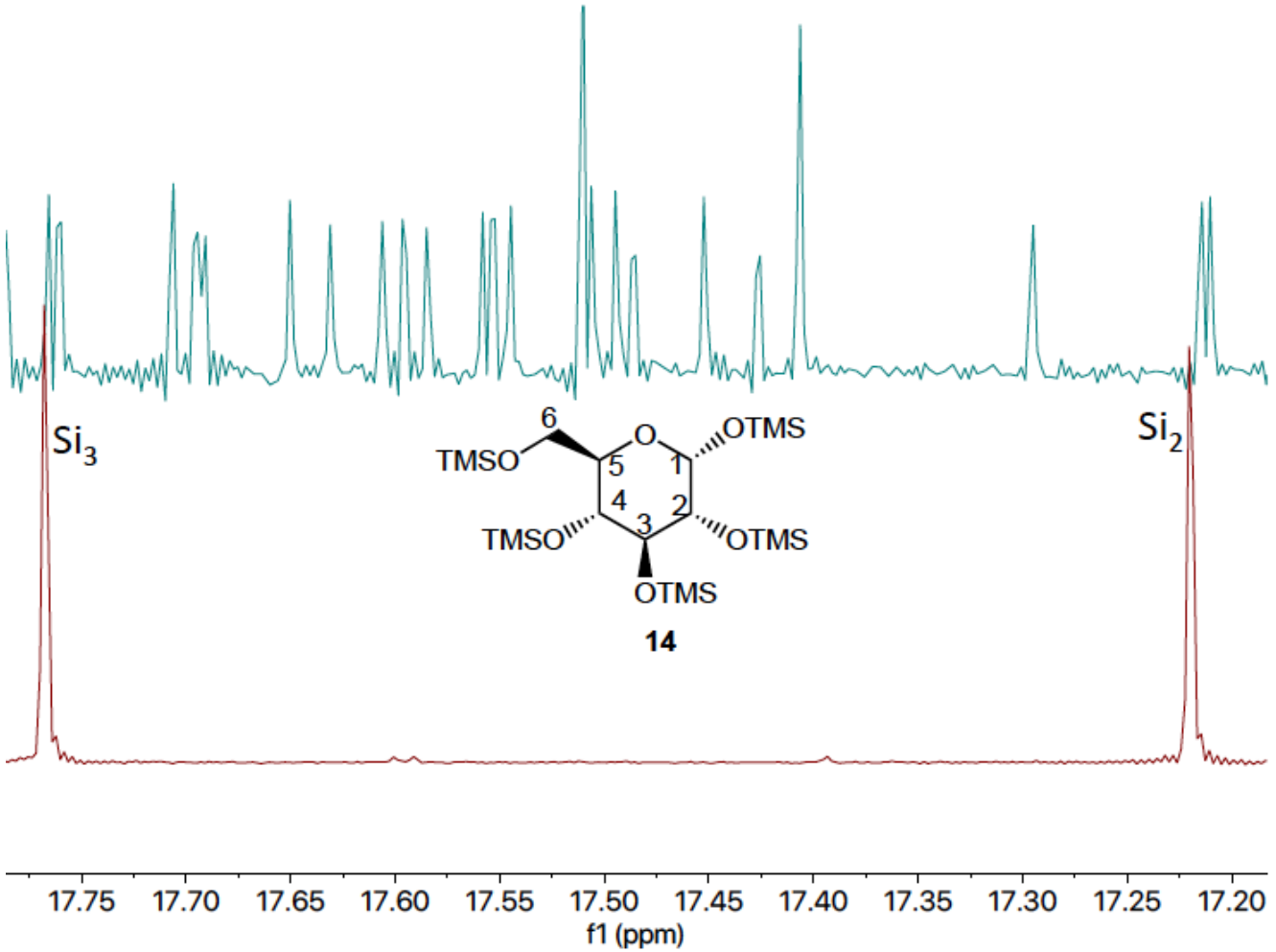

SI-Figure 2.16: The ^{29}Si NMR spectra overlapped between per-*O*-TMS glucose (**14**) and reaction mixture of 13 per-*O*-silylated derivatives in zoom in region of Si2 and Si3 comparison for peak identification.

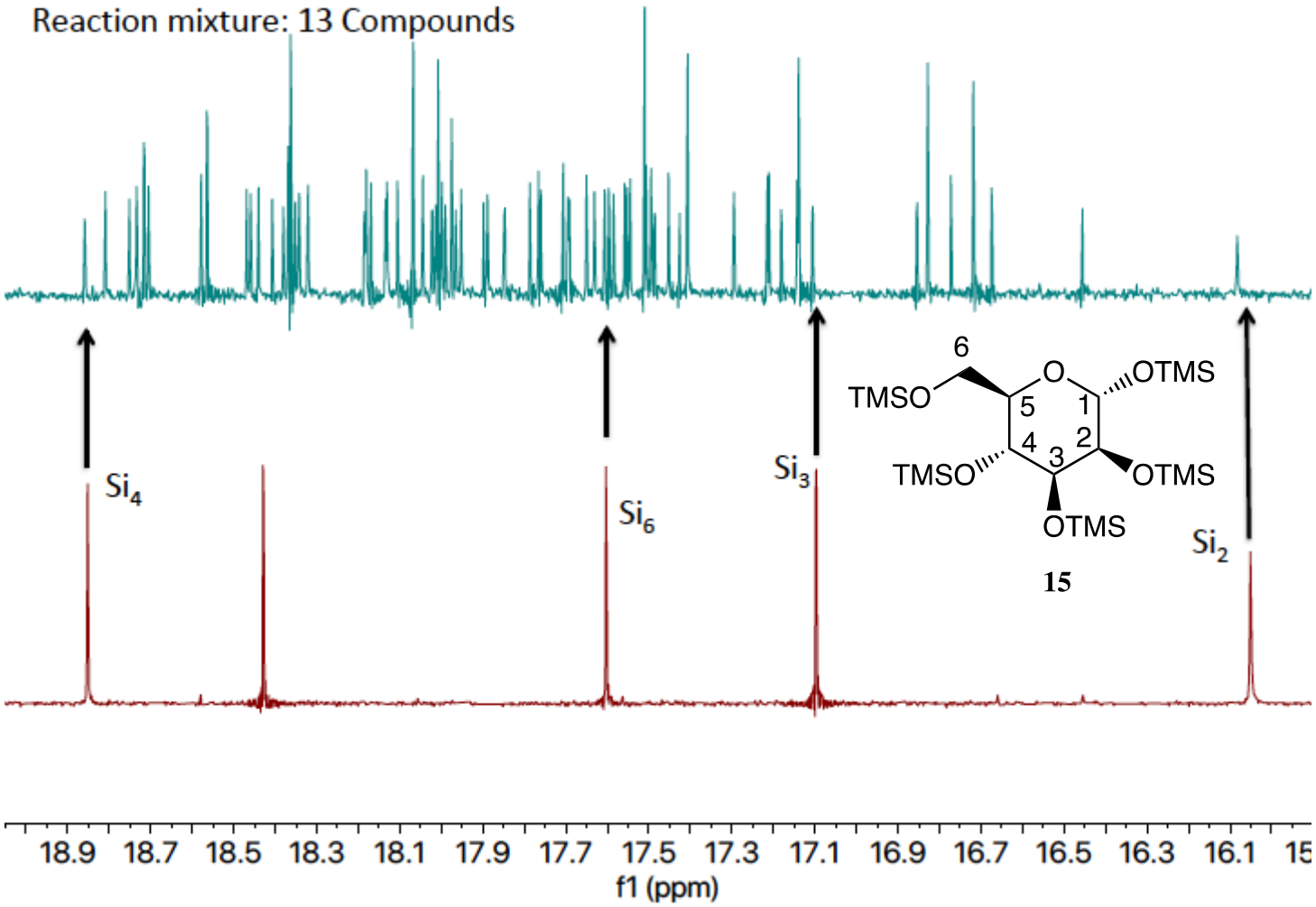

SI-Figure 2.17: The ^{29}Si NMR spectra overlapped between per-*O*-TMS mannose (**15**) and reaction mixture of 13 per-*O*-silylated derivatives.

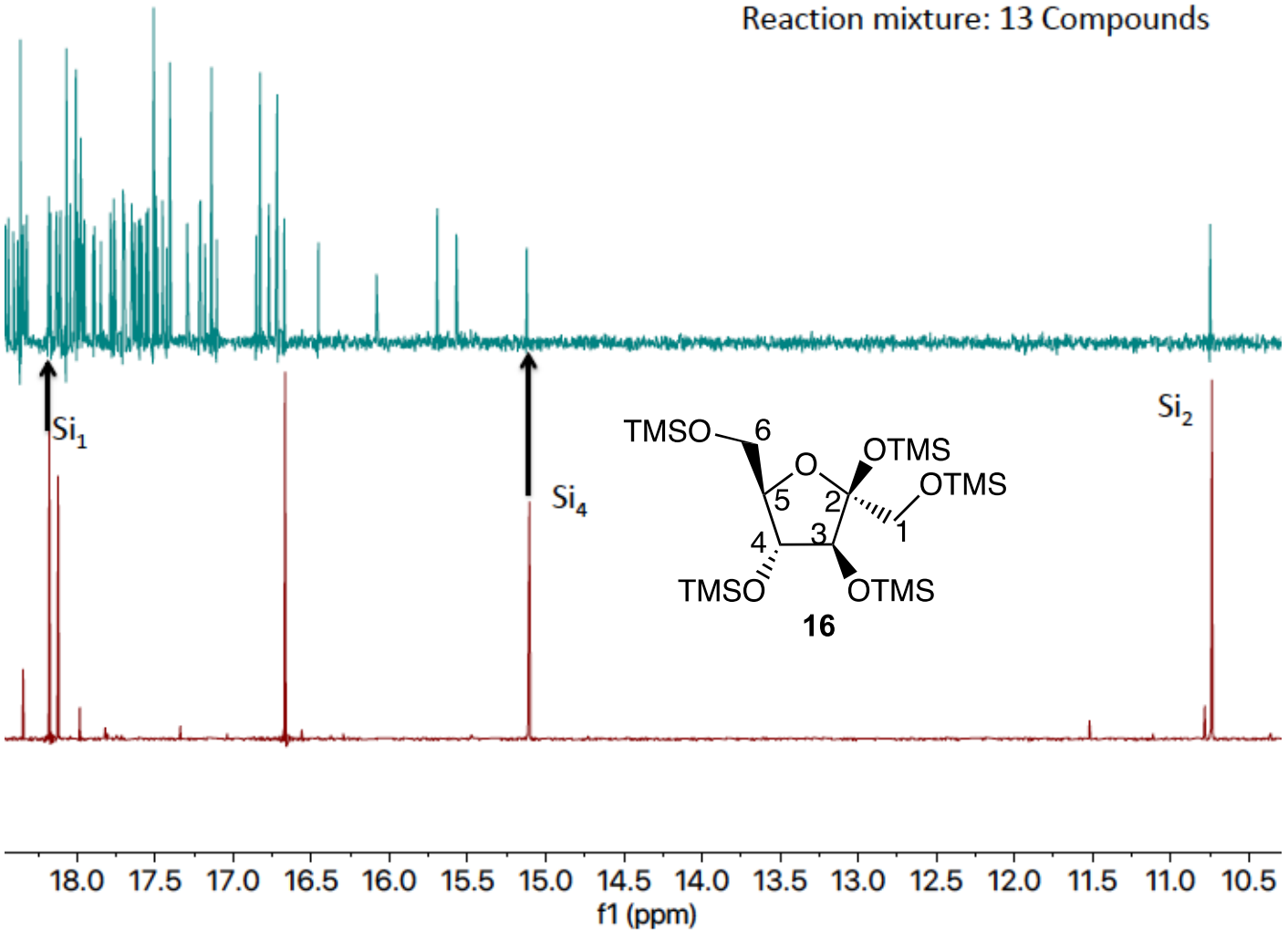

SI-Figure 2.18: The ^{29}Si NMR spectra overlapped between per-*O*-TMS fructose (**16**) and reaction mixture of 13 per-*O*-silylated derivatives.

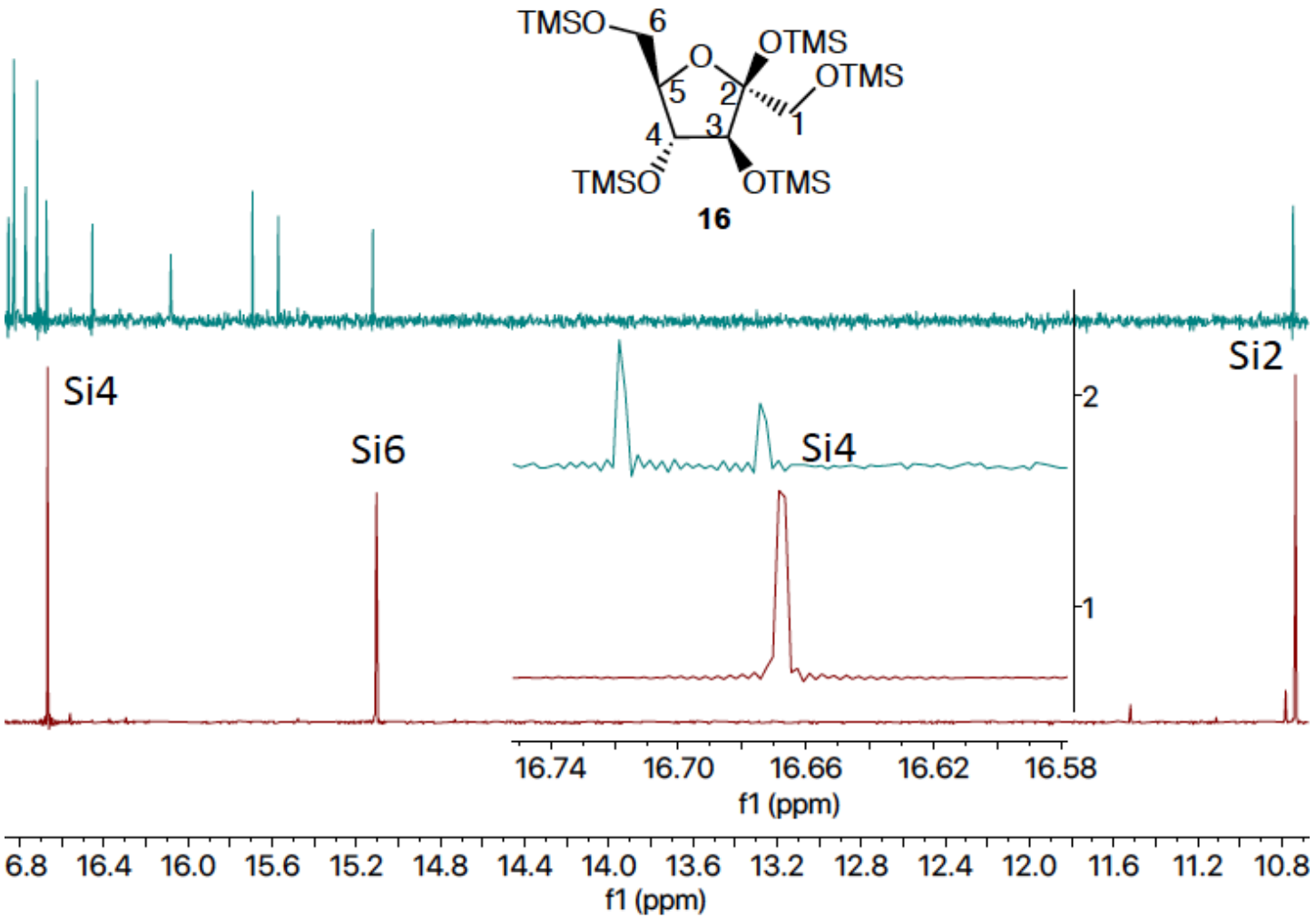

SI-Figure 2.19: The ^{29}Si NMR spectra overlapped between per-*O*-TMS fructose (**16**) and reaction mixture of 13 per-*O*-silylated derivatives showed zoom in region of Si4.

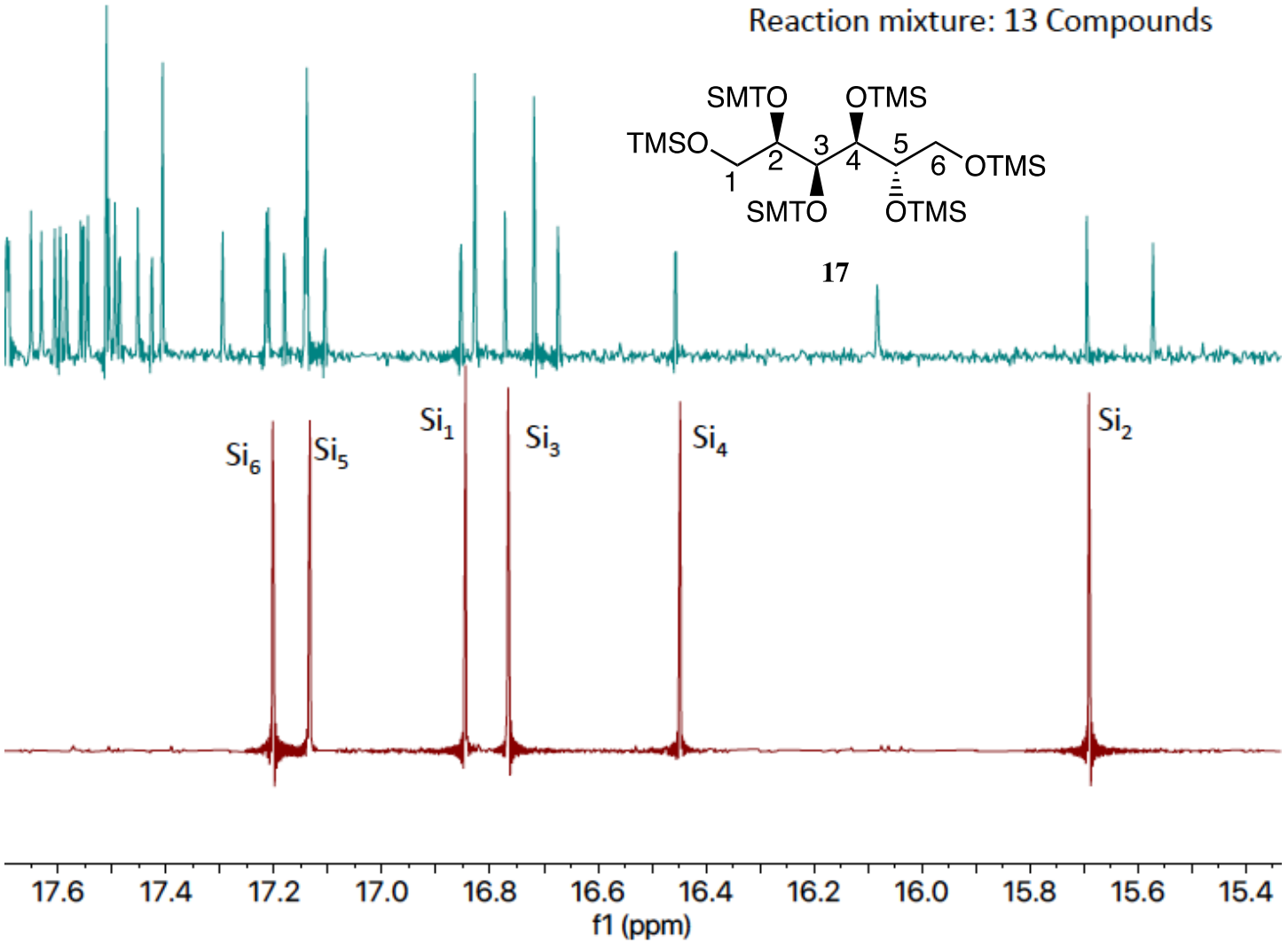

SI-Figure 2.20: The ^{29}Si NMR spectra overlapped between per-*O*-TMS sorbitol (**17**) and reaction mixture of 13 per-*O*-silylated derivatives.

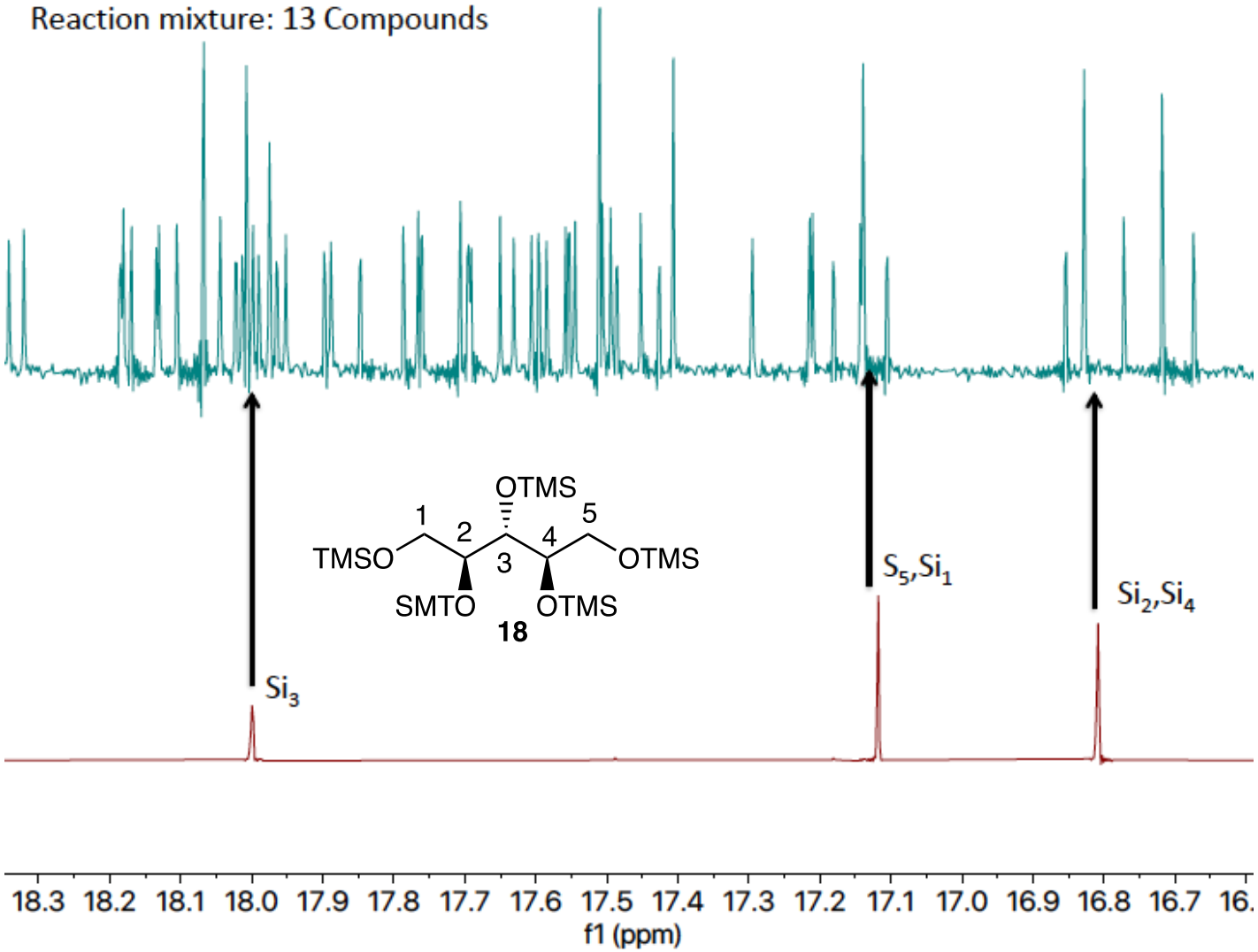

Si-Figure 2.21: The ^{29}Si NMR spectra overlapped between per-*O*-TMS ribitol (**18**) and reaction mixture of 13 per-*O*-silylated derivatives.

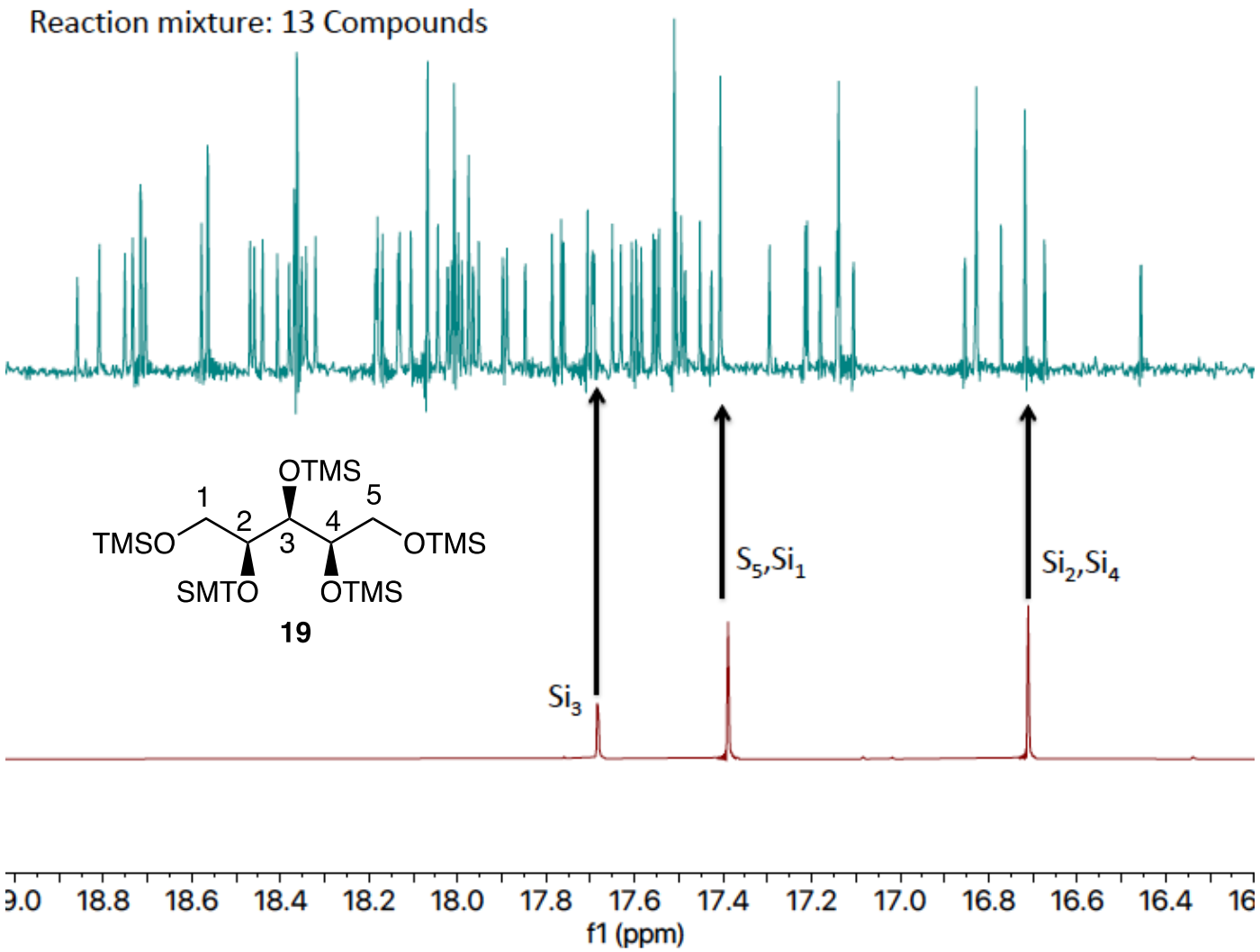

SI-Figure 2.22: The ^{29}Si NMR spectra overlapped between per-*O*-TMS xylitol (**19**) and reaction mixture of 13 per-*O*-silylated derivatives.

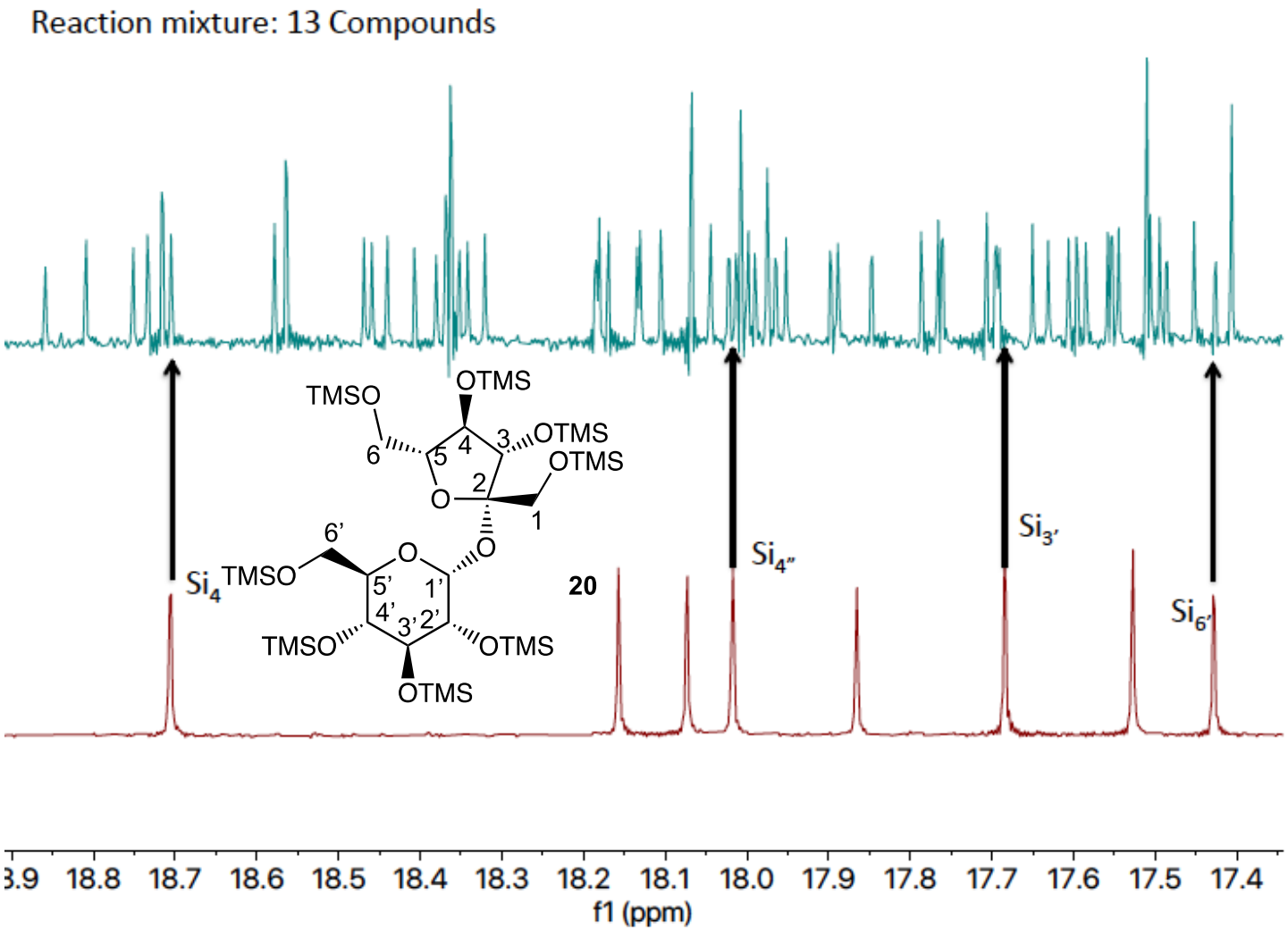

SI-Figure 2.23: The ^{29}Si NMR spectra overlapped between per-*O*-TMS sucrose (**20**) and reaction mixture of 13 per-*O*-silylated derivatives.

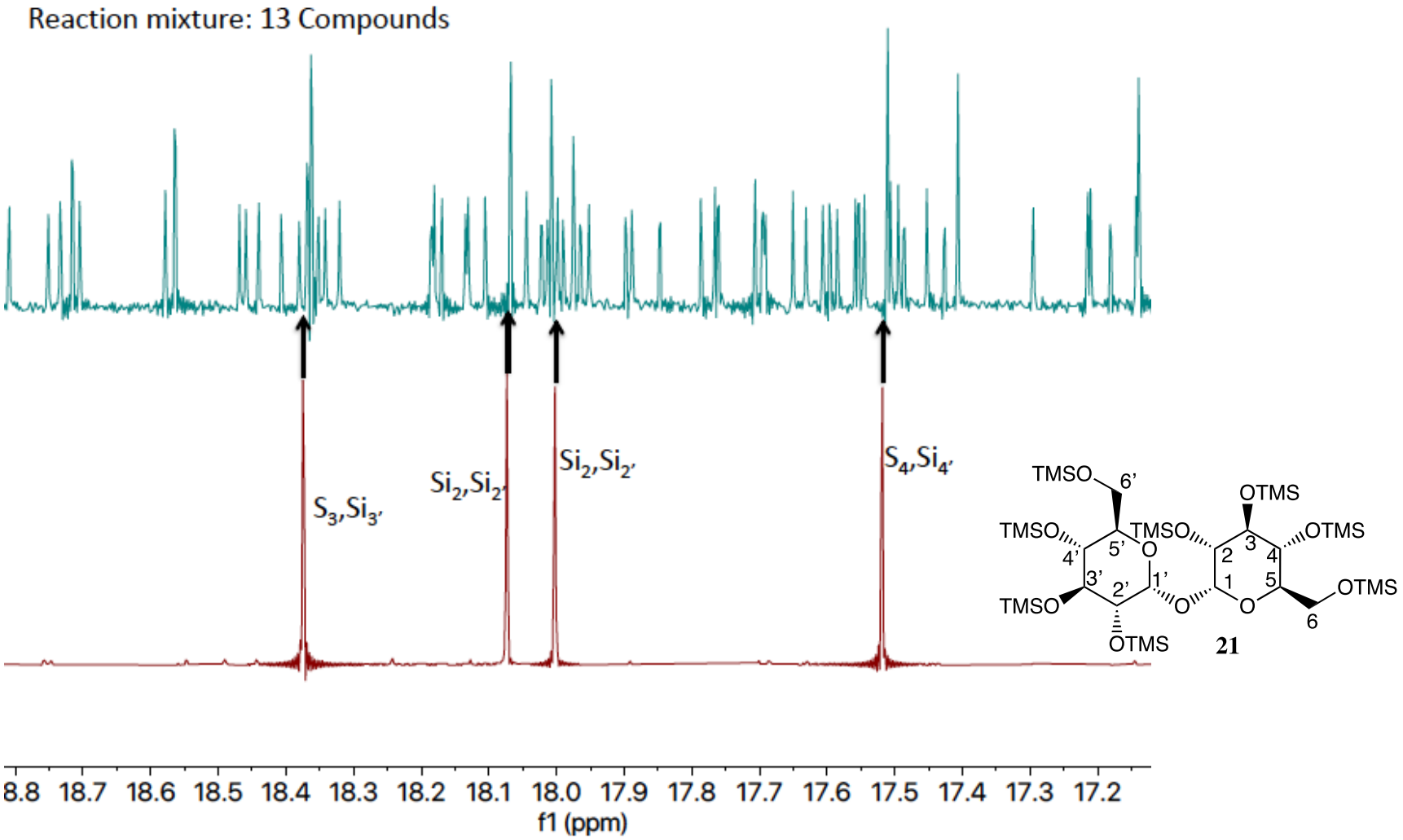

SI-Figure 2.24: The ^{29}Si NMR spectra overlapped between per-*O*-TMS trehalose (**21**) and reaction mixture of 13 per-*O*-silylated derivatives.

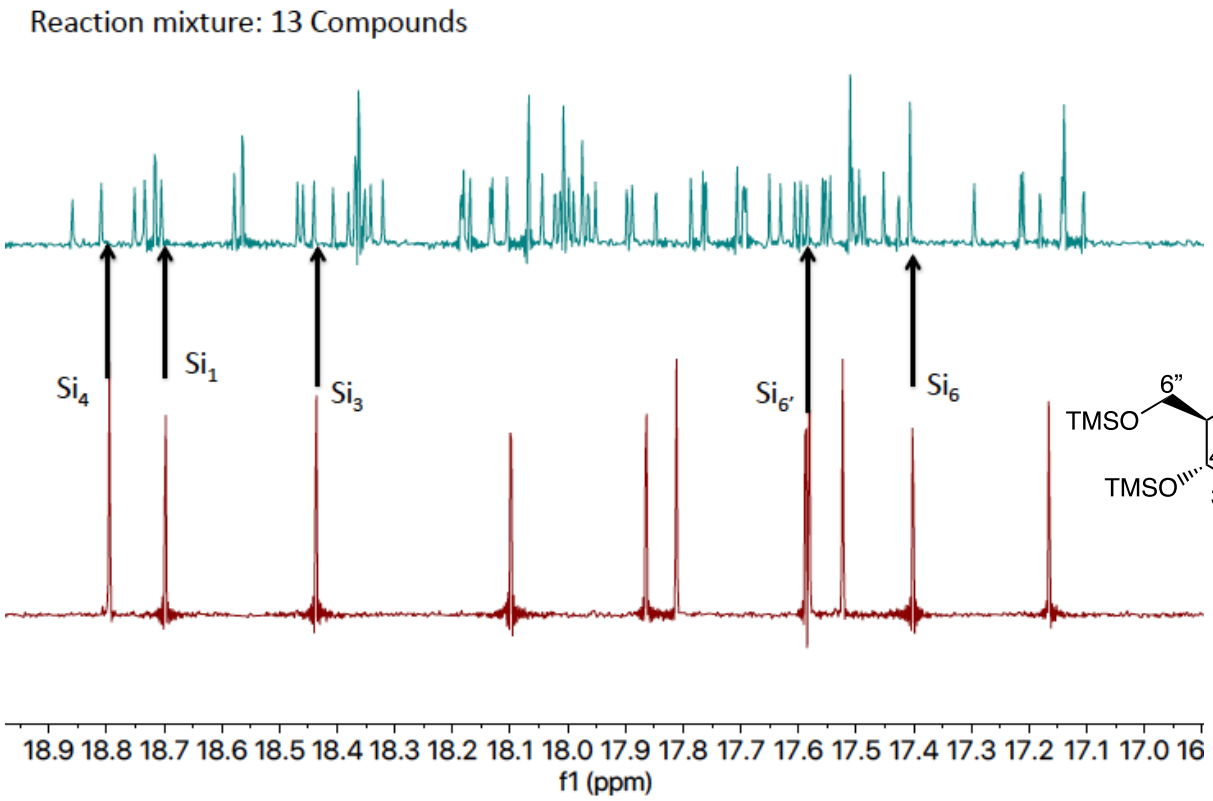

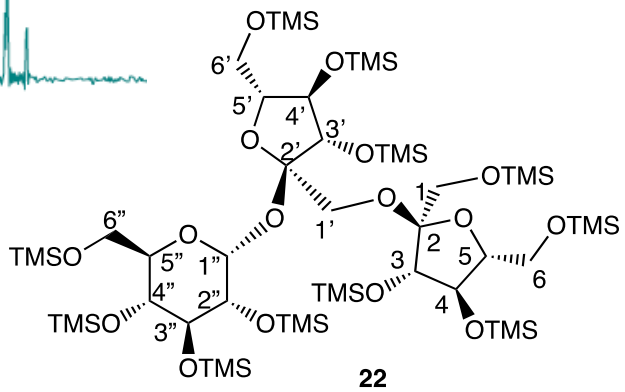

SI-Figure 2.25: The ^{29}Si NMR spectra overlapped between per-*O*-TMS kestose (**22**) and reaction mixture of 13 per-*O*-silylated derivatives.

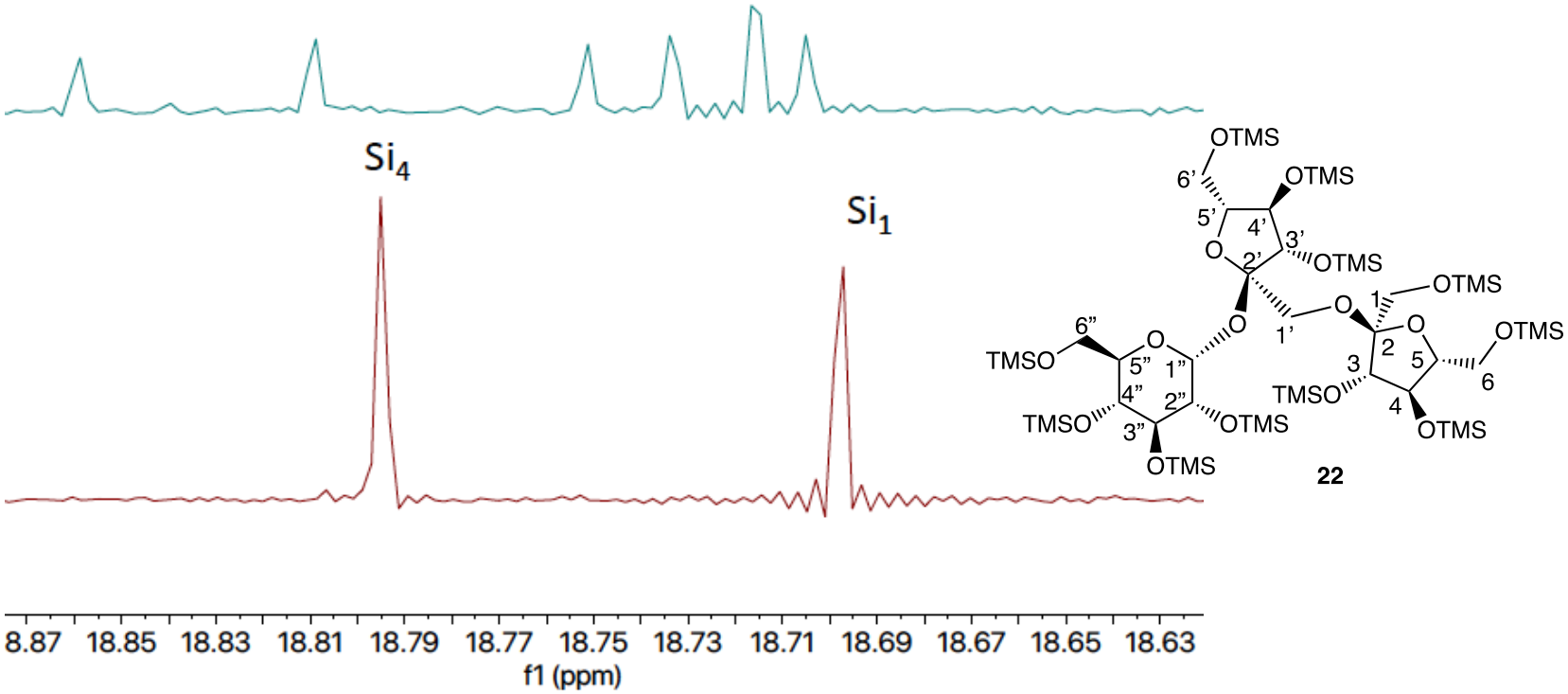

SI-Figure 2.26: The ^{29}Si NMR spectra overlapped between per-*O*-TMS kestose (**22**) and reaction mixture of 13 per-*O*-silylated derivatives. A zoom in region of Si1 and Si4 signals illustrate the deviation from compound in mixture to pure.

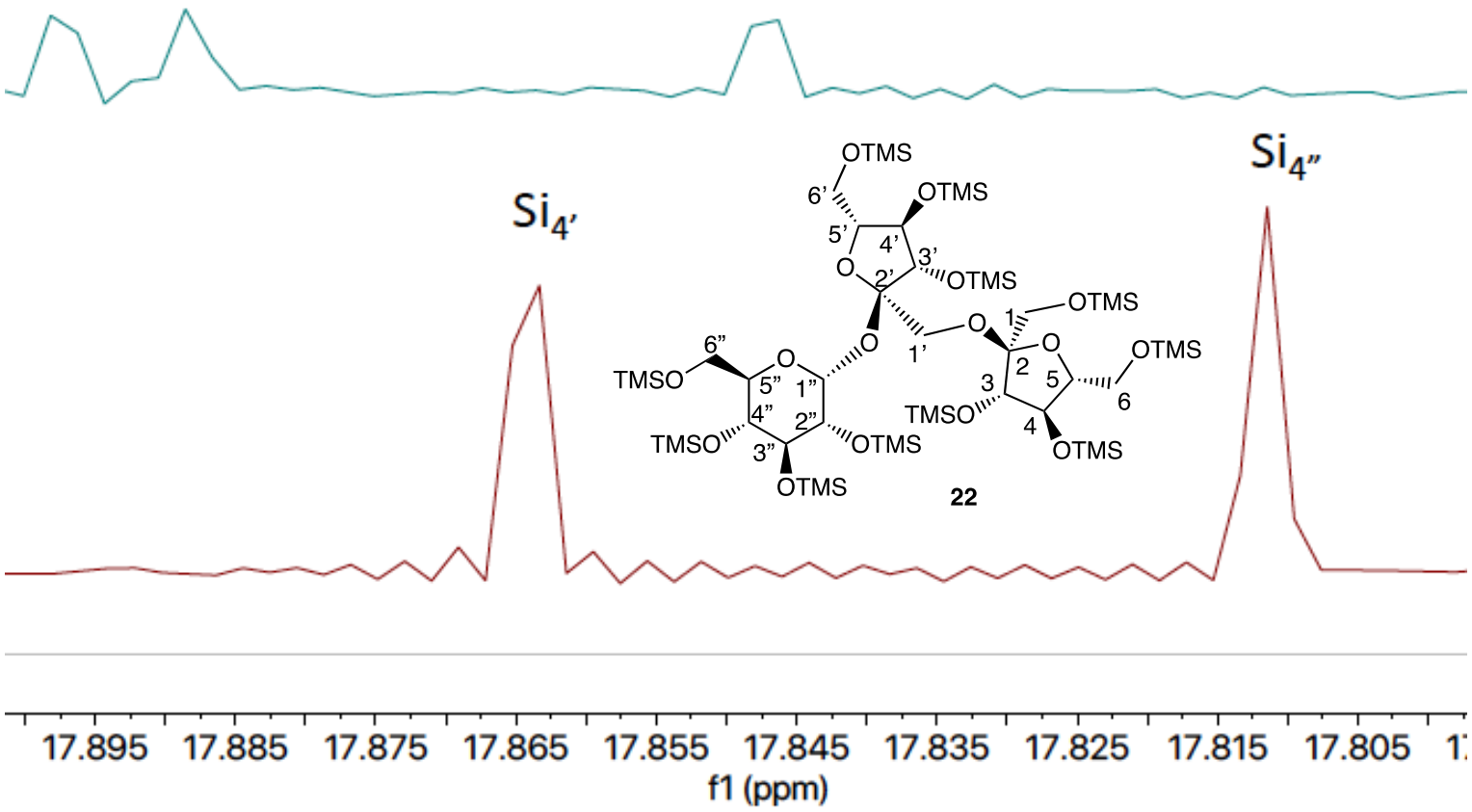

SI-Figure 2.27: The ^{29}Si NMR spectra overlapped between per-*O*-TMS kestose (**22**) and reaction mixture of 13 per-*O*-silylated derivatives. A zoom in region of Si4' and Si4" signals illustrate the deviation from compound in mixture to pure.

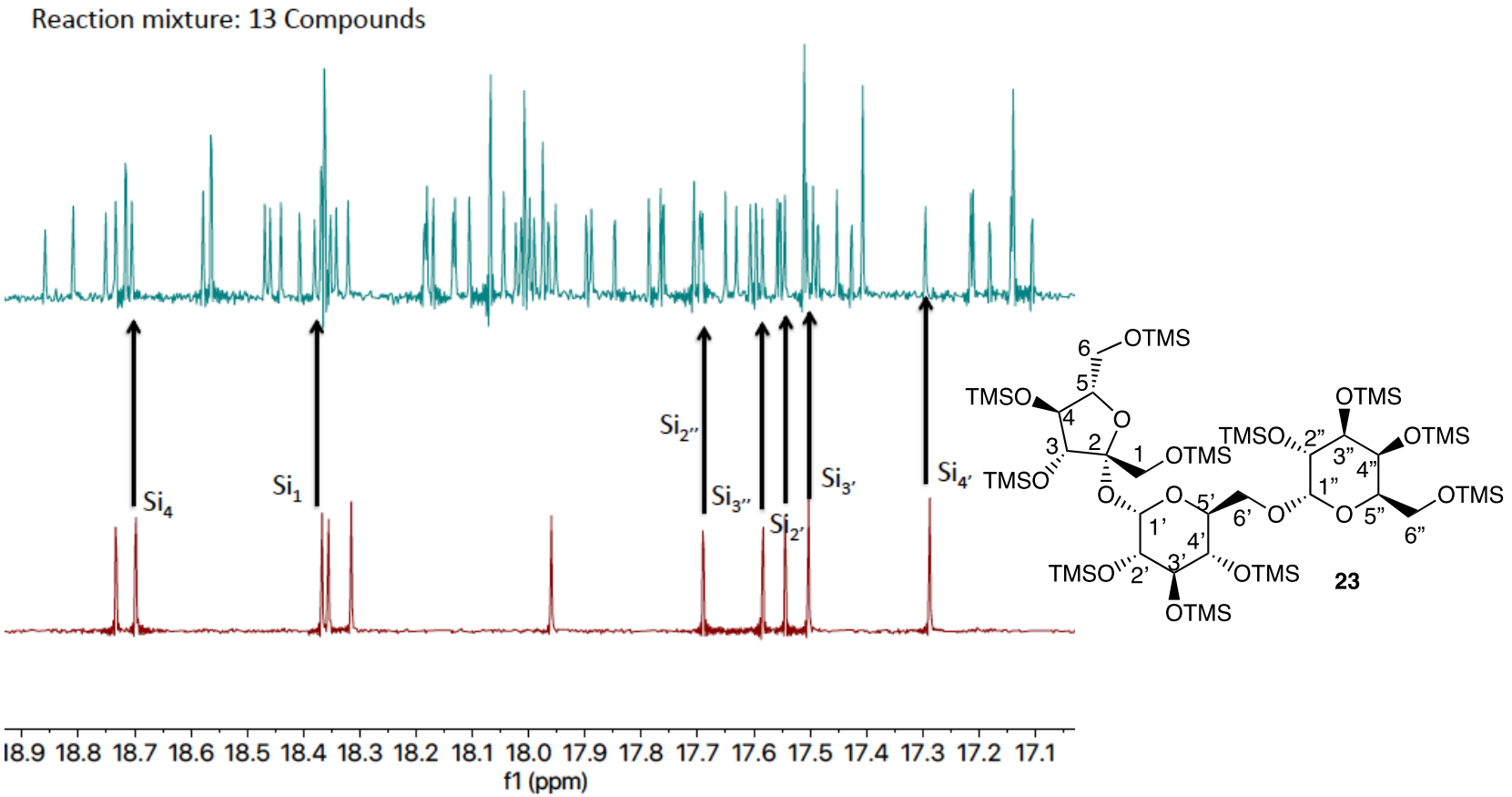

SI-Figure 2.28: The ^{29}Si NMR spectra overlapped between per-*O*-TMS raffinose (**23**) and reaction mixture of 13 per-*O*-silylated derivatives.

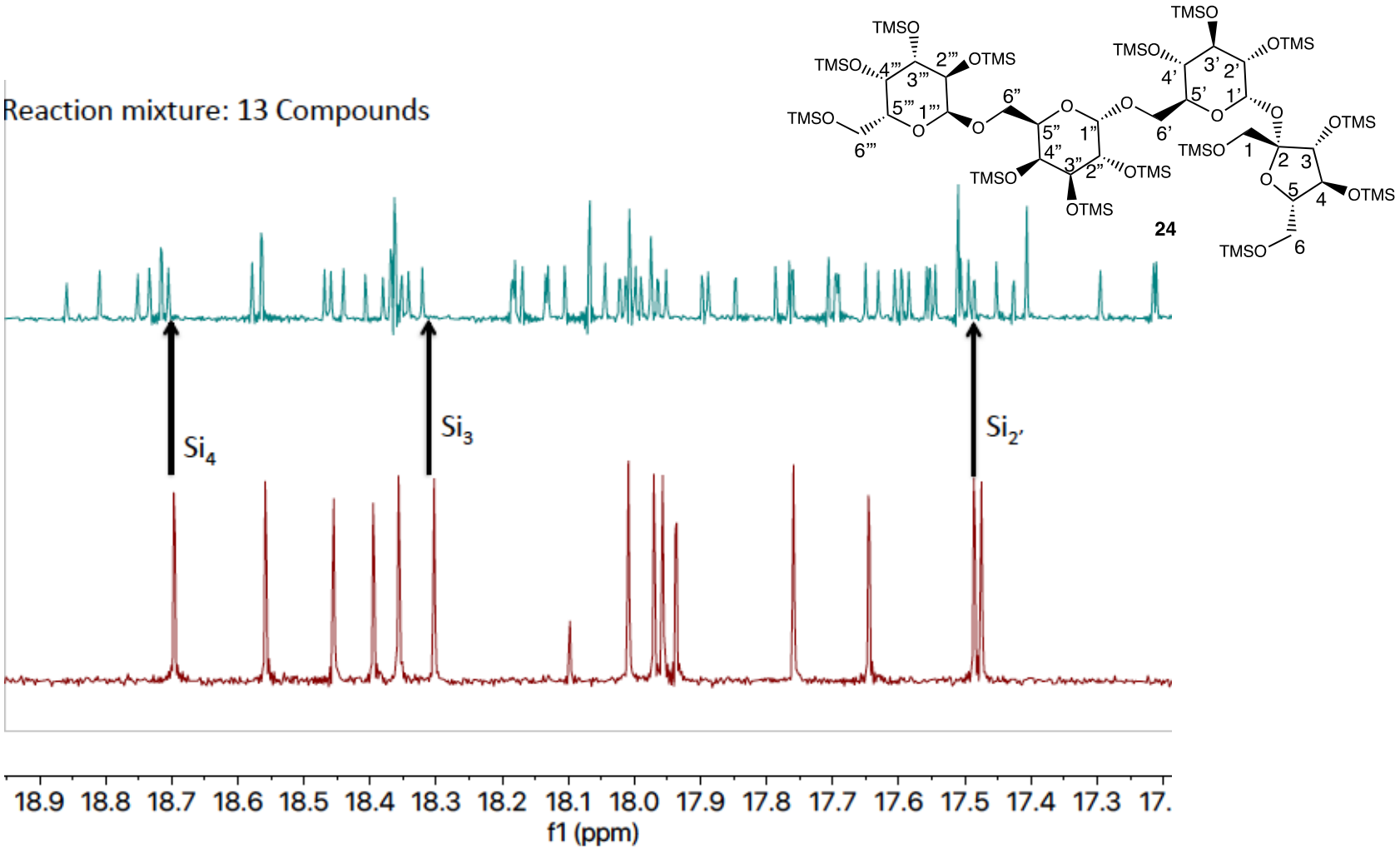

SI-Figure 2.29: The ^{29}Si NMR spectra overlapped between per-*O*-TMS styachose (**24**) and reaction mixture of 13 per-*O*-silylated derivatives.

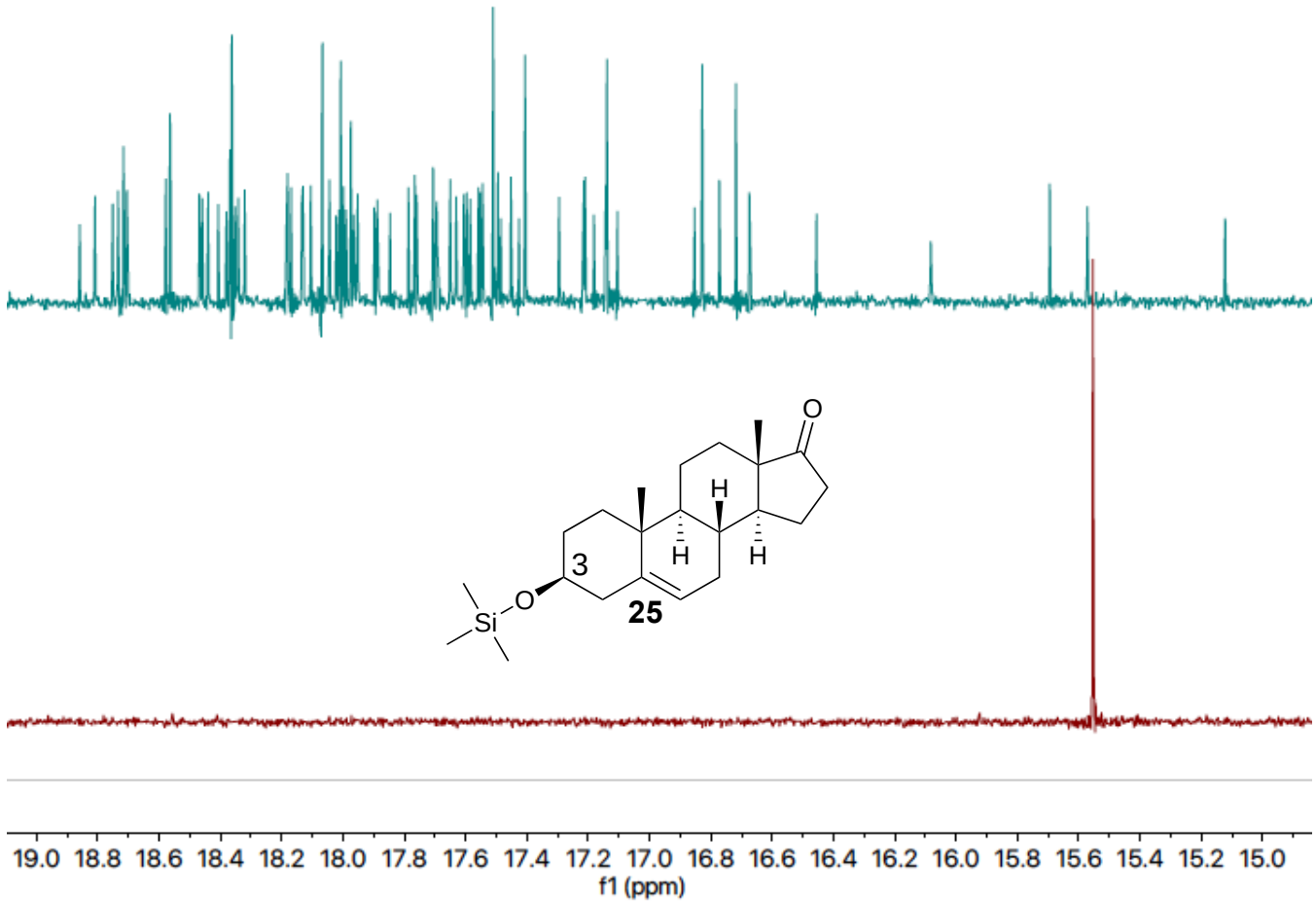

SI-Figure 2.30: The ^{29}Si NMR spectra overlapped between per-*O*-TMS DHEA (**25**) and reaction mixture of 13 per-*O*-silylated derivatives.

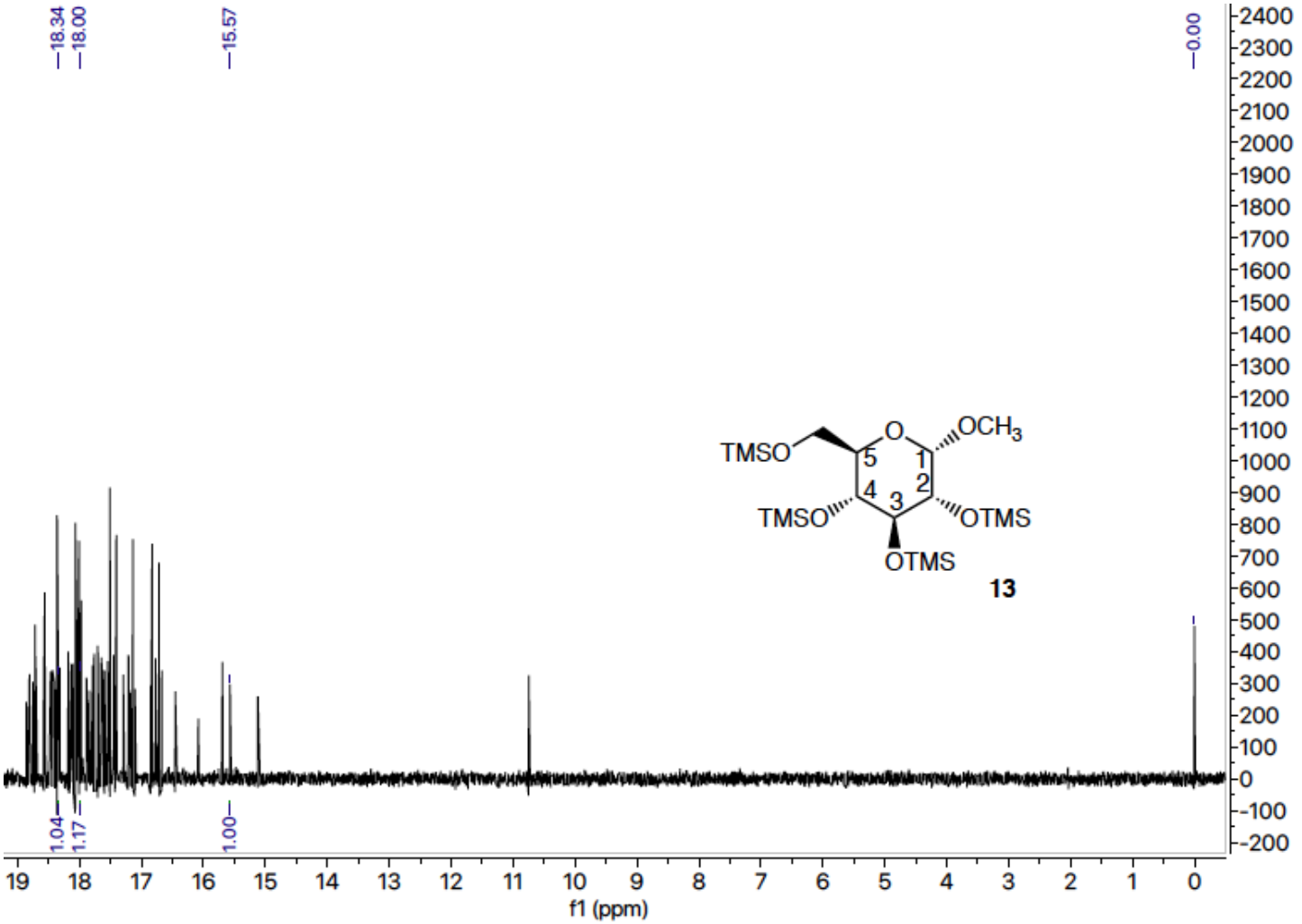

SI-Figure 2.31: The integration of assigned Si signals of α-per-*O*-TMS methylglucoside (**13**) in reaction mixture of 13 per-*O*-silylated derivatives.

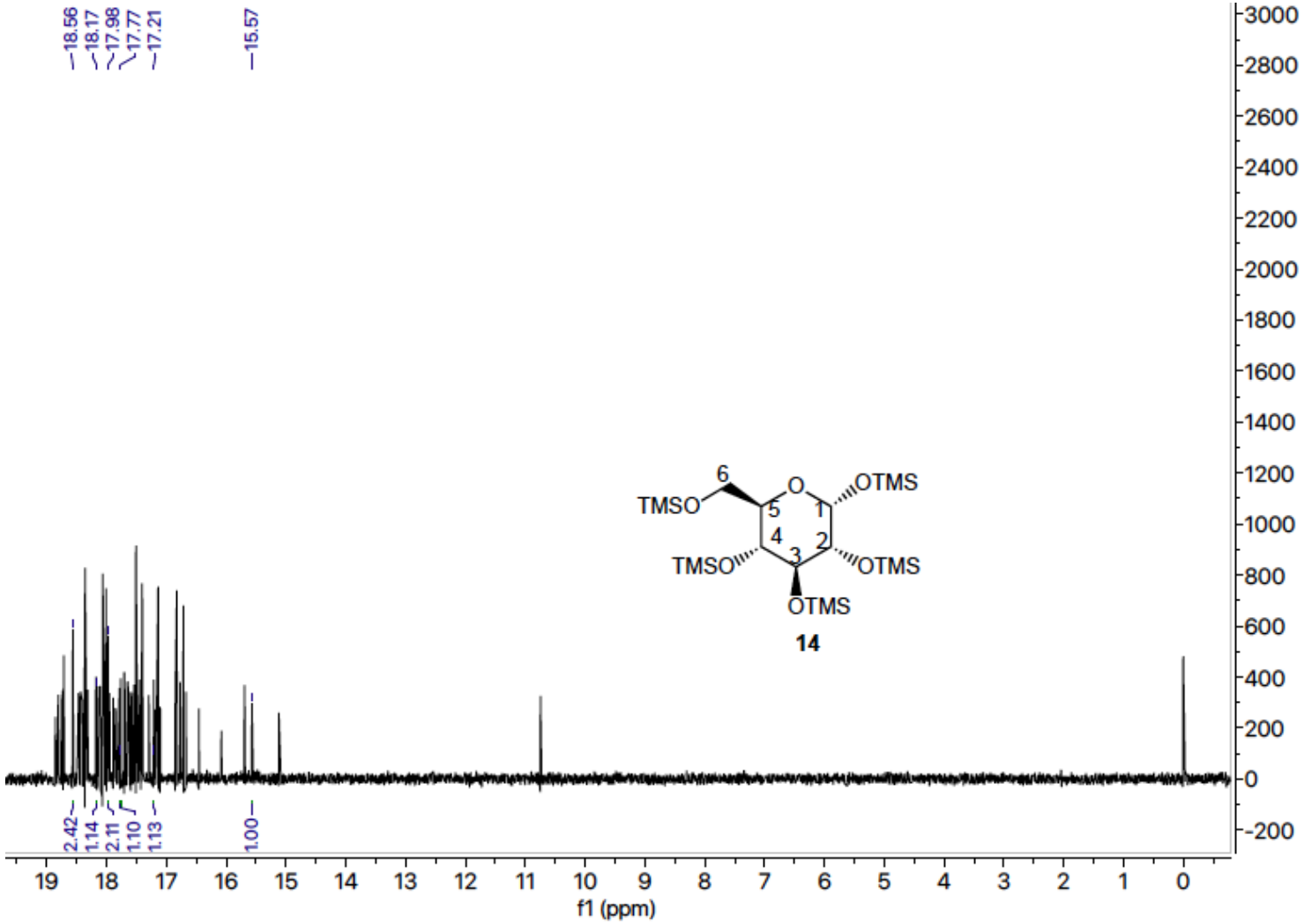

SI-Figure 2.32: The integration of assigned Si signals of α-per-*O*-TMS glucose (**14**) in reaction mixture of 13 per-*O*-silylated derivatives.

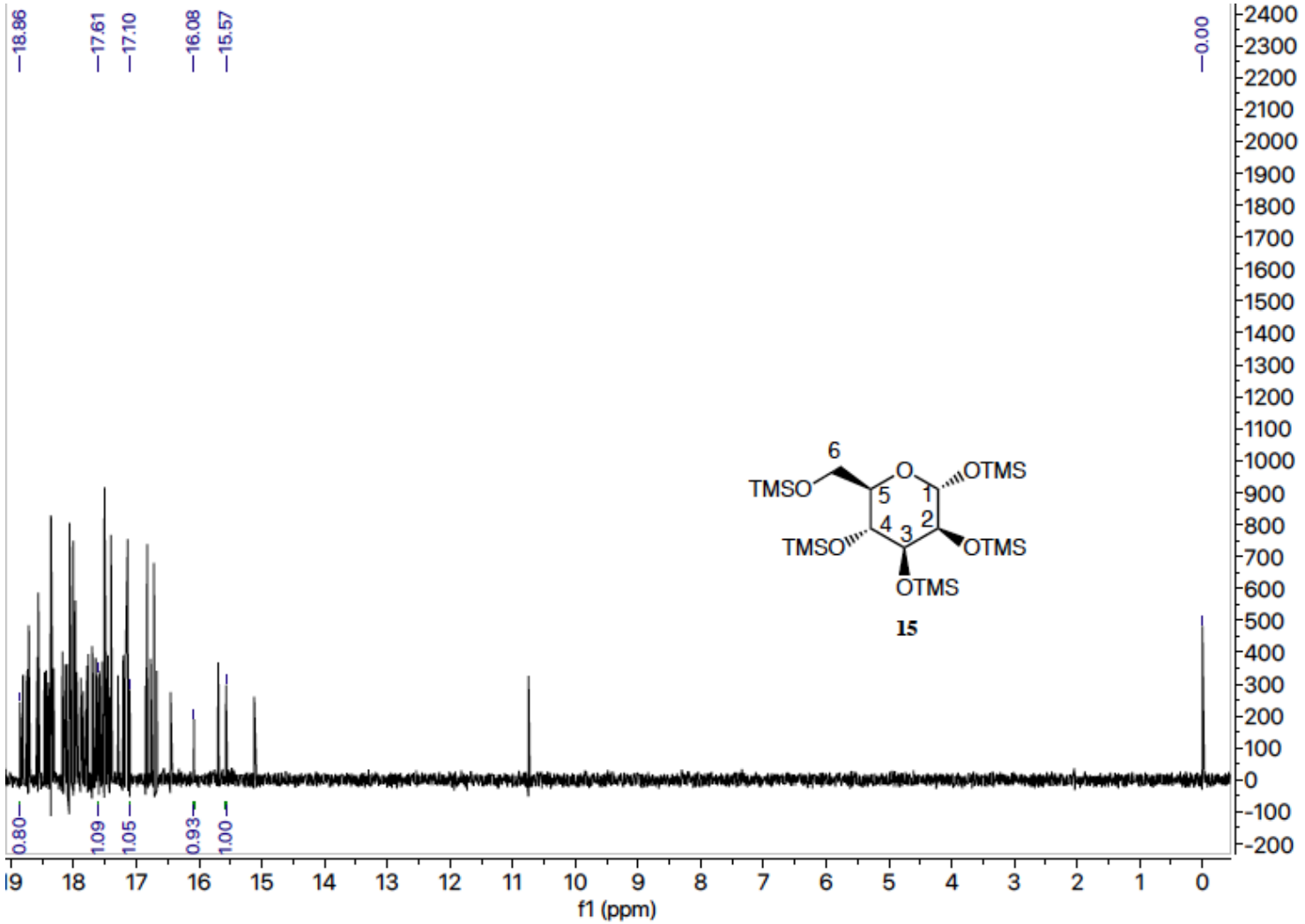

SI-Figure 2.33: The integration of assigned Si signals of α-per-*O*-TMS mannose (**15**) in reaction mixture of 13 per-*O*-silylated derivatives.

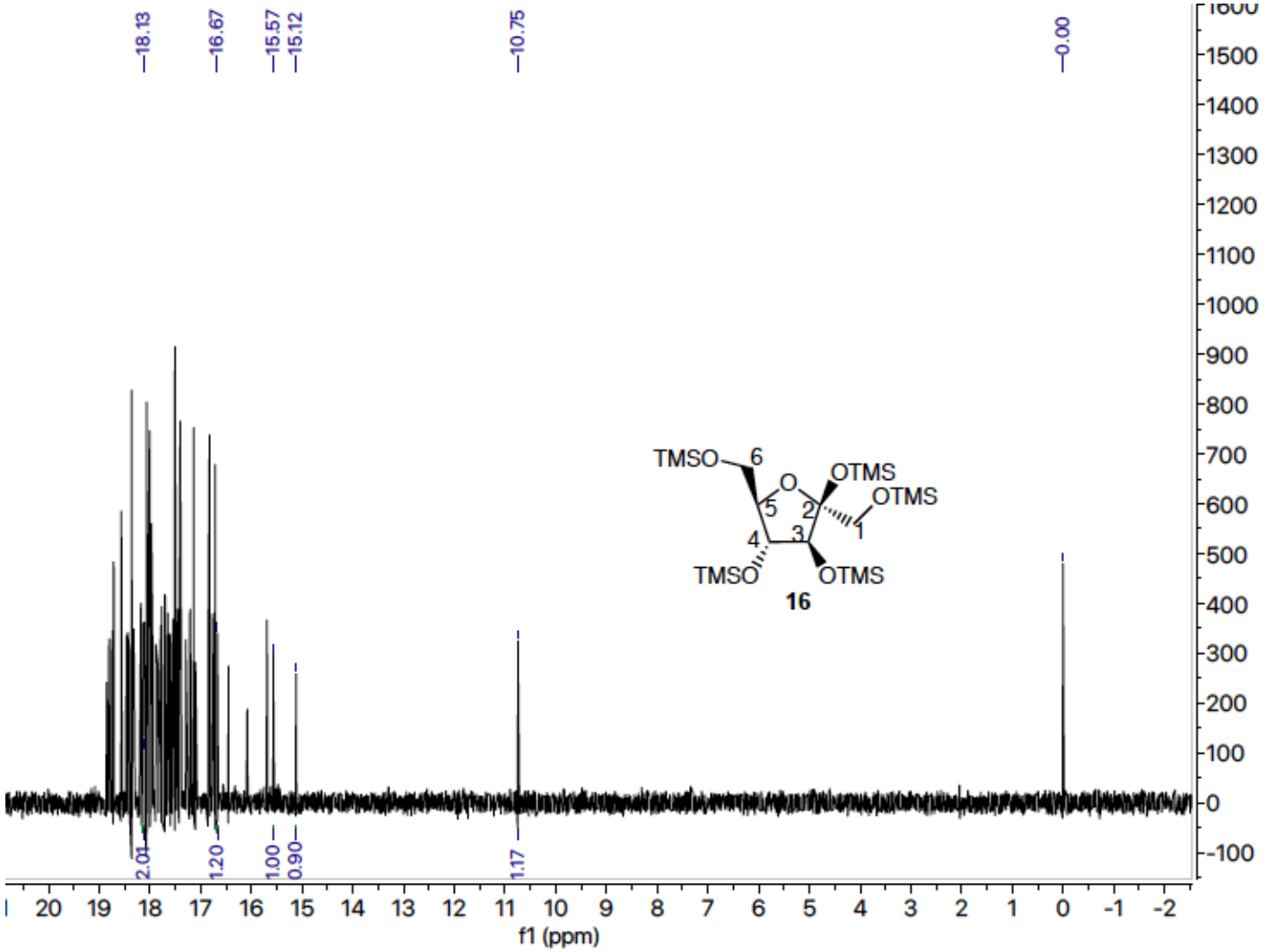

SI-Figure 2.34: The integration of assigned Si signals of -per-*O*-TMS mannose (**16**) in reaction mixture of 13 per-*O*-silylated derivatives.

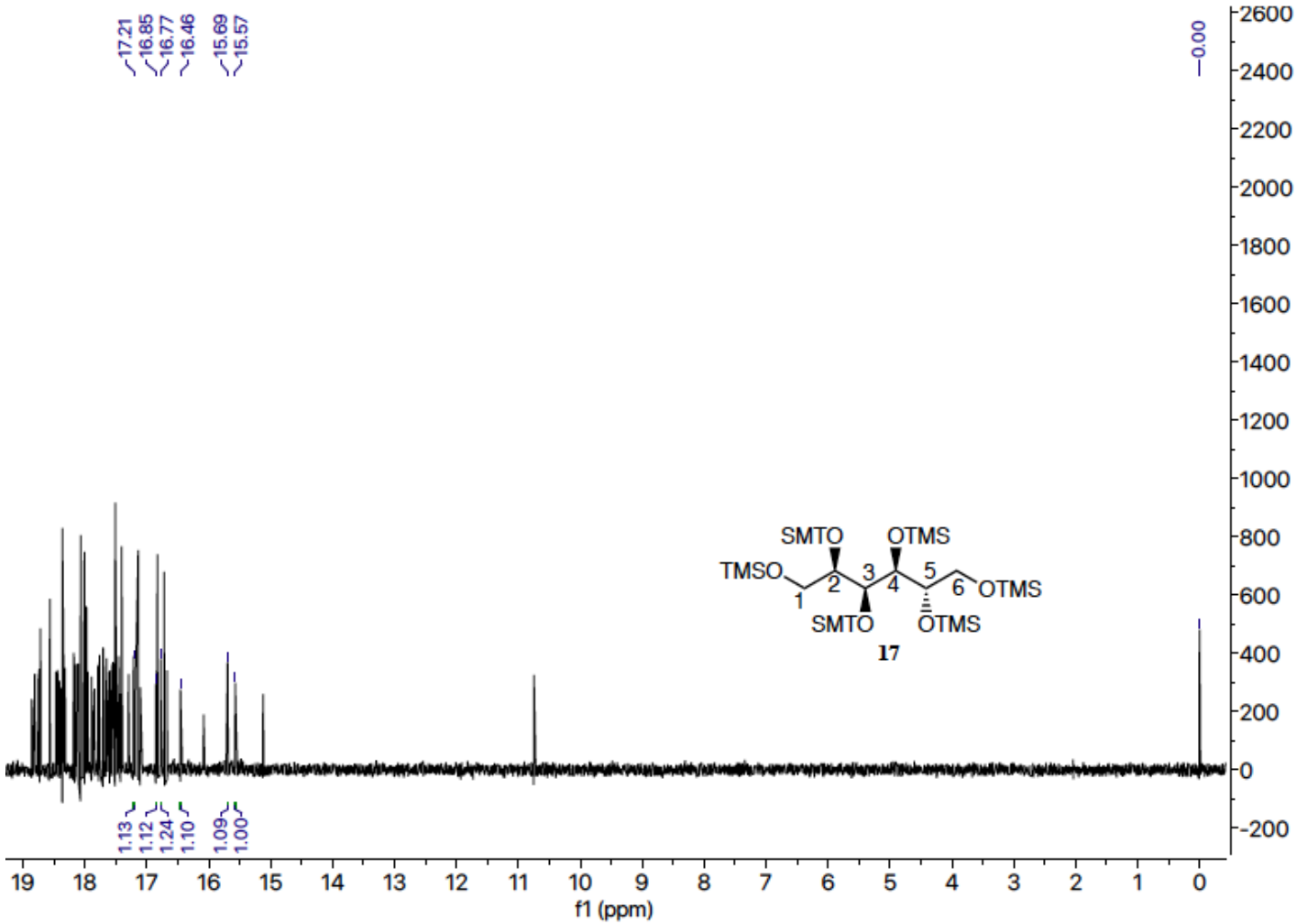

SI-Figure 2.35: The integration of assigned Si signals of per-*O*-TMS sorbitol (**17**) in reaction mixture of 13 per-*O*-silylated derivatives.

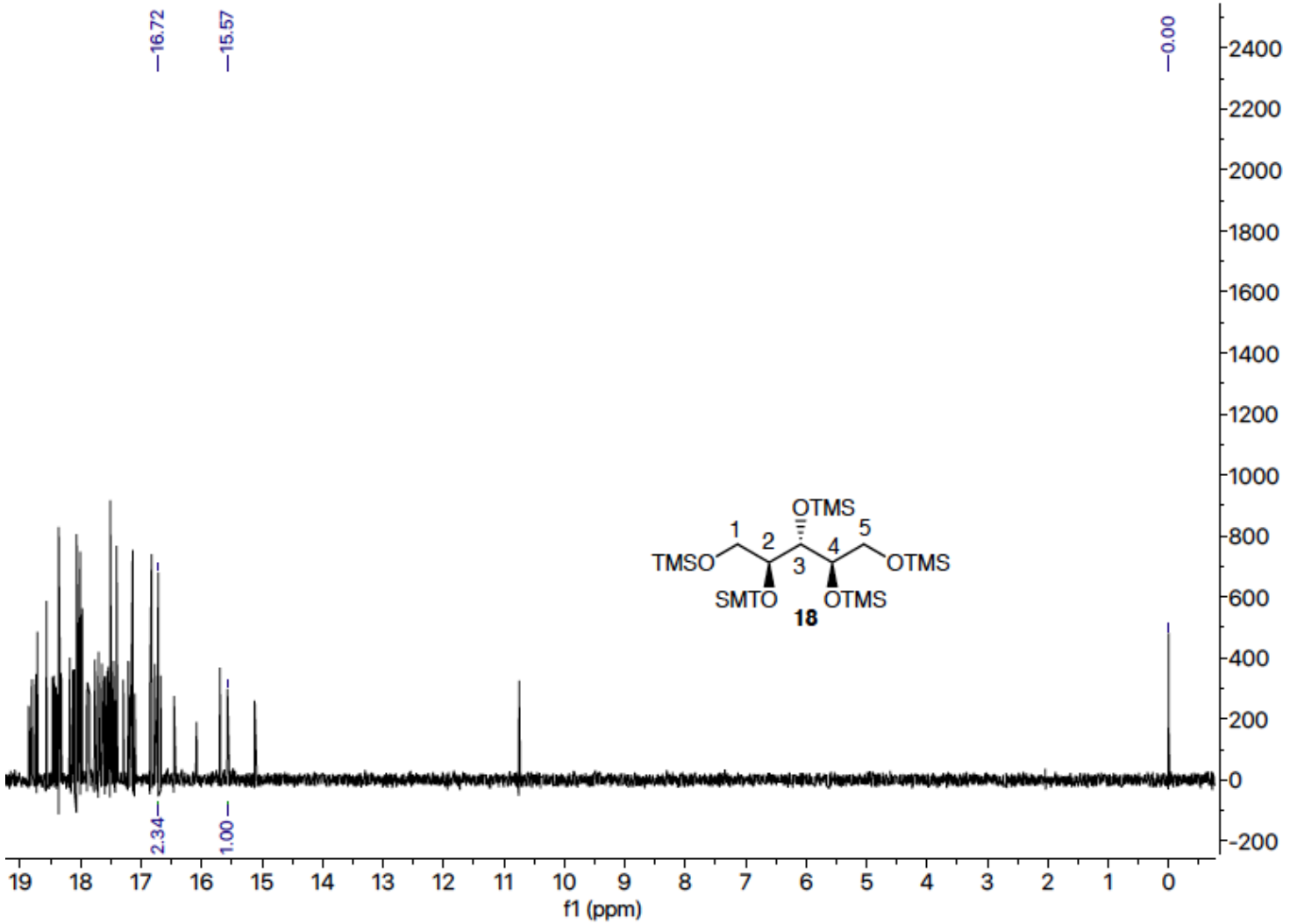

SI-Figure 2.36: The integration of assigned Si signals of per-*O*-TMS ribitol (**18**) in reaction mixture of 13 per-*O*-silylated derivatives.

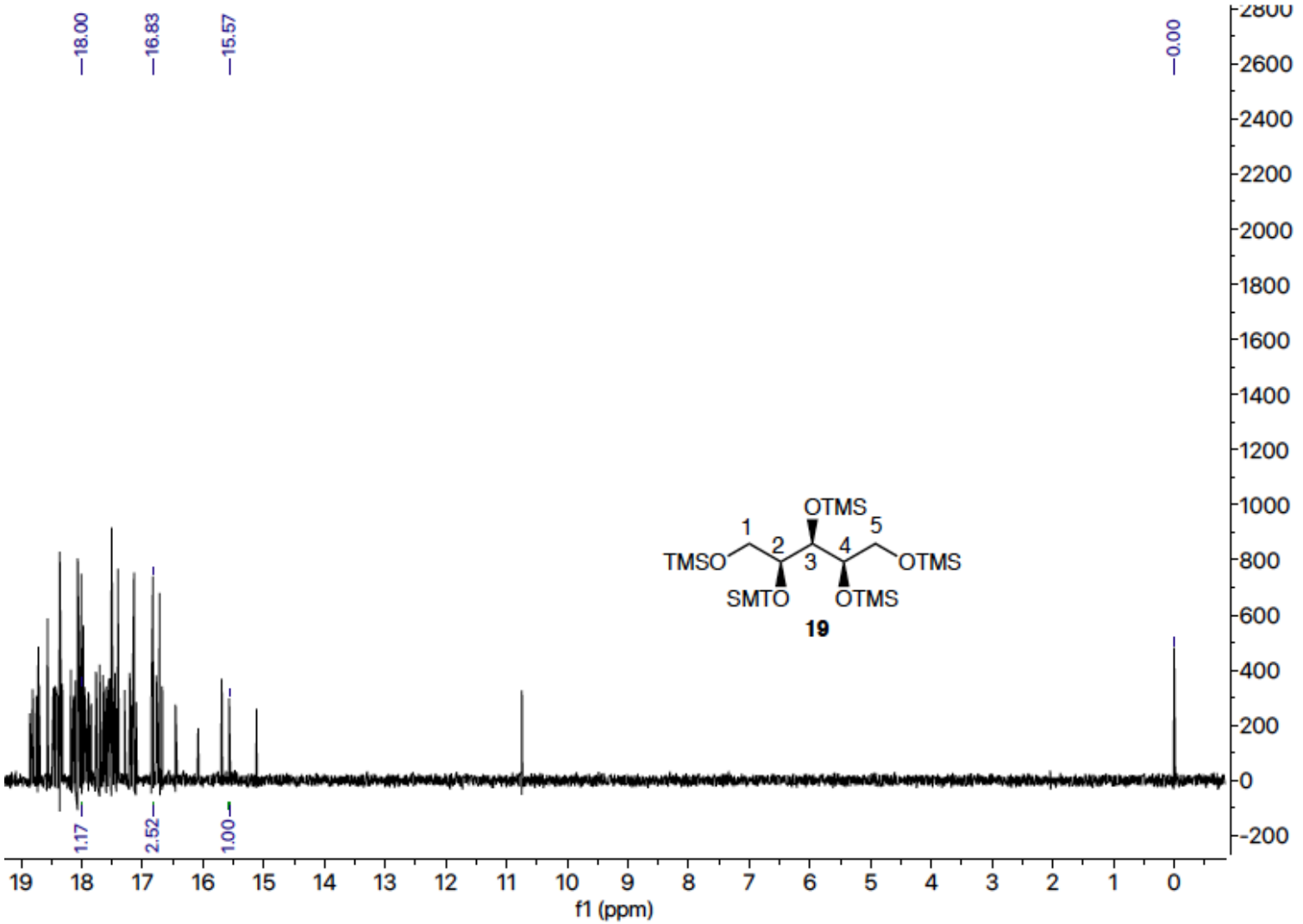

SI-Figure 2.37: The integration of assigned Si signals of per-*O*-TMS xylitol (**19**) in reaction mixture of 13 per-*O*-silylated derivatives.

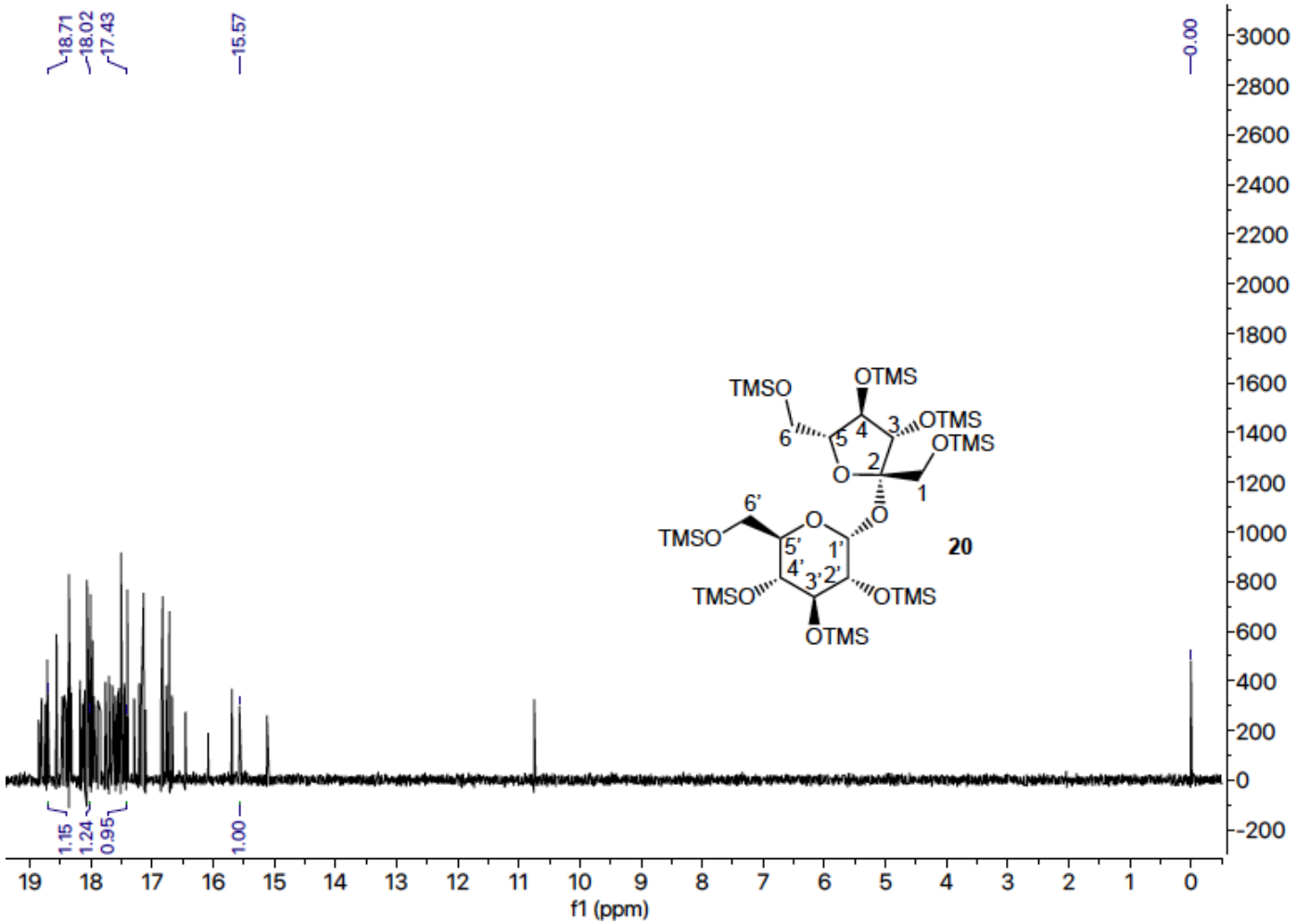

SI-Figure 2.38: The integration of assigned Si signals of per-*O*-TMS sucrose (**20**) in reaction mixture of 13 per-*O*-silylated derivatives.

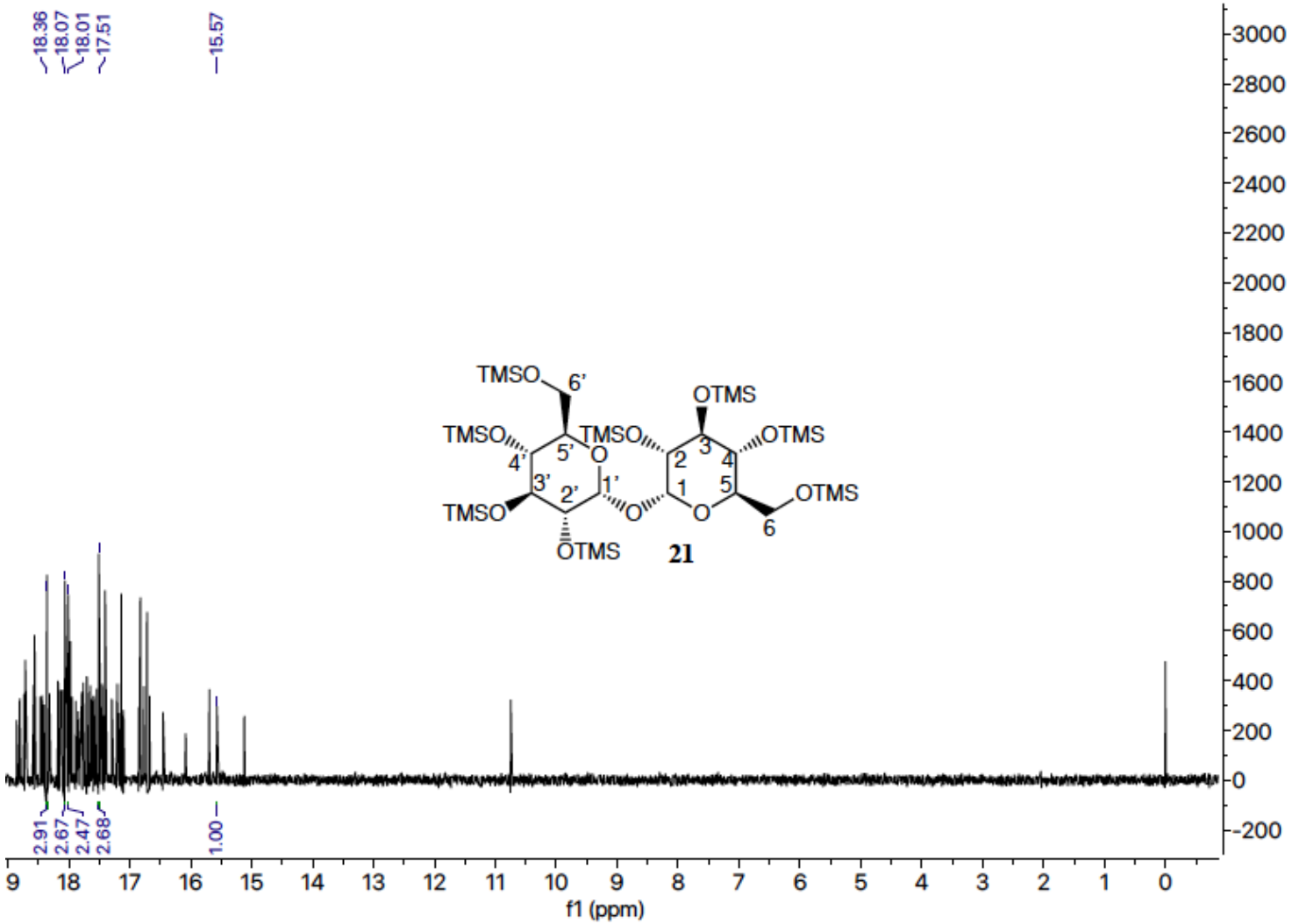

SI-Figure 2.39: The integration of assigned Si signals of per-*O*-TMS trehalose (**21**) in reaction mixture of 13 per-*O*-silylated derivatives.

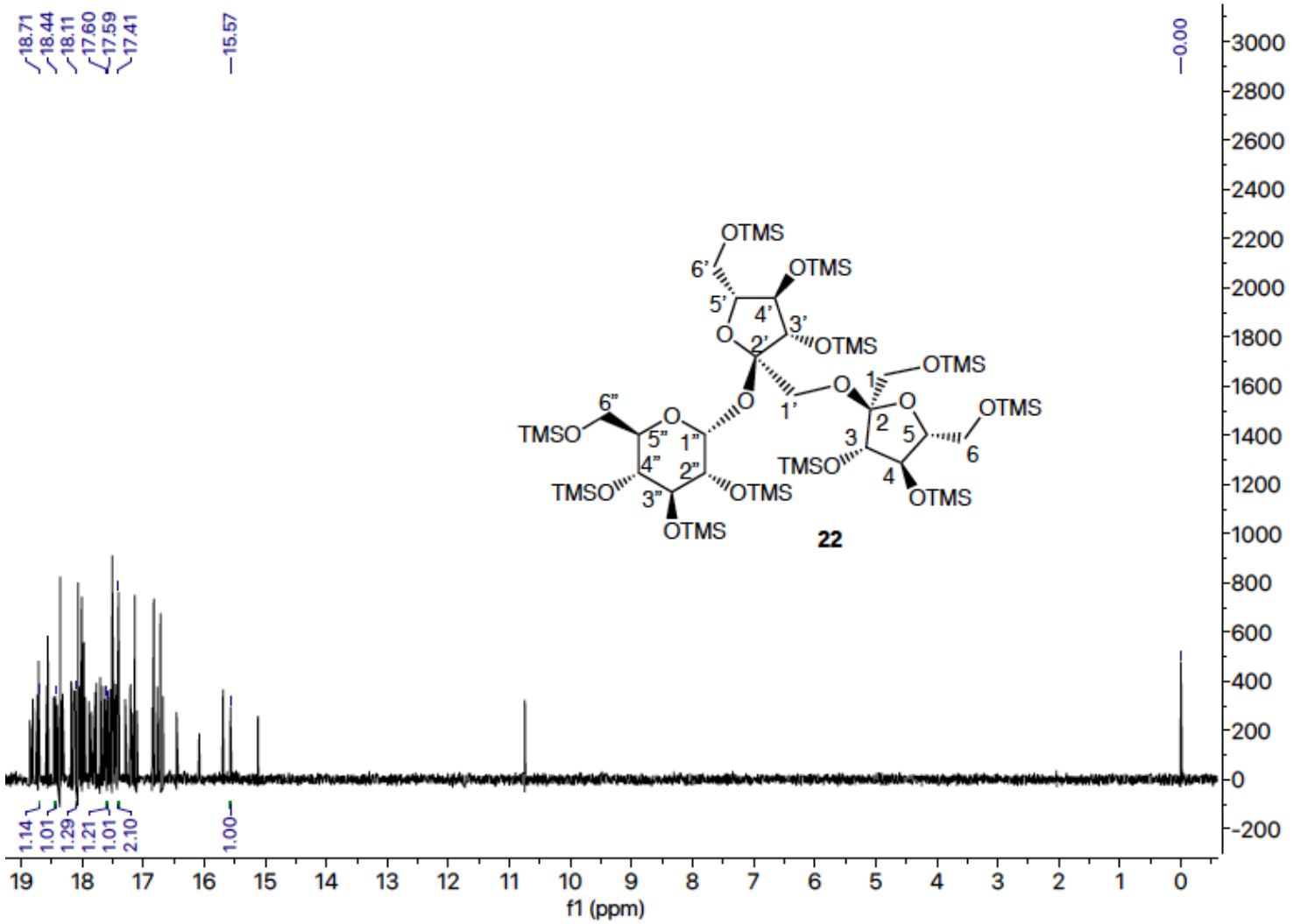

SI-Figure 2.40: The integration of assigned Si signals of per-*O*-TMS ketose (**22**) in reaction mixture of 13 per-*O*-silylated derivatives.

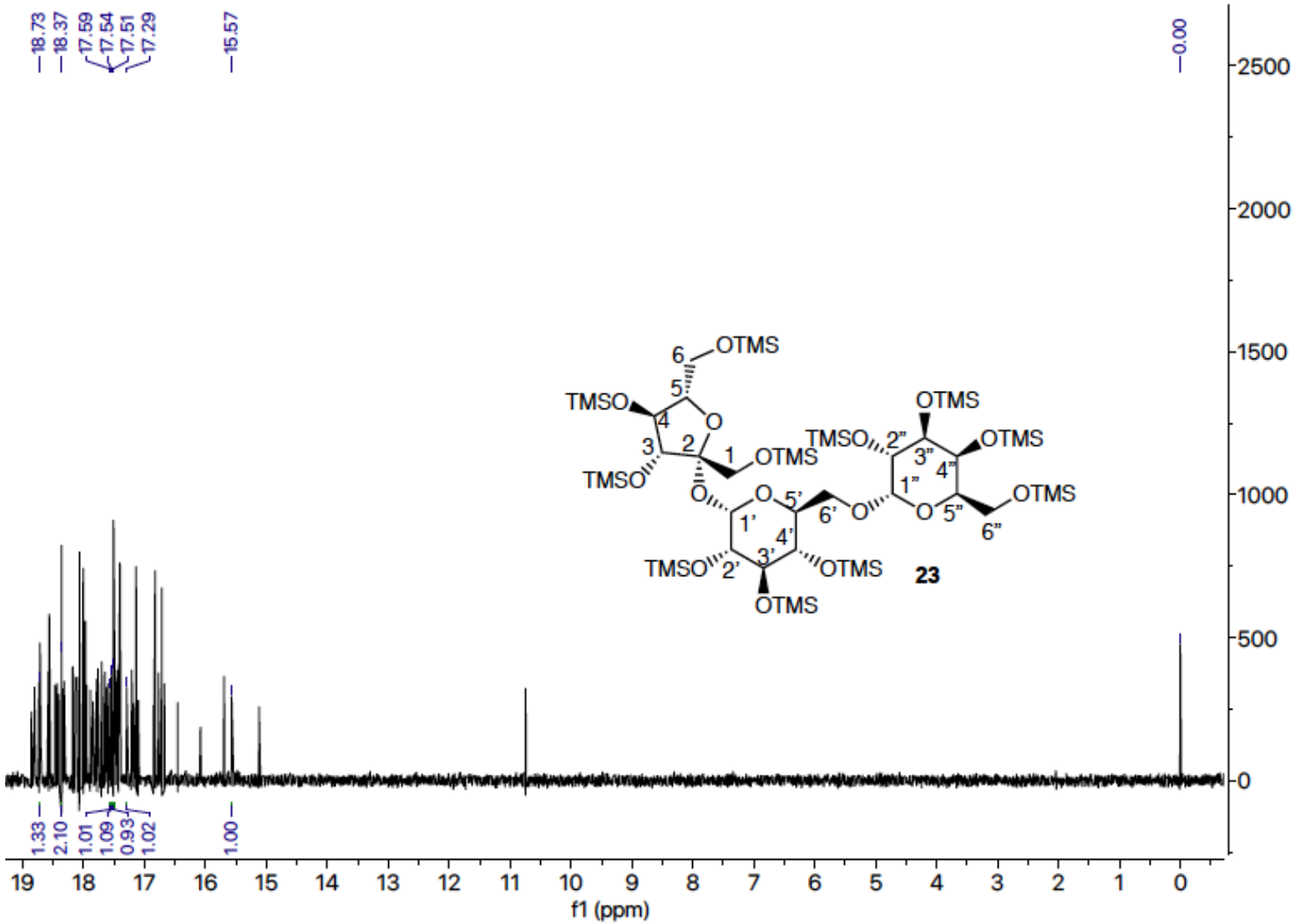

SI-Figure 2.41: The integration of assigned Si signals of per-*O*-TMS raffionse (**23**) in reaction mixture of 13 per-*O*-silylated derivatives.

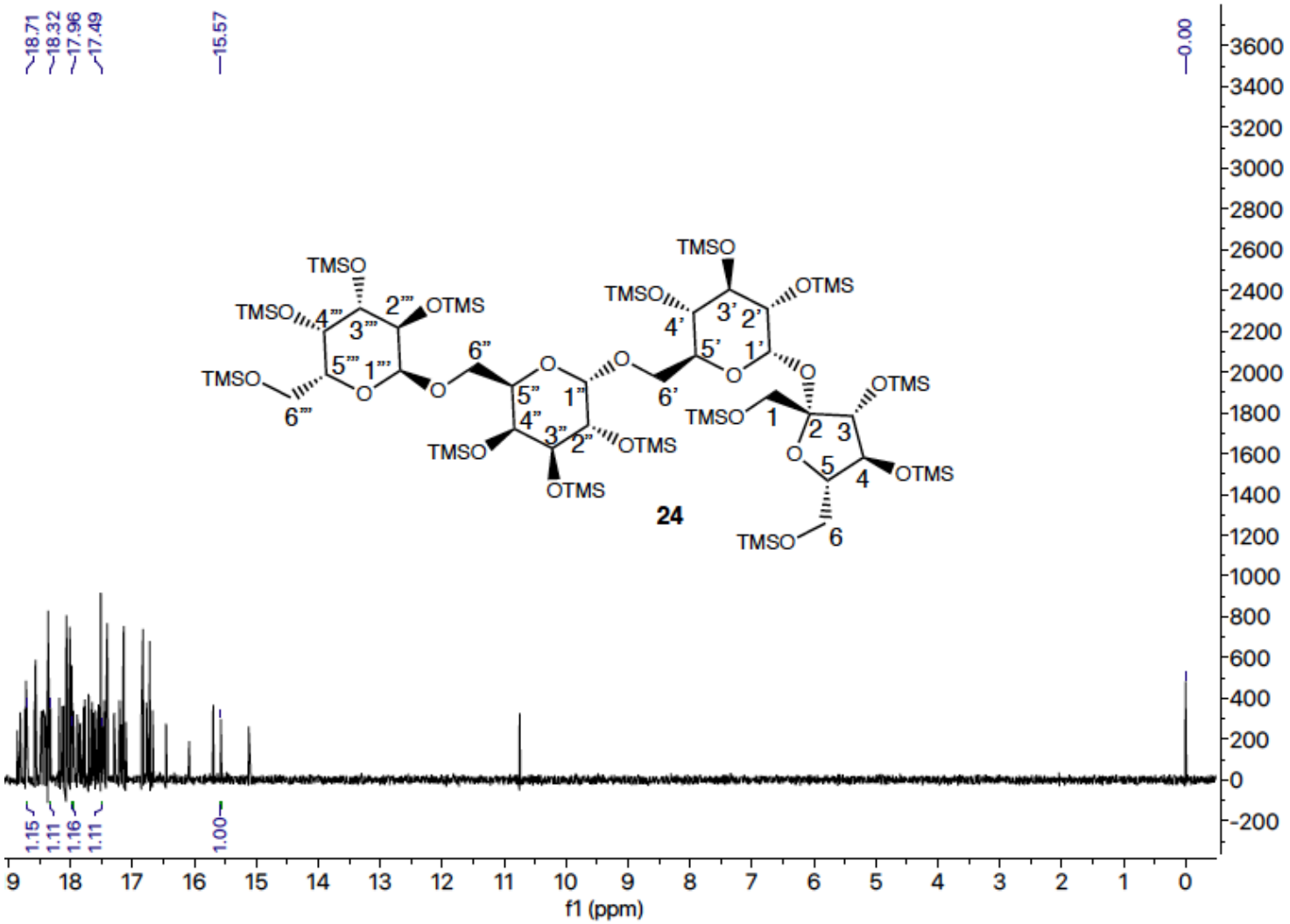

SI-Figure 2.42: The integration of assigned Si signals of per-*O*-TMS staychose **(24)** in reaction mixture of 13 per-*O*-silylated derivatives.

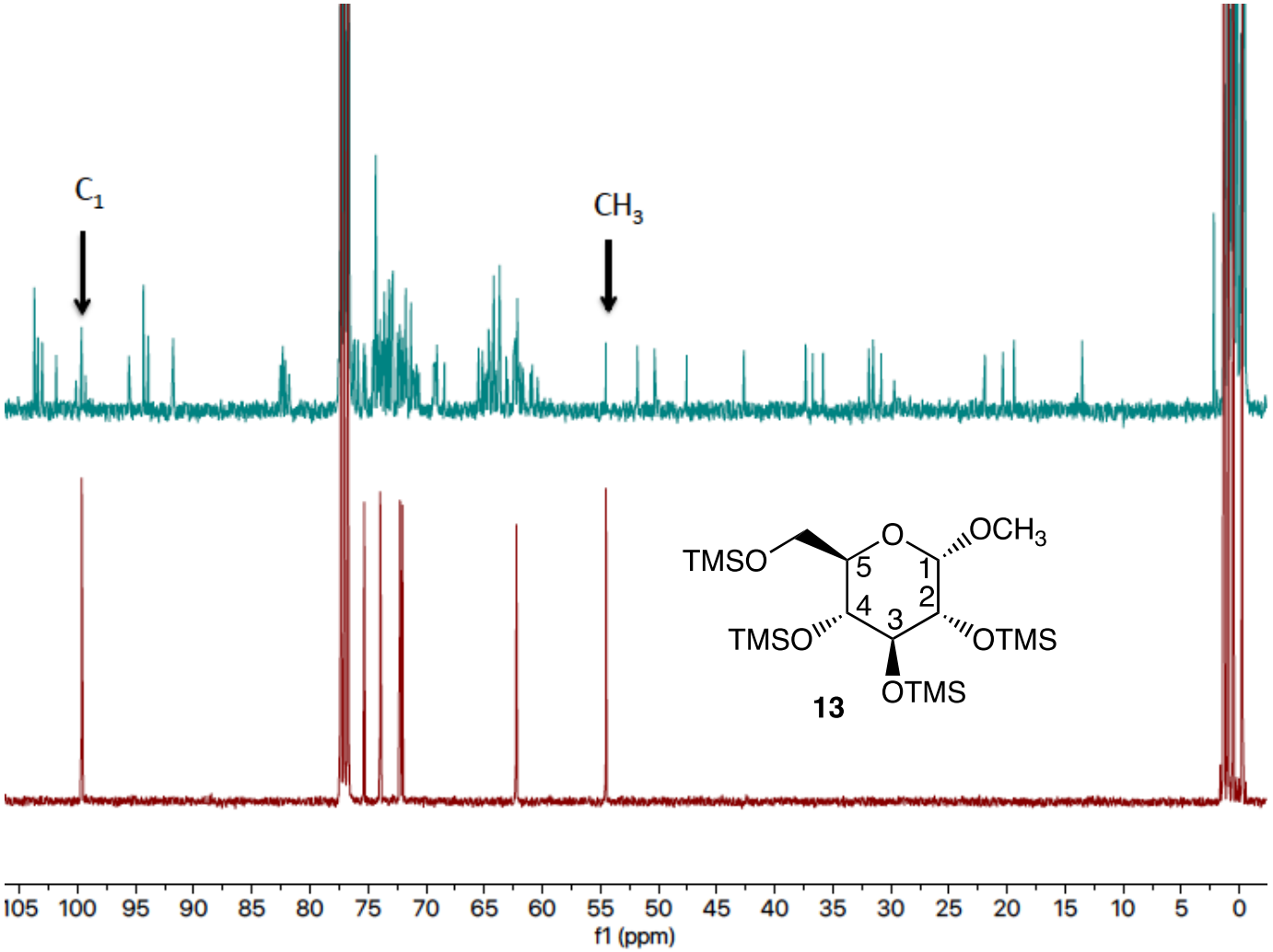

SI-Figure 2.43: The ^{13}C NMR spectra overlapped between per-*O*-TMS methylglucoside (**13**) and reaction mixture of 13 per-*O*-silylated derivatives.

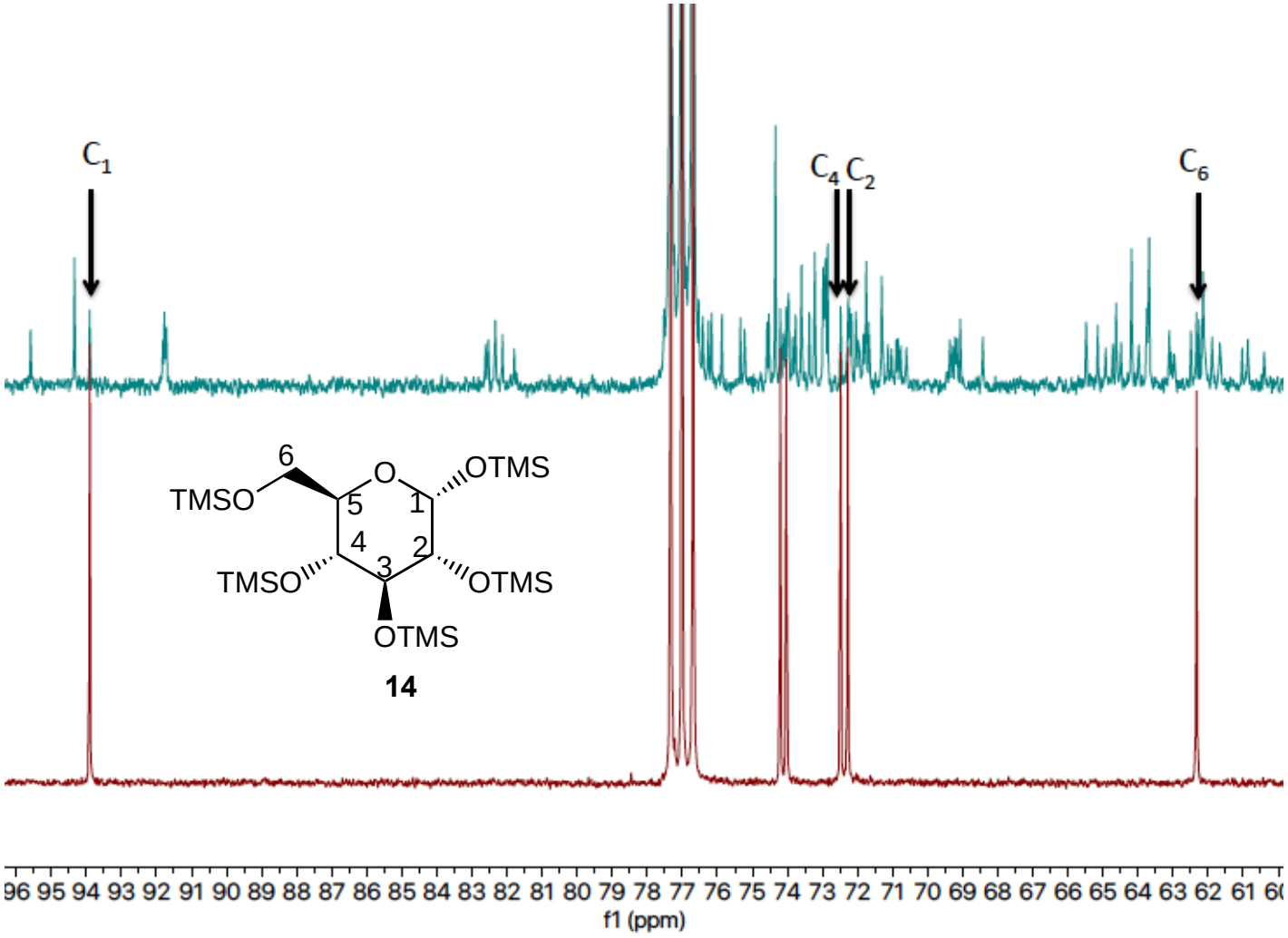

SI-Figure 2.44: The ^{13}C NMR spectra overlapped between per-*O*-TMS glucose (**14**) and reaction mixture of 13 per-*O*-silylated derivatives.

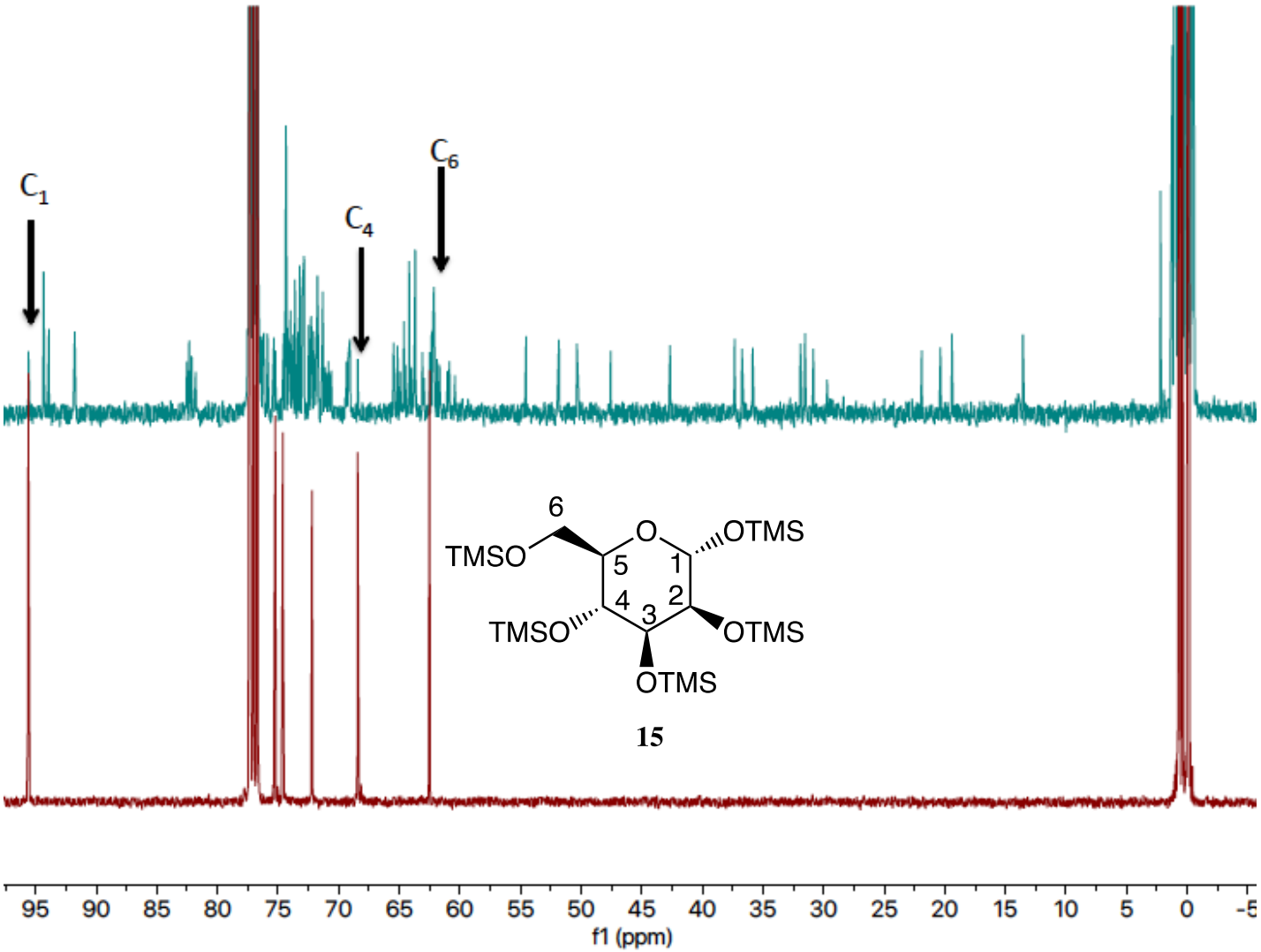

SI-Figure 2.45: The ^{13}C NMR spectra overlapped between per-*O*-TMS mannose (**15**) and reaction mixture of 13 per-*O*-silylated derivatives.

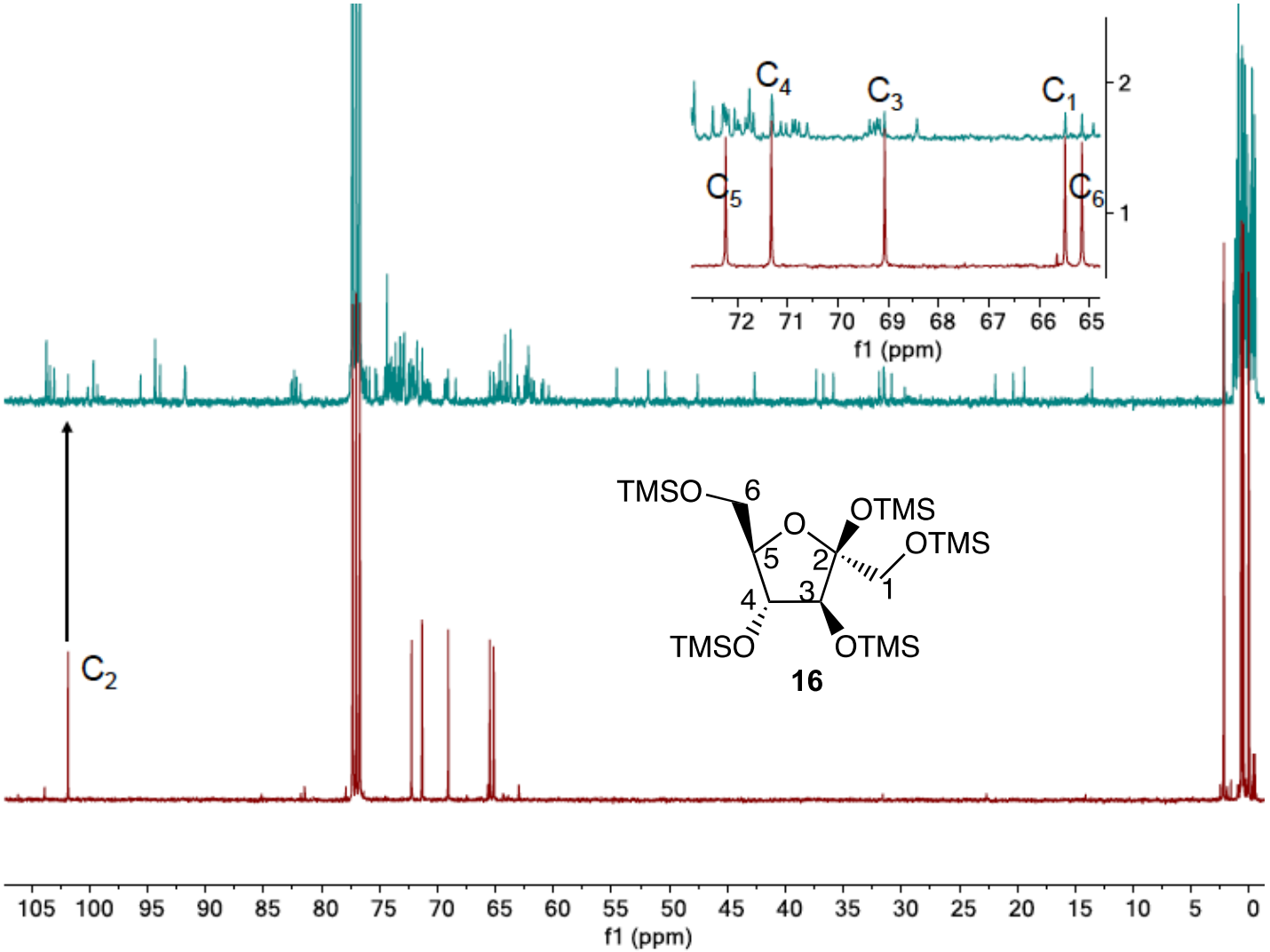

SI-Figure 2.46: The ^{13}C NMR spectra overlapped between per-*O*-TMS fructose (**16**) and reaction mixture of 13 per-*O*-silylated derivatives.

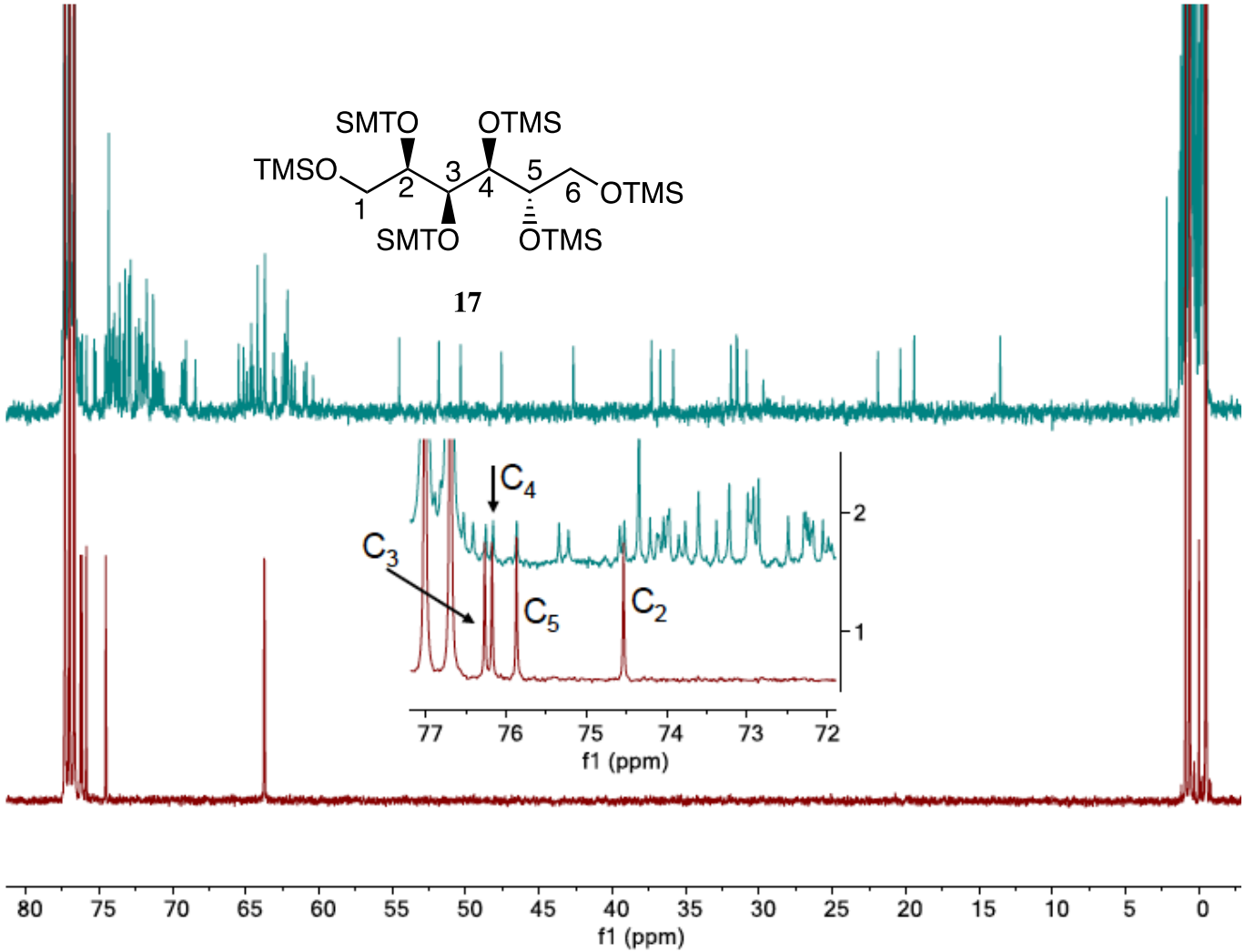

SI-Figure 2.47: The ^{13}C NMR spectra overlapped between per-*O*-TMS sorbitol (**17**) and reaction mixture of 13 per-*O*-silylated derivatives.

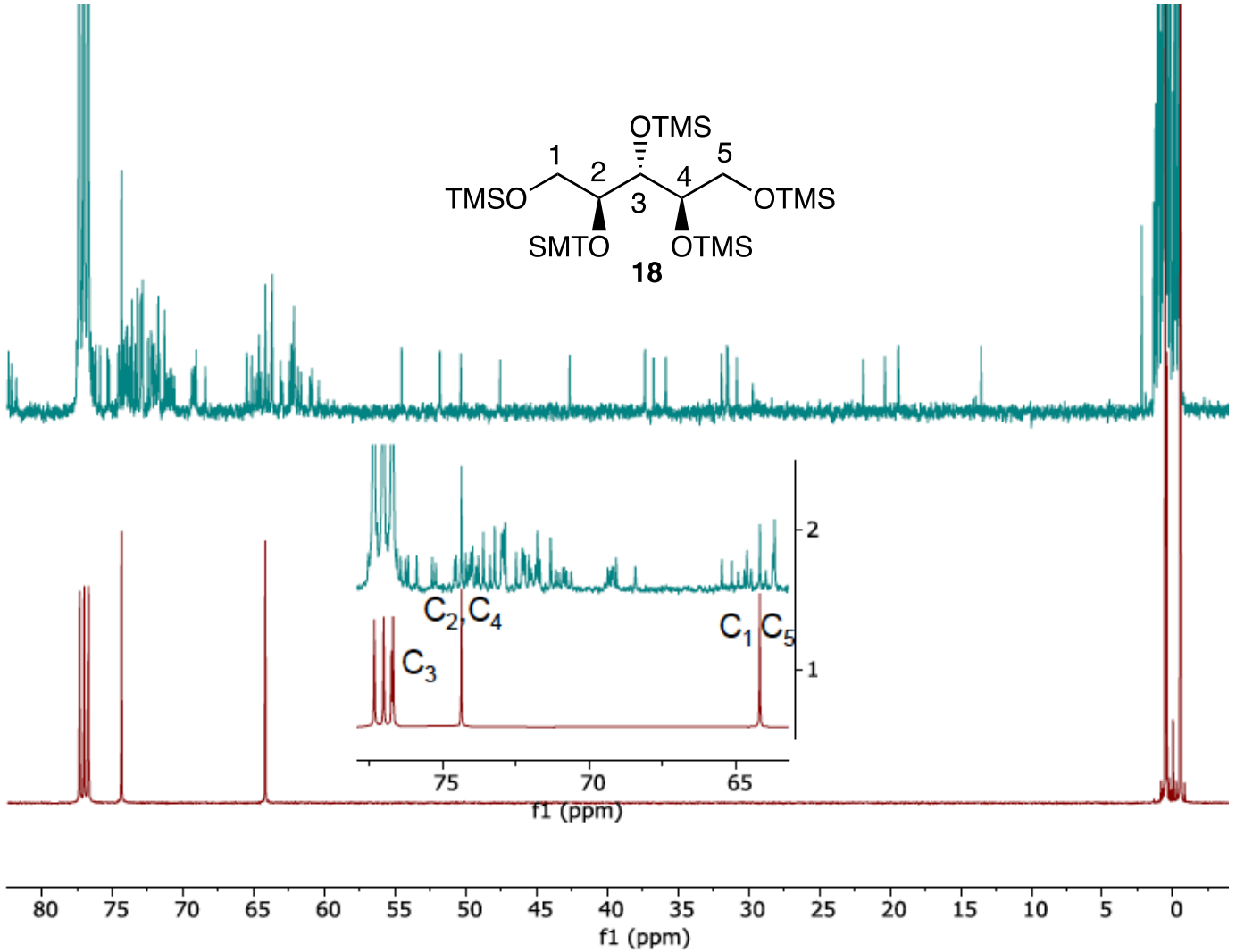

Si-Figure 2.48: The ^{13}C NMR spectra overlapped between per-*O*-TMS ribitol (**18**) and reaction mixture of 13 per-*O*-silylated derivatives.

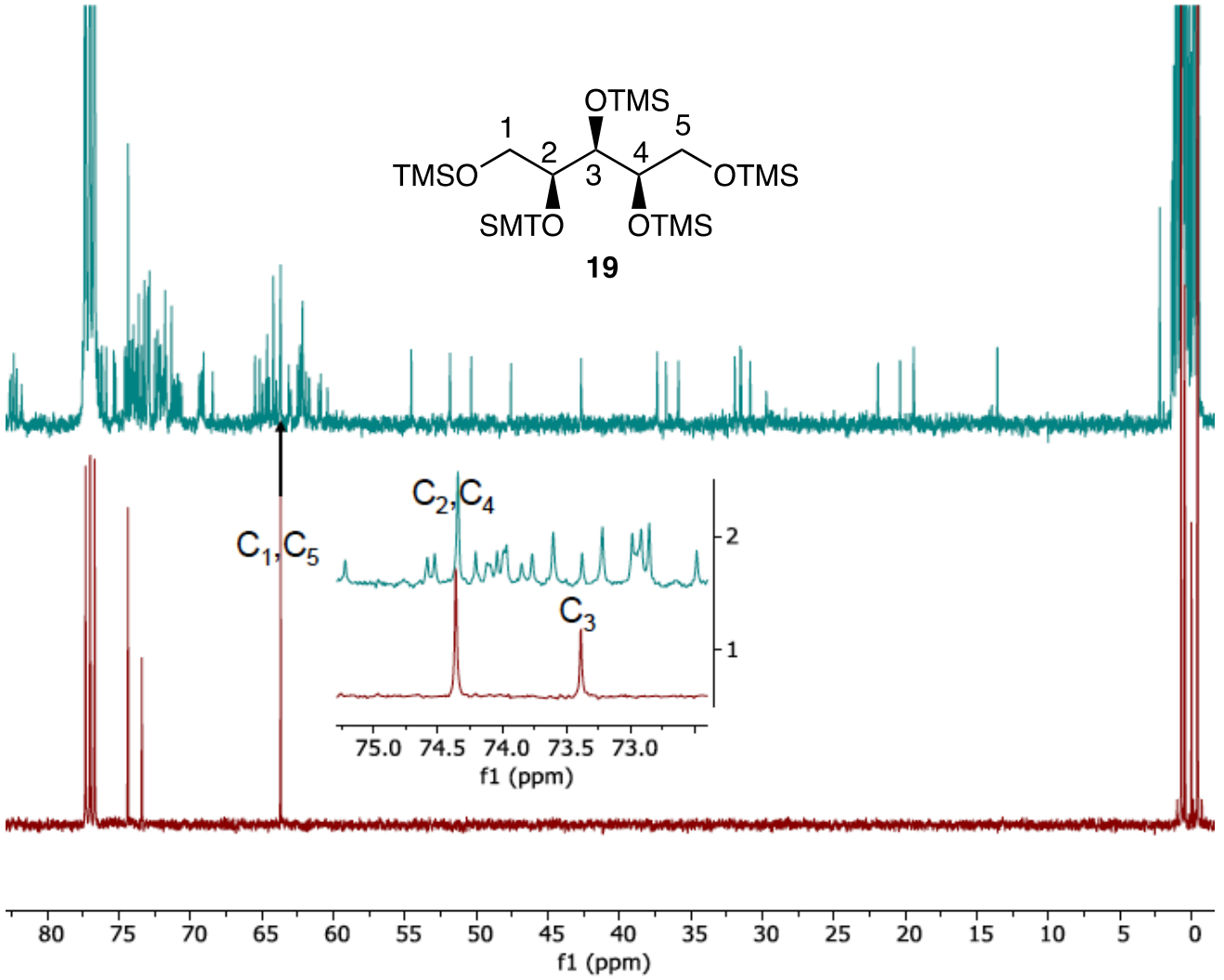

SI-Figure 2.49: The ^{13}C NMR spectra overlapped between per-*O*-TMS xylitol (**19**) and reaction mixture of 13 per-*O*-silylated derivatives.

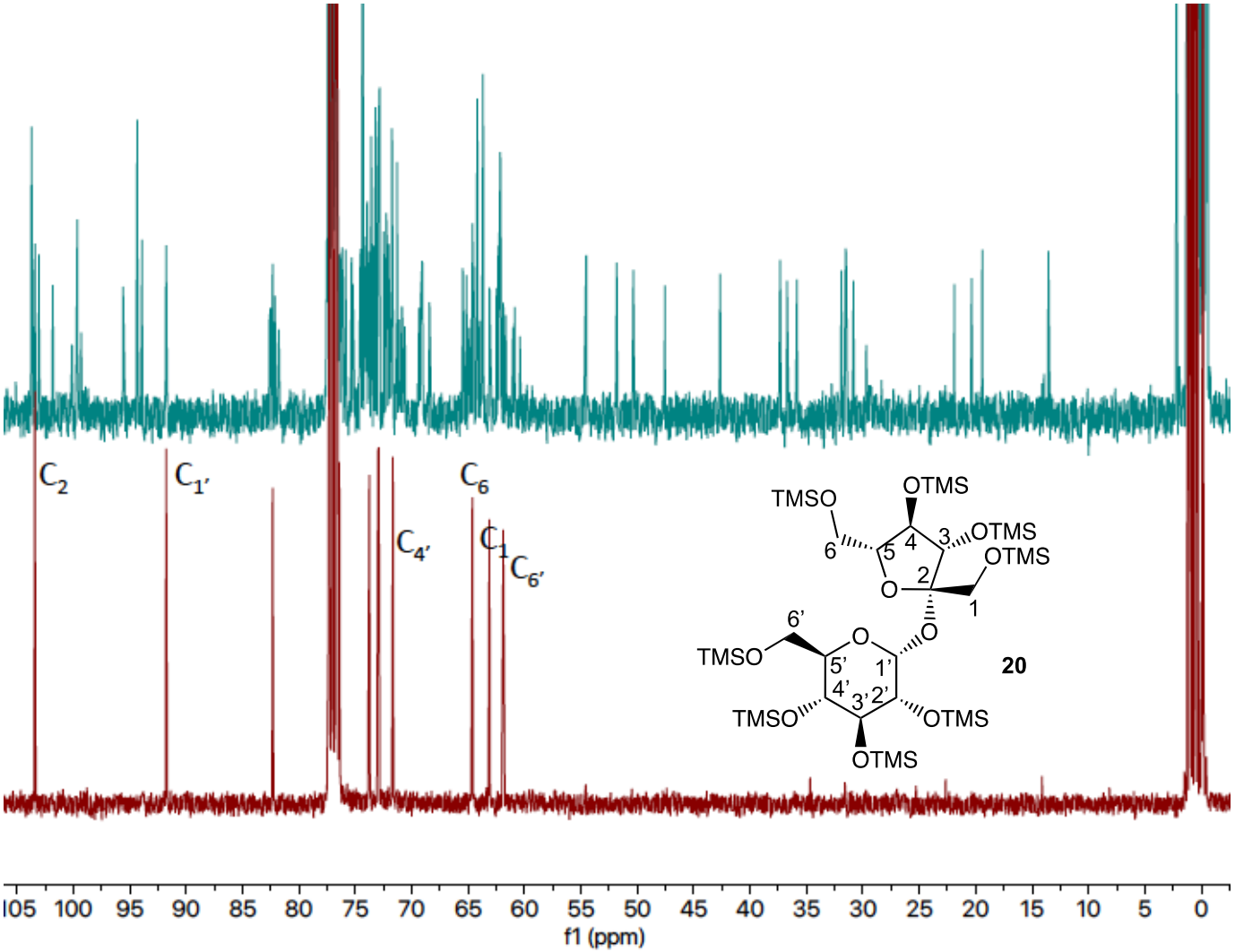

Si-Figure 2.50: The ^{13}C NMR spectra overlapped between per-*O*-TMS sucrose (**20**) and reaction mixture of 13 per-*O*-silylated derivatives.

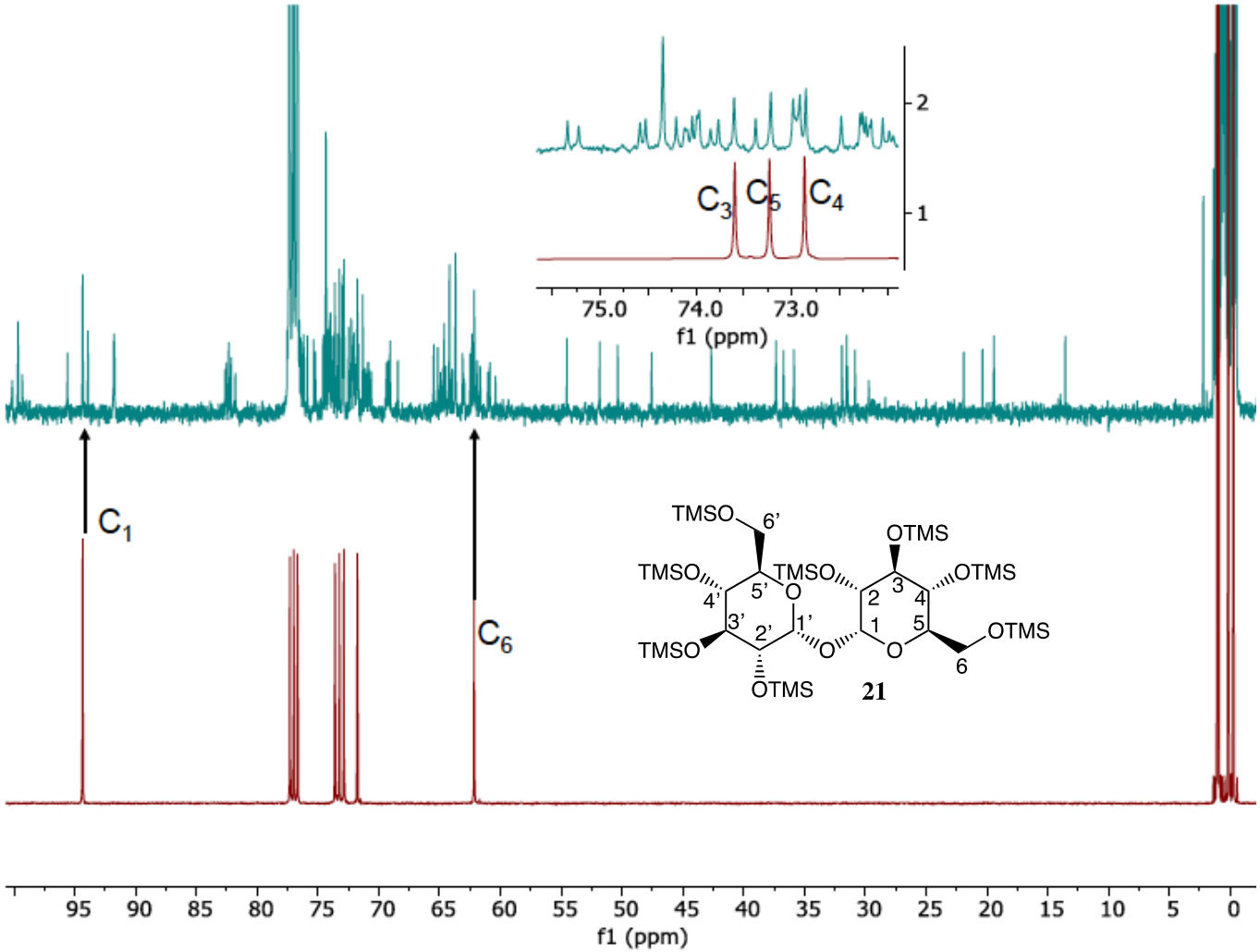

SI-Figure 2.51: The ^{13}C NMR spectra overlapped between per-*O*-TMS trehalose (**21**) and reaction mixture of 13 per-*O*-silylated derivatives.

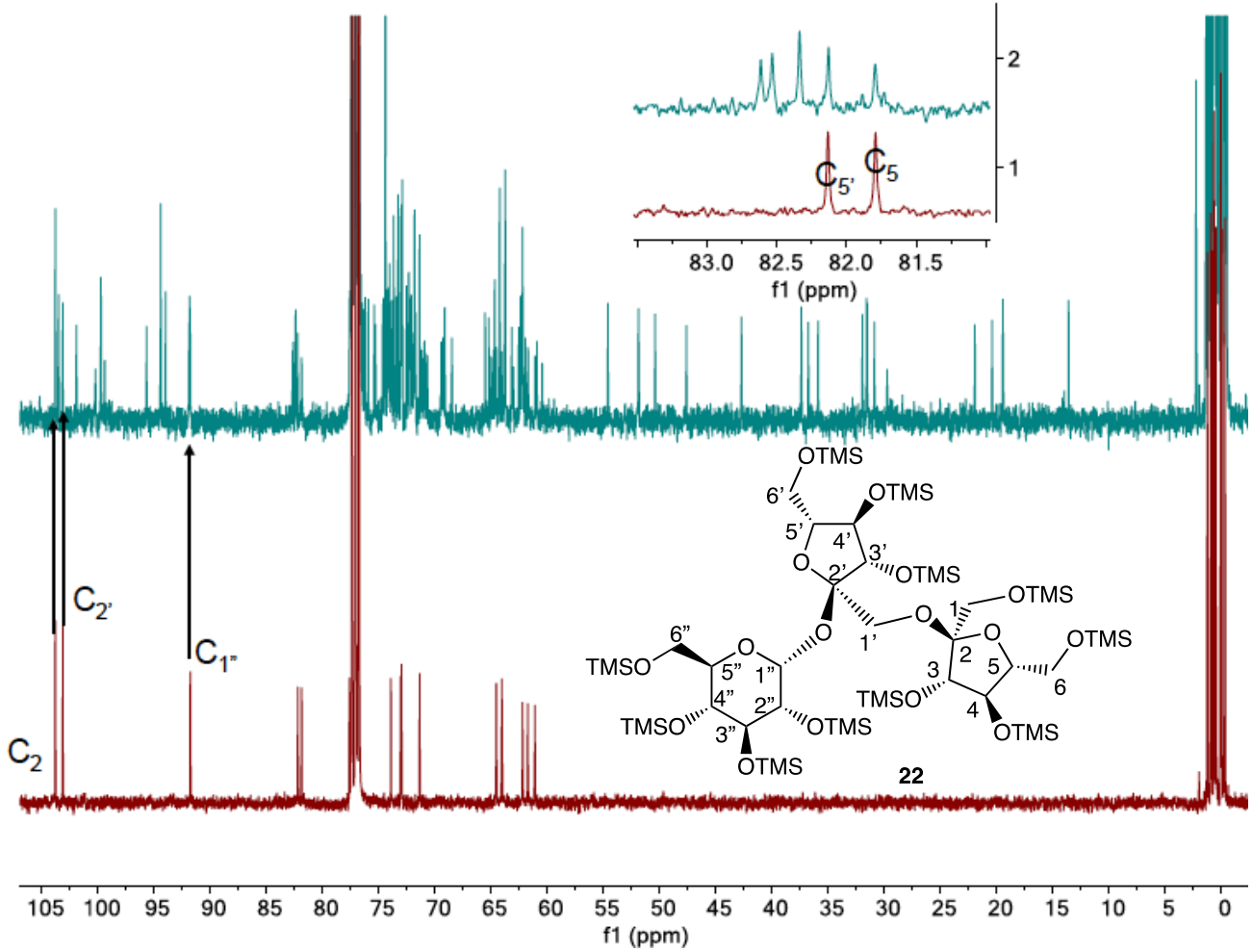

SI-Figure 2.52: The ^{13}C NMR spectra overlapped between per-*O*-TMS kestose (**22**) and reaction mixture of 13 per-*O*-silylated derivatives.

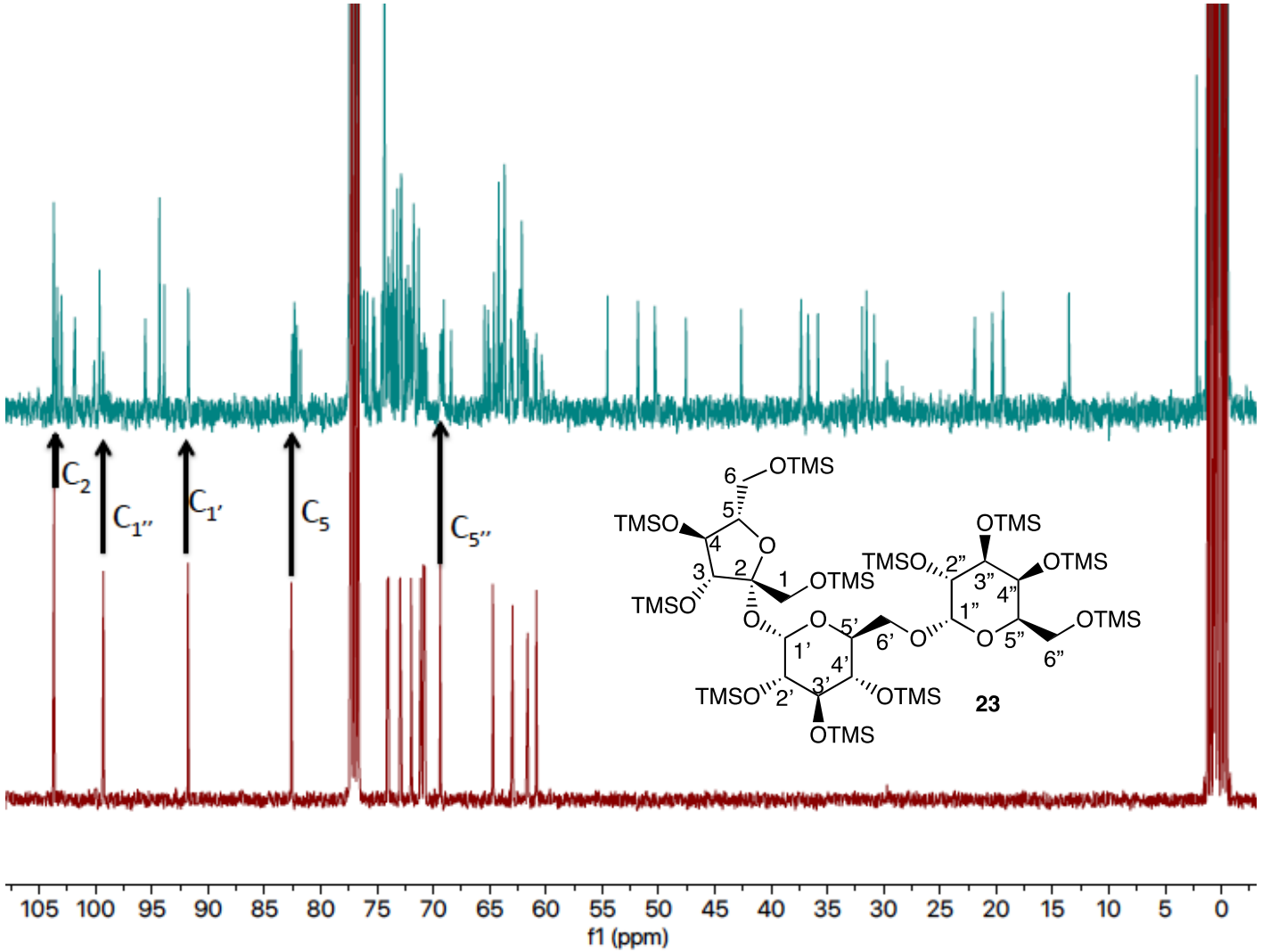

SI-Figure 2.53: The ^{13}C NMR spectra overlapped between per-*O*-TMS raffinose (**23**) and reaction mixture of 13 per-*O*-silylated derivatives.

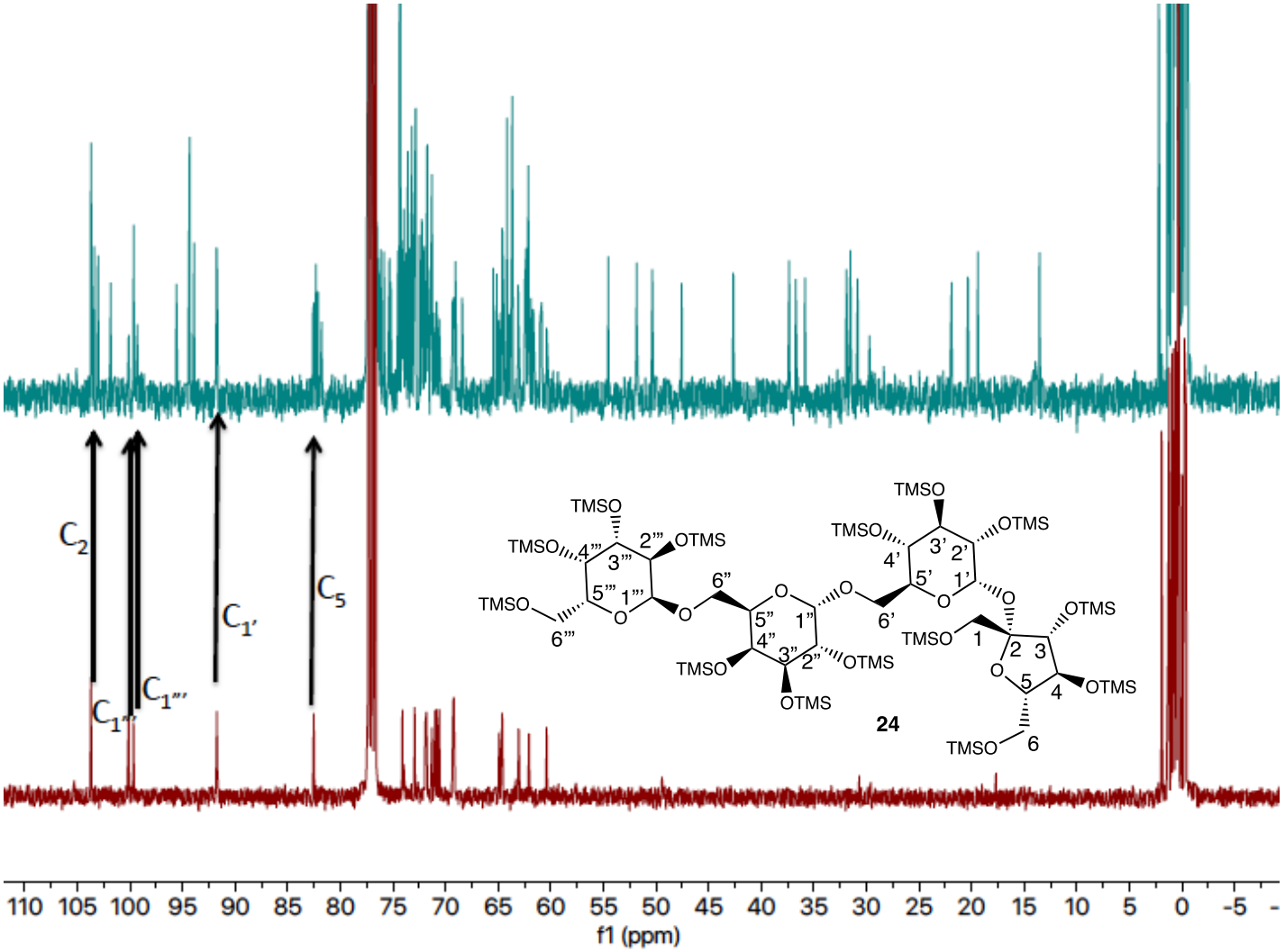

SI-Figure 2.54: The ^{13}CNMR spectra overlapped between per-*O*-TMS styachose (**24**) and reaction mixture of 13 per-*O*-silylated derivatives.

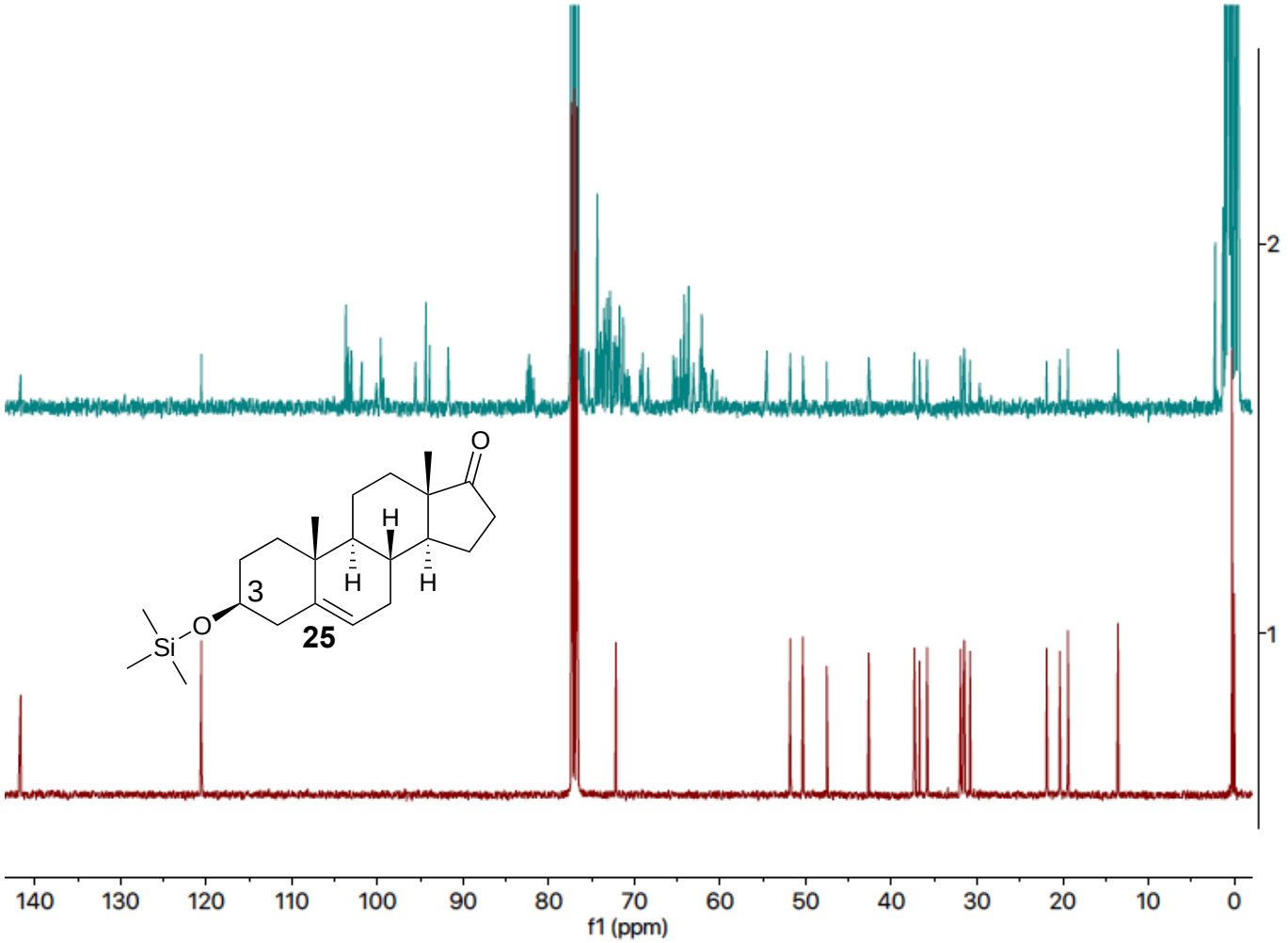

SI-Figure 2.55: The ^{13}C NMR spectra overlapped between per-*O*-TMS DHEA (**25**) and reaction mixture of 13 per-*O*-silylated derivatives.

Table 1: ^{29}Si NMR and ^{13}C NMR chemical shift values from individual 12 pure per-*O*-TMS compounds in $CDCl_3$ that are used to generate 2D graph (Figure 2.7 in text).

^{29}Si	^{13}C	Atom Number	Compound
17.99	72.24	2	**13**
17.77	75.33	3	**13**
18.57	73.95	4	**13**
18.34	62.24	6	**13**
18.17	93.91	1	**14**
17.22	74.21	2	**14**
17.77	74.03	3	**14**
18.57	72.28	4	**14**
17.97	62.33	6	**14**
18.43	95.61	1	**15**
16.05	74.61	2	**15**
17.1	72.2	3	**15**
18.85	68.43	4	**15**
17.6	62.51	6	**15**
18.08	65.48	1	**16**
10.69	101.84	2	**16**
18.08	69.07	3	**16**
16.63	72.23	4	**16**
15.05	65.15	6	**16**
16.85	63.75	1	**17**
15.69	75.87	2	**17**
16.77	76.27	3	**17**
16.45	76.18	4	**17**
17.13	74.54	5	**17**
17.2	63.72	6	**17**
17.12	63.68	1	**18**
17.12	63.68	5	**18**
16.81	74.36	2	**18**
16.81	74.36	4	**18**
18	73.39	3	**18**
17.68	76.73	3	**19**
17.39	64.19	1	**19**
17.39	64.19	5	**19**
16.71	74.35	2	**19**
16.71	74.35	4	**19**
18.16	63.12	1	**20**
18.07	76.54	3	**20**
18.71	76.42	4	**20**
17.87	64.63	6	**20**

17.53	72.99	2'	**20**
17.68	73.77	3'	**20**
18.02	71.68	4'	**20**
17.43	61.89	6'	**20**
18.08	72.87	2	**21**
18.08	72.87	2'	**21**
18.37	73.59	3	**21**
18.37	73.59	3'	**21**
17.62	71.75	4	**21**
17.62	71.75	4'	**21**
18.01	62.15	6	**21**
18.01	62.15	6'	**21**
18.7	62.21	1	**22**
18.44	76.9	3	**22**
18.8	76.82	4	**22**
17.59	63.98	6	**22**
18.1	76.95	3'	**22**
17.88	77.54	4'	**22**
17.4	64.48	6'	**22**
17.52	72.99	2"	**22**
17.58	73.85	3"	**22**
17.81	71.3	4"	**22**
17.17	61.05	6"	**22**
18.36	62.98	1	**23**
18.32	77.21	3	**23**
18.73	76.72	4	**23**
17.96	64.72	6	**23**
17.54	72.97	2'	**23**
17.5	74.1	3'	**23**
17.29	71.98	4'	**23**
17.69	70.9	2"	**23**
17.58	74	3"	**23**
18.7	71.13	4"	**23**
18.37	60.86	6"	**23**
18.4	63.06	1	**24**
18.3	76.77	3	**24**
18.7	77.22	4	**24**
17.96	64.62	6	**24**
17.48	72.94	2'	**24**
15.55	72.16	3	**24**

References:

1. Provera, S.; Davalli, S.; Raza, G. H.; Contini, S.; Marchioro, C., Long-range two-dimensional1H-29Si heteronuclear shift correlation using gradients. Application to tetra-TMS-*O*-methyl-D-glucopyranose and tetra-TES-*O*-methyl-D-glucopyranose. *Magnetic Resonance in Chemistry* **2001,** *39* (1), 38-42.

2. Hsieh, H. W.; Schombs, M. W.; Gervay-Hague, J., Integrating ReSET with glycosyl iodide glycosylation in step-economy syntheses of tumor-associated carbohydrate antigens and immunogenic glycolipids. *J Org Chem* **2014,** *79* (4), 1736-48.

3. Mouna Harket, B. D. J., Jean-Claude Lartigue, Michel Petraud, Max Ratier, Application of the 29Si NMR 2D INEPT spin-flip J-resolved technique to the structural analysis of trimethylsilylated glycosides. *Carbohydrate Research* **1994,** *263*, 155-161.

4. Gale, D. J.; Haines, A. H.; Harris, R. K., 29Si and13C NMR studies of organosilicon chemistry. V—Sugar derivatives. *Organic Magnetic Resonance* **1975,** *7* (12), 635-636.

5. Bhat, A., S., Gervay-Hague, J. , Efficient Syntheses of B-Cyanosugars Using Glycosyl Iodides Derived from Per-O-Silylated Mono and Disaccharides. *Organic Letters* **2001,** *3* (13), 2081-2081.

6. Schraml, J., 29Si NMR Spectroscopy of Trimethylsilyl Tags. *Progress in NMR Spectroscopy* **1990,** *22*, 289-348.

Chapter 3:

Quantitative ^{29}Si-NMR Spectroscopy as an Efficient Method for Quantification of Carbohydrate Mixtures

Abstract:

Nuclear magnetic resonance spectroscopy, a well-established technique, serves to analyze structures of molecules both small and large. Notably, ^{1}H NMR quantitative nuclear magnetic resonance (qNMR) has risen to prominence as a precise means for quantifying components within complex mixtures. Despite its usefulness, proton NMR has limitations such as constrained chemical shift dispersion, particularly evident in intricate biological samples where overlapping peaks from substantial compounds like metabolites or polysaccharides impede identification and quantification. Accurate carbohydrate measurement holds great importance across diverse sectors, including food, pharmaceuticals, and biofuels, due to the impact of carbohydrates on quality, safety, and regulatory adherence. The Gervay-Hague research group's focus involves employing ^{29}Si NMR signal to quantify glucose, sucrose, and fructose within mixtures, expanding this approach to evaluate these compounds within coffee and tea leaves. The exploration of ^{29}Si NMR analysis of sugar mixtures revealed significant insights. Integration of ^{29}Si NMR resonances closely mirrored observed ratios, confirming its reliability. By adopting a novel internal standard DHEA-TDBPSi (**26**), a 50% reduction in error compared to liquid HMDS (**27**) was achieved. Analyzing samples that are solid like per-*O*-TMS trehalose (**21**) using DHEA-TDBPSi (**26**) further reduced error to 8-15%. Notably, the ^{29}Si NMR

signal corresponding to the 2-hydroxyl position proved the most consistent ratio and a promising diagnostic signal for quantitative assessment of sample mixtures.

3.1.0 Introduction:

Nuclear magnetic resonance spectroscopy is a well-established analytical technique widely employed for structure elucidation in both small and macromolecules. Particularly, the ^{1}H NMR spectrum, which incorporates chemical shift and coupling constants, and offers valuable insights into the quantitative amount of a compound in a mixture.[1] The distinctive and unique peak patterns observed in proton NMR spectra provide valuable information about the chemical linkages between atoms and groups within each molecule.[2] As a result, 1D proton NMR has emerged as a convenient and efficient method for rapid identification and quantification of analytes. By closely analyzing these spectral features, researchers gain critical knowledge about the proton arrangements and interactions within a molecule, enhancing the understanding of molecular structure and properties.

The underlying principle of quantitative NMR lies in the direct correlation between the signal intensity observed in the NMR spectrum and the number of nuclei responsible for that particular resonance.[1,3] This correlation facilitates a straightforward determination of molar concentration, making qNMR a favored technique for characterizing compounds. By analyzing the spectral signatures, qNMR can predict and determine the compositions and ratios of products or composition within a sample, providing valuable insights into the chemical makeup of the analyzed

material.[3] Furthermore, the wide linear dynamic range of signal digitization in NMR enables the quantification of analytes across a broad concentration range.[2]

In addition, the qNMR method offers several benefits, including non-destructive and non-invasive characteristics, a relatively rapid sample preparation process, and the ability to simultaneously determine multiple analytes in a mixture without compound-specific recalibration.[3,4,5] More importantly, qNMR does not require authentic identical reference materials for quantitative analyses, making it possible to use any highly pure, chemically stable, and inert calibration standard of choice.[4,5,6] Furthermore, quantification using qNMR proves highly effective, delivering precision, accuracy, and cost-efficiency surpassing other established methods.[8] Compared to traditional chromatographic methods, qNMR is both easy to use and faster in obtaining results.[6] The extensive application of NMR in compound quantification further reinforces its prominence.

In 1963, Jungnickel and Forbes reported the first use of proton NMR spectroscopy as an analytical tool for quantifying the intra-molecular proton ratios in 26 pure organic substances.[9] Following this, in the same year (1963), Hollis utilized qNMR to analyze the fraction of aspirin, phenacetine, and caffeine in their respective mixtures.[10] Several papers in qNMR had been published between 1965 and 1990, focusing on the absolute quantitation of active drugs and their purity in various formulations, such as tablets, gelatin, ointments, and inhalants.[1] Since then multiple review articles have explored different aspects of quantitative proton NMR (qHNMR). This dissertation encompasses applications in pharmaceutical analysis and quality

control of traditional Chinese medicines, metabolomic profiling of plant extracts, an overview of quantitative metabolomics, and the theoretical foundation of quantitation by NMR.[5,11,12,13,14]

^{1}H qNMR has seen substantial growth as an analytical tool and become one of the most appropriate methods for quantitatively measuring multiple components in complex mixtures, such as cell extracts, tissue extracts, body fluids, [2,15,16] natural-product isolates,[4,6,17,18,19,20] microplastic mixtures,[21] and drug formulations.[8,10] Proton NMR preference is attributed to its high sensitivity, which surpasses other nuclei, thanks to its large magnetogyric ratio and high natural abundance. Additionally, proton NMR exhibits relatively fast relaxation recovery, making it advantageous for many analytical applications.[2] While qNMR applications to other nuclei like ^{31}P, ^{29}Si, ^{15},N and ^{13}C NMR are limited due to low sensitivity and/or natural abundance,[1,13,22] recent advancements in high-field magnets and CryoProbe technologies have significantly reduced the limit of detection (LOD).[1,22,23]

The level of major chemical ingredient can be determined by qNMR with remarkable accuracy and precision, surpassing 1-5 %, making it suitable for precise and accurate quantification.[1,6] Additionally, impurities can be quantified at levels of 0.1% or even lower.[6] The validation processes, including precision, accuracy, linearity, reproducibility, robustness, selectivity, and specificity, confirm NMR spectroscopy as a reliable technique for quantitative estimation.[1] However, careful optimization of acquisition and processing parameters, referencing techniques, and sample preparation is necessary to achieve high accuracy and precision. Bharti and

Roy[1] have thoroughly discussed the pertinent parameters to be considered, and below is a summary of some crucial aspects emphasized in their review.

- **Temperature**: Maintaining a constant temperature during the experiment is crucial for the reproducibility of quantitative results. Temperature variations can impact molecular relaxation properties and cause artifacts in signal baselines. Higher temperatures may induce signal shifts, making it essential to keep the temperature controlled and stable at 20–30 °C for optimal results in oil applications.[3]
- **Pulse Width**: In spectra recording for qNMR data, pulse angles between 30° and 90° are commonly used. While a 90° pulse provides maximum signal intensity, pulse widths below 90° are often preferred to achieve good data in a reasonable time. Specifically, 30° pulses are widely used to ensure resonance relaxation within a shorter experiment duration, ensuring uniformity in pulse width usage during measurement.[1,3,4]
- **Relaxation Delay (Repetition Time)**: The relaxation delay (D1) and pulse angle are crucial parameters for accurate quantification, and they are correlated with each other. Maximum sensitivity is typically achieved with a 90° pulse angle, and D1 needs to be five times greater than the longest longitudinal relaxation time (T1) for the quantification of protons. With a 30° pulse angle, D1 should be more than 7/3 times the T1 value.[1,3,4,24]
- **Number of Scans:** The number of scans in NMR experiments is a critical parameter influenced by sample concentration, desired signal-to-noise (S/N)

ratio, and limit of quantification (LOQ) requirements. For accurate and precise quantitative purposes (<1% error), a recommended S/N ratio of 1:250 is advised. Increasing the S/N ratio is proportional to the square root of the number of scans, impacting time consumption, especially for low-concentration analytes. Additionally, the number of scans is important for signal-to-noise (S/N) values, and using 16 scans ensures S/N values above 150.[1,3,24]

- **Acquisition Time:** The acquisition time is a crucial parameter in NMR experiments, as it affects the trade-off between spectral resolution and experimental time. Longer acquisition times lead to higher spectral resolution and better signal-to-noise ratio (S/N) but result in longer overall experiment duration. Optimizing the acquisition time is essential to balance the desired spectral quality and the practical constraints of the experiment. Factors like sample concentration, relaxation times, and desired spectral resolution influence the choice of acquisition time in NMR spectroscopy.[1]

Despite its broad applicability, there may be some limitations in terms of quantitative accuracy in certain situations. To ensure reliable results, careful consideration and validation are crucial for specific analytical purposes. Proton NMR has its limitations, such as limited chemical shift dispersion in the spectrum. In biological samples and products, severe peak overlap is common, especially in body fluids, tissue extracts, and vaccines.[2,17] Mixtures of endogenous metabolites or polysaccharides can lead to numerous NMR peaks, making identification and quantification challenging. Furthermore, the chemical shifts of ^{1}H NMR peaks may be

affected by solution matrix effects like pH, metal cations, and molecular interactions.[2] With these challenges using ^{1}H qNMR, other nuclei such as ^{13}C have been explored recently.

In particular, the implementation of ^{13}C NMR spectroscopy encompasses a range of fields, such as polymer chemistry, clinical chemistry, and food chemistry investigations. Numerous studies have delved into the quantitative analysis of lignin chemistry using ^{13}C NMR, along with a study utilizing magic angle spinning ^{13}C NMR to analyze crystal polymorphs of an organic compound within a complex solid matrix.[22,23,24,25,26] This progress has opened up opportunities to analyze samples with low concentrations in fields such as metabolomics, pharmaceuticals, and natural products. While ^{13}C qNMR has some advantages due to signal distribution, a drawback of employing ^{13}C NMR spectroscopy lies in the need for prolonged relaxation delays to achieve quantitative goals. This requirement results in extended data acquisition times to ensure satisfactory signal-to-noise ratios.

The examination of both ^{1}H and ^{13}C qNMR's pros and cons has revealed that there remains a need to explore additional nuclei. In this study, the quantification using ^{29}Si NMR will be explored in detail using pure samples of per-*O*-silylated-sugars (per-*O*-TMS sugars), mixtures of per-*O*-silylated sugars from synthesis, and mixtures of per-*O*-silylated from commercially pure products. The advantages offered by ^{29}Si NMR, such as its large chemical shift dispersion and reduced spectral congestion, make it a highly valuable tool for identifying components of mixtures, as shown in Figures 3.1 and 3.2 (per-*O*-TMS glucose (**14**), per-*O*-TMS fructose (**16**), and per-*O*-

TMS sucrose (**20**)). This capability arises from the unique chemical environment of silicon atoms in various compounds, allowing for distinct signals in the NMR spectrum. After analyzing these signals, it becomes clear that it is possible to differentiate between different components within a mixture. In addition, the silicon signals assigned to each sugar are more abundant to use for quantification and easier for identifications compared to proton signals.

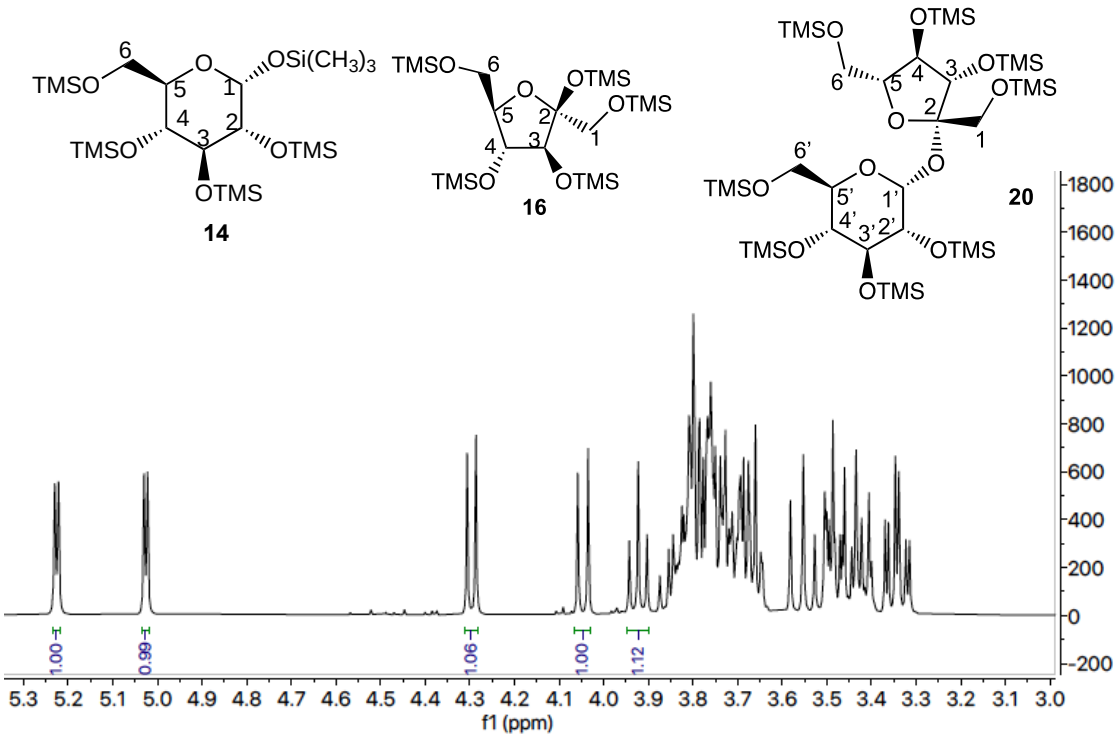

Figure 3. 1: ^{1}H NMR spectrum of a sample mixture containing per-*O*-TMS glucose (**14**), per-*O*-TMS fructose (**16**), and per-*O*-TMS sucrose (**20**).

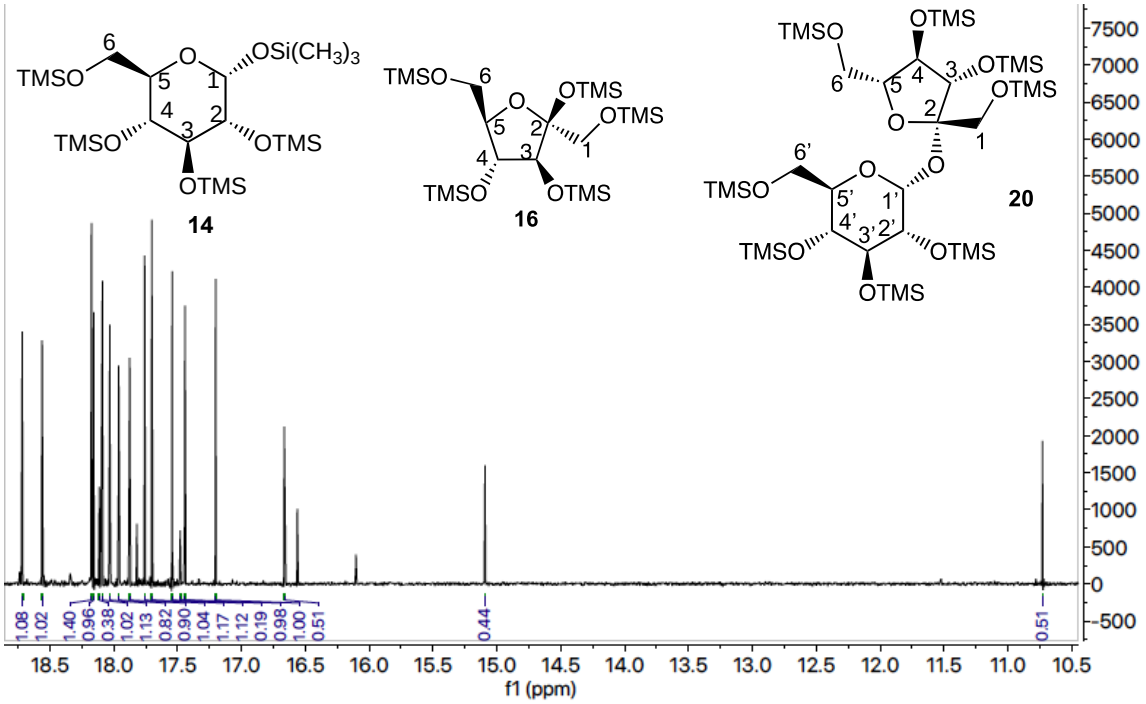

Figure 3.2: ^{29}Si NMR spectrum of a sample mixture containing per-*O*-TMS glucose (**14**), per-*O*-TMS fructose (**16**), and per-*O*-TMS sucrose (**20**). These spectra illustrated the difference of peak overlapped between ^{1}H and ^{29}Si spectra. All peaks are resolved in ^{29}Si NMR.

As explicitly stated in Chapter 1, carbohydrates stand as the foundational components of life, ubiquitously existing across all levels of organisms.[27] Having an accurate measurement of carbohydrates holds significance across diverse sectors such as the food and beverage industry, pharmaceutical industry, and biofuel industry. The pursuit of quantitatively measuring these fundamental compounds aligns with the focus of the Gervay-Hague research group. The primary objective is to employ ^{29}Si NMR in quantifying the levels of glucose, sucrose, and fructose within mixtures, and subsequently extend the applicability of this method to quantitatively assess the content of glucose, sucrose, fructose, raffinose, stachyose, kestose, and xylitol intrinsically existing within coffee and tea leaves. Meanwhile, prior research

has attempted quantification of these carbohydrates using well established methods like ^{1}H qNMR,[19] MS,[28,29,20,31] and HPLC,[28,32] it must be acknowledged that the limitations of these approaches persist, as highlighted earlier. More importantly, it was found that the precision of measuring hydroxyl and carboxyl groups could be notably improved by transforming OH groups into $Si(CH_3)_3$ groups. This alteration resulted in a remarkable nine-fold enhancement of the ^{1}H NMR signal, triggering a notable increase in the utilization of NMR quantification techniques of silyl derivatives in ^{1}H qNMR.[33] As a result, the quantification of silyl derivatives of OH natural products using ^{29}Si NMR becomes a more appropriate approach rather than relying solely on ^{1}H qNMR.

Despite the potential of ^{29}Si NMR for sample quantification, a significant gap exists in comprehensive investigations targeting silyl carbohydrate derivatives. This knowledge gap inhibits a thorough understanding of ^{29}Si NMR's applicability and constraints in this realm. To fully realize ^{29}Si NMR's quantitative prowess in carbohydrate analysis, it is imperative to undertake further research in silyl carbohydrate derivatives. Leveraging the unique strengths of ^{29}Si NMR and recognizing the untapped potential for multidimensional correlations, this study explores novel avenues for identifying and quantitatively analyzing carbohydrate silyl derivatives using ^{29}Si qNMR techniques.

3.2.0 Result and Discussion

3.2.1 Introduction to twelve per-*O*-silylated sugars

In the previous chapters, twelve per-*O*-TMS sugars; per-*O*-TMS-α-methylglucoside (**13**), α-per-*O*-TMS glucose (**14**), α-per-*O*-TMS mannose (**15**), β-per-

O-TMS fructose (**16**), per-*O*-TMS sorbitol (**17**), per-*O*-TMS ribitol (**18**), per-*O*-TMS xylitol (**19**), per-*O*-TMS sucrose (**20**), per-*O*-TMS trehalose (**21**), per-*O*-TMS kestose (**22**), per-*O*-TMS raffinose (**23**), and per-*O*-TMS stachyose (**24**) were synthesized and characterized. In the context of identifying carbohydrate components in a mixture, the utilization of ^{29}Si NMR peaks holds great potential as a quantification tool for carbohydrates and related natural products. The detailed work illustrated in Chapter 1 has successfully established a robust framework for the identification and characterization of distinct silyl sugars, revealing their unique chemical shift profiles. Building upon this foundation, the present chapter employs silyl derivatives of glucose, fructose, sucrose, and trehalose for the purpose of conducting quantitative studies.

3.2.2 Investigating the sensitivity of ^{29}Si NMR chemical shifts on concentration.

All silicon NMR experiments were conducted in deuterated chloroform. The ^{29}Si NMR spectra were recorded using the DEPT pulse sequence for polarization transfer as shown in Figure 3.3. Figure 3.4 depicts a generic pathway for conducting experiments and analyzing experimental data. Two sugar mixture syntheses were conducted, which will be discussed below, and additional quantification samples were derived from per-*O*-silylated sugars (per-*O*-TMS sugars), including α-per-*O*-TMS glucose (**14**), per-*O*-TMS fructose (**16**), per-*O*-TMS sucrose (**20**), and per-*O*-TMS trehalose (2**1**), which was prepared from each respective free sugar.

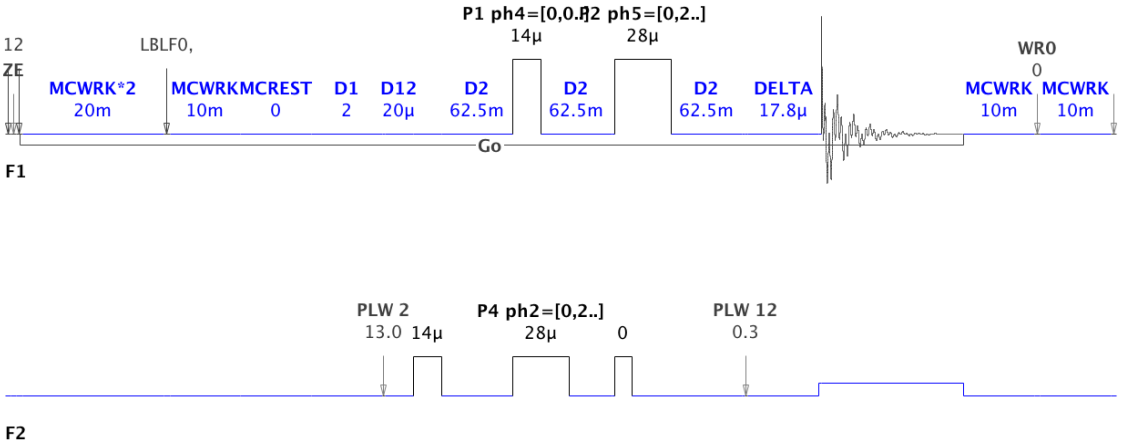

Figure 3.3:Pulse sequence of ^{29}Si DEPT experiment; f1 channel is the silicon and f2 channel is proton with 2 s delay relaxation and pulse length of 14 µs and 28 µs on both channels.

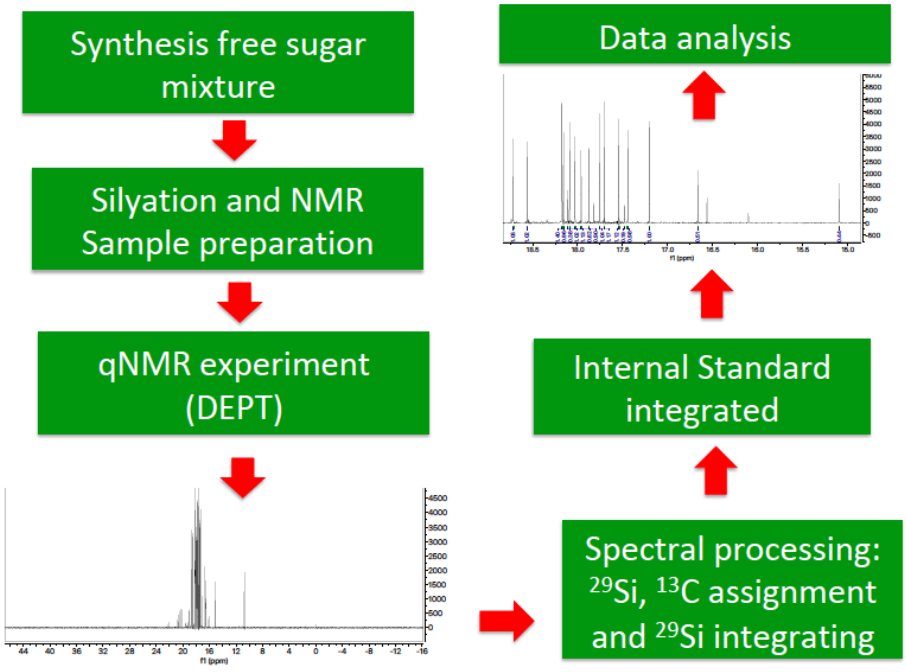

Figure 3.4: Optimizing ^{29}Si NMR quantification: a comprehensive guide to stepwise sample preparation and data processing.

Three different internal standards were used for testing the method. The first internal standard was hexamethyldisilazane (**27**). The other internal standards, 3-*O*-

tert-butyldiphenylsilyl-dehydroepiandrosterone (DHEA-*O*-TBDPSi **26**), and 3-*O*-trimethylsilyl-dehydroepiandrosterone (DHEA-*O*-TMS **25**), Figure 3.5, were synthesized for this project in the lab, but are also commercially available to be purchased at Sigma Aldrich. The benefits and limitations of the standard are discussed below.

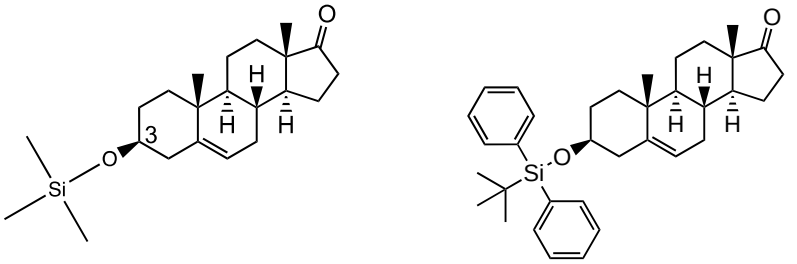

dehydroepiandrosterone-O-TMS (**25**) dehydroepiandrosterone-SiTBDP (**26**)

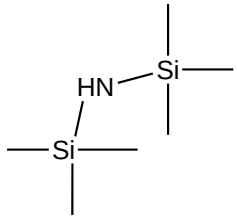

hexamethyldisilazane (HMDS **27**)

Figure 3.5: The three internal standard uses for the study of ^{29}Si NMR quantification. Internal standard **25** and **26** were synthesized in the lab as solids and HMDS (**26**) was purchased as a liquid.

Establishing the optimal mixture concentration that does not alter the chemical shifts (δ) of the Si signal, whether in the upfield or downfield region, is of utmost importance. Previous studies have demonstrated that the sensitivity of the ^{29}Si NMR chemical shift is dependent on concentration.[33] Therefore, a series of experiments was conducted with varying concentrations ranging from 0.0125 M to 0.500 M of α per-*O*-TMS glucose (**14**) to determine the most optimal concentration for quantification via ^{29}Si NMR experiments using a 400 HMz spectrometer. The

spectra presented in Figure 4.6 display seven different concentrations of **14**, ranging from 0.0125 M to 0.500 M in $CDCl_3$. It is evident that the signals from high concentrations, specifically 0.500 M were not well resolved compared to those from lower concentrations. Upon close examination of the superimposed spectra, it is noteworthy that concentrations within the range of 0.100 M to 0.125 M manifest superiorly resolved peaks as opposed to those observed at 0.250 M or 0.500 M. Furthermore, Si6 fails to exhibit a consistent chemical shift value or adhere to the observed trend in Si1 or Si4, wherein lower concentrations showcase a marginal downfield shift, and higher concentrations display a slight upfield shift. A subtle shift in Si3 is discerned at higher concentrations, occurring downfield, while at lower concentrations, it is situated upfield. Although the chemical shift is small, its change in value was observable as shown in Figure 3.6.

The variability in the chemical shifts of Si6 or Si2 is likely attributed to the specific chemical environment surrounding these silicon atoms. It is evident that their chemical environments exhibit heightened sensitivity to changes in concentration compared to other silicon atoms. This observation is substantiated by a meticulous analysis of the reference peak, where their chemical shifts remained constant despite variations in concentration. As illustrated in Figure 3.7, the reference peaks for HMDS at δ 2.45 PPM and TMS at δ 0.00 consistently maintained their positions across the concentration range from 0.0125 M to 0.500 M.

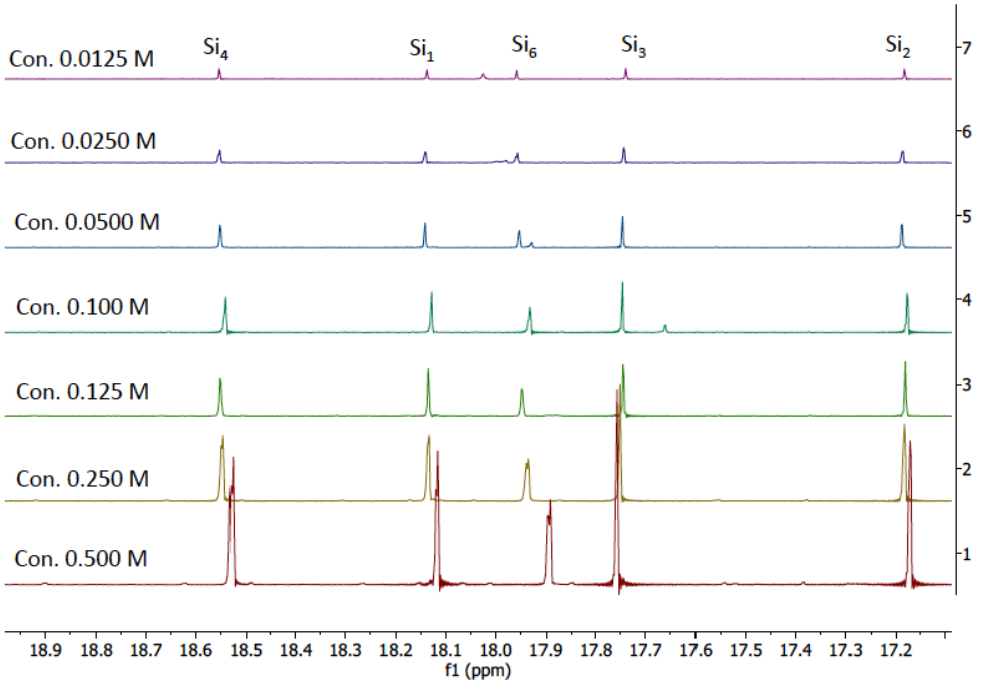

Figure 3.6: Stacked spectra of different concentrations from 0.0125 M to 0.500 M of α-per-*O*-TMS-glucose (**14**) spectra zoom in region of ^{29}Si NMR signal from glucose ring.

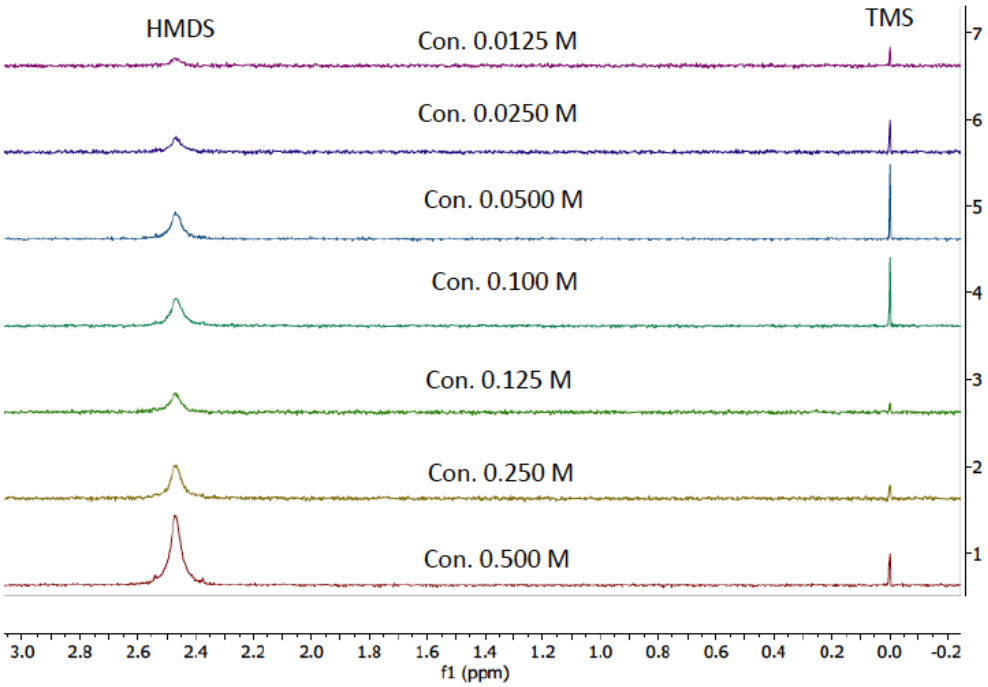

Figure 3.7: Stacked spectra of different concentrations from 0.0125 M to 0.500 M of α-per-*O*-TMS-glucose (**14**) spectra zoom in region of reference ^{29}Si NMR signals, HMDS and TMS.

Furthermore, upon analyzing the carbon spectra of all six concentrations, it was observed that the chemical shift of hexamethyldisilane remained unchanged, as illustrated in Figure 3.8. The chemical shift of ^{13}C NMR of HMDS at δ 2.45 ± 0.01 remained consistent throughout the variations in concentration. This observation is noteworthy in the context of experimental conditions, where $CDCl_3$ serves as the primary reference with a chemical shift of δ 76.98, Figure 3.9 and TMS at δ 0.00, Figure 3.8. The stability of the HMDS chemical shift under these conditions (6 different concentrations) lends credence to its role as a secondary ^{29}Si NMR chemical shift reference. In light of the standards set for solvent excess, the utilization of these consistent ^{13}C NMR chemical shift values of HMDS, $CDCl_3$, and TMS enhances the reproducibility and reliability of the experimental data, aligning with what is referred to as the standard or optimal conditions of this study. The data obtained at these concentrations align with Schraml's[33] findings, although they utilized a different internal standard reference, hexamethyldisilsane (HMDSS). The results are consistent and agreeable.

These results underscore the critical importance of carefully determining the optimal concentration to minimize changes in chemical shift. The observed shift from upfield to downfield as concentration decreases highlights the influence of concentration on the chemical environment of Si6. In contrast, other signals do not exhibit drastic changes and remain consistent once the concentration reaches 0.125 M or lower. These findings guide decisions regarding the concentration of per-*O*-silylated derivatives in ^{29}Si NMR quantification experiments. The optimal concentration range of 0.100 M to 0.125 M enhances the resolution and consistency

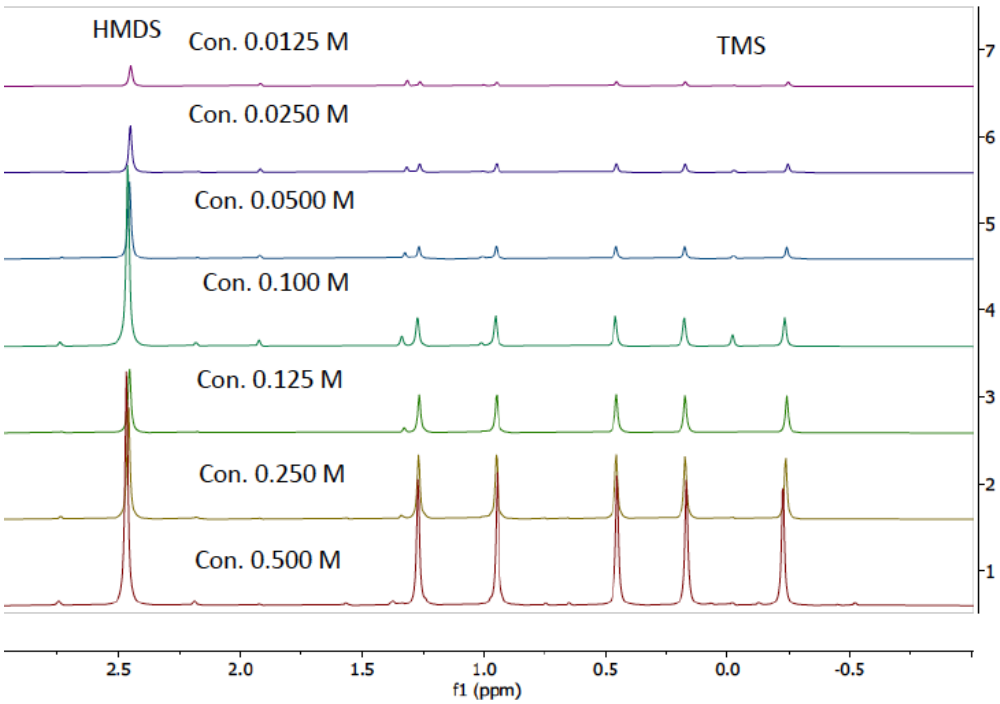

Figure 3.8: ^{13}C NMR spectra stacked spectra of different concentrations from 0.0125 M to 0.500 M of α-per-*O*-TMS glucose (**14**) in the HMDS δ 2.45 and TMS region.

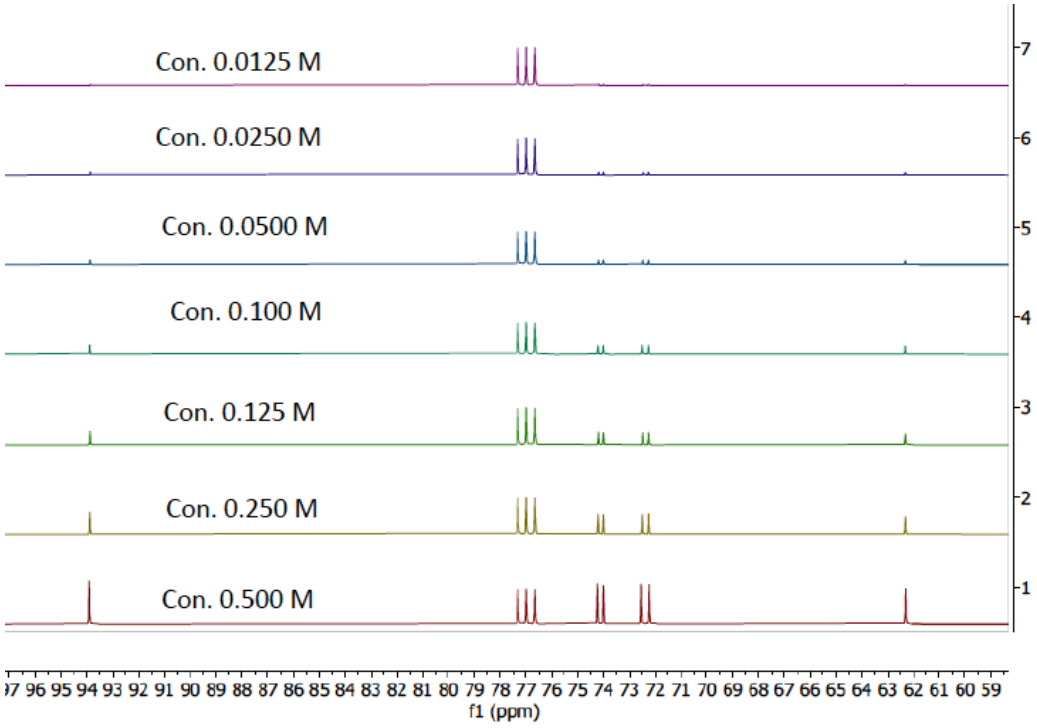

Figure 3.9: ^{13}C NMR spectra stacked spectra of different concentrations from 0.0125 M to 0.500 M of α-per-O-TMS glucose (**14**) in the $CDCl_3$ region where the middle peak at δ 76.98.

of Si signal interpretation. Overall, these results contribute to a deeper understanding of factors influencing Si chemical shifts and provide valuable guidelines for optimizing experimental conditions in NMR studies involving silylated carbohydrates.

3.2.3 Determination of the Integration Ration of α-Per-*O*-TMS Glucose (**14**), β-Per-*O*-TMS Fructose (**16**), and Per-*O*-TMS Sucrose (**20**) from ^{29}Si Integration in a Synthetic.

To study and validate the integration value of the silicon signal, a mixture of sugars commonly found in tea leaves: glucose, fructose, and sucrose[34,35,36] was combined and subjected to silylation. The same silylation method as discussed in Chapter 1 was followed. The synthesis of this mixture is depicted in Scheme 3.1. The sugars were combined in a 1:1:1 molar ratio and mixed with pyridine, HMDS, and TMSCl, and stirred at room temperature for 24 hours. Afterwards, the work-up process and NMR analysis was conducted.

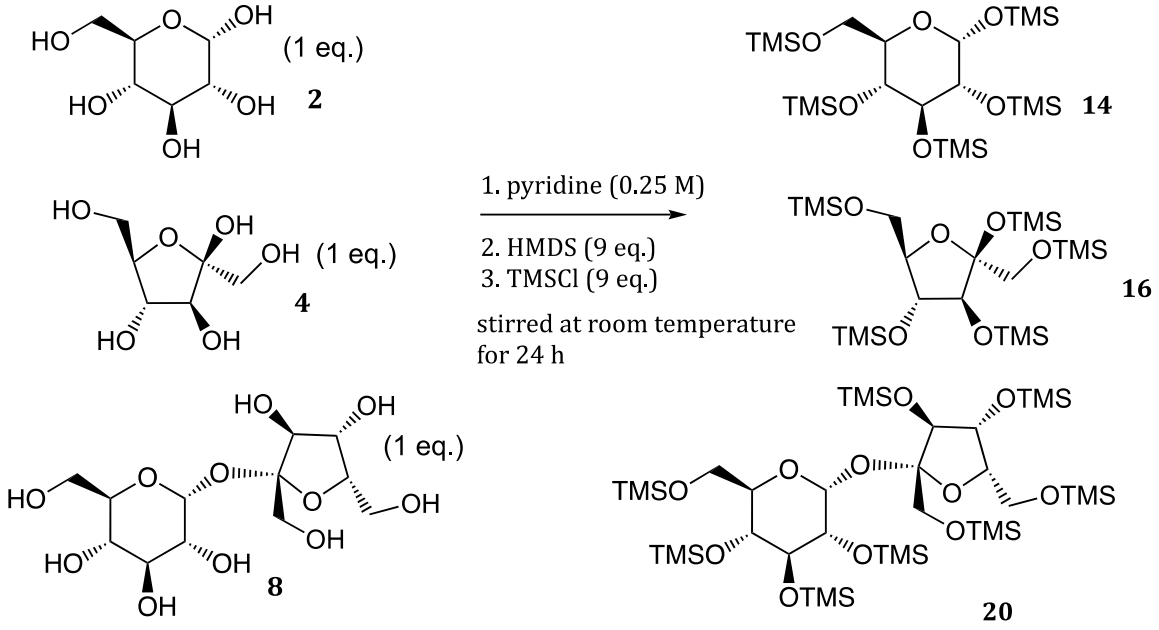

Scheme 3.1: Synthesis of α-per-*O*-TMS glucose (**14**), β-per-*O*-TMS fructose (**16**), and per-*O*-TMS sucrose (**20**) as reaction mixture.

The spectrum obtained from this mixture was overlaid with the pure per-*O*-TMS spectra, as shown in Figure 3.10. The overlay spectra revealed that the chemical shifts of each compound in the mixture remained the same as those of the pure compounds. For relative ratio analysis in this mixture, an integration of ^{29}Si NMR was signal conducted with respect to HMDS as 1.00 at δ 2.47. The NMR experiment was performed in triplicates and the ratio of each per-*O*-silylated sugar was calculated from each silicon signal of each compound and compared with the theoretical ratio from the starting material, free sugar.

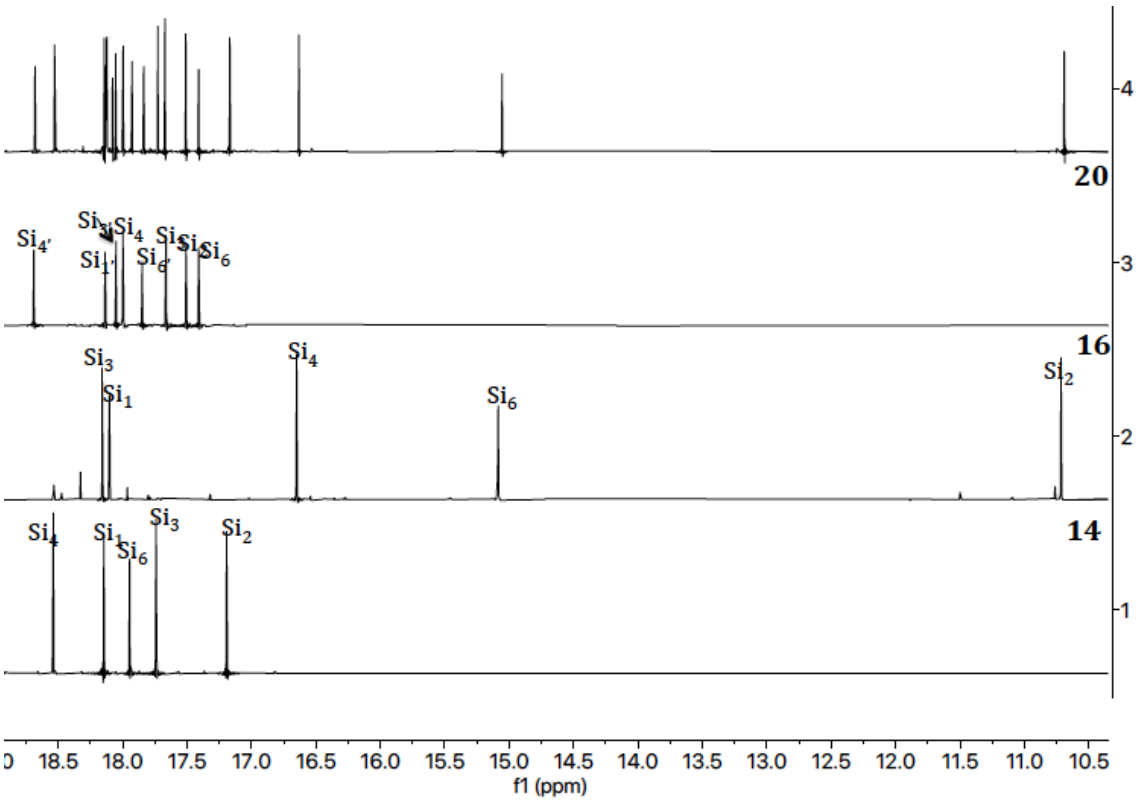

Figure 3.10: (4) is ^{29}Si NMR spectra of a reaction mixture containing (**14**), (**16**), and (**20**) in 1:1:1 ratio in $CDCl_3$ stirred at room temperature for 24 h. (3), (2), and (1) are pure ^{29}Si spectra of per-*O*-TMS sucrose (**20**), β-per-*O*-TMS fructose (**16**), and α-per-*O*-TMS glucose (**14**) respectively.

Triplicate NMR experiments of the same sample were prepared for the integration and ratio analysis of these syntheses. The oily per-*O*-silylated sugars were

weighed by mass difference and prepared according to the procedure outlined in Figure 3.11.

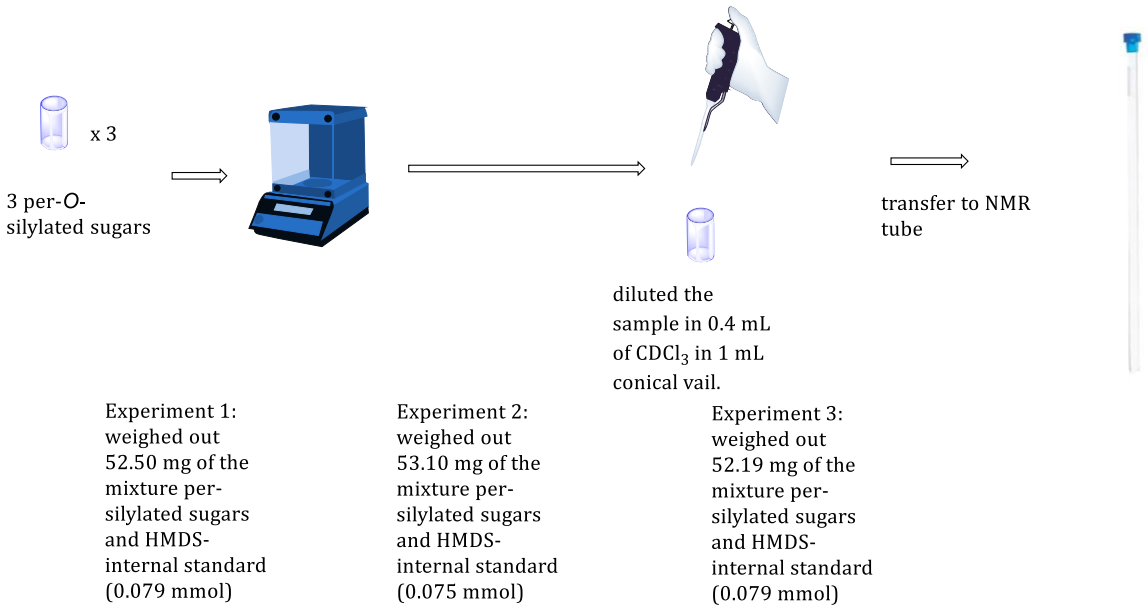

Figure 3.11: NMR samples preparation for ratio study of reaction mixture contained α-per-*O*-TMs glucose (**14**), β-per-*O*-TMS fructose (**16**), and per-*O*-TMS sucrose (**20**).

The signals in the mixture were integrated and assigned to their respective pure compounds. The internal standard, HMDS, was used as a reference with an integration value of 1.00. The integration values for all signals are listed in Table 3.1. Interestingly, the ^{29}Si NMR signals of Si3 from β-per-*O*-TMS fructose (**16**) and Si1' from per-*O*-TMS sucrose (**20**) are overlapped, making it impossible to collect accurate integration values for these two signals. Additionally, the integration values for the signals from per-*O*-silylated-fructose were slightly lower compared to glucose or sucrose. The possibility could be that the free sugars are hydrated with different amounts of water. The smallest integration value was observed for Si1 in β-per-*O*-TMS fructose (**16**), Si6' in per-*O*-TMS sucrose (**20**), and Si6 in α-per-*O*-TMS glucose (**14**). This exhibits a consistent integration pattern, wherein Si atoms attached to the

primary hydroxyl groups have smaller integration values compared to the rest of the Si atoms attached to the secondary hydroxyls or in the ring as their integration are generally close to each other. The distinction between these two types of silicon (Si) lies in the number of neighboring hydrogen atoms. The Si atom attached to the primary hydroxyl possesses 11 protons (9 protons from TMSi and 2 protons from 2° C position), whereas the secondary or ring hydroxyl has 10 protons. In the context of a DEPT ^{29}Si NMR experiments, hydrogen polarization transfer is used to selectively enhance the Si nuclei thus the difference in proton number can contribute to the disparity in the two types of integrations.

Table 3.1: ^{29}Si NMR integration values obtained from an equal mole ratio sample contained α-per-*O*-TMs glucose (**14**), β-per-*O*-TMS fructose (**16**), and per-*O*-TMS sucrose (**20**). Triplicate experiments were conducted in $CDCl_3$. HMDS was used as internal standard and set as reference at 1.00.

Integration Values: HMDS as Internal Standard									
Compound	Si_2	Si_3	Si_6	Si_1	Si_4	Si_{1f}	Si_{3f}	Si_{4f}	Si_{6f}
Experiment 1									
Sucrose	1.80	1.92	1.56	x	1.88	x	1.70	1.74	1.46
Fructose	1.60	x	1.40	1.26	1.62				
Glucose	1.64	1.70	1.30	1.54	1.72				
Experiment 2									
Sucrose	1.62	1.86	1.50	x	1.82	x	1.48	1.74	1.44
Fructose	1.60	x	1.40	1.24	1.48				
Glucose	1.60	1.60	1.32	1.48	1.70				
Experiment 3									
Sucrose	1.62	1.82	1.56	x	1.82	x	1.58	1.74	1.42
Fructose	1.56	x	1.32	1.18	1.56				
Glucose	1.60	1.64	1.16	1.46	1.66				

Notably, the Si2 signal exhibited the closest values between different molecules, differing only in the 100th place such as the example of experiment 2 of Si2. The integration values for β-per-*O*-TMS fructose (**16**) and α-per-*O*-TMS glucose (**14**) were the same at 1.60, while per-*O*-TMS sucrose (**20**) was 1.62. When comparing these integration values to the theoretical value, there was 50-60% error, which could be attributed to the Si attached to the N in HMDS (internal standard-IS) and Si attached to *O* in the sugar. In addition, the volatility of the HMDS and weighing by difference of oily sample could contribute to the large errors. Detailed explanation will be discussed later in the chapter.

To calculate the ratio of each signal from different compounds in all three replicate experiments, we used the equation mentioned earlier (equation 3.1). As shown in Table 3.2 and mentioned previously, the integration of Si3 and Si1 overlapped, making it impossible to obtain data for those signals. Therefore, in this ratio analysis, we will focus on three signals: Si4, Si6, and Si2. The other signals were used for comparison since it is only present in sucrose.

Equation 3. 1: Integration Ratio Calculation

$$ratio = \frac{Si\ of\ interest}{Si\ (smallest\ integration\ value\ from\ the\ same\ Si)}$$

Example:

$$ratio\ of\ Si_2\ (1.03\ (\alpha - \text{glucose})) = \frac{1.60}{1.56}$$

Table 3.2: The relative ratio obtained used ^{29}Si NMR integration values from an equal mole ratio sample containing α-per-*O*-TMS-glucose (**14**), β-per-*O*-TMS-fructose (**16**), and per-*O*-TMS-sucrose (**20**). Three experiments were conducted in $CDCl_3$. HMDS was used as internal standard and set as reference at 1.00.

Ratio by Integration: HMDS as Internal Standard									
Compound	Si_2	Si_3	Si_6	Si_1	Si_4	Si_{1f}	Si_{3f}	Si_{4f}	Si_{6f}
Theoretical Ratio									
Sucrose	1.00	1.00	1.00	x	1.00	1.00	1.00	1.00	1.00
Fructose	1.00	1.00	1.00	1.00	1.00				
Glucose	1.00	1.00	1.00	1.00	1.00				
Measured Ratio Used Integration Value									
Experiment 1									
Sucrose	1.15	1.20	1.34	x	1.27	x	1.15	1.00	1.03
Fructose	1.03	x	1.21	1.07	1.09				
Glucose	1.05	1.06	1.12	1.31	1.16				
Experiment 2									
Sucrose	1.04	1.16	1.29	x	1.23	x	1.10	1.00	1.01
Fructose	1.03	x	1.21	1.05	1.00				
Glucose	1.03	1.00	1.14	1.25	1.15				
Experiment 3									
Sucrose	1.04	1.14	1.34	x	1.23	x	1.07	1.00	1.00
Fructose	1.00	x	1.14	1.00	1.05				
Glucose	1.03	1.03	1.00	1.24	1.12				

The ratios obtained from the integration led to the following findings: For Si4, α-glucose and sucrose consistently exhibit ratios ranging from 1.12 to 1.16 across all three experiments. This indicates a stable relative proportion of Si4 within these compounds. Regarding Si6, fructose shows consistent ratios across all three experiments, while α-glucose exhibits some variation of ± 0.14 and sucrose shows slight variation ± 0.05 in the ratios. In terms of Si_2, fructose consistently displays ratios in all three experiments (± 0.01), α-glucose shows consistent ratios across the experiments (± 0.02) and sucrose exhibits some variation ± 0.09 in the ratios. Overall, within each compound, there is consistency in the ratios for certain signals

across the experiments, while other signals may exhibit more variation. There are two types of differences in integration, the integration difference between signals within the same compound and the difference between experiments. The first integration difference may be potentially due to the different chemical environments of the ^{29}Si nuclei or structural configurations. The second variation observed may be attributed to experimental measurement of uncertainties such as sample preparation or sample weighing by difference because the mixture is oil.

Upon analyzing the reaction mixtures in two experiments, an additional inference that can be made is that the silylation method employed did not exhibit selectivity towards any specific sugar. The initial composition of the reaction mixture consisted of a 1:1:1 ratio of free sugars. Interestingly, the integration and relative ratios observed in the resulting per-*O*-silylated sugars also corresponded closely to the initial proportions. While minor variations were detected, it is plausible to attribute them to experimental and integration measurement uncertainties. These findings highlight the lack of preferential reactivity of the silylation method towards individual sugars within the mixture. The absence of significant deviations from the initial sugar ratio implies that the synthetic reaction proceeds uniformly, without favoring any sugar species. This observation suggests that the silylation process does not discriminate between the sugars present in the starting mixture, indicating a lack of selective silylation based on sugar type. Moreover, the agreement between the integration and relative ratios of the pers-silylated sugars and the initial mixture ratios strengthens the reliability of the experimental measurements.

3.2.4 Determine the Mmol of α-Per-*O*-TMS Glucose (**14**), β-Per-*O*-TMS Fructose (**16**), and Per-*O*-TMS Sucrose (**20**) from Si Integration of Known Amount Mixture

Calculating the millimoles (mmol) of a mixture containing different ratios of α-per-*O*-TMS Glucose (**14**), β-per-*O*-TMS Fructose (**16**), and per-*O*-TMS Sucrose (**20)** was performed to further validate the accuracy of Si integration. To conduct this study, three replicate experiments were conducted wherein each pure per-*O*-silylated compound was individually weighed (according to Figure 3.12) and then mixed in $CDCl_3$ for the ^{29}Si NMR experiment. In the first experiment, the ratios of β-per-*O*-TMS fructose (**16**), per-*O*-TMS sucrose (**20**), and α-per-*O*-TMS glucose (**14**) were set at 1:2:4. The second experiment involved ratios of per-*O*-TMS sucrose (**20)**, α-per-*O*-TMS glucose (**14**) and β-per-*O*-TMS fructose (**16**) in the same 1:2:4 proportions. Finally, the third experiment consisted of ratios of α-per-*O*-TMS glucose (**14**), β-per-*O*-TMS fructose (**16**), and per-*O*-TMS sucrose (**20)**, also in a 1:2:4 ratios. Each per-silylated sugar was weighed individually by mass difference then transferred to a vial and dissolved in $CDCl_3$. The preparation scheme is illustrated in Figure 3.12. By performing these experiments with precisely controlled ratios of the per-*O*-silylated compounds, the integration values obtained through Si integration can be compared to the expected mmol values of each sample.

Similar to the previous study, the integration values within the same compound were generally within the same range, with the exception of the primary Si signal. The integration values, along with the relative ratios calculated from the integration (1.00, 2.43, 4.71), closely matched the mole ratio of 1:2:4 (fructose, sucrose, glucose respectively) as prepared, as shown in Table 3.3 with Si2 as an

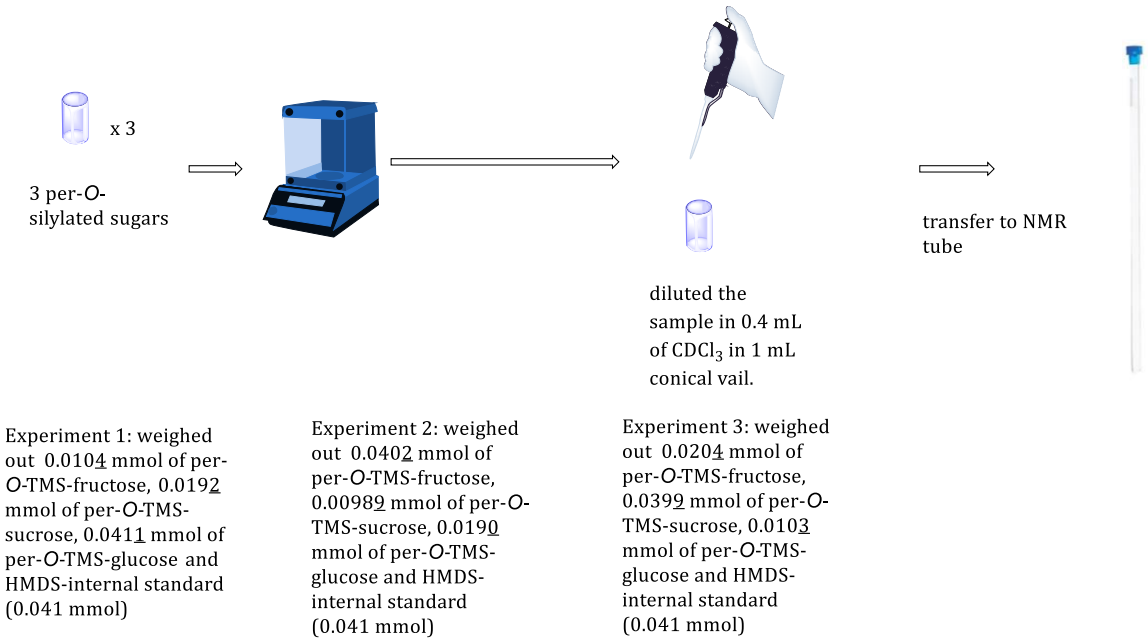

Figure 3.12: NMR samples preparation for calculating mmol (quantification study) of mixture contained α-per-*O*-TMS glucose (**14**), β-per-*O*-TMS fructose (**16**), and per-*O*-TMS sucrose (**20**).

example. For instance, in experiment 3, the mole ratio of α-per-*O*-silylated-glucose, β-per-*O*-silylated-fructose, and per-*O*-silylated-sucrose was 1:2:4, and the corresponding integration ratio calculated was also close at 1.00, 2.00, 4.26, respectively. An interesting observation was made with Si6, which typically displayed lower integration values. Surprisingly, even in experiment 3, it maintained a ratio of approximately 1:1.97 (~2): 4.10 (~4). This consistent ratio was also observed in experiments 1 and 2, where the ratio of per-*O*-silylated-sucrose, α-per-*O*-silylated-glucose, and β-per-*O*-silylated-fructose was 1:2:4. In experiment 2, the calculated ratios from integration for Si2 or Si4 were 1:2.18:4.08 and 1:2.24:4.22, respectively. A similar pattern was observed in experiment 1. These consistent findings confirm that the integration ratios of Si and the mole ratios are in alignment, highlighting the reliability of the experimental measurements. The close correlation between the

integration values and the mole ratios of the silylated compounds supports the Si-DEPT experiment for the quantification of unknown quantities.

Table 3.3: The integrations of α-per-*O*-TMs glucose (**14**), β-per-*O*-TMS fructose (**16**), and per-*O*-TMS sucrose (**20**) from mixtures of triplicate ^{29}Si NMR experiment at different ratios.

Integration Values: HMDS as Internal Standard (1.00)									
Compound	Si_2	Si_3	Si_6	Si_1	Si_4	Si_{1f}	Si_{3f}	Si_{4f}	Si_{6f}
Experiment 1: Ratio of mixture: Sucrose (2): Fructose (1): Glucose (4)									
Sucrose	3.26	3.36	3.02	x	3.08	x	3.00	3.16	2.68
Fructose	1.34	x	1.14	1.08	1.36				
Glucose	6.32	6.52	5.42	6.38	6.54				
Experiment 2: Ratio of mixture: Sucrose (1): Fructose (4): Glucose (2)									
Sucrose	1.38	1.36	1.18	x	1.32	x	1.04	1.30	1.06
Fructose	5.64	x	5.14	4.1	5.58				
Glucose	3.02	3.06	2.38	2.80	2.96				
Experiment 3: Ratio of mixture: Sucrose (4): Fructose (2): Glucose (1)									
Sucrose	5.72	5.54	5.10	x	5.96	x	5.30	5.60	4.28
Fructose	2.68	x	2.44	2.08	2.66				
Glucose	1.34	1.56	1.24	1.00	1.56				

To further validate the usefulness of ^{29}Si NMR integration values, the millimoles (mmol) of each signal were calculated using Equation 3.2. The mmol calculated from the individual signal is equal to the integration of that signal time the mole of the internal standard (HMDS) multiplies by the mole ratio of HMDS (2 Si)/ sugar (1 Si). In Experiment 1, the mmol calculated from the weight of each compound was 0.0412 mmol for α-per-*O*-TMS glucose (**14**), 0.0102 mmol for β-per-*O*-TMS fructose (**16**), and 0.0193 mmol for per-*O*-TMS sucrose (**20**). The experimental calculated mmol from the Si2 integration were 0.0536, 0.130, and 0.253 for β-per-*O*-TMS fructose (**16**), 0.0193 mmol of per-*O*-TMS sucrose (**20**), and 0.0412 mmol of α-per-*O*-TMs glucose (**14**), respectively. The calculated mmol and it expected mmol

were shown in Table 3.4. These calculated mmol values were considerably higher than the actual values. However, the calculated mmol ratios (1.00:2.43:4.71) were closed to the expected ratio (1:2:4). This pattern was observed consistently across all three experiments and for all signals. While the calculated mmol values may not precisely match the actual quantities, the consistency in the mmol ratios demonstrates the reliability of the Si integration quantification method in accurately representing the relative concentrations of the compounds within the mixture.

Equation 3.2: mmol calculation from integration

mmol of per-*O*-TMS sugar calculate from integration =

$$\frac{integration\ of\ per-O-TMS\ sugars\ x\ mass\ of\ HMDS\ (IS)}{molecular\ weight\ of\ HMDS}\ x\ \frac{2\ mmol\ of\ Si}{1\ mmol\ of\ HMDS}$$

Using ^{29}Si NMR integration value, we conducted studies to confirm the ratios in two different experiments. The first study involved a mixture of α-glucose, β-fructose, and sucrose in a 1:1:1 mole equivalence to produce α-per-*O*-TMS glucose (**14**), β-per-*O*-TMS fructose (**16**), and per-*O*-TMS sucrose (**20**). In the second study, we aimed to quantify the amounts present in the sample by individually weighing and mixing α-per-*O*-TMS glucose (**14**), β-per-*O*-TMS fructose (**16**), and per-*O*-TMS-sucrose (**20**) in different ratios, followed by NMR experiments. HMDS was used as the internal standard, and the calculated millimoles (mmol) were based on this internal standard.

Table 3.4: The calculated mmol from ^{29}Si NMR integration in a mixture contained α-per-*O*-TMS glucose (**14**), β-per-*O*-TMS fructose (**16**), and per-*O*-TMS sucrose (**20**) at different mol ratio and HMDS (**27**) was used as internal standard.

Mmol calculated by ^{29}Si Integration Value: HMDS as Internal Standard (1.00)									
	Si_2	Si_3	Si_6	Si_1	Si_4	Si_{1f}	Si_{3f}	Si_{4f}	Si_{6f}
Experiment 1:									
Anticipated mmol: Sucrose (0.02): Fructose (0.01): Glucose (0.04)									
Weighted mmol: Sucrose (0.019<u>3</u>): Fructose (0.010<u>2</u>): Glucose (0.041<u>2</u>)									
Calculated mmol:									
Sucrose	0.0130	0.134	0.121	x	0.123	x	0.120	0.126	0.107
Fructose	0.0536	x	0.0456	0.0432	0.0544				
Glucose	0.253	0.261	0.217	0.255	0.2620				
Experiment 2:									
Anticipated mmol: Sucrose (0.01): Fructose (0.04): Glucose (0.02)									
Weighted mmol: Sucrose (0.0098<u>9</u>): Fructose (0.040<u>3</u>): Glucose (0.019<u>1</u>)									
Calculated mmol:									
Sucrose	0.0550	0.0544	0.047	x	0.0528	x	0.0416	0.0520	0.0504
Fructose	0.225	x	0.206	0.164	0.223				
Glucose	0.121	0.122	0.0952	0.112	0.118				
Experiment 3:									
Anticipated mmol: Sucrose (0.04): Fructose (0.02): Glucose (0.01)									
Weighted mmol: Sucrose (0.039<u>9</u>): Fructose (0.020<u>5</u>): Glucose (0.010<u>2</u>)									
Calculated mmol:									
Sucrose	0.228	0.222	0.204	x	0.206	x	0.212	0.224	0.171
Fructose	0.107	x	0.0976	0.0832	0.100				
Glucose	0.0536	0.0624	0.0496	0.0400	0.0624				

The results from the experiments showed consistent ratios between each compound as illustrated in Table 3.1, experiment 2, Si2 as 1.62, 1.60, 1.50 for per-*O*-TMS sucrose (**20**), β-per-*O*-TMS fructose (**16**), α-per-*O*-TMs glucose (**14**). The mole ratio of each compound in the mixture was expected as 1:1:1 ratio. However, the calculated mmol values being approximately five times greater than the actual mmol presence as illustrated in Table 3.4 experiment 2, Si2 0.055, 0.22, 0.12 of per-*O*-TMS sucrose (**20**), β-per-*O*-TMS fructose (**16**), α-per-*O*-TMs glucose (**14**). The actual mmol for each was 0.01, 0.04, and 0.02 respectively. This consistent discrepancy in the calculated mmol values suggests a potential error stemming from the chosen internal standard, HMDS, or a possible error in weighing the sample by mass difference. To address this, further investigation into the experimental error led to the implementation of a new internal standard.

One possible explanation for the generated large error could be the evaporation of the internal standard (IS), HMDS, resulting in a lower actual amount in the solution compared to its initial quantity. This difference in mass could cause the integration value for the IS to be lower, while the integration of the sample becomes larger. Consequently, this discrepancy leads to an error in the mmol calculation, as the mass of the internal standard is incorporated into the calculation. Given that HMDS has a boiling point of 127 °C (Sigma Aldrich), it is plausible that some of it may have evaporated during the experiments. To investigate the hypothesis that the error might be attributed to the volatile nature of the internal standard, an alternative internal standard was utilized.

3.2.5 The Use 3-*O*-*Tert*-Butyldiphenylsilyl-Dehydroepiandrosterone (DHEA-TBDPSi) (**25**) as Internal Standard to Calculate the Mmol of Different Per-*O*-Silylated Mixtures.

A desirable internal standard or reference compound should be inert to the solvent, soluble in the solvent, have a single resonance line, be separated from the desired signals, and/or be present upfield from the region of the signal of interest.[8,37] Some internal standards that have been used in ^{29}Si NMR studies are octamethylcyclotetrasiloxane, polydimethylsiloxane, tetramethylsilane, tetramethoxysilane, tetraethoxysilane, and tetrafluorosilane.[37] One commonly used reference is tetraethoxysilane because its resonance line is upfield, it is commercially available, and it is relatively stable. However, it is one of the slowest relaxing Si nuclei among the other listed references.[38] Another very common and widely accepted silicon reference is tetramethylsilane, which has a short T1 at room temperature. Nevertheless, it is volatile and can only be used for low temperature studies.[37,38,39] Additionally, the structural similarity between sugar Si-*O* and DHEA Si-*O* is favored over HMDS Si-*N*-Si. The discrepancy in heteroatoms and the number of Si atoms may be another contributing factor to the error.

After carefully analyzing the internal reference criteria, we decided to use a solid silicon-containing internal standard, 3-*O*-*tert*-butyldiphenylsilane-dehydroepiandrosterone (DHEA-TBDPSi) (Figure 3.13). This compound only has one silicon signal, and the signal is present upfield at -6.21 ppm (Figure 3.13), whereas the peaks of interest are all above 10 ppm. Additionally, the solid DHEA-TBDPSi (**25**) is not volatile and easier to weigh out, which reduces the accumulation of errors.

Although this compound is commercially available and can be purchased through Sigma Aldrich, for this study, it was synthesized in the lab in high yield.

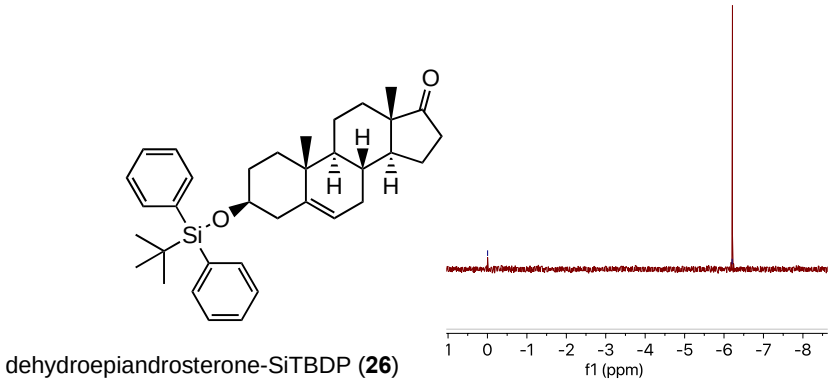

Figure 3.13: 3-O-tert-butyldiphenylsilane-dehydroepiandrosterone (**26**) is the internal standard used for the mmol calculated from per-O-TMS-sugars (left) and the ^{29}Si NMR of this IS on the right.

The novel internal standard, 3-*O*-*tert*-butyldiphenylsilane-dehydroepiandrosterone (**26**), was added to a mixture of three replicate samples: α-per-*O*-TMS glucose (**14**), β-per-*O*-TMS fructose (**16**), and per-*O*-TMS sucrose (**20**). These three compounds **14**, **16**, and **20** were synthesized from free sugar as a 1:1:1 ratio and used in this study as 1 mixture containing 3 compounds. The mmol calculated from the signal of each compound are shown in Table 3.5. The calculated millimoles (mmols) obtained from the silicon signal using Equation 3.2 in page 340, were twice the amount of the target mmols from the mixture. For example, the calculated mmol using Si2 for per-*O*-TMS sucrose (**20**), β-per-*O*-TMS fructose (**16**), and α-per-*O*-TMs glucose (**14**) in experiment 1 were 0.027, 0.0247, and 0.025, while the anticipated mmols were 0.018, 0.016, and 0.016 respectively. This pattern was consistent across the triplicate experiments. The half fold increase of the calculated mmol compared to the expected mmol in the sample could be attributed to an error in weighing the oily sample. This discrepancy arises because the mass of the sample

$$\frac{2.10\ (\text{Si2 of } \mathbf{20}\ x\ 6.96\ mg\ (TBDPSi - DHEA)}{526.83\ mg/mmol\ (TBDPSi - DHEA)}\ x\ \frac{1\ mmol\ of\ Si}{1\ mmol\ of\ TBDPsi - DHEA} = 0.027$$

Table 3. 5: The calculated mmol from ^{29}Si NMR integration in a mixture contained α-per-*O*-TMS glucose (**14**), β-per-*O*-TMS fructose (**16**), and per-*O*-TMS sucrose (**20**) with DHEA-TBDPSi (**25**) as internal standard.

Mmol calculated by ^{29}Si Integration Value: TBDPSi-DHEA as Internal Standard (0.0132)									
	Si_2	Si_3	Si_6	Si_1	Si_4	Si_{1f}	Si_{3f}	Si_{4f}	Si_{6f}
Experiment 1:									
Anticipated mmol: Sucrose (0.0185): Fructose (0.0161): Glucose (0.0167)									
Calculated mmol:									
Sucrose	0.0277	0.0310	0.0223	x	0.0281	x	0.0249	0.0269	0.0212
Fructose	0.0247	x	0.0199	0.0186	0.0239				
Glucose	0.0252	0.055	0.0190	0.0234	0.0256				
Experiment 2:									
Anticipated mmol: Sucrose (0.0185): Fructose (0.0161): Glucose (0.0167)									
Calculated mmol:									
Sucrose	0.0267	0.0289	.0223	X	.0274	x	0.0216	0.0262	0.0216
Fructose	0.0239	x	0.0195	0.0188	0.0231				
Glucose	0.0250	0.0241	0.01982	0.0225	0.0252				
Experiment 3:									
Anticipated mmol: Sucrose (0.0184): Fructose (0.0160): Glucose (0.0166)									
Calculated mmol:									
Sucrose	0.0283	.0291	0.0242	X	0.0270	x	0.0256	0.0275	0.0228
Fructose	0.0197	x	0.0215	0.0197	0.0251				
Glucose	0.0263	0.0266	0.0198	0.0235	0.0248				

might be higher due to the vial being removed from the balance each time a sample was taken. The weighing of the vial may not be accurate, raising suspicions about its precision.

When comparing the mmols calculated from experiments 1 to experiment 3, the variations are minimal. Specifically, the variation of Si2 in per-*O*-TMS sucrose (**20**) is ± 0.0011, in per-*O*-TMS glucose (**14**) is also ± 0.0011 and β-per-*O*-TMS fructose (**16**) is ± 0.0040. The small variations observed suggest a high degree of consistency and reliability in the calculated mmols across these experiments. This consistency indicates that the method used for measurement is stable and produces reliable results for the compounds under investigation.

Calculating the percentage error in each experiment assessed the accuracy of using DHEA-TBDPSi as a new internal standard. Analyzing the percent error demonstrates that Si_6 has the lowest percent error among all the signals. However, the values vary significantly between the three compounds within the same experiment and are inconsistent across the three experiments. For instance, in experiment 1, the percent error for per-*O*-TMS sucrose (**20**) is 20%, whereas for α-per-*O*-TMs glucose (**14**) it is 13%. Conversely, in experiment 3, the percent error for per-*O*-TMS sucrose (**20**) rises to 31%. This wide range of error within compounds in the same experiment and across different experiments renders the Si6 signal unsuitable as a diagnostic signal.

Similarly, Si4 also exhibits a broad range of percent error (calculated through equation 3), with variations of 7% to 10% within the same experiment, indicating poor consistency. On the other hand, the percent error for Si2 ranges from 45% to

60% across the three different experiments. However, the error remains relatively consistent within the same experiment, ranging from 4% to 5% difference. For example, in experiment 1, per-*O*-TMS sucrose (**20**) is 49%, α-per-*O*-TMS glucose (**14**) is 50%, and β-per-*O*-TMS fructose (**16)** is 53%. In experiment 3, per-*O*-TMS sucrose (**20**) is 53%, β-per-*O*-TMS fructose (**16**) is 54%, and α-per-*O*-TMS glucose (**14**) is 58%. Analyzing these percentage errors, it is reasonable to assert that Si2 provides more consistent integration values and can be utilized as a diagnostic signal. The analysis of percentage errors highlights that Si2 exhibits greater consistency in integration values, making it a suitable diagnostic signal. Conversely, Si6 and Si4 demonstrate wide variations in percent error, both within the same experiment and across different experiments, rendering them less reliable for diagnostic purposes.

Equation 3.3: Percent Error Calculation

$$percent\ error = \frac{actual\ mmol - calculated\ mmo}{actual\ mmol}\ x\ 100$$

$$50.8\% = \frac{0.0167 - 0.0252}{0.0167}\ x\ 100$$

3.2.6 Calculated the Mmol of Per-*O*-TMS Trehalose From Si Integration of Individual NMR Experiment With 3-*O*-Tert-Butyldiphenylsilane-Dehydroepiandrosterone as Internal Standard.

It has been illustrated that the calculated ratios of integration closely agree with the molar ratios of the reaction mixtures, as discussed in sections 3.2.2 Furthermore, the mmol calculated ratio or integration ratio of each weighted sample in section 3.2.3 also supports this finding. However, the results obtained from the mmol calculations in sections 3.2.3 indicate the presence of systematic errors in the preparation or measurement processes. As a result, a change in the internal standard

was implemented, as outlined in section 3.2.4. This change led to better results, with a lower percentage of error compared to using HMDS as the internal standard. Nonetheless, the percentage of errors remained considerable, prompting us to conduct additional studies to investigate the sources of these additional errors.

The search to validate the utility of ^{29}Si NMR integration as a quantification method further intensified by refocusing on a single sample with a precisely known weight (mass), thereby eliminating any potential ambiguities. To conduct this experiment, a carefully measured mass of a solid sample is required. As demonstrated previously in the above experiments, the oily sample was weighed by mass difference leading to large error in the calculation.

There is a choice from a total of twelve per-*O*-silylated compounds investigated in this project, comprising four monosaccharides, two disaccharides, three free sugar alcohols, two trisaccharides, and one tetrasaccharide. Notably, among these twelve compounds, per-*O*-TMS trehalose (**21**) and per-*O*-TMS stachyose (**24**) were found to be in solid form. For the per-*O*-TMS trehalose (**21**) samples, three replicate measurements were conducted; involving the precise weighing of each sample followed by the addition of the internal standard, DHEA-TBDPSi (**25**), and subsequent ^{29}Si NMR experiment. From the integration, the calculated millimoles (mmol) were derived from Equation 3.2 as shown below and data shown in Table 3.6.

$$\frac{2.22\ (\text{Si2 of } \mathbf{21})\ x\ 13.17\ mg\ (TMS-DHEA)}{360.61\ \frac{mg}{mmol}\ (TMS-DHEA)}\ x\ \frac{1\ mmol\ of\ Si}{1\ mmol\ of\ TMS-DHEA}$$

$$= 0.0555\ mmol\ of\ 2Si$$

$$\frac{0.055}{2}\ (2\ Si\ in\ 1\ signal) = \ 0.0277$$

Note: In 1 atom of Si2 or Si2', the mmol is 0.0227

Table 3.6: The calculated mmol from ^{29}Si NMR integration of per-*O*-TMS trehalose (**21**) using DHEA-TBDPSi (**25**) was used as internal standard. The experiments were carried out as 1:1, 0.5:1 and 0.25:1 ratio of per-*O*-TMS trehalose (**21**) to DHEA-TBDPSi (**25**)

mmol Calculated by ^{29}Si NMR: *TBDPSi-DHEA as Internal Standard (0.0250)*				
Compounds	Si_4, $Si_{4'}$	Si_3, Si_3	Si_6, Si_6	Si_2, Si_2
	Experiment 1: 0.0249 mmol Trehalose			
Trehalose	0.0555 (0.0277)	0.0577 (0.0288)	0.0505 (0.0252)	0.0555 (0.0277)
	Experiment 2: 0.0126 mmol Trehalose			
Trehalose	0.0227 (0.0113)	0.0272 (0.0136)	0.0190 (0.0095)	0.0220 (0.0110)
	Experiment 3: 0.00635 mmol Trehalose			
Trehalose	0.0107 (0.00537)	0.0130 (0.00650)	0.0100 (0.0050)	0.0112 (0.00562)

Table 3.7: The percent error from ^{29}Si NMR integration of per-*O*-TMS trehalose (**21**) using DHEA-TBDPSi (**25**) was used as internal standard. The experiments were carried out as 1:1, 0.5:1 and 0.25:1 ratio of per-*O*-TMS trehalose (**21**) to DHEA-TBDPSi (**25**)

% Error Calculated by ^{29}Si NMR: *TBDPSi-DHEA as Internal Standard (0.0250)*				
Compounds	Si_4, $Si_{4'}$	Si_3, Si_3	Si_6, Si_6	Si_2, Si_2
	Experiment 1: Actual mmol 0.0249			
Trehalose	11%	15%	1.3%	11%
	Experiment 2: Actual mmol 0.0126			
Trehalose	12%	8%	24%	9%
	Experiment 3: Actual mmol 0.00635			
Trehalose	15%	2%	21%	11%

Furthermore, the mmol values obtained from each of the three experiments exhibited a narrow range, despite differing mole ratios between the compound of interest and the internal standard. The ratios observed throughout these experiments remained consistent, with ratios of 1:1, 0.5:1, and 0.25:1 being used. Notably, the mmol calculated from the integration closely mirrored the ratio of the internal standard, similar to the actual mmol values. In Table 3.6, show the mmol calculated from each signal the number in the parentheses is the mmol of one Si signal. It was previous stated that trehalose is a symmetrical dissacharide, with only 4 signals representing 8 Si atoms per mol, therefore the number on the left is for two mol of in the signal Si, but the number inside the parentheses is per one mole.

The results from all three experiments indicate a consistent trend of underestimation in the calculated mmol values for Si4 when compared to the true values. This trend is observed in Experiment 1 (0.0277 vs. 0.0249), Experiment 2 (0.0113 vs. 0.0126), consistently show a lower value for Si4 mmol, suggesting a systematic underestimation. On the other hand, the calculated mmol values for Si3 tend to be higher than the true values in all three experiments. This pattern observed in Experiment 1 (0.0288 vs. 0.0249), Experiment 2 (0.0136 vs. 0.0126), and Experiment 3 (0.00650 vs. 0.00635). In contrast to Si4, these results indicate a consistent overestimation of Si3 mmol in the ^{29}Si NMR signal measurement. However, the calculated mmol values for Si6 appear to be relatively close to the true values across the experiments, with minor variations. There seems to be a consistent relationship or ratio between the mmol values of Si2 and Si4 throughout all three experiments. For instance, in Experiment 1, the calculated mmol value for Si_4

(0.0277) is the same as the mmol value for Si2. Similar mmol values are also observed in Experiment 2 and 3, as shown in Table 3.6. Overall, Si4 and Si2 exhibit a comparable chemical environment, as their integration values consistently demonstrate similarity across the experiments. They also share similar signal sensitivity, leading to both being consistently underestimated during the integration process.

As expected, since the mmol values are closer, the percentage error is also smaller. The percentage error has decreased from 50-60% to 10-15%, Table 3.7 when using a solid study sample. When comparing the percentage error between the mixtures and per-*O*-TMS-glucose (**14**), where the sample was in the form of oil/gel, to a solid sample like per-*O*-TMS-trehalose (**21**), the error reduction was significant. The difference in percentage error indicates that the large error generated was due to the weighing of the oil/gel sample compared to weighing a solid sample. This suggests that weighing a sample by difference could lead to more errors than weighing a solid sample on the scale.

When comparing the percentage errors of all four signals, it becomes evident that Si4 and Si2 exhibit more consistent percentage errors, ranging from 11% to 15% and 9% to 11% for Si4 and Si2, respectively (refer to Table 3.7 for details). On the other hand, Si3 and Si6 display inconsistent percentage errors with a wide range of values for both signals (Table 3.7). The observed percentage errors align with the calculated mmol trend, indicating that Si4 and Si2 share a similar chemical environment or experience a similar systematic error. However, since these signals originate from the same compound and the integration measurements for each signal are based on the same distance in ppm, this eliminates the possibility of a systematic

error. This leads us to consider the chemical environment of Si4 and Si2, which generate the same sensitivity in the magnetic field. The chemical environment plays a crucial role in NMR integration, as it directly influences the observed signal intensities and the integration values obtained from the NMR spectrum. The integration values are used to deduce the relative concentrations and ratios of nuclei in various chemical environments, thereby explaining the similarity in the calculated mmol values for Si4 and Si2.

3.2.7 Calculating the Mmol of Per-*O*-Silylated-Trehalose (**21**) From Si Integration Individual Run NMR Experiment With 3-*O*-Trimethylsilane-Dehydroepiandrosterone (**25**) as Internal Standard.

To investigate the variation in percent error observed previously, an additional internal standard was examined. The purpose was to ascertain whether the variation (percent error) originated from the lack of fewer protons for polarization transfer in DEPT experiment when use 3-*O*-tert-butyldiphenylsilane-dehydroepiandrosterone (**26**) as internal standard. This internal standard only has one $^{2}J_{\mathrm{Si,H}}$ coupling proton, unlike of the *O*-TMS sugars, which possesses nine $^{2}J_{Si\text{-},H}$ coupling protons from three methyl groups. It was suspected that the $^{2}J_{Si\text{-},H}$ coupling proton in silicon NMR could potentially impact the line shape, signal broadening, relaxation rates, and relative intensities of the NMR signals. These factors can introduce errors during integration measurements and calculations of mmol. To address this concern, a new internal standard, 3-*O*-trimethylsilane-dehydroepiandrosterone (Figure 3.14), an internal standard that poses nine $^{2}J_{Si\text{-},H}$ coupling protons from the methyl groups like the *O*-TMS sugars, was utilized. However, it is worth noting that the signal for 3-*O*-trimethylsilane-

dehydroepiandrosterone appears in the same region (15.55 pm) as the signals of interest in the per-*O*-silylated sugars study. However, it showed in Chapter 2 that the signal generated from **25** did not overlap with any of the silylated sugars in the mixtures studied.

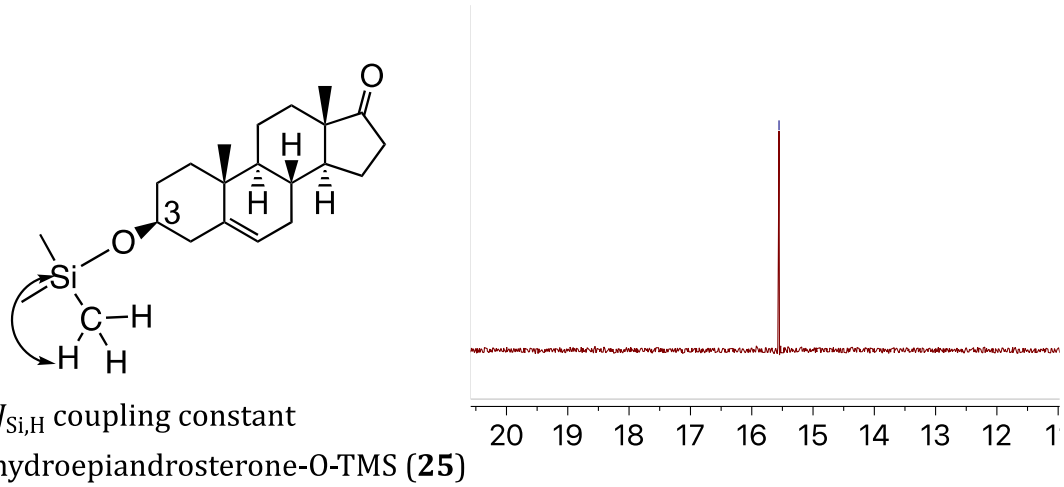

$^{2}J_{Si,H}$ coupling constant

dehydroepiandrosterone-O-TMS (**25**)

Figure 3.14: 3-*O*-trimethylsilane-dehydroepiandrosterone (**25**) is the internal standard used for the mmol calculated from per-*O*-TMS trehalose (**21**) and the ^{29}Si NMR of this IS.

The internal standard, 3-*O*-trimethylsilane-dehydroepiandrosterone, was synthesized in our laboratory using the same procedure employed for the silylated sugar. However, this compound is also commercially available and can be purchased through Sigma Aldrich. For the NMR experiments, three samples were prepared, and the sample preparation process followed the same method as previously described. Each sample was individually weighed, and an internal standard was added. The spectra obtained from the experiments were then integrated and calculated for mmol using Equation 3.2.

The ^{29}Si NMR analysis yielded mmol values that reflect the relative amount of per-*O*-silylated trehalose in the sample. The true mmol values for Experiment 1, 2,

and 3 in Table 3.8 were determined as 0.0247 mmol, 0.0246 mmol, and 0.0246 mmol, respectively. By integrating the obtained spectra, it was possible to identify the presence of Si4, Si2, Si6, and Si3 signals in varying amounts across the experiments. Table 3.9 displays the calculated mmol values for Si2, Si4, Si6 and Si3.

Upon analyzing and comparing the data, it becomes evident that the true values remained consistent across all three experiments. For instance, the mmol calculated for Si2 were 0.0257, 0.0271, and 0.0271 for Experiment 1, 2, and 3, respectively, indicating the reliability of the measurement technique. Similarly, the mmol values for Si4, Si6, and Si3 were consistently observed in all three experiments (see Table 3.8), suggesting their stability within the sample. Although there were slight variations in the mmol values for Si3, the overall trend indicates relative consistency. Notably, experiment 1 exhibited an offset in all mmol calculations. Consistent with previous findings, Si2 and Si4 displayed more consistent results compared to Si3. However, the utilization of the new internal standard resulted in more accurate and consistent mmol calculations for Si6, with values of 0.0241, 0.0244, and 0.0242 for Experiment 1, 2, and 3, respectively. These findings provide valuable insights into the composition of silicon species in the sample highlight the stability and consistency of the ^{29}Si NMR analysis technique.

When analyzing the percentage error for each experiment, the average of all signals was calculated, and the percent error was determined (Table 3.8). Interestingly, the percent errors for Experiment 2 and 3 are in close agreement, with values of 8.13% and 8.09% respectively, while Experiment 1 shows a slightly higher percent error of 9.74%. Nonetheless, the percentage errors for all three experiments

Table 3.8: The calculated mmol from ^{29}Si NMR integration of per-*O*-TMS-trehalose (**21**) using DHEA-*O*-TMS (**26**) as internal standard. The experiments were carried out as 1:1 ratio of per-*O*-TMS-trehalose (**21**) to DHEA-*O*-TMS (**26**). The percentage error of each experiment is shown in the right column and each signal shown at bottom.

mmol Calculated by ^{29}Si NMR: *TBDPSi-DHEA as Internal Standard (0.0250)*						
Compounds	Si_4, $Si_{4'}$	Si_3, Si_3	Si_6, Si_6	Si_2, Si_2	Average	% Error
	Experiment 1:		*0.0247 mmol*			
Trehalose	0.0292	0.0288	0.0241	0.0257	0.0269	9.74%
	Experiment 2:		*0.0246 mmol*			
Trehalose	0.0281	0.0267	0.0244	0.0271	0.0266	8.13%
	Experiment 3:		*0.0246 mmol*			
Trehalose	0.0286	0.0269	0.0242	0.0271	0.0269	8.09%
Average	0.0286	0.0272	0.0242	0.0266		
% Error	16%	11.0%	1.17%	8.00%		

$$\frac{2.02\ (\text{Si2 of } \mathbf{21}\ x\ 9.21\ mg\ (TMS-DHEA)}{360.61\ mg/mmol\ (TMS-DHEA)}\ x\ \frac{1\ mmol\ of\ Si}{1\ mmol\ of\ TMS-DHEA} = 0.0515$$

$$\frac{0.0515}{2}(2\ Si\ in\ 1\ signal) = 0.0257$$

$$4.04\% = \frac{0.0247 - 0.0257}{0.0247}\ x\ 100$$

can still be considered relatively low. Furthermore, the percentage error was calculated for each individual signal by using the average values. It was observed that Si4 had the highest percent error (16%), while Si6 exhibited the lowest percent error of 1.17%. Interestingly, Si2 showed a similar percentage error to Experiment 2 and 3. This indicates that the integration of Si2 is reliable and consistent across all experiments, suggesting its suitability for accounting for the overall signal of the compound. This information is of great importance to our study, as it consistently demonstrates that Si2 provides reliable integration and can be used as a diagnostic signal.

Furthermore, it is crucial to highlight that the percent error calculated when using 3-*O*-trimethylsilyl-dehydroepiandrosterone (**26**) as the internal standard (8%-9% for Si2) was similar to the percent error obtained when 3-*O*-tert-butyldiphenylsilane-dehydroepiandrosterone used as internal standard (9%-11% for Si2). The spectra including integration can be found in the Supplemental Information on page 382-387 and table for mmol calculated on page 421-426.

3.2.8 Determining the Percent Conversion of α-Per-*O*-TMS Glucose (**14**), β-Per-*O*-TMS Fructose (**16**), and Per-*O*-TMS Sucrose (**20**), Per-*O*-TMS Kestose (**22**), Per-*O*-TMS raffinose (**23**), and Per-*O*-TMS Stachysoe (**24**) Using 3-*O*-Trimethylsilane-Dehydroepiandrosterone (**26**) as Internal Standard.

It has been demonstrated above that DEPT ^{29}Si NMR is a reliable quantification technique. The use of 3-*O*-trimethylsilane-dehydroepiandrosterone (**25**) as an internal standard further supports this idea. To validate the hypothesis of using ^{29}Si NMR and internal standard **25** for quantification, a mixture of six saccharides, including mono, di, tri, and tetra saccharides, was synthesized from free sugar in a

1:1:1:1:1:1:1 ratio with the internal standard. The same silylation method as described above was followed. The sugars included glucose (**2**), fructose (**4**), sucrose (**8**), raffinose (**10**), kestose (**11**), and stachyose (**12**), and DHEA mixed with HMDS and TMSCl in pyridine, stirred for 24 hours, and worked up to obtain an oily sample.

The results from the replicated syntheses demonstrate a 100 percent conversion of reactant to product using the silylation method, as indicated by the ^{29}Si integration value shown in Figure 3.15. The spectrum displays the integration of Si2 from α-per-*O*-TMS glucose (**14**), β-per-*O*-TMS fructose (**16**), per-*O*-TMS sucrose (**20**), per-*O*-TMS kestose (**22**), per-*O*-TMS raffinose (**23**), and per-*O*-TMS stachysoe (**24**), along with Si3 from the internal standard **25**. The spectrum clearly reveals a 1:1:1:1:1:1:1 ratio in the integration of each signal to the internal standard. The chemical shift and integration values for each individual signal are provided in Table 3.9, showing small changes in chemical shifts of the mixture from the pure. All replicates' experiments illustrated the same pattern, and their data can be found at the Supplemental Information section on page 406-411 (spectra) and 427-429 tables.

Table 3.9: The integration and chemical shifts (**δ)** from a reaction mixture synthesized from free sugars to produce α-per-*O*-TMS glucose (**14**), β-per-*O*-TMS fructose (**16**), per-*O*-TMS sucrose (**20**), per-*O*-TMS kestose (**22**), per-*O*-TMS raffinose (**23**), per-*O*-TMS stachysoe (**24**) and DHEA-*O*-TMS (**26**).

Compound	**Si signal**	**Integration**	**δ mixture**	**δ pure**	**Δ**
Glucose (**14**)	2	1.22	17.2242	17.2204	0.0038
Fructose (**16**)	2	1.19	10.7613	10.7358	0.0255
Surcose (**20**)	2'	1.18	17.5278	17.5271	0.0007
Kestose (**22**)	4"	1.23	17.8659*	17.8115	0.0544
Raffinose (**23**)	2"	1.03	17.7103*	17.6907	0.0196
Stachyose (**24**)	2'	1.12	17.5028*	17.4750	0.0278
DHEA (**25**)		1.00	15.5470	15.5425	0.0045

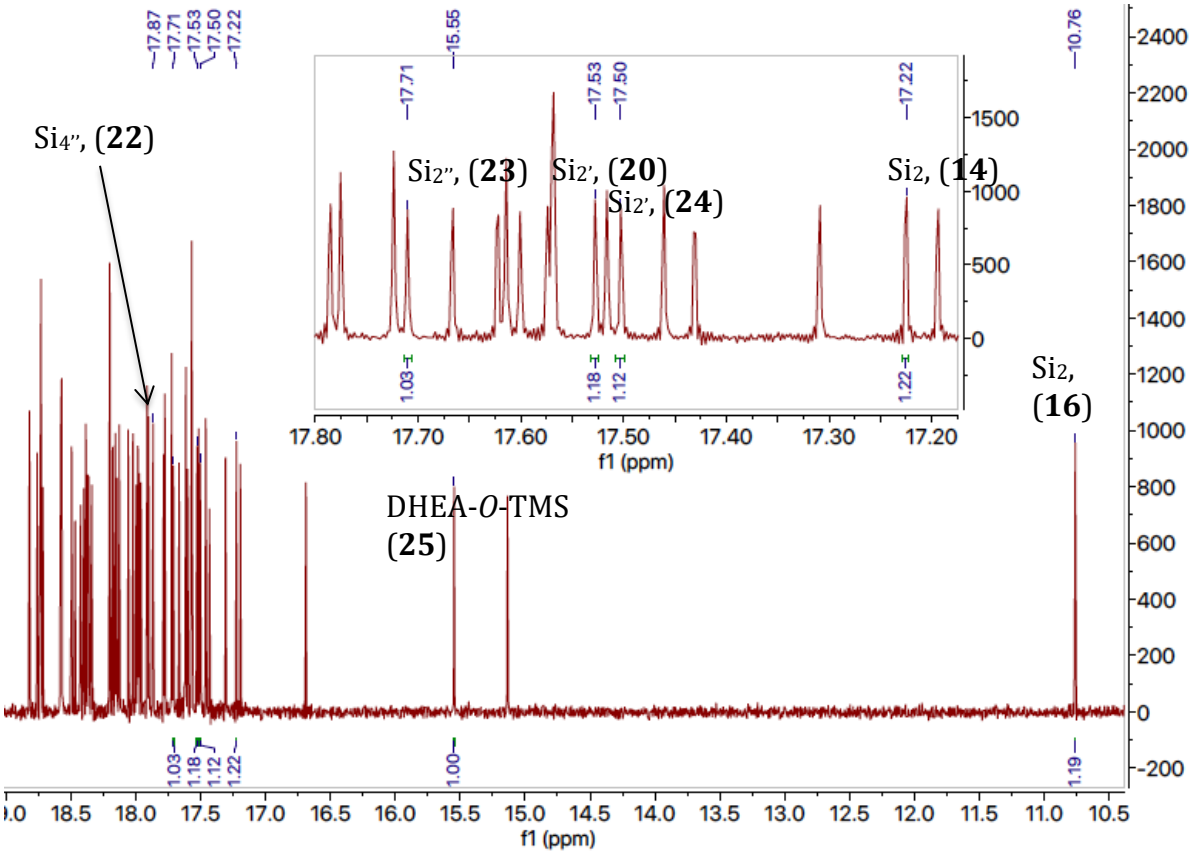

Figure 3.15: ^{29}Si NMR spectrum of α-per-*O*-TMS glucose (**14**), β-per-*O*-TMS fructose (**16**), per-*O*-TMS sucrose (**20**), per-*O*-TMS kestose (**22**), per-*O*-TMS raffinose (**23**), and per-*O*-TMS stachysoe (**24**) with internal standard, DHEA-*O*-TMS (**26**) as a mixture synthesized from free sugar and DHEA.

The difference (**Δ**) in chemical shift between the pure and mixture may be attributed to the variations in concentration. This discrepancy arises from the distinct concentrations of the pure compounds versus mixture, leading to a slight shift. Specifically, the concentration of the pure sample is 0.10 M, whereas in the mixture, the concentration of individual compounds of the mixture is less than 0.10 M. The total concentration of the sample is 0.179 M. The theoretical molar concentration, calculated based on theoretical mmol from each silylated sugar, is 0.030 M, which is three times lower than the concentration calculated from the pure spectrum. Consequently, the chemical shift of the pure compounds vs. mixture exhibits slight

differences. Despite this, certain peaks, as shown, remain identifiable and can be utilized for integration. The concentration of the solution and the percentage yield were calculated as in Table 3.10 and calculation below.

Table 3.10: The mmol of free sugars and theoretical mmol of the per-silylated sugars use to calculate the theoretical concentration of each individual silylated sugar.

Free sugar	mmol	Silylated sugar	Theoretical mmol	Theoretical mass (mg)
glucose (**2**)	0.0152	**14**	0.0152	8.20
fructose (**4**)	0.0153	**16**	0.0153	8.26
sucrose (**8**)	0.0155	**20**	0.0155	14.26
kestose (**10**)	0.0144	**22**	0.0144	18.74
raffinose (**11**)	0.0150	**23**	0.0150	17.95
stachyose (**12**)	0.0152	**24**	0.0152	25.37
DHEA	0.0151	**24**	0.0151	5.44
Total	0.0905		0.0905	98.22

Percent yield = $\frac{77.9\ mg}{98.22\ mg}\ x100$ = 79%

Total Concentration = 0.0905 x 0.793 (percent yield) = 0.0717/0.4 mL =<u>0.179 M</u>

Individual = (0.0152 *0.793) = 0.0120/0.4 mL = <u>0.030 M</u>

To further validate the capability of DEPT ^{29}Si NMR as a quantification method, a known equivalent of compound **26** was introduced into the solution, and its integration was examined. As anticipated, the integration of internal standard **26** was found to be double (Table 3.11) compared to the other signals from the sugar mixture. Given our precise knowledge of the quantity of internal standards incorporated into the sample, the observed integration alteration is in direct proportion to the amount added. The initial synthesis established a 1:1 ratio of each sugar to DHEA, and with a 1 equivalence of **25** added, the doubling of integration unequivocally affirms the reliability of the DEPT ^{29}Si NMR method.

Table 3.11: The integration and chemical shifts (**δ**) from a reaction mixture synthesized from free sugars to produce α-per-*O*-TMS glucose (**14**), β-per-*O*-TMS fructose (**16**), per-*O*-TMS sucrose (**20**), per-*O*-TMS kestose (**22**), per-*O*-TMS raffinose (**23**), and per-*O*-TMS stachysoe (**24**) and additional 1 equiv. of DHEA-*O*-TMS (**26**) added.

Compound	**Si signal**	**Int.**	**Δ mixture**	**δ pure**	**Δ**
O-TMS Glucose (**14**)	2	1.15	17.2261	17.2204	0.0057
O-TMS Fructose (**16**)	2	1.00	10.7632	10.7160	0.0472
O-TMS Surcose (**20**)	2'	1.00	17.5259	17.5271	0.0012
O-TMS Kestose (**22**)	4"	1.09	17.8678*	17.8115	0.0563
O-TMS Raffinose (**23**)	2"	1.01	17.7084*	17.6907	0.0177
O-TMS Stachyose (**24**)	2'	0.99	17.5028*	17.4750	0.0278
O-TMS DHEA (**25**)		2.15	15.5470	15.5425	0.0078

*Indicated chemical shift is not aligned with the pure compound, the possibility of chemical shifts listed are in the upfield and downfield of the pure compound.
Note: Int. → Integration

3.3.0: Conclusion

In summary, the consistent and reliable results obtained through DEPT ^{29}Si NMR underscore its remarkable efficacy in accurately quantifying the presence of substances in a mixture of complex carbohydrates. The study, conducted with a mixture of α-per-*O*-TMS glucose (**14**), β-per-*O*-TMS fructose (**16**), and per-*O*-TMS sucrose (**20**) alongside HMDS as an internal standard, revealed the method's resilience, maintaining mmol ratios even with a calculated mmol deviation of 50%. Notably, the inclusion of a solid internal standard, such as **26**, reduced the error to 20%, and further modifications using a solid silylated sample like per-*O*-TMS trehalose (**21**) with internal standard **26** yielded a remarkable percent error of less than 10%.

The success achieved by employing both solid silyl sugar and a solid internal standard, resulting in a lower percent error in calculated mmol from integration, underscores the reliability of ^{29}Si NMR as a quantification technique for determining

unknown substance amounts in a mixture. Additionally, the utilization of another internal standard, **26**, in a mixture of mono, di, tri, and tetra saccharides during synthesis demonstrated the feasibility and reliability of ^{29}Si NMR signal quantification, confirming the robustness of the method.

In conclusion, the amassed data substantiate the hypothesis that DEPT ^{29}Si NMR serves as a viable alternative for quantifying unknown substance amounts in a mixture. This research marks the first documented instance of using DEPT ^{29}Si NMR signal for quantification, and the reliability of the data supports this innovative approach. Through a thorough literature search, no prior reports of such utilization were found, further emphasizing the novelty and validity of employing DEPT ^{29}Si NMR signal as a quantification method.

3.4.0: Experimental Section

3.3.1: NMR Experimental Method:

All silicon NMR experiments were conducted in deuterated chloroform. Integration was carried out using a 0.01 Hz signal difference for all integration processes. Quantitative experiments were executed with an internal standard of known concentration. The experiments were conducted at room temperature (20-21 °C). The ^{29}Si NMR spectra were recorded using the DEPT pulse sequence for polarization transfer. A pulse length of 180 degrees was used on the f1 channel and 90 degrees on the f2 channel. The pulse lengths were 14 µs and 28 µs respectively. The waltz16 decoupling sequence was applied for a relaxation delay of 2s. The spectra width was 10000 Hz, and 128 scans were performed with an acquisition time of 3.2s.

*3.3.2: Global silylation of per-O-silylated (TMS) mono and disaccharides as mixture stirred at room temperature (mixture of glucose (**2**), fructose (**4**), glucose (**8**)).*

In a 50 mL 2 neck round bottom flask, 91.2 mg (0.510 mmol) of fructose, 91.23 mg of (0.510 mml) of α-glucose and 171.8 mg (0.510 mmol) of sucrose were dissolved in 7.50 mL of pyridine. The flask was purged with argon gas using a balloon followed by addition of 0.96 mL (3 x 3 equiv.) of hexamethyldisilazane and 0.57 mL (3 equiv. x 3) of chlorotrimethylsilane. The solution was stirred at room temperature for 24 hours. After 24 hours, the solution is removed from oil bath and extracted with hexane (50 mL x 3) and rinsed with deionized water (50 mL x 3) then dried over sodium sulfate. The dried organic layer was concentrated to clear oil. ^{29}Si NMR integration ratio shown 1:1:0.98 for per-*O*-TMS-sucrose (**20**): α-per-*O*-TMS-glucose (**14**): per-*O*-TMS-fructose (**16**). Percent yield is 92%.

*3.3.3: Global silylation of per-O-silylated (TMS) mono and disaccharides as mixture stirred at room temperature (glucose (**2**), fructose (**4**), sucrose (**8**), raffinose (**10**), kestose (**11**), stachyose (**12**), and DHEA).*

Trial 1:

In a 20 mL 2 neck round bottom flask, 2.73 mg (0.0152 mmol) glucose (**2**), 2.75 mg (0.0153 mmol) fructose (**4**), 5.33 mg (0.0155 mmol) sucrose (**8**), 7.60 mg (0.0150 mmol) raffinose (**10**), 7.61 mg (0.0144 mmol) kestose (**11**), 10.10 mmg (0.0152 mmol) stachyose (**12**), and 4.35 mg (0.0151 mmol) of DHEA dissolved in 0.40 mL of pyridine. The flask was purged with argon gas using a balloon followed by addition of 0.120 mL (3 x 3 equiv.) of hexamethyldisilazane and 0.07 mL (3 equiv. x 3) of chlorotrimethylsilane. The solution was stirred at room temperature for 24 hours. After 24 hours, the solution was removed from oil bath and extracted with hexane (5

mL x 3) and rinsed with deionized water (5 mL x 3) then dried over sodium sulfate. The dried organic layer was concentrated to clear oily. ^{29}Si NMR integration ratio shown 1:1:1:1:1:1:1 ratio of α-per-*O*-TMS glucose (**14**): β-per-*O*-TMS fructose (**16**): per-*O*-TMS sucrose (**20**): per-*O*-TMS raffinose (**22**): per-*O*-TMS kestose (**23**): and per-*O*-TMS stachysoe (**24**): per-*O*-TMS DHEA (**26**). The percent yield is 79%.

Trial 2:

The following table included the mass of each sugar used and its mmols. The HMDS (0.12 mL) and TMSCl (0.07 mL) in 0.7 mL of pyridine were added. The percent yield is 67%.

Table 3.12: Mass and theoretical mass of free sugars and per-*O*-silylated (TMS) in mg used in synthesis trail 2.

Free sugar	**mg**	**mmol**	**Theoretical mmol**	**Theoretical mass (mg)**
glucose (**2**)	2.67	0.0148	0.0148	8.03
fructose (**4**)	2.67	0.0148	0.0148	8.03
sucrose (**8**)	5.27	0.0154	0.0154	14.13
raffinose (**10**)	7.28	0.0144	0.0144	17.71
kestose (**11**)	7.36	0.0146	0.0146	18.98
stachyose (**12**)	10.14	0.0153	0.0153	25.56
DHEA (**25**)	4.30	0.0149	0.0149	5.37
Total		0.104	0.104	97.81

Trial 3:

The following table included the mass of each sugar used and its mmols. The HMDS (0.12 mL) and TMSCl (0.07 mL) in 0.7 mL of pyridine were added. The percent yield is 90%.

Table 3.13: Mass and theoretical mass of free sugars and per-*O*-silylated (TMS) in mg used in synthesis trail 3.

Free sugar	**mg**	**mmol**	**Theoretical mmol**	**Theoretical mass (mg)**
glucose (**2**)	2.75	0.0153	0.0153	8.26
fructose (**4**)	2.80	0.0155	0.0155	8.41
sucrose (**8**)	5.30	0.0155	0.0155	14.21
raffinose (**10**)	7.71	0.0153	0.0153	18.75
kestose (**11**)	7.70	0.0153	0.0153	19.83
stachyose (**12**)	10.30	0.0155	0.0155	25.89
DHEA (**25**)	4.35	0.0151	0.0151	5.44
Total		0.108	0.108	100.79

3.3.4: Silylation DHEA-TBDPO.

This compound was synthesized by Matthew Orellana in Dr. Jacquelyn Gervay-Hague Laboratory as part of his dissertation.[40]

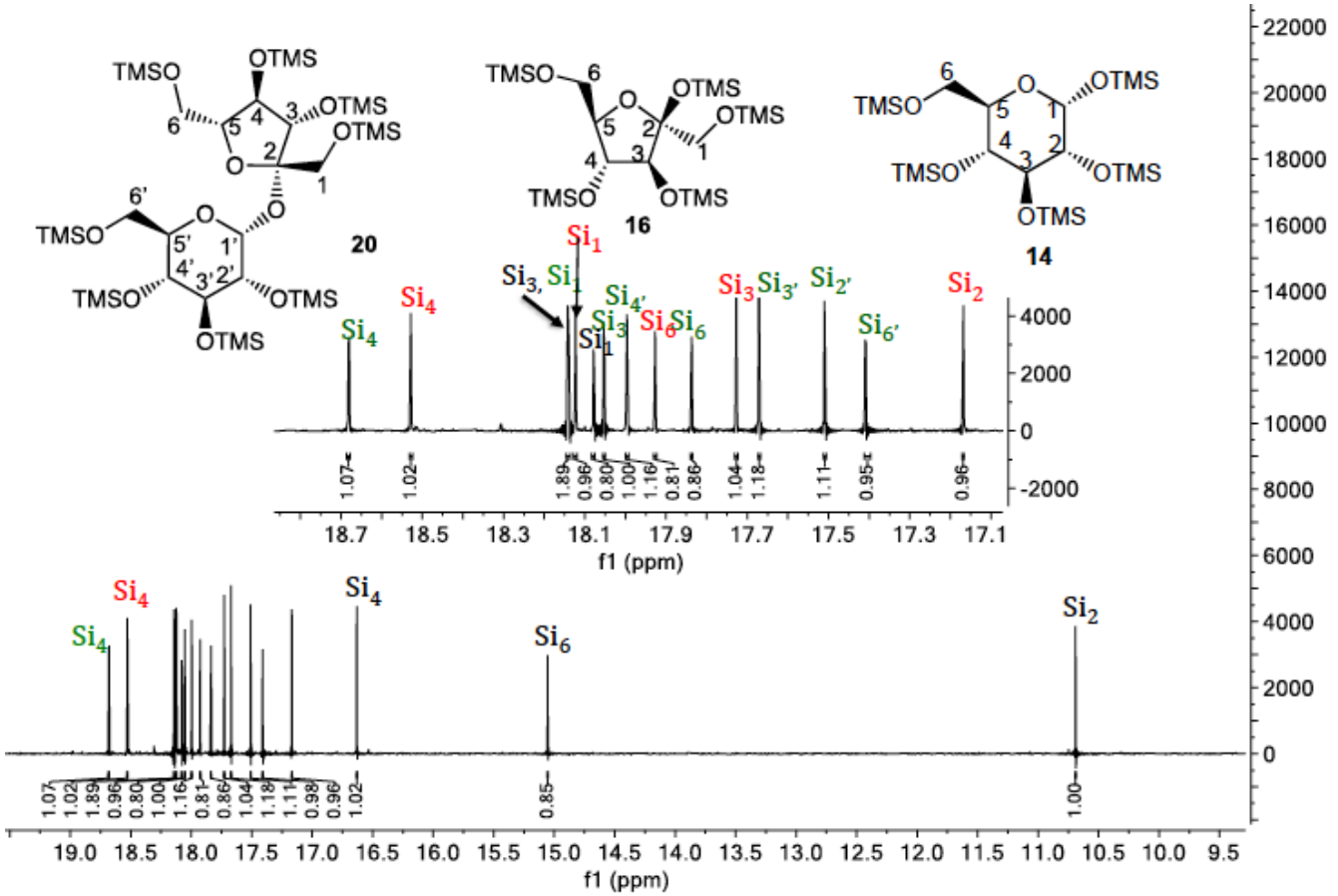

SI-Figure 3.1: ^{29}Si NMR spectrum of a reaction mixture stirred at room temperature for 24 h containing α-per-*O*-TMS glucose (**14**), β-per-*O*-TMS fructose (**16**), and per-*O*-TMS sucrose (**20**) in $CDCl_3$. The reaction started as equal mole (1:1:1) of α-glucose, β-fructose, and sucrose. Color code represent

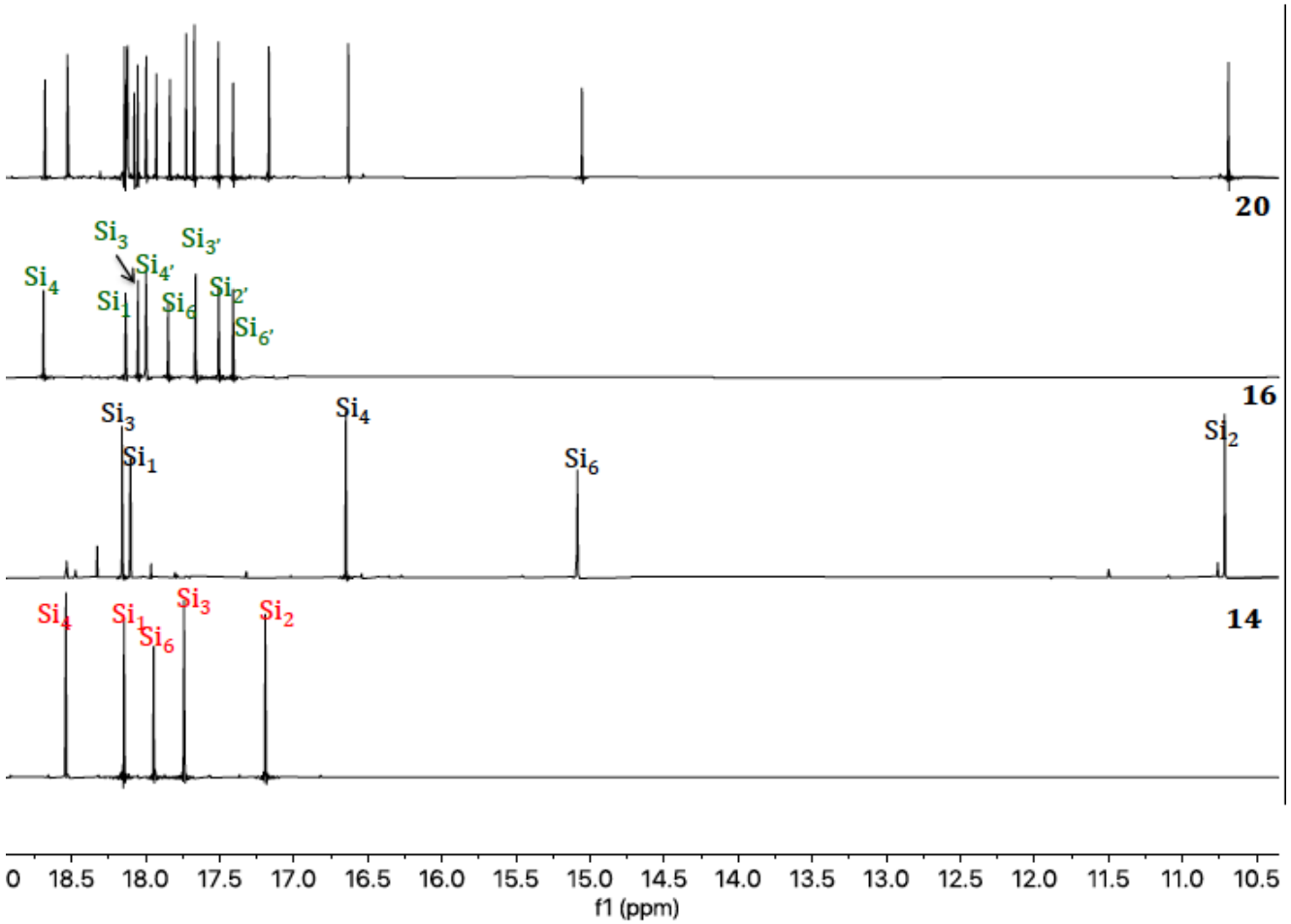

SI-Figure 3.2: An Overlap spectrum is ^{29}Si NMR of a reaction mixture containing α-per-*O*-TMS-glucose, β-per-*O*-TMS-fructose, and per-*O*-TMS-sucrose in $CDCl_3$ stirred at room temperature for 24 hours with pure ^{29}Si spectra of per-*O*-TMS sucrose (**20**), β-per-*O*-TMS fructose (**16**), and α-per-*O*-TMS glucose (**14**) respectively.

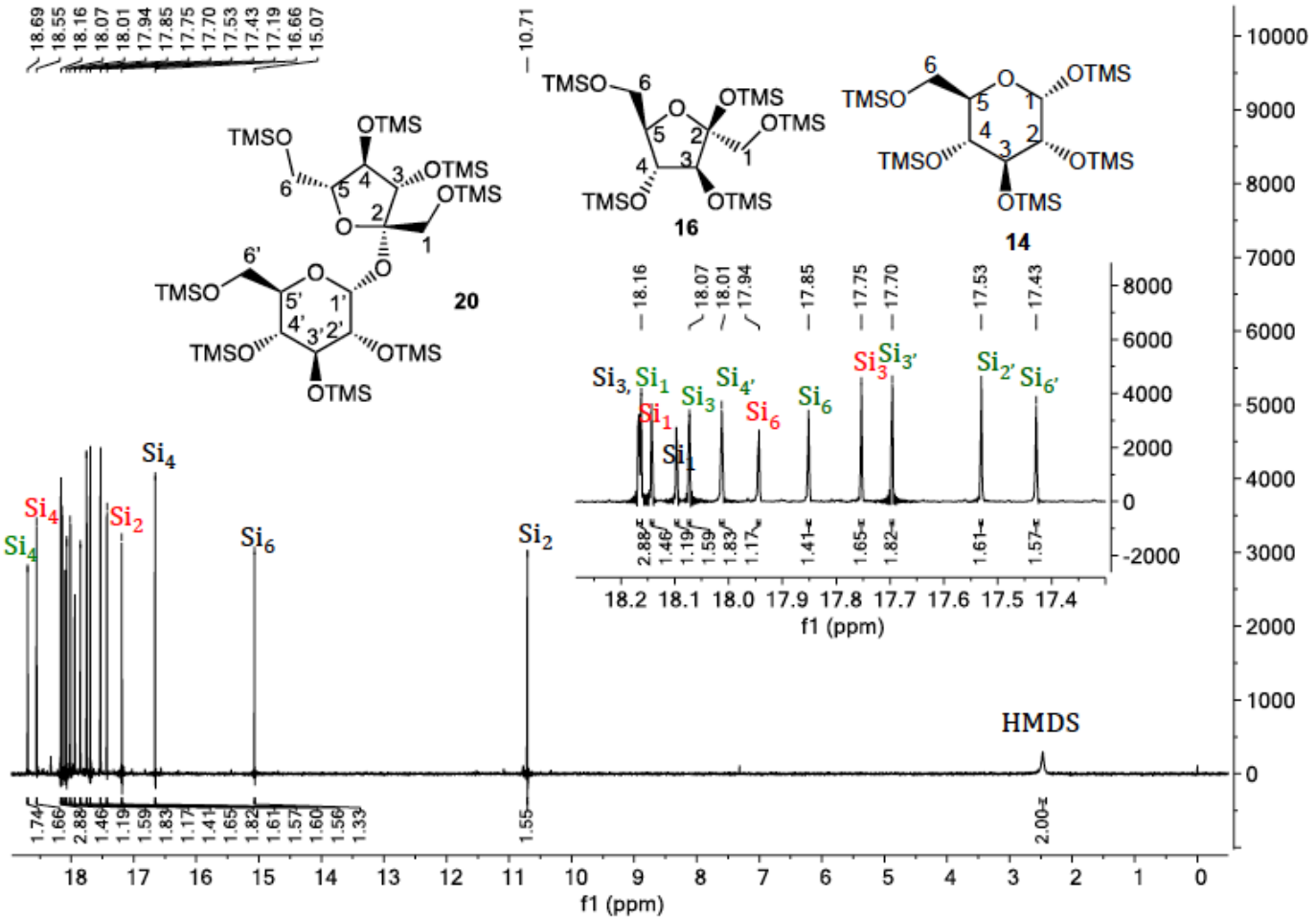

SI-Figure 3.3: (Triplicate 1: Section 3.2.3): ^{29}Si NMR spectrum and integrations of a mixture containing equal mole (1:1:1:1) of α-per-*O*-TMS glucose (**14**): β-per-*O*-TMS fructose (**16**): per-*O*-TMS sucrose (**20**) in $CDCl_3$ and HMDS used as internal standard. The sugars were mixture from reaction and added HMDS as internal standard for the integration values.

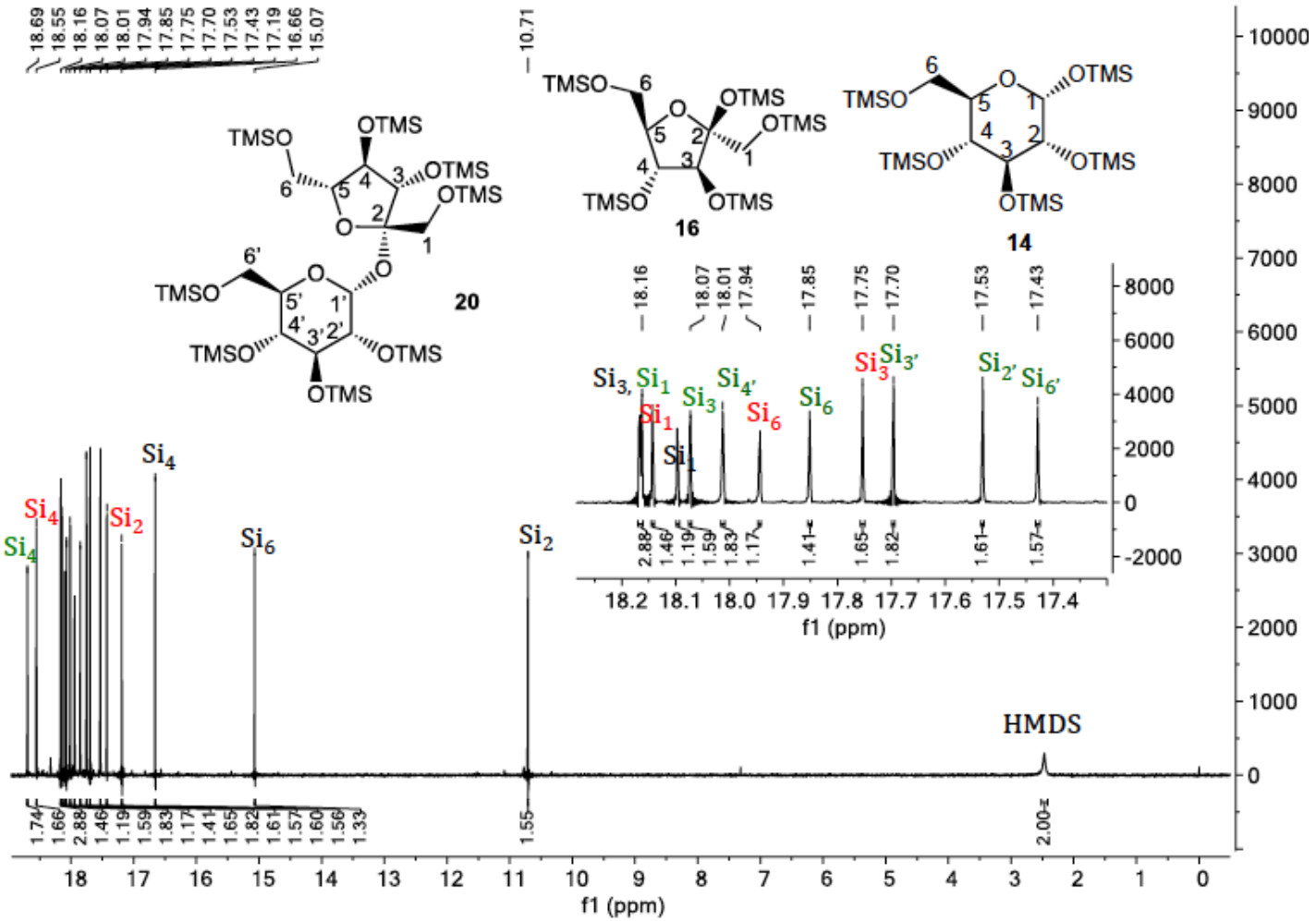

SI-Figure 3.4: (Triplicate 2: Section 3.2.3): ^{29}Si NMR spectrum and integrations of a mixture containing equal mole (1:1:1:1) of α-per-*O*-TMS glucose (**14**): β-per-*O*-TMS fructose (**16**): per-*O*-TMS sucrose (**20**) in $CDCl_3$ and HMDS used as internal standard. The sugars were mixture from reaction and added HMDS as internal standard for the integration values.

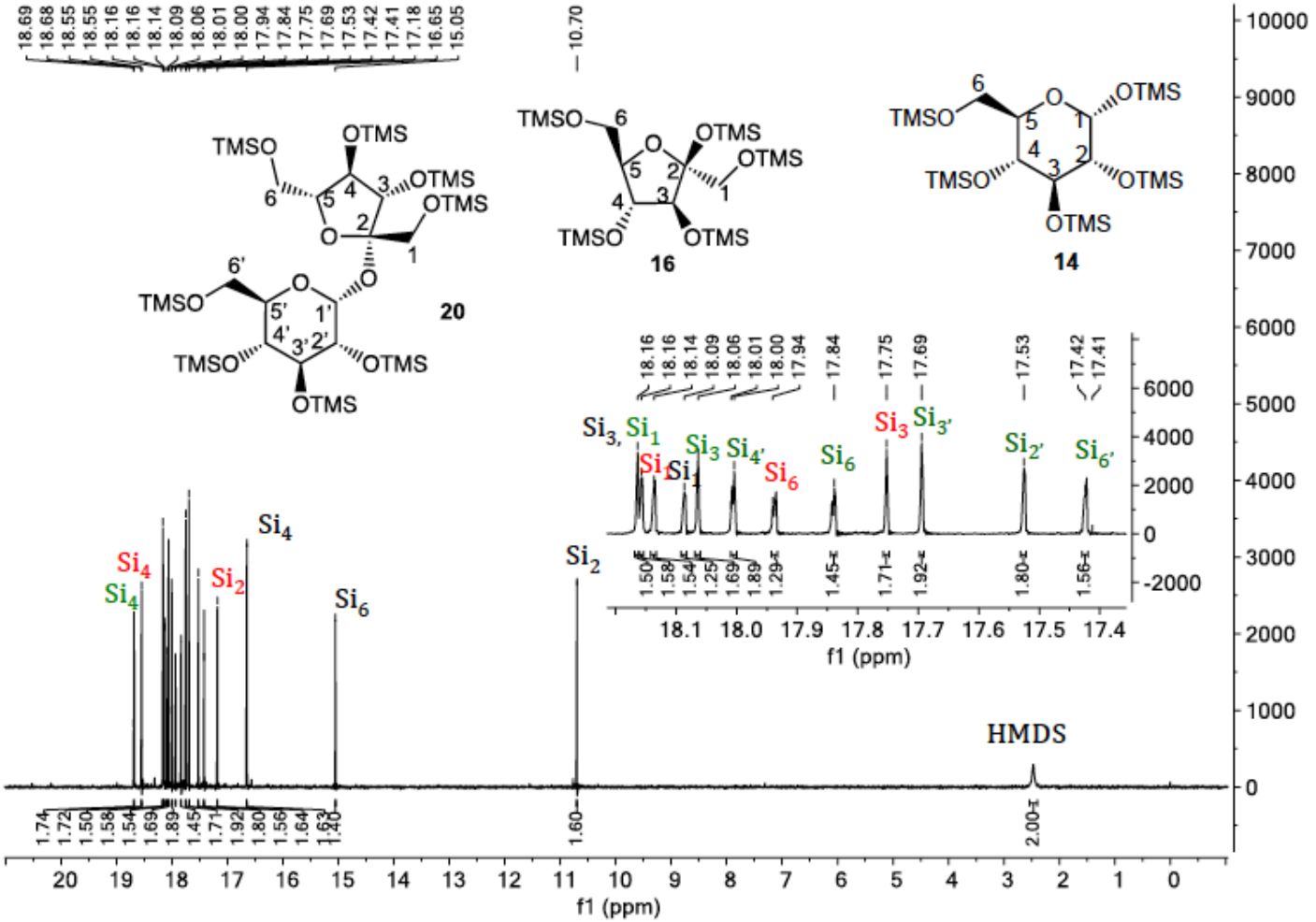

SI-Figure 3.5: (Triplicate 3: Section 3.2.3): ^{29}Si NMR spectrum and integrations of a mixture containing equal mole (1:1:1:1) of α-per-*O*-TMS glucose (**14**): β-per-*O*-TMS fructose (**16**): per-*O*-TMS sucrose (**20**) in $CDCl_3$ and HMDS used as internal standard. The sugars were mixture from reaction and added HMDS as internal standard for the integration values.

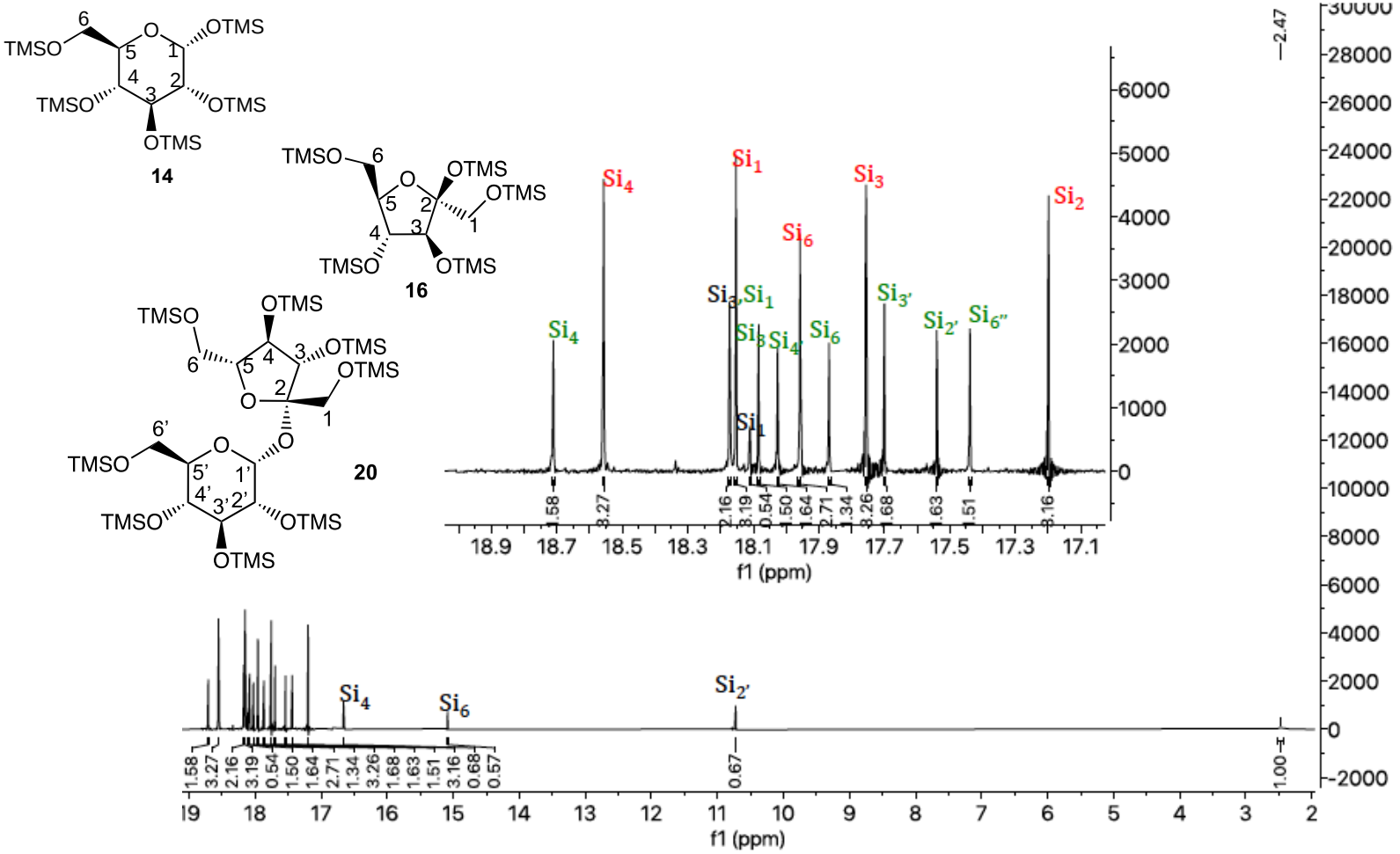

SI-Figure 3.6: (Triplicate 1-section 3.2.4) ^{29}Si NMR of three different sample α-per-*O*-TMS glucose (**14**)-label red (0.10 M), β-per-*O*-TMS fructose (**16**)-label black (0.025 M), and per-O-TMS sucrose (**20**)-label green (0.050 M) in $CDCl_3$ with HMDS used as internal standard. All peaks integrate respect to HMDS as base reference of 1.00.

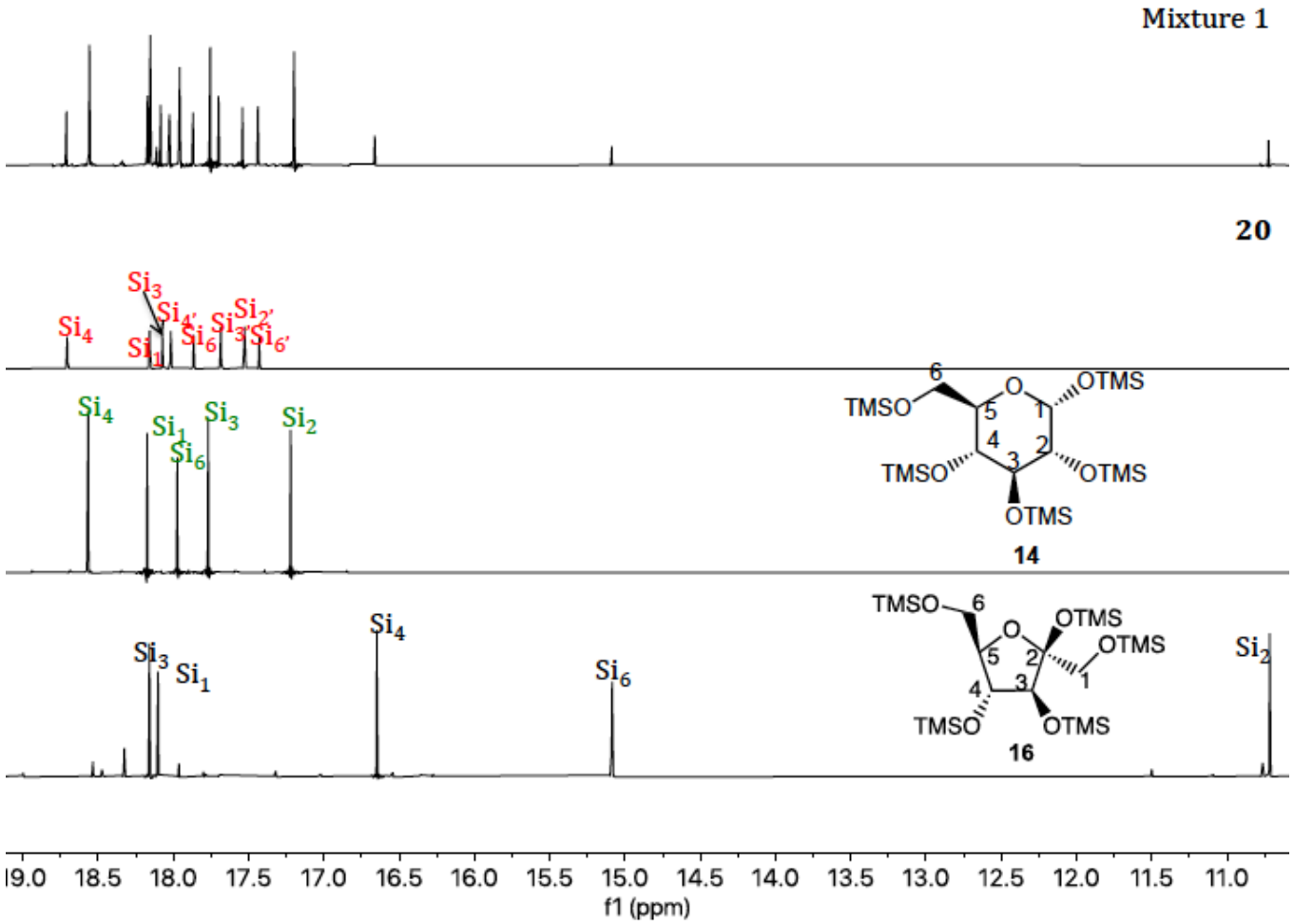

SI-Figure 3.7: (Triplicate 1-section 3.2.4) Three different sample α-per-*O*-TMS glucose (**14**): β-per-*O*-TMS fructose (**16**): per-*O*-TMS sucrose (**20**) in $CDCl_3$ with different concentration stacked with pure sample. The chemical shifts in the mixture are confirmed to be the same value as in the pure sample.

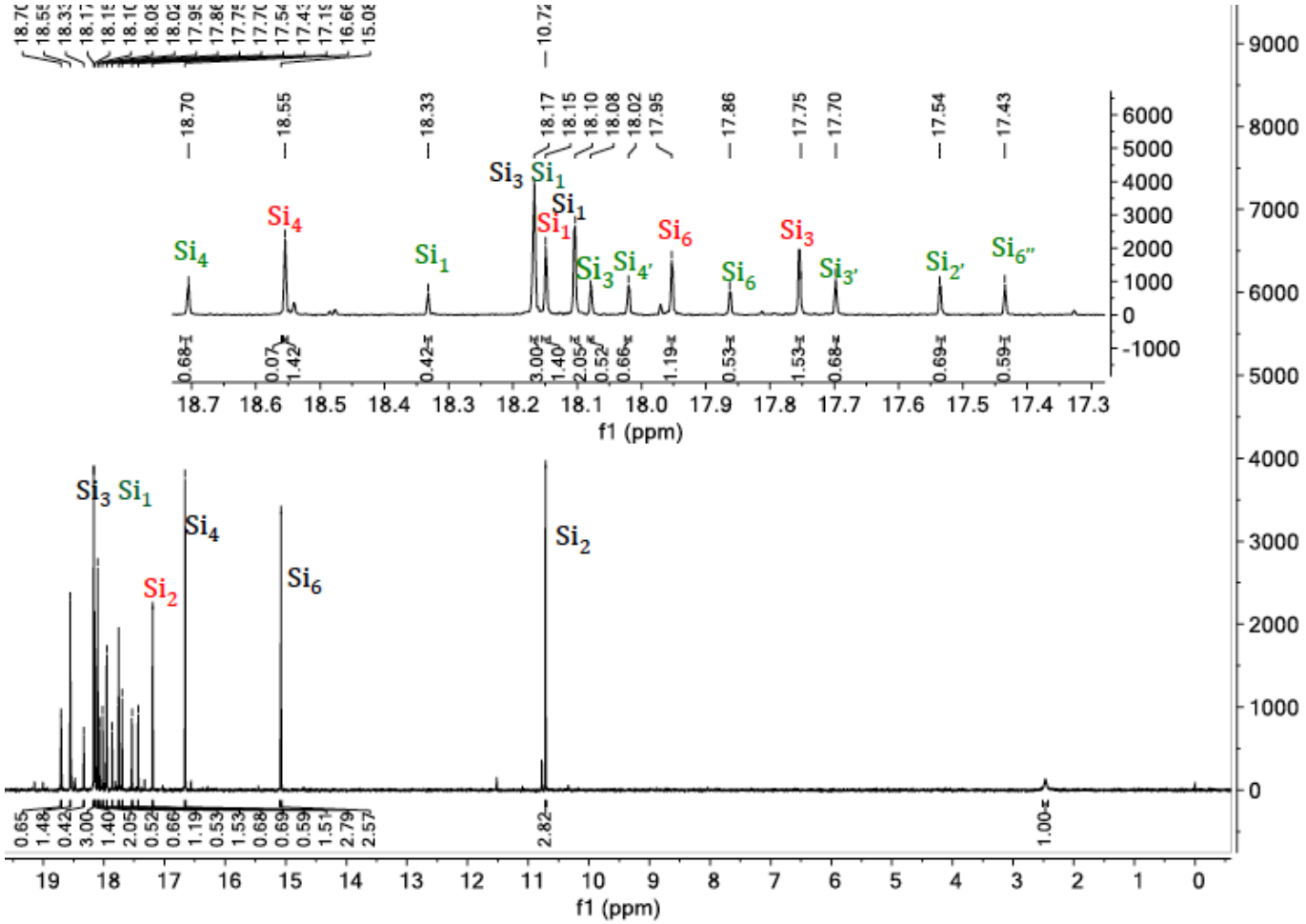

SI-Figure 3.8: (Triplicate 2-section 3.2.4): ^{29}Si NMR of three different samples α-per-*O*-TMS glucose (**14**)-red (0.050 M), β-per-*O*-TMS fructose (**16**)-black (0.10 M), and per-O-TMS sucrose (**20**)-green (0.025 M) in $CDCl_3$ with HMDS used as internal standard. All peaks integrate respect to HMDS as base reference 1.00.

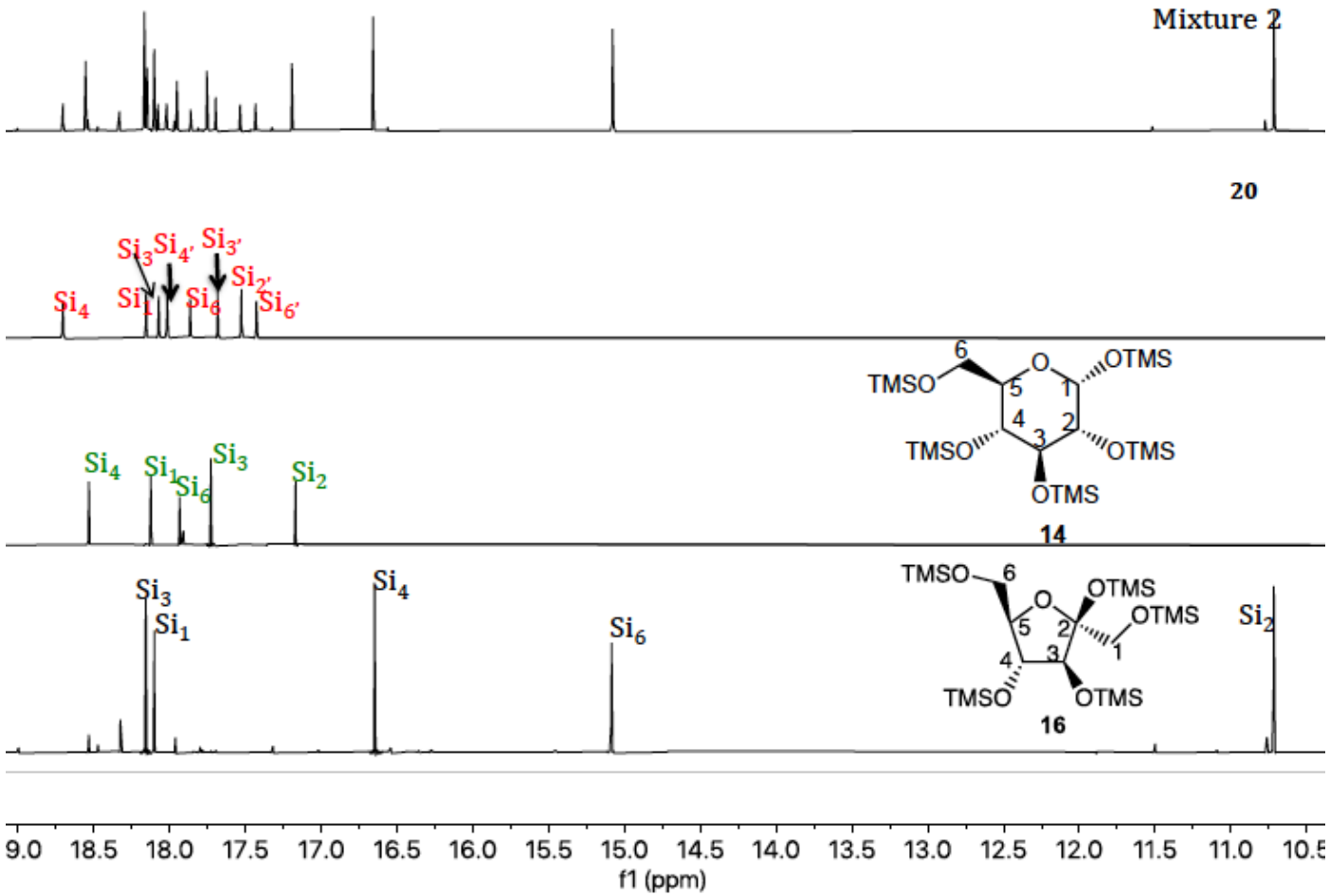

SI-Figure 3.9: (Triplicate 2-section 3.2.4): Three different sample α -per-*O*-TMS glucose (**14**), β-per-*O*-TMS fructose (**16**), and per-O-TMS sucrose (**20**) in $CDCl_3$ with different concentration stacked with pure sample. The chemical shifts in the mixture are confirmed to be the same value as in the pure sample.

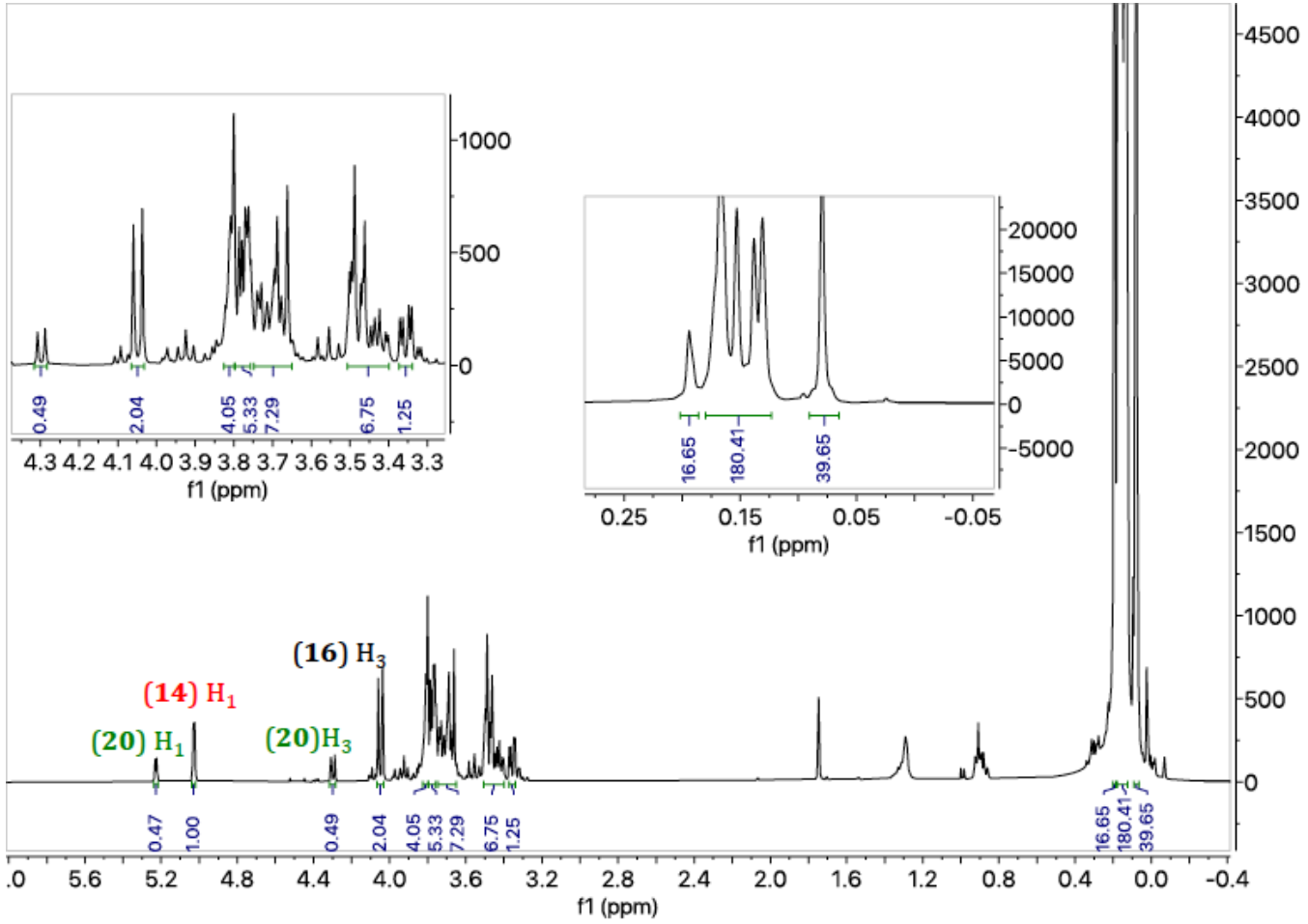

SI-Figure 3.10: (Triplicate 2-section 3.2.4): ^{1}H NMR of three different samples α-per-*O*-TMS glucose (**14**) (0.050 M), β-per-*O*-TMS fructose (**16**) (0.10 M), and per-O-TMS sucrose (**20**) (0.025 M) in $CDCl_3$ with HMDS as internal standard. These signals were integrated using H_1-glucose as the base reference of 1.00.

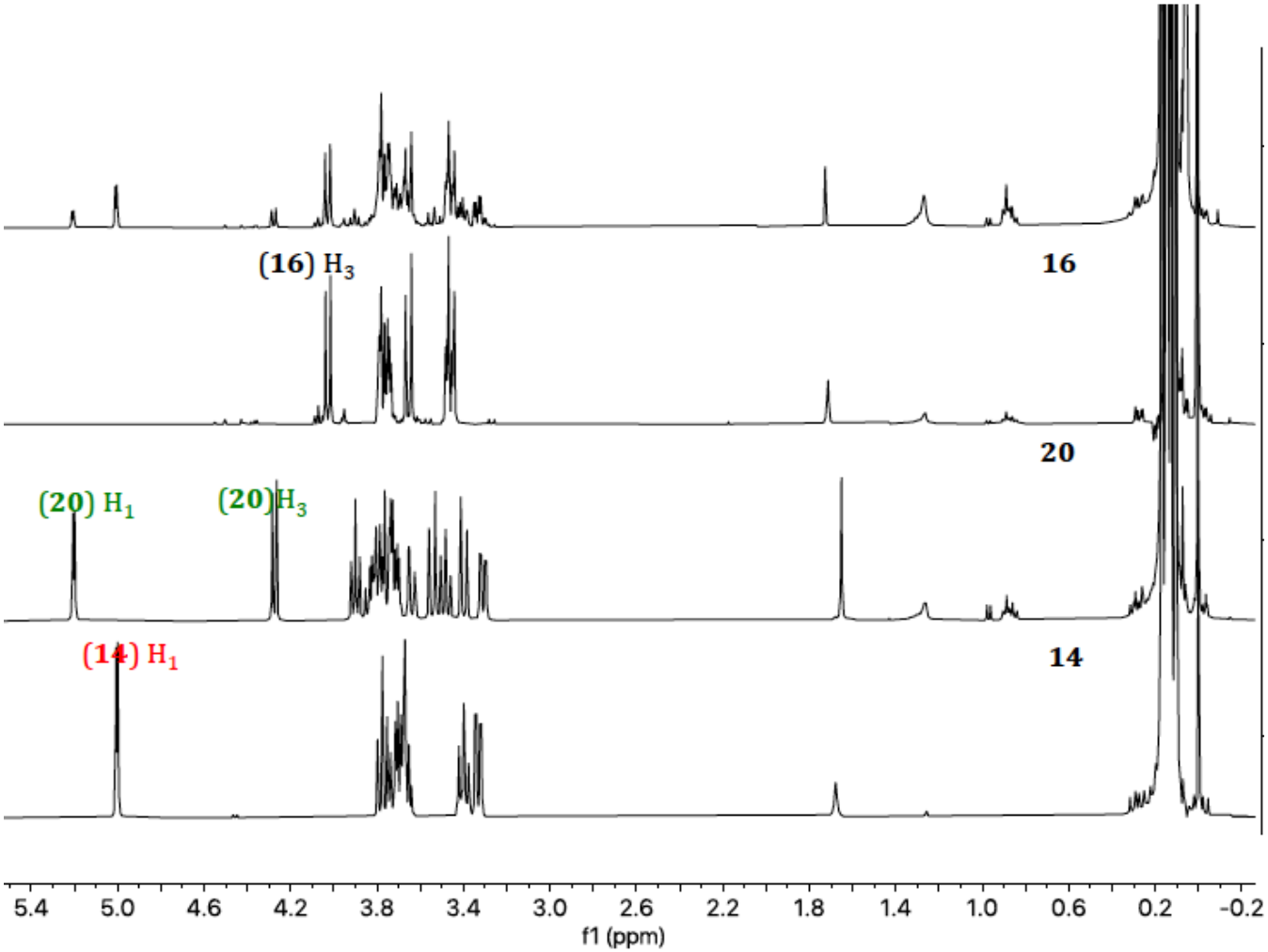

SI-Figure 3.11: (Triplicate 2-section 3.2.4): ^{1}H NMR of three of different samples α-per-*O*-TMS glucose (**14**) (0.050 M), β-per-*O*-TMS fructose (**16**) (0.10 M), and per-O-TMS sucrose (**20**) (0.025 M) in $CDCl_3$ with different concentration stacked with the pure compound (1,2,3).

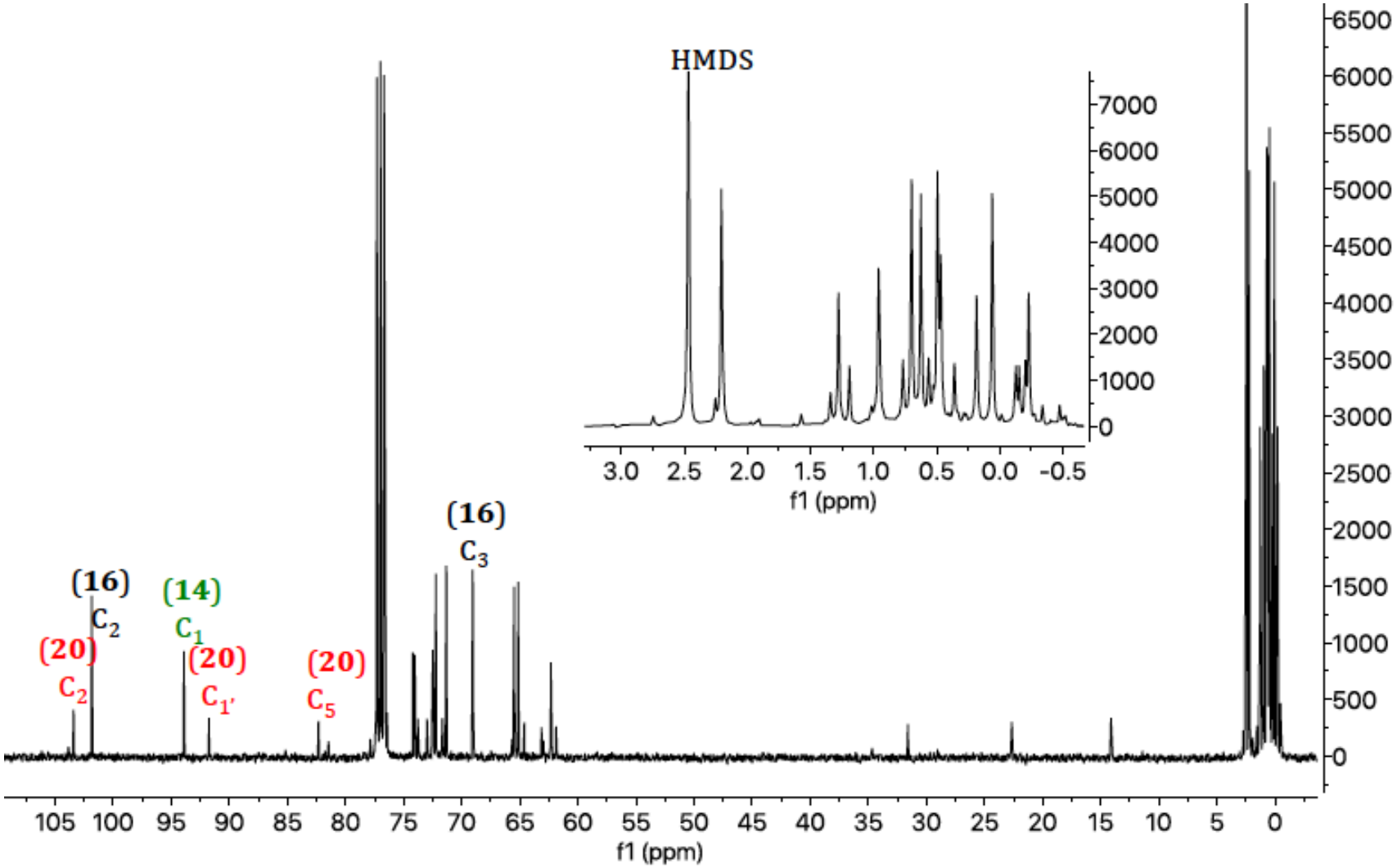

SI-Figure 3.12: (Triplicate 2-section 3.2.4): ^{13}C NMR of three different compounds α-per-*O*-TMS glucose (**14**) (0.050 M), β-per-*O*-TMS fructose (**16**) (0.10 M), and per-O-TMS sucrose (**20**) (0.025 M) in $CDCl_3$ use HMDS as reference peak.

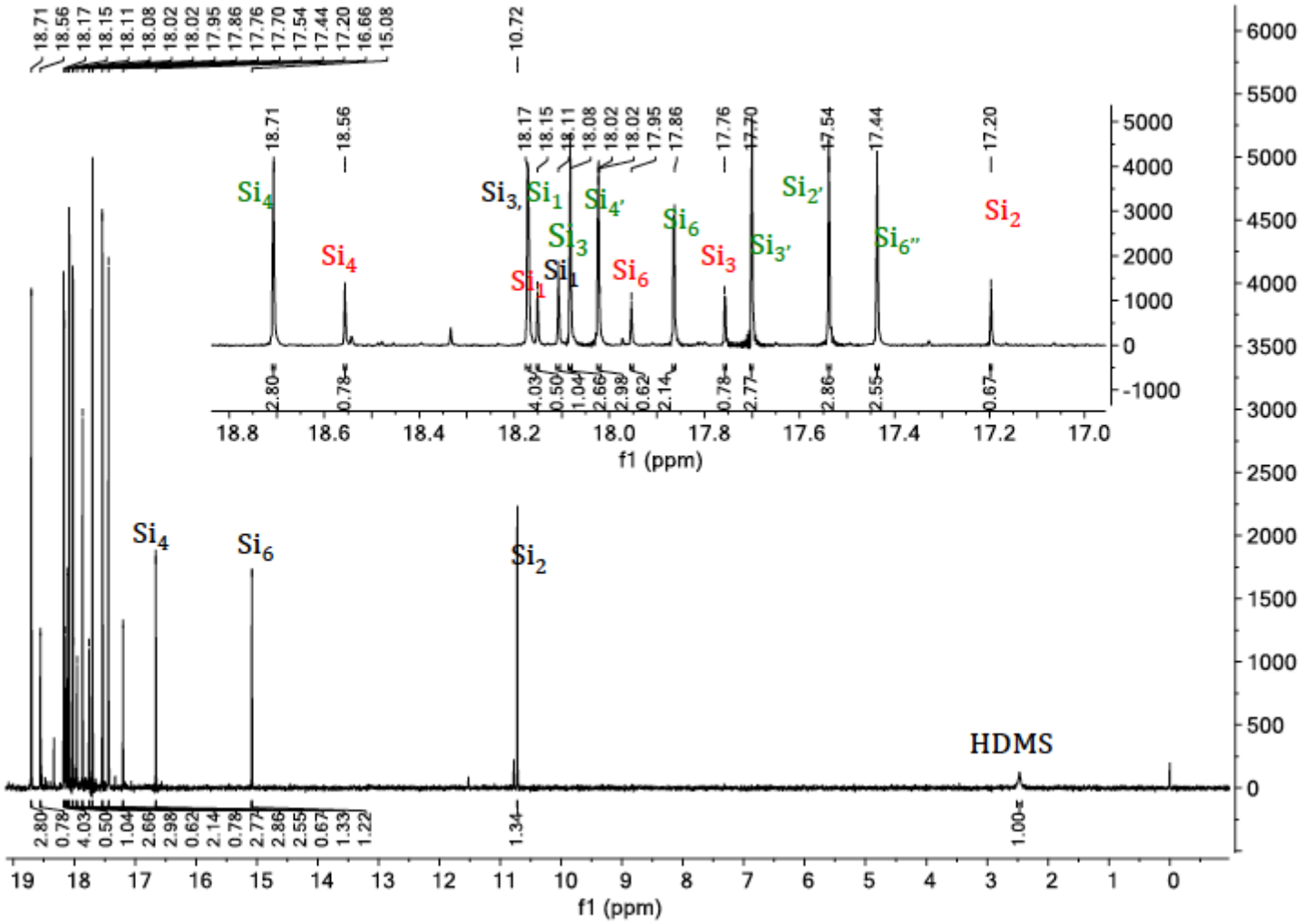

SI-Figure 3.13: (Triplicate 3-section 3.2.4): ^{29}Si NMR of three different compounds, α-per-*O*-TMS-glucose (0.025 M), β-per-*O*-TMS-fructose (0.050 M), and per-O-TMS-sucrose (0.10 M) in $CDCl_3$ HMDS used as internal standard. All peaks integrate respect to HMDS as base reference 1.00.

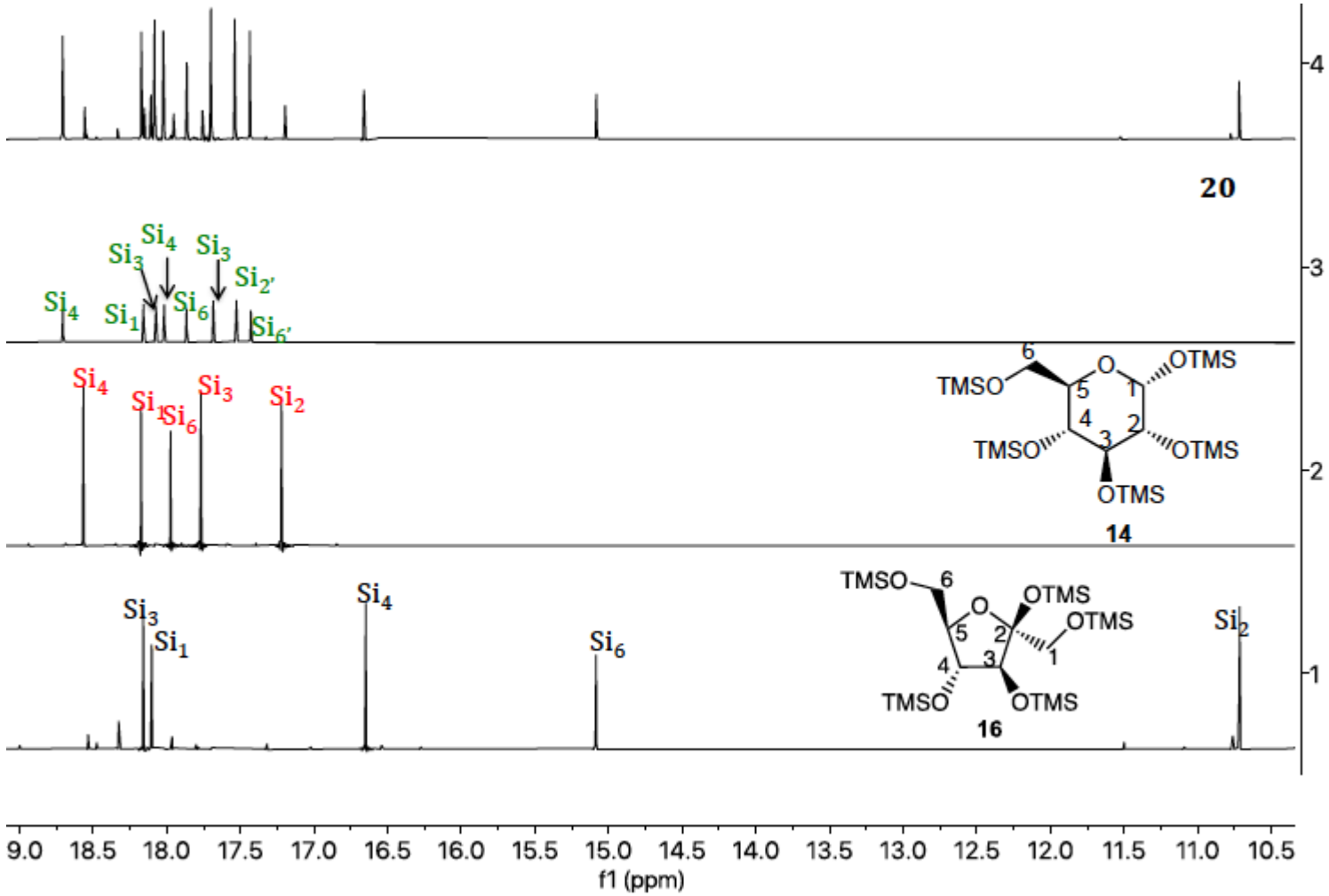

SI-Figure 3.14: (Triplicate 3-section 3.2.4): ^{29}Si NMR of three different compounds, α -per-*O*-TMS glucose (**14**) (0.025 M), β-per-*O*-TMS fructose (**16**) (0.050 M), and per-O-TMS sucrose (**20**) (0.100 M) mixture in $CDCl_3$ stacking against its pure compound (1,2,3).

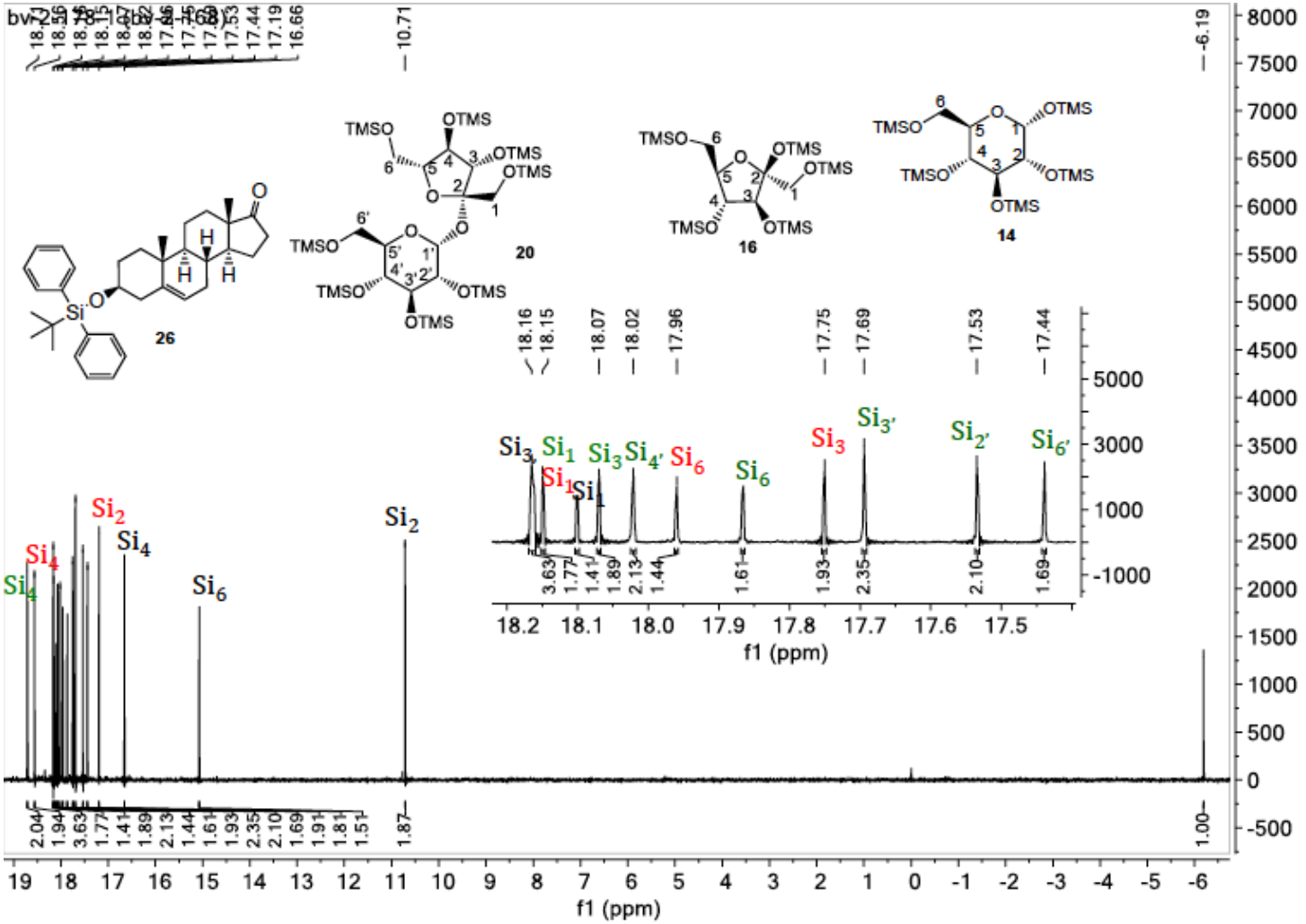

SI-Figure 3.15: (Replicate 1: Section 3.2.5): ^{29}Si NMR spectrum and integrations of a mixture containing equal mole (1:1:1:1) of α-per-*O*-TMS glucose (**14**): β-per-*O*-TMS fructose (**16**): per-*O*-TMS sucrose (**20**) in $CDCl_3$ using DHEA-*O*-TBDPSi (**26**) as internal standard as reference of 1.00 at δ -6.19.

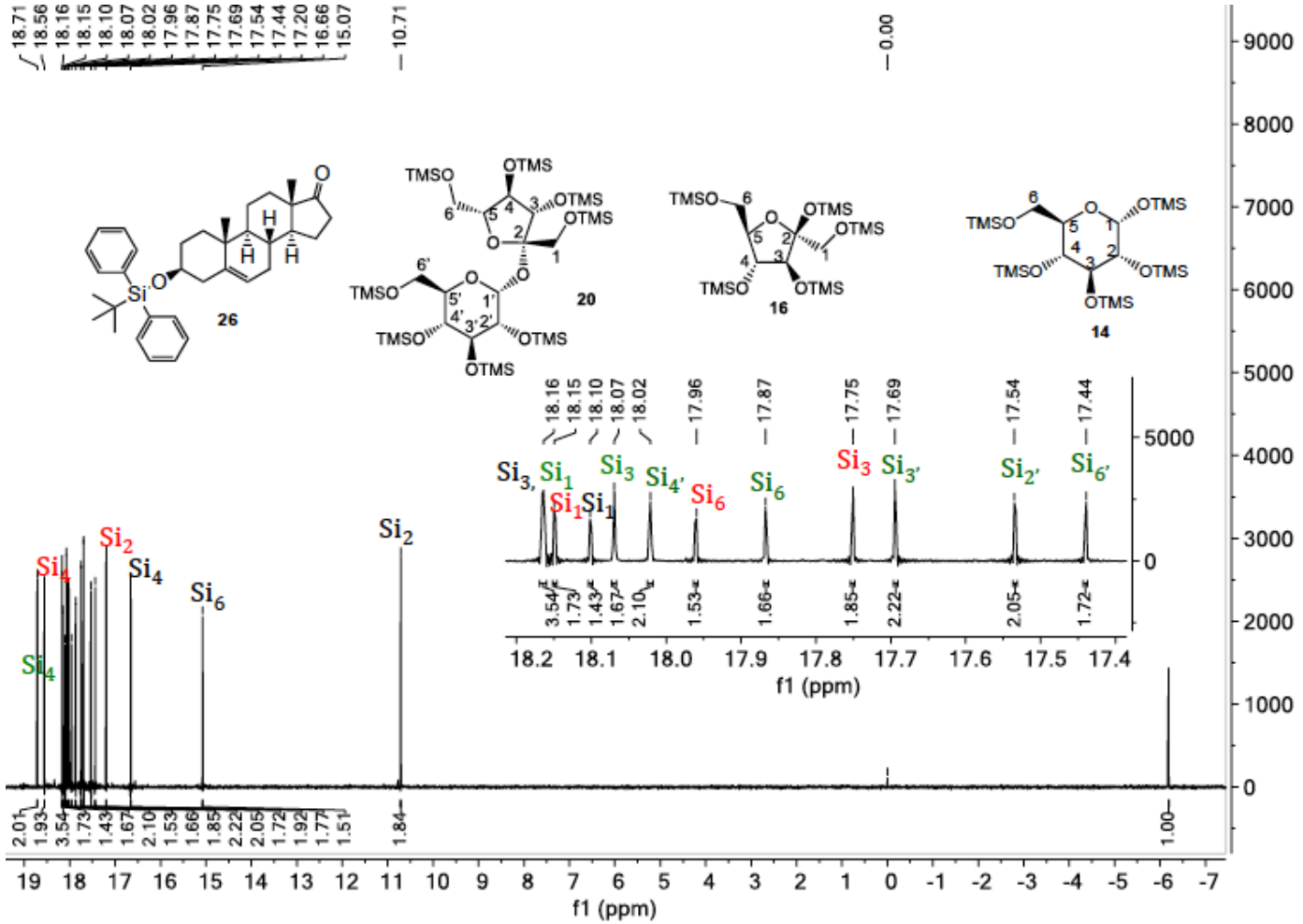

SI-Figure 3.16: (Replicate 2: Section 3.2.5): ^{29}Si NMR spectrum and integrations of a mixture containing equal mole (1:1:1:1) of α-per-*O*-TMS glucose (**14**): β-per-*O*-TMS fructose (**16**): per-*O*-TMS sucrose (**20**) in $CDCl_3$ using DHEA-*O*-TBDPSi (**26**) as internal standard as reference of 1.00 at δ -6.19.

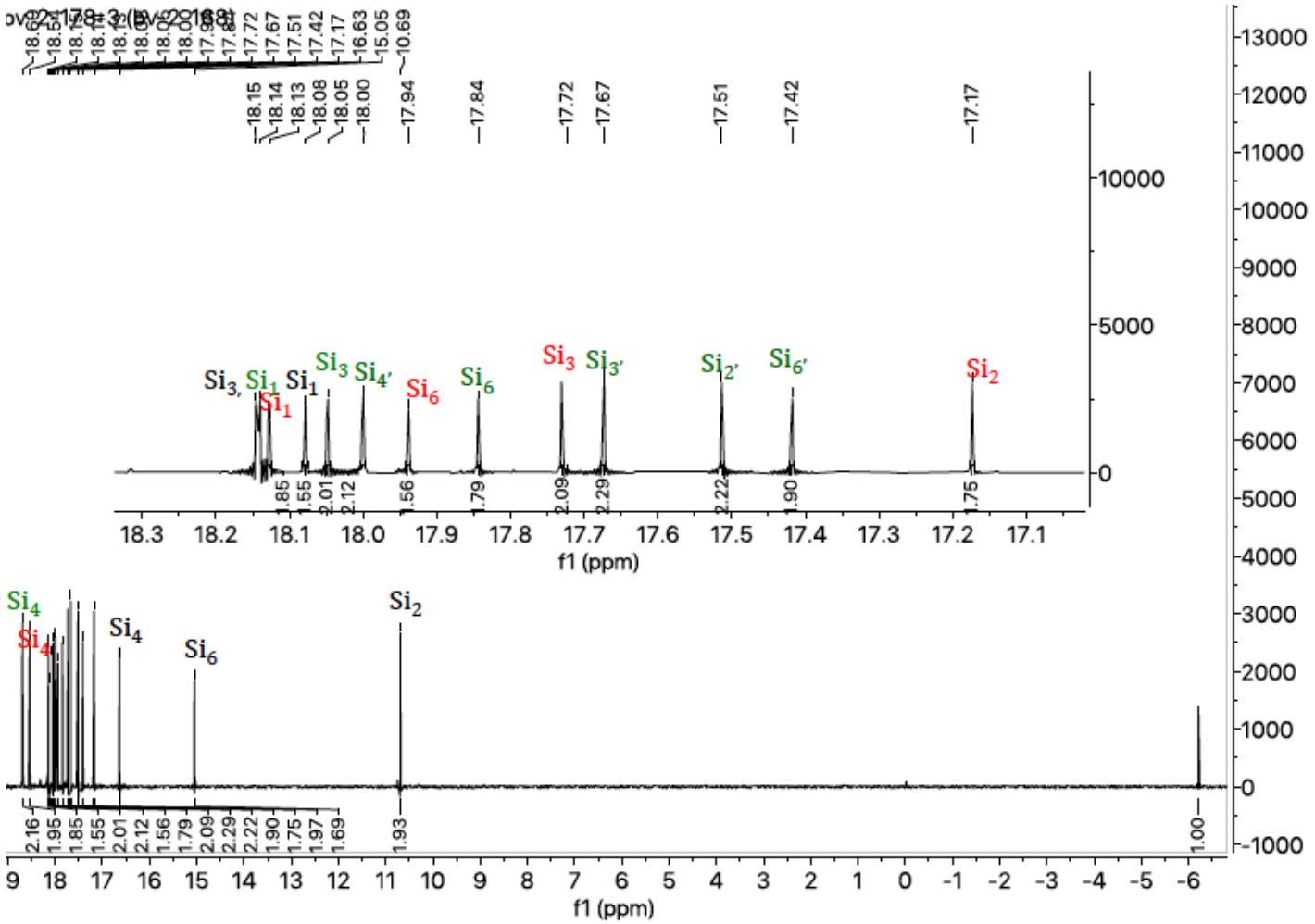

SI-Figure 3.17: (Replicate 3: Section 3.2.5): ^{29}Si NMR spectrum and integrations of a mixture containing equal mole (1:1:1:1) of α-per-*O*-TMS glucose (**14**): β-per-*O*-TMS fructose (**16**): per-*O*-TMS sucrose (**20**) in $CDCl_3$ using DHEA-*O*-TBDPSi (**26**) as internal standard as reference of 1.00 at δ -6.19.

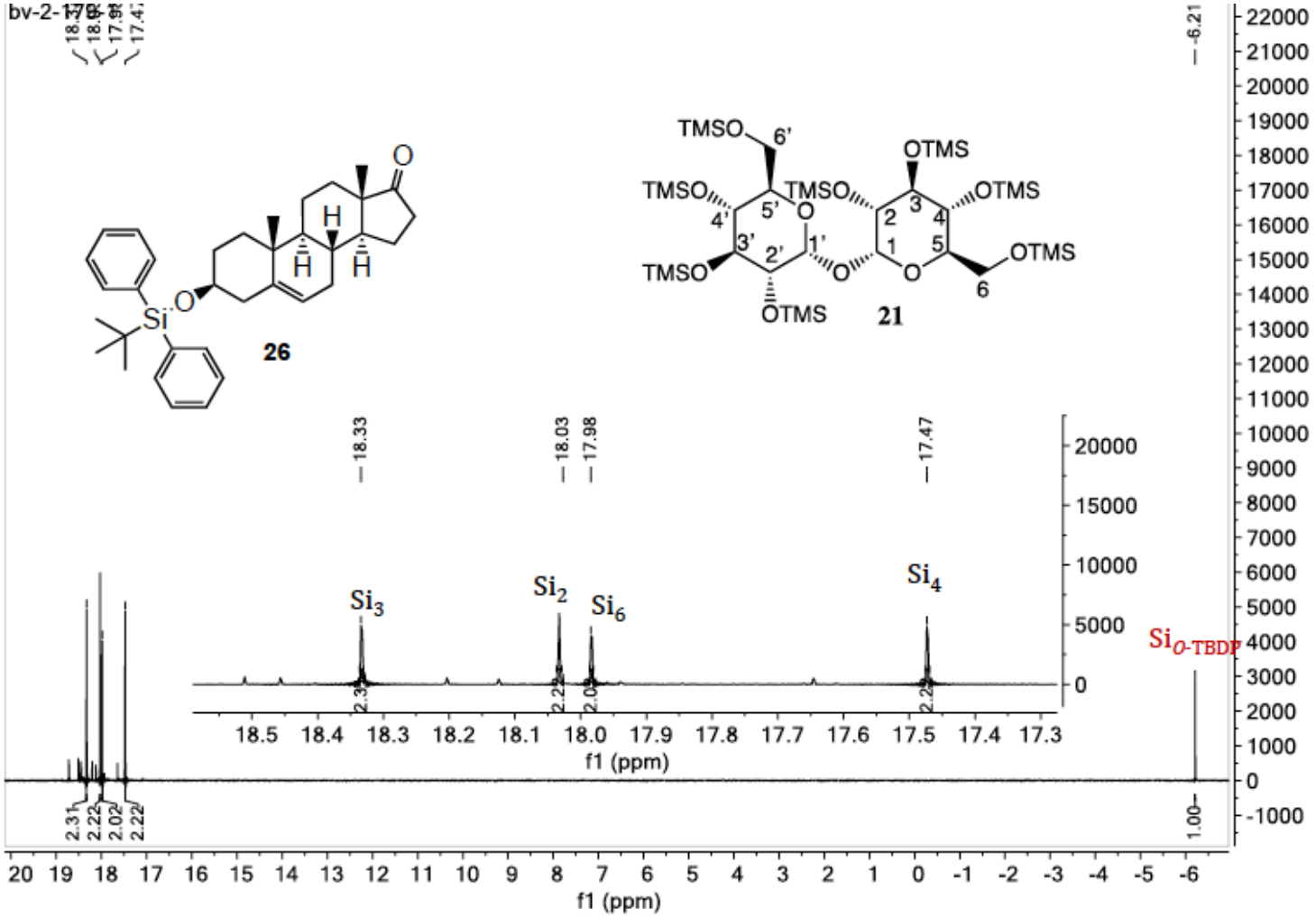

SI-Figure 3.18: (Replicate 1 Section 3.2.6): ^{29}Si NMR experiment of α-per-O-TMS trehalose (**21**) and DHEA-*O*-TBDPSi (**26**) as internal standard to calculate mmol from Si integration. The mole ratio of α-per-O-TMS trehalose (**21**) and DHEA-*O*-TBDPSi (**26**) is 1:1.

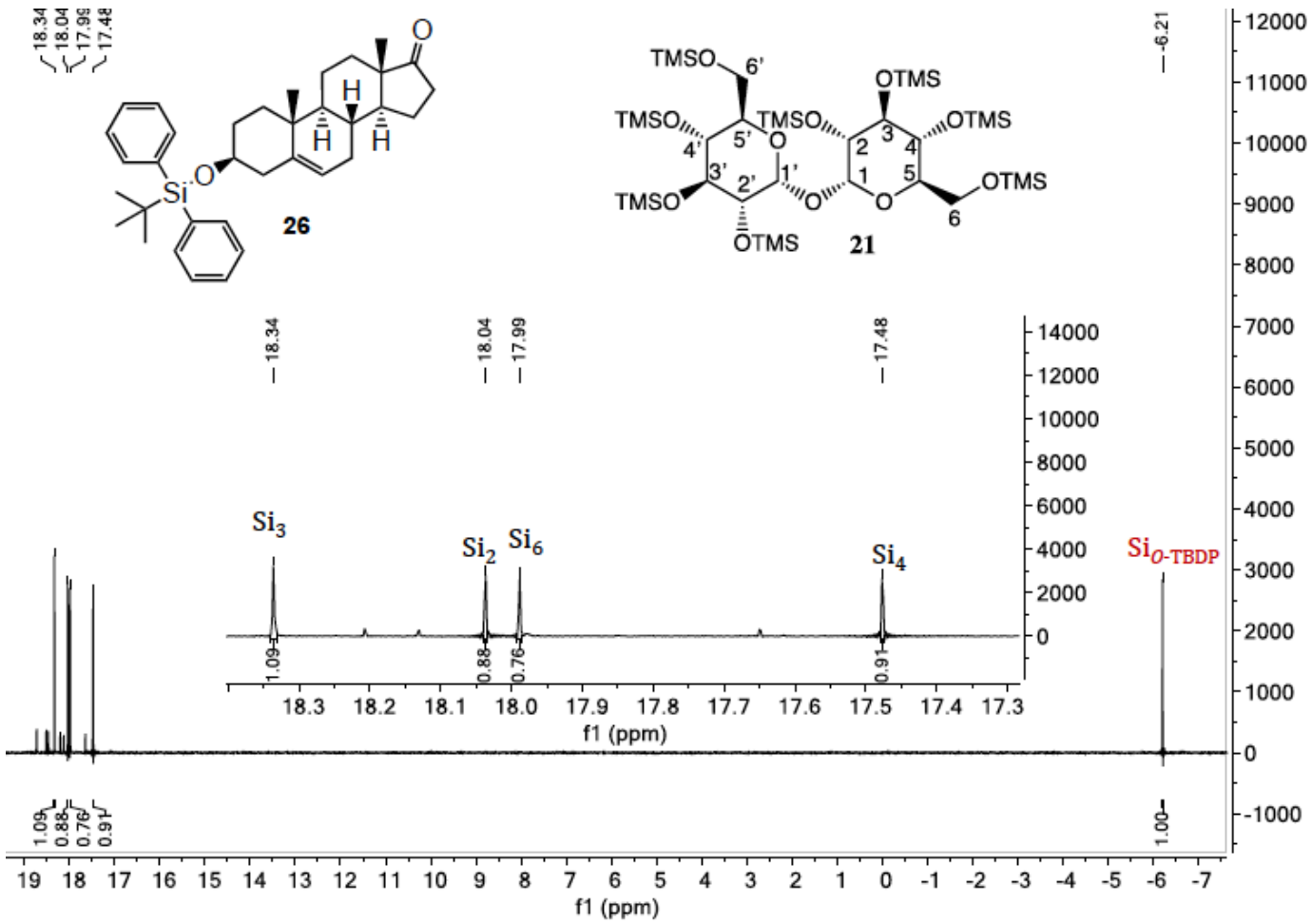

SI-Figure 3.19: (Replicate 2 Section 3.2.6): ^{29}Si NMR experiment of α-per-O-TMS trehalose (**21**) and DHEA-*O*-TBDPSi (**26**) as internal standard to calculate mmol from Si integration. The mole ratio of α-per-O-TMS trehalose (**21**) and DHEA-TBDPSi (**26**) is 0.5:1.

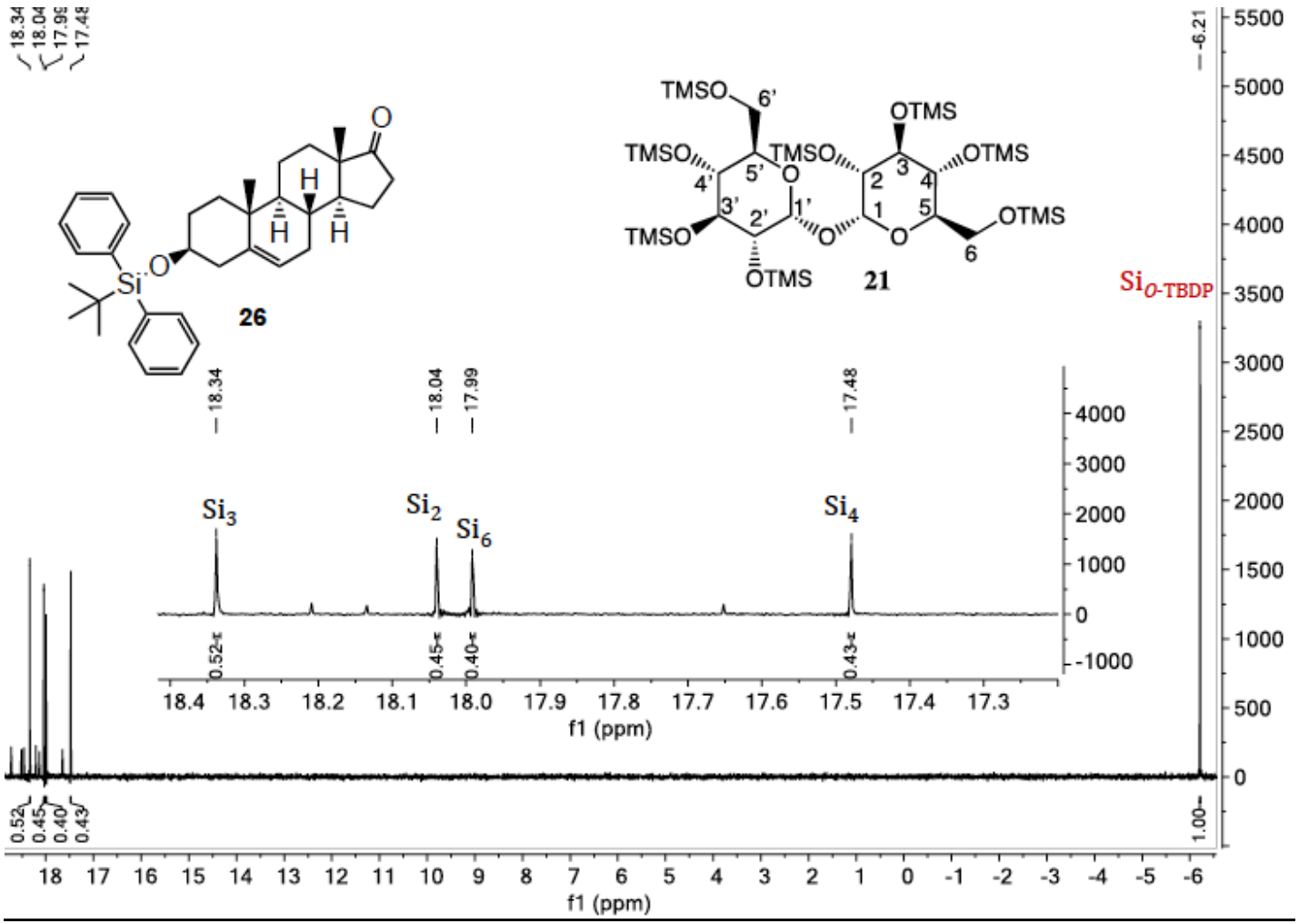

SI-Figure 3.20: (Replicate 3 Section 3.2.6): ^{29}Si NMR experiment of α-per-O-TMS trehalose (**21**) and DHEA-*O*-TBDPSi (**26**) as internal standard to calculate mmol from Si integration. The mole ratio of α-per-O-TMS trehalose (**21**) and DHEA-TBDPSi (**26**) is 0.25:1.

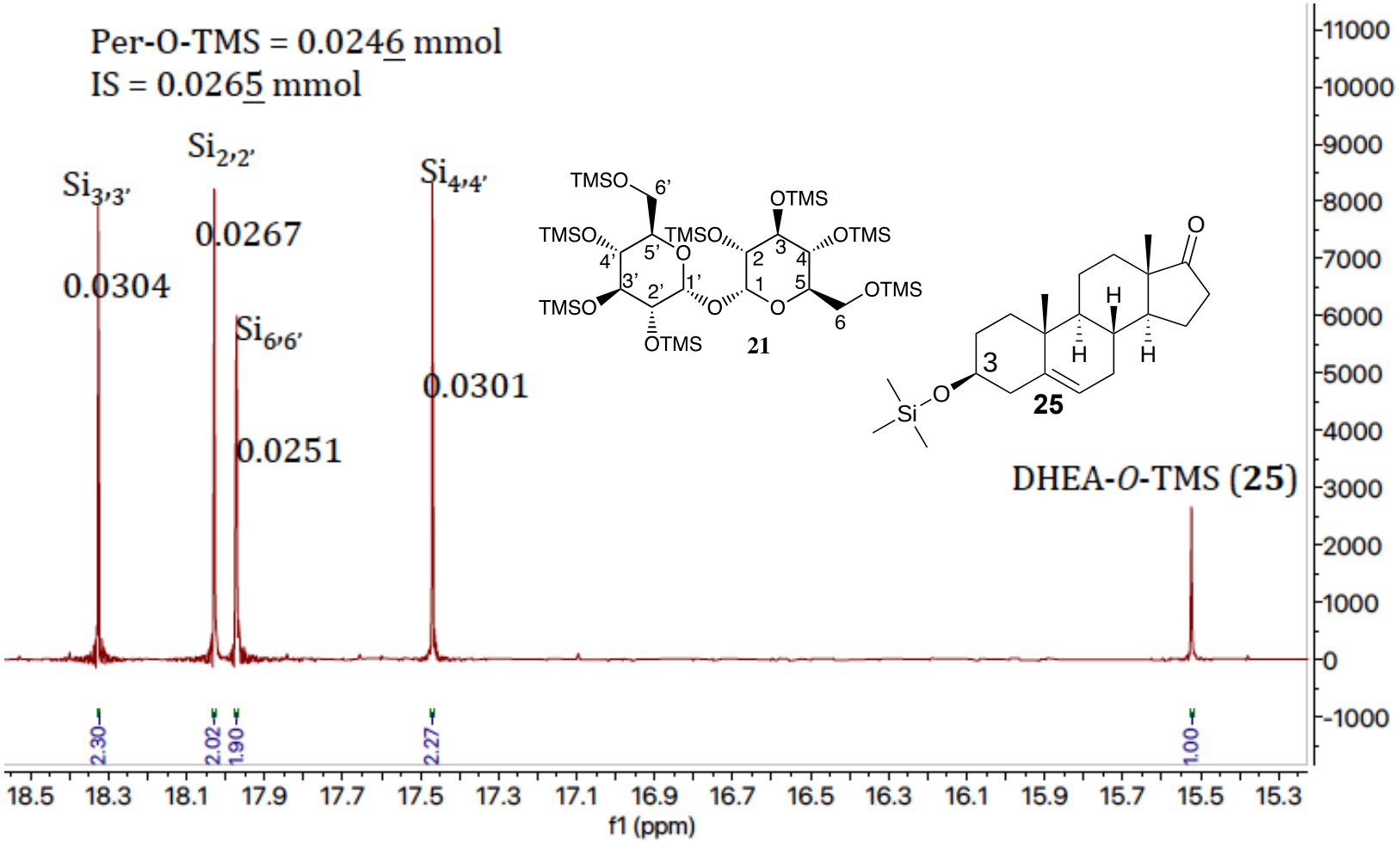

SI-Figure 3.21: (Replicate 1 Section 3.2.7): ^{29}Si NMR experiment of α-per-O-TMS trehalose (**21**) and DHEA-*O*-TMS (**25**)) as internal standard to calculate mmol from Si integration. The mole ratio of α-per-O-TMS trehalose (**21**) and DHEA-*O*-TMS (**25**) is 1:1.

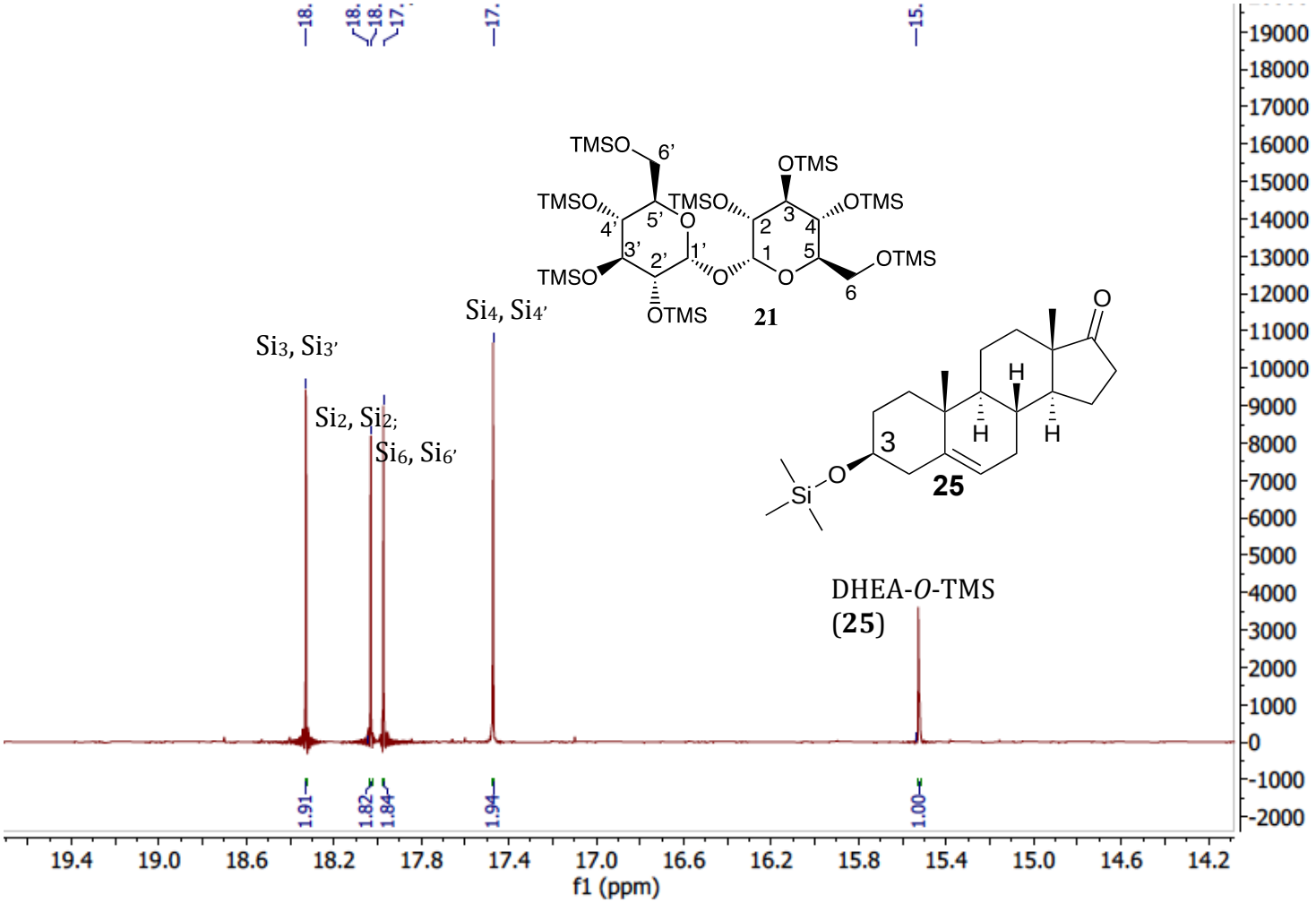

SI-Figure 3.22: (Replicate 2 Section 3.2.7): ^{29}Si NMR experiment of α-per-O-TMS trehalose (**21**) and DHEA-*O*-TMS (**25**) as internal standard to calculate mmol from Si integration. The mole ratio of α-per-O-TMS trehalose (**21**) and DHEA-*O*-TMS (**25**) is 1:1.

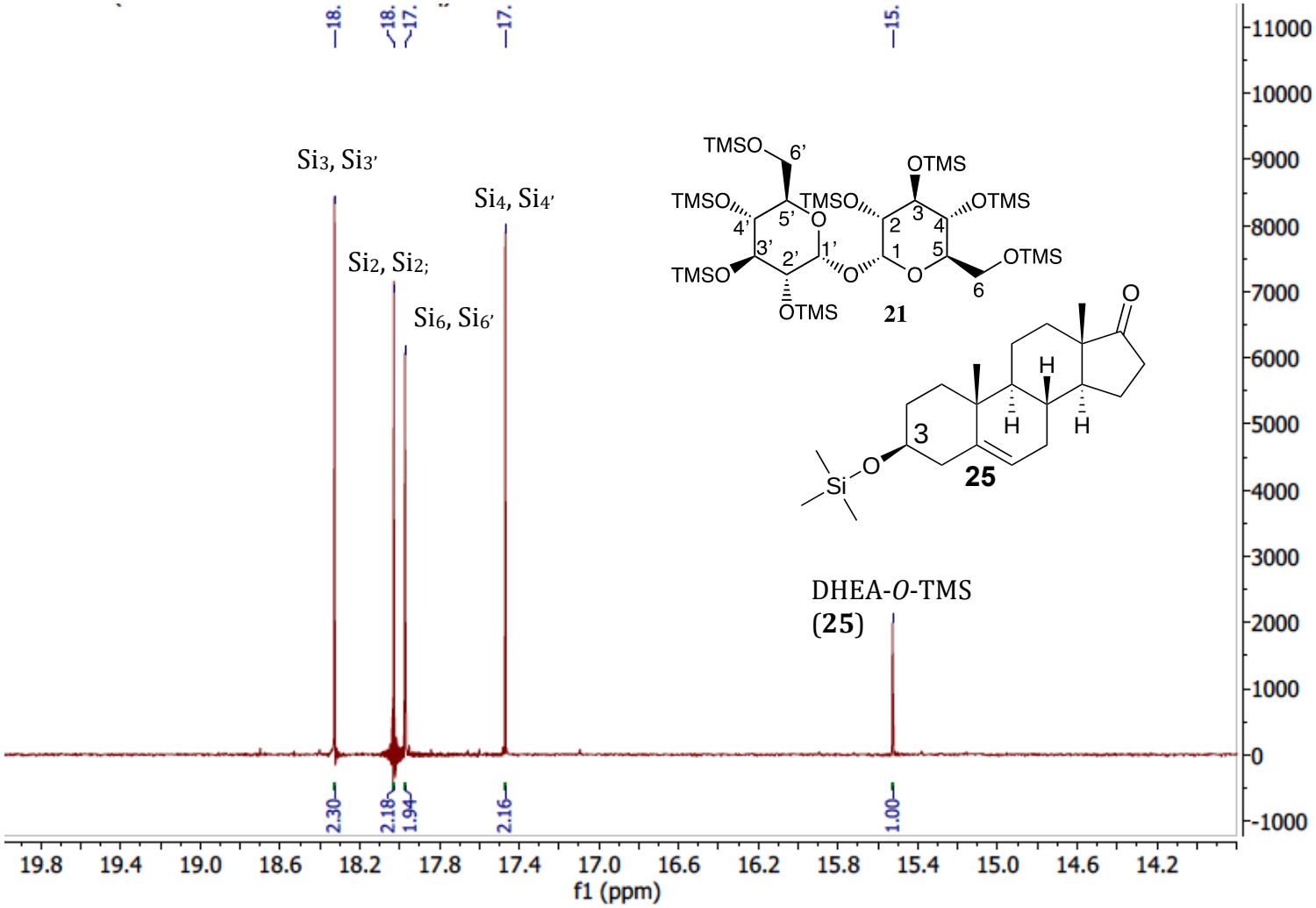

SI-Figure 3.23: (Replicate 3 Section 3.2.7): ^{29}Si NMR experiment of α-per-O-TMS trehalose (**21**) and DHEA-*O*-TMS (**25**) as internal standard to calculate mmol from Si integration. The mole ratio of α-per-O-TMS trehalose (**21**) and DHEA-*O*-TMS (**25**) is 1:1.

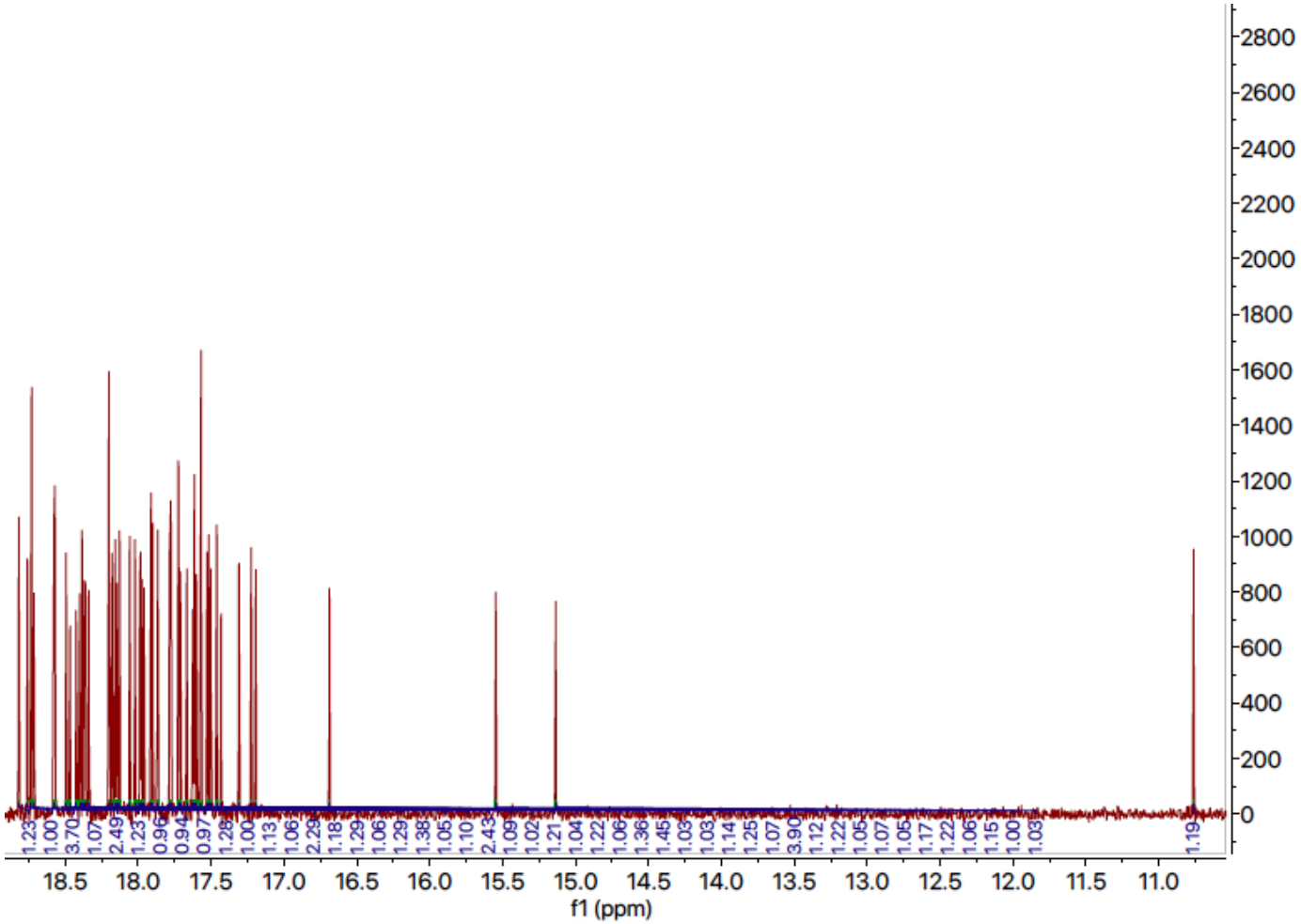

SI-Figure 3.24: (Replicate 1 Section 3.2.8): ^{29}Si NMR experiment of α-per-*O*-TMS glucose (**14**), β-per-*O*-TMS fructose (**16**), per-*O*-TMS sucrose (**20**), per-*O*-TMS kestose (**22**), per-*O*-TMS raffinose (**23**), per-*O*-TMS staychose (**24**) and DHEA-*O*-TMS (**25**) synthesized from free sugar as mixture in 1:1:1:1:1:1:1 mole ratio.

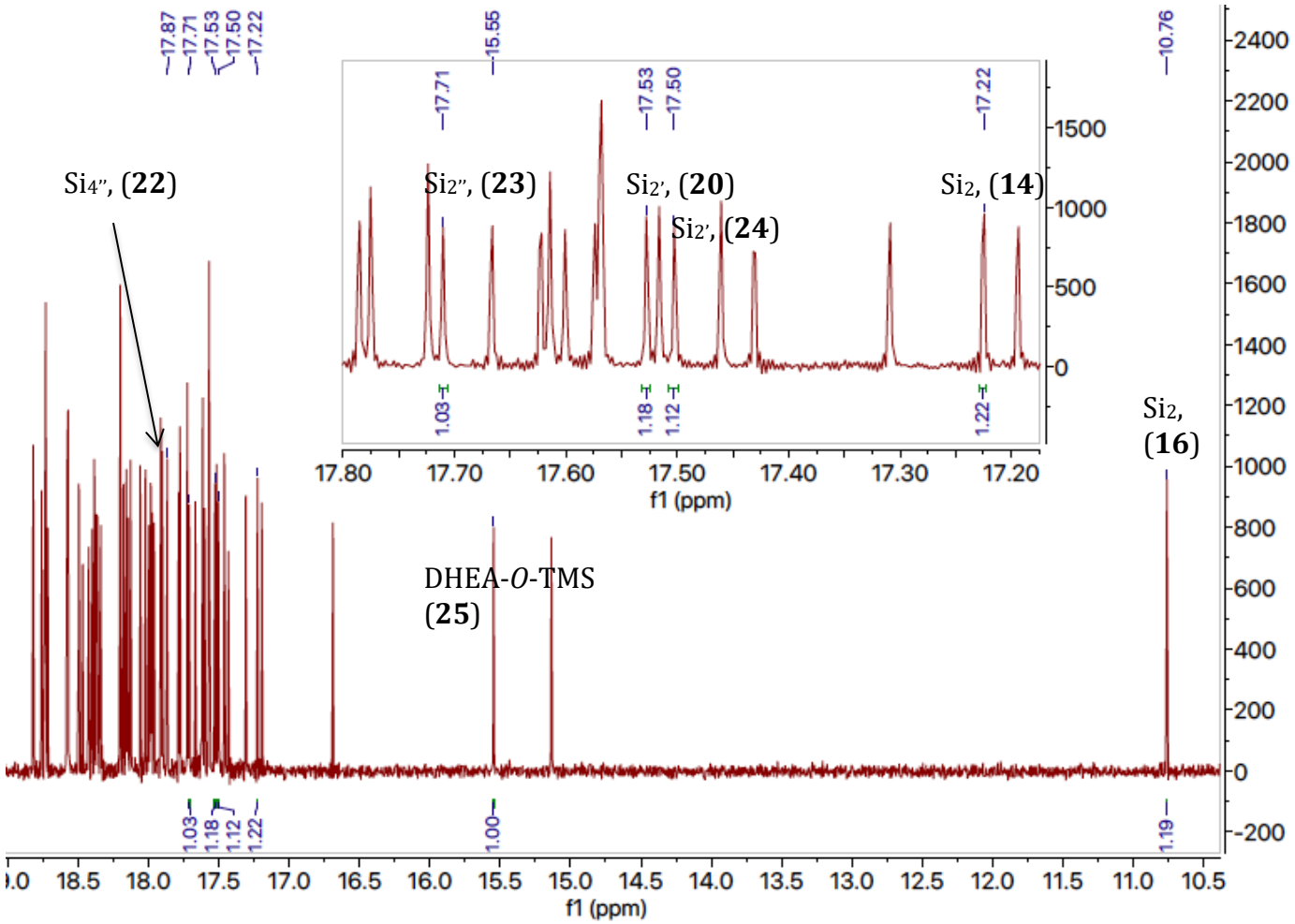

SI-Figure 3.25: (Replicate 1 Section 3.2.8): ^{29}Si NMR experiment of α-per-*O*-TMS glucose (**14**), β-per-*O*-TMS fructose (**16**), per-*O*-TMS sucrose (**20**), per-*O*-TMS kestose (**22**), per-*O*-TMS raffinose (**23**), per-*O*-TMS staychose (**24**) and DHEA-*O*-TMS (**25**) synthesized from free sugar as mixture in 1:1:1:1:1:1:1 mole ratio. The select Si2, Si2', Si2" and Si4" for integration.

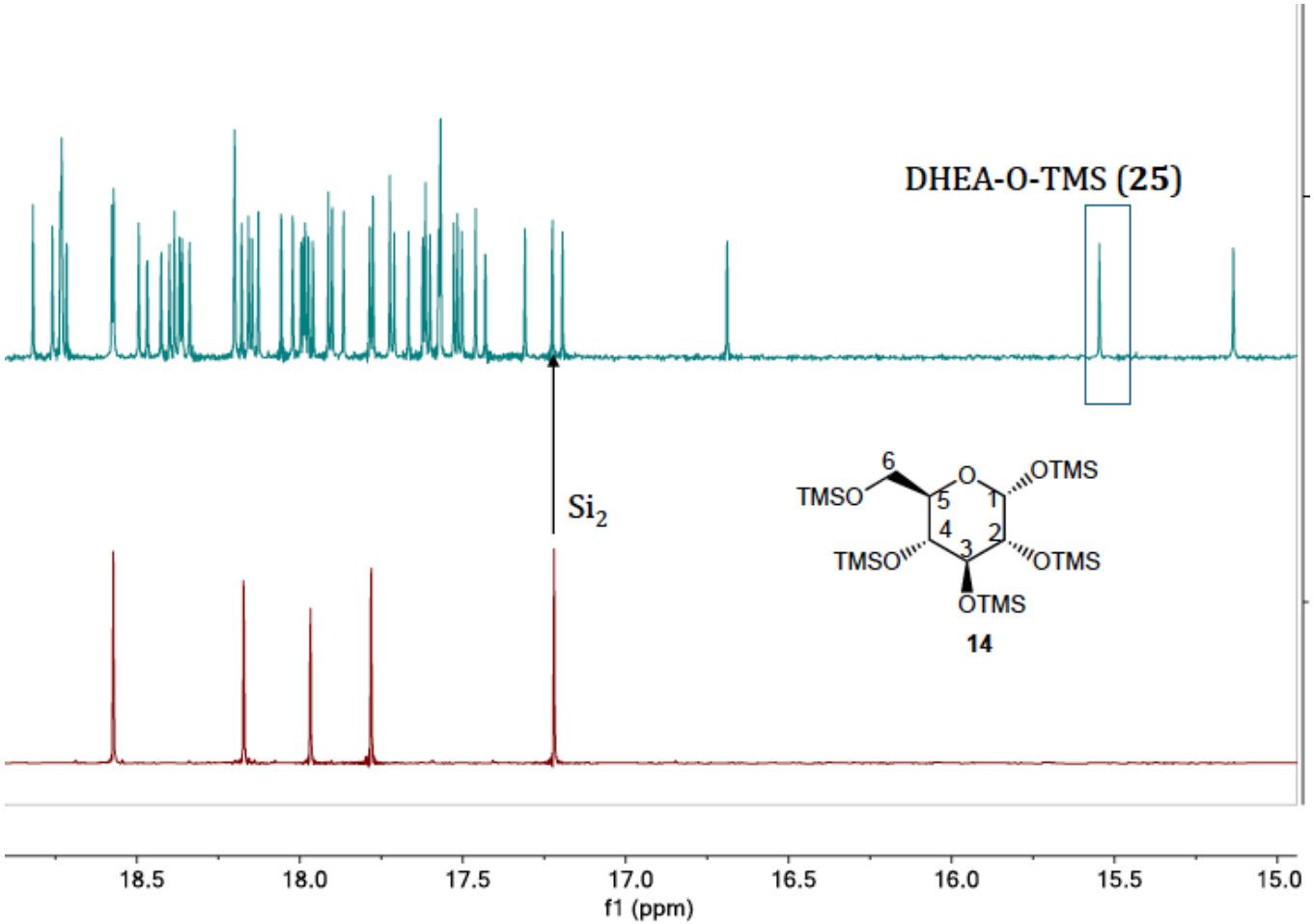

SI-Figure 3.26: (Replicate 1 Section 3.2.8): Overlap of ^{29}Si NMR experiment of α-per-*O*-TMS glucose (**14**), β-per-*O*-TMS fructose (**16**), per-*O*-TMS sucrose (**20**), per-*O*-TMS kestose (**22**), per-*O*-TMS raffinose (**23**), per-*O*-TMS staychose (**24**) and DHEA-*O*-TMS (**25**) synthesized from free sugar as mixture in 1:1:1:1:1:1:1 mole ratio synthesized from free sugar as mixture in 1:1:1:1:1:1:1 mole ratio with pure per-*O*-TMS glucose (**14**).

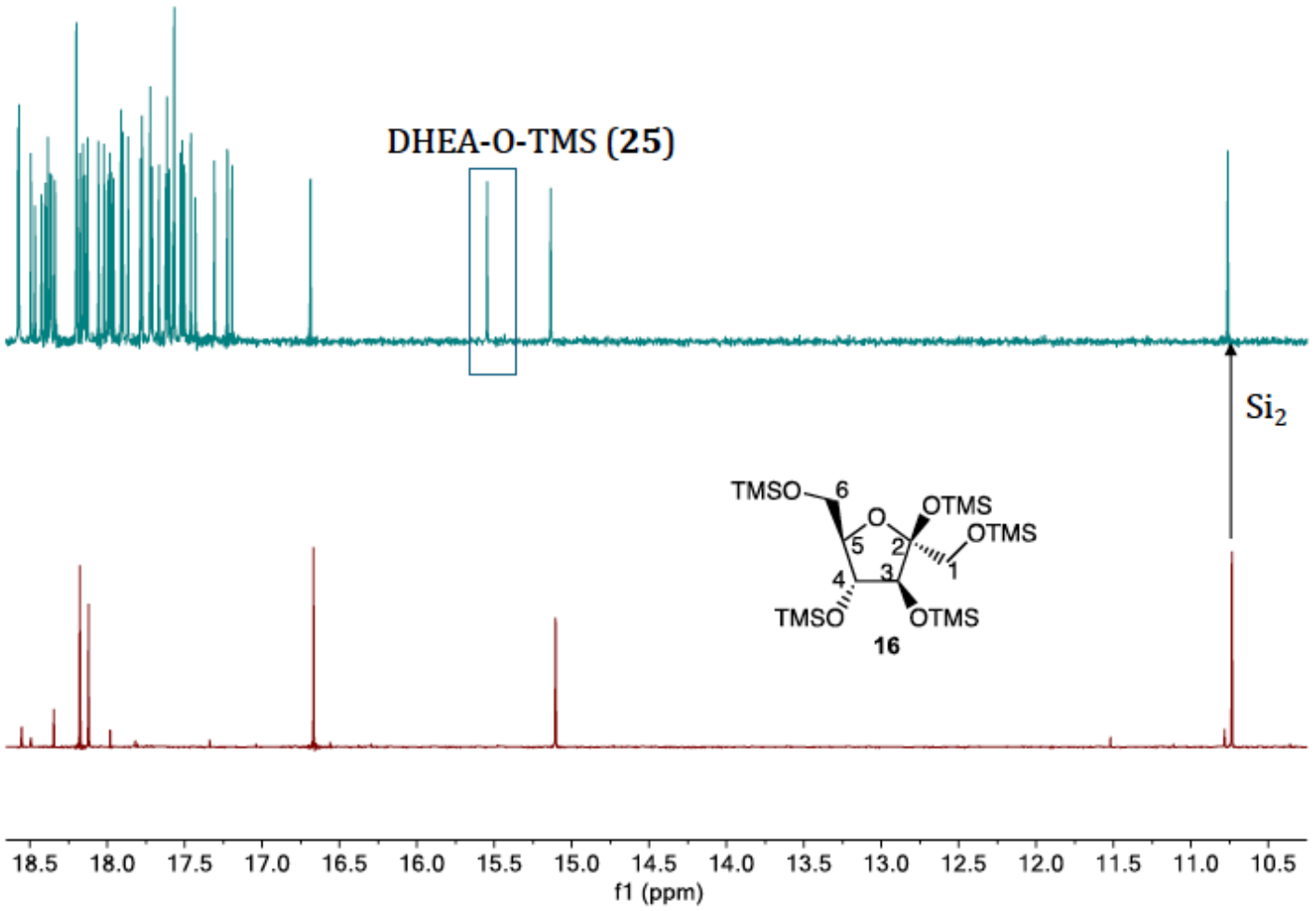

SI-Figure 3.27: (Replicate 1 Section 3.2.8): Overlap of ^{29}Si NMR experiment of α-per-*O*-TMS glucose (**14**), β-per-*O*-TMS fructose (**16**), per-*O*-TMS sucrose (**20**), per-*O*-TMS kestose (**22**), per-*O*-TMS raffinose (**23**), per-*O*-TMS staychose (**24**) and DHEA-*O*-TMS (**25**) ,ynthesized from free sugar as mixture in 1:1:1:1:1:1:1 mole ratio with pure per-*O*-TMS fructose (**16**).

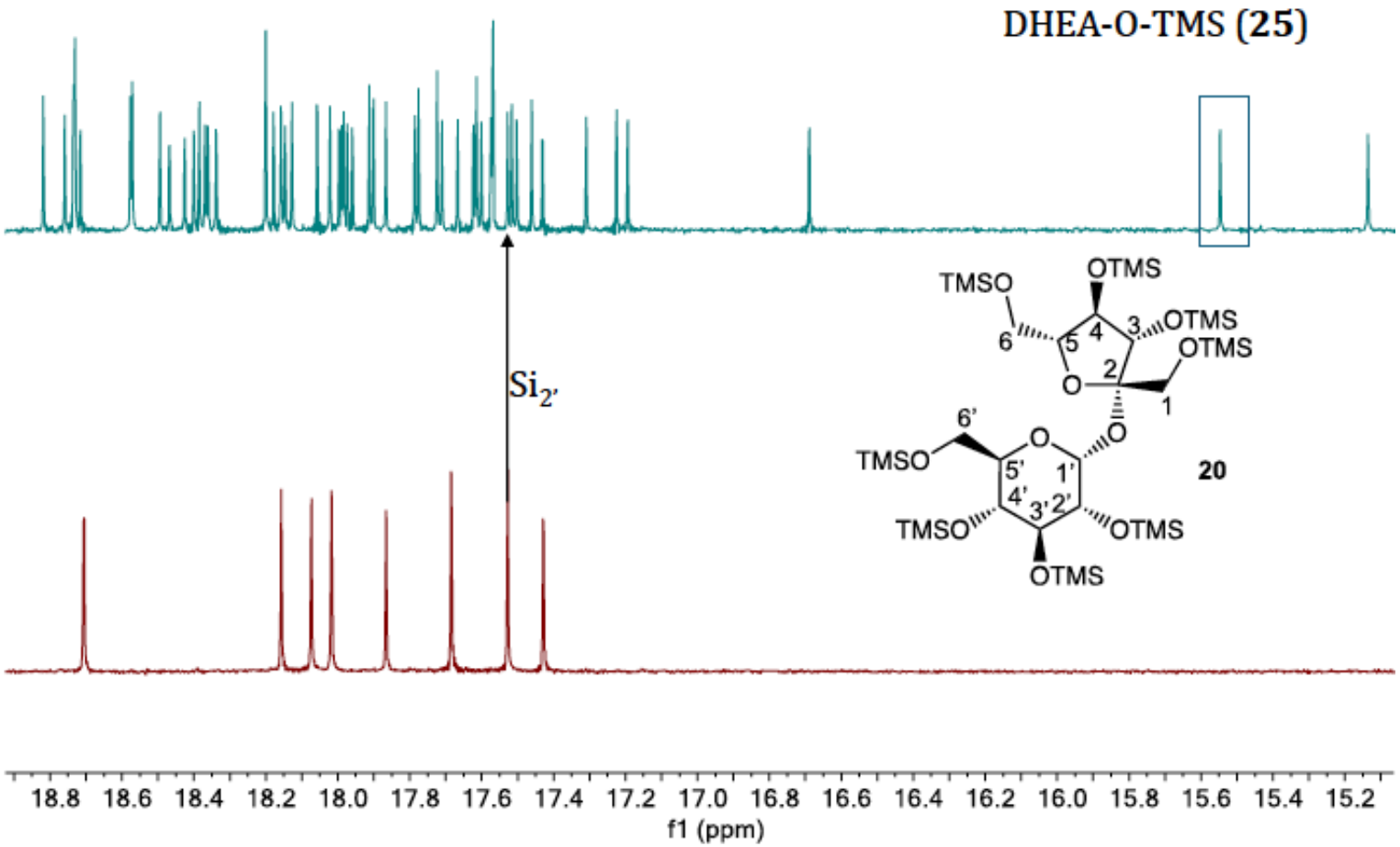

SI-Figure 3.28: (Replicate 1 Section 3.2.8): Overlap of ^{29}Si NMR experiment of α-per-*O*-TMS glucose (**14**), β-per-*O*-TMS fructose (**16**), per-*O*-TMS sucrose (**20**), per-*O*-TMS kestose (**22**), per-*O*-TMS raffinose (**23**), per-*O*-TMS staychose (**24**) and DHEA-*O*-TMS (**25**) synthesized from free sugar as mixture in 1:1:1:1:1:1:1 mole ratio with pure per-*O*-TMS surcose (**20**).

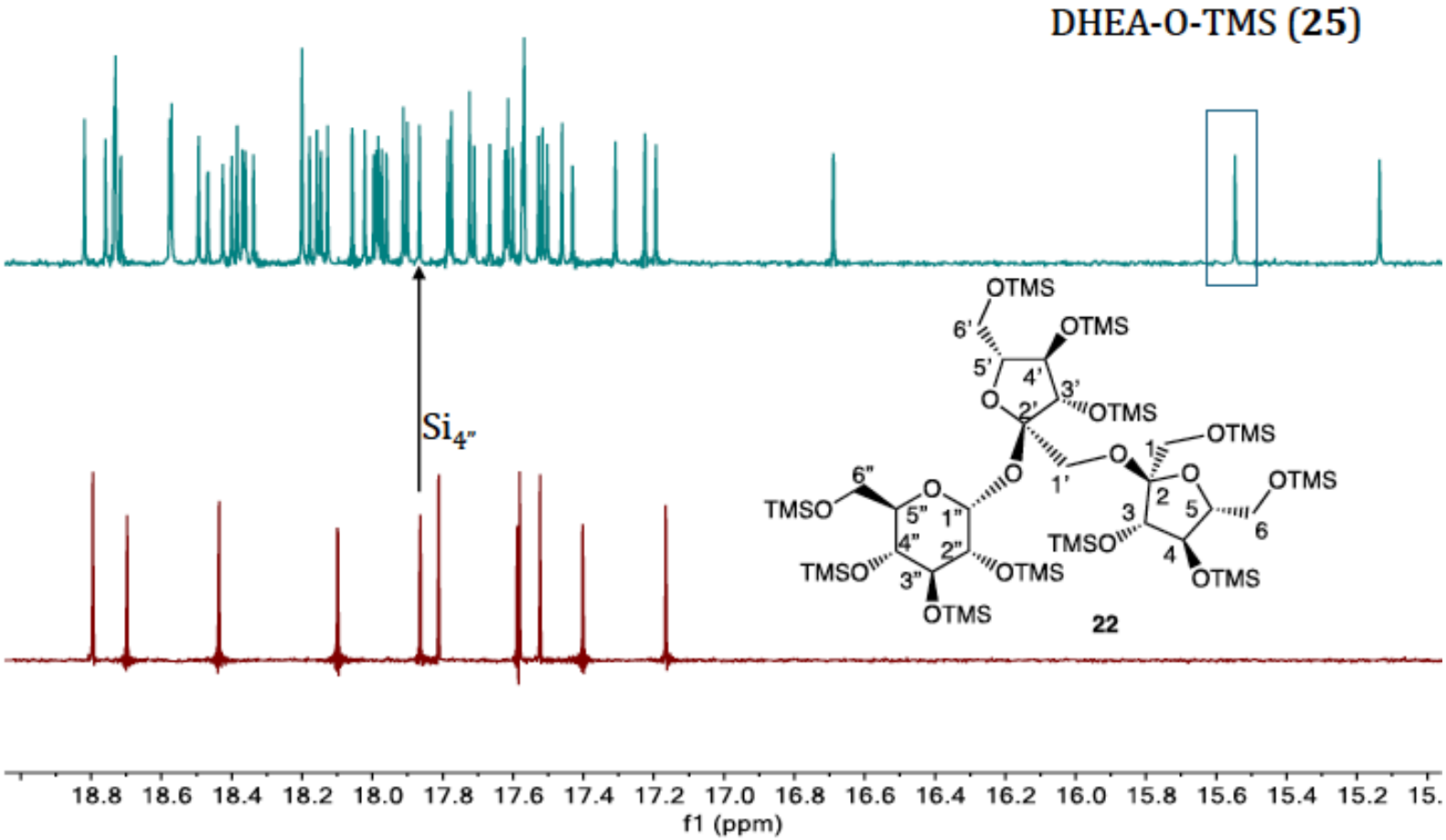

Si-Figure 3.29: (Replicate 1 Section 3.2.8): Overlap of ^{29}Si NMR experiment of α-per-*O*-TMS glucose (**14**), β-per-*O*-TMS fructose (**16**), per-*O*-TMS sucrose (**20**), per-*O*-TMS kestose (**22**), per-*O*-TMS raffinose (**23**), per-*O*-TMS staychose (**24**) and DHEA-*O*-TMS (**25**) synthesized from free sugar as mixture in 1:1:1:1:1:1:1 mole ratio with pure per-*O*-TMS kestose (**22**).

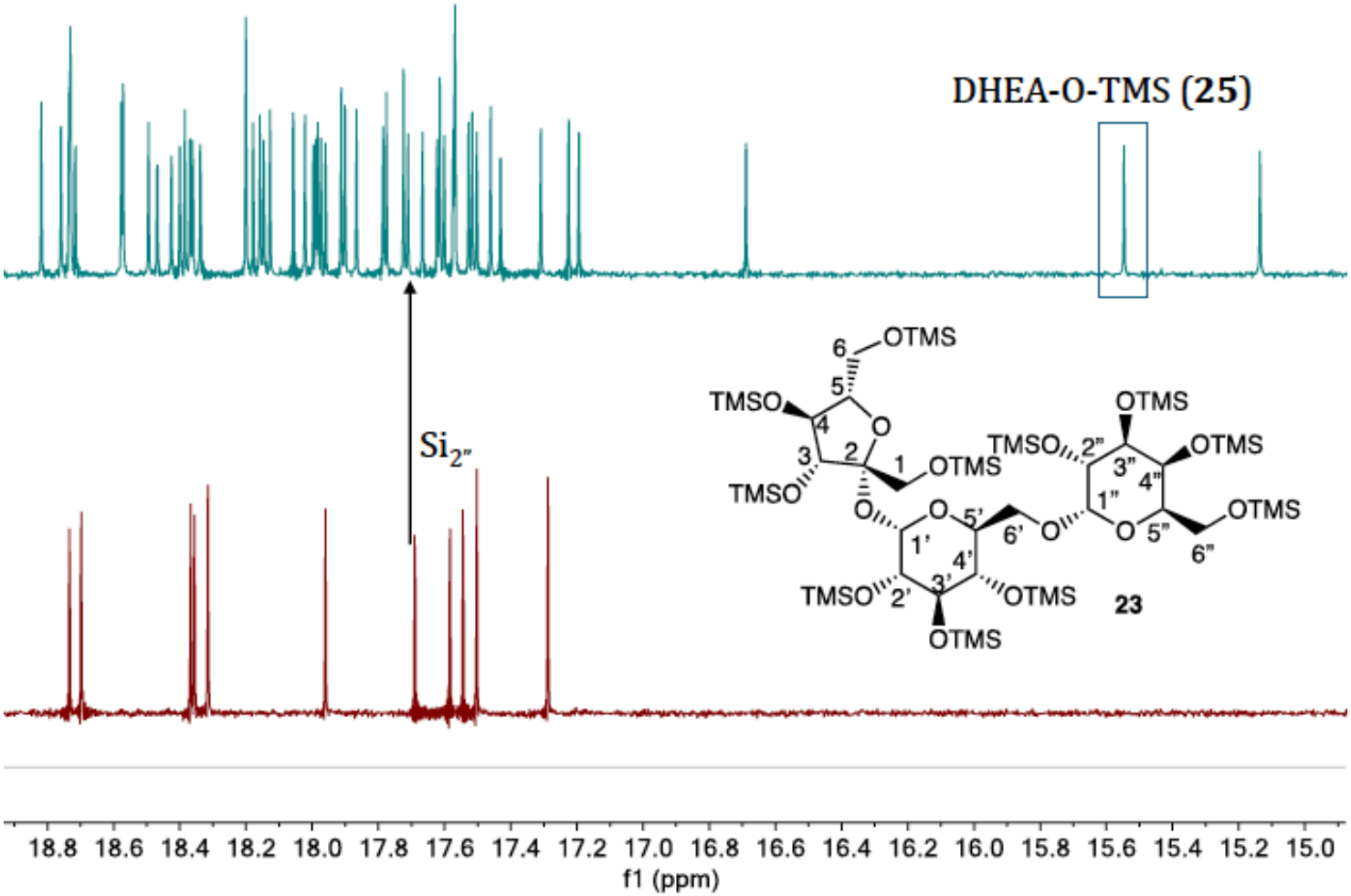

SI-Figure 3.30: (Replicate 1 Section 3.2.8): Overlap of ^{29}Si NMR experiment of α-per-*O*-TMS glucose (**14**), β-per-*O*-TMS fructose (**16**), per-*O*-TMS sucrose (**20**), per-*O*-TMS kestose (**22**), per-*O*-TMS raffinose (**23**), per-*O*-TMS staychose (**24**) and DHEA-*O*-TMS (**25**) synthesized from free sugar as mixture in 1:1:1:1:1:1:1 mole ratio with pure per-*O*-TMS raffinose (**23**).

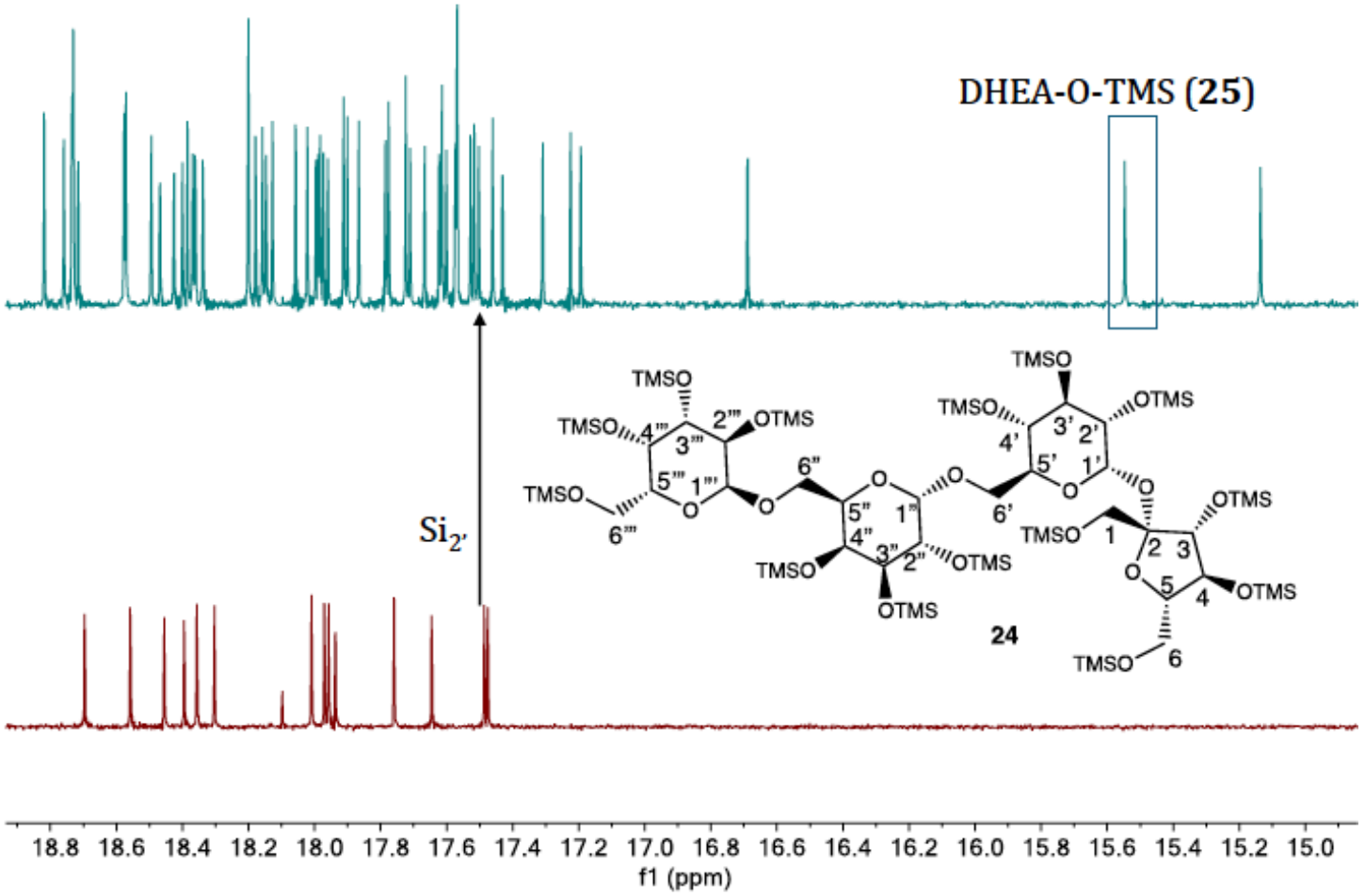

SI-Figure 3.31: (Replicate 1 Section 3.2.8): Overlap of ^{29}Si NMR experiment of α-per-*O*-TMS glucose (**14**), β-per-*O*-TMS fructose (**16**), per-*O*-TMS sucrose (**20**), per-*O*-TMS kestose (**22**), per-*O*-TMS raffinose (**23**), per-*O*-TMS staychose (**24**) and DHEA-*O*-TMS (**25**) synthesized from free sugar as mixture in 1:1:1:1:1:1:1:1 mole ratio with pure per-*O*-TMS stachysoe (**24**).

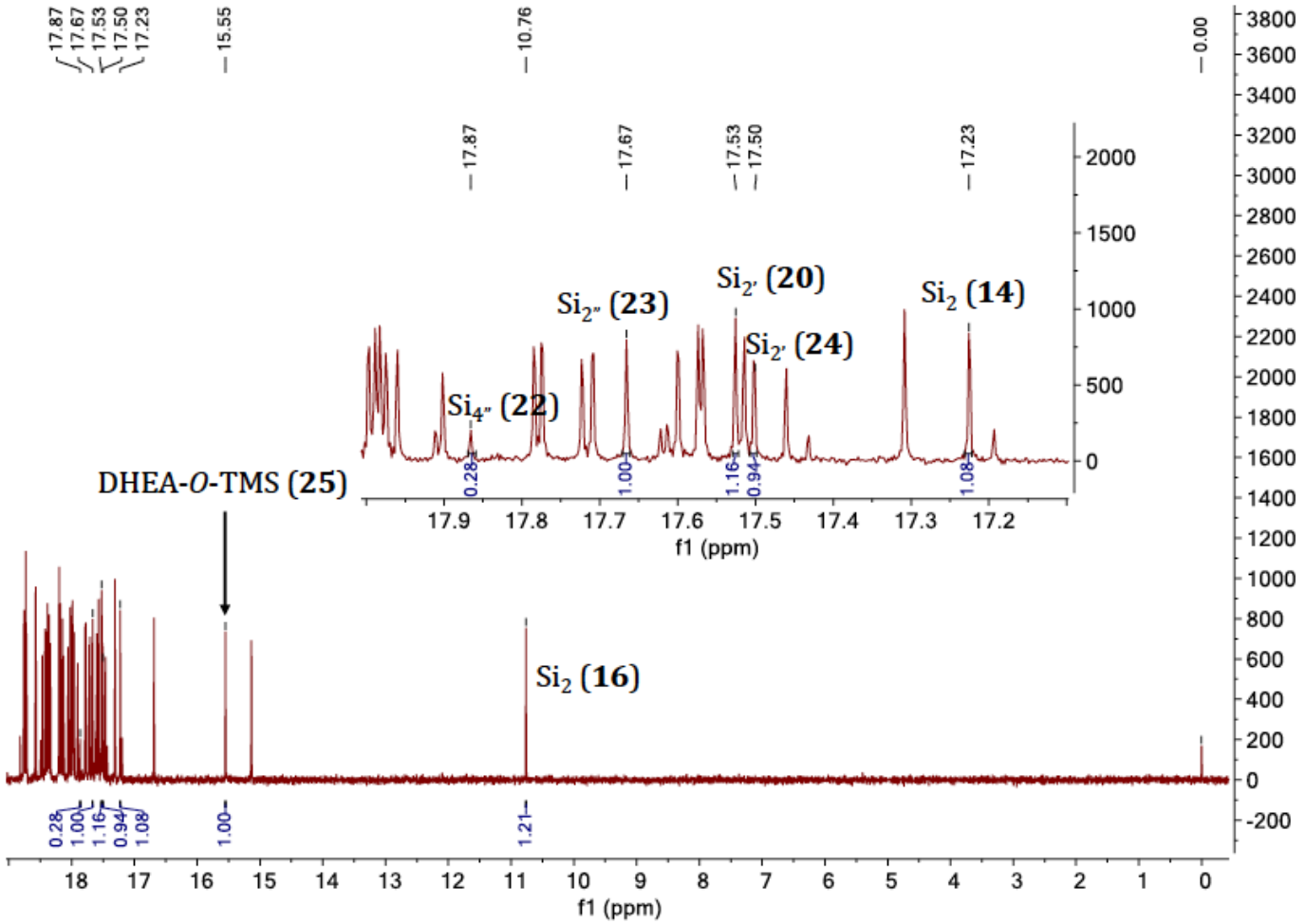

SI-Figure 3.32: (Replicate 2 Section 3.2.8): ^{29}Si NMR experiment of α-per-*O*-TMS glucose (**14**), β-per-*O*-TMS fructose (**16**), per-*O*-TMS sucrose (**20**), per-*O*-TMS kestose (**22**), per-*O*-TMS raffinose (**23**), per-*O*-TMS staychose (**24**) and DHEA-*O*-TMS (**25**) synthesized from free sugar as mixture in 1:1:1:1:1:1:1 mole ratio. The select Si2, Si2', Si2" and Si4" for integration.

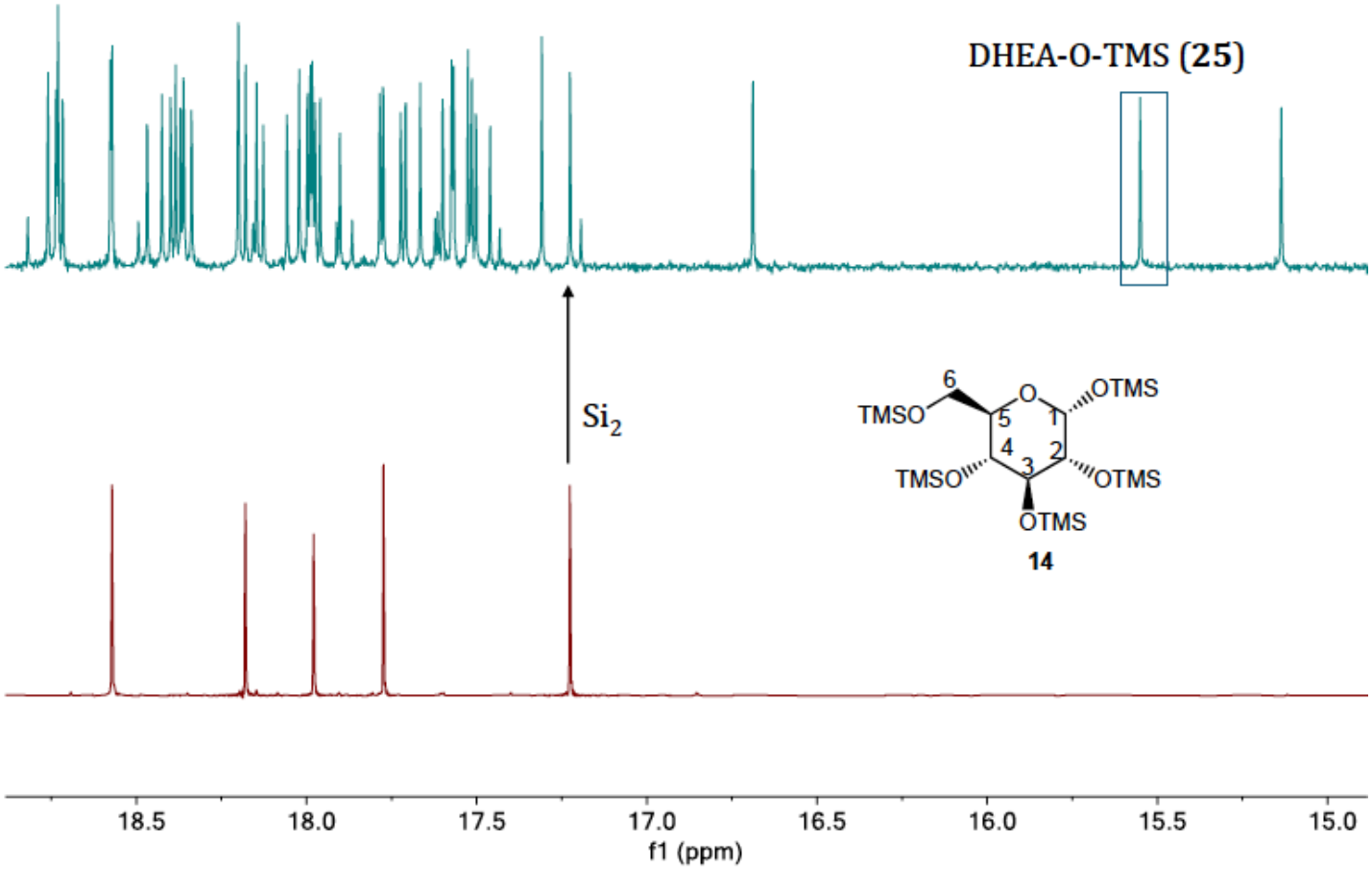

SI-Figure 3.33: (Replicate 2 Section 3.2.8): Overlap of ^{29}Si NMR experiment of α-per-*O*-TMS glucose (**14**), β-per-*O*-TMS fructose (**16**), per-*O*-TMS sucrose (**20**), per-*O*-TMS kestose (**22**), per-*O*-TMS raffinose (**23**), per-*O*-TMS staychose (**24**) and DHEA-*O*-TMS (**25**) synthesized from free sugar as mixture in 1:1:1:1:1:1:1 mole ratio with pure per-*O*-TMS glucose (**14**).

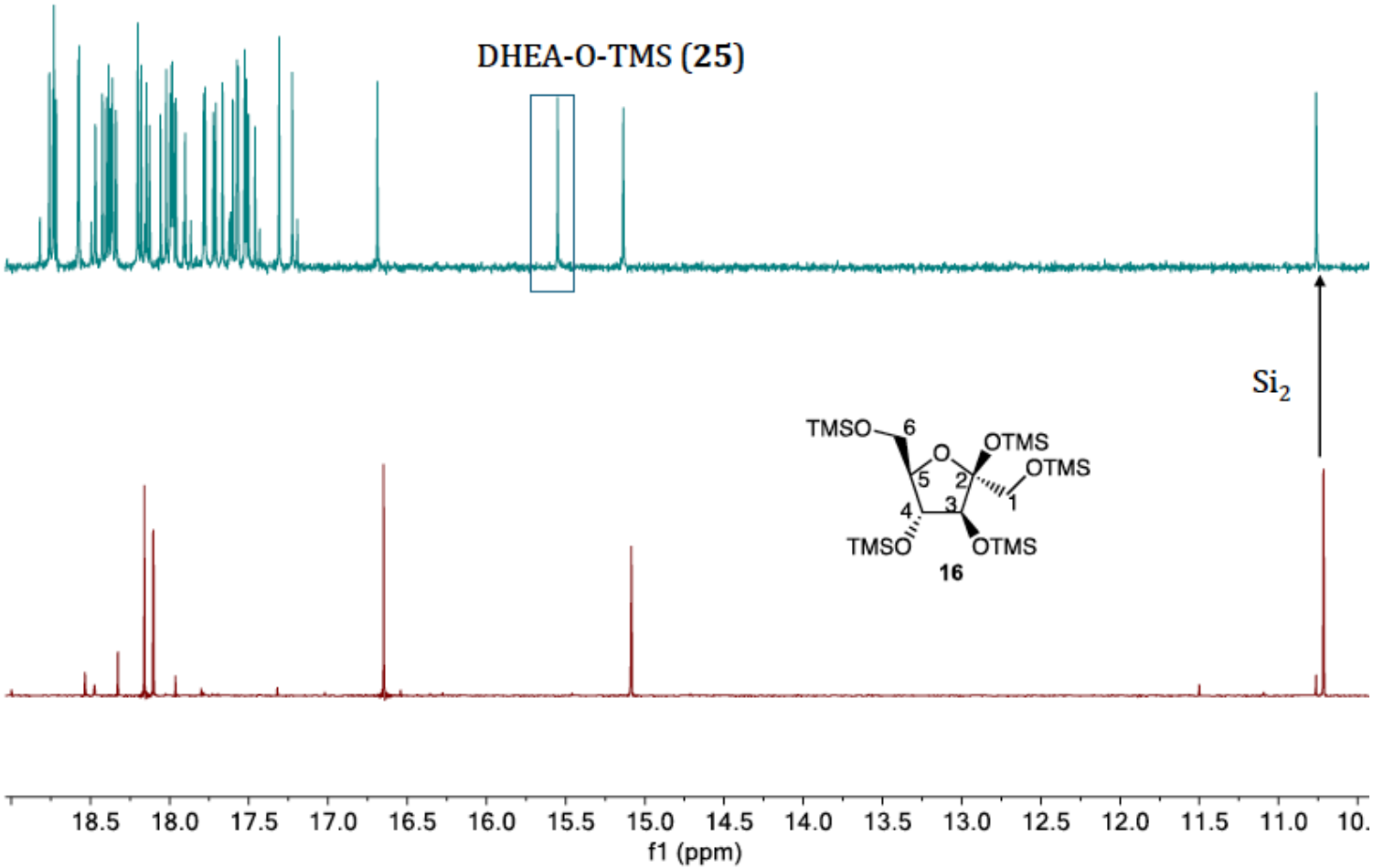

Si-Figure 3.34: (Replicate 2 Section 3.2.8): Overlap of ^{29}Si NMR experiment of α-per-*O*-TMS glucose (**14**), β-per-*O*-TMS fructose (**16**), per-*O*-TMS sucrose (**20**), per-*O*-TMS kestose (**22**), per-*O*-TMS raffinose (**23**), per-*O*-TMS staychose (**24**) and DHEA-*O*-TMS (**25**) synthesized from free sugar as mixture in 1:1:1:1:1:1:1 mole ratio with pure per-*O*-TMS fructose (**16**).

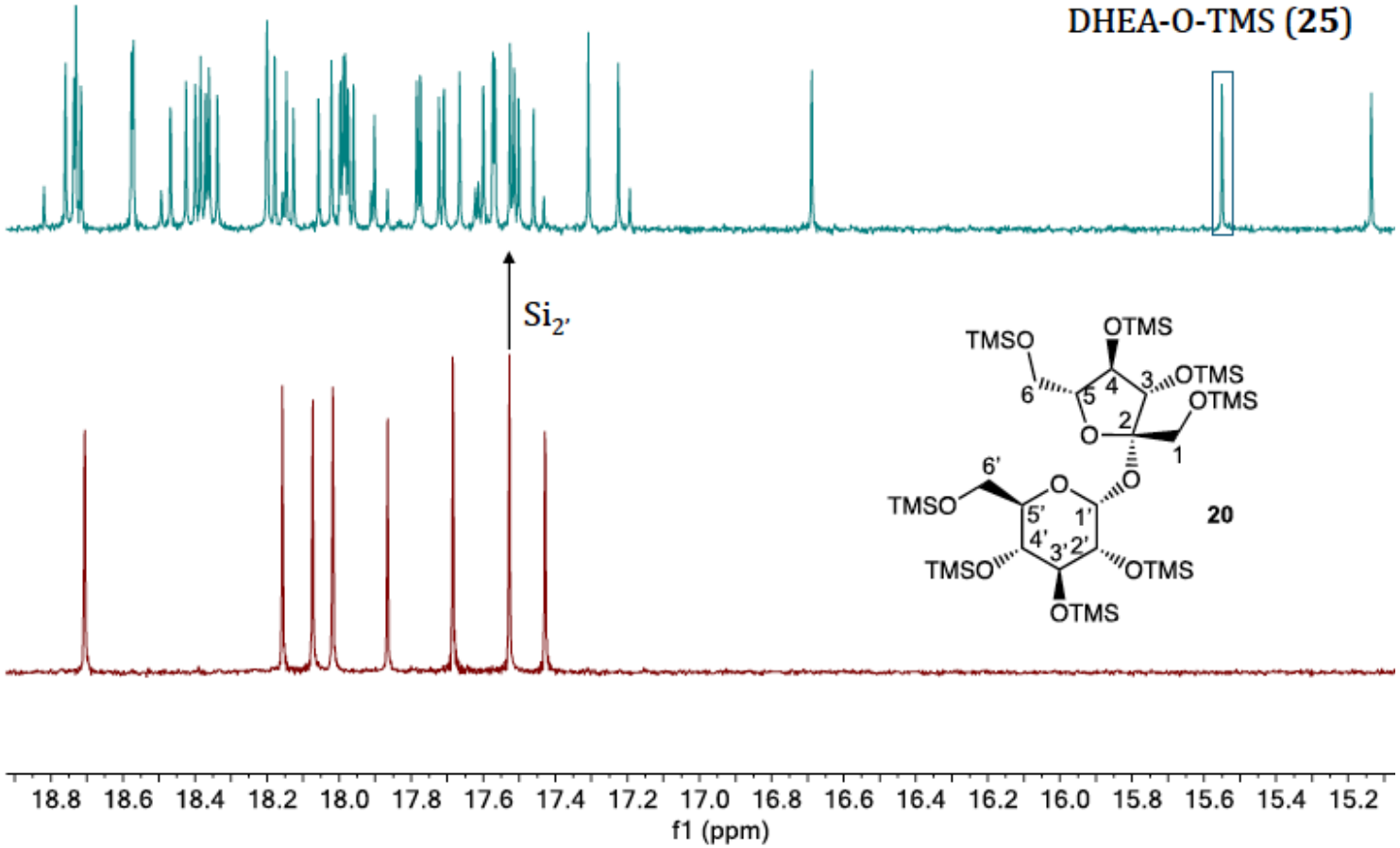

SI-Figure 3.35: (Replicate 2 Section 3.2.78): Overlap of ^{29}Si NMR experiment of α-per-*O*-TMS glucose (**14**), β-per-*O*-TMS fructose (**16**), per-*O*-TMS sucrose (**20**), per-*O*-TMS kestose (**22**), per-*O*-TMS raffinose (**23**), per-*O*-TMS staychose (**24**) and DHEA-*O*-TMS (**25**) synthesized from free sugar as mixture in 1:1:1:1:1:1:1 mole ratio with pure per-*O*-TMS surcose (**20**).

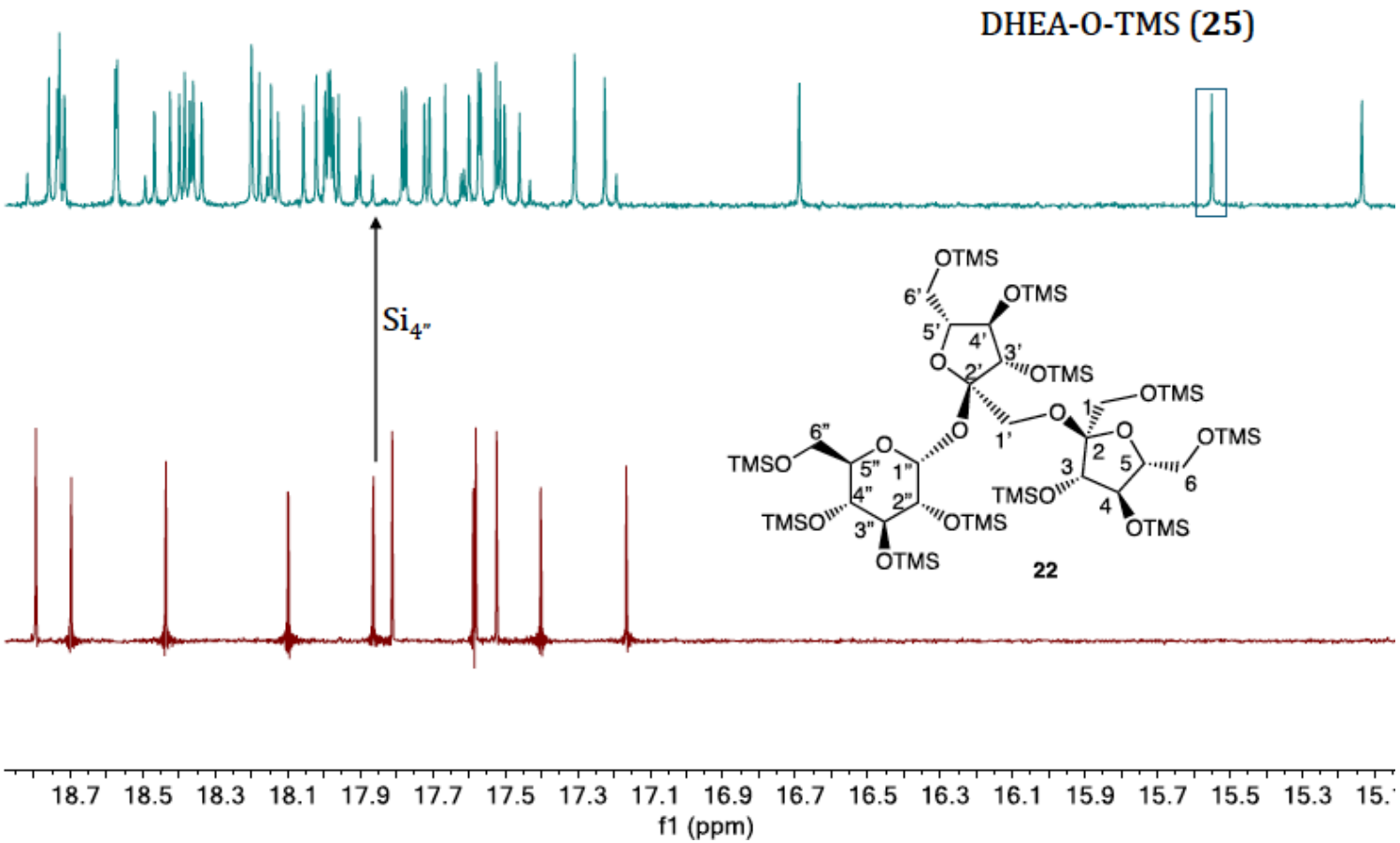

SI-Figure 3.36: (Replicate 2 Section 3.2.8): Overlap of ^{29}Si NMR experiment of α-per-*O*-TMS glucose (**14**), β-per-*O*-TMS fructose (**16**), per-*O*-TMS sucrose (**20**), per-*O*-TMS kestose (**22**), per-*O*-TMS raffinose (**23**), per-*O*-TMS staychose (**24**) and DHEA-*O*-TMS (**25**) synthesized from free sugar as mixture in 1:1:1:1:1:1:1 mole ratio with pure per-*O*-TMS raffinose (**22**).

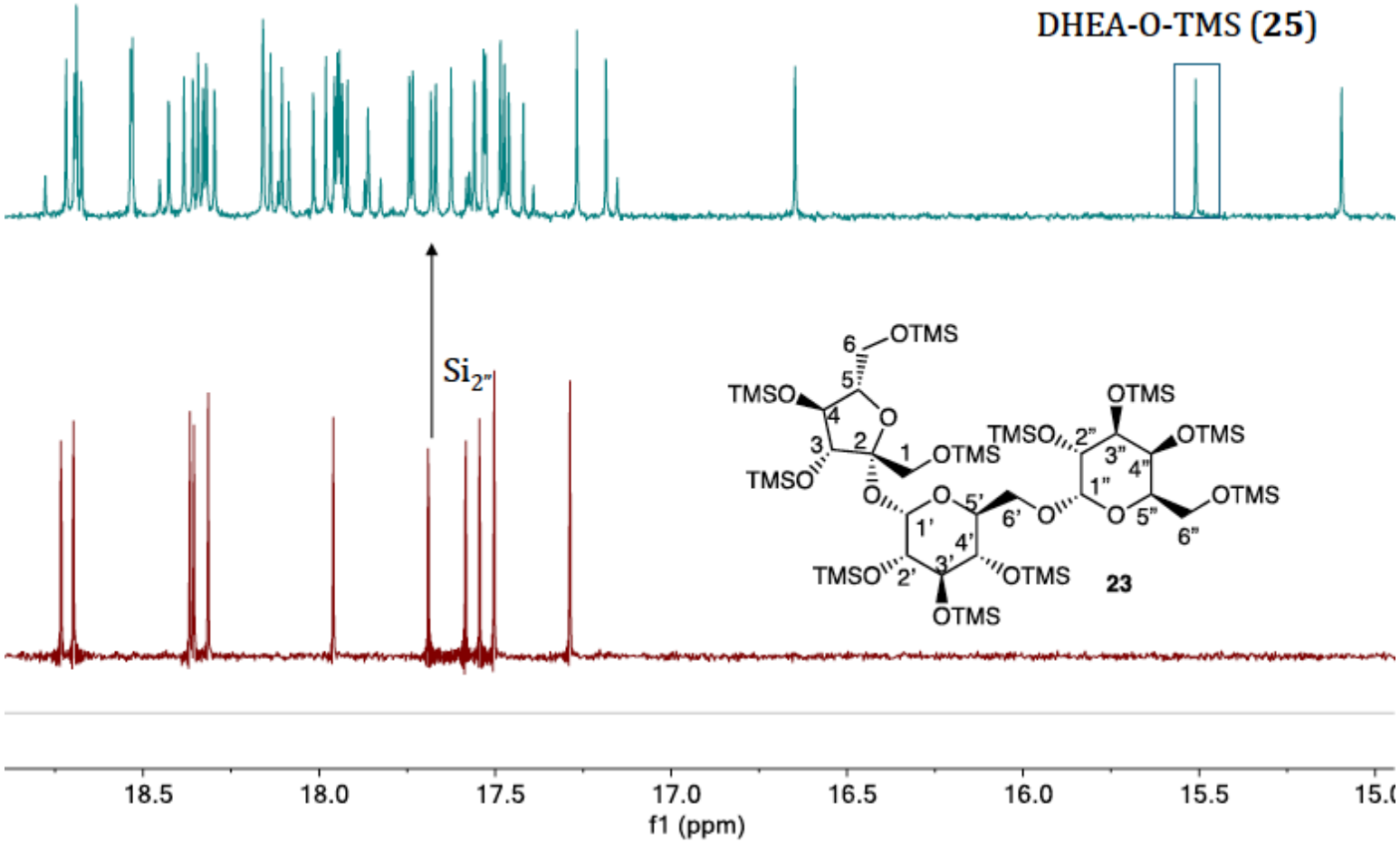

SI-Figure 3.37: (Replicate 2 Section 3.2.8): Overlap of ^{29}Si NMR experiment of α-per-*O*-TMS glucose (**14**), β-per-*O*-TMS fructose (**16**), per-*O*-TMS sucrose (**20**), per-*O*-TMS kestose (**22**), per-*O*-TMS raffinose (**23**), per-*O*-TMS staychose (**24**) and DHEA-*O*-TMS (**25**) synthesized from free sugar as mixture in 1:1:1:1:1:1:1 mole ratio with pure per-*O*-TMS kestose (**23**).

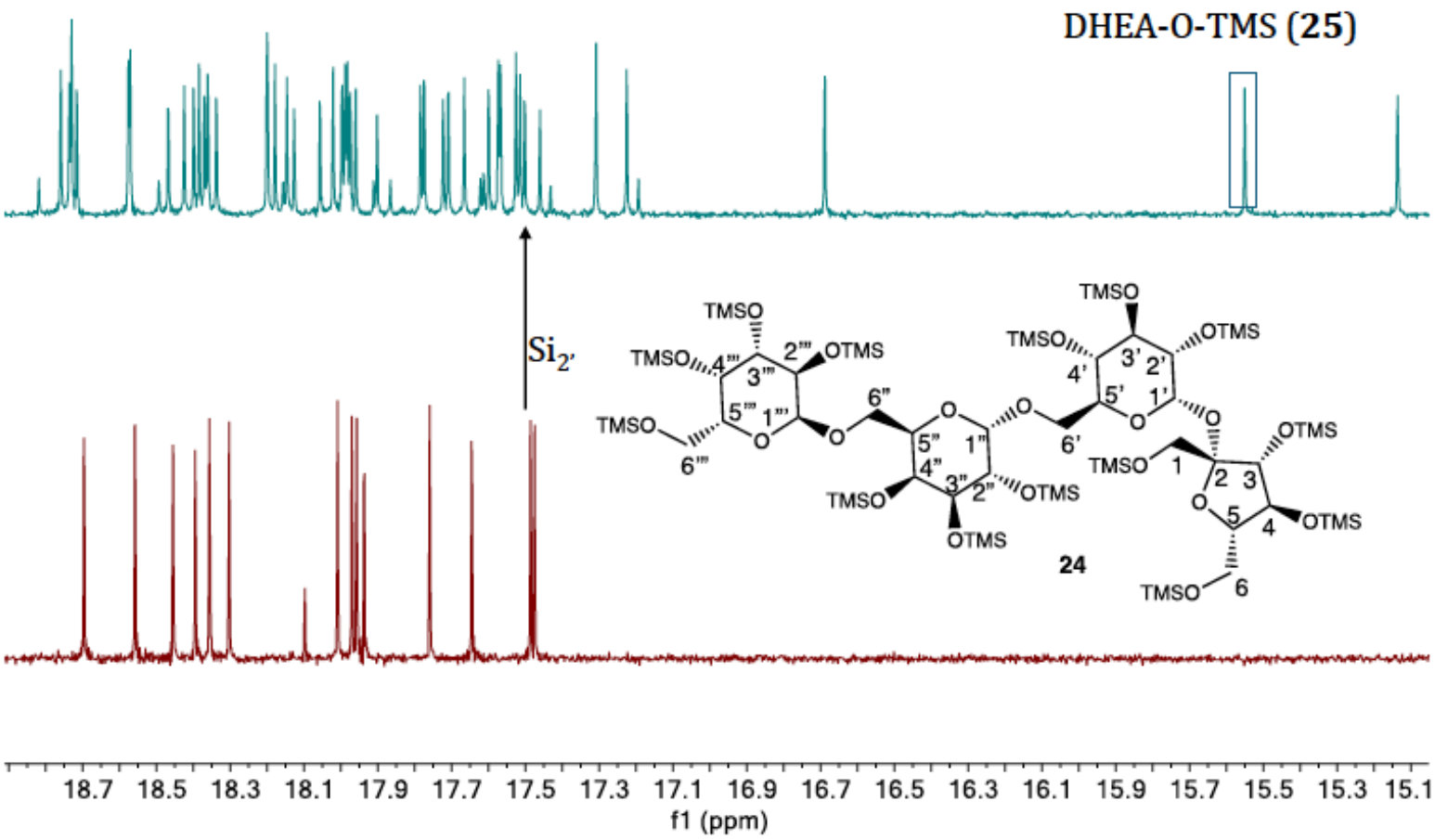

SI-Figure 3.38: (Replicate 2 Section 3.2.8): Overlap of ^{29}Si NMR experiment of α-per-*O*-TMS glucose (**14**), β-per-*O*-TMS fructose (**16**), per-*O*-TMS sucrose (**20**), per-*O*-TMS kestose (**22**), per-*O*-TMS raffinose (**23**), per-*O*-TMS staychose (**24**) and DHEA-*O*-TMS (**25**) synthesized from free sugar as mixture in 1:1:1:1:1:1:1 mole ratio with pure per-*O*-TMS stachysoe (**24**).

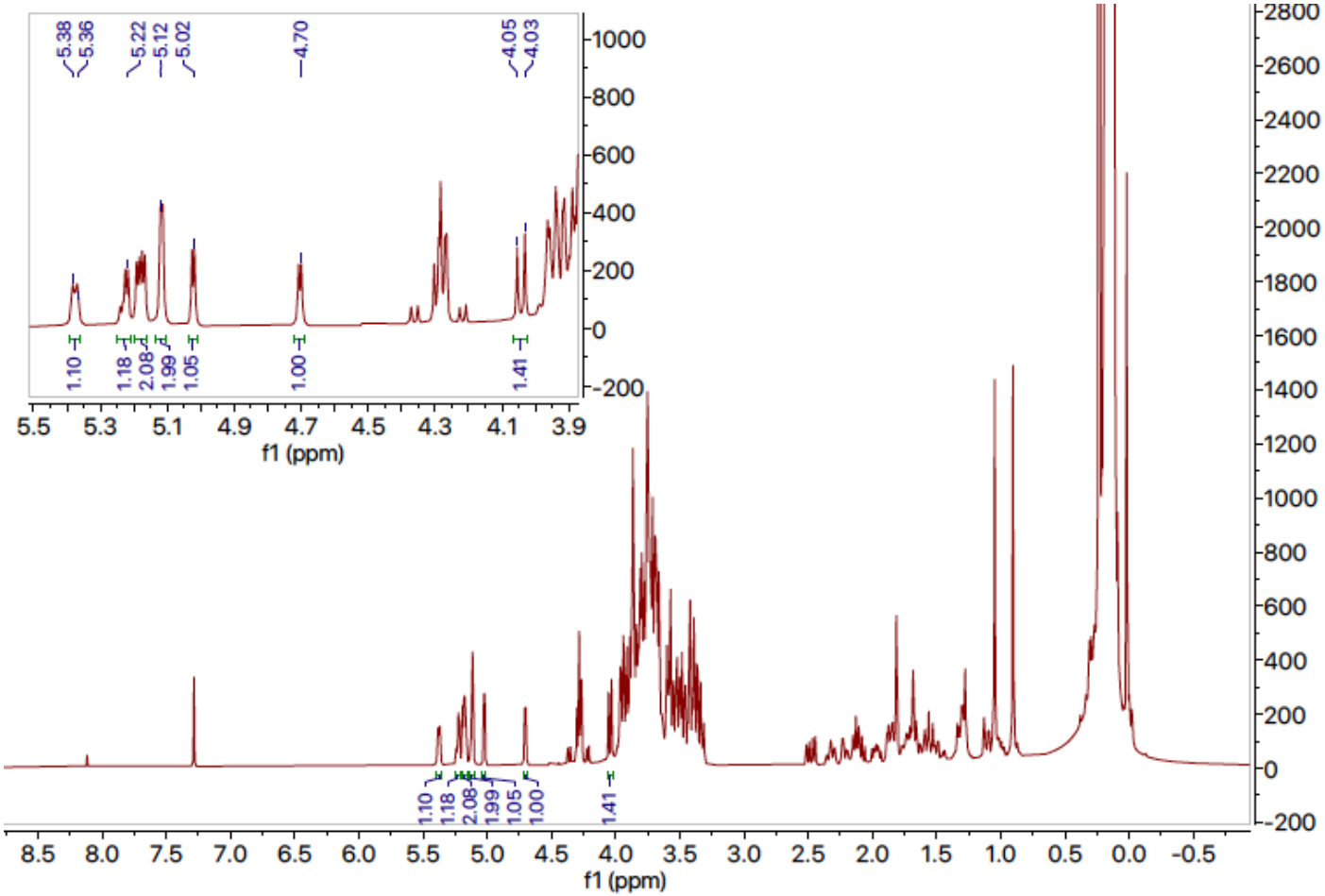

SI-Figure 3.39: (Replicate 2 Section 3.2.8): ^{1}H NMR experiment of α-per-*O*-TMS glucose (**14**), β-per-*O*-TMS fructose (**16**), per-*O*-TMS sucrose (**20**), per-*O*-TMS raffinose per-*O*-TMS kestose (**22**), per-*O*-TMS raffinose (**23**), per-*O*-TMS staychose (**24**) and DHEA-*O*-TMS (**25**) synthesized from free sugar as mixture in 1:1:1:1:1:1:1 mole ratio.

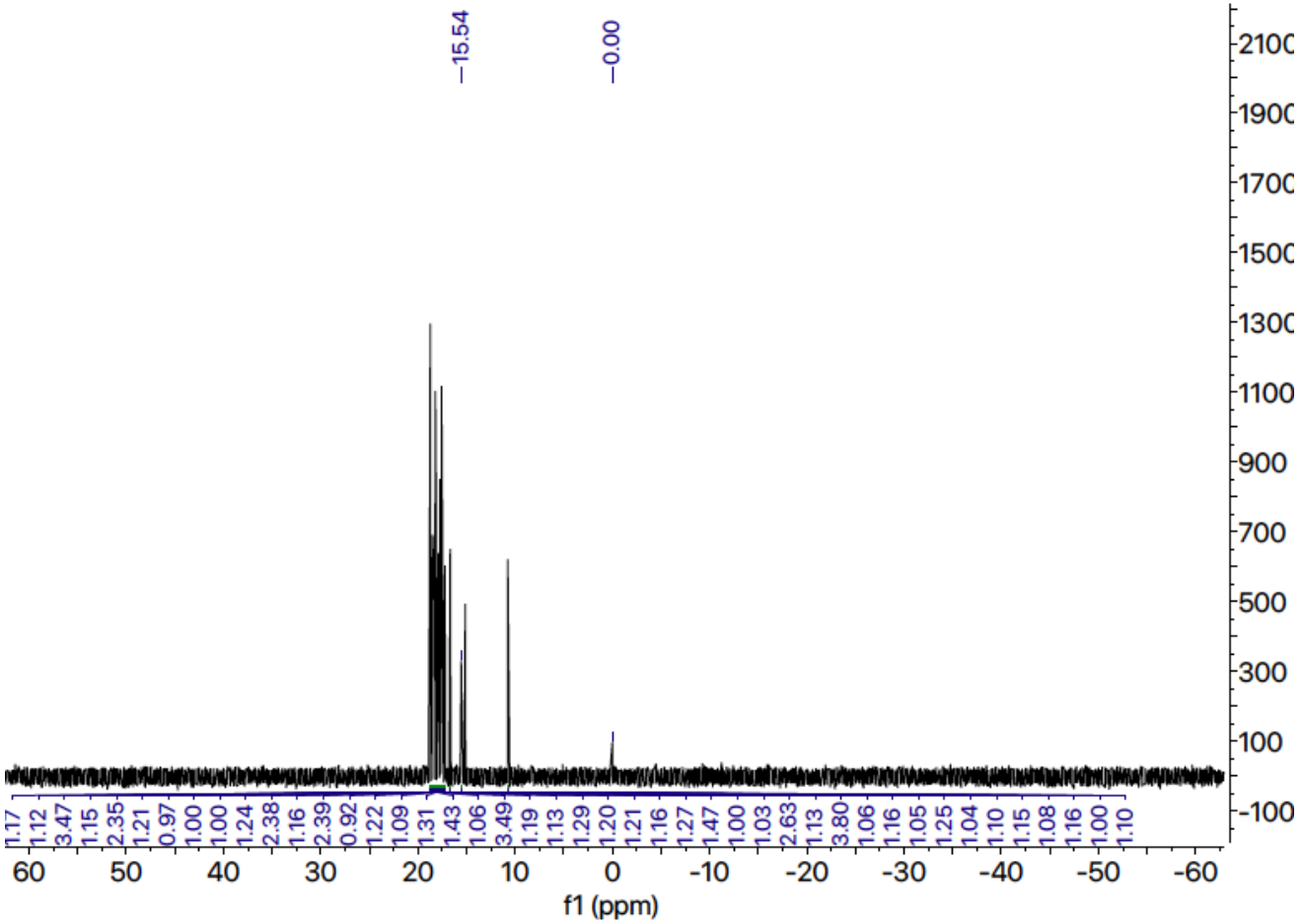

SI-Figure 3.40: (Replicate 3 Section 3.2.8): ^{29}Si NMR experiment of α-per-*O*-TMS glucose (**14**), β-per-*O*-TMS fructose (**16**), per-*O*-TMS sucrose (**20**), per-*O*-TMS kestose (**22**), per-*O*-TMS raffinose (**23**), per-*O*-TMS staychose (**24**) and DHEA-*O*-TMS (**25**) synthesized from free sugar as mixture in 1:1:1:1:1:1:1 mole ratio.

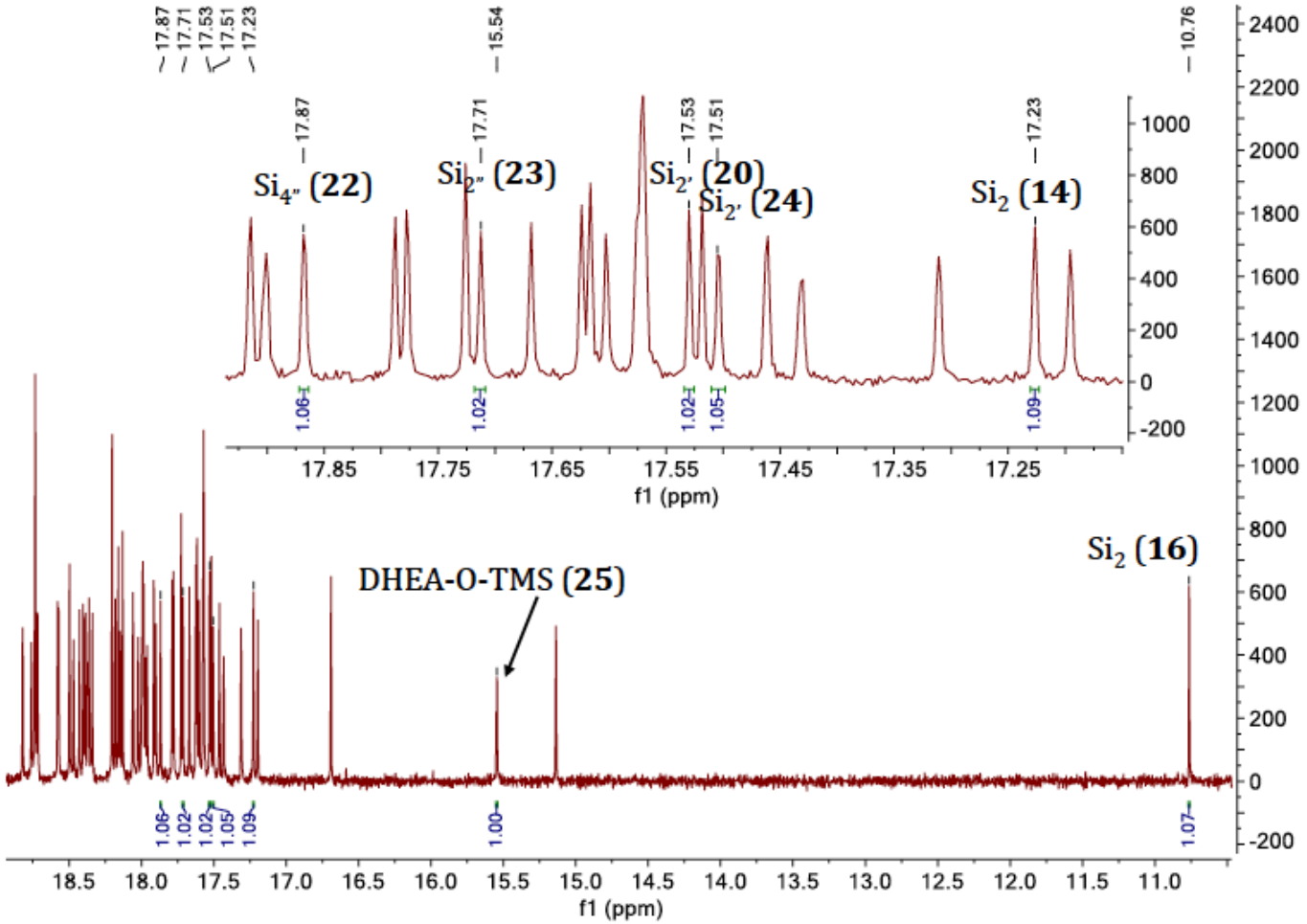

SI-Figure 3.41: (Replicate 3 Section 3.2.8): ^{29}Si NMR experiment of α-per-*O*-TMS glucose (**14**), β-per-*O*-TMS fructose (**16**), per-*O*-TMS sucrose (**20**), per-*O*-TMS raffinose (**22**), per-*O*-TMS kestose (**23**), per-*O*-TMS stachysoe (**24**) and per-*O*-TMS DHEA (**25**) synthesized from free sugar as mixture in 1:1:1:1:1:1:1 mole ratio. The select Si2, Si2', Si2" and Si4" for integration.

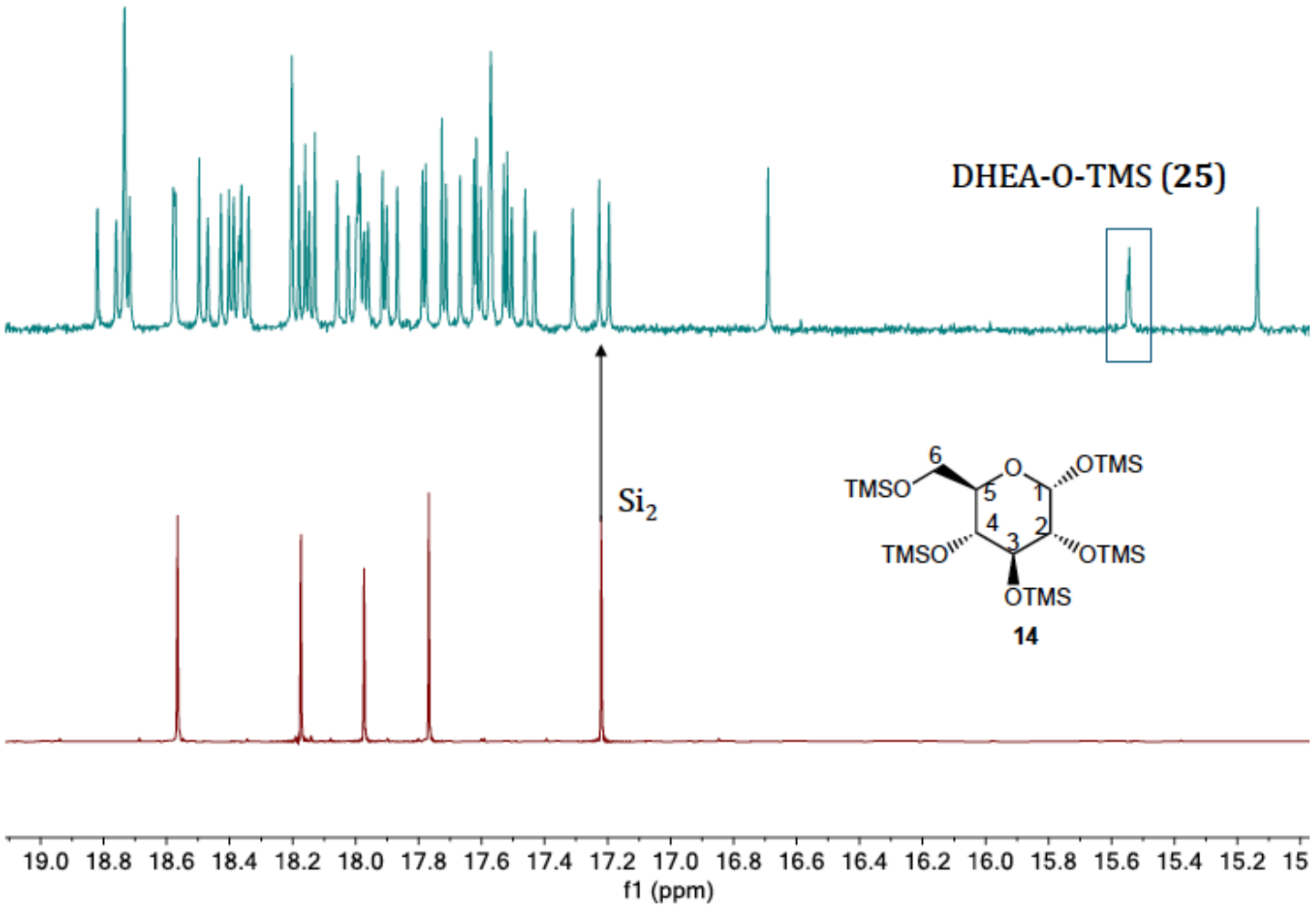

SI-Figure 3.42: (Replicate 3 Section 3.2.8): Overlap of ^{29}Si NMR experiment of α-per-*O*-TMS glucose (**14**), β-per-*O*-TMS fructose (**16**), per-*O*-TMS sucrose (**20**), per-*O*-TMS raffinose (**22**), per-*O*-TMS kestose (**23**), per-*O*-TMS stachysoe (**24**) and per-*O*-TMS DHEA (**25**) synthesized from free sugar as mixture in 1:1:1:1:1:1:1 mole ratio with pure per-*O*-TMS glucose (**14**).

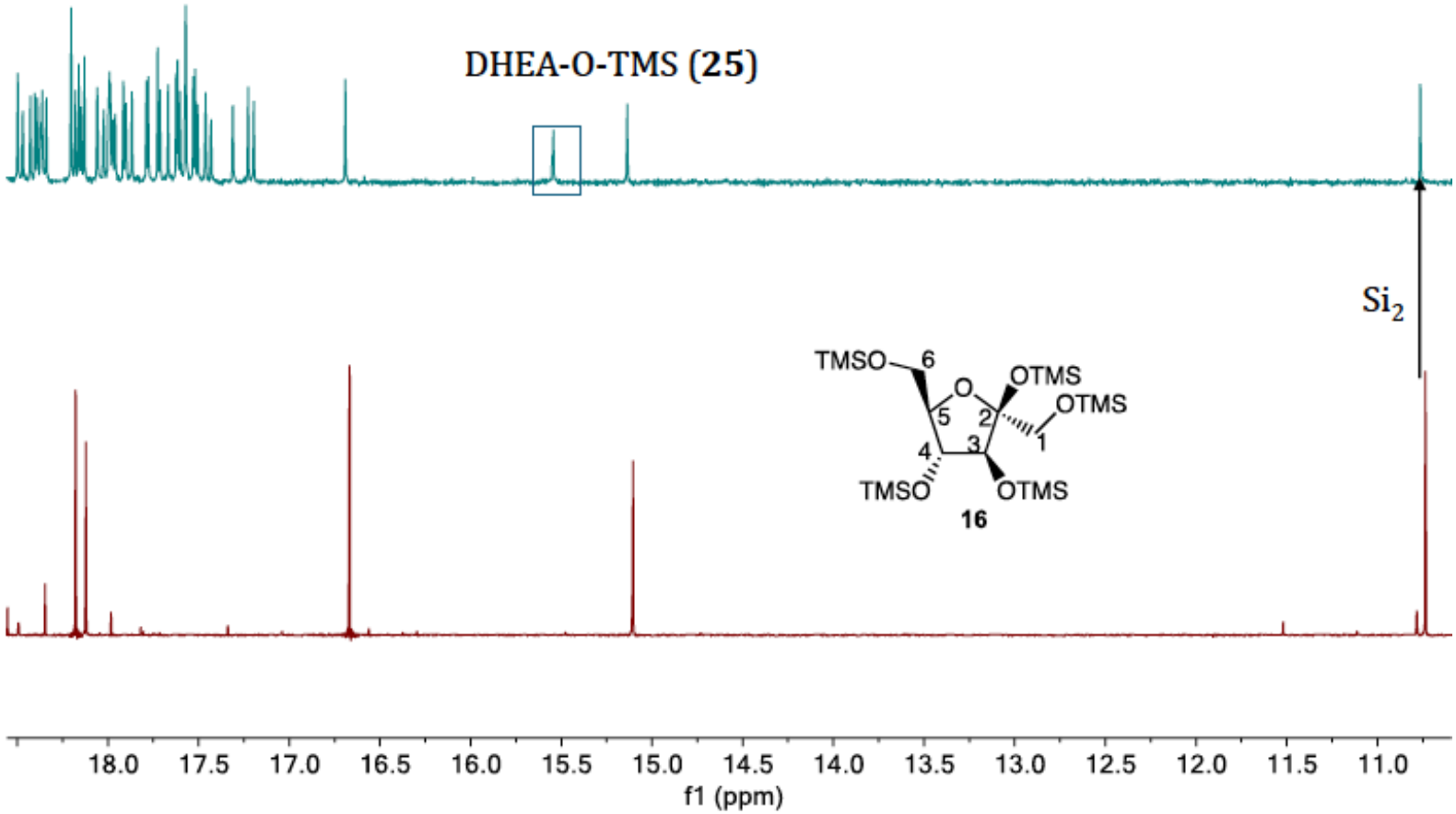

SI-Figure 3.43: (Replicate 3 Section 3.2.8): Overlap of ^{29}Si NMR experiment of α-per-*O*-TMS glucose (**14**), β-per-*O*-TMS fructose (**16**), per-*O*-TMS sucrose (**20**), per-*O*-TMS raffinose (**22**), per-*O*-TMS kestose (**23**), per-*O*-TMS stachysoe (**24**) and per-*O*-TMS DHEA (**25**) synthesized from free sugar as mixture in 1:1:1:1:1:1:1 mole ratio with pure per-*O*-TMS fructose (**16**).

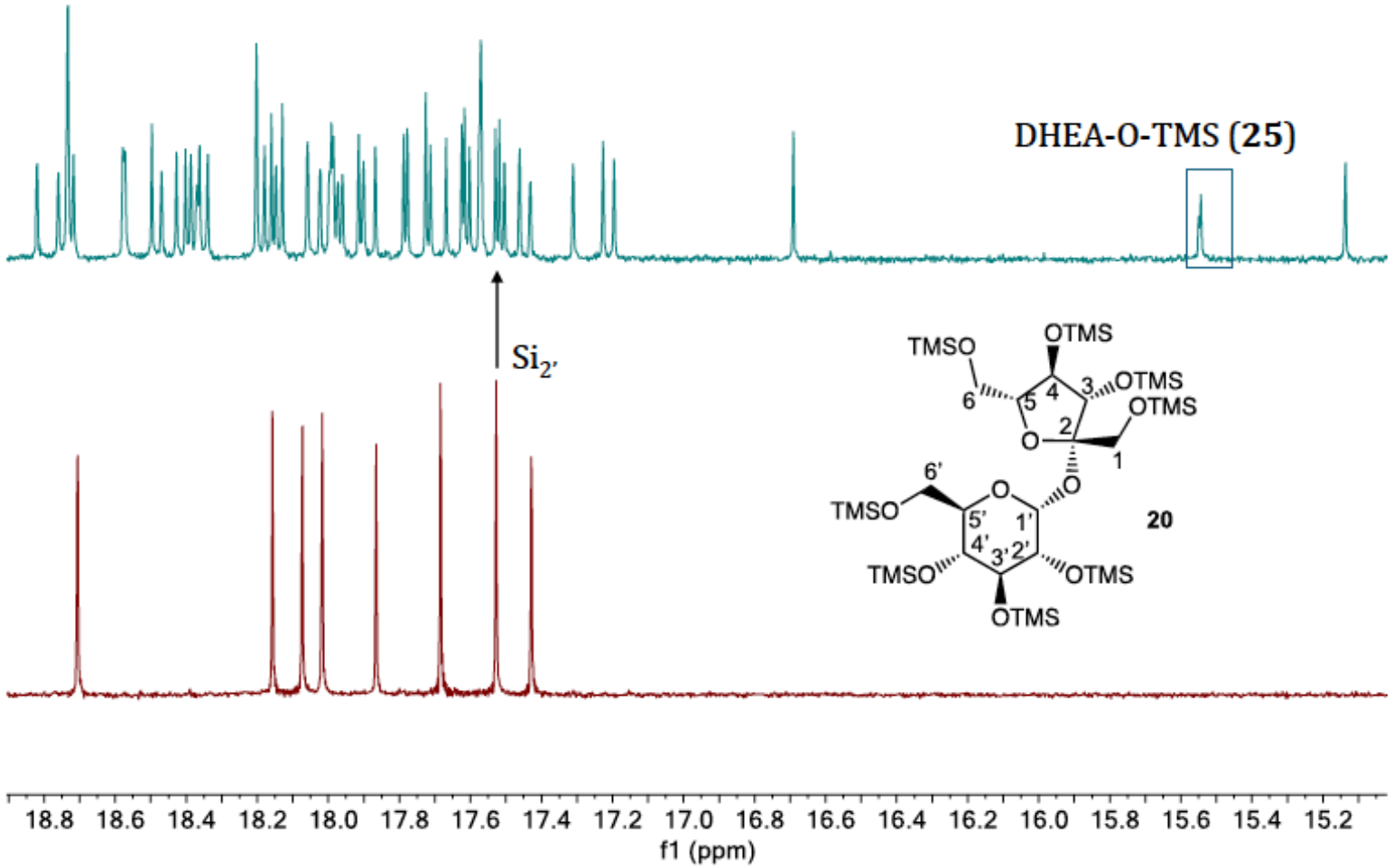

SI-Figure 3.44: (Replicate 3 Section 3.2.8): Overlap of ^{29}Si NMR experiment of α-per-*O*-TMS glucose (**14**), β-per-*O*-TMS fructose (**16**), per-*O*-TMS sucrose (**20**), per-*O*-TMS raffinose (**22**), per-*O*-TMS kestose (**23**), per-*O*-TMS stachysoe (**24**) and per-*O*-TMS DHEA (**25**) synthesized from free sugar as mixture in 1:1:1:1:1:1:1 mole ratio with pure per-*O*-TMS surcose (**20**)**.**

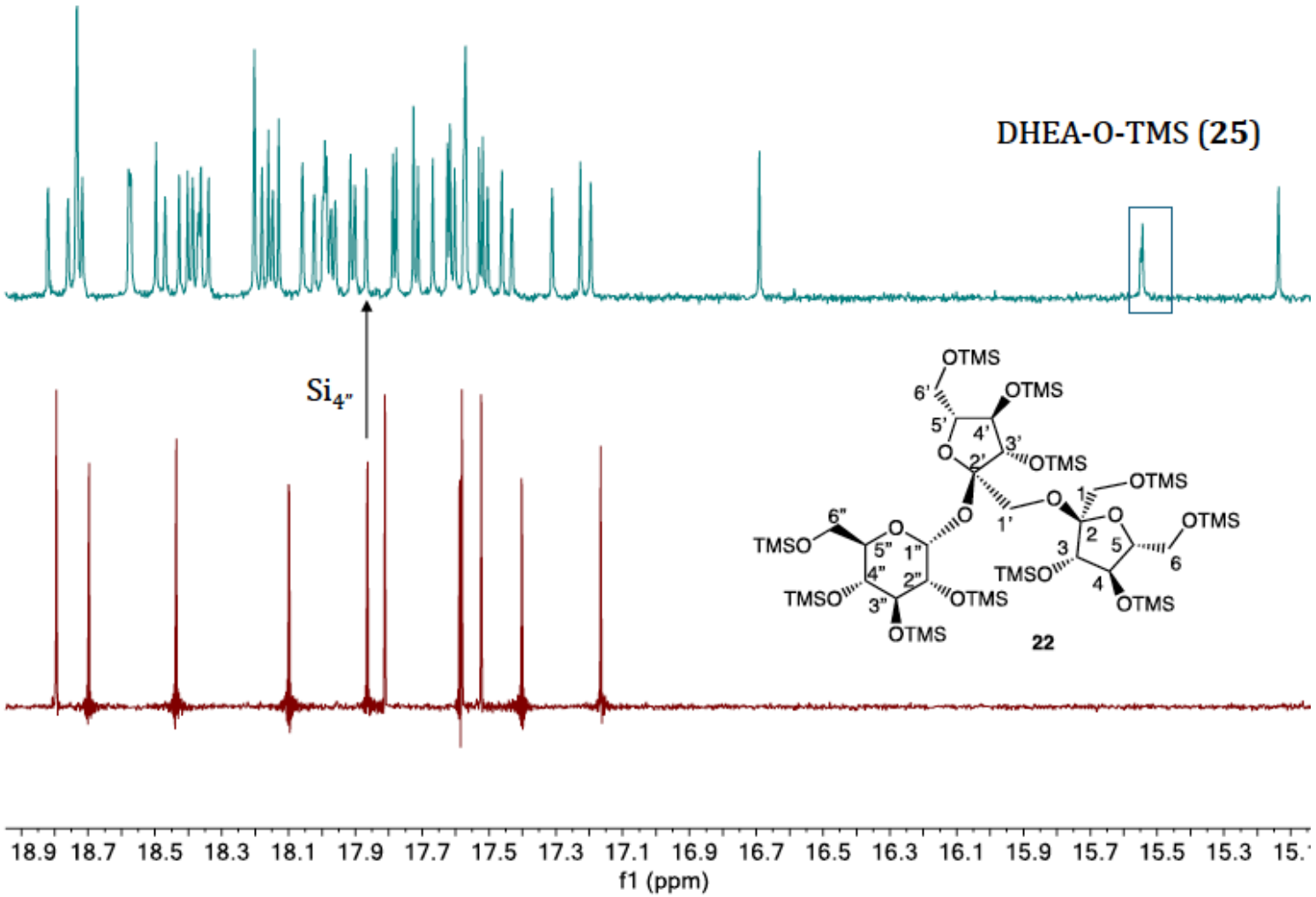

SI-Figure 3.45: (Replicate 3 Section 3.2.8): Overlap of ^{29}Si NMR experiment of α-per-*O*-TMS glucose (**14**), β-per-*O*-TMS fructose (**16**), per-*O*-TMS sucrose (**20**), per-*O*-TMS raffinose (**22**), per-*O*-TMS kestose (**23**), per-*O*-TMS stachysoe (**24**) and per-*O*-TMS DHEA (**25**) synthesized from free sugar as mixture in 1:1:1:1:1:1:1 mole ratio with pure per-*O*-TMS raffinose (**22**).

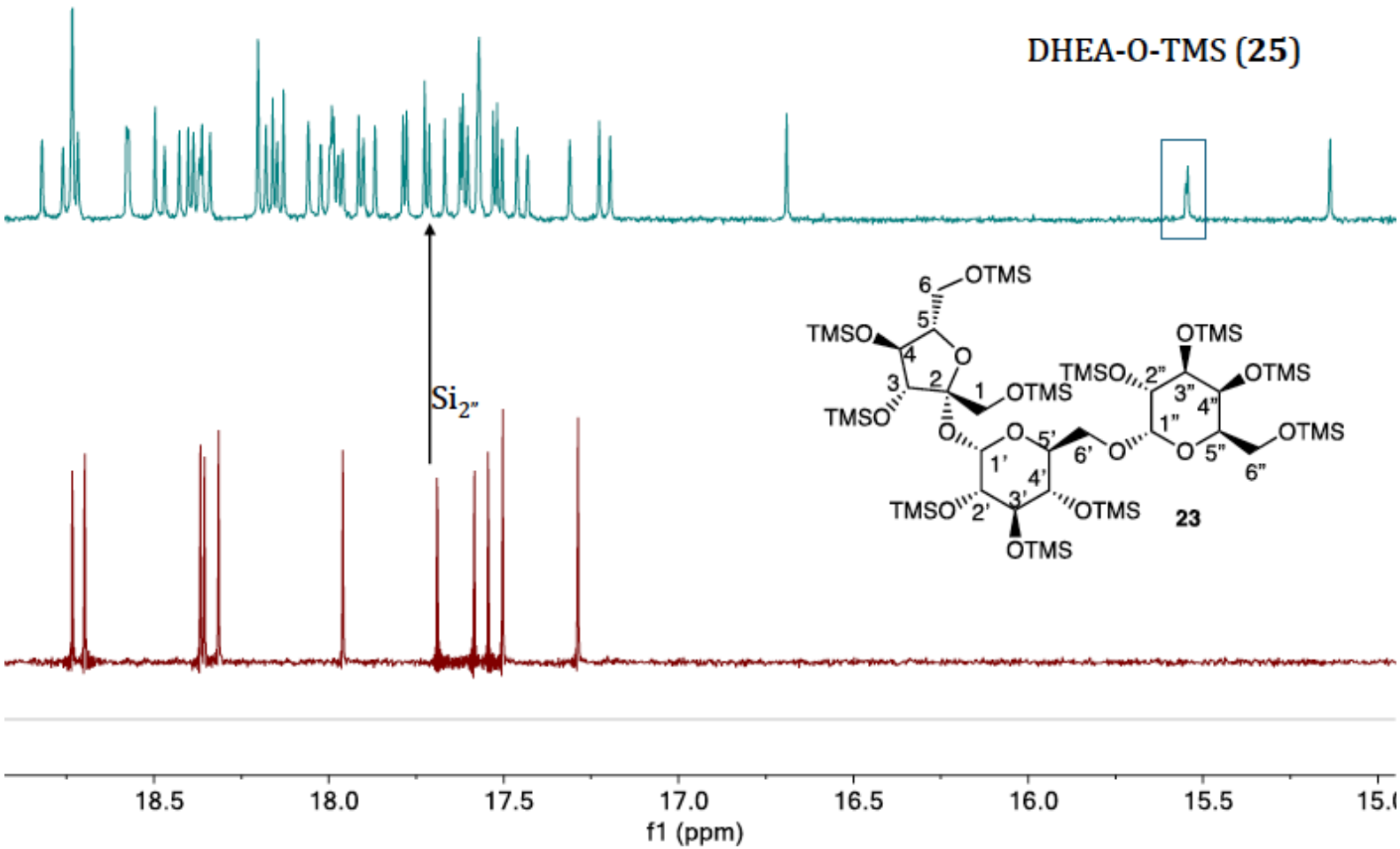

SI-Figure 3.46: (Replicate 3 Section 3.2.8): Overlap of ^{29}Si NMR experiment of α-per-*O*-TMS glucose (**14**), β-per-*O*-TMS fructose (**16**), per-*O*-TMS sucrose (**20**), per-*O*-TMS raffinose (**22**), per-*O*-TMS kestose (**23**), per-*O*-TMS stachysoe (**24**) and per-*O*-TMS DHEA (**25**) synthesized from free sugar as mixture in 1:1:1:1:1:1:1 mole ratio with pure per-*O*-TMS kestose (**23**).

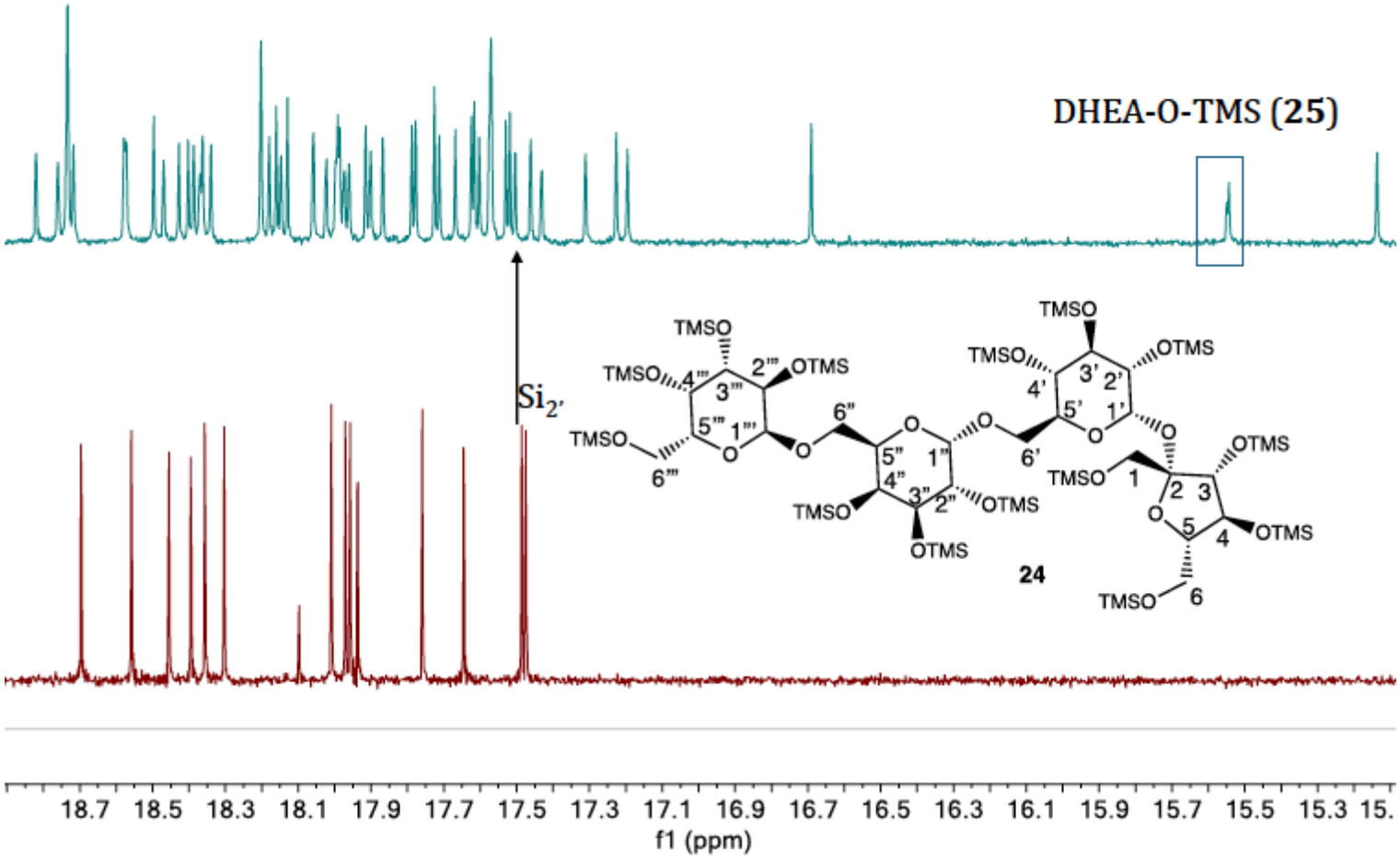

SI-Figure 3.47: (Replicate 3 Section 3.2.8): Overlap of ^{29}Si NMR experiment of α-per-*O*-TMS glucose (**14**), β-per-*O*-TMS fructose (**16**), per-*O*-TMS sucrose (**20**), per-*O*-TMS raffinose (**22**), per-*O*-TMS kestose (**23**), per-*O*-TMS stachysoe (**24**) and per-*O*-TMS DHEA (**25**) synthesized from free sugar as mixture in 1:1:1:1:1:1:1 mole ratio with pure per-*O*-TMS stachysoe (**24**).

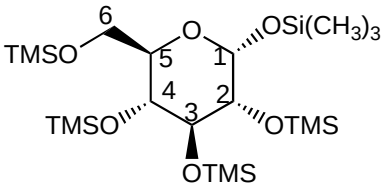

14

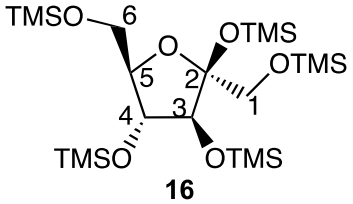

16

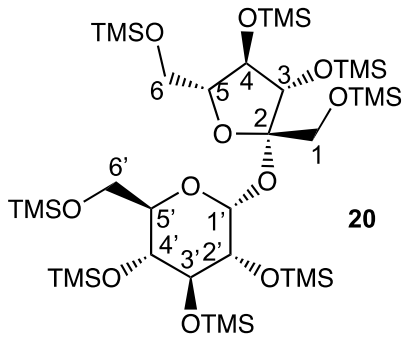

20

SI-Table 3.1: The measured integration of three ^{29}Si NMR experiments of α-per-*O*-TMS glucose (**14**), β-per-*O*-TMS fructose (**16**), and per-*O*-TMS sucrose (**20**) in $CDCl_3$, with reference to TMS at 0 and use HMDS (**27**) as internal standard as 1.00. The mixture was synthesized in a reaction as a 1:1:1 equal mole ratio and the reaction was run for 24 hours.

Integration Values: HMDS as Internal Standard									
Compound	Si_2	Si_3	Si_6	Si_1	Si_4	Si_{1f}	Si_{3f}	Si_{4f}	Si_{6f}
Experiment 1									
Sucrose (**20**)	1.80	1.92	1.56	x	1.88	x	1.70	1.74	1.46
Fructose (**16**)	1.60	x	1.40	1.26	1.62				
Glucose (**14**)	1.64	1.70	1.30	1.54	1.72				
Experiment 2									
Sucrose (**20**)	1.62	1.86	1.50	x	1.82	x	1.48	1.74	1.44
Fructose (**16**)	1.60	x	1.40	1.24	1.48				
Glucose (**14**)	1.60	1.60	1.32	1.48	1.70				
Experiment 3									
Sucrose (**20**)	1.62	1.82	1.56	x	1.82	x	1.58	1.74	1.42
Fructose (**16**)	1.56	x	1.32	1.18	1.56				
Glucose (**14**)	1.60	1.64	1.16	1.46	1.66				

SI-Table 3.2: The ratio of triplicate ^{29}Si NMR experiments of α-per-*O*-TMS glucose (**14**), β-per-*O*-TMS fructose (**16**), and per-*O*-TMS sucrose (**20**) in $CDCl_3$, with reference to TMS at 0 and use HMDS as internal standard as 1.00. The mixture was synthesized in a reaction as a 1:1:1 equal mole ratio and reaction was run for 24 hours. The ratio calculated from the integration values.

Ratio by Integration: HMDS as Internal Standard									
Compound	Si_2	Si_3	Si_6	Si_1	Si_4	Si_{1f}	Si_{3f}	Si_{4f}	Si_{6f}
Theoretical Ratio									
Sucrose (**20**)	1.00	1.00	1.00	x	1.00	1.00	1.00	1.00	1.00
Fructose (**16**)	1.00	1.00	1.00	1.00	1.00				
Glucose (**14**)	1.00	1.00	1.00	1.00	1.00				
Measured Ratio Used Integration Value									
Experiment 1									
Sucrose (**20**)	1.15	1.20	1.34	x	1.27	x	1.15	1.00	1.03
Fructose (**16**)	1.03	x	1.21	1.07	1.09				
Glucose (**14**)	1.05	1.06	1.12	1.31	1.16				
Experiment 2									
Sucrose (**20**)	1.04	1.16	1.29	x	1.23	x	1.10	1.00	1.01
Fructose (**16**)	1.03	x	1.21	1.05	1.00				
Glucose (**14**)	1.03	1.00	1.14	1.25	1.15				
Experiment 3									
Sucrose (**20**)	1.04	1.14	1.34	x	1.23	x	1.07	1.00	1.00
Fructose (**16**)	1.00	x	1.14	1.00	1.05				
Glucose (**14**)	1.03	1.03	1.00	1.24	1.12				

SI-Table 3.3: The mmols calculated from integration of triplicate ^{29}Si NMR experiments of α-per-*O*-TMS glucose (**14**), β-per-*O*-TMS fructose (**16**), and per-*O*-TMS sucrose (**20**) in $CDCl_3$, with reference to TMS at 0 and use HMDS (**27**) as internal standard as 1.00.

Mmol calculated by ^{29}Si Integration Value: HMDS as Internal Standard (1.00)									
	$Si_{2'}$	$Si_{3'}$	$Si_{6'}$	$Si_{1'}$	$Si_{4'}$	Si_1	Si_3	Si_4	Si_6
Experiment 1:									
Anticipated mmol: Sucrose (0.030): Fructose (0.027): Glucose (0.025)									
Calculated mmol:									
Sucrose (**20**)	0.143	0.15<u>2</u>	0.124	x	0.149	x	0.138	0.116	0.212
Fructose (**16**)	0.127	x	0.111	0.100	0.129				
Glucose (**14**)	0.130	0.135	0.103	0.122	0.137				
Experiment 2:									
Anticipated mmol: Sucrose (0.018<u>5</u>): Fructose (0.016<u>1</u>): Glucose (0.016<u>7</u>)									
Calculated mmol:									
Sucrose (**20**)	0.128	0.147	0.119	x	0.144	x	0.117	0.138	0.114
Fructose (**16**)	0.127	x	0.110	0.098	0.117				
Glucose (**14**)	0.128	0.127	0.105	0.117	0.135				
Experiment 3:									
Anticipated mmol: Sucrose (0.018<u>4</u>): Fructose (0.016<u>0</u>): Glucose (0.016<u>6</u>)									
Calculated mmol:									
Sucrose (**20**)	0.127	0.143	0.122	x	0.143	x	0.124	0.136	0.111
Fructose (**16**)	0.122	x	0.104	0.093	0.122				
Glucose (**14**)	0.126	0.129	0.091	0.115	0.130				

SI-Table 3.4: The chemical shift (δ) of α-per-*O*-TMS glucose (**14**), β-per-*O*-TMS fructose (**16**), and per-*O*-TMS sucrose (**20**) with reference to TMS at 0 and use HMDS (**27**) as internal standard. The mixtures were prepared at different ratio from pure silylated sugar for each experiment.

Experiment 1 - Internal Standard (HMDS= 0.10M): δ 2.47										
Compound	Conc.	δ Si_2	δ Si_3	δ Si_6	δ Si_1	δ Si_4	δ $Si_{1'}$	δ $Si_{3'}$	δ $Si_{4'}$	δ $Si_{6'}$
Fructose	0.025 M	10.72	Overlap 18.17	15.08	18.11	16.66	x	x	x	x
Sucrose	0.050 M	17.54	17.70	17.44	x	18.03	Overlap 18.17	18.08	18.71	17.87
Glucose	0.10 M	17.20	17.76	17.96	18.15	18.56	x	x	x	x
Experiment 2										
Compound	Conc.	δ Si_2	δ Si_3	δ Si_6	δ Si_1	δ Si_4	δ $Si_{1'}$	δ $Si_{3'}$	δ $Si_{4'}$	δ $Si_{6'}$
Fructose	0.10 M	10.72	Overlap 18.17	15.08	18.10	16.66	x	x	x	x
Sucrose	0.025 M	17.54	17.70	17.43	x	18.02	Overlap 18.17	18.08	18.70	17.86
Glucose	0.05 M	17.19	17.70	17.95	18.15	18.55	x	x	x	x
Experiment 3										
Compound	Conc.	δ Si_2	δ Si_3	δ Si_6	δ Si_1	δ Si_4	δ $Si_{1'}$	δ $Si_{3'}$	δ $Si_{4'}$	δ $Si_{6'}$
Fructose	0.050 M	10.72	Overlap 18.17	15.08	18.11	16.66	x	x	x	x
Sucrose	0.10 M	17.54	17.70	17.44	x	18.02	Overlap 18.17	18.08	18.70	17.86
Glucose	0.025 M	17.20	17.76	17.95	18.15	18.55	x	x	x	x

SI-Table 3.5: The integration of α-per-*O*-TMS glucose (**14**), β-per-*O*-TMS fructose (**16**), and per-*O*-TMS sucrose (**20**) in $CDCl_3$, with reference to TMS at 0 and use HMDS (**27**) as internal standard integrated as 1.00.

Integration Values: HMDS as Internal Standard (1.00)

Compound	Si_2	Si_3	Si_6	Si_1	Si_4	Si_{1f}	Si_{3f}	Si_{4f}	Si_{6f}
Experiment 1: Ratio of mixture: Sucrose (2): Fructose (1): Glucose (4)									
Sucrose (**20**)	3.26	3.36	3.02	x	3.08	x	3.00	3.16	2.68
Fructose (**16**)	1.34	x	1.14	1.08	1.36				
Glucose (**14**)	6.32	6.52	5.42	6.38	6.54				
Experiment 2: Ratio of mixture: Sucrose (1): Fructose (4): Glucose (2)									
Sucrose (**20**)	1.38	1.36	1.18	x	1.32	x	1.04	1.30	1.06
Fructose (**16**)	5.64	x	5.14	4.1	5.58				
Glucose (**14**)	3.02	3.06	2.38	2.80	2.96				
Experiment 3: Ratio of mixture: Sucrose (4): Fructose (2): Glucose (1)									
Sucrose (**20**)	5.72	5.54	5.10	x	**5.96**	x	5.30	5.60	4.28
Fructose (**16**)	2.68	x	2.44	2.08	**2.66**				
Glucose (**14**)	1.34	1.56	1.24	1.00	1.56				

SI-Table 3.6: The mmol calculated from ^{29}Si NMR integration from α-per-*O*-TMS glucose (**14**), β-per-*O*-TMS fructose (**16**), and per-*O*-TMS sucrose (**20**) in $CDCl_3$, with reference to TMS at 0 and use HMDS (**27**) as internal standard as 1.00.

Mmol calculated by ^{29}Si Integration Value: HMDS as Internal Standard (1.00)									
	$Si_{2'}$	$Si_{3'}$	$Si_{6'}$	$Si_{1'}$	$Si_{4'}$	Si_1	Si_3	Si_4	Si_6
Experiment 1:									
Anticipated mmol: Sucrose (0.02): Fructose (0.01): Glucose (0.04)									
Weighted mmol: Sucrose (0.0193): Fructose (0.0102): Glucose (0.0412)									
Calculated mmol:									
Sucrose (**20**)	0.0130	0.134	0.121	x	0.123	x	0.120	0.126	0.107
Fructose (**16**)	0.0536	x	0.0456	0.0432	0.0544				
Glucose (**14**)	0.253	0.261	0.217	0.255	0.2620				
Experiment 2:									
Anticipated mmol: Sucrose (0.01): Fructose (0.04): Glucose (0.02)									
Weighted mmol: Sucrose (0.00989): Fructose (0.0403): Glucose (0.0191)									
Calculated mmol:									
Sucrose (**20**)	0.0550	0.0544	0.047	x	0.0528	x	0.0416	0.0520	0.0504
Fructose (**16**)	0.225	x	0.206	0.164	0.223				
Glucose (**14**)	0.121	0.122	0.0952	0.112	0.118				
Experiment 3:									
Anticipated mmol: Sucrose (0.04): Fructose (0.02): Glucose (0.01)									
Weighted mmol: Sucrose (0.0399): Fructose (0.0205): Glucose (0.0102)									
Calculated mmol:									
Sucrose (**20**)	0.228	0.222	0.204	x	0.206	x	0.212	0.224	0.171
Fructose (**16**)	0.107	x	0.0976	0.0832	0.100				
Glucose (**14**)	0.0536	0.0624	0.0496	0.0400	0.0624				

SI-Table 3.7: The Integration of triplicate ^{29}Si NMR experiment of α-per-*O*-TMS glucose (**14**), β-per-*O*-TMS fructose (**16**), and per-*O*-TMS sucrose (**20**) in $CDCl_3$, using DHEA-*O*-TBDPSi (**26**) as internal standard. This mixture was synthesized from free sugar of 1:1:1 mol ratio at room temperature for 24 h. The mass of each experiment was weighed independently of each other. The solution is 0.125 M concentration.

Integration Values: *TBDPSi-DHEA as Internal Standard (1.00)*									
Compound	Si_2	Si_3	Si_6	Si_1	Si_4	Si_{1f}	Si_{3f}	Si_{4f}	Si_{6f}
Ratio of mixture: Sucrose (1): Fructose (1): Glucose (1)									
Experiment 1:									
Sucrose (**20**)	2.10	2.35	1.69	**x**	2.13	**x**	1.89	2.04	1.61
Fructose (**16**)	1.87	**x**	1.51	1.41	1.81				
Glucose (**14**)	1.96	1.93	1.44	1.77	1.94				
Experiment 2:									
Sucrose (**20**)	2.05	2.22	1.71	**x**	2.10	**x**	1.66	2.01	1.66
Fructose (**16**)	1.84	**x**	1.50	1.44	1.77				
Glucose (**14**)	1.92	1.85	1.52	1.73	1.93				
Experiment 3:									
Sucrose (**20**)	2.22	2.29	1.90	**x**	2.12	**x**	2.01	2.16	1.79
Fructose (**16**)	1.93	**x**	1.69	1.55	1.97				
Glucose (**14**)	2.07	2.09	1.56	1.85	1.95				

SI-Table 3.8: The mmol calculated from integration values of α-per-*O*-TMS glucose (**14**), β-per-*O*-TMS fructose (**16**), and per-*O*-TMS sucrose (**20**) in $CDCl_3$, using DHEA-*O*-TBDPSi (**26**) as internal standard. This mixture was synthesized from free sugar of 1:1:1 mol ratio at room temperature for 24 h. The mass of each experiment was weighed independently of each other. The solution is 0.125 M concentration.

Mmol calculated by ^{29}Si Integration Value: TBDPSi-DHEA as Internal Standard (0.0132)									
	Si_2	Si_3	Si_6	Si_1	Si_4	Si_{1f}	Si_{3f}	Si_{4f}	Si_{6f}
Experiment 1:									
Anticipated mmol: Sucrose (0.0185): Fructose (0.0161): Glucose (0.0167)									
Calculated mmol:									
Sucrose (**20**)	0.0277	0.0310	0.0223	x	0.0281	x	0.0249	0.0269	0.0212
Fructose (**16**)	0.0247	x	0.0199	0.0186	0.0239				
Glucose (**14**)	0.0252	0.055	0.0190	0.0234	0.0256				
Experiment 2:									
Anticipated mmol: Sucrose (0.0185): Fructose (0.0161): Glucose (0.0167)									
Calculated mmol:									
Sucrose (**20**)	0.0267	0.0289	.0223	x	.0274	x	0.0216	0.0262	0.0216
Fructose (**16**)	0.0239	x	0.0195	0.0188	0.0231				
Glucose (**14**)	0.0250	0.0241	0.01982	0.0225	0.0252				
Experiment 3:									
Anticipated mmol: Sucrose (0.0184): Fructose (0.0160): Glucose (0.0166)									
Calculated mmol:									
Sucrose (**20**)	0.0283	.0291	0.0242	x	0.0270	x	0.0256	0.0275	0.0228
Fructose (**16**)	0.0197	x	0.0215	0.0197	0.0251				
Glucose (**14**)	0.0263	0.0266	0.0198	0.0235	0.0248				

SI-Table 3.9: The percent error of mmol calculated from integration values of α-per-*O*-TMS glucose (**14**), β-per-*O*-TMS fructose (**16**), and per-*O*-TMS sucrose (**20**) in $CDCl_3$, using DHEA-*O*-TBDPSi (**26**) as internal standard. This mixture was synthesized from free sugar of 1:1:1 mol ratio at room temperature for 24 h. The mass of each experiment was weighed independently of each other. The solution is 0.125 M concentration.

% Error of mmol calculated by ^{29}Si Integration Value: TBDPSi-DHEA as Internal Standard (1.00)									
	Si_2	Si_3	Si_6	Si_1	Si_4	Si_{1f}	Si_{3f}	Si_{4f}	Si_{6f}
Experiment 1:									
Sucrose (**20**)	49%	67%	20%	x	51%	x	35%	45%	14%
Fructose (**16**)	53%	x	23%	15%	48%				
Glucose (**14**)	50%	52%	13%	39%	53%				
Experiment 2:									
Sucrose (**20**)	44%	56%	20%	x	48%	x	16%	41%	17%
Fructose (**16**)	49%	x	22%	17%	43%				
Glucose (**14**)	50%	44%	18%	35%	50%				
Experiment 3:									
Sucrose (**20**)	53%	58%	31%	x	46%	x	39%	49%	24%
Fructose (**16**)	54%	x	34%	23%	57%				
Glucose (**14**)	58%	60%	19%	41%	49%				

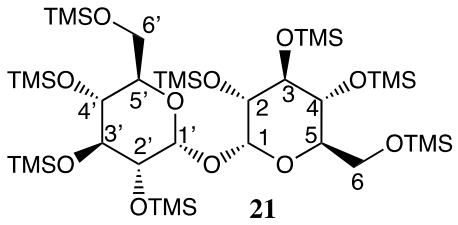

21

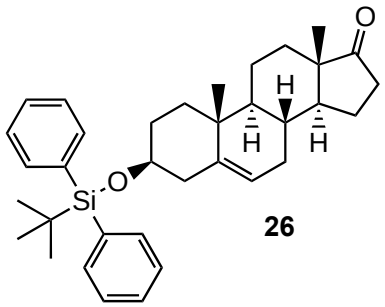

26

SI-Table 3.10: Integration values of per-*O*-TMS trehalose (**21**) in $CDCl_3$ using DHEA-*O*-TBDPSi (**26**) as internal standard. The weighted mole ratio of per-*O*-TMS trehalose (**21**) and internal standard is 1:1 in experiment 1, 0.5:1 in experiment 2, and 0.25:1 in experiment 3. The internal standard measured from a solution and per-*O*-TMS trehalose (**21**) was weighed out for each experiment.

Integration Values: *TBDPSi-DHEA as Internal Standard (1.00)*				
Compounds	Si_4, $Si_{4'}$	Si_3, Si_3	Si_6, Si_6	Si_2, Si_2
	Experiment 1: (1:1 ratio of IS: Trehalose)			
Trehalose (**21**)	2.22 (1.11)	2.31 (1.15)	2.02 (1.01)	2.22 (1.11)
	Experiment 2: (1:0.5 ratio of IS: Trehalose)			
Trehalose (**21**)	0.95 (0.47)	1.09 (0.55)	0.84 (0.42)	0.96 (0.0.48)
	Experiment 3: (1:0.25 ratio of IS: Trehalose)			
Trehalose (**21**)	0.44 (0.22)	0.52 (0.26)	0.40 (0.20)	0.45 (0.225)

SI-Table 3.11: The mmol calculated from integration values of per-*O*-TMS trehalose (**21**) in $CDCl_3$ using DHEA-*O*-TBDPSi (**26**) as internal standard. The weighted mole ratio of per-*O*-TMS trehalose (**21**) and internal standard is 1:1 in experiment 1, 0.5:1 in experiment 2, and 0.25:1 in experiment 3. The internal standard measured from a solution and per-*O*-TMS trehalose (**21**) was weighed out for each experiment.

mmol Calculated by ^{29}Si NMR: *TBDPSi-DHEA as Internal Standard (0.0250)*				
Compounds	Si_4, $Si_{4'}$	Si_3, Si_3	Si_6, Si_6	Si_2, Si_2
	Experiment 1: 0.0249 mmol Trehalose			
Trehalose	0.0555 (0.0277)	0.0577 (0.0288)	0.0505 (0.0252)	0.0555 (0.0277)
	Experiment 2: 0.0126 mmol Trehalose			
Trehalose	0.0227 (0.0113)	0.0272 (0.0136)	0.0190 (0.0095)	0.0220 (0.0110)
	Experiment 3: 0.00635 mmol Trehalose			
Trehalose	0.0107 (0.00537)	0.0130 (0.00650)	0.0100 (0.0050)	0.0112 (0.00562)

SI-Table 3.12: The percent errors of mmol calculated from integration values of per-*O*-TMS trehalose (**21**) in $CDCl_3$ using DHEA-*O*-TBDPSi (**26**) as internal standard. The weighted mole ratio of per-*O*-TMS trehalose (**21**) and internal standard is 1:1 in experiment 1, 0.5:1 in experiment 2, and 0.25:1 in experiment 3. The internal standard measured from a solution and per-*O*-TMS trehalose (**21**) was weighed out for each experiment.

% Error Calculated by ^{29}Si NMR: *TBDPSi-DHEA as Internal Standard (0.0250)*				
Compounds	Si_4, $Si_{4'}$	Si_3, Si_3	Si_6, Si_6	Si_2, Si_2
		Experiment 1: Actual mmol 0.0249		
Trehalose	11%	15%	1.3%	11%
		Experiment 2: Actual mmol 0.0126		
Trehalose	12%	8%	24%	9%
		Experiment 3: Actual mmol 0.0635		
Trehalose	15%	2%	21%	11%

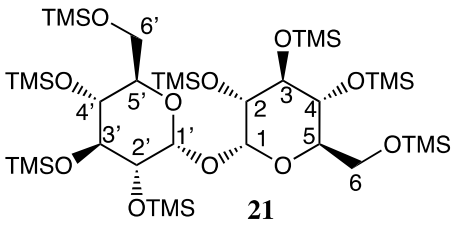

21

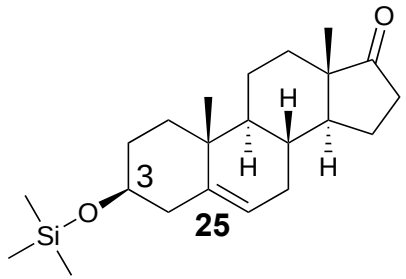

25

SI-Table 3.13: Integration values of per-*O*-TMS trehalose (**21**) in $CDCl_3$ using DHEA-*O*-TMS (**25**) as internal standard. The mole ratio of per-*O*-TMS trehalose (**21**) and internal standard is 1:1 for the triplicate experiment.

Integration Values: *TMSi-DHEA as Internal Standard (1.00)*				
Compounds	Si_4, $Si_{4'}$	Si_3, Si_3	Si_6, Si_6	Si_2, Si_2
	Experiment 1: (1:1 ratio of IS: Trehalose)			
Trehalose	2.27 (1.11)	2.30 (1.15)	1.90 (0.95)	2.02 (1.01)
	Experiment 2: (1:1 ratio of IS: Trehalose)			
Trehalose	2.26 (1.13)	2.15(1.07)	1.96 (0.98)	2.18 (1.09)
	Experiment 3: (1:1 ratio of IS: Trehalose)			
Trehalose	2.30 1.15)	2.16 (1.08)	1.94 (0.97)	2.18 (1.09)

SI-Table 3.14: The mmol calculated and percent error (for each experiment) and for each signal from the triplicate of per-*O*-TMS trehalose (**21**) in $CDCl_3$ using DHEA-*O*-TMS (**25**) as internal standard. The mole ratio of per-*O*-TMS trehalose (**21**) and internal standard is 1:1 for the triplicate experiment.

mmol Calculated by ^{29}Si NMR: *TBDPSi-DHEA as Internal Standard (0.0250)*						
Compounds	Si_4, $Si_{4'}$	Si_3, Si_3	Si_6, Si_6	Si_2, Si_2	Average	% Error
Experiment 1: 0.0247 mmol Trehalose						
Trehalose	0.0292	0.0288	0.0241	0.0257	0.0269	9.74%
Experiment 2: 0.0246 mmol Trehalose						
Trehalose	0.0281	0.0267	0.0244	0.0271	0.0266	8.13%
Experiment 3: 0.0246 mmol Trehalose						
Trehalose	0.0286	0.0269	0.0242	0.0271	0.0269	8.09%
Average	0.0286	0.0272	0.0242	0.0266		
% Error	16%	11.0%	1.17%	8.00%		

SI-Table 3.15: The percent error of per-*O*-TMS trehalose (**21**) in $CDCl_3$ using DHEA-*O*-TMS (**25**) as internal standard. The mole ratio of per-*O*-TMS trehalose (**21**) and internal standard is 1:1 for the triplicate experiment.

% Error Calculated by ^{29}Si NMR: *TBDPSi-DHEA as Internal Standard (0.0250)*				
Compounds	Si_4, $Si_{4'}$	Si_3, Si_3	Si_6, Si_6	Si_2, Si_2
		Experiment 1: 0.0247 mmol Trehalose		
Trehalose	18%	4.0%	2.4%	16%
		Experiment 2: 0.0246 mmol Trehalose		
Trehalose	14%	10%	0.08%	8.1%
		Experiment 3: 0.0246 mmol Trehalose		
Trehalose	16%	10%	1.6%	9.3%

SI-Table 3.16: (Replicate 1): The integration and chemical shifts **(δ)** (Si2, S2', Si2", Si4") of a reaction mixture synthesized from free sugars to produce α-per-*O*-TMS glucose (**14**), β-per-*O*-TMS fructose (**16**), per-*O*-TMS sucrose (**20**), per-*O*-TMS raffinose (**22**), per-*O*-TMS kestose (**23**), per-*O*-TMS stayhose (**24**) and DHEA-*O*-TMS (**25**).

Compound	**Number**	**Si signal**	**Integration**	**δ mixture**	**δ pure**	**Δ**
Glucose (**14**)	6	2	1.22	17.2242	17.2204	0.0038
Fructose (**16**)	8	2	1.19	10.7613	10.7358	0.0255
Surcose (**20**)	12	2'	1.18	17.5278	17.5271	0.0007
Raffinose (**22**)	14	2"	1.03	17.7103*	17.6907	0.0196
Kestose (**23**)	15	4"	1.23	17.8659*	17.8115	0.0544
Styachose (**24**)	16	2'	1.12	17.5028*	17.4750	0.0278
DHEA (**25**)	18		1.00	15.5470	15.5425	0.0045

SI-Table 3.17: (Replicate 1): The integration and chemical shifts **(δ)** (Si2, S2', Si2", Si4") of a reaction mixture synthesized from free sugars to produce α-per-*O*-TMS glucose (**14**), β-per-*O*-TMS fructose (**16**), per-*O*-TMS sucrose (**20**), per-*O*-TMS raffinose (**22**), per-*O*-TMS kestose (**23**), per-*O*-TMS stayhose (**24**) and DHEA-*O*-TMS (**25**) after addition of 1 eq. of DHEA-*O*-TMS (0.0151→5.43 mg/360.61 =0.151).

Compound	**Number**	**Si signal**	**Integration**	**δ mixture**	**δ pure**	**Δ**
Glucose (**14**)	6	2	1.15	17.2261	17.2204	0.0057
Fructose (**16**)	8	2	1.00	10.7632	10.7160	0.0472
Surcose (**20**)	12	2'	1.00	17.5259	17.5271	0.0012
Raffinose (**22**)	14	2"	1.01	17.7084*	17.6907	0.0177
Kestose (**23**)	15	4"	1.09	17.8678*	17.8115	0.0563
Styachose (**24**)	16	2'	0.99	17.5028*	17.4750	0.0278
DHEA (**25**)	18		2.15	15.5470	15.5425	0.0078

* Indicated chemical shift is not aligned with the pure compound, the possibility of chemical shifts listed are in the upfield and downfield of the pure compound.

SI-Table 3.18: (Replicate 2): The integration and chemical shifts **(δ)** (Si2, S2', Si2", Si4") of a reaction mixture synthesized from free sugars to produce α-per-*O*-TMS glucose (**14**), β-per-*O*-TMS fructose (**16**), per-*O*-TMS sucrose (**20**), per-*O*-TMS raffinose (**22**), per-*O*-TMS kestose (**23**), per-*O*-TMS stayhcose (**24**) and DHEA-*O*-TMS (**25**).

Compound	Number	Si signal	Integration	δ mixture	δ pure	Δ
Glucose (**14**)	6	2	1.08	17.2258	17.2204	0.0054
Fructose (**16**)	8	2	1.21	10.7609	10.7358	0.0251
Surcose (**20**)	12	2'	1.16	17.5255	17.5271	0.0016
Raffinose (**22**)	14	2"	1.00	17.6657	17.6907	0.025
Kestose (**23**)	15	4"	0.28	17.8655	17.8115	0.054
Styachose (**24**)	16	2'	0.94	17.5005	17.4750	0.0255
DHEA (**25**)	18		1.00	15.5506	15.5425	0.0081

SI-Table 3.19: (Replicate 1): The integration and chemical shifts **(δ)** (Si2, S2', Si2", Si4") of a reaction mixture synthesized from free sugars to produce α-per-*O*-TMS glucose (**14**), β-per-*O*-TMS fructose (**16**), per-*O*-TMS sucrose (**20**), per-*O*-TMS raffinose (**22**), per-*O*-TMS kestose (**23**), per-*O*-TMS stayhcose (**24**) and DHEA-*O*-TMS (**25**) after addition of 1 eq. of DHEA-*O*-TMS (**25**).

Compound	Number	Si signal	Integration	δ mixture	δ pure	Δ
Glucose (**14**)	6	2	1.00	17.2224	17.2204	0.002
Fructose (**16**)	8	2	1.05	10.7556	10.7358	0.0198
Surcose (**20**)	12	2'	1.05	17.5183	17.5271	0.0088
Raffinose (**22**)	14	2"	0.91	17.6604	17.6907	0.0303
Kestose (**23**)	15	4"	0.23	17.8602	17.8115	0.0487
Styachose (**24**)	16	2'	0.88	17.4971	17.4750	0.0221
DHEA (**25**)	18		1.98	15.5548	15.5425	0.0123

SI-Table 3.20: (Replicate 3): The integration and chemical shifts **(δ)** (Si2, S2', Si2", Si4") of a reaction mixture synthesized from free sugars to produce α-per-*O*-TMS glucose (**14**), β-per-*O*-TMS fructose (**16**), per-*O*-TMS sucrose (**20**), per-*O*-TMS raffinose (**22**), per-*O*-TMS kestose (**23**), per-*O*-TMS stayhcose (**24**) and DHEA-*O*-TMS (**25**).

Compound	Number	Si signal	Integration	δ mixture	δ pure	Δ
Glucose (**14**)	6	2	1.09	17.226	17.220	0.006
Fructose (**16**)	8	2	1.07	10.764	10.736	0.028
Surcose (**20**)	12	2'	1.02	17.530	17.527	0.003
Raffinose (**22**)	14	2"	1.02	17.713	17.691	0.022
Kestose (**23**)	15	4"	1.06	17.868	17.812	0.057
Styachose (**24**)	16	2'	1.05	17.505	17.475	0.030
DHEA (**25**)	18		1.00	15.544	15.543	0.001

SI-Table 3.21: (Replicate 3): The integration and chemical shifts **(δ)** (Si2, S2', Si2", Si4") of a reaction mixture synthesized from free sugars to produce α-per-*O*-TMS glucose (**14**), β-per-*O*-TMS fructose (**16**), per-*O*-TMS sucrose (**20**), per-*O*-TMS raffinose (**22**), per-*O*-TMS kestose (**23**), per-*O*-TMS stayhcose (**24**) and DHEA-*O*-TMS (**25**) after addition of 1 eq. of DHEA-*O*-TMS (**25**).

Compound	Number	Si signal	Integration	δ mixture	δ pure	Δ
Glucose (**14**)	6	2	1.09	17.224	17.220	0.003
Fructose (**16**)	8	2	0.99	10.759	10.736	0.023
Surcose (**20**)	12	2'	1.00	17.522	17.527	0.006
Raffinose (**22**)	14	2"	0.89	17.706	17.691	0.015
Kestose (**23**)	15	4"	1.05	17.862	17.812	0.050
Styachose (**24**)	16	2'	0.96	17.499	17.475	0.024
DHEA (**25**)	18		2.16	15.552	15.543	0.010

References:

1. Bharti, S. K.; Roy, R., Quantitative 1H NMR spectroscopy. *TrAC Trends in Analytical Chemistry* **2012,** *35*, 5-26.

2. Qiuwei Xu, J. R. S., Ting-Chuan Wang, and William H. Schaefer, Quantification and Identification of Components in Solution Mixtures from 1D Proton NMR Spectra Using Singular Value Decomposition. *Anal. Chem.* **2006,** *78*, 7175-7185.

3. Triyasmono, L.; Holzgrabe, U., Combination quantitative 1H NMR and chemometric approaches for the assessment of quality control in commercially available products of red fruit (Pandanus conoidues, Lam.) oil. *Journal of Pharmaceutical and Biomedical Analysis Open* **2023,** *1*, 100010.

4. Gödecke, T.; Napolitano, J. G.; Rodríguez-Brasco, M. F.; Chen, S.-N.; Jaki, B. U.; Lankin, D. C.; Pauli, G. F., Validation of a Generic Quantitative 1
H NMR Method for Natural Products Analysis. *Phytochemical Analysis* **2013,** *24* (6), 581-597.

5. Eriko Fukuda, M. Y., Masaki Baba, Yoshihiro Uesawa, Ryuichiro Suzuki, Osamu Kamo, Koji Tsubono, Kazunori Arifuku, Kazuhisa Yatsunami, and Yoshihito Okada, Application to Classification of Mulberry Leaves using Multivariate Analysis of Proton NMR Metabolomic Data. *Natural Product Communications* **2011,** *6* (11), 1621-1625.

6. Chauthe, S. K.; Sharma, R. J.; Aqil, F.; Gupta, R. C.; Singh, I. P., Quantitative NMR: An Applicable Method for Quantitative Analysis of Medicinal Plant Extracts and Herbal Products. *Phytochemical Analysis* **2012,** *23* (6), 689-696.

7. Caligiani, A.; Acquotti, D.; Palla, G.; Bocchi, V., Identification and quantification of the main organic components of vinegars by high resolution 1H NMR spectroscopy. *Analytica Chimica Acta* **2007,** *585* (1), 110-119.

8. Singh, S.; Roy, R., The application of absolute quantitative1H NMR spectroscopy in drug discovery and development. *Expert Opinion on Drug Discovery* **2016,** *11* (7), 695-706.

9. Forbes, J. L. J. a. J. W., Quantitative Measurement of Hydrogen Types by Intergrated Nuclear Magnetic Resonance Intensities. *Analytical Chemistry 35* (8), 938-942

10. Hollis, D. P., Quantitative Analysis of Aspirin, Phenacetin, and Caffeine Mixtures by Nuclear Magnetic Resonance Spectrometry. *Anal. Chem.* **1963,** *35* (11), 1682–1684.

11. Wang, R. C. C.; Campbell, D. A.; Green, J. R.; Čuperlović-Culf, M., Automatic 1D 1H NMR Metabolite Quantification for Bioreactor Monitoring. *Metabolites* **2021,** *11* (3), 157.

12. Jiang, Y.; David, B.; Tu, P.; Barbin, Y., Recent analytical approaches in quality control of traditional Chinese medicines—A review. *Analytica Chimica Acta* **2010,** *657* (1), 9-18.

13. Emwas, A.-H.; Roy, R.; McKay, R. T.; Tenori, L.; Saccenti, E.; Gowda, G. A. N.; Raftery, D.; Alahmari, F.; Jaremko, L.; Jaremko, M.; Wishart, D. S., NMR Spectroscopy for Metabolomics Research. *Metabolites* **2019,** *9* (7), 123.

14. Wishart, D. S., Quantitative metabolomics using NMR. *TrAC Trends in Analytical Chemistry* **2008,** *27* (3), 228-237.

15. Kostidis, S.; Addie, R. D.; Morreau, H.; Mayboroda, O. A.; Giera, M., Quantitative NMR analysis of intra- and extracellular metabolism of mammalian cells: A tutorial. *Analytica Chimica Acta* **2017,** *980*, 1-24.

16. Madrid-Gambin, F.; Oller, S.; Marco, S.; Pozo, Ó. J.; Andres-Lacueva, C.; Llorach, R., Quantitative plasma profiling by 1H NMR-based metabolomics: impact of sample treatment. *Frontiers in Molecular Biosciences* **2023,** *10*.

17. Napolitano, J. G.; Gödecke, T.; Lankin, D. C.; Jaki, B. U.; McAlpine, J. B.; Chen, S.-N.; Pauli, G. F., Orthogonal analytical methods for botanical standardization: Determination of green tea catechins by qNMR and LC–MS/MS. *Journal of Pharmaceutical and Biomedical Analysis* **2014,** *93*, 59-67.

18. Pauli, G. F.; Gödecke, T.; Jaki, B. U.; Lankin, D. C., Quantitative 1H NMR. Development and Potential of an Analytical Method: An Update. *Journal of Natural Products* **2012,** *75* (4), 834-851.

19. del Campo, G.; Zuriarrain, J.; Zuriarrain, A.; Berregi, I., Quantitative determination of carboxylic acids, amino acids, carbohydrates, ethanol and hydroxymethylfurfural in honey by 1 H NMR. *Food Chemistry* **2016,** *196*, 1031-1039.

20. del Campo, G.; Berregi, I.; Caracena, R.; Zuriarrain, J., Quantitative determination of caffeine, formic acid, trigonelline and 5-(hydroxymethyl)furfural in soluble coffees by 1H NMR spectrometry. *Talanta* **2010,** *81* (1-2), 367-371.

21. Peez, N.; Imhof, W., Quantitative 1H-NMR spectroscopy as an efficient method for identification and quantification of PVC, ABS and PA microparticles. *The Analyst* **2020,** *145* (15), 5363-5371.

22. Grzegorz Maniara, K. R., Srinivasan Rajan, and Gerald W. Stockton, Method Performance and Validation for Quantitative Analysis by 1H and 31P NMR Spectroscopy. Applications to Analytical Standards and Agricultural Chemicals. *Anal. Chem.* **1998,** *70* (23), 4921–4928.

23. Wang, R.; Luo, Y.; Jia, H.; Ferrell, J. R.; Ben, H., Development of quantitative 13C NMR characterization and simulation of C, H, and O content for pyrolysis oils based on 13C NMR analysis. *RSC Advances* **2020,** *10* (43), 25918-25928.

24. Zhang, Y.-Y.; Zhang, J.; Zhang, W.-X.; Wang, Y.; Wang, Y.-H.; Yang, Q.-Y.; Wu, S., Quantitative 1H Nuclear Magnetic Resonance Method for Assessing the Purity of Dipotassium Glycyrrhizinate. *Molecules* **2021,** *26* (12), 3549.

25. Otte, D. A. L.; Borchmann, D. E.; Lin, C.; Weck, M.; Woerpel, K. A., 13C NMR Spectroscopy for the Quantitative Determination of Compound Ratios and Polymer End Groups. *Organic Letters* **2014,** *16* (6), 1566-1569.

26. Johnson, R. L.; Schmidt-Rohr, K., Quantitative solid-state 13C NMR with signal enhancement by multiple cross polarization. *Journal of Magnetic Resonance* **2014,** *239*, 44-49.

27. Leong, S. Y.; Duque, S. M.; Abduh, S. B. M.; Oey, I., Carbohydrates. In *Innovative Thermal and Non-Thermal Processing, Bioaccessibility and Bioavailability of Nutrients and Bioactive Compounds*, Editorial, M. R. B., Ed. Charlotte Cockle Acquisition: 2019; pp 171-206.

28. Wang, X.; Zhang, L.-H.; Ye, X.-S., Recent development in the design of sialyltransferase inhibitors. *Medicinal Research Reviews* **2003,** *23* (1), 32-47.

29. Rojas-Escudero, E.; Alarcón-Jiménez, A. L.; Elizalde-Galván, P.; Rojo-Callejas, F., Optimization of carbohydrate silylation for gas chromatography. *Journal of Chromatography A* **2004,** *1027* (1-2), 117-120.

30. Ruiz-Matute, A. I.; Hernández-Hernández, O.; Rodríguez-Sánchez, S.; Sanz, M. L.; Martínez-Castro, I., Derivatization of carbohydrates for GC and GC–MS analyses. *Journal of Chromatography B* **2011,** *879* (17-18), 1226-1240.

31. Gorwitz, M. Silylation of Carbohydrate Syrups. Western Michigan University, 1979.

32. Valliyodan, B.; Shi, H.; Nguyen, H. T., A Simple Analytical Method for High-Throughput Screening of Major Sugars from Soybean by Normal-Phase HPLC with Evaporative Light Scattering Detection. *Chromatography Research International* **2015,** *2015*, 1-8.

33. Schraml, J., 29Si NMR Spectroscopy of Trimethylsilyl Tags. *Progress in NMR Spectroscopy* **1990,** *22*, 289-348.

34. Nelum P. Piyasena, K. G.; Hettiarachchi, L. S. K.; D. P. S. Jayawardhane, S. A.; U. Edirisinghe, E. N.; Jayasinghe, W. S., Evaluation of inherent fructose, glucose and sucrose concentrations in tea leaves (Camellia sinensis L.) and in black tea. *Applied Food Research* **2022,** *2* (1), 100100.

35. Knopp, S.; Bytof, G.; Selmar, D., Influence of processing on the content of sugars in green Arabica coffee beans. *European Food Research and Technology* **2005,** *223* (2), 195-201.

36. Shevchuk, A.; Megías-Pérez, R.; Zemedie, Y.; Kuhnert, N., Evaluation of carbohydrates and quality parameters in six types of commercial teas by targeted statistical analysis. *Food Research International* **2020,** *133*, 109122.

37. Williams, E. A.; Cargioli, J. D., Silicon-29 NMR Spectroscopy. **1979,** *9*, 221-318.

38. George C. Levy, J. D. C., Peter C. Juliano, and Tyrone D. Mitchell, Silicon-29 Spin-Lattice Relaxation in Organosilicon Compounds. *Journal of the American Chemical Society* **1973,** *95* (11), 3445-3454.

39. Kimber, R. K. H. a. B. J., 29Si and 13 C Nuclear Magnetic Resonance Studies of Organosilicon Chemistry. I. Trimethylsilyl Compounds. *Journal of Magnetic Resonance* **1974,** *17*, 174-188.

40. Orelllana, M. "Title" Dissertation of Philosophy **2024,** Univeristy of California, Davis, California.